Ontario Geological Survey
Miscellaneous Paper 113

Geoscience Research Grant Program

Summary of Research 1982-1983

edited by
E.G.Pye

1983

Ontario
Ministry of Natural Resources

Hon. Alan W. Pope
Minister

W. T. Foster
Deputy Minister

ISSN 0704-2752 (Series)
ISSN 0225-5316 (Sub-series)

Publications of the Ontario Ministry of Natural Resources are available from the following sources. Orders for publications should be accompanied by cheque or money order payable to the *Treasurer of Ontario*.

Reports, maps, and price lists (personal shopping or mail order):

Public Service Centre, Ministry of Natural Resources
Room 1640, Whitney Block, Queen's Park
Toronto, Ontario M7A 1W3

Reports and accompanying maps (personal shopping):

Ontario Government Bookstore
Main Floor, 880 Bay Street
Toronto, Ontario

Reports and accompanying maps (mail order or telephone orders):

Publications Services Section, Ministry of Government Services
5th Floor, 880 Bay Street
Toronto, Ontario M7A 1N8
Telephone (local calls), 965-6015
Toll-free long distance, 1-800-268-7540
Toll-free from Area Code 807, 0-ZENITH-67200

Van Loon, Jon C.
1983: Direct Trace Elemental Analysis of Solid Samples by Techniques of Atomic Spectrometry; Grant 140, p.177-182 *in* Geoscience Research Grant Program, Summary of Research 1982-1983, edited by E.G. Pye, Ontario Geological Survey, Miscellaneous Paper 113, 199p.

Scientific Editor: Z.L. Mandziuk

1000-83-Regency

CONTENTS

Page

Introductory Remarks iv
1982-1983 Geoscience Research Grant Recipients vi

Barker, J.F., Macqueen, R.W., and Fritz, P.; Grant 114 Source, Correlation, and Thermal Maturation History of Hydrocarbon Deposits of Southern Ontario 1

Borthwick, A.A. and Naldrett, A.J.; Grant 106 Neutron Activation Analysis for Platinum Group Elements in Chromitites 7

Brand, Uwe and Terasmae, Jaan; Grant 131 Source Rock Geochemistry of Pleistocene Tills of Southern Ontario 13

Card, J.W. and Bell, Keith; Grant 105 Latter-Stage Decay Products of ^{222}Rn — Use in Radioactive Waste Management and Uranium Exploration 21

Crocket, J.H., McNutt, R.H., Schwarcz, H.P., Rees, C.E., Blum N., Hurley, T., Bowins, R., and Kabir, A.; Grant 132 Isotopic and Geochemical Characterization of Archean Iron Formations and Associated Volcanic Rocks — Some Preliminary Results from the Temagami and Boston Iron Formations 29

Edwards, N., Lo, B., Cheesman, S., Nabighian, M., and Opplinger, G.; Grant 145 Cross-Hole Magnetometric Resistivity (MMR) 41

Fralick, Philip W., Miall, A.D., and Abdel-Rahman; Grant 136 Rock Geochemistry as a Placer Exploration Tool in the Southeastern District of Algoma 55

Fyfe, W.S., Kronberg, B.I., Long, D.F., Murray, F., Powell, M., Try, C., van der Flier, E., Winder, C.G., and Brown, J.R.; Grant 134 Stratigraphy and Geochemistry of Northern Ontario Carbonaceous Deposits: Onakawana Lignites 63

Gale, J.E., Nadon, R.L., McKay, D.A., and Sweezey, R.A.; Grant 92 Impact of Groundwater on Surface and Subsurface Mining Activities in the Niagara Escarpment 83

Greenhouse, J.P., Karrow, P.F., and Farvolden, R.N.; Grant 128 Subsurface Quaternary Stratigraphy Using Borehole Geophysics 93

Greenhouse, J.P. and Monier-Williams, M.; Grant 127 A Gravity Survey of the Dundas Buried Valley West of Copetown, Ontario 97

Hudec, Peter P.; Grant 112 Petrographic Number Re-Evaluation: Phase 2 109

Kenny, T.C.; Grant 113 Investigation of Factors Controlling Changes of Groundwater Pressure in Clay Slopes 117

Lesher, C.M., Campbell, I.H., Coad, P., Franklin, J.M., Gibson, H.L., Goodwin, A.M., Gorton, M.P., Hart, T.R., Sowa, J.M., and Thurston, P.C.; Grant 80 Rare Earth Elements in Felsic Volcanic Rocks Associated with Cu-Zn Massive Sulphide Mineralization 127

Mereu, R.F.; Grant 57 A Microearthquake Survey of the Gobles Oil Field Area of Southwestern Ontario 135

Rao, B.V., Naldrett, A.J., Evensen, N.M., and Dressler, B.O.; Grant 146 Contamination and Genesis of the Sudbury Ores 139

Rowell, W.F. and Edgar, A.D.; Grant 100 Petrology, Geochemistry, and Economic Potential of the Nipissing Gabbro 153

Strangway, D.W., Ilkisik, O.M., and Redman, J.D.; Grant 118 Surface Electromagnetic Mapping in Selected Positions of Northern Ontario, 1982-1983 159

Symons, D.T.A. and Stupavsky, M.; Grant 143 Analysis of Aeromagnetic Anomalies over Algoman-Type Iron Formations 175

Van Loon, Jon C.; Grant 140 Direct Trace Elemental Analysis of Solid Samples by Techniques of Atomic Spectrometry 177

Watkinsin, D.H., Whittaker, P.J., and Jones, P.L.; Grant 107 Platinum Group Elements in the Eastern Gabbro, Coldwell Complex, Northwestern Ontario 183

Wicks, F.J., Schandl, E.S., Ozoray, Judit, and Pu, Wan; Grant 138 Mineralogy and Geochemistry of the Chrysotile Asbestos Deposits of Ontario 193

INTRODUCTORY REMARKS

The Ontario Geoscience Research Grants Program was initiated in early 1978, as a means of supporting mission-oriented research at Ontario universities, to complement the work of the Ontario Geological Survey in response to the various issues within its mandate:

> *"To stimulate exploration for, and facilitate sound planning in all matters related to, mineral and other earth resources by providing an inventory and analysis of the geology and mineral deposits of Ontario."*

The Grants Program is administered by a committee reporting to the Director of the Ontario Geological Survey and is made up of 3 representatives of the minerals industry, 3 representatives of the university community, 4 representatives of the Survey, and a chairman. Appointments of industry and Ontario university representatives are up to 3 years, renewable once. The members of the present committee are:

S.N. Charteris, Chairman	Corporation Falconbridge Copper
A. Becker	Questor Surveys Limited
N. Paterson	Paterson, Grant and Watson Limited
J.H. Crocket	McMaster University
P.F. Karrow	University of Waterloo
W.S. Fyfe	University of Western Ontario
J.A. Coope	Newmont Explorations of Canada Limited
A.C. Colvine	Ontario Geological Survey
P.C. Thurston	Ontario Geological Survey
P.G. Telford	Ontario Geological Survey
J.A.C. Fortescue	Ontario Geological Survey

The role of the committee is to receive, review, and rank proposals from research workers at Ontario universities with respect to scientific merit and relevance to the objectives and activities of the Ontario Geological Survey; and to recommend funding or rejection. A feature of the appraisal process is that each submission is referred by the committee to at least 4 geoscientists in industry, the university community, and/or government outside the Ontario Geological Survey, and 1 member of the Survey for critical review and comment to ensure the most thorough and objective appraisal possible.

Proposals for projects up to 3 years duration are acceptable. Original and renewal applications must be submitted by November 15 preceding the fiscal year (April 1 - March 31) for which grants are awarded. Successful applicants are expected to submit a brief report for publication in the annual Summary of Research, and to participate in an annual seminar to present the results of their research to the community at large. Publication in scientific journals is encouraged, and a final report is required by the Ontario Geological Survey within 6 months of the termination of funding.

Nine final reports on research projects partially or wholly funded under the Ontario Geoscience Grant Program in 1982-1983 will be published as Ontario Geological Survey Open File Reports by May 1984. They are:

Grant 57: A Microearthquake Survey of the Gobles Oil Field Area of Southwestern Ontario; R.F. Mereu, University of Western Ontario.

Grant 80: Rare Earth Elements in Felsic Volcanic Rocks; I.H. Campbell, University of Toronto.

Grant 92: Impact of Groundwater on Surface and Subsurface Mining Activities in the Niagara Escarpment; J.E. Gale, University of Waterloo.

Grant 105: Latter-Stage Decay Products of ^{222}Rn — Use in Radioactive Waste Management; K. Bell, Carleton University.

Grant 112: Petrographic Number Re-Evaluation; P.P. Hudec, University of Windsor.

Grant 113: Field Investigation of Factors Controlling Changes of Groundwater Pressure in Clay Slopes; T.C. Kenney, University of Toronto.

Grant 127: Gravity Survey of the Upper Dundas Buried Valley; J.P. Greenhouse, University of Waterloo.

Grant 136: Rock Geochemistry as a Placer Exploration Tool; A.D. Miall, University of Toronto.

Grant 143: Analysis of Aeromagnetic Anomalies over Algoman-Type Iron Formations; D.T.A. Symons, University of Windsor.

This publication is the fifth annual Summary of Research, and presents brief descriptions of the projects funded for the fiscal year ending March 31, 1983. Of the 22 projects approved for funding in 1982-1983, 11 were renewal projects.

UNIVERSITY	APPROVED			REJECTED	
Brock	$ 20,440	1	.....	$ 12,900	1
Carleton	37,622	2	.....	11,400	1
Guelph	—	0	.....	—	0
Lakehead	—	0	.....	—	0
Laurentian	*	(1)	.....	12,000	1
McMaster	45,000	1	.....	22,946	1
Ottawa	—	0	.....	8,600	1
Queen's	—	0	.....	68,291	2
Toronto	206,444	9	.....	22,285	1
Waterloo	71,004	4	.....	9,350	1
Western	81,723*	3	.....	44,000	2
Windsor	37,740	2	.....	13,720	1
York	—	0	.....	—	0
Total	$499,973	22	.....	$225,942	12

*A grant for $48,500 was submitted by the University of Western Ontario but was held jointly with Laurentian University.

The undersigned would like to thank the chairman and the members of the committee for their hard work and participation in the program during the past year, and to the large number of dedicated scientists who gave freely of their time and expertise to review the proposals and provide objective appraisals to serve as a basis for selecting the projects reported on in this publication. The work of the individual researchers also is gratefully acknowledged, for it is only through their endeavours and commitment to scientific excellence that the objectives of the program can be achieved. Finally, special thanks are due to Ms. W. Pacquette, who served as Grants Administrator and Secretary.

E.G. Pye
Director
Ontario Geological Survey

Ontario Geoscience Research Grant Recipients 1982-1983

GRANT NUMBER	PRINCIPAL APPLICANT	UNIVERSITY	TITLE
57	R.F. Mereu	Western	A Microearthquake Survey of the Gobles Oil Field Area of Southwestern Ontario
80	I.H. Campbell	Toronto	Rare Earth Elements in Felsic Volcanic Rocks Associated with Cu-Zn Massive Sulphide Mineralization
92	J.E. Gale	Waterloo	Impact of Groundwater on Surface and Subsurface Mining Activities in the Niagara Escarpment
100	A.D. Edgar	Western	Petrology, Geochemistry, and Economic Potential of the Nipissing Gabbro
105	K. Bell	Carleton	Latter-Stage Decay Products of ^{222}Rn — Use in Radioactive Waste Management and Uranium Exploration
106	A.J. Naldrett	Toronto	Platinum Group Elements in Layered Intrusions
107	D.H. Watkinson	Carleton	Platinum Group Elements in Alkaline Rocks of Northwestern Ontario
112	P.P. Hudec	Windsor	Petrographic Number Re-Evaluation
113	T.C. Kenney	Toronto	Field Investigation of Factors Controlling Changes of Groundwater Pressure in Clay Slopes
114	J.F. Barker	Waterloo	Source, Correlation, and Thermal Maturation History of Hydrocarbon Deposits of Southern Ontario
118	D.W. Strangway	Toronto	Surface Electromagnetic Mapping in Selected Positions of Northern Ontario
127*	J.P. Greenhouse	Waterloo	Gravity Survey of the Upper Dundas Buried Valley
128*	R.N. Farvolden	Waterloo	Subsurface Quaternary Stratigraphy Using Borehole Geophysics
131*	U. Brand	Brock	Source Rock Geochemistry of Pleistocene Tills of Southern Ontario
132*	J.H. Crocket	McMaster	Genesis of Precambrian Iron Formations — Links with Base and Precious Metal Mineralization
134*	W.S. Fyfe and D. Long	Western/ Laurentian	Stratigraphy and Geochemistry of Northern Ontario Carbonaceous Deposits: Onakawana Lignites and James Bay Peats
136*	A.D. Miall	Toronto	Rock Geochemistry as a Placer Exploration Tool
138*	F.J. Wicks	Toronto	Mineralogy and Geochemistry of the Chrysotile Asbestos Deposits of Ontario
140*	J.C. Van Loon	Toronto	Direct Trace Elemental Analysis of Solid Samples by Techniques of Atomic Spectrometry
143*	D.T.A. Symons	Windsor	Analysis of Aeromagnetic Anomalies over Algoman-Type Iron Formations
145*	R.N. Edwards	Toronto	Cross-Hole Magnetometric Resistivity
146*	A.J. Naldrett	Toronto	Contamination and Genesis of the Sudbury Ores

*New OGRF projects initiated in fiscal 1982-1983.

Conversion Factors for Measurements in Ontario Geological Survey Publications

If the reader wishes to convert imperial units to SI (metric) units or SI units to imperial units the following multipliers should be used:

CONVERSION FROM SI TO IMPERIAL			CONVERSION FROM IMPERIAL TO SI		
SI Unit	*Multiplied by*	*Gives*	*Imperial Unit*	*Multiplied by*	*Gives*
			LENGTH		
1 mm	0.039 37	inches	1 inch	**25.4**	mm
1 cm	0.393 70	inches	1 inch	**2.54**	cm
1 m	3.280 84	feet	1 foot	**0.304 8**	m
1 m	0.049 709 7	chains	1 chain	20.116 8	m
1 km	0.621 371	miles (statute)	1 mile (statute)	**1.609 344**	km
			AREA		
1 cm^2	0.155 0	square inches	1 square inch	**6.451 6**	cm^2
1 m^2	10.763 9	square feet	1 square foot	**0.092 903 04**	m^2
1 km^2	0.386 10	square miles	1 square mile	2.589 988	km^2
1 ha	2.471 054	acres	1 acre	0.404 685 6	ha
			VOLUME		
1 cm^3	0.061 02	cubic inches	1 cubic inch	**16.387 064**	cm^3
1 m^3	35.314 7	cubic feet	1 cubic foot	0.028 316 85	m^3
1 m^3	1.308 0	cubic yards	1 cubic yard	0.764 555	m^3
			CAPACITY		
1 L	1.759 755	pints	1 pint	0.568 261	L
1 L	0.879 877	quarts	1 quart	1.136 522	L
1 L	0.219 969	gallons	1 gallon	**4.546 090**	L
			MASS		
1 g	0.035 273 96	ounces (avdp)	1 ounce (avdp)	28.349 523	g
1 g	0.032 150 75	ounces (troy)	1 ounce (troy)	**31.103 476 8**	g
1 kg	2.204 62	pounds (avdp)	1 pound (avdp)	**0.453 592 37**	kg
1 kg	0.001 102 3	tons (short)	1 ton (short)	**907.184 74**	kg
1 t	1.102 311	tons (short)	1 ton (short)	**0.907 184 74**	t
1 kg	0.000 984 21	tons (long)	1 ton (long)	**1016.046 908 8**	kg
1 t	0.984 206 5	tons (long)	1 ton (long)	**1.016 046 908 8**	t
			CONCENTRATION		
1 g/t	0.029 166 6	ounce (troy)/ ton (short)	1 ounce (troy)/ ton (short)	34.285 714 2	g/t
1 g/t	0.583 333 33	pennyweights/ ton (short)	1 pennyweight/ ton (short)	1.714 285 7	g/t

OTHER USEFUL CONVERSION FACTORS

1 ounce (troy)/ton (short)	20.0	pennyweights/ton (short)
1 pennyweight/ton (short)	0.05	ounce (troy)/ton (short)

NOTE—Conversion factors which are in bold type are exact. The conversion factors have been taken from or have been derived from factors given in the Metric Practice Guide for the Canadian Mining and Metallurgical Industries published by The Mining Association of Canada in cooperation with the Coal Association of Canada.

Grant 114 Source, Correlation, and Thermal Maturation History of Hydrocarbon Deposits of Southern Ontario

J.F. Barker, R.W. Macqueen, and P. Fritz
Department of Earth Sciences, University of Waterloo

ABSTRACT

Conventional oil deposits occur in reservoirs of Cambrian to Devonian age in southern Ontario, even though some Silurian and all Devonian source rocks are insufficiently mature thermally to have generated significant oil pools. Conventional organic geochemical studies and carbon isotope studies have identified 3 oil groups: Devonian-reservoired, Silurian-reservoired, and Cambrian/Ordovician-reservoired oils. The Silurian-reservoired oils are geochemically and isotopically correlated with Silurian (Guelph Formation) source rocks. The Cambrian/Ordovician oils could have been produced from sediments of that age but no specific sources have been identified. The source of Devonian oils is still very uncertain.

Natural gases have chemical characteristics consistent with generation from mainly immature sediments, but most isotopic maturity indicators point to a mature-to-overmature source which would necessitate gas migration either from the Precambrian basement or over hundreds of kilometres from deeper parts of the Appalachian and Michigan Basins. A reinterpretation of the isotopic data which emphasizes kinetic factors rather than thermal factors in the generation of the observed carbon and hydrogen isotope distributions has been made. This permits essentially all the data on Ontario natural gases to be *rationalized with a rather immature, perhaps very local,* source.

Unconventional energy sources, namely oil shales, are the topic of current studies. Three possible oil shales are recognized: the Upper Devonian Kettle Point Formation, the Middle Devonian Marcellus Formation, and the Upper Ordovician Collingwood Member of the Lindsay Formation. Resource assessment is continuing, as is an attempt to establish a preliminary conceptual model which considers the geological and geochemical controls of organic richness (and so shale oil potential).

INTRODUCTION

This report presents the progress made from June 1982 until June 1983 in the study of the occurrence and origin of both conventional oil and gas pools and also unconventional hydrocarbon deposits, namely oil shales, in southern Ontario. The research into the conventional deposits is essentially complete and is the subject of 2 papers being prepared for submission to journals. The oil shale studies are continuing through 1984 and so only the preliminary progress will be described here.

OIL AND GAS DEPOSITS

The study of the occurrence and origin of these deposits has three specific aims:

1. to establish the thermal maturation level of selected sedimentary sequences through conodont colour alteration studies, organic geochemical studies, and kerogen reflectance measurements
2. to determine the probable thermal history of these deposits and host rocks
3. to apply, improve, and assess organic geochemical and isotopic methods for correlation of oil and gas pools and for correlation of petroleum deposits with their source rocks.

The thermal history of sedimentary organic matter, mainly kerogen, is usually discussed relative to the optimum time-temperature conditions for hydrocarbon (oil) generation. Immature kerogen has not been heated sufficiently to produce oil, but the sediment may contain associated hydrocarbon gases, mainly biogenic methane. At perhaps 40-80°C maximum paleotemperature, the kerogen should have been sufficiently matured to produce oil as well as natural gas. At higher paleotemperatures, 120-160°C, only hydrocarbon gases should be present, as liquid hydrocarbons are no longer stable. The associated kerogen is considered overmature. A number of thermal maturation indicators are commonly employed. Vitrinite reflectance, thermal alteration index (T.A.I.), and the conodont colour alteration index (C.A.I.) utilize the temperature-dependent change in colour or light reflectance of various kerogen components. The hydrocarbon proportion of bitumen from mature sediments generally exceeds 40% and this maturation indicator is also utilized in southern Ontario.

Table 1 summarizes maturation level indicators for organic matter in the Paleozoic strata of southern Ontario. Only a few samples have been examined to date, but the conclusions are consistent with the more extensive studies in southern Ontario by Legall *et al.* (1981). Individual indicators alone rarely provide a definitive indication of thermal maturation, but when considered together, they provide a reasonably consistent picture. Only Cambrian to Middle Silurian age sediments should have produced oil; Upper Silurian and Devonian strata should only be

TABLE 1 MATURATION LEVEL INDICATORS FOR ORGANIC MATTER IN PALEOZOIC STRATA OF SOUTHERN ONTARIO.

	SYSTEM	VITRINITE REFLECTANCE R_O, %	THERMAL ALTERATION INDEX, TAI	CONODONT COLOURATION INDEX, CAI	BITUMEN CHARACTER	INFERRED HYDROCARBON POTENTIAL
DEVONIAN	UPPER	0.39	2-	1.5	—	Immature
	MIDDLE	0.32 to 0.53	1+ to 2-	1.5	Immature-mature	
	LOWER	—	—	1.5	—	
SILURIAN	UPPER	—	—	1.5	Immature	
	MIDDLE	0.40 to 0.93	2 to 2+	1.5	Immature-mature	
	LOWER	—	—	1.5	—	
ORDOVICIAN	UPPER	0.41 to 1.38	2- to 3-	1.5	Mature	Mature
	MIDDLE	0.36 to 1.00	2+ to 3-	1.5 to 2.5	—	
CAMBRIAN	UPPER	0.81	—	—	Mature	

capable of producing natural gas and perhaps condensate (very light oil products).

T.G. Powell of the Geological Survey of Canada has examined about 35 crude oil samples and over 30 sedimentary rock samples from southern Ontario. Oil-oil correlation studies revealed 3 distinct groups. One group includes all oils found in Silurian reservoirs. These have organic geochemical characteristics typical of oils associated with evaporite/carbonate sequences. Oils from Devonian and from Cambrian and Ordovician reservoirs have many similarities and have a generally immature organic geochemical character. However, subtle differences have not noted between Devonian and Cambro-Ordovician oils (Macqueen *et al.* in preparation). Carbon isotope differences in the saturate and aromatic fractions of oils from these reservoirs support this 3-fold division of Ontario oils (Figure 1).

Geochemical methods of oil-source rock correlation have been attempted to identify the source of these oil pools. Organic geochemical techniques suggest a local Silurian source, perhaps within the Middle Silurian Guelph (Eramosa) Formation, for Silurian oils. Organic matter in Cambrian and Ordovician sedimentary rocks appears to be sufficiently mature to have produced oils reservoired in these rocks but no specific source materials could be correlated with these oils. Devonian age sediments were likely not sufficiently mature in organic matter to have generated Devonian oils, at least in terms of generally accepted concepts, and no source for them has been identified. Carbon isotope correlation techni-

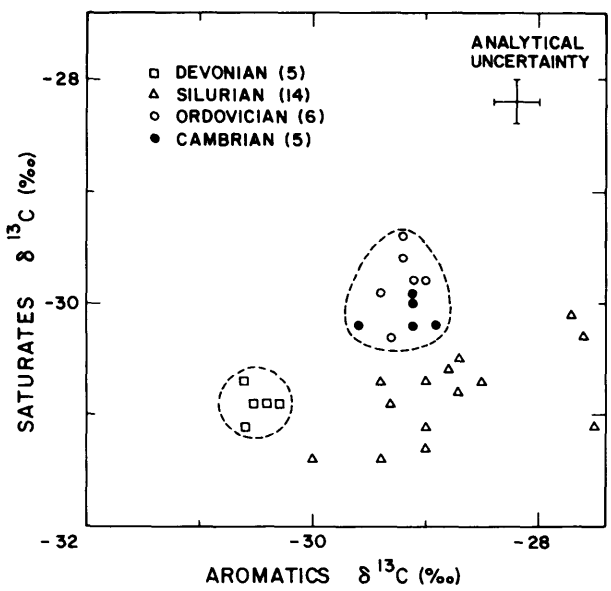

Figure 1. Oil-oil correlations using the carbon isotope ratios of saturate and aromatic fraction (after Bree 1983).

ques also identified the Guelph (Eramosa) Formation as a potential source for Silurian oil pools, and the Devonian Kettle Point Formation for some Devonian oils, but failed to suggest potential sources for the other oils (Bree 1983). It has become obvious that the simple isotope correlation techniques described in the literature are of very limited applicability in southern Ontario.

Sixty-two natural gas samples from southern Ontario and 6 samples from the adjacent United States have been analyzed for hydrocarbon and nonhydrocarbon gas composition, and most methane, ethane, and propane plus butane fractions have been analyzed for $^{13}C/^{12}C$ and $^{2}H/^{1}H$ ratios. Additional chemical data were obtained from Paper 70-72, Ontario Department of Mines and Northern Affairs (1970) and from the files of the Petroleum Resource Section, Ministry of Natural Resources.

The gases are quite dry (mean CH_4 concentration is 85% with other hydrocarbons comprising only 8.5% by volume) and so could have been generated from immature or overmature sources. The major hydrocarbon gas is N_2. This is characteristic of immature gas. Other chemical indicators of source maturation (isobutane/normal butane ratios, ethane/propane ratios) are equivocal.

Gas deposits in southern Ontario occur in both the Appalachian and Michigan Basins and along the Algonquin Arch, a generally positive structural feature separating the basins during much of Lower Paleozoic time. There are very few systematic chemical differences between gases in the 2 basins. However, a separation is evident if the ratio of ethane to propane is divided by the ratio of isobutane to normal butane (Nantais 1982). The resulting ratio exceeds 3.5 in the Appalachian Basin and is less than 3.5 in the Michigan Basin. Some mixing of gases derived from these basins is evident from the imperfect geographical distribution of these ratio values along the Algonquin Arch (Figure 2).

Figure 3 combines hydrocarbon chemistry (methane/total hydrocarbon) and methane carbon isotope ratios, both of which are sensitive to source thermal maturation level (Stahl 1977; Fuex 1977). This plot suggests that the dominant source of methane in southern Ontario is thermally mature to overmature. This is somewhat at odds with the dominance of N_2 in the nonhydrocarbon gas fraction and the immature to only marginally mature maturation level of the enclosing strata.

A number of explanations are possible. One possibility is that there was migration of a major portion of the hydrocarbon components of the natural gas from more mature (deeper?) areas in the basins. However, from studies of thermal maturation in these basins and the few analyses carried out on U.S.A. gases in this study, this possibility is unlikely. A second hypothesis is that significant

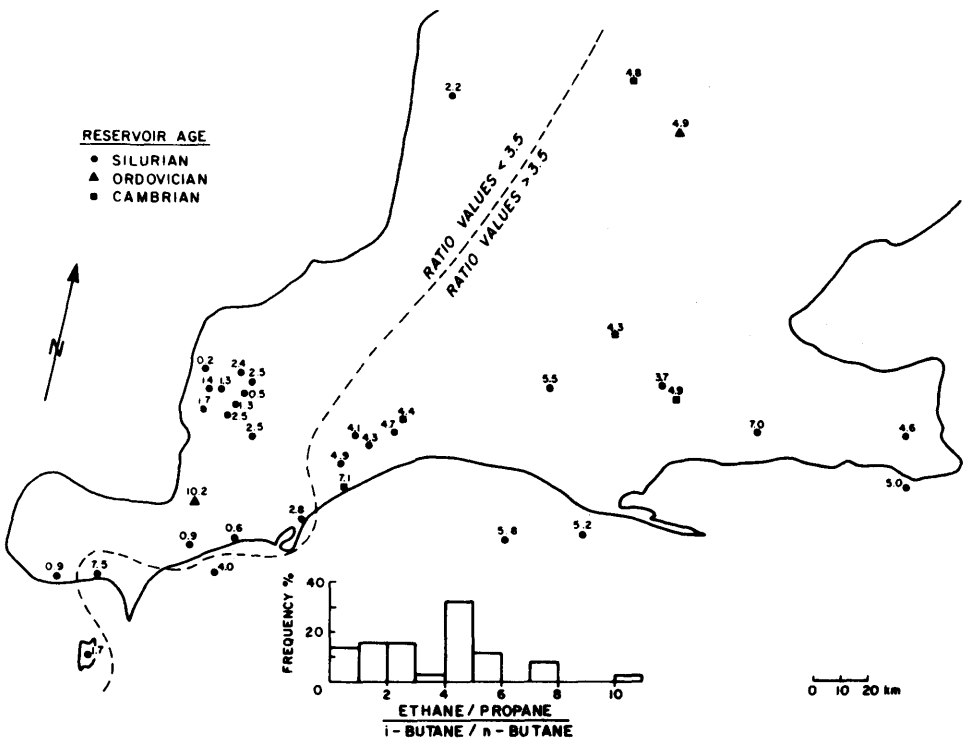

Figure 2. Distribution of the ethane to propane divided by isobutane to normal butane ratios for natural gases in southern Ontario (from Nantais 1982)

overmature methane entered the gas pools via diffusion from the Precambrian basement rocks. The presence of overmature methane in deep crustal and perhaps in mantle materials has been proposed by Gold (1982) and substantiated by studies of rift zones, ocean-spreading centres, and deep groundwaters of the Canadian Shield. However, there is little evidence to support deep sources for Ontario natural gases. A third possibility is that apparently overmature methanes can be generated at much lower temperatures if unusually long and stable time periods are available for gasification. The geochemical data from Paleozoic-age pools can be rationalized with this hypothesis and certainly a long period has been available for natural gas generation.

The concept of petroleum and natural gas generation recognizes the importance of both temperature and time. The interpretation of natural gas chemistry and isotope composition has generally emphasized temperature. The generation of apparently "overmature" gases from thermally immature organic matter suggests that the application of maturation indicators in natural gas studies must recognize the importance of time-dependent (kinetic) processes, especially for pools hosted in pre-Tertiary hosted rocks.

OIL SHALES

There is no geological or chemical definition of an oil shale. Any rock yielding oil in commercial quantities upon pyrolysis can be considered an oil shale. Pyrolysis involves the nonoxidative thermal breakdown of the large, complex kerogen molecules, yielding smaller, oil-like products. Three possible oil shales are found in Ontario: the Upper Devonian Kettle Point Formation, the Middle Devonian Marcellus Formation, and the Upper Ordovician Collingwood Member of the Lindsay Formation (previously included in the Whitby Formation). Figure 4 indicates the outcrop or subcrop distribution of these units. Studies of these units have been undertaken by the Ontario Geological Survey, by the Federal Department of Energy, Mines and Resources, and by the authors through Ontario Geoscience Research Grant 114.

Thermal maturation has been defined by a number of techniques in addition to those employed in the oil and gas studies. These include pyrolysis with the determination of bitumem/kerogen ratio and H and C analysis of kerogen. Results are in agreement with maturation levels indicated in Table 1. The Billings Formation (the equivalent of the Whitby Formation in the Ottawa area) is mature to overmature. Its oil yields upon pyrolysis are less than 5 l/t, which is consistent with the observation that only immature to marginally mature sediments are possible oil shales. More mature sediments have already yielded oil by natural pyrolysis. The presence of a significant (10-40%) portion of bitumen in sample of the Collingwood Member reflects its marginal maturation level and may

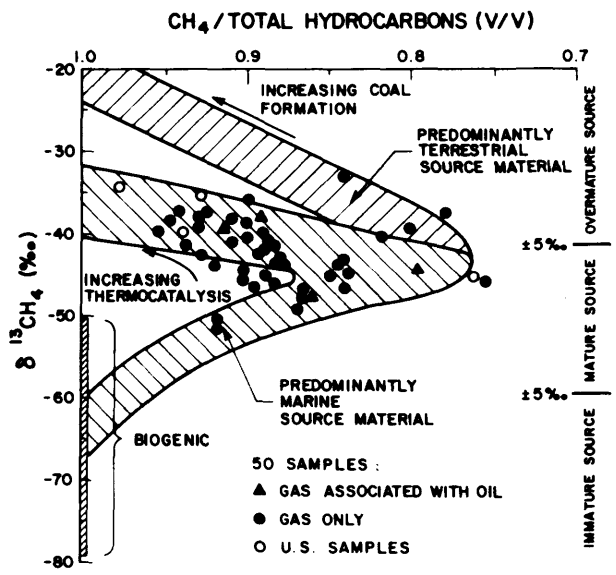

Figure 3. The relationship between hydrocarbon chemistry and carbon isotope ratio of methane in Ontario natural gases. Worldwide trends are from Stahl (1977) and source maturation conditions were suggested by Fuex (1977).

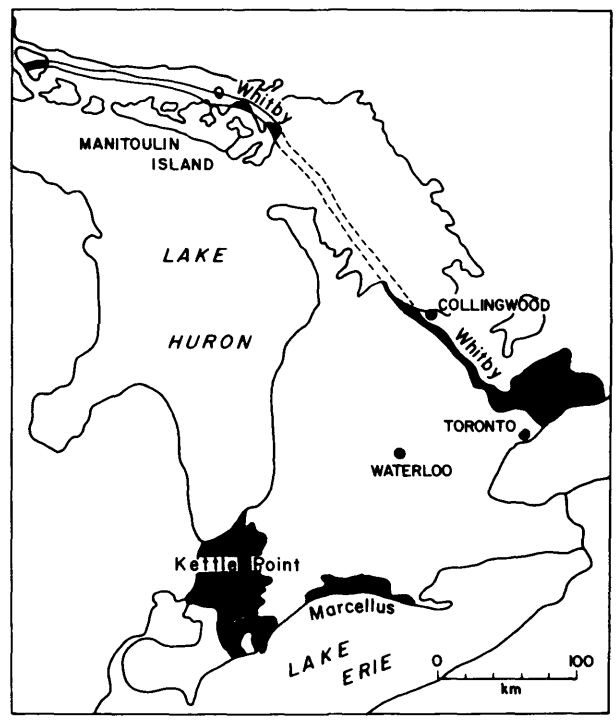

Figure 4. The distribution of outcrops and subcrops of possible oil shales in southern Ontario.

cause these shales to provide unusually high oil yields (up to 60 l/t) for the rather low total organic carbon contents (<10% TOC usually). The yields of the Kettle Point and Marcellus Formations (up to 72 l/t and 65 l/t, respectively) are typical of immature Devonian black shales containing up to 15% TOC being studied in the eastern United States.

Marine, sapropelic organic matter (type I and type II) is more hydrogen-rich than nonmarine humic organic matter (type III) and so will yield more oil per unit weight of organic matter because oil shale yields are inevitably hydrogen-limited, not carbon-limited. The organic matter type has been determined by kerogen studies. Visual assessment of maceral types (P. Gunther, Petro-Canada, personal communication, 1983), H/C ratio measurement, infrared spectrometry, and pyrolysis typing of kerogens have shown all formations to contain dominantly type I or type II material at a relatively low thermal maturation level. In the Lindsay and Whitby Formations, the most hydrogen-rich kerogen occurs in the Manitoulin Island to Collingwood area. This corresponds to the most organic-rich part of the subcrop-outcrop trend and so should be the focus of future exploration.

Pyrolysis, coupled with gas chromatographic and mass spectrometric identification of pyrolysis products, is currently being employed to evaluate some geological controls on organic richness in these formations. It is hoped to combine these results with geological investigations being conducted by the Ontario Geological Survey and others to produce a depositional model that will facilitate future exploration and possible exploitation of these resources.

ACKNOWLEDGMENTS

R.D. Dickhout and his staff provided oil shale analyses. S.J. Pollock provided analyses and assisted with the interpretation of the natural gases. Inspectors of the Petroleum Resources Section of the Ontario Ministry of Natural Resources assisted with the oil and gas sample collection and provided data and encouragement; and scientists of the Engineering and Terrain Geology Section of the Ontario Geological Survey provided oil shale samples and geological information. Parts of this research were supported by grants the Federal Department of from Energy, Mines and Resources and by research contracts with the Ontario Geological Survey as well as Grant 114 from the Ontario Geoscience Research Fund. Co-investigators and their organizations, particularly P. Gunther of PetroCanada and T.G. Powell, I.S.P.G. (Geological Survey of Canada) are also acknowledged.

REFERENCES

Barker, J.F., Macqueen, R.W., Telford, P.G., Russell, D.J., Riediger, C.L., and Gunther, P.R.
1982: Potential Oil Shales in Southern Ontario; Abstracts: International Association of Sedimentologists Congress, 1982, Hamilton, Ontario, p.90.

Barker, J.F., Dickhout, R.D., Russell, D.J., Johnson, M.D., and Gunther, P.R.
1983: The Organic Geochemistry of the Ordovician Whitby Formation - A Possible Ontario Oil Shale; American Chemical Society, Fuel Chemistry Division Preprints of Papers Presented at Seattle, Washington, March 20-25, 1983, Volume 28, p.39-44.

Bree, D.G.
1983: Oil Correlations in Southern Ontario Using Stable Carbon Isotopes; Unpublished B.Sc. Thesis, University of Waterloo, 62p.

Fuex, A.N.
1977: The Use of Stable Carbon Isotopes in Hydrocarbon Exploration; Journal of Geochemical Exploration, Volume 7, p.155-188.

Gold, T.
1979: Terrestrial Sources of Carbon and Earthquake Outgassing; Journal of Petroleum Geology, Volume 1, p.3-19.

Legall, F.D., Barnes, C.R. and Macqueen, R.W.
1981: Thermal Maturation, Burial History and Hotspot Development, Paleozoic Strata of Southern Ontario-Quebec, from Conodont and Acritarch Alteration Studies; Bulletin of Canada Petroleum Geology, Volume 29, p.492-539

Nantais, P.T.
1982: Geochemistry of Natural Gases in Southern Ontario; Unpublished B.Sc. Thesis, University of Waterloo, 64p.

Stahl, W.J.
1977: Carbon and Nitrogen Isotopes in Hydrocarbon Research and Exploration; Chemical Geology, Volume 10, p.121-150.

Grant 106 Neutron Activation Analysis for Platinum Group Elements in Chromitites

A.A. Borthwick and A.J. Naldrett
Department of Geology, University of Toronto

ABSTRACT

Noble metals are inhomogeneously distributed as discrete minerals and to a limited extent also occur in solid solution in sulphides, silicates, and chromian spinel. A fire assay technique has been adapted to analyse noble metals in chromite-rich rocks and chromitites. To ensure representative analyses, a large sample size (30 g) is required. The fire assay technique concentrates the noble metals into a nickel sulphide button. The fire assay button is dissolved in hydrochloric acid and the solution filtered. The noble metal residue obtained on the filter paper is analyzed quantitatively by INAA technique. This method allows the rapid determination of noble metals in chromite-rich rocks.

INTRODUCTION

The noble metals occur naturally as discrete minerals and, to some extent, in solid solution in sulphides, silicates, and chromian spinel. In chromite, they can be seen as inclusions of sulphides and other minerals (Figure 1). They possibly also occur in solid solution (Crocket *et al.* 1979; Crocket 1981; Naldrett and Cabri 1976; Greenland 1971; Razin and Khomenko 1969). The inhomogeneous distribution of noble metals in many environments, and particularly in chromite ores, necessitates using a large sample size for analysis in order that the sample is representative. Hoffman *et al.*(1978) described a simple analytical technique suitable for large sample sizes in which a nickel-nickel sulphide bead fire assay preconcentration was combined with acid leach and instrumental neutron activation analysis of the leach residue. Although highly effective for treating sulphide and silicate ores, the fire assay procedure proved ineffective with chromite ores. This paper describes a modification of the fire assay method which, when combined with neutron activation, permits the rapid determination of noble metals in chromite-rich rocks.

Figure 1. Stillwater chromite grain (grey, angular) with a sulphide inclusion (white, spherical). Field of view is 0.4 mm by 0.2 mm.

PREVIOUS METHODS

Most analytical methods for the noble metals are limited to a small sample size, tend to be time consuming, and are not suited to analysis of all 7 metals (Haffety and Ridley 1968; Razin and Khomenko 1969; Greenland *et al.* 1971). The combined fire assay and neutron activation technique developed by Hoffman *et al.* (1978), and used successfully in determining noble metals in silicates and sulphides, has proved to be unsuitable for chromite-rich samples. As can be seen in an illustration comparing an early attempt to analyze a chromite-rich ore (Figure 2) and the chromite mill product (Figure 3), the flux does not attack the chromite grains. The noble metals will thus remain trapped within the chromite grains as inclusions and also possibly within the chromite structure. Furthermore, the presence of undissolved chromite grains, which tend to settle to become incorporated in the assay bead, gives rise during the neutron activation stage to interferences and a deterioration in the resolution of the noble metal peaks.

Robert and van Wyk (1975) describe a modification of the fire assay and leach procedure for the treatment of chrome-rich ores. This involves a change in the proportions of the flux, a higher temperature of fluxing, and a higher temperature for the acid leach (under hydrogen sulphide saturated conditions); but it is our experience that this also fails to break down individual grains of chromite.

EXPERIMENTAL METHODS

The method and equipment used in this study is the same as that described by Hoffman *et al.* (1978), except that lithium tetraborate was substituted for sodium metaborate in the flux and during the filtering stage a 'Millipore' filtering system was used.

FUSION

For the fusion, a 30 g sample of chrome-rich ore was thoroughly mixed with 60 g of lithium tetraborate, 30 g of sodium carbonate, 10 g of nickel, 6 g of sulphur, and 6 g of silica. The mixture was placed in a furnace at 1000°C. After 2 hours, the assay crucibles were removed and allowed to cool to room temperature.

DISSOLUTION AND FILTRATION

The cold crucible was split with a hammer and the nickel sulphide button carefully removed. The button was crushed in a hardened steel piston-type device to a fine powder, dissolved in concentrated hydrochloric acid by simmering on a hot plate for 2 to 3 hours, filtered, and the residue after filtering irradiated and analyzed following the procedure of Hoffman *et al.* (1978).

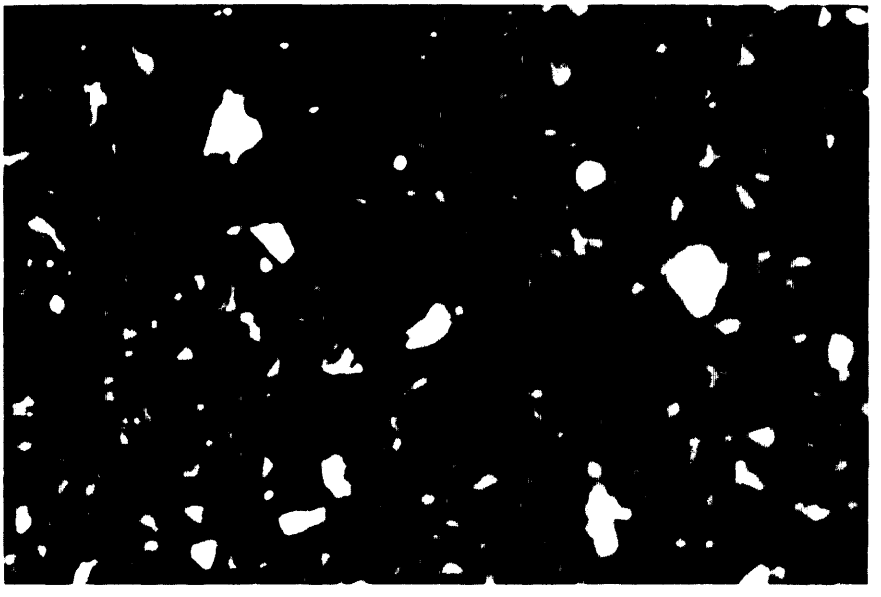

Figure 2. Polished cross-section of the slag (pitted grey and black background) after using the technique of Hoffman et al. (1978). The chromite grains (angular, grey) have not reacted with the flux (dark grey background), and sulphide droplets (white spherical blebs) remain trapped in the flux. Field of view is 0.4 mm by 0.2 mm.

YIELD AND PRECISION

In order to test whether the noble metals are lost during the fire assay, the yield was determined by spiking the fusion mixture with noble metal radiotracers. A radioactive filtrate of noble metals was obtained by fusing South African ore standard (South African Bureau of Standards, Platinum Ore SARM 7, Lot #12) followed by the same dissolution, filtration, and irradiation procedure referred to above. After 5 days of radioactive decay, the sealed filter papers were placed in the lithium tetraborate fusion mix, along with 30 g of chromite, and fused according to the procedure previously described. The noble metal concentrations in the filtration residue were determined by counting immediately after filtration. The results for the radiotracer experiments are compared with the accepted values for the South African Standard in Table 1.

Repeated analyses of a sample of noble metal-bearing chromite from the Stillwater complex listed in Table 3 provide an indication of the precision of the method.

REAGENTS

It is stressed that all reagents must be analyzed for noble metals to eliminate the possibility of contamination. It has been found that commercially available nickel powder has a high noble metal content and it is important to acquire a supply of high purity nickel.

The following reagents were used in our fusion procedure: lithium tetraborate (SPEX); calcined, dry, purified sodium carbonate (Fisher Scientific S-261); silica floated powder, ca. 240 mesh (Fisher Scientific S-153); sublimed sulphur (J.T. Baker Chemical Company 5-4088); nickel powder produced by the carbonyl process (INCO Metals Limited); 30 g fire assay crucibles (Canlab 8522-30C). Hydrochloric acid (12M, J.T. Baker Chemical Company, 3-9535) was used for dissolving the buttons and Millipore 'Durapore' (poresize 0.5 μm, 47 mm) or Metricel GA-1 (poresize 5.0 μm, 47 mm) filterpapers (Gelman Filtration products, #60003) were used in the filtration.

DISCUSSION OF RESULTS

Unlike the sodium metaborate-bearing flux, the lithium tetraborate mixture reacts with chromite incongruently to leave a solid residue of Cr, Al, Fe sesquioxide (Table 2) with the balance entering the liquid. It can be seen from Figure 4 that the sesquioxide remains, mimicking the original chromite grains, whose original outlines are clearly visible. However, provided the chromite has been ground finely, the reaction goes to completion and all of the noble metals in inclusions or in the chromite structure (?) will be freed from their chromite armour, and be able to react with the liquid and thus enter the sulphide button.

The radiotracer analyses indicate good recoveries (Table 1); the analyses are not significantly different from the accepted values for the standard. From these results, it is also seen that platinum-group elements and gold do not partition into the sesquioxide phase.

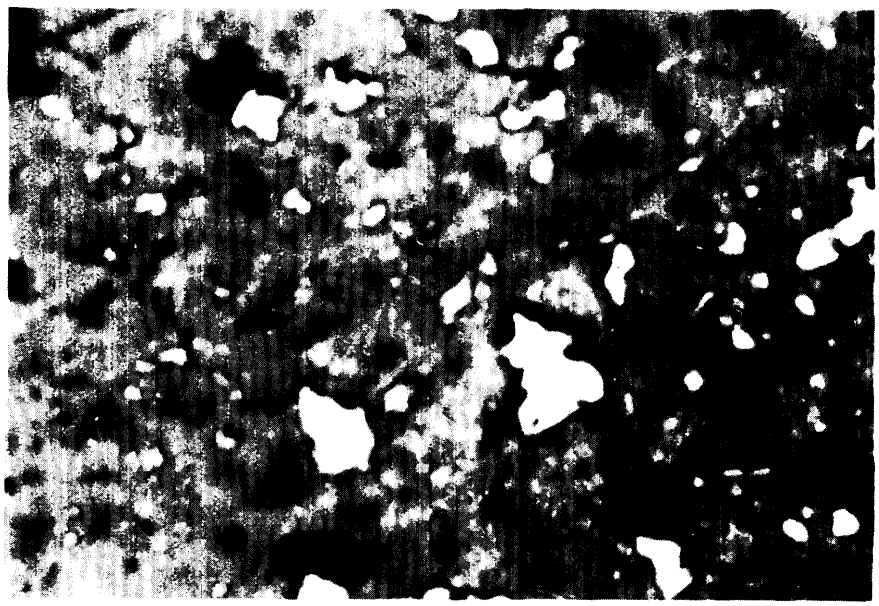

Figure 3. Chromite grains (light grey, angular) after milling are similar in appearance to the unreacted chromite grains in Figure 2. Field of view is 0.4 mm by 0.2 mm.

TABLE 1 RADIO TRACER YIELDS COMPARED TO THE SOUTH AFRICAN ORE STANDARD.

Element	SA STD	*SA AA	yield	*SA AX	yield	*SA EE	yield	*SA W	yield
Os	0.063	0.066	105	0.073	115	0.071	112	0.063	100
Pt	3.740	4.208	112	3.840	102	4.140	111	3.392	91
Ir	0.074	0.071	95	0.073	98	0.076	102	0.069	93
Au	0.310	0.332	107	0.390	125	0.341	110	0.331	109
Ru	0.430	0.404	94	0.471	109	0.387	90	0.431	100

SA = South African Ore Standard
* denotes South African Ore Standard used as a radiotracer
platinum group elements and Au in ppb, yield in percent)

TABLE 2 ELECTRON MICROPROBE ANALYSES OF CHROMITE AND SESQUIOXIDE RESIDUE FROM A SAMPLE OF CHROME-RICH ORE.

	Chromite (wt. percent)	Sesquioxide
SiO_2	.32	.49
Al_2O_3	.95	17.86
TiO_2	.74	.00
FeO	25.08	16.14
MnO	.41	.51
MgO	11.21	6.12
Cr_2O_3	43.93	70.05
NaO_2	.53	.00
Total:	100.07	94.25

TABLE 3 RESULTS OF PRECISION EXPERIMENTS FOR A STILLWATER CHROMITE SAMPLE.

Element	Chr#1	Chr#2	Chr#3	Chr#4
Rh	0.113	0.123	0.115	0.114
Pd	0.000	0.000	0.000	0.000
Os	0.016	0.016	0.014	0.008
Pt	0.088	0.061	0.062	0.074
Ir	0.022	0.029	0.023	0.024
Ru	0.064	0.169	0.101	0.114

(platinum group elements in ppb)

Figure 4. A cross-section of the slag (dark grey background) showing the sesquioxide (clusters of light grey blebs) mimicking the original form of this unusually coarse chromite grain. No sulphide droplets are visible in the slag. Field of view is 0.4 mm by 0.2 mm.

The short half-lives of palladium and rhodium precluded determination of their yields by this method. The similar chemical behaviour of these 2 metals with others of the platinum group lead us to believe that their yields should be no different than the others.

REFERENCES

Crocket, J.H.
1979: Platinum-Group Elements in Mafic and Ultramafic Rocks: A Survey; Canadian Mineralogist, Volume 17, p.391-402.

1981: Geochemistry of Platinum-Group Elements; p.47-64 *in* Platinum-Group Elements: Mineralogy, Geology, and Recovery, edited by L.J. Cabri, Canadian Institute of Mining and Metallurgy, Special Volume 23.

Greenland, L.P., Rowe, J.J., and Dinnin, J.I.
1971: Application of Triple Coincidence Counting and Fire-Assay Separation to the Neutron-Activation Determination of Iridium; United States Geological Survey, Professional Paper 750B, p.B175-B179.

Haffty, J., and Riley, L.B.
1968: Determination of Palladium, Platinum, and Rhodium in Geologic Materials by Fire-Assay and Emission Spectrology; Talanta, Volume 15, p.111-117.

Hoffman, E.L., Naldrett, A.J., Van Loon, J.C., Hancock, R.G.V., and Mason, A.
1978: The Determination of all the Platinum Group Elements and Gold in Rocks and Ore by Neutron Activation Analyses after Preconcentration by Nickel Sulfide Fire-Assay Technique on Large Samples; Analytica Chimica Acta, Volume 102, p.157-166.

Naldrett, A.J., and Cabri, L.J.
1976: Ultramafic and Related Mafic Rocks: Their Classification and Genesis with Special Reference to the Concentration of Nickel Sulfides and Platinum-Group Elements; Economic Geology, Volume 71, p.1131-1158.

Razin, L.V., and Khomenko, G.A.
1969: Accumulation of Osmium, Ruthenium, and the Other Platinum-Group Metals in Chromite Spinel in Platinum-Bearing Dunites; Geochemistry International, Volume 6, Number 6, p.546-557.

Robert, R.V.D., and van Wyk, E.
1975: The Effects of Various Matrix Elements on the Efficiency of the Fire-Assay Procedure using Nickel Sulfide as a Collector; National Institute of Metallurgy, S.A., Report Number 1705.

Grant 131 Source Rock Geochemistry of Pleistocene Tills of Southern Ontario

Uwe Brand and Jaan Terasmae
Department of Geological Sciences, Brock University

ABSTRACT

This investigation was designed to: (1) develop geochemical techniques for the characterization of glacial tills and their source rocks, (2) apply these techniques to an actual glacial model, and (3) determine the usefulness of the techniques in defining the origin and source rocks of glacial deposits of the Dummer Moraine.

Approximately 400 bedrock and 40 till samples were collected in the study area northeast of Peterborough, extending across the Paleozoic-Precambrian boundary and the Dummer Moraine. About 108 matrix samples of the Ordovician Gull River, Bobcaygeon, and Verulam Formations were analyzed for Ca, Mg, Sr, Na, Mn, Fe, Zn, and Al, and similar analyses were carried out for till samples

The 3 Paleozoic formations (Gull River, Bobcaygeon, and Verulam) are chemically distinct. Till samples show strong chemical relationship to the underlying bedrock formation. Correlation of till and bedrock data suggests that provenance of the till can be defined by Sr, Fe, and Mn values.

This preliminary phase of the study has provided a data base for further refinement of geochemical techniques, an improved field sampling system, and the testing and verification of the conceptual model.

INTRODUCTION

Although several studies (Karrow 1974; Dreimanis 1977; Prest 1970; Terasmae 1980; Terasmae *et al.* 1972; Terasmae and Dreimanis 1976) have been carried out during *the last few decades* in southern Ontario, there are still problems relating to the stratigraphic correlation of glacial deposits. In part this is due to the complex lobate configuration of the ice sheet margin in Late Wisconsinan time.

Other problems exist with respect to the genesis of the Dummer Moraine (Figure 1). Early workers suggested that the Dummer is a terminal moraine (e.g. Coleman 1937; Chapman and Putnum 1966). However, this concept of a terminal end moraine origin has been challenged recently by Schluchter (1979), who concluded that the Dummer Moraine could have been produced by the dynamics of the retreating ice sheet. Conversely, Gadd (1980) suggested that the Dummer Moraine was formed as a consequence of its position relative to the Precambrian-Paleozoic contact, and thus is a facies equivalent of the basal till to the south. Terasmae (1980) reviewed the Dummer Moraine problem within the regional context of deglaciation and concluded that:

"It is quite possible that when the southward flowing ice of the Lake Simcoe lobe thinned over the Algonquin Highlands, large masses of ice became stagnant to the lee of these highlands and the melt-out of englacial debris resulted in the disintegration topography that characterizes the Dummer Moraine."

This interpretation is in agreement with all the described characteristics of the "Dummer Moraine".

There also have been attempts to correlate till material with bedrock, and thus determine its provenance (Warren and Delavault 1961; May and Dreimanis 1973; Shilts 1973; Stea and Fowler 1979). A major difficulty, however, is that most tills include large amounts of quartz, feldspars, and associated minerals derived from the rocks of the Precambrian Shield. This has the effect of homogenizing tills and their geochemical properties if bulk sampling methods are employed.

One of the objectives of this study is to modify existing analytical methods for bedrock-till samples, and to devise a model, which uses sedimentological and geochemical techniques, to define the origin and source rock of glacial deposits of the Dummer Moraine.

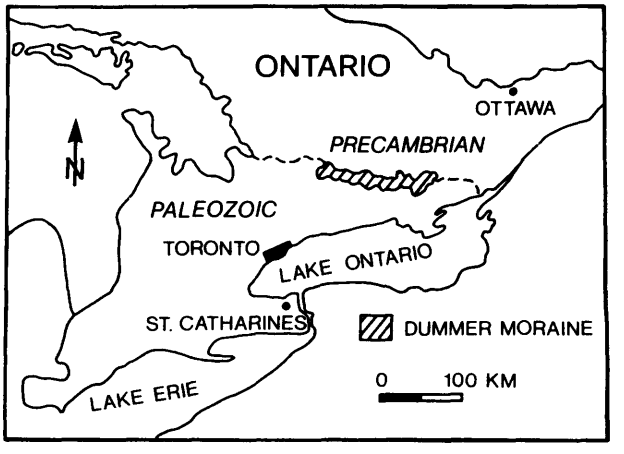

Figure 1. Locality map of the Dummer Moraine in southeastern Ontario.

BEDROCK GEOLOGY

The bedrock samples were collected from outcrops along traverses that approximately parallel the ice flow direction of the last ice sheet (Figure 2). Samples of 3 Paleozoic carbonate formations were collected for each traverse. About 30 samples per formation per traverse were collected for a total of about 400 samples. This allows for the effects of any geochemical differentiation along ice-flow lines as well as on a regional scale.

GULL RIVER FORMATION

The Gull River Formation is a grey to light grey mudstone with variable amounts of fossils and bird's-eye structures. The Gull River samples from the contact with the underlying Shadow Lake Formation contain detrital quartz and feldspar grains. The micrite matrix of the Gull River shows signs of alteration to microspar. In one locality, the micrite is replaced by microspar-dolomite. Only minor amounts of crinoids, gastropods, and bryozoans were noted. Peloids are the most abundant allochems. Also some rip-up clasts are present in the unit.

BOBCAYGEON FORMATION

The unit overlying the Gull River Formation is the Bobcaygeon Formation. It is highly fossiliferous and grey to dark grey in colour. Its composition is that of a packstone. The most abundant allochems are peloids, coral fragments, crinoids, trilobites, and brachiopods. The peloids are preserved as micrite balls. The matrix is highly variable with a complete transition from micrite to pseudospar and sparite. However, the last two are the most abundant. Some minor silicification of the fossil allochems has occurred. Also, large rounded fossil-micrite rip-up clasts are present. Stylolite-fractures are common in the unit. These can be infilled by either calcite sparite or quartz-clay detrital material.

VERULUM FORMATION

The Verulam Formation, which overlies the Bobcaygeon Formation, is a dark grey, argillaceous packstone with shale intercalations. Fossil allochems are very abundant with gastropods, bryozoans, crinoids, trilobites, and brachiopods being the major representatives. Minor allochems are conodonts and *Tetrachium*. Some of the fossils show replacement by chert. The matrix is mostly microspar and pseudospar, and some dolomitization of the matrix took place in selective localities. The crinoid fragments are generally rimmed by syntaxial overgrowth cement. The unit is replete with clay and silt-clay seams.

TILL GEOLOGY

North of the Dummer Moraine (and north of the limit of Paleozoic rocks) the till is generally thin and discontinuous. The landscape physiography is controlled by bedrock surface topography and the regional ice flow direction was generally from north to south. Pebble lithology of the till clearly reflects changes in bedrock types and indicates that glacial abrasion was an active process during till genesis. Till north of the Dummer Moraine is characteristically stony and has a sandy matrix.

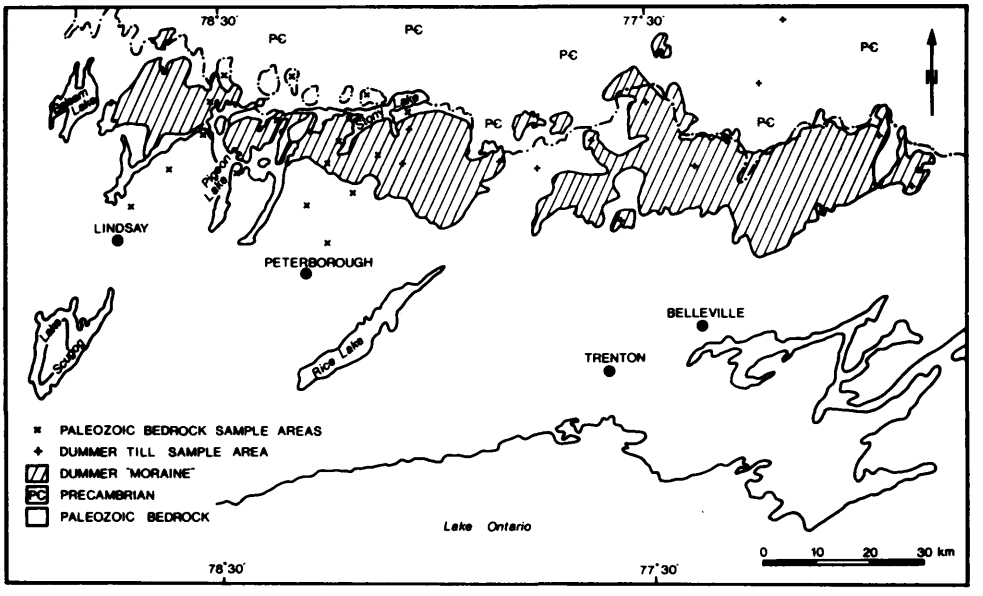

Figure 2. Sample distribution and locality map of the till and bedrock samples (modified after Carson 1980).

A marked change occurs in till characteristics at the limit of Paleozoic outcrop and the area of Dummer Moraine south of this limit. Perhaps the most obvious aspect of this change is the sudden increase to predominance of Paleozoic rock fragments of all sizes in the till. The till cover becomes more continuous although its thickness varies greatly. The till surface is characterized by hummocky topography and an abundance of boulders. Clasts of Precambrian rocks are relatively rare in the "Dummer till" which is typically very stony and has a fine sandy to silty matrix.

ANALYTICAL METHODS

BEDROCK SAMPLES

About 108 matrix samples of the Ordovician Gull River, Bobcaygeon, and Verulum Formations were cleaned and powdered for standard chemical analysis. Half a gram of each sample was leached with 18 ml of 1.8% (5% v/v) HCl for 5 hours (Brand and Veizer 1980). The samples were analyzed for Ca, Mg, Sr, Na, Mn, Fe, Zn, and Al on a Varian 1475 atomic absorption spectrophotometer with HP-85 control. For complete description of analytical techniques *see* Brand and Veizer (1980).

Average accuracy and precision as compared with standard rocks NBS-631 and NBS-634 was better than 5 relative percent for Ca, Mg, Sr, Mn, and Fe; and better than 10 relative percent for Na, Al, and Zn (Brand and Veizer 1980). Insoluble Residue (I.R.) was determined gravimetrically and precision was better than 7 relative percent. All chemical data were reported on a 100 percent carbonate basis (residue-free calculated) to facilitate intersample correlation.

TILL SAMPLES

Till samples are generally a mixture of various lithologies. Consequently, the leaching process devised for carbonate samples (Brand and Veizer 1980) had to be modified to fit the till lithology. An experiment was devised to test the approach. First, 2 till samples, one high in sand and one high in clay fraction, were sieved at 1/4 ϕ intervals. Two batches of each sample were prepared for dissolution. One sample set was leached with 18 ml (uniform volume—UV) of 1.8% (5% v/v) HCl. Another sample set was leached with variable volume (VV) of 1.8% (5% v/v) HCl. The amount of acid was calculated on the soluble portion of each till sample previously determined by leaching experiments. The Insoluble Residue of sandy tills (DT 29D) increases less rapidly than that of clayey tills (DT 4BD) (Figure 3). Furthermore, the I.R. trend is similar for samples leached by uniform (UV) and variable (VV) acid volume. The sandy till shows a smaller degree of elemental leaching from I.R. than the clayey till (Figure 4). Elements associated mainly with I.R. (e.g. Al, Zn, Cd, Cu) are readily leached. However, this leaching can be controlled, especially for elements which are partly associated with the $CaCO_3$ (Figure 4). Thus elements such as Sr, which are solely associated with the calcium carbonate lattice, and partly associated elements such as Fe and Mn, can be used as till-bedrock correlation tools. The chemical data of till is recalculated in a similar fashion to the bedrock samples to allow intersample correlation.

All till samples were sieved at 1/2 ϕ intervals. However, only the -2.0, -1.5, -1.0, +1.0, +3.0, and pan fraction were chosen for full geochemical analysis. The coarser fractions will be used to correlate the till to the bedrock samples. The others have been analyzed for comparison purposes.

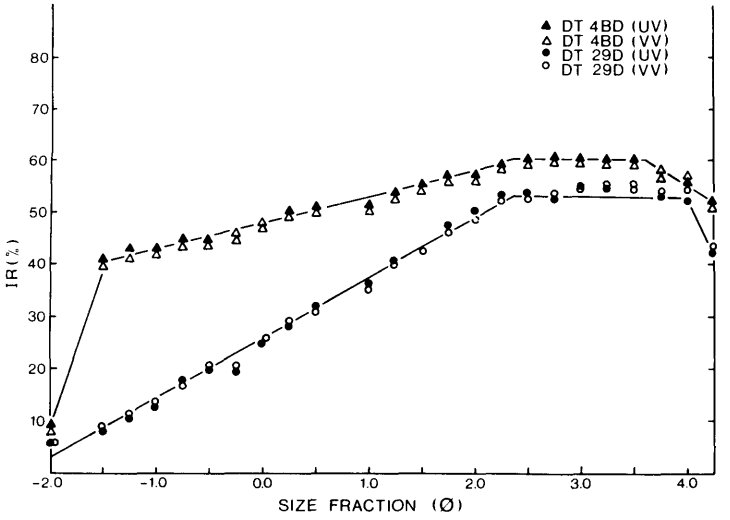

Figure 3. Leaching experiment of till samples from the Dummer Moraine. UV = uniform volume of acid; VV = variable volume of acid.

RESULTS AND DISCUSSION

These results are based on preliminary bedrock and till samples (*see* Tables 1, 2) from the Stony Lake area of the Dummer Moraine. The 3 Paleozoic formations, Gull River, Bobcaygeon, and Verulam, are chemically distinct lithologies (Figure 5). The till sample data can be compared to bedrock geochemistry to help resolve provenance. Till sample DT 26, which is situated on the Gull River Formation, shows strong chemical affinities to this formation. This is apparent for Sr, Fe, and Mn (Figure 5). A similar affinity was determined for till samples DT 27, DT 29, and DT 32. These 3 tills are located on the Gull River Formation, and also show a strong chemical relationship to the underlying formation.

Till sample DT 30, based on Sr, Fe, and Mn, displays both a spatial and a chemical relationship to the noncarbonates (Figure 5). This till is related to sands and silts derived from the Precambrian Shield area to the north of the Dummer Moraine and the Paleozoic formations (Figure 2).

In contrast, till sample DT 31 has chemical affinities, based on Sr and Mn, to the underlying Gull River Formation (Figure 5). However, the Fe values are outside the range determined for this formation (Figure 5). Leaching from insoluble residue is probably not the dominant factor. Instead, an admixture of some till material derived from a Precambrian source could account for this anomaly of Fe enrichment.

Till samples DT 33 and DT 34 were collected from exposures overlying the Gull River and Bobcaygeon Formations, respectively. This relationship is supported by the Mn and Fe data (Figure 5). However, Sr data suggests that the tills from these localities are admixed with detritus from the Verulam Formation (Figure 5).

Sample DT 35 is from an exposure of till at the top of the Bobcaygeon Formation. Only the Mn data support this relationship of superposition unequivocally (Figure 5). Conversely, the Sr and Fe data of the till sample suggest that the major portion of the till was contributed by the Bobcaygeon Formation with a minor portion being derived from the Gull River Formation (Figure 5).

A similar study showed that it was possible to determine provenance of tills by analyzing for trace elements (Leyland-Mihychuk and Brand 1982). However, a problem in that study and in others (May and Dreimanis 1973; Shilts 1973; Stea and Fowler 1979) is that the extent of leaching of elements during till digestion was not accounted for. Thus, it is possible that the observed chemical affinities of tills in those studies represent mixtures of values derived from both the carbonate and noncarbonate portions of the till samples.

CONCLUSIONS

A modified selective leaching method allows for the geochemical analysis of till samples and correlation with bedrock chemistry. This new technique is especially effective for Sr, with slightly less accurate correlations for Fe and Mn values. The correlation of till and bedrock data suggests that provenance of till materials can be resolved by these elements. In addition, extraneously derived material in the till can also be identified by this method.

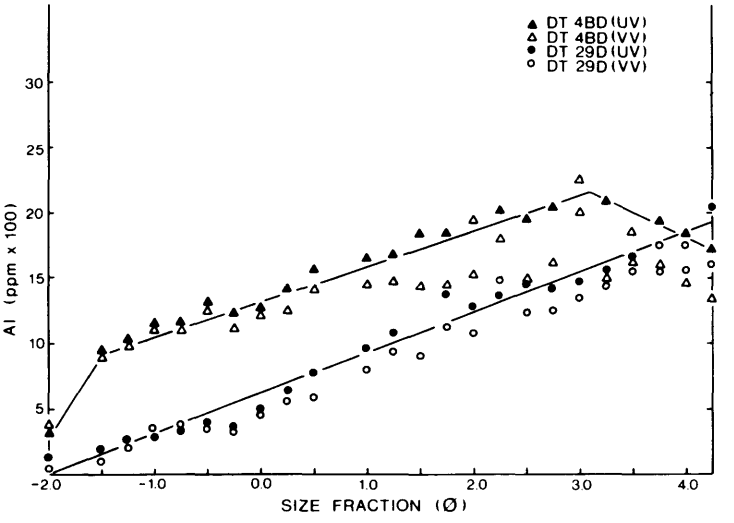

Figure 4. Distribution diagram of Al in the various size fractions from the Dummer Till leaching experiment. Explanations as in Figure 3.

TABLE 1 CHEMICAL ANALYSES OF BEDROCK SAMPLES FROM THE STONY LAKE AREA OF THE DUMMER MORAINE.

Sample	SP	LM	IR	Ca	Mg	Sr	Na	Fe	Al	Mn	Zn
17142	7	17	15.7	295230	43500	350	180	3250	370	2260	7
17143	7	17	9.7	350010	16330	370	210	1350	260	770	7
17144	7	17	11.8	369640	6360	410	170	660	270	380	6
17145	7	17	74.2	304850	15010	310	140	2600	1420	3070	10
17146	7	17	23.7	297260	22360	210	220	4100	490	2310	5
17148	7	17	34.1	289170	26400	260	100	2570	450	2720	7
17149	7	17	10.6	322450	16640	360	110	1970	330	1220	6
17150	7	17	7.4	376180	6030	370	80	770	240	690	5
17151	7	17	10.1	375470	4510	420	170	680	220	350	5
17152	7	17	9.1	371830	4290	410	90	670	240	450	5
17153	7	17	8.2	342280	4470	400	80	640	220	420	10
17154	7	17	12.4	310130	3240	420	190	490	260	270	10
17155	7	17	13.0	317980	3000	420	170	510	240	300	8
17156	7	17	7.5	390530	3680	360	140	420	70	280	0
17157	7	17	12.2	296200	3470	400	170	440	230	320	7
17158	7	17	4.8	288190	2950	330	150	360	20	350	6
17159	7	17	2.3	370090	3090	310	100	610	40	570	1
17160	7	17	3.5	374650	3090	330	110	480	60	460	1
17161	7	17	3.4	378140	3390	420	110	530	40	520	1
17162	7	17	2.9	353930	3480	350	100	600	60	590	1
17163	7	17	6.6	287760	2710	310	140	420	50	450	10
17164	7	17	4.3	355100	3930	340	110	350	110	280	5
17165	7	17	3.0	349260	2270	260	60	400	60	400	0
17166	7	17	2.7	337150	1850	170	50	340	0	350	8
17168	8	17	2.5	367270	3720	520	110	260	40	260	3
17169	8	17	4.5	336560	3660	460	110	320	20	340	9
17170	8	17	5.9	324770	3270	520	80	360	20	350	8
17170	8	17	2.3	322720	3410	470	80	390	20	400	6
17171	8	17	4.7	329360	3840	540	100	430	80	380	6
17172	8	17	2.2	315930	3780	630	100	290	30	280	6
17173	8	17	3.5	382840	3530	580	100	340	40	330	1
17174	8	17	3.2	352540	4550	500	100	250	50	250	6
17175	8	17	4.5	335970	3730	470	120	330	40	320	4
17176	8	17	5.7	334150	4790	430	130	200	50	210	8
17177	8	17	5.1	361790	4000	490	110	340	60	330	1
17178	8	17	1.9	385850	3850	330	100	200	30	240	4
17179	8	17	4.7	395010	3200	370	140	430	0	490	1
17180	8	17	3.7	356990	3920	390	120	350	80	350	7
17181	8	17	17.7	406770	4190	440	140	430	60	420	10
17182	8	17	6.9	336360	2480	340	100	370	30	340	8
17183	8	17	2.6	374840	2380	300	80	300	0	360	1
17184	8	17	5.3	339400	4390	370	110	340	80	280	6
17185	8	17	4.3	362820	4520	340	120	290	90	330	8
18186	7	18	6.9	328940	4400	290	110	580	120	630	9
18187	7	18	4.4	318910	3450	270	110	570	60	740	7
18188	7	18	3.0	351940	4460	230	110	1100	30	1140	1
18189	7	18	6.9	333820	12720	190	110	2550	40	1660	1
18190	7	18	4.6	371620	3170	220	110	890	40	1270	2
18191	7	18	4.2	324210	3260	240	120	580	60	1010	10
18192	7	18	4.0	320990	3310	260	110	690	60	1200	7
18194	7	18	7.0	302040	14110	230	110	1510	120	1020	7
18195	7	18	3.7	382510	3420	280	140	670	20	850	1
18196	7	18	3.1	322640	3430	270	130	660	30	1060	8
18197	7	18	3.6	361420	3540	290	130	680	90	980	7
18198	7	18	14.5	384350	3430	380	160	470	160	210	3
18199	7	18	6.3	353130	3880	310	160	510	40	280	2
18200	7	18	2.4	352890	3800	320	130	410	30	420	6
18201	7	18	3.0	381460	3830	290	100	700	100	440	5
18202	7	18	2.7	318150	3230	320	120	660	90	410	20
18203	7	18	3.1	350190	3660	370	110	510	50	370	5
18204	7	18	3.1	343490	3990	320	120	500	50	340	5
18205	7	18	3.8	331400	3700	320	100	450	30	330	5
18206	7	18	3.0	335540	3730	300	100	370	50	250	5
18207	7	18	3.3	334050	4420	300	140	280	50	140	6
18208	7	18	5.6	358860	3580	420	110	490	70	390	1
18209	7	18	6.7	362550	4090	420	140	370	90	270	3
18210	7	18	3.3	340930	4530	390	120	280	50	210	8
18211	7	18	6.6	354800	4430	430	170	270	50	250	6
18212	7	18	4.7	355220	4870	360	150	250	20	220	7
18213	7	18	3.6	367850	4540	460	120	280	20	260	7
18214	7	18	3.1	341930	3510	410	130	400	60	390	7
18215	7	18	6.5	354660	3620	500	120	220	90	160	1
18216	7	18	6.4	372870	3860	480	180	180	150	220	6
18217	7	18	1.7	340730	3810	530	130	230	20	230	7
18218	7	18	3.6	315520	4520	440	110	400	120	230	5
18219	7	18	5.0	355650	3330	420	110	310	60	360	7
18220	7	18	3.9	331330	3780	480	130	270	30	330	8
20221	8	20	3.2	342430	3060	410	110	380	30	500	10
20222	8	20	2.7	356490	4470	470	110	330	70	310	4
20223	8	20	2.3	341980	4150	500	110	370	70	300	4
20224	8	20	4.0	358850	3070	430	100	410	20	440	1
20225	8	20	3.3	368350	3370	490	120	370	60	440	7
20226	8	20	5.6	389100	4000	480	120	350	60	400	7
20227	8	20	3.0	345490	4660	430	90	310	70	250	8
20228	8	20	3.0	347470	4370	630	100	310	70	310	4
20229	8	20	3.0	367060	4510	580	120	220	90	220	5
20230	8	20	2.5	362960	4060	500	110	190	20	210	6
20231	8	20	2.1	386830	4360	420	130	190	90	100	5
20233	8	20	3.5	390970	4400	600	110	4580	30	230	10
20234	8	20	4.6	356890	4270	600	100	5210	30	300	9
20235	8	20	3.6	368620	3990	400	90	260	100	220	4
21236	9	21	5.6	416960	2890	840	290	680	170	230	0
21237	9	21	3.1	418820	2900	840	110	790	70	230	1
21238	9	21	4.2	396430	3750	830	150	440	100	200	0
21239	9	21	2.0	397860	2320	810	90	550	40	220	0
21240	9	21	2.4	394860	2870	830	100	420	40	210	0
21241	9	21	2.6	369970	3880	940	100	490	120	180	5
21242	9	21	2.6	346050	11120	910	80	1760	50	300	1
21243	9	21	2.0	386190	2680	970	80	360	40	170	1
21244	9	21	3.5	369200	3370	1020	80	280	50	180	0
21245	9	21	3.3	374950	3770	940	100	320	80	210	1
21246	9	21	7.0	370820	4150	1050	100	400	100	190	1
21247	9	21	3.3	362190	2160	850	50	360	90	130	5
21248	9	21	4.0	361520	4170	900	100	350	180	140	5
21249	9	21	2.8	368830	4130	1070	120	300	80	140	2
21250	9	21	5.1	398460	3850	900	130	400	100	140	1
21251	9	21	4.2	390850	3680	910	100	490	120	160	1
21252	9	21	4.8	399050	3530	740	80	710	110	190	1

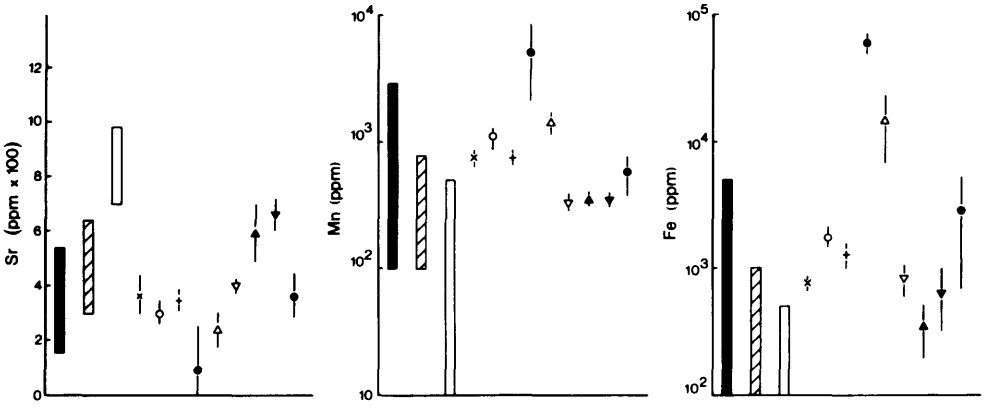

Figure 5. Geochemical correlation graph. Comparison of till and bedrock chemistry. The ■, ▨, and □ represent ranges of the Gull River, Bobcaygeon, and Verulam Formations respectively. The x, o, +, •, Δ, ▽, ▲, ▼, and ⊕ represent till samples DT 26, DT 27, DT 29, DT 30, DT 31, DT 32, DT 33, DT 34, and DT 35, respectively.

TABLE 2 CHEMICAL ANALYSES OF TILL SAMPLES FROM THE STONY LAKE AREA OF THE DUMMER MORAINE.

Sample	SP	LM	IR	Ca	Mg	Sr	Na	Fe	Al	Mn	Zn
58226	1	26	15.4	324890	3810	440	190	710	280	620	6
58226	2	26	15.9	303070	3820	460	190	700	280	580	5
58226	3	26	17.9	306260	3750	360	180	890	350	800	5
58226	4	26	28.8	298550	3780	320	150	770	500	870	6
58226	5	26	46.0	298280	3760	310	140	1660	1370	1130	7
58226	6	26	49.0	285820	4370	330	120	2870	2220	1400	10
58227	1	27	35.6	257540	24870	360	560	1430	760	960	20
58227	2	27	37.2	248360	25460	260	350	1700	1020	990	10
58227	3	27	39.2	254630	26270	270	520	1810	1050	970	10
58227	4	27	44.0	262480	28520	280	510	2020	1200	1230	10
58227	5	27	54.4	259040	35030	320	370	2290	1660	1540	20
58227	6	27	45.5	249390	29360	300	400	1940	1170	1130	30
58229	1	29	18.4	402700	7740	370	190	1000	110	690	5
58229	2	29	22.0	381760	14750	300	170	1580	270	840	5
58229	3	29	23.0	368430	12730	300	170	1340	310	680	5
58229	4	29	40.6	434440	12080	330	160	2170	510	800	5
58229	5	29	79.6	307450	13090	370	170	4690	1780	1010	9
58229	6	29	77.6	342400	20420	370	180	5330	2000	1130	20
58230	1	30	94.2	15740	3290	140	2130	13580	12460	930	20
58230	2	30	97.9	74020	12250	390	4070	73730	76750	8680	110
58230	3	30	97.7	67410	18750	0	5450	77500	91400	5490	80
58230	4	30	97.7	53540	9290	0	1950	51330	35270	2170	70
58230	5	30	97.6	62920	10000	0	1170	67500	49110	1420	40
58230	6	30	95.9	129560	9110	0	540	54330	37050	1330	50
58231	1	31	67.4	345700	8010	230	950	5870	3090	1470	20
58231	2	31	82.8	259390	12190	290	1740	26320	13040	1940	60
58231	3	31	72.2	327500	6330	290	710	5160	2490	1180	20
58231	4	31	88.0	278220	12060	280	1760	17450	9940	1330	50
58231	5	31	94.6	237590	13520	150	2930	21960	11850	1430	140
58231	6	31	92.1	263270	9570	200	1620	16720	9720	1570	70
58232	1	32	13.5	423670	4100	390	190	770	100	380	6
58232	2	32	20.7	404070	4230	440	190	890	210	290	6
58232	3	32	22.3	395530	4140	400	160	1280	230	360	6
58232	4	32	33.0	441410	3680	400	160	830	230	410	6
58232	5	32	40.3	431250	3650	370	180	550	200	530	6
58232	6	32	42.6	441720	3860	380	150	1650	730	590	20
58233	1	33	7.6	394590	3720	590	140	520	60	340	3
58233	2	33	8.2	398860	3880	710	140	460	50	380	3
58233	3	33	9.3	406640	3850	720	130	510	70	360	3
58233	4	33	22.8	409980	3380	540	120	230	0	350	2
58233	5	33	34.0	400760	3200	440	80	250	0	410	5
58233	6	33	31.1	387760	3370	510	100	200	0	460	7
58234	1	34	8.3	439140	3840	690	200	650	110	270	4
58234	2	34	13.5	416040	3680	660	150	700	170	320	3
58234	3	34	14.6	418390	3740	710	190	740	130	360	3
58234	4	34	28.4	372840	3620	650	180	340	120	370	4
58234	5	34	39.4	369370	3540	550	150	370	160	410	4
58234	6	34	38.9	339210	3630	670	180	1190	340	460	9
58235	1	35	37.1	380990	3960	470	170	1120	270	270	6
58235	2	35	65.4	349620	4200	310	390	5620	2610	850	10
58235	3	35	56.0	344680	8610	430	240	2500	1240	420	8
58235	4	35	79.6	339480	5650	320	240	7480	5560	580	20
58235	5	35	87.5	319760	6880	260	200	11030	8060	780	30
58236	6	35	78.5	314450	4890	350	210	7560	7170	670	30

ACKNOWLEDGMENTS

We thank J. Morrison and J. Pinder for assistance with chemical analyses. Also our thanks go to A.M. Fulton for typing the manuscript.

REFERENCES

Brand, U., and Veizer, J.
1980: Chemical Diagenesis of a Multicomponent Carbonate System-1: Trace Elements; Journal of Sedimentary Petrology, Volume 50, p.1219-1236.

Carson, D.M.
1980: Paleozoic Geology of the Burleigh Falls-Peterborough Area, District of Southern Ontario; Ontario Geological Survey, Preliminary Map P.2337, Geological Series, scale 1:50 000. Geology 1979.

Chapman, L.J., and Putnam, D.F.
1966: The Physiography of Southern Ontario; University of Toronto Press, 2nd edition, 386p.

Coleman, A.P.
1937: Geology of the North Shore of Lake Ontario; Ontario Department of Mines, Annual Report for 1936, Volume 45, Part 7, p.75-116. Accompanied by Map 45f, scale 1:316 800 or 1 inch to 5 miles.

Dreimanis, A.
1977: Correlation of Wisconsin Glacial Events between the Eastern Great Lakes and the St. Lawrence Lowlands; Geographie Physique et Quaternaire, Volume 31, p.37-51.

Gadd, N.R.
1980: Late-Glacial Regional Ice-Flow Patterns in Eastern Ontario; Canadian Journal Earth Sciences, Volume 17, p.1439-1453.

Karrow, P.F.
1974: Till Stratigraphy in Parts of Southwestern Ontario; Geological Society of America, Bulletin, Volume 85, p.761-768.

Leyland-Mihychuk, M., and Brand, U.
1982: Sedimentology and Geochemical Analysis of Late Wisconsin Glacial Sediments and Paleozoic Bedrock, Havelock, Ontario; Geological Association Canada, Program with Abstracts, Volume 7, p.63.

May, R.W., and Dreimanis, A.
1973: Differentiation of Glacial Tills in Southern Ontario, Canada, Based on Their Cu, Zn, Cr, and Ni Geochemistry; Geological Society America, Memoir 16, p.221-228.

Prest, V.K.
1970: Quaternary Geology of Canada; p.675-764 *in* Geology and Economic Minerals of Canada, edited by R.J.W. Douglas; Geological Survey Canada, Economic Geology Report.

Schluchter, C.
1979: The Dummer Moraine in Southern Ontario - Its Sedimentology and Origin; Geological Association Canada, Program with Abstracts, Volume 4, p.77.

Shilts, W.W.
1973: Glacial Dispersion of Rocks, Minerals, and Trace Elements in Wisconsin Till, Southeastern Quebec, Canada; Geological Society America, Memoir 16, p.189-219.

Stea, R.R., and Fowler, J.H.
1979: Minor and Trace Element Variations in Wisconsinan Tills, Eastern Shore Region, Nova Scotia; Nova Scotia Department of Mines and Energy, Paper 79-4, 30p.

Terasmae, J.
1980: Some Problems of Late Wisconsin History and Geochronology in Southeastern Ontario; Canadian Journal Earth Sciences, Volume 17, p.361-381.

Terasmae, J., and Dreimanis, A.
1976: Quaternary Stratigraphy of Southern Ontario; p.51-63 *in* Quaternary Stratigraphy of North America, edited by W.C. Mahaney; Dowden, Hutchinson and Ross, Stroudsburg, Pa.

Terasmae, J., Karrow, P.F., and Dreimanis, A.
1972: Quaternary Stratigraphy and Geomorpholoy of the Eastern Great Lakes Region of Southern Ontario; 24th International Geological Congress, Field Excursion A42 Guidebook, 75p.

Warren, H.V., and Delavault, R.E.
1961: The Lead, Copper, Zinc and Molybdenum Content of Some Limestone and Related Rocks in Southern Ontario; Economic Geology, Volume 56, p.1264-1272.

Grant 105 Latter-Stage Decay Products of ^{222}Rn - Use in Radioactive Waste Management and Uranium Exploration

J.W. Card and Keith Bell
Department of Geology, Carleton University

ABSTRACT

Geochemical anomalies related to uranium mineralization have been outlined by ^{210}Po and ^{210}Pb analyses of soil samples from 3 uranium occurrences in Ontario: the South March occurrence, the Quirke "discovery zone", and a pegmatite in Palmerston Township. The analytical technique used in this study involved plating out ^{210}Po onto copper surfaces from acidic solutions; samples were prepared by leaching with 10% nitric acid or complete hydrofluoric acid digestion.

In general, the ^{210}Po and ^{210}Pb anomalies are more closely related to the presence of ^{226}Ra in the soils than to the presence of migrating ^{222}Rn. Soil tests from samples overlying a pegmatite in Blithfield Township, where an in situ ^{222}Rn anomaly occurs without a corresponding soil ^{226}Ra anomaly, were ineffective in delineating any ^{210}Po and ^{210}Pb anomalies.

Studies at the Pronto uranium and copper tailings area, near Elliot Lake, indicated that although measurable quantities of ^{210}Po and ^{210}Pb occur in the uranium tailings, their absence in the overlying copper tailings suggests that migration here has been negligible.

INTRODUCTION

A study of ^{210}Po and ^{210}Pb distributions, both in soils overlying uranium mineralization and in uranium tailings, has been conducted during the last 2 years under the support of the Ontario Geoscience Research Grant Program. Because both ^{210}Pb and ^{210}Po are "latter-stage decay products" of ^{222}Rn, it was thought that their occurrence in *unconsolidated geological* materials might be useful both in prospecting and health-hazard monitoring.

During the first year of work, we adapted an analytical technique for measuring ^{210}Po and ^{210}Pb in soils and tailings, and conducted some preliminary field tests (Card and Bell 1982b). Our work during the second year of support, described here, included extensive sample measurement, as well as further evaluation of the ^{210}Po spontaneous deposition method of analysis.

ANALYTICAL METHODS

The analytical method for measuring ^{210}Po in soils and tailings is based on alpha-counting of the ^{210}Po deposited on copper plates from sample leachates. A step-by-step summary of the analytical procedures eventually adopted is presented in our 1981-1982 report (Card and Bell 1982b). Although the current year's work was primarily devoted to measurement of soil and tailings samples and interpretation of the data, additional tests were made to assess the analytical methods. These are described in the Appendix.

Soil samples from 4 uranium occurrences, as well as samples from tailings areas in the Elliot Lake district, have now been studied for ^{210}Po and ^{210}Pb following a 10% nitric acid leach. Samples at 2 of the uranium exploration test sites were analyzed for both nuclides following a complete digestion with hydrofluoric acid. In addition, ^{226}Ra was measured using either the collector method (Card and Bell 1979, 1982a) or its commercial version, the Alphacard System.

APPLICATIONS TO EXPLORATION

The results of ^{210}Po and ^{210}Pb studies at the various test sites are summarized below.

(1) THE SOUTH MARCH URANIUM OCCURRENCE

The South March uranium occurrence has been extensively studied. Pertinent references are included in our 1981-1982 report, as well as our first results from the latter-stage decay product study (Card and Bell 1982b). The South March results now include all 4 latter-stage decay product methods. Presented in Figure 1 are the 4 profiles as well as a schematic illustration of the location of the mineralization. In each case, the peaks on the profiles correspond to the mineralization, clearly confirming the viability of the latter-stage decay product method as a prospecting tool. Some features of the profiles do, however, merit further investigation. The third peak, which shows up in 3 surveys at the southwest section of the traverse, is unrelated to known mineralization; this may relate to the fact that these samples were all high in organic content. Also, the northeast peak from the ^{210}Pb (HF) survey is somewhat suppressed.

The results of a statistical comparison of the 4 surveys with each other, and also with the in situ ^{222}Rn and

soil ^{226}Ra surveys (*reported in* Card and Bell 1979) are shown as a correlation matrix in Table 1, prepared after log-transformation of the data. At the 95% confidence level, all but 2 of the correlation coefficients are significant. In both cases, the data from the ^{210}Pb (HF) survey are involved. For further comparison, the results of a cluster analysis using the weighted pair-group method (Sokal and Sneath 1963) are presented as a dendrogram in Figure 2. Using cluster analysis, closely related groups of variables form clusters at high correlation levels. The dendrogram shows that although the surveys relate to each other at reasonably high correlation levels, the tendency for clusters to form is small.

The South March test site has been studied by a variety of uranium exploration methods over the years; all have clearly delineated the anomaly. To the list of successful techniques can now be added the ^{210}Po and ^{210}Pb methods.

(2) THE QUIRKE "DISCOVERY SHOWING"

Results of our 1981-1982 research (Card and Bell 1982b) outlined a ^{210}Po anomaly at the "discovery showing" of the Quirke Mine, near Elliot Lake, Ontario. The geological setting of this area is described by Robertson (1968, 1976); an associated ^{222}Rn anomaly has been reported by Dyck (1972). ^{210}Pb measurements made during 1982-1983 outlined a pattern similar to the ^{210}Po anomaly (Figure 3). An interesting, though as yet unexplained, feature of the profiles is that the ^{210}Pb activities (after adjustment to anticipated equilibrium values) average 4½ times those from the ^{210}Po work. The correlation coefficient between the ^{210}Po and ^{210}Pb data (log-transformed) is 0.87, which is significant at the 95% confidence level.

Both the ^{210}Po and ^{210}Pb results have some measure of correlation with the ^{226}Ra survey (*shown in* Figure 3b), significant at the 95% confidence level (r = 0.51 with ^{210}Po, and 0.79 with ^{210}Pb).

TABLE 1 CORRELATION MATRIX FOR THE SURVEYS AT THE SOUTH MARCH URANIUM OCCURRENCE, USING LOG-TRANSFORMED DATA.

			10 % nitric		HF	
	Rn-222	Ra-226	Po-210	Pb-210	Po-210	Pb-210
Rn-222		0.49	0.37	0.30	0.49	0.22
Ra-226			0.50	0.63	0.81	0.38
Po-210 (nitric)				0.63	0.43	0.25
Pb-210 (nitric)					0.73	0.61
Po-210 (HF)						0.44
Pb-210 (HF)						

N = 34

r is significant if greater than 0.29 (95% confidence level)

(3) GRENVILLE PEGMATITES

Sampling sites included 2 uranium-bearing pegmatites in the Grenville Province, 1 in Palmerston Township, and the other in Blithfield Township. Previous work had shown that although clear in situ ^{222}Rn anomalies are associated with both pegmatites, a soil ^{226}Ra anomaly only occurs at Palmerston.

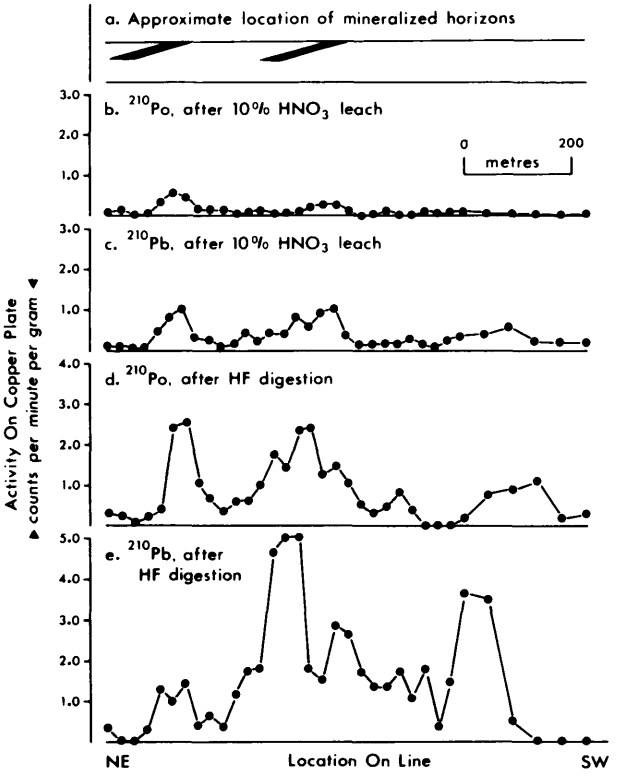

Figure 1. Comparative profiles across the South March uranium occurrence.

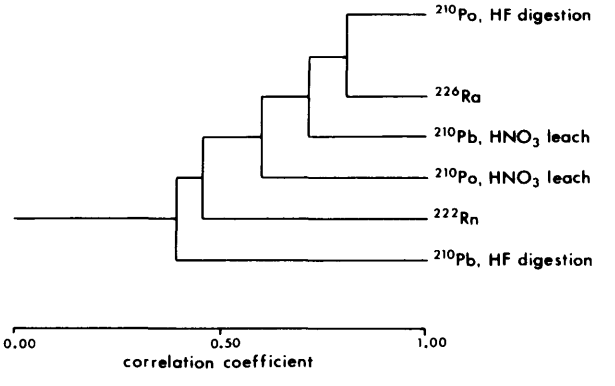

Figure 2. Dendrogram of the surveys at the South March uranium occurrence.

TABLE 2 CORRELATION MATRIX FOR THE SURVEYS AT THE URANIUM-BEARING PEGMATITE IN PALMERSTON TOWNSHIP, USING LOG-TRANSFORMED DATA.

			10 % nitric		HF	
	Rn-222	Ra-226	Po-210	Pb-210	Po-210	Pb-210
Rn-222		0.19	0.41	0.21	0.36	0.55
Ra-226			0.63	0.70	0.42	0.44
Po-210 (nitric)				0.63	0.33	0.28
Pb-210 (nitric)					0.63	0.56
Po-210 (HF)						0.41
Pb-210 (HF)						

N = 21

r is significant if greater than 0.37 (95% confidence level)

A summary of the Palmerston data is presented in Figure 4. All 4 latter-stage decay product methods produce anomalies, and all broadly agree with the site of known uranium mineralization. A statistical comparison of the data, including the ^{222}Rn and ^{226}Ra results (*see* Table 2), shows some measure of correlation between the surveys. Several correlation coefficients are significant at the

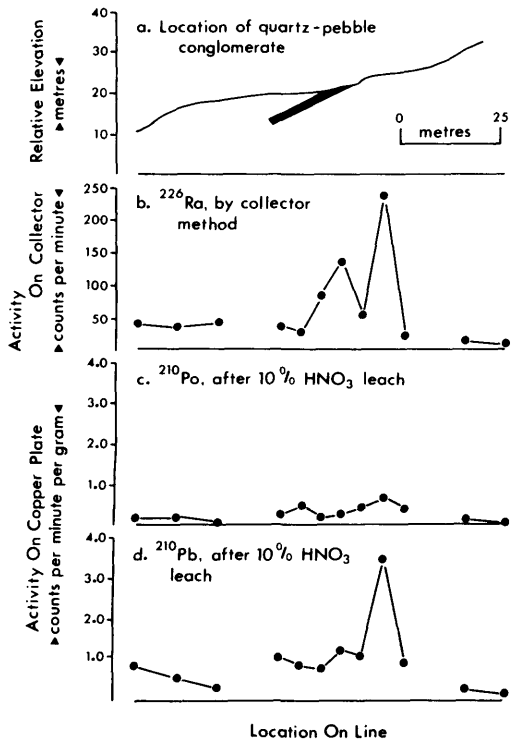

Figure 3. Comparative profiles across the discovery showing of the Quirke Mine, near Elliot Lake, Ontario.

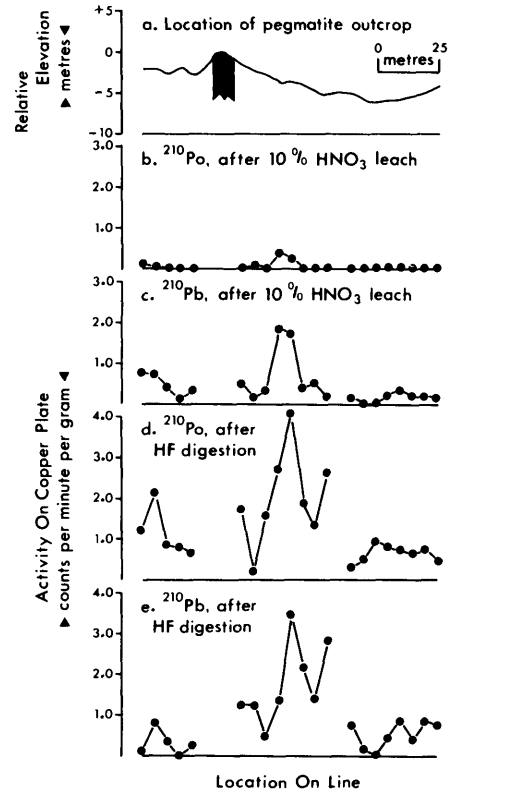

Figure 4. Comparative profiles across a uranium-bearing pegmatite in Palmerston Township, Ontario.

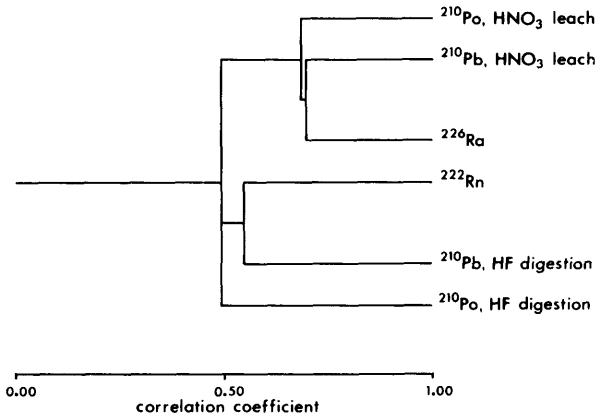

Figure 5. Dendrogram of the surveys at the pegmatite in Palmerston Township, Ontario.

95% confidence level. Although the corresponding dendrogram (Figure 5) shows some clustering, no readily interpretable patterns are observed.

Thus far, the data from the South March, Quirke, and Palmerston sites have delineated ^{210}Po and ^{210}Pb anomalies related to known uranium occurrences. Common to all is the presence of corresponding in situ ^{222}Rn and soil-sample ^{226}Ra anomalies.

Earlier work at Blithfield Township indicated a clear in situ ^{222}Rn anomaly, but one that was not associated with a soil ^{226}Ra anomaly (Bell and Card 1980). Measurements of ^{210}Po and ^{210}Pb, unlike those from the other 3 localities, failed to satisfactorily locate any anomalies. If any ^{210}Po or ^{210}Pb were produced by migrating ^{222}Rn, their abundance is so low that we are unable to detect them using our present analytical methods. On the basis of our results to date, it would seem that latter-stage decay product anomalies are related more to the presence of ^{226}Ra in the soil than to ^{222}Rn migrating from depth.

APPLIED TESTS AT URANIUM MINE TAILINGS AREAS

Because ^{210}Po and ^{210}Pb are abundant in uranium mill tailings piles, evaluation of the ^{210}Po plating method for environmental measurements forms one aspect of the current study. Involved were ^{210}Po and ^{210}Pb studies of the tailings, and comparative gamma-ray, ^{222}Rn, and ^{226}Ra measurements. Other work included measurement of nuclides in the natural environment adjacent to the tailings. The Pronto tailings area, in the Elliot Lake district, was used for our 1982-1983 studies.

The Pronto tailings area covers about 60 ha. Uranium milling operations ceased in the late 1950s, and subsequently the mill was used to process copper ore. Copper tailings cover a considerable area of old uranium tailings. Stations were located for in situ readings and sample collection by a pace-and-compass traverse across the tailings surface and along the outflowing stream channel (Figure 6). In situ gross-count gamma-ray measurements were taken at all stations, and some in situ ^{222}Rn readings made. Samples, collected at 10 cm and 50 cm depths, were subsequently analyzed for ^{210}Po, ^{210}Pb, and ^{226}Ra. Figure 7 summarizes the results.

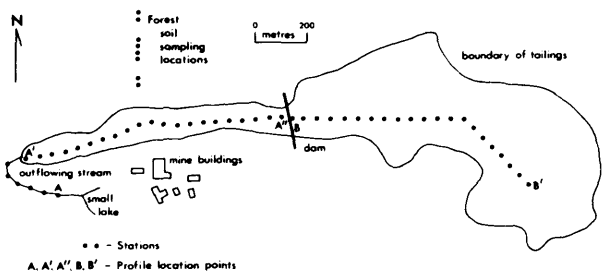

Figure 6. The Pronto tailings area.

Gamma-ray readings were generally low in the area covered by copper tailings, and very high where uranium tailings remain uncovered. Of particular interest is the high reading just to the east of the dam, an area that consists predominantly of copper tailings. The high readings in the stream channel appear to reflect erosion of material from the tailings pile.

The ^{222}Rn survey, with the exception of 1 station, was restricted to the area where copper tailings occur at the surface. The readings were generally quite low, suggesting negligible ^{222}Rn migration throughout most of the area. However, the presence of radioactive material immediately east of the dam, first noted during the gamma-ray survey, was further confirmed by an in situ ^{222}Rn reading.

In the uranium-tailings area, large numbers of counts were obtained during the ^{226}Ra, ^{210}Po, and ^{210}Pb surveys. High values from stream sediments probably reflect mixing of tailings with the natural stream-bottom material. With only 1 exception, high values in the uranium tailings for ^{210}Po, ^{210}Pb, and ^{226}Ra were observed at both the 10 and 50 cm depths. Although the values are extremely variable from different depths at the same site, the ^{226}Ra, ^{210}Po, and ^{210}Pb profiles are similar. The relationships between the various surveys are summarized by a correlation matrix (Table 3), in which all correlation coefficients are significant at the 95% confidence level, and by a dendrogram (Figure 8). From the latter, it is clear that the

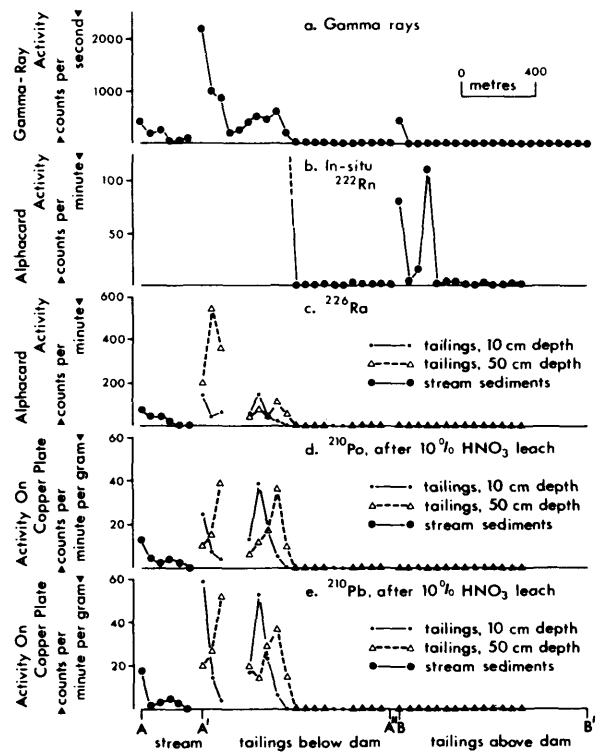

Figure 7. Comparative profiles of the survey results from the Pronto tailings area.

TABLE 3 CORRELATION MATRIX FOR THE SURVEYS AT THE PRONTO TAILINGS AREA, USING UNTRANSFORMED DATA.

	Ra-226		Pb-210		Po-210		Gamma
	10 cm	50 cm	10 cm	50 cm	10 cm	50 cm	Rays
Ra-226 (10 cm)		0.49	0.96	0.58	0.93	0.50	0.79
Ra-226 (50 cm)			0.38	0.74	0.32	0.67	0.70
Pb-210 (10 cm)				0.44	0.96	0.34	0.78
Pb-210 (50 cm)					0.48	0.97	0.67
Po-210 (10 cm)						0.38	0.63
Po-210 (50 cm)							0.58
Gamma rays							

N = 30

r is significant if greater than 0.31 (95% confidence level)

highest levels of clustering relate to depth values rather than to nuclide species. Inhomogeneity with depth, a feature commonly characteristic of uranium tailings, has thus been further demonstrated by the present work.

An interesting additional test at the Pronto area involved a more detailed investigation of the gamma-ray anomaly at the east side of the dam (*see* Figure 7). Samples at 3 adjacent stations were collected at 5 different depths between 10 and 50 cm, and analyzed for ^{210}Po, ^{210}Pb, and ^{226}Ra. The ^{210}Po and ^{226}Ra results, summarized in Figure 9, clearly show a layer of radioactive tailings at the 20 to 30 cm depth. From these results, it is clear that the ^{210}Po, ^{210}Pb, and ^{226}Ra methods can be helpful in identifying pockets of radioactive material.

To test whether the adjacent natural woodland area might have been contaminated by airborne material, 8 soil samples were collected from a traverse running north

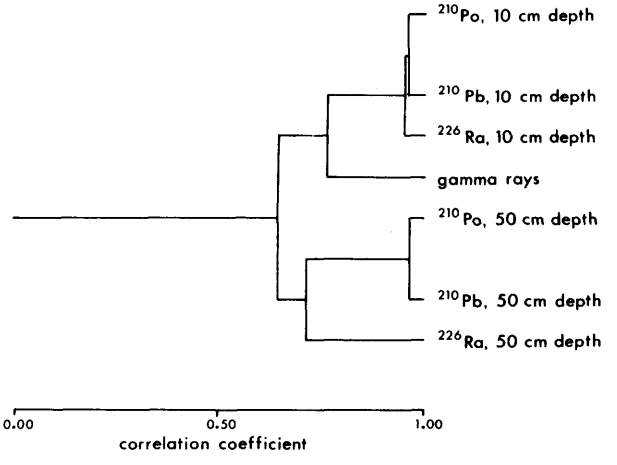

Figure 8. Dendrogram of the surveys at the Pronto tailings area.

from the tailings (*see* Figure 6). The ^{210}Po and ^{210}Pb levels were quite low, suggesting minimal contamination.

Although the distribution of the radioactive tailings below the material from the copper milling operations is not known, our work has shown that the copper tailings at most sites contain negligible ^{210}Po and ^{210}Pb. This suggests that the copper tailings act as an effective cover, minimizing ^{222}Rn migration from any underlying radioactive tailings. Such migration should produce detectable amounts of ^{222}Rn, as well as ^{210}Po and ^{210}Pb, but none were found.

CONCLUSIONS

Our study of the use of latter-stage ^{222}Rn decay products, ^{210}Po and ^{210}Pb, in uranium exploration covers 4 occurrences in 3 quite different geological environments. The method is effective only where ^{226}Ra occurs in the soil. In those cases where there is only ^{222}Rn migration without an associated ^{226}Ra anomaly, the results are unsatisfactory. The model in which ^{222}Rn leaves a residue of ^{210}Po and ^{210}Pb, as it migrates through the soil, thus requires further study.

At the Pronto area, the uranium tailings contain abundant ^{210}Po and ^{210}Pb, in contrast to negligible concentrations in the copper tailings. This suggests that the latter may act as an effective barrier to ^{222}Rn migration.

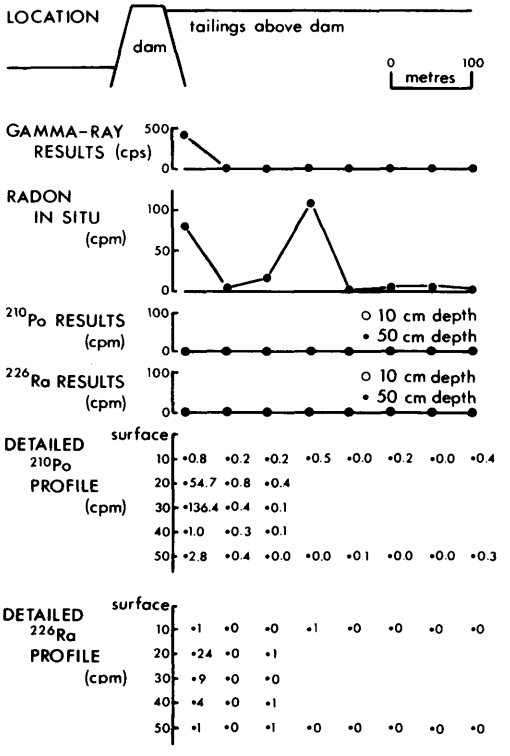

Figure 9. Comparative measurements at the east side of the dam at the Pronto tailings area.

ACKNOWLEDGMENTS

The authors are grateful to Rio Algom Mines Limited, A.J.M. Limited, and Metcalfe Realties Limited who permitted access to their respective properties for the in situ measurements and sample collection.

APPENDIX: ANALYTICAL DETAILS

^{210}Pb IN CANMET STANDARDS

Following collection of ^{210}Po, the leach solutions were saved for a number of weeks and ^{210}Po grown in from the ^{210}Pb present in solution collected on the copper plates. The counts were then adjusted to expected values for equilibrium with ^{210}Pb, using the known half-lives of ^{210}Po and ^{210}Bi, yielding a measure of ^{210}Pb present in the solution. Measurements of ^{210}Pb in leach solutions from the CANMET Standards, BL-3, BL-2, and DH-1 are shown in Table 4. In all cases, the ^{210}Pb activity was significantly higher than that from ^{210}Po. Table 4 also shows that the higher ^{210}Po measurements occur regardless of the strength of the nitric acid used for leaching.

TABLE 4 COMPARISON OF Pb-210 AND Po-210 READINGS FROM THE CANMET STANDARDS.

Standard	Trial	Po-210 Activity (cpm/g)	Po-210 Mean (cpm/g)	Pb-210 Activity (cpm/g)	Pb-210 Mean (cpm/g)	Ratio: Pb-210/Po-210
BL-3 (1.02% U)	1	756	717	978	943	1.31
	2	690		958		
	3	708		932		
	4	715		903		
BL-2 (0.453% U)	1	368	351	370	389	1.11
	2	354		402		
	3	353		380		
	4	327		407		
DH-1 (0.177% U; 0.104% Th)	1	137	144	174	167	1.16
	2	154		165		
	3	137		173		
	4	147		157		
BL-3 0.1% HNO_3 leach		607		847		1.40
1.0% " "		741		927		1.25
10% " "		736		849		1.15
70% " "		820		965		1.18

OBSERVATION OF ^{210}Po DECAY CURVES

Plates exposed in leach solutions from the CANMET Standards were counted shortly after plating, and again about 2 months later (Card and Bell 1982b). These results, together with the activity counted again about 1 year after plating, are presented in Table 5. The theoretical values are based on the subsequent activity predicted from the initial counting results. The good agreement of the observed and predicted values confirms that the activity is entirely due to ^{210}Po, and that the possibility of contamination by either longer or shorter lived nuclides is negligible.

COLLECTION OF ^{210}Po ON ALPHACARDS

Although we used a scintillation counter for most of our work, a few tests were undertaken to measure activity using a diffused junction detector. For this purpose, cards from the Alphacard ^{222}Rn detection system were modified by replacing the 2.5 cm diameter aluminized mylar disc with copper and brass discs; the converted Alphacards were then exposed in leach solutions from CANMET Standards and subsequently counted in an Alphacard reader. Counts were similar in magnitude to those from the copper plates, indicating that the diffused junction detecting is just as efficient as scintillation counting.

TABLE 5 THEORETICAL AND OBSERVED Po-210 DECAY PATTERNS.

Source of Po-210	Initial Activity (cpm/g)	Waiting Period (days)	Predicted Activity After Waiting Period (cpm/g)	Observed Activity After Waiting Period (cpm/g)	% Observed/ Predicted
CANMET Standard BL-3 (1.02% U); mean of 4 trials	738	62	541	552	102
		351	127	119	94
CANMET Standard BL-2 (0.453% U); mean of 3 trials	325	61	239	237	99
		351	56	54	96
CANMET Standard DH-1 (0.177% U; 0.104% Th); mean of 4 trials; initial activity is after correcting for Bi-212 contamination	154	60	114	117	103
		352	26	27	104

DETECTION EFFICIENCY

The detection efficiency of the scintillation counting technique was estimated using a ^{241}Am standard provided by D.R. Wiles of the Chemistry Department, Carleton University. The energy of the alpha particles emitted by ^{210}Po (5.305 MeV; 100% yield) is similar to that of ^{241}Am (5.486 MeV, 86% yield; 5.443 MeV, 12.7% yield), and hence a reasonable estimate can be made of the detection efficiency. The results in this report can be converted to pCi by dividing the reported activity by the calibration factor of 1.42 cpm/pCi. The detection efficiency was estimated to be 64%.

REFERENCES

Bell, K., and Card, J.W.
1980: Further Investigations of the Radon Decay Product Collector Method of Uranium Exploration; Grant 38, p.24-38 *in* Geoscience Research Grant Program, Summary of Research, 1979-1980, edited by E.G. Pye, Ontario Geological Survey, Miscellaneous Paper 93, 263p.

Card, J.W., and Bell, K.
1979: Radon Decay Products and their Application to Uranium Exploration; Canadian Institute of Mining and Metallurgy Bulletin, Volume 72, Number 812, p.81-87.

1982a: Collection of Radon Decay Products - A Uranium Exploration Technique; Journal of Geochemical Exploration, Volume 17, p.63-76.

1982b: Latter-Stage Decay Products of ^{222}Rn - Use in Radioactive Waste Management; Grant 105, p.29-36 *in* Geoscience Research Grant Program, Summary of Research, 1981-1982, edited by E.G. Pye, Ontario Geological Survey, Miscellaneous Paper 103, 219p.

Dyck, W.
1972: Radon Methods of Prospecting in Canada; p.212-243 *in* Uranium Prospecting Handbook, The Institution of Mining and Metallurgy, London, 346p.

Robertson, J.A.
1968: Geology of Township 149 and Township 150; Ontario Department of Mines, Report 57, 162p.

1976: The Blind River Uranium Deposits: The Ores and their Setting; Ontario Division of Mines, Miscellaneous Paper 65, 45p.

Sokal, R.R., and Sneath, H.A.
1963: Principles of Numerical Taxonomy; W.H. Freeman and Company, San Francisco and London, 359p.

Grant 132 Isotopic and Geochemical Characterization of Archean Iron Formations and Associated Volcanic Rocks - Some Preliminary Results from the Temagami and Boston Iron Formations

J.H. Crocket, R.H. McNutt, H.P. Schwarcz, C.E. Rees, N. Blum, T. Hurley, R. Bowins, and A. Kabir
Department of Geology, McMaster University

ABSTRACT

Iron formations from the Sherman Mine, Temagami, and the Adams Mine, Boston Township, were subjected to isotopic, trace element, mineralogical, and petrographic study, including sulphur and oxygen isotopic measurements together with determination of metals including gold, arsenic, antimony, and tungsten. Selected areas in the volcano-sedimentary piles hosting these iron formations are being mapped with an overall objective of characterizing the volcanic activity closely associated with iron formation deposition. Detailed studies of metal distribution are included as a part of the assessment of the volcanic rocks.

The immediate objective of the research reported here is to characterize the isotopic and heavy metal distribution properties of the iron formation and associated volcanic rocks, while a longer range study is directed toward establishing whether the metal content of iron formation is genetically linked to volcanic evolution. Such evaluation is expected to provide some constraints on whether gold in banded iron formation is essentially synvolcanic or an epigenetic introduction of metal fixed by virtue of the distinctive physical and chemical properties of iron formation.

The preliminary results suggest that biogenic sulphur is a major component of iron formation pyrite and that such pyrite carries most of the gold, arsenic, and antimony. The thermal and metamorphic history of iron formations appears to have a significant bearing on the metal content of these deposits. Some features of the gold distribution in volcanic rocks associated with the Sherman Mine iron formation tentatively suggest distribution patterns not commonly found in volcanic rocks.

INTRODUCTION

Algoman type banded iron formation (BIF) is considered by many investigators to represent a volumetrically minor lithology genetically related to Archean volcanism. Goodwin (1973) noted that such BIF is preferentially localized in the stratigraphically uppermost rocks of mafic-to-felsic volcanic cycles, and that it probably constitutes a volcanogenic component of the pile. The occurrence of economic concentrations of gold in BIF is well-known, but the genetic relationships between this mineralization and the iron formation is not well-understood. Such uncertainty contributes to inefficient exploration for auriferous iron formation. At least 2 types of genetic relationship are advocated in recent studies of gold-bearing BIF. One is that gold is introduced after lithification of BIF by fluids that deposit auriferous quartz veins and replace magnetite by gold-bearing pyrite. Fyon *et al.* (1983) suggested such a process for the gold-bearing Carshaw-Malga BIF in the Timmins area. In this model, it was proposed that BIF served as a chemogenic sink for gold, and represents a lithology favourable to sulphide replacement of oxides. According to another model, as advocated for the Contoyowo Lake deposits by Page (1983), sulphide facies BIF concentrated gold during sedimentation. In this model, the depositional environment hosting the BIF is thought to be enriched in gold as a consequence of exhalative volcanism.

If metal enrichment in BIF was essentially a synvolcanic phenomenon, then the associated volcano-sedimentary pile may be marked by characteristic petrographic and geochemical indicators resulting from the magma fractionation and evolution that contributed to the enrichment. However, if metals such as gold were introduced epigenetically into the BIF, then other factors assume major importance. For example, proximity of the BIF to younger, large plutonic intrusions, which may have generated sufficient thermal energy to effect circulation of large volumes of fluid, or proximity to major fault systems, which could have channeled fluid flow, must be critically appraised. Thus, evaluation of both an iron formation and its host volcanic pile are essential to a better understanding of mineralization processes and metal sources. It also follows that an understanding of mineralization processes may provide a means of assessing the economic mineral potential of the associated volcano-sedimentary pile.

Two iron formations, the Temagami iron formation in Strathy, Strathcona, and Briggs Townships (District of Nipissing) and the Boston iron formation in Boston Township (District of Timiskaming), were selected for study.

These 2 areas provide important geological constraints useful for assessing factors which may be critical to the understanding of the BIF depositional environment. In this report, the preliminary results of some isotopic and geochemical studies are reported.

GEOLOGY

The geology of the Temagami area was mapped at a scale of 1:31 680 by Bennett (1978), and the petrography and stratigraphy of the northern band of Sherman Mine iron formation were discussed by Campbell (1978). Boston Township and the Boston iron formation were mapped by Lawton (1958) and the geology presented on a 1:12 000 scale map. Additional discussion of the Boston iron formation and Adams Mine geology has been contributed by Lovell (1972), Ridler (1970, 1972), and Jensen (1978). Certain comparative aspects of the general regional geology are of importance in the choice of these 2 areas for study. Firstly, the volcanic lithologies in the 2 areas differ, in that rocks of the komatiite suite occur in close association with the Boston iron formation (Jensen 1978), but have not been reported in the Sherman Mine area. Secondly, the regional metamorphic grade of the Boston iron formation is higher than the regional grade of the volcanic rocks in the Sherman Mine area. Jolly (1974) indicated an upper greenschist to lower amphibolite grade for rocks of the Adams Mine area; grunerite, cummingtonite, and garnet are common in the silicate-facies BIF. Lower greenschist facies (quartz-albite-muscovite-chlorite subfacies) rocks prevail in the Sherman Mine area (Bennett 1978), and silicate facies iron formation locally carries minnesotaite whereas garnet is absent. Both areas have been affected by the intrusion of large granitoid plutons. Much of the iron formation in the Adams Mine area is within 1.5 km of the Lebel Stock. The Sherman Mine iron formation is approximately the same distance from the Spawning Lake Stock at its western extremities. However, it strikes away from this intrusion so that some pits (e.g. the North Pit) are at least 4 km distant from major intrusive plutons. Thermal overprinting thus can be expected to be more severe in the Adams Mine area. Finally, on a regional basis, the Boston iron formation is associated with a major gold camp (Kirkland Lake) whereas the Sherman Mine iron formation is not. These differences in geological setting may provide guidelines to the explanation of geological or geochemical properties distinctive to each area.

In the Sherman Mine area, a unit of felsic to intermediate volcanic rocks (Bennett 1978, Map 2322), which stratigraphically underlies the north iron formation band, is being mapped to establish the physical, petrological, and geochemical characteristics of volcanism which occurred just prior to iron formation deposition. In the Adams Mine area a series of volcanic, volcaniclastic, and possible interflow sedimentary rocks west of the South and Central Pits is being mapped to establish possible correlation with volcanic and sedimentary rocks in the immediate vicinity of the Central Pit. In this report, geochemical data from the iron formations and the Sherman Mine volcanic section are presented.

METHODOLOGY

SAMPLING PROCEDURES

Samples of volcanic rocks were collected from the Sherman Mine area during detailed mapping some 500 m north of the North Pit (*see* Figure 4). Also, some samples were obtained from volcanic rocks in the footwall and immediately underlying the south-dipping West Pit iron formation as indicated in Figure 2. Other volcanic-rock samples were taken at the northeastern end of the South Pit, within 10 m of the stratigraphic base of the iron formation. Iron formation samples also were taken across pit face exposures, at the western ends of the South and West Pits, representing complete stratigraphic sections of approximately 70 m and 20 m, respectively. Another exposure was sampled toward the eastern end of the West Pit (*see* Figure 2) and represents an incomplete section extending from the footwall into the iron formation for approximately 67 m.

At the Adams Mine, samples of iron formation were taken from the Central, Northern, and Peria Pits (Figure 1). In the Northern and Peria Pits, samples were collected from pit wall faces and from large dislocated blocks within the pit. At the Central Pit, sampling of all major iron formation facies was possible by collecting from pit wall faces.

ANALYTICAL PROCEDURES

Sulphur isotope analyses were carried out on SO_2 gas obtained by direct burning of pyrite, as described by Thode and Rees (1971) and Rees (1978). Precision of an individual determination was ±0.1‰ and all $\delta^{34}S$ data are expressed relative to Canyon Diablo troilite. Sulphide-rich areas of mesobands were cut out using a diamond saw, crushed to pass a −100 mesh screen, and digested with hydrofluoric acid on a steam bath for 1 to 2 days. After decanting the acid and washing with water, a pyrite concentrate of very high purity was produced. No significant difference in isotopic composition between chemically and mechanically concentrated pyrites from the same mesoband were found.

The BrF_5 method of Clayton and Mayeda (1963) was used to liberate oxygen from chert. The gas was converted to CO_2 for isotopic analysis. Reproducibility was within ±0.015‰. Chert mesobands were crushed to pass −325 mesh and the powder treated with aqua regia to remove iron oxides and silicates.

Determination of Au, As, Sb, and W was carried out by epithermal instrumental neutron activation analysis while Cu and Zn were determined by XRF analysis. Sulphur was determined by iodine titration using a Leco Model WR-12 furnace system to outgas samples. For the

activation analysis, the approximate sensitivity limits are 1 ppb for Au and 50 ppb for As, Sb, and W in the iron formation samples. For volcanic rocks, the sensitivities are somewhat poorer and estimated at 2 ppb for Au and 100 ppb for the other metals.

DISCUSSION

SULPHUR ISOTOPE COMPOSITION

The isotopic compositions of pyrite from the Adams Mine and Sherman Mine iron formations are summarized in Table 1, and shown in Figure 3. Samples are classified according to the nature of the host rock as either oxide-facies or sulphide-facies pyrites. Oxide-facies host rocks are mainly magnetite-rich mesobands in which the pyrite usually occurs as disseminated subhedral grains or as quartz-pyrite veinlets filling microfractures. The pyrite is dominantly discordant on a hand specimen scale. Sulphide-facies host rocks are mostly dark green, very fine-grained, chloritic rocks which are commonly interlayered with and conformable on an outcrop scale with oxide-facies mesobands and are usually of comparable lateral extent. These rocks, which are major carriers of sulphide, are tentatively considered to be pyroclastic rocks and are termed chloritic tuff. The pyrite occurs as disseminated grains in the chloritic tuff, and locally as laminated masses. Sulphide-facies host rocks also include a graphitic schist bed, with nodular pyrites overlying the Sherman South Pit iron formation.

For the entire population of 24 samples, the range in $\delta^{34}S$ is 18.9‰ (from −14.3‰ to +4.6‰), with an arithmetic mean of −2.5‰. The sulphide-facies pyrites are characterized by light sulphur in that all samples but

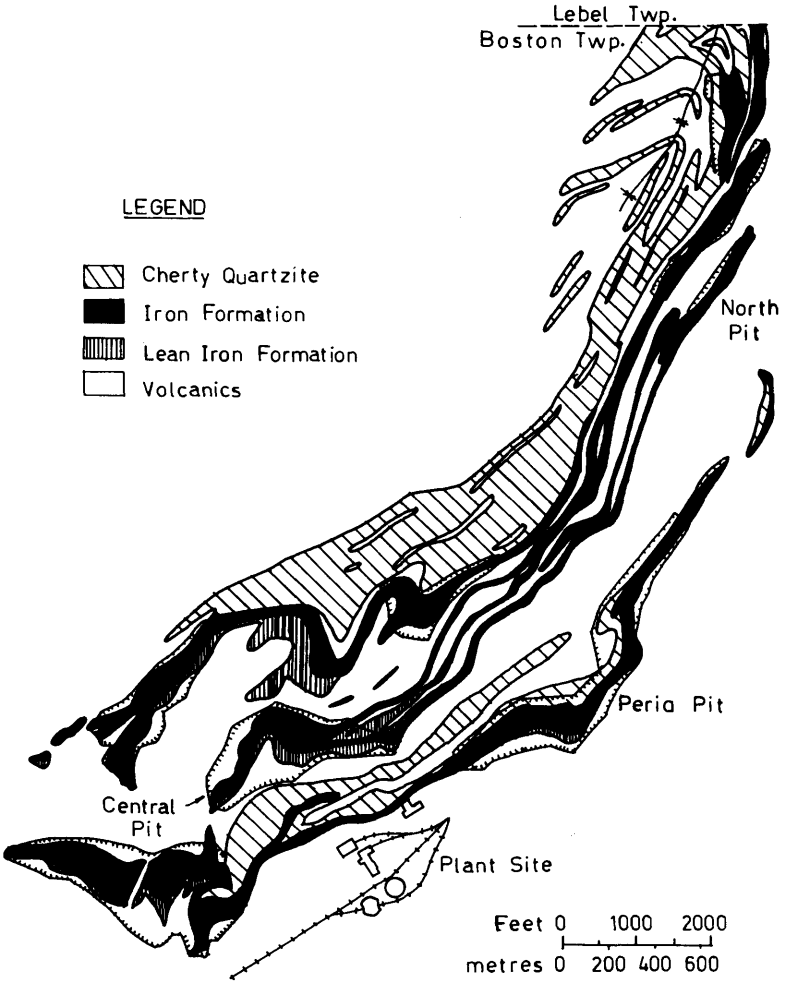

Figure 1. Adams Mine iron formations showing pits sampled for isotopic and geochemical studies.

1 have negative values. The majority of oxide-facies pyrites are positive although 2 samples have distinctly light sulphur with $\delta^{34}S$ values of −6.2‰ and −11.0‰. The nodular pyrite from the South Pit graphite schist has $\delta^{34}S$ = −0.5‰.

It is suggested that an isotopic distinction can also be drawn between the oxide-facies and sulphide-facies populations in that the pyrites of the chloritic tuff are characterized by lighter sulphur than those of the magnetite-rich mesobands. Sulphide-facies pyrites have an average $\delta^{34}S$ = −3.3‰ in comparison with oxide-facies pyrites with an average $\delta^{34}S$ = −0.5‰. The ranges in isotopic composition of the 2 populations are nearly identical: 15.2 and 15.6‰, respectively. The histogram (*shown in* Figure 3) shows the tendancy of the oxide-facies pyrite samples to cluster in the positive field.

It is suggested that the sulphur in the chloritic tuff-hosted pyrite is mainly biogenic. The predominance of isotopically light sulphur, the relatively large range in isotopic composition (15‰), and the stratabound character of the pyrite are properties favouring metallogenesis involving bacterial reduction of marine sulphate. An important constraint on a biogenic-reduction model for sulphate production is that Archean seawater sulphate probably had a mean isotopic composition of $\delta^{34}S$ = 0 as argued by Thode and Goodwin (1983). The isotopic dis-

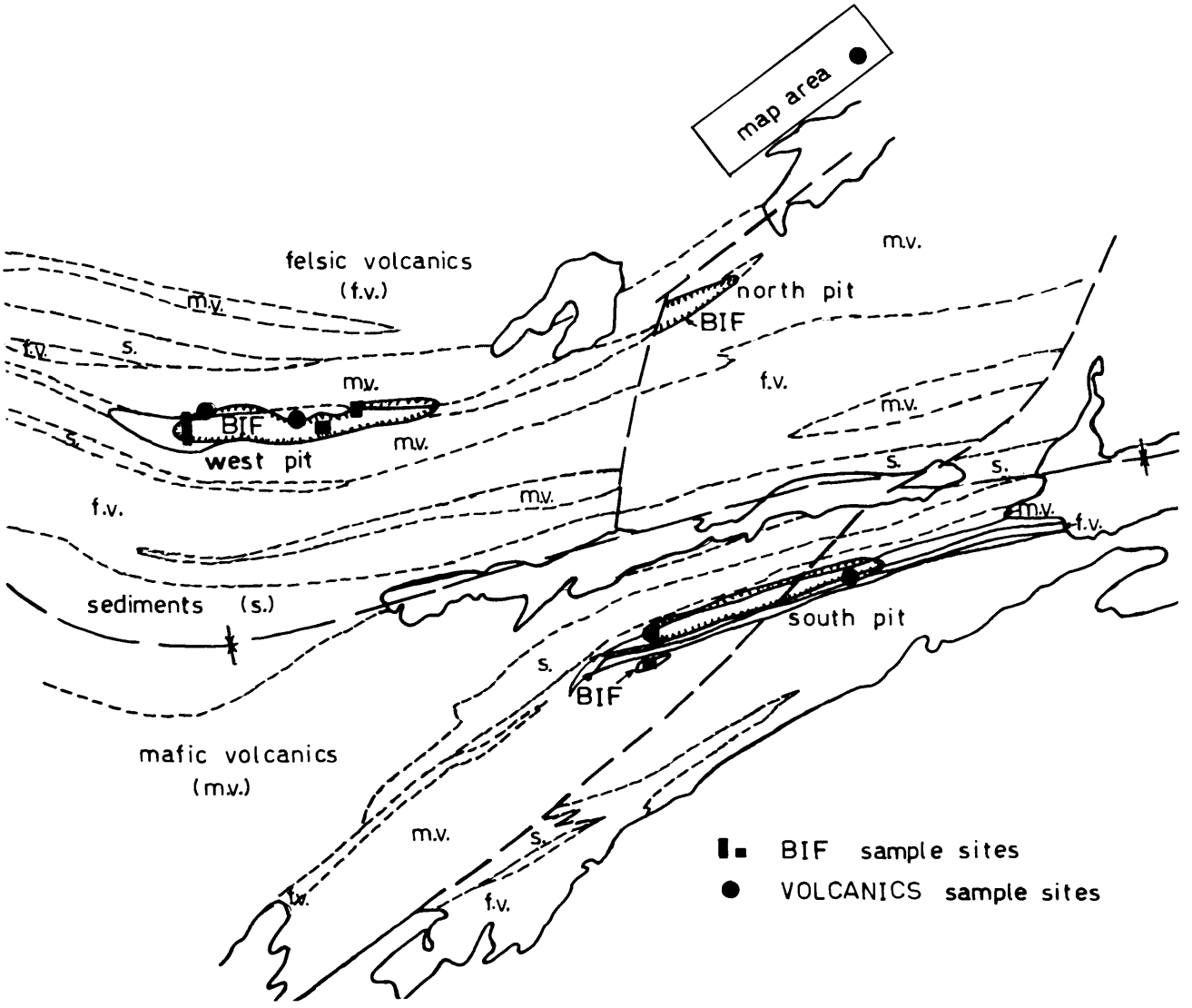

Figure 2. Location map showing: sampling traverses (bars) across the West and South Pits BIF, sampling sites for hanging wall and footwall volcanic rocks (circles), and a map area in felsic volcanic rocks underlying the northern band of iron formation at the Sherman Mine. Geology after Bennett (1978).

tribution observed in the chloritic tuff must have been produced by a relatively complete reduction of sulphate from a nearly fixed source, that is, under conditions of a closed system. The physical process of sedimentation most conducive to producing closed-system conditions with respect to a single bed would be rapid accumulation such as might result from the falling of fine volcanic ash from a distal source. Rapid accumulation would minimize the time the sediment was in direct contact with a seawater reservoir and effectively limit the exchange rate of sulphate between sediment pore fluid and seawater to that set by slow diffusion processes. This, in turn, would limit the sulphate supply to bacteria, promote high consumption of available sulphate, and tend to push the mean isotopic composition of sulphide towards that of the original sulphate. Thus, the observed mean $\delta^{34}S$ of sulphide facies pyrite of $-3.3‰$ is probably reasonable if an initial sulphate source with $\delta^{34}S$ of approximately 0‰ was almost completely reduced to sulphide without significant sulphate replenishment.

The source of sulphur in the dominantly discordant pyrite filling microfractures in magnetite-rich chert mesobands is uncertain. One possibility is remobilization of sulphide from chloritic tuff beds. Both oxide-facies and sulphide-facies populations show the same range in $\delta^{34}S$, about 15‰; however, the oxide-facies population is characterized by sulphur which on average is 2.8‰ heavier. Although an obvious explanation of the fractionation processes that concentrate ^{34}S in remobilized pyrites is lacking, chloritic tuff-hosted pyrite is probably the major sulphur source, and its dissolution and reprecipitation in response to metamorphism and deformation seems probable. Another sulphur source suggested by the clustering of oxide-facies sulphide near $\delta^{34}S = 0$ is volcanogenic sulphur. The occurrence of much oxide-facies sulphide in discordant settings indicates post-lithification emplacement. An ultimate source of such sulphur in the underlying volcanic pile is perhaps more likely than a direct exhalative addition to the depositional basin.

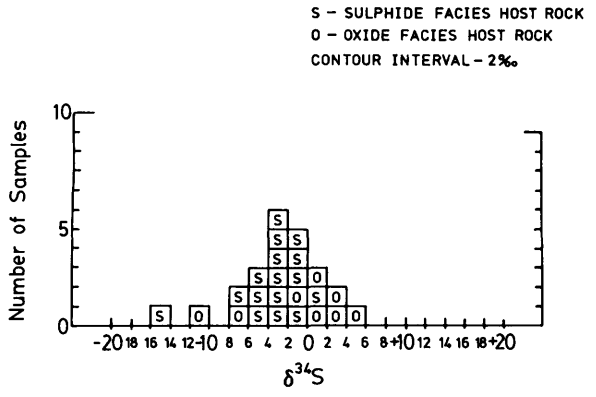

Figure 3. Sulphur isotopic composition of pyrite from the Adams Mine and Sherman Mine. Samples from the sulphide facies (chloritic tuff mesobands) and the oxide facies (magnetite-rich or jasper mesobands) are differentiated by S and O respectively.

TABLE 1 SULPHUR ISOTOPE COMPOSITION OF PYRITES FROM ADAMS AND SHERMAN MINES BANDED IRON FORMATIONS.

Locality	$\delta^{34}S$, oxide facies	$\delta^{34}S$, sulphide facies
ADAMS MINE		
North pit	+1.5, +1.9	−0.2, −1.25, −2.7, −4.1
Central pit		+0.9, −0.5, −3.2, −4.8, −5.1, −7.3
Peria pit		−2.1, −3.1, −3.8
SHERMAN MINE		
West pit	−11.0, −6.2, +2.8, +3.0	−1.6, −2.7, −14.3
South pit	+4.6	−0.5

OXYGEN ISOTOPIC COMPOSITION

The oxygen isotopic compositions of some 70 purified quartz separates from chert mesobands were measured to evaluate the thermal history of the iron formations. This study will ultimately test the quartz-magnetite isotopic geothermometer to search for possible thermal anomalies in the depositional environment and to evaluate the thermal aspects of metamorphism of the iron formations. The latter studies may provide important data to determine if primary metallogenic signatures are recognizable or whether redistribution of metals in response to metamorphism and deformation is the major control on metal distribution.

The oxygen isotopic compositions of quartz separates from the chert mesobands from 2 different iron formation units exposed in the Central and North Pits at the Adams Mine were determined. As indicated by the comparison in Table 2, the oxygen of the quartz separates from the Central Pit cherts is 2.6% heavier on average than that of quartz separates from the North Pit, and there is no overlap of data between the 2 populations. In both iron formation units, a systematic increase in $\delta^{18}O$ was observed from hanging wall to footwall. Detailed evaluation of the thermal significance of the isotopic data is not be attempted here as the magnetite isotopic compositions remain to be established. However, some pre-

liminary comments on estimated isotopic and mineral assemblage temperatures can be noted.

According to Jolly (1974), volcanic rocks in the Adams Mine area have compositions which represent upper greenschist- to lower amphibolite-facies conditions. Grunerite, cummingtonite, and almandine are characteristic minerals. A temperature of at least 330°C is suggested by the absence of minnesotaite, and the minimum temperature for the breakdown of minnesotaite to grunerite.

An isotopic temperature can be roughly estimated by assigning seawater an isotopic composition of $\delta^{18}O = 0$, recognizing that either or both the isotopic composition and temperature of Archean seawater were different than those of modern seawater. Using the quartz-water fractionation curve of Knauth and Epstein (1976), i.e. $-10^3 \ln\alpha^{quartz}_{water} = (3.09 \times 10^6)T^{-2} - 3.29$ and the oxygen isotopic compositions from Table 2, an upper temperature of 155°C (i.e. $-\delta^{18}O_{quartz} = 18‰$) is obtained. Allowing for adjustment due to uncertainty of Archean seawater isotopic composition, it seems that a significantly higher isotopic compositon prevails than that required for an equilibrium established at the regional metamorphic grade represented by the mineral assemblages. Tentatively, the comparison suggests that a post-regional metamorphic isotopic re-equilibration has affected these rocks. The systematic variations in isotopic composition across the Central and North Pit iron formations, which are less than 50 m thick, were probably caused by a thermal front generated by the intrusion of the Lebel syenite stock some 1.5 km to the northwest.

In the Sherman Mine area, where metamorphic grade is lower, similar isotopic results were obtained. The entire South Pit and the western section of the West Pit are characterized by $\delta^{18}O_{quartz}$ ranging from 15.0 to 17.9‰ indicating metamorphic temperatures of approximately 145° to 110°C. The occurrence of grunerite indicates metamorphic temperatures of at least 330°C, suggesting isotopic disequilibrium and/or re-equilibration. However, east of the Iron Lake Fault (Campbell 1978), which cuts the West Pit, an abrupt change in isotopic signature and mineralogy is found. Here, in the eastern section of the West Pit, minnesotaite rather than grunerite is the prominent iron silicate and jasper becomes much more abundant. Assuming a greenalite precursor, a temperature range of 200° to 300°C (at 5 kbar) is suggested by the presence of minnesotaite, in that dehydration of pure greenalite begins at 200° to 220°C, where minnesotaite becomes stable. Further, the occurrence of both magnetite and hematite in this section of the pit indicates a metamorphic temperature of approximately 200°C (Melnik 1982). $\delta^{18}O_{quartz}$ in this area of the West Pit ranges from 12.0 to 13.1‰, equivalent to a temperature range of 180° to 165°C thus making the concordance of isotopic and metamorphic mineral assemblage temperatures much greater than in other areas studied. Apparently this area preserved an isotopic record indicating equilibration at relatively low-temperature metamorphic conditions. Thus, a comparison of metal distribution patterns and metal abundance levels in the western and eastern sectors of the pit may provide useful insight into the effects of metamorphism on mobilization of metals.

TABLE 2 OXYGEN ISOTOPIC COMPOSITION OF QUARTZ FROM CHERT MESOBANDS, ADAMS AND SHERMAN MINES.

Location	$\delta^{18}O$, ‰			
	$\bar{X}$	σ	range	n
Central Pit, Adams	17.3	0.63	16.6-18.0	15
North Pit, Adams	14.7	0.87	13.4-15.6	15
South Pit, Sherman	16.2	0.63	15.0-17.9	15
West Pit, Sherman				
western section	16.7	0.96	15.0-17.9	15
eastern section	13.1	0.05	12.0-14.0	10

GOLD, ARSENIC, ANTIMONY, AND TUNGSTEN IN BIF

Favourable structures (faults, major folds) in deformed iron formation often are loci of gold mineralization; however, it is difficult to determine if the mineralization resulted from an introduction of gold from an external source, or a remobilization of syngenetic gold. Detailed knowledge of gold distribution and concentration levels in undeformed iron formation should provide some guide to metal characteristics inherited as a result of concentration processes, which in turn may establish a basis for recognition of metal distribution patterns suggestive of introduction versus redistribution. In practice, however, the interpretation of trace metals in iron formation involves several uncertain factors. Aside from the probable lack of any Algoman BIF which has entirely escaped deformation, the effects of dewatering, lithification, diagenesis, and burial metamorphism are highly uncertain. With these reservations in mind, the gold contents of oxide-facies and sulphide-facies rocks from the Sherman Mine and Adams Mine iron formations have been determined. In addition, the concentrations of arsenic, antimony, and tungsten, any one of which may be occasionally concentrated in gold-quartz veins, were also measured. The results of trace element analyses of pyrite from the Adams Mine and Sherman Mine iron formations are given in Tables 3 and 4.

PYRITE

The pyrite samples are mineral separates having about 98% purity. The average contents of some trace elements, particularly arsenic and antimony, are strongly biased by a few very high values. For purposes of comparison and discussion, only averages which exclude samples differing by more than 2σ from the total population mean are used. In comparison with oxide-facies

TABLE 3 GOLD AND OTHER METALS IN BANDED IRON FORMATION FROM THE SHERMAN AND ADAMS MINES[1].

No.	Sample Description[2]	Facies[3]	Gold ppb	Arsenic ppm	Antimony ppm	Tungsten ppm
West Pit						
W1	M	O,SIL	4.0	0.47	0.85	0.68
W1	J		7.5	0.47	0.60	0.54
W6	J_1	O,CARB	5.9	0.16	1.4	0.37
W6	J_2		4.4	1.1	1.8	0.95
W9	J_1	O	70	1.0	0.94	1.4
W9	J_2		12	0.94	1.2	1.4
W13	J_1		20	0.82	1.0	2.7
W13	J_2	O	15	0.78	1.1	2.5
W13	J_3		11	0.35	1.2	1.7
W14	J	O	20	0.50	0.64	2.8
W15	M_1		11	1.6	0.41	29
W15	M_2		7.5	1.9	5.6	38
W15	M_3,J_3	O	6.1	1.9	4.8	36
W15	M_4,J_4		7.5	2.1	5.2	39
W15	J_1		7.4	0.68	1.1	2.5
W15	J_2		6.9	1.6	4.9	37
W37D	$C(J)_1$	O	7.1	1.5	0.55	5.0
W37D	$C(J)_2$		5.0	0.72	0.61	2.9
W20	P	SUL	260	0.61	1.8	0.33
W23	P	O	93	770	4.8	0.67
W29	P	O	450	12	0.27	0.50

Notes

1. Sample locations - Adams Mine: C, Central Pit; N, North Pit; P, Peria Pit.
Sherman Mine: S, South Pit; W, West Pit.

2. Sample Descriptions
Discrete mesobands and purified pyrite mineral separates were analysed. The pyrite separates are designated by P. The mesobands are designated by the dominant mineralogical component as follows: M-magnetite, C-chert (quartz), J-jasper (hematite-quartz), C(J)-chert bands with minor jasper, CARB-carbonate (mainly siderite).
Bands from the same hand specimen are indicated by the same sample mumber, for example C34. Different bands with the same dominant mineralogical properties are distinguished by subscripts 1,2,3 etc. when they are cut from the same hand-specimen. For example four magnetite bands, one chert band and one jasper-bearing chert band were cut from sample S9C.

3. The host rock is assigned to a specific facies according to the mineralogical character of the most common mesobands. Abbreviations used are: O-oxide facies, magnetite-quartz and hematite-quartz mesobands; CARB-carbonate facies, siderite; SIL-silicate facies, mesobands with an iron silicate mineral such as minnesotaite, stilpnomelane, grunerite, cummingtonite and actinolite; SUL-sulphide facies, mesobands with abundant pyrite usually hosted in chlorite-biotite-tremolite bearing rocks.

TABLE 3 (Continued)

No.	Sample Description[2]	Facies[3]	Gold ppb	Arsenic ppm	Antimony ppm	Tungsten ppm
			ADAMS MINE			
Central Pit						
C34	M	O	4.7	0.81	0.17	1.4
C34	C(J)		10	0.86	0.15	1.0
C35	M	O	9.4	0.97	0.29	0.66
C35	C(J)		10	0.52	0.17	0.51
C38	M(S)	O	14	0.88	0.18	1.2
C38	C(S)		3.3	0.29	0.18	1.1
C39	J	O	5.7	0.61	0.49	1.1
C36	P	SUL.	99	5.2	0.27	0.40
C37	P	SUL.	79	6.8	0.20	1.0
North Pit						
N23	J	O, SIL	13	0.10	0.18	0.30
N17	P	SUL-O	45	19	0.48	0.28
N18	P	O	18	25	0.28	0.34
Peria Pit						
P13	P	SUL	220	19	0.41	0.84
			SHERMAN MINE			
South Pit						
S9C	M_1		0.64	1.6	1.2	0.20
S9C	M_2		0.68	0.71	0.37	0.80
S9C	M_3	O,CARB	0.80	0.38	0.46	0.71
S9C	M_4		1.3	0.44	0.36	0.41
S9C	C		2.9	1.1	0.25	0.67
S9C	C(J)		2.9	0.46	0.30	0.91
S9D	M		0.94	1.0	0.83	0.56
S9D	C	O	7.4	0.55	0.20	0.17
S9D	C(J)		7.5	1.1	0.39	1.8
S7	C	CARB	4.4	0.40	0.11	2.2
S7	CARB		3.3	5.7	0.24	1.8
S22	$C(J)_1$	O	11	0.88	0.40	1.2
S22	$C(J)_2$		10	1.0	0.36	0.61
S11	P	Graphite Schist	260	600	69	0.40

TABLE 4 MEAN VALUES AND OTHER STATISTICS FOR GOLD, ARSENIC, ANTIMONY, AND TUNGSTEN IN BANDED IRON FORMATION FROM THE ADAMS AND SHERMAN MINES.

Sample	n	Gold, ppb			Arsenic, ppm			Antimony			Tungsten		
		$\bar{X}$	σ	r	$\bar{X}$	σ	r	$\bar{X}$	σ	r	$\bar{X}$	σ	r
Pyrite separates	9	169	139	18-450	162	300	0.61-770	8.6	23	0.20-69	0.53	0.25	0.28-1.0
	8[1]				86	208	0.61-600	1.1	1.6	0.20-4.8			
Magnetite mesobands	13	5.3	4.4	0.64-14	1.1	0.51	0.38-2.1	1.6	2.1	0.17-5.6	11	17	0.20-39
	7										5.8	13	0.53-35.5
Jasper and jasper-bearing chert mesobands	21	9.2	4.6	2.9-20	0.87	0.53	0.10-2.1	1.3	1.6	0.17-5.2	6.7	13	0.30-39
	18[2]										3.1	6.6	0.30-29

Notes

1. Excludes samples which exceed the mean by more than 2σ
2. Sample W15 is unusually high in tungsten. Mesoband subsamples from W15 are averaged and this sample is represented by one value only.

mesobands, pyrite separates generally have high concentrations of gold, arsenic, and antimony, but are significantly depleted in tungsten (*see* Table 4).

Pyrite separates were obtained from 3 distinct host rock settings. Samples C36, C37, N17, and W20 are pyrites from chloritic tuff bands. Separates N18, W23, and W29 are from magnetite mesobands in which sulphides occur as discordant fracture fillings with quartz, and sometimes carbonate. A third lithology sampled was a black, graphite schist which overlies the main iron formation units in the Sherman South Pit, and contains concentrically laminated pyrite nodules up to 2 cm in diameter.

All pyrite separates except N18 are strongly enriched in gold compared to oxide-facies mesoband samples. On average, pyrite separates carry 32 times more gold than magnetite mesobands and 18 times as much gold as jasper-bearing mesobands. Although their arsenic contents are extremely variable, pyrite separates carry approximately 12 times as much arsenic as the oxide-facies mesobands, neglecting the arsenic value of 770 ppm for sample W23. There are no large differences in the antimony contents of sulphide-facies and oxide-facies pyrite separates, while tungsten is strongly depleted in pyrite separates relative to oxide mesobands. Pyrite nodules from the graphite schist have a high gold content (260 ppb) and very high arsenic and antimony contents. The precursor sediment was probably an organic-rich, highly reducing mud in which reduction of multivalent metals such as gold, arsenic, and antimony led to their coprecipitation with pyrite during diagenesis. Although a quantitative assessment is lacking, the most commonly observed occurrence of pyrite is in chlorite tuff bands, and it is suggested that these bands represent the major sinks for sulphides and metals in both iron formations.

OXIDE-BEARING MESOBANDS

On average, magnetite- and jasper-bearing mesobands vary by less than a factor of 2 in metal contents. Magnetite mesobands carry 20% more arsenic and antimony, 80% more tungsten, but 80% less gold. Some of the most anomalous rocks are the jasper-rich samples from the eastern section of the Sherman West Pit (W13, W14, W15, W37D) where the oxygen isotopic data and mineralogy tentatively suggest a simpler and probably lower-temperature thermal history. Metal contents which significantly exceed the total population average are found in a number of these rocks. Tungsten, for example, is particularly anomalous. With 1 exception (sample S7), tungsten is less than 2 ppm in magnetite, jasper, and chert mesobands, except in the W13 to W37D series where all samples but 1 exceed 2 ppm. The highest tungsten values, averaging 30 ppm in the W15 sample series, are found in both magnetite and jasper mesobands. Antimony behaves similarly, although less extremely. Few magnetite or chert bands carry more than 1 ppm antimony (excepting S9C-M_1, W6, and W9-J_2) whereas 2 of the 4 eastern section sample suites from the West Pit exceed 1 ppm, with the W15 suite carrying an average of 3.7 ppm antimony. Arsenic is not markedly enriched in these rocks except in the W15 sample suite. Excluding magnetite and chert mesoband samples, which carry more than a trace of sulphide (sample C38), there are no samples which exceed 10 ppb gold, except for those of the West Pit suite in which W13 and W14 jasper bands contain up to 20 ppb gold. Although only a tentative generalization can be drawn with the data available, it is suggested that the jasper-rich eastern section of the Sherman West Pit iron formation is significantly enriched in 3 metals gold, antimony, and tungsten. If this area represents a low-grade

metamorphic "window", the suggested metal enrichment may be primary. A further supportive observation is that the Adams Mine samples, which represent a higher metamorphic-grade suite, are significantly poorer in tungsten and antimony than the Sherman West Pit samples. To speculate further, the overall effect of metamorphism may have been to mobilize those metals which are generally incompatible with oxide structures, leading to either their concentration in sulphide-rich mesobands, or their loss from the BIF.

METALS IN VOLCANIC ROCKS FROM THE SHERMAN MINE AREA

Metals determined in Sherman Mine volcanic rocks are copper, zinc, arsenic, antimony, gold, and also sulphur, the distributions of which were studied in a section stratigraphically underlying the West and North Pits, and in samples taken from the immediate hanging wall and footwall units of the South and West Pits. The section of volcanic rocks sampled is located approximately 500 m north of the North Pit (*see* Figure 4) and consists of flows and fragmental rocks of felsic, intermediate, and mafic compositions. About 75% of the analyzed rocks are basalts with a few andesites, while the remaining 25% are dacites and rhyolite according to the Jensen (1976) cation plot classification. The samples taken from the pit areas are mainly dacite but include some basalt and andesite.

The analytical data are presented in Table 5, in which rocks are grouped according to physical character (flows or fragmentals) and composition. In flows from the map area north of the North Pit, the base metals show an increase in concentration from felsic to mafic rocks, while gold and arsenic contents vary in the opposite sense. Antimony trends are less distinct but more comparable with those of gold and arsenic. Fragmental rocks (tuff-breccia, lapilli-tuffs, and crystal tuffs) are mainly mafic and, compared to mafic flows, they contain slightly higher contents of all metals.

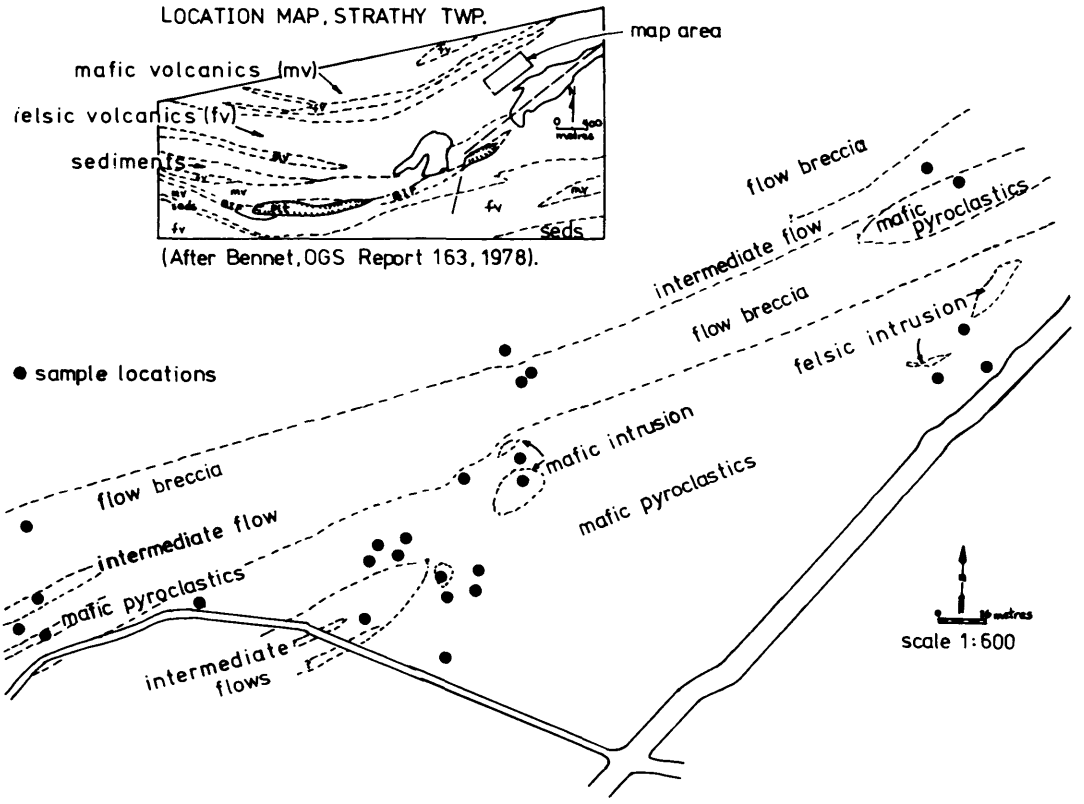

Figure 4. Preliminary geological map of volcanic rocks underlying the northern band of iron formation at the Sherman Mine. The main units are differentiated according to physical character into fragmentals, flows, and possible intrusive varieties. Compositional characterization into felsic, intermediate, and mafic volcanic rocks correspond to rhyolite-dacite, andesite, and basalt from a petrographic classification according to a Jensen (1976) cation plot.

TABLE 5 METAL CONTENTS OF VOLCANIC ROCKS FROM THE SHERMAN MINE AREA.

Sample Description	Rock[1] type	Location	n[2]	S ppm	Cu ppm	Zn ppm	Au ppb	As ppm	Sb ppm
Felsic intrusion or flow	rhyolite	Map area[3]	3	400	<5	19	63	3.7	0.21
Felsic and intermediate flows, dacites and andesites		Map area & SM Road	5	1000	9	76	5.7	2.8	0.55
Mafic flows, basalt		Map area	3	300	38	107	4.2	1.4	0.50
Mafic and intermediate fragmental volcanics	mainly basalt	Map area	13	1800	48	155	7.2 5.9[4]	6.4 3.6[4]	1.6 0.74[4]
Felsic and intermediate fragmental volcanics	dacite and andesite	West Pit	8	265	50 9[4]	67	4.9	0.75	0.48
Felsic and intermediate fragmental volcanics	dacite and andesite	South Pit	2	125	22	82	6.3	3.7	0.45
Mafic fragmental volcanics	basalt	South Pit	1	16,000	26	86	220	4.3	0.35
Mafic fragmental volcanics	basalt	South Pit	1	100	<5	120	7.6	0.12	0.42

Notes
1. Petrographic classification according to Jensen Cation Plot (1976).
2. number of samples
3. as indicated on Fig. 4
4. arithmetic mean excluding samples which exceed the total population mean by more than 2σ .

The base-metal trends, that is increasing concentrations with increasing mafic content of the host rocks, are those normally found in volcanic rocks. The general trends of gold and arsenic with variation in silica content in volcanic rocks are not well established, but in the case of gold, 2 points may be noted. Specific studies (Gottfried *et al.* 1972; Kwong and Crocket 1978) and literature surveys (Crocket 1974) suggest that the gold content of mafic rocks is higher than or comparable to that of felsic rocks. Secondly, average gold in felsic rocks for large suites of samples is usually found to average 1 to 2 ppb (*for example* Crocket 1974: 1.5 ppb for 188 samples, literature survey; Gottfried *et al.* 1972: 1.4 ppb for 125 samples, mainly U.S. southwest; Kwong and Crocket 1978: 1.5 for 35 samples, Kakagi Lake). Thus, the Sherman Mine suite represents a trend in gold content with volcanic rock bulk composition which is opposite to that usually found, and the average gold content of the felsic and intermediate volcanic rocks is approximately 4 times higher than the average gold content of felsic volcanic rocks as found in previous studies noted above.

Volcanic rocks from the immediate hanging walls and footwalls of the West and South Pits are mainly felsic and intermediate fragmental rocks (dacite and andesite). They are generally comparable in metal content to the suite just discussed. Finally, it is noted that gold content is usually highly anomalous if the sulphide content is high. Thus the highest gold content found, 220 ppb, is in a fragmental mafic volcanic rock from the South Pit area, which carries 1.6% sulphur as very fine-grained disseminated pyrite. In the majority of samples, sulphur is less than 0.05% by weight.

CONCLUSIONS

The following tentative generalizations are drawn with respect to the Temagami and Boston iron formations and associated volcanic rocks:

1. Iron formation sulphide strongly concentrates gold, arsenic, and antimony relative to oxide-facies mesobands. In most cases, sulphides in metal-rich oxide-facies mesobands occur as quartz-pyrite fracture fillings.
2. Chloritic tuff mesobands are frequently sulphide-rich, and their abundance and distribution are probably the major control on metal distribution in the iron formations investigated.
3. The sulphur in chloritic tuff mesobands has an isotopic composition compatible with biogenic reduction of marine sulphate if these mesobands were rapidly deposited.
4. The oxygen isotopic composition of chert together with BIF mineralogy and regional metamorphic grade

suggests that some iron formation in the Sherman Mine is significantly less altered by post-lithification events. Isotopic trends in both the Sherman and Adams Pits indicates that the thermal effects of nearby granitoid intrusions causes significant re-equilibration of oxygen isotopes.

5. The suggested low intensity metamorphic "window" in the Sherman West Pit is characterized by weakly anomalous metal enrichment of oxide facies rocks, particularly jaspar-rich rocks.

6. Volcanic rocks stratigraphically underlying the Sherman northern band of iron formation show trends in gold distribution which are unusual in comparison with gold distribution suggested by literature surveys and studies of specific areas elsewhere.

ACKNOWLEDGMENTS

We are grateful to Mr. Bob Garrett of Sherman Mines and Mr. Keith Oliver, Adams Mine for geological introductions to their respective areas.

REFERENCES

Bennett, G.
1978: Geology of the Northeast Temagami Area, District of Nipissing; Ontario Geological Survey, Report 163, 128p. Accompanied by Maps 2323 and 2324, scale 1:31 680 or 1 inch to ½ mile and 1 chart.

Campbell, G.
1978: Petrography and Stratigraphy of the North Band of Iron Formation, Sherman Mine, Temagami, Ontario; M.Sc. Thesis, Laurentian University, Sudbury, 75p.

Clayton, R.N., and Mayeda, T.K.
1963: The Use of Bromine Pentafluoride in the Extraction of Oxygen from Oxides and Silicates; Geochimica et Cosmochimica Acta, Volume 27, p.43-52.

Crocket, J.H.
1974: Gold; Sections B-O *in*Handbook of Geochemistry, Volume II/4, edited by H. Wedepohl, Springer, Berlin.

Fyon, J.A., Crocket, J.H., and Schwarcz, H.P.
1983: The Carshaw and Malga Iron-formation-hosted Gold Deposits of the Timmins Area; p.98-110 *in* The Geology of Gold in Ontario, edited by A.C. Colvine, Ontario Geological Survey, Miscellaneous Paper 11, 298p.

Goodwin, A.M.
1973: Archean Iron-Formations and Tectonic Basins of the Canadian Shield; Economic Geology, Volume 65, p.915-933.

Gottfried, D., Rowe, J.J., and Tilling, R.I.
1972: Distribution of Gold in Igneous Rocks; United States Geological Survey, Professional Paper 727, 42p.

Jensen, L.S.
1976: A New Cation Plot for Classifying Subalkalic Volcanic Rocks; Ontario Division of Mines, Miscellaneous Paper 66, 22p.

1978: Archean Komatiitic, Tholeiitic, Calc-alkalic and Alkaline Volcanic Sequences in the Kirkland Lake Area; *in*Toronto '78 Field Trip Guidebook, edited by A.L. Currie and W.O. MacKasey, Geological Association of Canada, 361p.

Jolly, W.
1974: Metamorphism in the Canada Shield; Geological Survey of Canada, Paper 78-10, p.63-79.

Knauth, L. and Epstein, S.
1976: Hydrogen and Oxygen Ratios of Nodular and Bedded Cherts; Geochimica et Cosmochimica Acta, Volume 40, p.1095-1108.

Kwong, J., and Crocket, J.H.
1978: Background and Anomalous Gold in Rocks of an Archean Greenstone Assemblage, Kakagi Lake Area, Northwestern Ontario; Economic Geology, Volume 73, p.50-63.

Lovell, H.L.
1972: The Kirkland Lake Area; p.27-57 *in*Precambrian Geology and Mineral Deposits of the Temagami, Cobalt, Kirkland Lake and Timmins Region, Ontario, Guidebook A39, 24th International Geological Congress, Montreal, 96p.

Melnik, V.
1982: Precambrian BIF: Physicochemical Conditions of Formation; Elsevier, Amsterdam, 310p.

Page, C.
1983: The Geology of the Cullaton Lake B-Zone Gold Deposit, Northwest Territories; M.Sc. Thesis, University of Waterloo, Waterloo.

Rees, C.E.
1978: Sulphur Isotope Measurements Using SO_2 and SF_6; Geochemica et Cosmochimica Acta, Volume 42, p.383-389.

Ridler, R.H.
1970: Relationship of Mineralization to Volcanic Stratigraphy in the Kirkland-Larder Lake Area, Ontario; Geological Association of Canada, Volume 21, p.33-42.

1972: Volcanic Stratigraphy of the Kirkland Lake Area; p.33-55 *in* Precambrian Volcanism of the Noranda-Kirkland Lake-Timmins, Michipicoten, and Mamainse Point Areas, Quebec and Ontario; Guidebook A40, 24th International Geological Congress, Montreal, 93p.

Thode, H.G., and Goodwin, A.M.
1983: Further Sulphur and Carbon Isotope Studies of Late Archean Iron-formations of the Canadian Shield and the Rise of Sulfate Reducing Bacteria; Precambriam Research.

Thode, H.G., and Rees, C.E.
1971: Measurements of Sulphur Concentrations and the Isotope Ratios $^{33}S/^{32}S$, $^{34}S/^{32}S$ and $^{36}S/^{32}S$ in Apollo 12 samples; Earth and Planetary Science Letters, Volume 12, p.434-438.

Grant 145 Cross-Hole Magnetometric Resistivity (MMR)

N. Edwards[1], B. Lo[1], S. Cheesman[1], M. Nabighian[2], and G. Oppliger[2]
[1]Department of Physics, University of Toronto
[2]Newmont Exploration Limited, Tucson, Arizona

ABSTRACT

The Magnetometric Resistivity (MMR) method is an electrical method of exploration for conductive, mineralized bodies. The cross-hole variant, introduced by us in 1980, requires 2 boreholes in the vicinity of a target. In the first hole, 2 fixed current electrodes are located, one above the other, and are effectively joined by a single cable carrying the low frequency transmitter current. In the second hole, a sensitive coil measures, as a function of depth, the component of the magnetic field of the transmitted current parallel to the hole. For a uniform earth, if both holes are vertical, the measured magnetic component vanishes. However, the presence of an anomalous conductor locally channels current and causes an 'MMR anomaly', which may be interpreted to indicate the position, orientation, and relative conductance of the conductor. The type of mineralization may be identified by the change in the MMR anomaly with frequency.

The theory of the method is described in detail. The pattern of current flow in the earth from the transmitter and its perturbation by a 3-dimensional structure are shown. The numerical calculations involve a new, integral equation technique for a lamellar body which can be simply programmed and which has applications beyond the MMR method for general resistivity, IP, and VLF interpretation.

Although new equipment has now been constructed for the method, field data are not yet available from Ontario. In their place, a brief case history of a successful experiment in the United States is presented. The principal targets were massive sulphides occurring as fracture fillings, a few metres thick, at depths in excess of 500 m.

INTRODUCTION TO THE MMR METHOD

The MMR method is an electrical prospecting method suitable for mapping lateral changes in earth conductivity to depths of several kilometres. Most geophysicists are familiar with the resistivity method of prospecting. The MMR method differs from it in that the potential electrodes are replaced by a coil. A component of the magnetic field, due to low frequency galvanic current flow in the ground between 2 current electrodes, is measured instead of a component of the electric field. The MMR anomalies are caused by the magnetic field of channelled currents. We have used the method to map regional geology, to explore for geothermal resources, to study hard rock sites for nuclear waste disposal, to map reef structures in sedimentary basins and, most recently, to probe the electrical conductivity of the floor of a shelf sea. The method has been used extensively by a number of companies for base-metal mineral exploration. It offers the advantage that it is not unduly influenced by superficial features and works well in regions of severe terrain or areas covered by conductive overburden.

Historically, the MMR method dates back to a patent by Jakosky (1933), but it met with little success experimentally at that time. In Europe, S.S. Stefanescu and his students undertook a theoretical consideration of the method by calculating the MMR responses of some very simple geologic structures, such as a geological contact.

A viable, experimental method was introduced by Edwards (1974) and Edwards and Howell (1976). They describe suitable apparatus, the field procedures, the factors which influence the location of the current electrodes, the reduction and normalization of the observations, and the definition and interpretation of the 'MMR Anomaly'.

The mathematical and analytic aspects of the method are described in a review paper by Edwards, Lee, and Nabighian (1978). The characteristic anomalies for an anisotropic earth, for vertical and dipping contacts, for thin and thick dikes, and semicylindrical and hemispherical depressions as well as 'alpha' media are described in some detail. Edwards (in press) has extended some of this work to include the effect of a thin conductive overburden.

The MMR anomalies of 2-dimensional structures can be computed numerically. Gomez-Trevino and Edwards (1979) have described an inexpensive, rapid, integral equation technique. A computer programme, MMR2D, based on an algorithm presented by Edwards and Gomez-Trevino (1980) is available to potential users. Pai and Edwards (1983) have published a more flexible finite difference algorithm based on the programs of Dey and Morrison (1976).

Joint work on the MMR method by Newmont Exploration Limited and the University of Toronto began almost ten years ago. The present MMR variant is a cross-hole system for very deep exploration. Its development is not being undertaken in isolation. Much of the equipment and expertise are already at hand, the result of a considerable, steady effort over the years.

THE CROSS-HOLE MMR VARIANT

The interest in a cross-hole MMR system stems from a problem presented to Newmont Exploration Limited, Tucson, Arizona, in the spring of 1980. One of the company's prospects occurs at a depth of about 500 m, and assays in places over 2½% copper. The deposit has been intersected by 1 exploratory hole. Several others were drilled, but missed the deposit. The role of the geophysicist is clear, to find the deposit by making suitable measurements in the drillholes.

The terrain above the prospect is rugged. Further, local gradients of 1:1 over a distance of a few hundred feet are typical. The MMR method had been tried as a surface technique with little success. Electrodes were also lowered into individual boreholes in an attempt to improve the coupling to the buried conductor.

A theoretical study of the problem indicated that the lowering of electrodes in a borehole in the vicinity of the deposit could *not* improve the surface MMR response. On the other hand, the lowering of a magnetic detector could produce significant increases in the observed anomaly. The concept is illustrated in the theory section in this report by a numerical calculation. The geometry of the subsequent field experiment is illustrated in Figure 1, both in plan and section. The results are encouraging and the case history will be discussed later.

Further development of the method requires both theoretical and experimental advances. The theory presented here is brief, and concentrates on explaining the behaviour of current flow in the earth, its perturbation by a conductivity anomaly, and the subsequent MMR anomaly produced. The identification of the intrinsic induced polarization parameters of a body from measurements of the frequency response of the MMR anomaly is also straightforward. Edwards and Nabighian (1981) introduced the concept of a *current channelling number* to explain simply both the MMR and the induced polarization response. This work has been extended and some of the results are described.

New apparatus is being constructed, but at the time of writing of this report the equipment had not been tested in the field. In this progress report, the design criteria for the sensor are given and our signal processing techniques are described.

THEORY

CURRENT FLOW IN A UNIFORM EARTH

The pattern of current flow from a single current electrode located at the surface of a uniform half space representing the earth is easily pictured. The current flow has radial symmetry and the current density decreases with the inverse square power of distance away from the source.

The pattern of current flow from 2 buried electrodes with a finite vertical separation is more difficult to estimate. However, it may be readily calculated as the superposition of radial current flow from the 2 buried electrodes and the 2 Maxwell image sources. These are located to satisfy the boundary conditions at the free surface of the earth, across which no current must flow. The combined current flow retains the axial symmetry of the simple flow from a single source, and by Ampere's Circuital Law, no vertical component of the magnetic field is generated. On the other hand, a vertical magnetic component is generated if this flow is distorted or channelled by a conductor. Generally, the more the conductor 'gathers' the local horizontal current flow, the more enhanced the local vertical

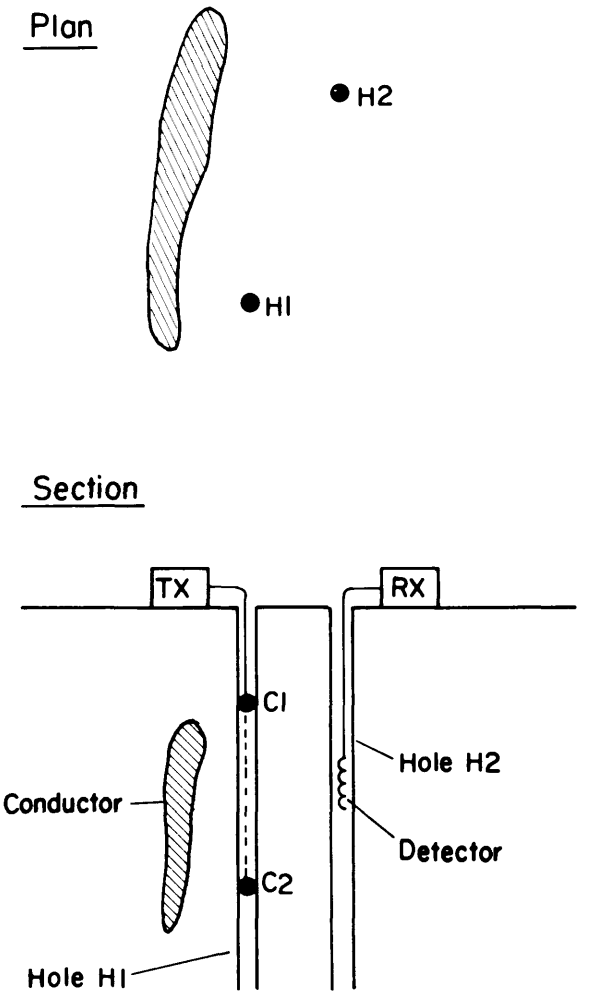

Figure 1. The geometry of the cross-hole MMR method.

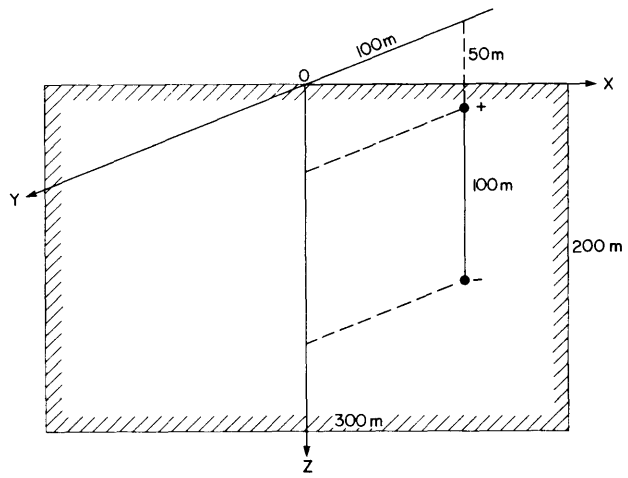

Figure 2. A bipole current transmitter located behind a vertical plane rectangular area within the earth.

magnetic field becomes. Consequently, contour maps of the local horizontal current flow within the earth are essential as a first step in the design of a cross-hole MMR experiment.

Consider the set of coordinate axes shown in Figure 2. The origin O is at the surface of the earth. The z-direction is downward. A 200 m by 300 m section of the x, z plane is shown shaded. A vertical current bipole is located symmetrically behind the shaded area. The coordinates of the positive and negative sources are (0, -100, 50) and (0, -100, 150) respectively.

The y or normal component of the current density over the shaded area is contoured in nAm^{-2}, in Figure 3a. The pattern is characterized by a broad positive region *near the surface* of the earth, and a similar but less intense negative region centred beneath the projection of the negative source. Between these 2 zones lies a region where there is little horizontal current flow. Clearly, the intensity and direction of any horizontal current channelled by a local inhomogeneity, and hence the sign and amplitude of the local vertical magnetic field produced, are strong functions of depth. The geophysicist must generate the set of appropriate maps of this type at the commencement of an MMR cross-hole survey.

THE EFFECT OF CONDUCTIVE OVERBURDEN

A thin conductive layer at the earth's surface reduces the surface horizontal electric field to a very low value. Its effect on the current flow *beneath the layer* may again be calculated simply as the superposition of radial current flow from the 2 down-hole electrodes and 2 Maxwell images. The images are in the same position as those described earlier, but are of opposite sign. The horizontal current flow immediately beneath the conductive surface layer is zero. This is the principal difference between the resulting current density map, Figure 3b, and the corresponding map for a uniform half-space, Figure 3a. The zone of positive current flow is also displaced downward and reduced substantially in intensity. Clearly, the vertical magnetic field generated by a local inhomogeneity is likewise reduced. This overburden shielding effect is not apparent for anomalies which are in electrical contact with the overburden and can gather current directly from it.

THE PERTURBATION OF CURRENT BY A THREE-DIMENSIONAL CONDUCTOR

A conductive deposit within the earth channels an impressed source current and causes anomalous magnetic and electric fields in its vicinity. In order to derive simply the form of the electric and magnetic anomalies, Stefanescu introduced the concept of a current dipole which is a complete, miniature, self-contained current system. It is an infinitesimal version of the bipole current system described previously and used as a transmitter, a short current element linking a point source and a point sink such that the combined current flow is divergence free.

A very common and useful representation of a base-metal mineral deposit is a conductive thin sheet or, more generally a lamella: a warped or folded sheet. The current channelling into, out of, and inside the sheet can be represented by a distribution of current dipoles lying within the sheet. A rectangular lamella may be divided into smaller rectangles. Within each small rectangle, 2 orthogonal dipoles are distributed uniformly. (A resistive lamella, in contrast to a conductive lamella, requires only 1 distributed dipole per rectangle directed normal to the plane of the rectangle).

A set of simultaneous equations for the strengths of the current dipoles are generated by calculating the 2 components of the tangential electric field at the centre of each small rectangle both inside and outside the lamella and equating them, a Maxwell boundary condition. The field outside is a sum over all dipoles, including the transmitter. The field inside is related only to the local dipole and the local lamella conductance which may vary from small rectangle to small rectangle. (The cole-cole parameters for any IP effect of the lamella may also vary from place to place).

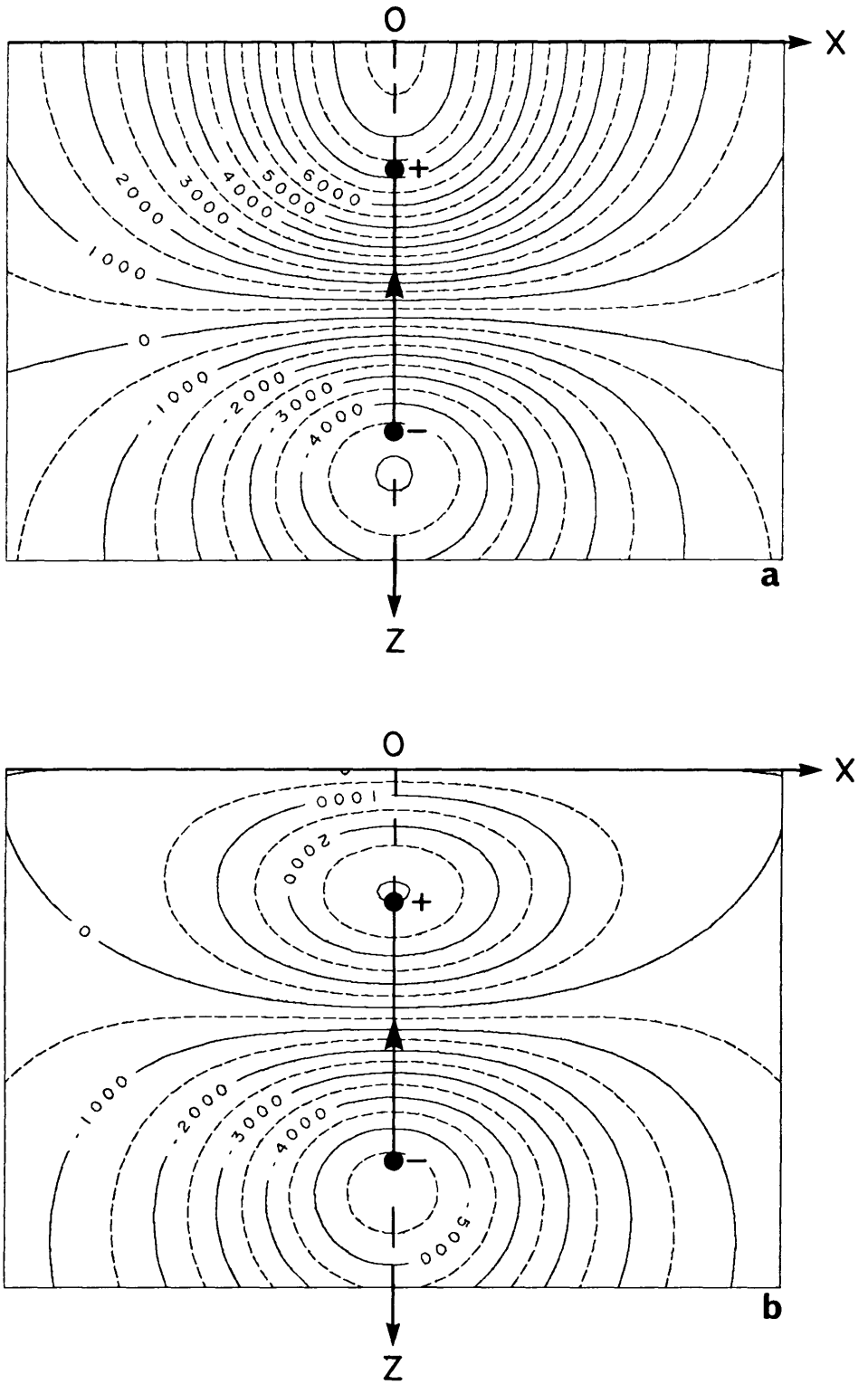

Figure 3. The component of current density crossing the shaded rectangular area of Figure 2 when (a) the upper half-space is very resistive (air), and (b) the upper region is very conductive

THE CURRENT CHANNELLING NUMBER

The ability of an inhomogeneity to channel a regional current flow is a function both of geometry and of the electrical conductivity contrast between the body and its environment. With increasing conductivity contrast, the channelled current at first increases linearly, but ultimately, saturation occurs. For plate structures, one can define a dimensionless channelling number representing the ratio of the effective inverse resistance of the plate to that of the host rock when these 2 elements are seen by the transmitter as resistors in parallel. For a simple, square plate of size L, thickness t, conductance S in a host medium of resistivity ρ, the channelling number α is of the order of ρSL^{-1}. The ratio of the current channelled in the plate to the total current flowing in the vicinity of the plate is of the order of $\alpha/(1+\alpha)$, i.e. the ratio of the inverse resistance of the plate to the total inverse resistance. The validity of this expression, important for 'guessing' the approximate MMR anomaly associated with a given structure, is examined numerically. A more elaborate discussion of channeling numbers is given by Jones (in press).

THE INDUCED POLARIZATION EFFECT

In the mathematical, parametric, macroscopic theory of induced polarization (IP), the electrical resistivity of the earth is not constant but varies with frequency. The simplest description of the intrinsic effect is the polarizability *m* defined as

$$[\rho(f_1) - \rho(f_2)]/\rho(f_1)$$

where the frequencies f_1 and f_2 are 'very low' and 'very high' respectively.

For the cross-hole system, estimates of the IP effect are made as

$$-[B_z(f_1) - B_z(f_2)]/B_z(f_1)$$

where B_z is the anomalous (and total) magnetic z-component. Under field conditions, f_1 may be of the order of 1 Hz and f_2 is an order of magnitude larger.

For a simple plate which has an IP response, we may define an IP effect as the ratio

$$\frac{[B_z(f_1) - B_z(f_2)]/B_z(f_1)}{[S(f_1) - S(f_2)]/S(f_1)}.$$

Now S and B_z are proportional to α and $\alpha/(1+\alpha)$ respectively. Hence, the IP effect reduces simply to $1/(1+\alpha)$. This approximation, too, is important for estimating responses of real structures and its validity is examined.

NUMERICAL RESULTS

A number of points mainly concerned with the physics of cross-hole MMR have been made in the foregoing discussion. These are now illustrated through 3-dimensional numerical modelling. All the models are of plate-like bodies. An in-depth examination of the numerical error inherent in representing a plate by a finite number of current dipoles has not yet been carried out. However, we believe the calculations shown are within 10% of the correct result. The computation of the magnetic field of a given dipole is analytic, and is based on the work described in Edwards (1974).

MOVING SOURCE OR MOVING RECEIVER?

The real benefit of making MMR measurements by *moving* a magnetic field detector in a borehole is the key reason for developing the cross-hole method. Improving the coupling of current sources to a body does improve its detection, but the increase in MMR anomaly produced at a given point is often very small. In contrast, when the detector is moved downwards from the surface towards the body, the anomaly observed can increase by an order of magnitude.

The plate shown in Figure 4 has a channelling number 3.3 and is excited by a single current source located in order at points C1, C2, and C3 respectively. The MMR anomalies in the vertical magnetic field measured along the x-axis and in the nearby vertical borehole are plotted in Figures 5a and 5b.

The anomalies are made dimensionless by expressing them as a percentage of the horizontal magnetic field to be expected at the origin O for this single down-hole source in a uniform half-space. Notice that the variation in anomaly strength with electrode position is at most 2%, even though the proximity of the electrode to the body changes significantly. Clearly, there is no great gain in placing electrodes in boreholes for near-surface exploration. In contrast, the down-hole sensor measures a magnetic field almost twice that of the surface. Obviously, surface source to downhole receiver is a better system than surface receiver to down-hole source. The cross-hole system for deep exploration is a natural development, the advantages of a fixed source, moving receiver system being retained.

THE CROSS-HOLE SYSTEM ANOMALY VARIATION WITH DEPTH

MMR anomalies in the vertical magnetic field are generated by local concentrations of horizontal current flow. The importance of preparing maps of the normal current flow in a half-space for a given survey geometry has al-

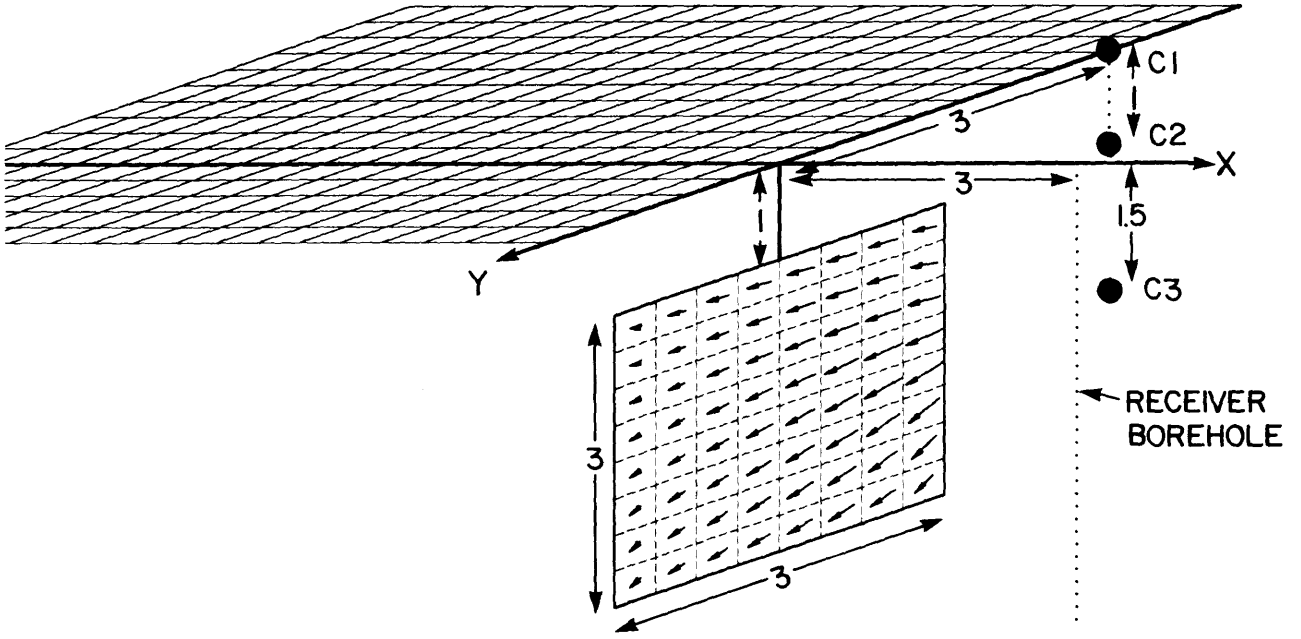

Figure 4. The geometry of a vertical plate located near 3 alternate current electrodes C1, C2, C3 and a receiver borehole. The pattern of current flow in the plate is that excited by electrode C3.

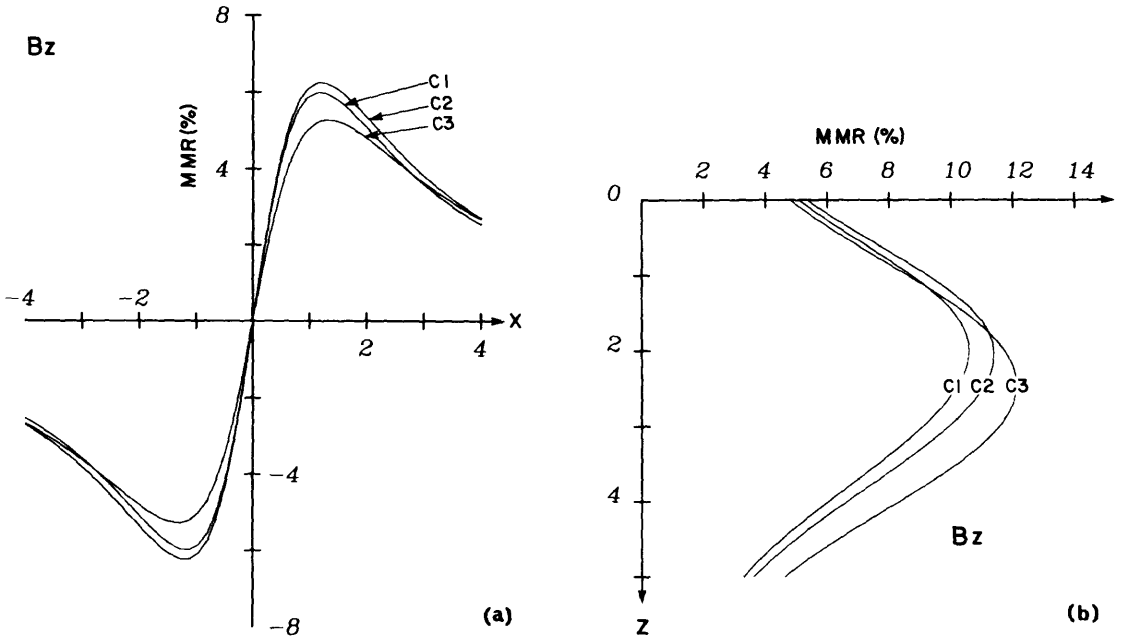

Figure 5. The vertical MMR anomalies in % for the 3 alternate electrode locations shown in Figure 4 measured (a) along the x-axis, and (b) in the nearby borehole shown.

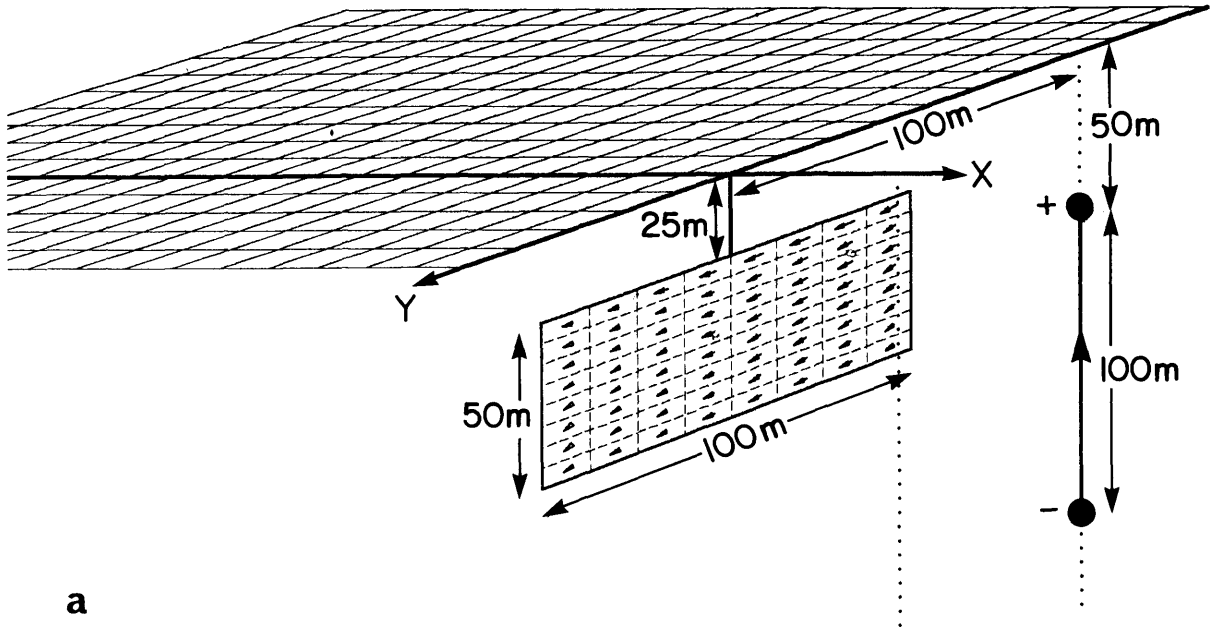

Figure 6a. The pattern of current flow in a vertical plate excited by a single vertical bipole transmitter when the plate is shallow and influenced mainly by the upper positive electrode.

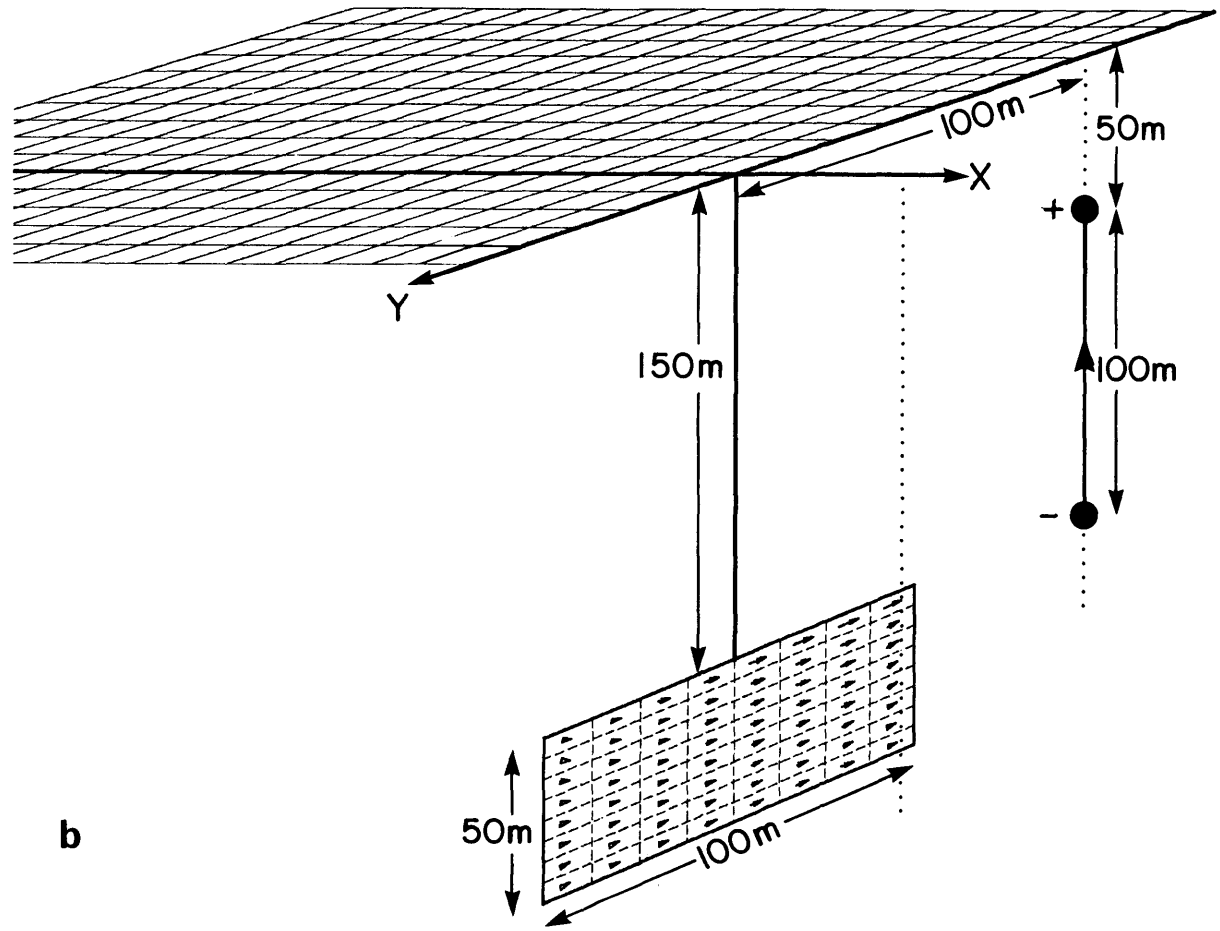

Figure 6b. The pattern of current flow in a vertical plate excited by a single vertical bipole transmitter when the plate is deep and influenced mainly by the lower negative electrode.

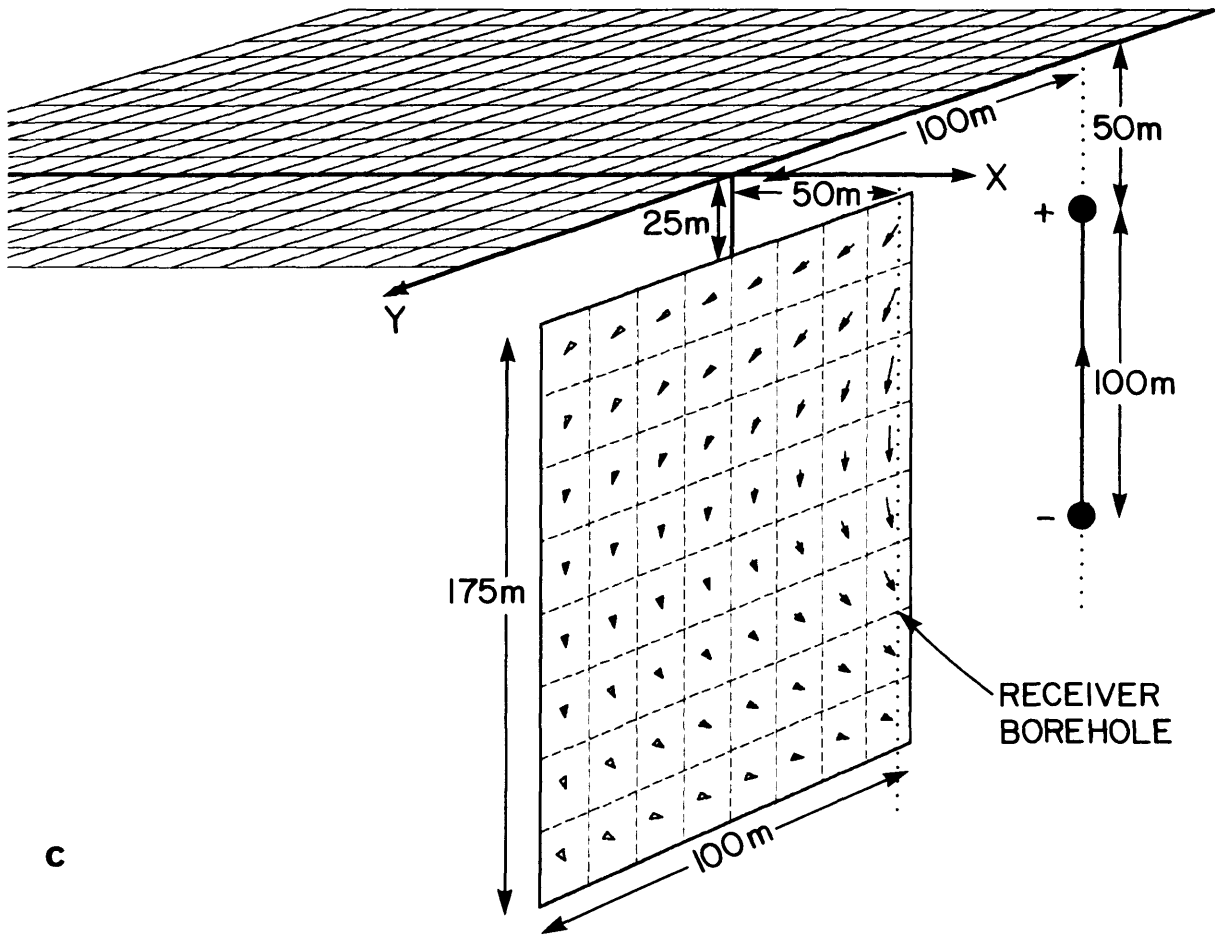

Figure 6c. The pattern of current flow in a vertical plate excited by a single vertical bipole transmitter when the plate is relatively large and influenced by both electrodes.

ready been emphasized, because the intensity and direction of the horizontal current flow are strong functions of depth. The resulting effect of depth on, in particular, the sign and the extrema of the MMR anomaly can now be illustrated numerically.

Figures 6a, 6b, and 6c show a series of plates excited by a bipole transmitter located relative to a set axes as shown previously in Figure 2. The small plate near the surface, Figure 6a, lies within the outward zone of horizontal current flow from the positive electrode (*see* Figure 3c). The vertical MMR anomaly (not shown) in the nearby borehole peaks over the centre of the plate and is negative. The small plate at depth, Figure 6b, lies within the return zone of horizontal current flow toward the negative electrode. The anomaly (not shown) peaks over the centre of the plate and is positive. The large plate, Figure 6c, lies within the influence of all the current flow. The MMR anomalies, shown in Figure 7 for a range of channelling numbers, are characterized by a cross-over over the centre of the plate and are both positive and negative. Interpreter beware!

THE CHANNELLING NUMBER, ESTIMATING MMR AND IP RESPONSES

The magnitude of the borehole anomalies plotted in Figure 7 clearly increase with increasing channelling number. They do not increase indefinitely. Eventually, at large numbers, saturation occurs and the anomaly of a perfect conductor is obtained. If the anomalies at finite response are normalized by the perfect conductor values, the ratio obtained is that shown as the solid curve in Figure 8a. It is almost independent of depth. It is very similar in shape to the function $\alpha/(1+\alpha)$, the 'guess', shown as a dashed line.

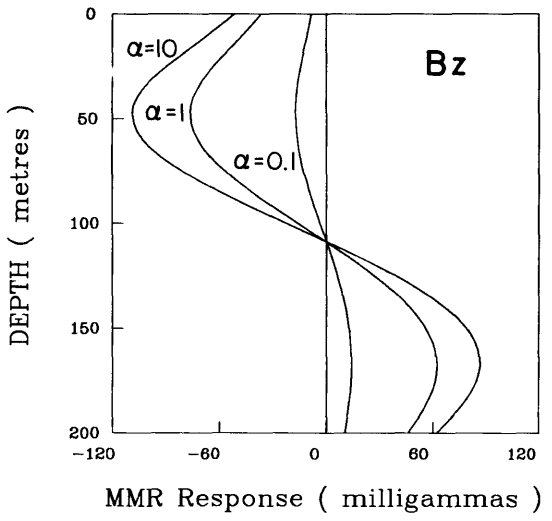

Figure 7. The vertical magnetic field measured in the borehole shown in Figure 6c for a range of plate channelling numbers.

This is a most important result. Often, the MMR response of a very good conductor can be simply estimated analytically. If the dominant response number involved can also be obtained, then a whole suite of type curves may be sketched.

The 'guessed' IP effect, as defined previously, varies as $1/(1+\alpha)$, the dashed curve in Figure 8b. The IP effect is small at large channelling numbers where a large change in plate conductance produces little change in the MMR anomaly but increases to a value of unity, by definition, at small channelling numbers where the anomaly is proportional to the conductance. The solid curve is the curve of the IP effect of the large plate shown in Figure 6c. Again, the 2 curves are very similar in form. The basic physical behaviour is predictable, with obvious consequences for the interpreter. At low response numbers, the polarizability measured in the field actually equals the intrinsic polarizability of the rock. The IP response is also independent of depth. For simple structures, containing only 1 polarizable target, measurements of the IP response magnetically are required only at 1 field point. The latter theorems, although tested here only for a simple plate, appear to be generally valid for all simple models in a uniform, layered earth.

A BRIEF CASE HISTORY

GEOLOGICAL ENVIRONMENT

The country rock in the vicinity of the Newmont prospect consists of an altered, fractured granodiorite with associated dacite porphyry plugs. Sulphide mineralizaton is present in both disseminated and massive forms, the latter occurring occasionally as fracture fillings a few metres thick. The massive sulphide bodies, which have an electrical conductivity many times that of the country rock, are the principal targets. Any interpretation is likely to be confused by barren fracture zones and highly altered material which act as moderately conductive current channels.

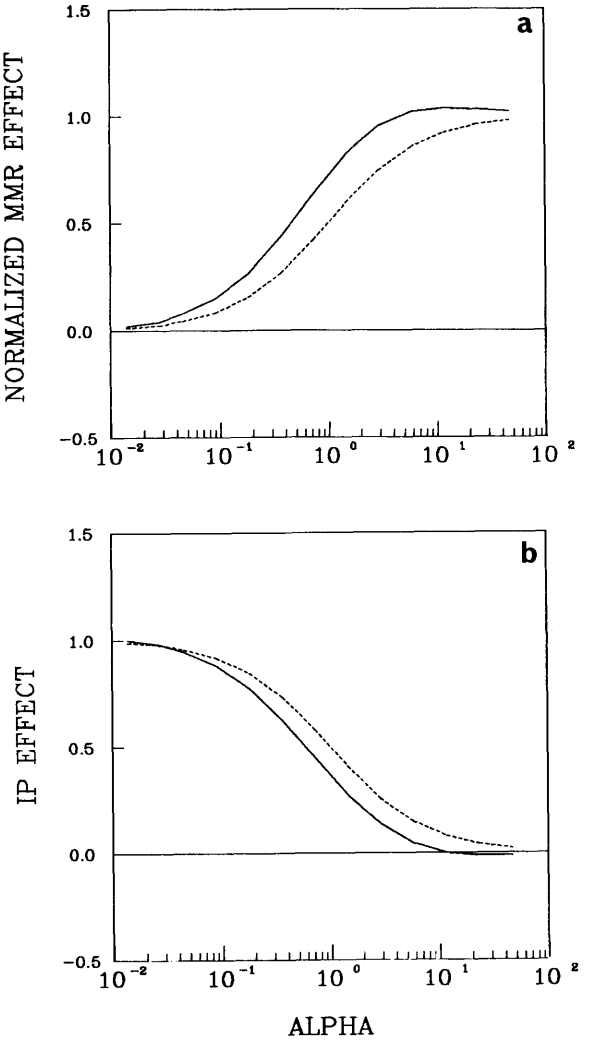

Figure 8. (a) The behaviour of the vertical borehole magnetic field (solid line) with increasing channelling number compared with a simple theoretical function (dashed line); (b) the behaviour of the vertical borehole magnetic IP effect (solid line) with increasing channelling number compared with a simple theoretical function (dashed line).

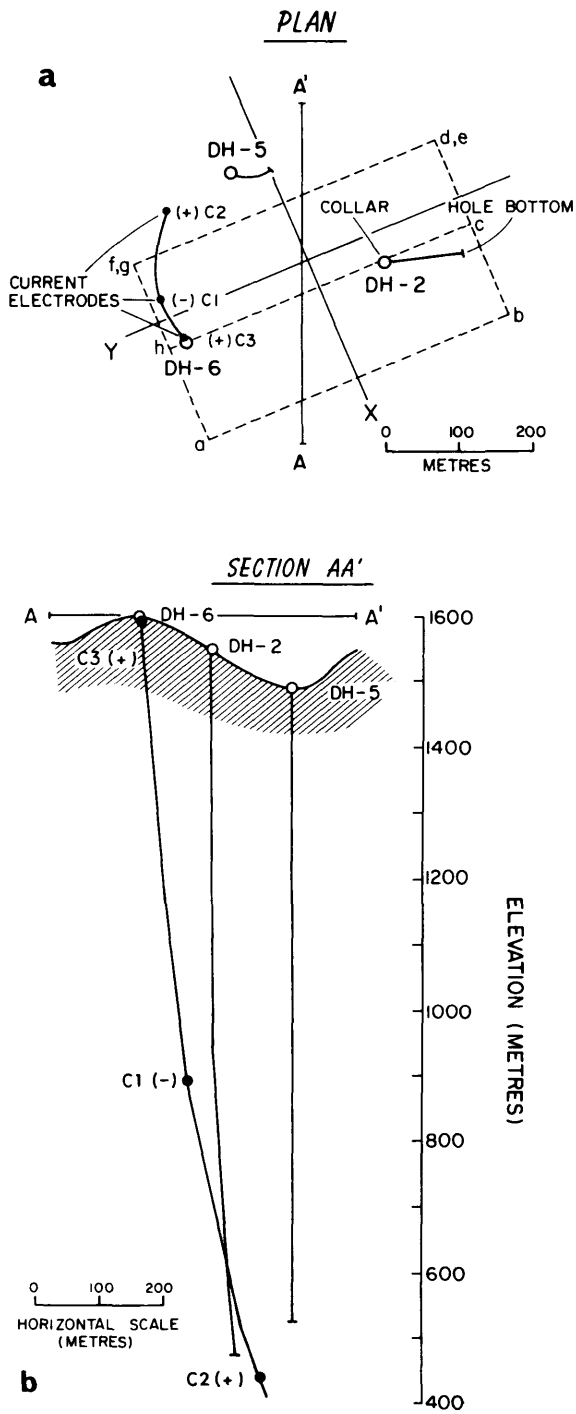

Figure 9. The 'Newmont' Prospect shown (a) in plan, and (b) in section.

DRILLING RESULTS

Three holes drilled in the vicinity of the prospect are shown in plan and section in Figures 9a and 9b respectively. Hole DH-6 intersected sulphide, assaying at up to 2½% copper, between markers C1 and C2. Hole DH-2 intersects sulphide between the 1300 and 1400 m levels. Hole DH-5 is barren.

METHOD

The objective of the MMR survey is to trace the possible extension of the mineral deposit intersected at depth in DH-6.

The cross-hole method was employed. Axial magnetic fields due to bipole transmitters between C3, C1 and C2, C1 were measured down-hole in DH-2 and DH-5 respectively. The current injected was approximately 2 amperes, the frequency 3Hz.

DATA

The data are presented as down-hole profiles in Figures 10a, 10b, and 10c respectively. On each figure, there are 3 graphs. The first shows the measurements actually made. The second is the non-zero field generated by the inclined bipole. The third is the difference or anomalous field, resolved into the vertical direction for interpretation purposes.

MODEL FITTING

The data are fitted very well by a bent plate model of varying conductance. The model generates all the character

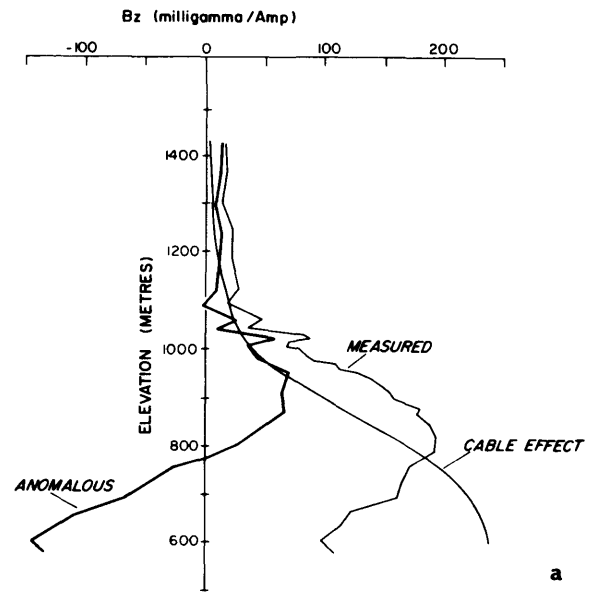

Figure 10a. The vertical magnetic fields in borehole DH-2, transmitter bipole C1, C3.

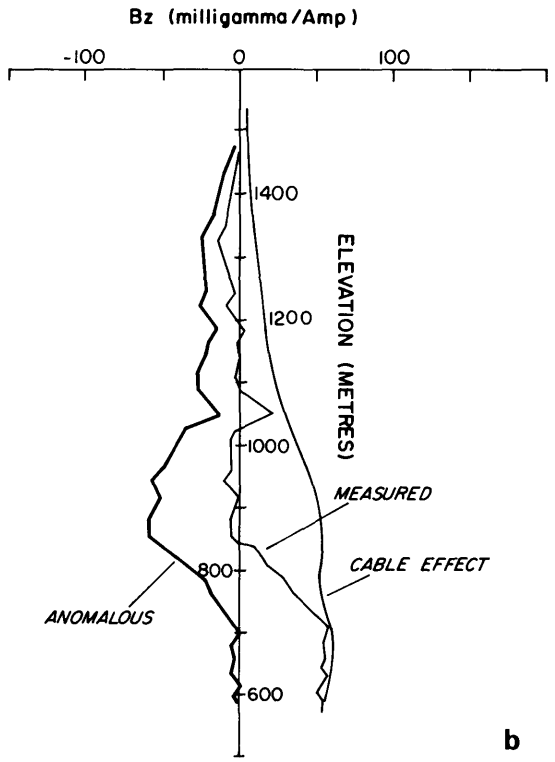

Figure 10b. The vertical magnetic fields in borehole DH-2, transmitter bipole C1, C2.

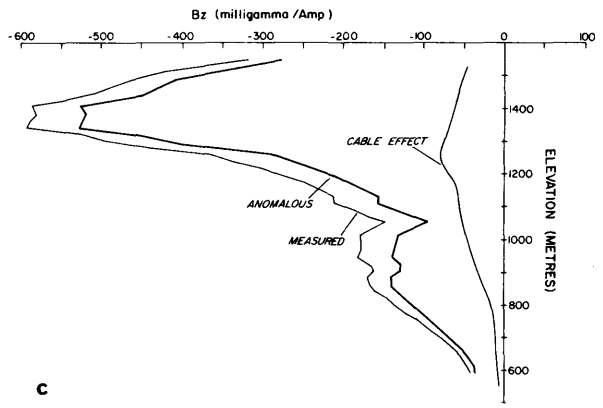

Figure 10c. The vertical magnetic fields in borehole DH-5, transmitter bipole C1, C2.

of the data: sign, locations of extrema, and cross-overs. Model amplitudes match the smoothed data on any one profile to better than 5% of the peak anomaly on the profile.

A plan view of the plate is shown as the dashed outline in Figure 9a. The plate is folded along lines parallel to the y-axis. The plate intersects DH-2 and DH-6 at levels where sulphide has been identified. The curvature of the plate and its relationship to the drillholes is evident in the x-axis section sketched in Figure 12.

The conductance of the plate is listed in Table 1 in terms of the channelling numbers of the individual rectangles forming it. Codes 1, 2, 3, represent the ρSL^{-1} values

TABLE 1 THE CONDUCTANCE OF THE PLATE MODEL EXPRESSED IN TERMS OF THE RESPONSE NUMBER α.

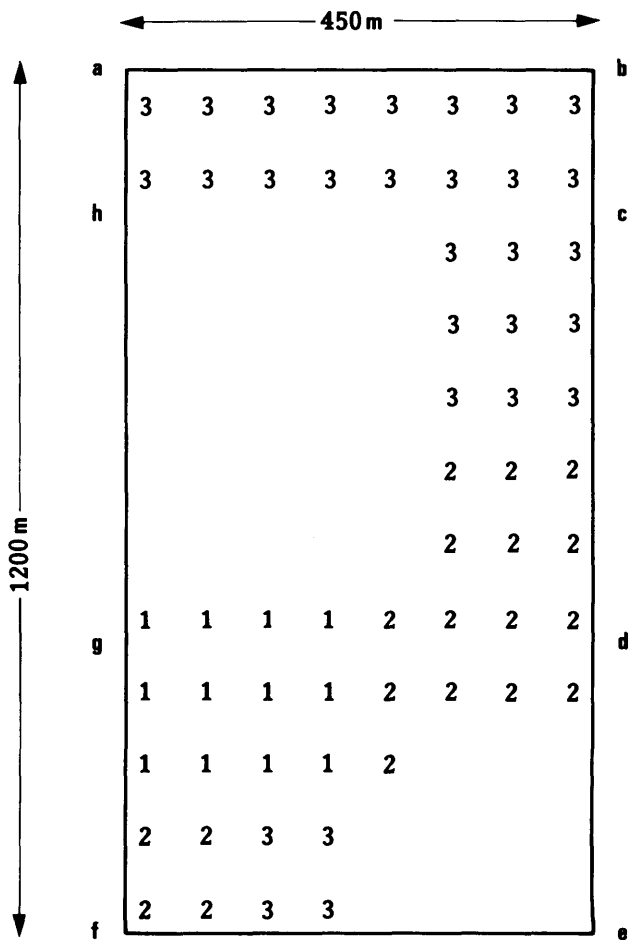

CODE	1	2	3
α	.15	.3	10.

.15, .3, and 10, where L, here, is the length of the longer of the 2 sides of the plate. The electrical current flow in the model is shown in Figures 11a and 11b for bipole transmitter C1, C3 and C1, C2. Clearly, there are several zones of anomalous conductance excited by cross-hole systems. The very large conductances could be interpreted as mapping the extent of massive sulphide. Other identifiable zones within the plate are not as conductive, and may be merely expressions of a barren fracture. The model is certainly not unique but it does provide the geologist with enough guidance as to the location of the deep conductive zone to stimulate further drilling. To this extent, the interpretation is adequate.

INSTRUMENTATION

The prototype field instrumentation used to collect the data for the case history was developed by Newmont Exploration Limited. It consists of:

1. An Elliot 4 km I.P. transmitter, modified to output a constant current 3 Hz bipolar squarewave. Power is provided by a gasoline motor-generator. Typical currents delivered to the electrodes are on the order of 2 amperes.
2. A radio transmitter connected to the current transmitter to send current polarity information to the MMR receiver.
3. A down-hole MMR sensor composed of a ferrite core coil tuned to 3 Hz, and a voltage-to-frequency converter which is used to provide interference-free transmission of the measured signal up a 2-wire cable to a frequency-to-voltage converter at the surface. The coil axis is of necessity oriented along the direction of the drillhole.
4. The MMR receiver, which is basically a phase-locked integrator which digitally displays the measured signal amplitude every 32 cycles. Synchronization with the transmitter is maintained through a radio link. Measurements are made only while the down-hole sensor is stationary.

The instrumentation presently being completed at the University of Toronto has many of the same specifications. Major differences include:

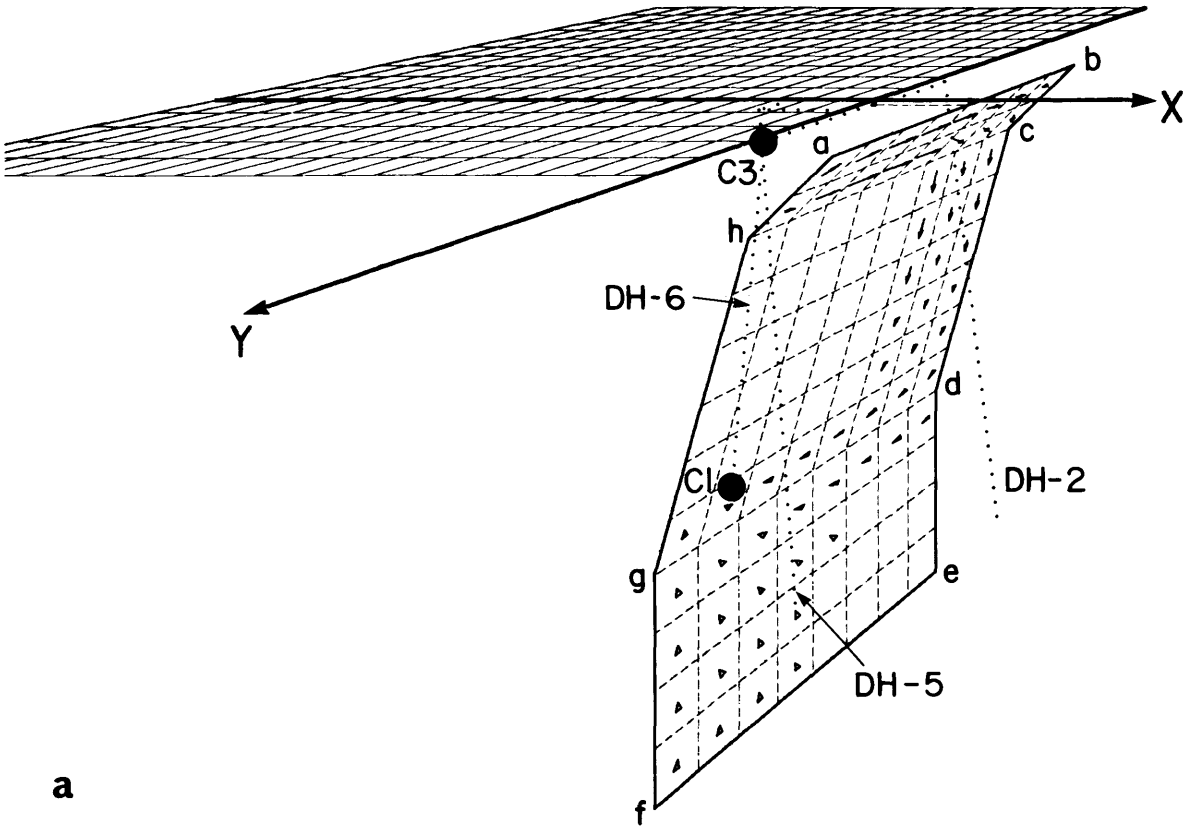

Figure 11. The current flow in the interpreted plate model for: (a) current bipole C1, C3, and (b) (following page) current bipole C1, C2.

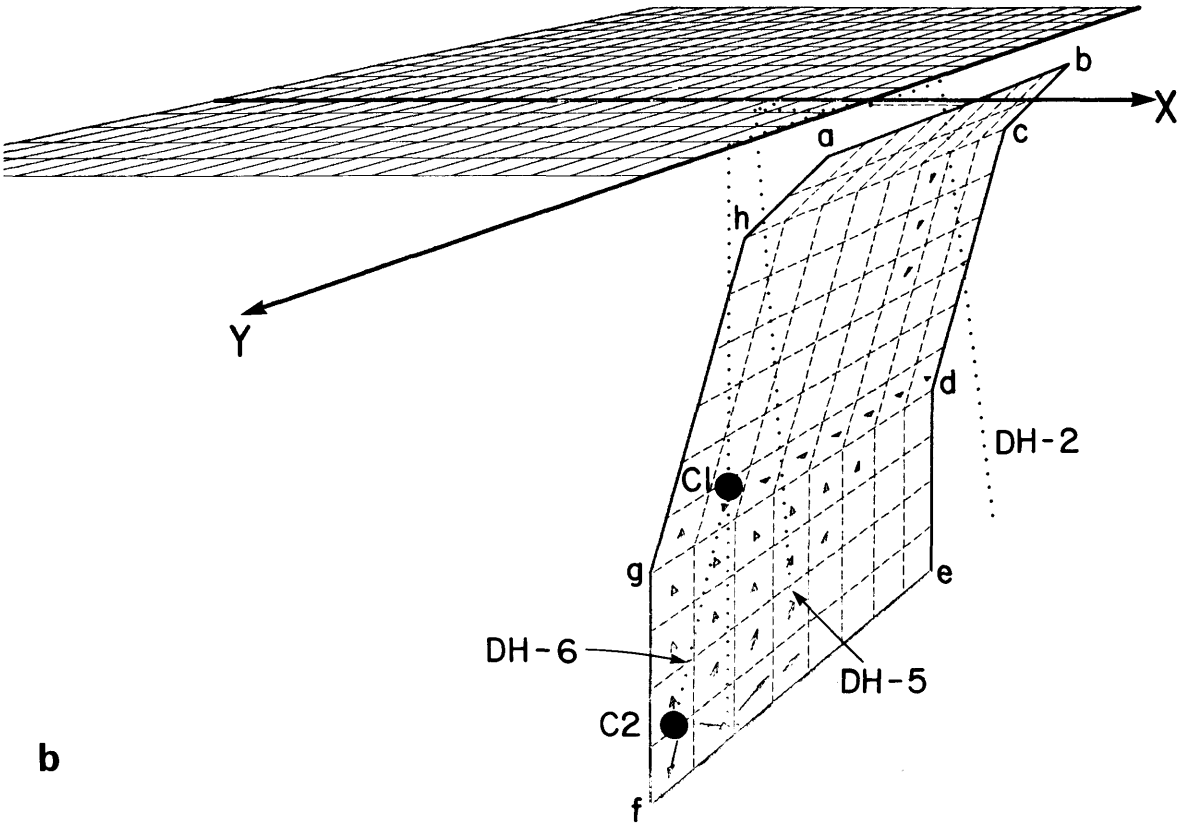

b

1. The use of 2 separate matched crystals to provide the required synchronization of transmitter and receiver.
2. The use of our own digital receiver and/or a DATA6000 processor for recovering weak signals in the presence of noise.

CONCLUDING REMARKS

Many of the original objectives of Ontario Geoscience Research Grant 145 have already been achieved, including the acquistion and/or design of a down-hole sensor with associated winch and cable, and the development of software for experimental design and interpretation. The project will be completed by collecting field data within Ontario. These will be interpreted, and some of the results should be available by the end of the 1983 calendar year.

REFERENCES

Dey, A., and Morrison, H.F.
1976: Resistivity Modelling for Arbitrarily Shaped Two Dimensional Structures, Parts I and II; Lawrence Berkeley Laboratory, Reports 5223 and 5283, NTIS, Springfield, Va.

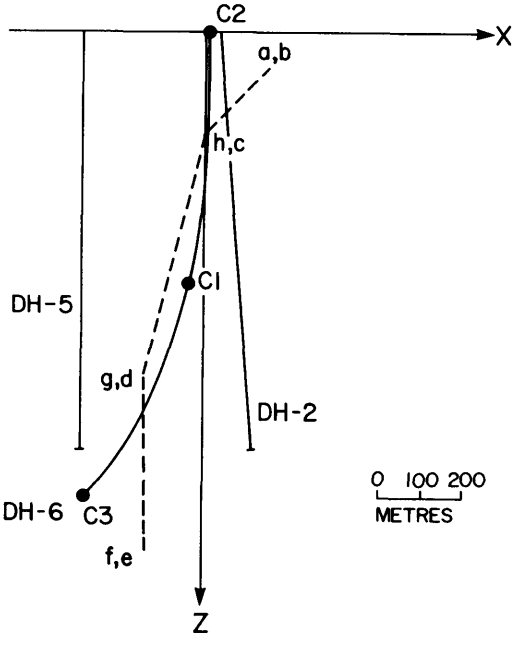

Figure 12. A section through the 'Newmont' Prospect showing the curvature and location of the interpreted plate model.

Edwards, R.N.
1974: The Magnetometric Resistivity (MMR) Method and Its Application to the Mapping of a Fault; Canadian Journal of Earth Sciences, Volume 11, p.1136-1156.

in press: An Approximate Model of the Magnetometric Resistivity (MMR) and Magnetic Induced Polarization (MIP) Responses of Dipping Dikes Beneath a Conductive Overburden; Bulletin of the Australian Society of Exploration Geophysicists.

Edwards, R.N., and Gomez-Trevino, E.
1980: MMR2D - A Programme for the Computation of Magnetometric Resistivity (MMR) Anomalies of Two-Dimensional Structures; Report available from Macquarie University, School of Earth Sciences, North Ryde, Australia.

Edwards, R.N., and Howell, E.C.
1976: A Field Test of the Magnetometric Resistivity (MMR) Method; Geophysics, Volume 41, p.1170-1183.

Edwards, R.N., and Nabighian, M.N.
1981: Extensions of the Magnetometric Resistivity (MMR) Method; Geophysics, Volume 46, p.459.

Edwards, R.N., Lee, H., and Nabighian, M.N.
1978: On the Theory of Magnetometric Resistivity (MMR) Methods; Geophysics, Volume 43, p.1176-1203.

Gomez-Trevino, E., and Edwards, R.N.
1979: Magnetometric Resistivity (MMR) Anomalies of Two-Dimensional Structures; Geophysics, Volume 41, p.947-958.

Jakosky, J.J.
1933: Method and Apparatus for Determining Underground Structure; U.S. Patent #1906271.

Jones, A.G.
in press: The Problem of Current Channelling; A Critical Review; Geophysical Surveys.

Pai, D., and Edwards, R.N.
1983: Programme MMR2DFD: Finite Difference Modelling of MMR Anomalies; Reports in Applied Geophysics Number 25, University of Toronto, Department of Geophysics.

Grant 136 Rock Geochemistry as a Placer Exploration Tool in the Southeastern District of Algoma

Philip W. Fralick[1], A.D. Miall[2], and Abdel-Rahman[2]
[1]Department of Geology, Lakehead University
[2]Department of Geology, University of Toronto

ABSTRACT

Even though placer deposits contribute substantially to the world's metal resources, exploration techniques aimed at predicting hidden placer occurrences are not well developed. In this study the authors examined mineral zonation surrounding the uraniferous conglomerates in the Matinenda Formation at Elliot Lake, Ontario, in an attempt to develop a whole-rock geochemical placer exploration technique. Mineral zonation, reflected by geochemical variation, occurs on 2 levels. Locally, uraninite (specific gravity 9) is concentrated in the highest energy portions of a stream system in well-packed cobble and pebble conglomerates. Rutile-brannerite, monazite (s.g. 5.2), and zircon (s.g. 4.5) progressively dominate the heavy mineral assemblage as the water velocity depositing the sediment decreases. This produces localized mineral variation which may be used to predict areas of economic importance in a zone of placer enrichment. On a regional scale, heavy minerals are depleted in the sediment-water mass away from the stream's entry point(s) into the basin. This leads to a widespread and rapid decrease of elements associated with heavy minerals down the paleoslope away from possible placer deposits. Trends reflecting regional zonation thus may be used to identify areas favourable to placer development.

INTRODUCTION

The mineralogy of a siliciclastic sedimentary deposit is controlled by a number of factors: the mineralogy of the source area; chemical and physical alteration of the sediment during transport; hydraulic sorting at the depositional site; diagenesis and metamorphism. The combined effect of these variables makes every sedimentary deposit unique to some degree. During placer formation, the main factors are the presence of economic minerals in the source area and hydraulic sorting at the depositional site. Hydraulic sorting depends on the size, shape, and specific gravity of the sediment particles; the velocity, depth, density, and viscosity of the transporting fluid; and the stream bed roughness. In any system undergoing deposition, these variables change both spatially and temporally. Systematic change in flow variables causes the mineral assemblages being deposited also to change systematically. Thus placer deposits should not be isolated mineralogic entities. Rather they should be surrounded by detrital assemblages which reflect a progressive trend in depositional processes towards those that favour placer formation.

Placer development is also dependent on the availability of economic minerals travelling in the water-sediment mass. As the heavy mineral load is preferentially depleted in the alluvium down-paleoslope, less of these minerals become available for concentration in suitable sites.

Two types of heavy mineral zonation should occur. The first type is on a local scale, where changes in mineralogy reflect lateral and vertical changes in lithofacies. The second type is on a regional scale, where the heaviest constituents of the sediment load are concentrated source-proximal and their content in the sediment gradually decreases down paleoslope (Smith and Minter 1979). Both types of systematic mineralogical zonation can be used to predict occurrences of economic placer deposits once the nature of the variations is understood.

In this study mineralogical zonation was investigated in the large, uraniferous placers of the early Proterozoic Matinenda Formation of the Elliot Lake area, Ontario (Figure 1). Debate has centred on the origin of these deposits. However, Robertson (1962), Roscoe (1969), Theis (1979), and Robinson (1982) have clearly shown that mineralization was syndepositional in origin. The uranium is believed to have been concentrated in gravel and cobble sheets in the lower and middle portions of the Matinenda Formation. Coarse grained sandstone occurs as lenses within the gravel sheets, and as beds separating the gravel sheets. Sandstone also makes up the formation above and below the gravel sheets. The depositional environment appears to reflect a broad area where unchannelized, sheet-flood deposition dominated. With time, and a decrease in slope caused by marine flooding in the south, lower energy, more highly channelized deposits formed, though a fairly high width-to-depth ratio probably still dominated the stream system. The highest Matinenda sandstones represent glacial erosion of unconsolidated Matinenda material from the north, and redeposition of this material in the Huronian Basin by glacial outwash processes.

Mineralogical zonation within the Matinenda Formation was investigated using geochemical instead of point-counting techniques. The advantages of geochemistry over point-counting are:

1. large numbers of grains per sample are analyzed (in this study approximately 15 000 per sample)
2. fine grain sizes are included in the identifications
3. mineral inclusions are taken into account
4. if the chemical system is closed, alteration of minerals is not a problem
5. mineral misidentification is not a part of the process.

The obvious drawback with geochemistry is that a particular element will occur in more than 1 mineral. Thus, to define the mineral assemblage of a sample from geochemistry, the common minerals in the rock must be known.

GEOCHEMICAL TRENDS

MINERALOGY

The mineralogy of the Matinenda sandstones and conglomerates reflects the granite-"greenstone" source terrain from which they were derived. The conglomerates consist essentially of quartz and chert pebbles in a matrix of sericitic, feldspathic quartzite that contains grains of pyrite, titanium minerals, monazite, and zircon. The radioactive mineral suite includes uraninite, brannerite, thucolite, uranothorite, uranothorianite, coffinite, allanite, xenotime, and gummite (Roscoe 1969). By far the most important uranium-bearing minerals are uraninite and brannerite. The Matinenda sandstones contain a mineral suite similar to that of the conglomerates, though with a very much reduced proportion of heavy minerals (Table 1).

The Lower Huronian strata have undergone a limited amount of post-depositional alteration. The most pronounced change is the transformation of microcline to sericite (Robinson 1982). This has resulted in a net loss of potassium, which was presumably carried out of the system in pore-water. Other diagenetic alteration effects discussed by Robinson (1982) concern the accessory mineral assemblage typical of the ore conglomerates. He found: (1) uraninite is sometimes replaced by coffinite and quartz, liberating U and Th; (2) uraninite is also occasionally altered to a phosphate containing Y, as well as some U and REEs; (3) the U and Th liberated into the pore-water by the alteration of uraninite caused some of the monazite to be replaced by uranothorite; and (4) U in the pore-water reacted with rutile remnants of detrital magnetite-ilmenite grains to form brannerite. These alteration effects probably did not result in any marked depletion of the elements involved from the system. Rather, simple exchange seems to have taken place.

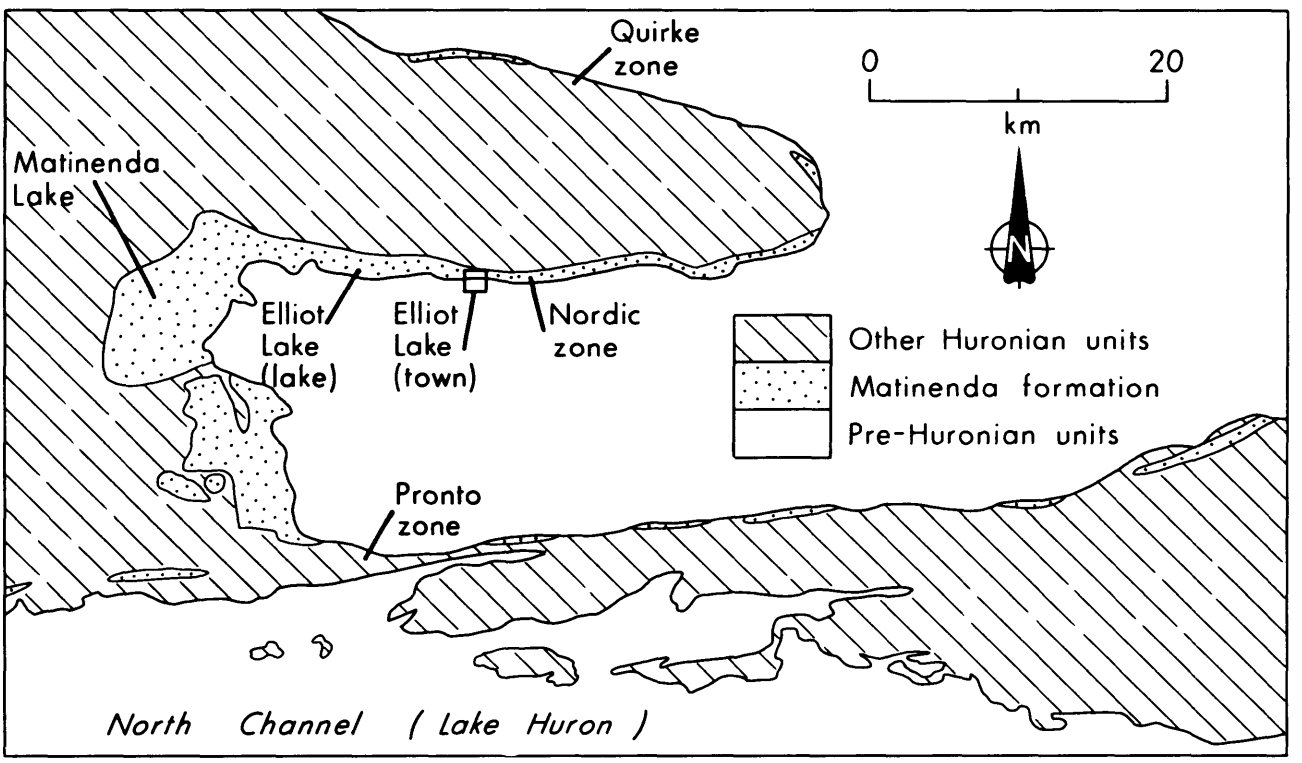

Figure 1. Area covered in this study.

TABLE 1 MINERAL ABUNDANCES IN THE LOWER HURONIAN SUPERGROUP. DATA FROM PARVIANINEN (1973).

MAJOR MINERALS

wt. %	Matinenda Formation			Ramsay Lake Formation
	Mineralized Conglomerate	Middle	Upper	Upper
quartz	26.7	51.1	59.0	44.6
orthoclase	.8	4.4	5.4	2.5
microcline	5.8	8.6	7.1	4.0
plagioclase	.7	.3	1.1	1.0
carbonate	1.8	.7	-	.1
fine material	5.6	18.7	13.6	14.4
chlorite	.1	-	1.0	5.5
muscovite/sc.	1.4	1.1	1.6	2.2
biotite	-	.1	.7	2.0
pyrite	16.6	1.6	1.3	1.7
accessories	6.9	1.6	2.6	2.0
igenous intrusive	32.4	9.3	5.5	13.6
igneous extrusive	1.4	1.1	.5	4.2
metamorphic	-	.9	.3	1.5
sedimentary	-	-	.9	.4

HEAVY MINERALS

cumulative weight % from mineral separates	Matinenda Formation			Ramsay Lake Formation
	Mineralized Conglomerate	Middle	Upper	Upper
pyr./pyrrh.	72.3	22.0	18.3	24.5
ilmenite	1.4	14.4	9.3	18.7
leucoxene	16.5	40.2	29.6	35.2
other opq.	2.3	4.2	1.2	4.8
biotite	.9	4.2	3.7	.9
chlorite	3.7	4.8	20.6	8.1
penninite	.2	.5	12.7	-
hyncinth	.5	4.0	2.6	4.3
malachon	.2	.3	.6	.3
tourmaline	-	.2	-	.9
rutile	.3	2.1	-	-
apatite	.8	.5	.9	2.1
hornblende	.8	-	-	-
trem./act.	-	2.1	-	-
garnet	-	.2	-	-
epid./grb.	-	.2	.5	-

In addition to the alteration effects, there also is the possibility that a large amount of the pyrite is secondary (Robinson 1982). Roscoe (1969) and Theis (1979) considered most of the pyrite to be primary. However, Robinson (1982) considered most of the pyrite to have been introduced post-depositionally, possibly replacing a primary heavy mineral. The abundance of pyrite in ripple laminae (Figures 2 and 3), in agreement with the observed hydrodynamic behaviour of heavy minerals (McQuivey and Keefer 1969), and its increased concentration in areas favourable to heavy mineral deposition (Figure 4), weigh in favour of much of the pyrite occurring as detrital grains or replacements of detrital grains. The pyrite is treated as a syndepositional constituent in the remaining sections of this report.

LOCALIZED MINERAL ZONATION

Systematic variation in mineralogy on a local scale probably reflects the hydraulics of the depositional environment rather than changes in the availability of minerals for sedimentation (Smith and Minter 1979). That is, the flow velocity and turbulence probably governed which minerals were deposited from the sediment-water mass, and thus variations in velocity and turbulence are believed to have caused localized mineralogical changes. Roscoe (1969) referred to this process to explain the mineral zonation of the ore conglomerates when he stated: "The bulk of the uraninite grains, which were .05 to .20 mm in diameter, were entrapped in this part (upstream end) of the deposit, whereas the bulk of other, more abundant, lighter types of heavy minerals were carried farther downstream." Robertson (1962) and Theis (1979) also noted a down-paleoslope zonation of minerals in extensive ore conglomerates. They found that zircon, monazite, and rutile-brannerite aggregates are more abundant in the finer grained conglomerates to the south (down-paleoslope) of the uraninite-rich ore zones. It can be inferred that, in the higher-velocity upstream areas, quartz-cobble-conglomerate-uraninite deposits formed and, as velocity decreased downstream, the lighter heavy minerals began to dominate the deposits.

R-mode factor analysis was employed in this study to investigate the existence of the mineral zonation described above. Factor analysis is a data reduction technique which is employed to define underlying factors controlling the variance in a data set. The conglomerates proved to be very strongly zoned in the manner described by Roscoe (1969). The uraninite zone forms the most distinct entity while the monazite, zircon, and rutile zones overlap each other. It was also discovered that the sandstones throughout the study area show a similar zonation.

Rare earth element patterns for typical Matinenda sandstones and conglomerates provide another means

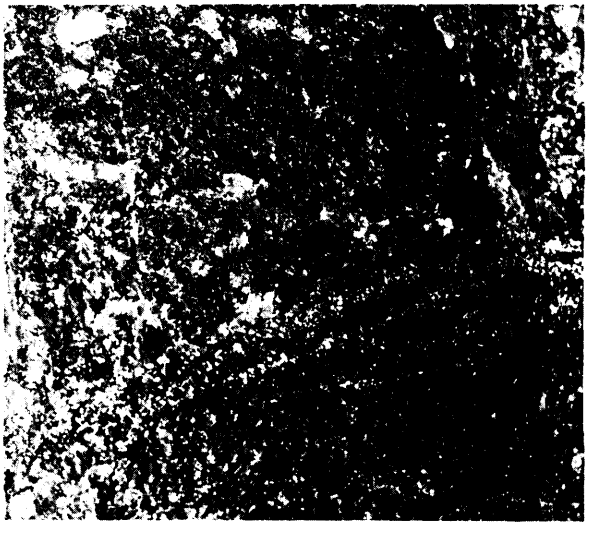

Figure 2. Pyrite accentuating ripple lamination in a small sandy area of a uraniferous ore reef (actual size).

of studying mineralogical variation. Figure 5 shows how the rare earth element (REE) values are elevated as the ore zone is approached. This is to be expected as monazite, the main REE-bearing mineral, increases markedly in abundance proximal to the ore zones. The most interesting feature of the REE trend is the gradational nature of the increase. Samples of sandstone not in the immediate proximity of the ore zone, i.e. within a few metres, have background values; sandstones intimately associated with the ore zone have intermediate values; and the ore conglomerate itself has extremely elevated values. The systematic rise in REE concentrations reflects a gradational increase in monazite deposited by the fluvial system as the ore reefs began to form.

This type of extremely localized zonation is, of course, of very little use when designing a regional exploration program. However, the existence of mineralogical variation controlled by local hydraulic conditions in the transport-depositional system must be kept in mind and may be used to advantage when conducting regional exploration.

Figure 3. Print obtained from a thin-section showing heavy mineral ripple laminae accentuated by opaque pyrite grains (photo 2.5 cm across).

VERTICAL MINERAL VARIATION

Samples of coarse grained Matinenda sandstone were collected throughout the stratigraphic column at a number of locations in the eastern District of Algoma. This sampling was conducted to examine the regional variation both laterally and vertically. Samples collected, analyzed, and plotted for individual stratigraphic sections not containing uraniferous conglomerates exhibited very little variation throughout their thickness. Obviously, fairly constant depositional environments lead to little variation in the mineralogy of the sediment deposited.

Figure 4. Print obtained from a thin-section. Notice the high concentration of pyrite associated with the quartz-pebble conglomerate as opposed to the relatively low pyrite concentration in the overlying coarse sandstone.

Contrasting with the above are a group of samples collected at intervals throughout the entire Lower Huronian Supergroup near the Quirke ore zone (Figure 6). Matinenda sandstones below the area containing ore conglomerates (missing section) show an increase in U, Th, and Zr up-section. This occurs in conjunction with an increase in grain size with stratigraphic height, reflecting higher energy conditions. Sandstones above the ore zone continue the upward trend towards higher U, Th, and Zr values. The reason for the increase is unknown, as the grain size remains relatively constant. The transition to Ramsay Lake Formation of possible glacial origin occurs immediately after the fourth sample above the main ore zone. This section of the column represents the glacially resedimented upper Matinenda Formation. The large increase in U content occurring here is probably caused by incorporation of material from glacially scoured ore zones up paleoslope and proximal resedimentation of that material during ablation. Uranium and thorium in the overlying marine/lacustrine Pecors Formation were probably concentrated by geochemical processes rather than as detrital grains (Roscoe 1969). The coarsening-upward trend in the lower Mississagi Formation (top unit in the column) controls the increase in U and Th content in this portion of the section. It is evident that even minor grain size changes are reflected by considerable "jumps" in U, Th, and Zr concentration. Thus, when sampling material in a regional exploration program, grain size should be held constant to remove, as much as possible, the variation arising from this source.

A detailed examination of the vertical variation exhibited in the uraniferous conglomerates and related lithologies was also undertaken. Figure 7 shows a hypothetical, composite view of variation through a series of ore conglomerates. In the lower conglomerate, the well-packed pebbles have a highly elevated U content, a moderately elevated Th content, and a depressed Zr content relative to the sample taken immediately below the sandstone lens. Also, the U/Zr ratio shows a relative increase in Zr from the well-packed conglomerate to the sandstone lens. These observations are compatible with uraninite concentration in areas of highest stream velocity; with increasing amounts of monazite and zircon being

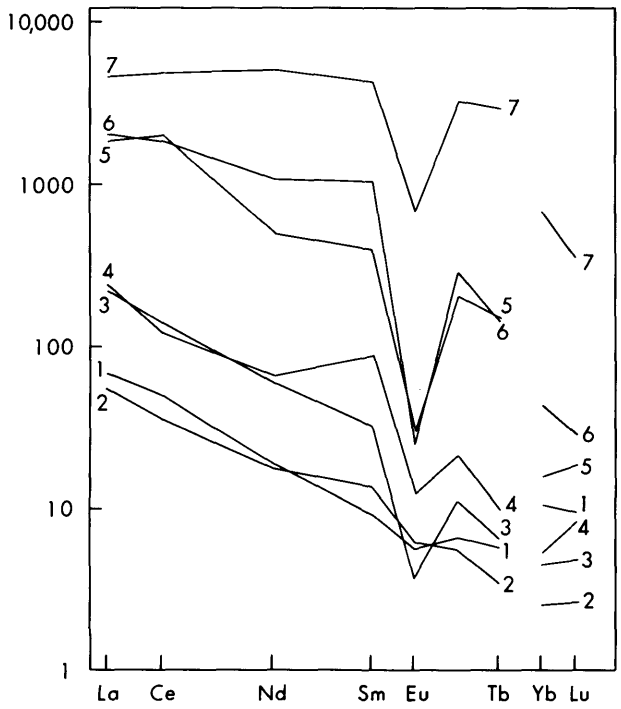

Figure 5. Chondrite normalized REE patterns for samples from the Matinenda Formation and monazite (curve 7, Wildeman and Condie 1973). Curve 1 = sandstone distal to the ore zone, curve 2 = sandstone proximal to the ore zone, curve 3 = 2 m thick sandstone between 2 ore conglomerates, curve 4 = sandstone lens within an ore conglomerate, curve 5 = U-poor section of ore conglomerate, curve 6 = U-rich section of ore conglomerate. Notice the similarity between curves 6 and 7, suggesting monazite is the main mineral contributing REEs to the ore conglomerate.

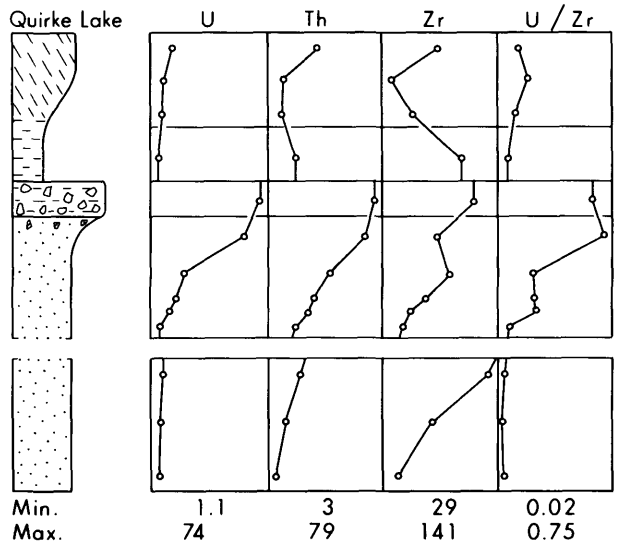

Figure 6. Vertical U, Th, and Zr variation in a section through the Lower Huronian Supergroup from the northern limb of the Quirke Syncline near Quirke Lake. The units are from bottom to top: the Matinenda Formation (missing the ore zones), the Ramsay Lake Formation, the Pecors Formation, and the Mississagi Formation. The total section is approximately 200 m thick. The U/Zr ratio reflects uraninite/zircon and thus should be higher in areas of increased paleoflow velocity (not drawn to scale).

concentrated as the stream velocity decreases. The upper conglomerate exhibits the same relationship, with the U, and Th to a lesser degree, concentrated in the basal, well-packed conglomerate; and Zr and Th concentrated in the upper pebbly sandstone. The sandstone lens in the upper conglomerate exhibits extremely elevated values compared to the other sandstones in the section and contains abundant heavy mineral laminae. The reason for the preferential enrichment in this lens is unknown, though destruction of a U-rich upstream bar may have provided a presorted sediment. Obviously, the hydrodynamics at the site of deposition of the sand lens governed density sorting of minerals to some degree, as evidenced by the relatively low U/Zr ratio compared to the U-rich conglomerates.

LATERAL TRENDS

Mineral zonation controlled by depositional environment has been documented in the preceeding sections. Zonation also may be caused by the heaviest (volume x specific gravity) constituents of the sediment load being deposited proximal to the source. Down-paleoslope depletion, and a regional mineral gradient increasing toward the fluvial entry point(s) into the basin is thereby produced. From Figure 8, it is apparent that zonation of Zr (reflecting zircon) is occurring on a regional scale with values increasing towards the north. This type of pattern also is observed when U, Th, Y, the REEs, Hf, and Ta are plotted. The denser the mineral that a particular element is associated with, the steeper the gradient is toward the north, and the quicker the gradient flattens toward the south. It is obvious that this type of regional trend can be used to specify areas favourable for placer development within a large basin.

HYDRAULIC VERSUS SOURCE CONTROL OF PLACER DEVELOPMENT

Two of the views commonly held concerning formation of placer deposits are that a rich source is needed to supply detritus to a stream system, and that these economic heavy minerals do not travel very far before forming a placer deposit. If this is so, it implies that exploration should occur only in areas proximal to presumed rich paleosources. This takes the emphasis away from depositional controls as the primary factor creating placer deposits, though of course the correct depositional setting is still required when dealing with a source-controlled placer depositional model.

The Zr/Hf ratio of samples from the Matinenda Formation was used to ascertain whether a rich source terrain combined with proximal deposition was the key factor which led to creation of the uraniferous placers. Hafnium content increases with progressive differentiation of a melt (Wedepohl 1978) leading to lower Zr/Hf zircon ratios. Thus, if the Elliot Lake uraniferous placers were derived from a granitic pegmatite source terrain, the probable source of the uraninite and quartz pebbles (Robinson 1982), their Zr/Hf ratios should be lower than surrounding Matinenda sediments. The ratios of all sediments studied were found to be very similar: (i) for the Matinenda sandstones from throughout the southeastern District of Algoma, 27; (ii) sandstones from locations near ore grade conglomerate, 26; (iii) sandstones intimately associated with ore grade conglomerates, 25; (iv) ore grade conglomerates, 28; (v) glacial mixtites, 28. The variation within these groupings was also found to be minimal. The

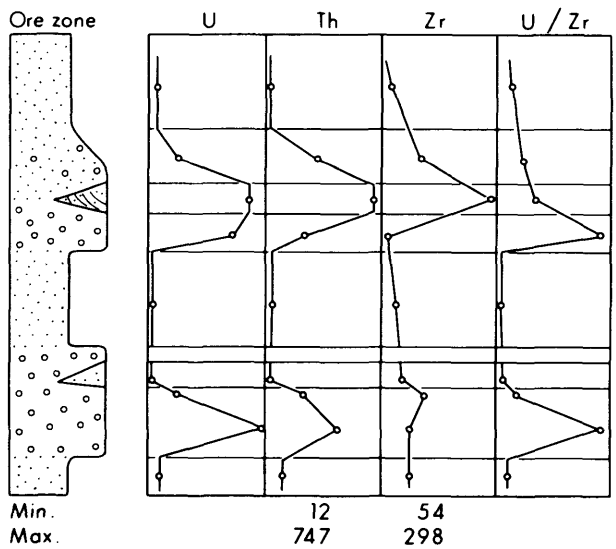

Figure 7. Vertical U, Th, and Zr variation in a section through a hypothetical, composite ore zone. See text for details.

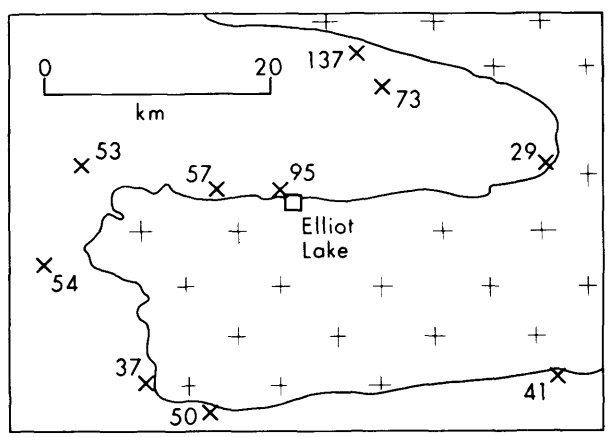

Figure 8. Regional variation in Zr content (ppm) of Matinenda sandstones. Notice the southward decrease (down paleoslope) of the values. Each data point represents the average of a number of samples collected throughout the stratigraphic section at that location.

above data are in direct contrast with possible granitic source material, the ratios of which range from 16 to 54. Increased values coincide with more mafic granites (*sensu lato*). The Zr/Hf ratio of possible volcanic source rocks also vary from 38 to 45, averaging 43. The Matinenda sediments deposited in the southeastern District of Algoma thus were extremely well mixed prior to entering the basin. Thus it is obvious that depositional environment played by far the key role in creating the uraniferous deposits.

CONCLUSIONS

HYDRODYNAMIC SORTING IN THE STUDY AREA

Factor analysis has confirmed that the Matinenda conglomerates of the Elliot Lake area are mineralogically zoned as described by other authors (Robertson 1962; Roscoe 1969; Theis 1979). Uraninite forms the most distinctive zone with greater overlap occurring between the brannerite, monazite, and zircon zones. Roscoe (1969) demonstrated that the uraninite-rich zone formed furthest upstream, with the lighter heavy minerals progressively dominating the heavy mineral assemblages downcurrent. The U concentration also systematically varies vertically through the conglomerates. The uraninite was concentrated in areas of maximum stream velocity, indicated by well packed sedimentary fabrics (Theis 1979). Monazite and zircon increasingly dominate the sequence along with evidence of decreasing depositional velocity. These trends resulted when conglomerate layers with uraninite concentrated near the bottom of bars and lag gravels, while monazite tended to concentrate upwards. Lag deposits rich in uraninite may exist at the top of a conglomerate or along minor internal disconformities. The immediately overlying sandstones are generally enriched in zircon, implying their formation at slightly greater stream flow velocities than other sandstones in the region. R-mode factor analysis performed on sandstones indicated that they contain the same progressive mineral zonation exhibited by the ore conglomerates.

In addition to the localized trends discussed above, a regional mineral gradient also occurs. As the premixed sediment debouched into the basin from the north-northwest (Fralick and Miall 1982), the heaviest minerals were sedimented first and thus were depleted in the material available for deposition further down the paleoslope. This process created a regional depletion in heavy mineral percentages away from the sediment entry points.

For more information on the study described briefly in this report *see* Fralick and Miall (in preparation).

ASSESSMENT OF EXPLORATION TECHNIQUE

This study demonstrates that whole-rock geochemistry is a valuable placer exploration technique. However, it must be borne in mind that lithofacies variation in the Matinenda Formation is minimal. With increased lithofacies variation, local variability of mineral concentrations increases and the regional pattern is more difficult to assess.

Important findings for geochemical placer exploration are summarized below:

1. Two types of variation exist in the mineral assemblages. On the local scale, hydrodynamic fluctuations through space and time create pronounced size, specific-gravity-related zonation. On the regional scale, the heavier mineral suites dominate in source-proximal areas. This causes downstream depletion in these minerals and a widespread concentration gradient is set up.
2. Regional exploration models should focus on the proximal-to-distal depletion of very heavy minerals. Exploration of a mineralized zone should focus on the pronounced local variations.
3. Samples used for regional contouring should all have the same grain size, preferably the coarsest sand size common throughout the area.
4. Samples containing heavy-mineral-rich ripple laminae, and especially pebble bands, are useful for determining the heavy mineral suite capable of being deposited at specific locations.
5. Elements to be analyzed vary with the commodity sought and the hypothesized source rock. Zirconium, titanium, and iron are probably the 3 most versatile elements which could be employed as pathfinders. In this study, a wide variety of elements were found to exhibit gradients decreasing away from the Quirke ore zone.
6. The number of samples required to establish a trend differs from target to target. In this study, relatively low numbers produced good results. Of course the more data points obtained the better the control and the more accurate the trend.
7. Whole-rock geochemistry techniques should be combined with a paleocurrent study to provide information on paleoslope and sediment entry points into the basin. An analysis of depositional environments, vital for determining the paleohydraulics of the system, should also be conducted.
8. When conducting a detailed study on a mineralized zone, local variation should be carefully monitored. The heavier trace element suite usually concentrates in the up-paleoslope portion of deposits in paleobars and paleochannels. For more information on localized zonation *see* Roscoe (1969, p.139-146).

ACKNOWLEDGMENTS

Grateful appreciation is extended to Ross Gunning and Allen MacEachern of Denison Mines Limited and Doug

Sprague of Rio Algom Mines Limited and the geologic staff of both operations for access to underground workings and valuable discussions on the geology of the area.

REFERENCES

Fralick, P.W., and Miall, A.D.
1982: Sedimentology of Huronian Deposits, Including Uranium Bearing Rocks; Ontario Geoscience Research Grant Number 84, Ontario Geological Survey, Open File Report 5375, 28p.

in preparation: Rock Geochemistry as a Placer Exploration Tool; Ontario Geoscience Research Grant Number 136, Ontario Geological Survey, Open File Report.

McQuivey, R.S., and Keefer, T.N.
1969: The Relation of Turbulence to Deposition of Magnetite over Ripples; United States Geological Survey, Professional Paper 650-D, p.244-247.

Parviainen, E.A.V.
1973: The Sedimentology of the Huronian Ramsay Lake and Bruce Formations, North Shore of Lake Huron, Ontario; Ph.D. Thesis, University of Western Ontario, London, Ontario, Canada, 426p.

Robertson, D.S.
1962: Thorium and Uranium Variations in the Blind River Ores; Economic Geology, Volume 57, p.1175-1184.

Robinson, A.G.
1982: The Origin and Modification of a Uraninite-Bearing Placer, Elliot Lake, Ontario; Unpublished M.Sc. Thesis, University of Toronto, Toronto, Ontario, Canada, 208p.

Roscoe, S.M.
1969: Huronian Rocks and Uraniferous Conglomerates in the Canadian Shield; Geologic Survey of Canada, Paper 68-40, 205p.

Smith, N.D., and Minter, W.E.L.
1979: Sedimentological Controls of Gold and Uranium in Local Developments of the Leader Reef, Welkom Goldfield, and Elsburg No. 5 Reef, Klerksdorp Goldfield Witwatersrand Basin; Economic Geology Research Unit, University of the Witwatersrand, Johannesburg, Information Circular Number 137, 21p.

Theis, N.J.
1979: Uranium-Bearing and Associated Minerals in Their Geochemical and Sedimentological Context, Elliot Lake, Ontario; Geological Survey of Canada, Bulletin 304, 50p.

Wedepohl, K.H.
1978: Handbook of Geochemistry; Springer Verlag, New York, p.72-A-1 to 72-0-1.

Wildeman, T.R., and Condie, K.C.
1973: Rare Earths in Archean Greywackes from Wyoming and from the Fig Tree Group, South Africa; Geochimica et Cosmochimica Acta, Volume 37, p.439-453.

Grant 134 Stratigraphy and Geochemistry of Northern Ontario Carbonaceous Deposits: Onakawana Lignites

W.S. Fyfe[1], B.I. Kronberg[1], D.F. Long[2], F. Murray[1], M. Powell[1], C. Try[2], E. van der Flier[1], C.G. Winder[1], and J.R. Brown[3]

[1]Department of Geology, University of Western Ontario
[2]Department of Geology, Laurentian University
[3]CANMET, Ottawa

ABSTRACT

The Lower Cretaceous Mattagami Formation of the Moose River Basin consists of plastic shales, unconsolidated sands, and lignite. This erosional outlier unconformably overlies Devonian shales and limestones. The maximum known thickness is 127 m, but Pleistocene glacial erosion has resulted in much local variation. The Grand Rapids High separates shales, lignites, and minimal sands to the east from coarse white sand, shale, and minimal lignite to the west. A continental fluvial-to-lacustrine model indicates that a large river, the ESOOM, deposited channel sand as it flowed westward to the Mowry Sea, while to the east, peat was deposited in swamps, marshes, and lakes.

An anticlinal structure along the bed of Adam Creek has resulted from the unloading of Pleistocene sediments through erosion resulting from hydro reservoir overflow and a vertical hydraulic head in water-saturated unconsolidated coarse sand causing an upward rise of the Mattagami Formation sediments.

Geochemical investigations show that the general weathering environment produced kaolin-gibbsite. The distribution of such elements as uranium is highly variable as is the distribution of thorium-uranium ratios. Zirconium concentrations are low to the east and high to the west. Anomalous concentrations of gold, platinum, and palladium are common in ashed lignite, reaching 0.1 ppm. A few samples contain arsenic but the sulphur contents are low. Sulphates and sulphides are common in lignites and seem to have formed by diagenetic processes.

GENERAL GEOLOGY

INTRODUCTION

The Lower Cretaceous Mattagami Formation of Northern Ontario is a semi-elliptical lens of sediments, approximately 170 km in east-west length and 80 km in north-south width (Figure 1). The boundaries are the Abitibi River on the east, the Cheepash River on the north, and the headwaters of the Rabbit and Soweska Rivers to the west. The southern margin is an east-trending fault along which a sharp contact occurs with Archean metamorphic rocks exposed just north of the Hydro Electric Power Commission (H.E.P.C.) of Ontario stations on the Mattagami and Missinaibi Rivers.

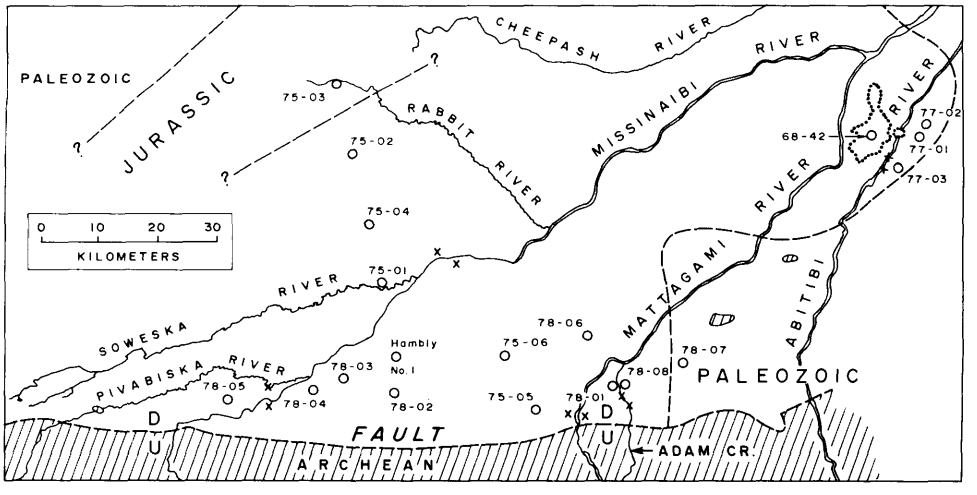

Figure 1. Mesozoic sediments in the Moose River Basin, selected drill sites, and Onakawana lignite field.

TABLE 1 SELECTED DATA FROM DRILLING OF THE MATTAGAMI FORMATION, MOOSE RIVER BASIN. DRILL LOCATIONS IN FIGURE 1. SOURCES: HOPKINS AND SWEET (1976), GUILLET (1979), TELFORD AND VERMA (1979).

	Drift (M)	Mattagami (M) (+ incomplete)	% sand	Lignite THICK (M)/No. Beds	Paleozoic Depth (Elev)(M)
Manalta 68-42	24	46	3	13/2	69(60)
OGS 77-01	26	0	0	0	27(42)
OGS 77-02	48+	0	0	0	?
OGS 77-03	30	16	0	0	47(1)
Aquit. Hambly 1	64	123	85	0	188(-77)
OGS 75-01	13	33+	40	0	-
OGS 75-02	99	9	0	0	(Jur)
OGS 75-03	116	0	0	0	(Jur)
OGS 75-04	152	20+	100	0	-
OGS 75-05	23	62+	30	0	-
OGS 75-06	51	84	65	0	137(-40)
OGS 78-01	40	124+	66	8.7/10	-
OGS 78-02	113	76+	43	0.8/1	-
OGS 78-03	56	127+	56	0	-
OGS 78-04	96	39+	74	0	-
OGS 78-05	73	48	0	2.4/1?	121(-3)
OGS 78-06	43	78+	61	8.1/3	-
OGS 78-07	102	-	-	-	102(4)
OGS 78-08	78	40+	55	1.1/1	-

ROCK TYPES

Sparse outcrops are of black, grey, green, orange, and red plastic shales, grey silts and fine sandstone, coarse white sands, and low rank lignite. Shales and lignite are exposed on the Abitibi River south of Onakawana. A small outcrop of grey shale occurs at the junction of the Mattagami and Missinaibi Rivers. In the western part of the area, the coarse unconsolidated sands are evident along Adam Creek, below the generating station at Smoky Falls; along the Missinaibi River, between the mouths of the Soweska and Opasatika Rivers; and along the Missinaibi River near the mouth of the Pivabiska River (Curran Bend) (Sanford *et al.* 1968; Price 1978). On Adam Creek, conglomerate lenses in the white sand contain red chert pebbles similar to the jasper pebbles of the Lorraine Quartzite, north of Lake Huron. Generally, the white sands are exposed topographically above stream level whereas shales tend to be at stream level.

Lignite outcrops near Onakawana have encouraged local trenching, exploratory underground mining, strip mining, and drilling. Over 430 closely spaced drillholes have indicated proven reserves of 185 000 000 tons in the Onakawana field. Drilling has been carried out in the western part of the basin into the Cretaceous sediments for lignite, silica sand, ceramic clay, and, into the older rocks for kimberlites. Most of these records are not available or considered unreliable.

Table 1 summarizes records of drillholes bored from 1968 to 1978; drillhole locations are shown in Figure 1. The maximum known thickness of the Mattagami Formation is 127 m (drillhole OGS 78-03) without reaching the underlying Devonian sedimentary rocks. The data show that the Mattagami Formation has great thickness irregularities in short distances. The unconformable surface with Pleistocene glacial sediments has substantial topographic relief. Insufficient data, however, are available on the relief of the unconformity with the underlying Devonian sedimentary rocks to ascertain whether notable irregularity here has had any influence on the thicknesses of the Mattagami Formation.

In summary, on the basis of outcrop and drillhole data, the Mattagami Formation is characterized by shale and lignite with minor sand toward the east. In the western part of the area, the Mattagami Formation contains sands with a few lignite beds of a metre or more in thickness. The most western drillhole, OGS 78-05, reveals shale, some sand, and 1 bed, 2.4 m in thickness, of lignite and lignitic shale. In the drillholes to the north, OGS 75-02 and 75-03, the Mattagami Formation is very thin or absent.

GEOLOGICAL STRUCTURE

Since Devonian sedimentary rocks outcrop north of the Mesozoic outlier and occur at an elevation of 77 m below

sea level in the Hambly Number 1 well, the Paleozoic rocks must dip gently to the south. In an east-west direction, an anticlinal structure with a northwest-trending axis exposes Devonian limestones at Grand Rapids on the Mattagami River (Figure 2). To the south, drillhole OGS 78-07 encountered Devonian limestones below the Pleistocene cover. Two topographically high Archean inliers occur to the southeast. Devonian black shales outcrop along the Abitibi River at Williams Island.

Figure 2 shows the general stratigraphic and structural configuration of the Grand Rapids Anticline, which would seem to plunge to the northwest. The origin of this structure is unknown. Solution of Devonian-age evaporites in the area around Gypsum Mountain may have caused the synclinal feature of the Onakawana field (Price 1978, Figure 7). Presumably, the Mattagami Formation is regionally conformable with the Devonian.

The gentle flexures of the Paleozoic rocks in the Moose River Basin are post-Mattagami in age. However, the 2 Archean inliers in the Grand Rapids anticline are higher than the present surface. These hills must have stood above the depositional surface of the Mattagami sediments and formed high ground between the "shale-lignite" environment to the east from the "sandstone-shale" environment to the west.

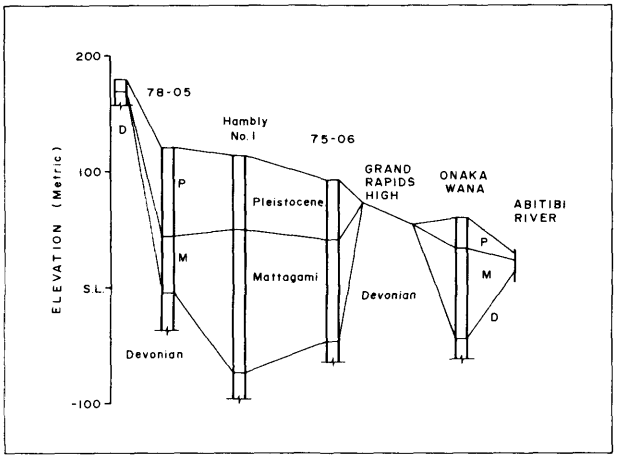

Figure 2. Surface topography, drift thickness, Mattagami Formation thickness, and flexures of the Devonian across the southern margin of the Moose River Basin (diagramatic).

AGE

Palynology has established a Lower Cretaceous age (Hopkins and Sweet 1976; Legault and Norris 1982) for the Mattagami Formation. The palynomorphs are indicative of fresh water lacustrine and upland environments. Evidence for marine deposition has not been found (Norris *et al.* 1976). The Manville Group of Alberta, with the Athabasca tar sands (Stewart and MacCallum 1978) and subsurface fluvial channel sandstones near Lloydminster (Putnam 1982), is correlative.

PALEOGEOGRAPHY

The Mattagami Formation represents a segment of a major large scale river system which drained an extensive tract of the Canadian Shield. A high-constructive system is indicated by the abundance of mudrocks in the formation and the absence of point bar surfaces or fining upwards sequences in the channel sandstones. Details of the proposed model are given in a paper by Try, Long, and Winder (in press) and are summarized in Figure 3.

Mudstones are interpreted as overbank deposits. They show great variation in colour and organic content and often exhibit well-developed soil textures. Flat and wavy, laminated, very fine grained sandstones and siltstones are interpreted as levee and splay deposits. White medium to very coarse grained sandstones and granule conglomerates occur in units from 2 to 20 m thick. They may be interpreted in terms of channel fill and channel lag deposits. Lack of fining upwards sequences and absence of well-developed point bar surfaces (epsilon cross-beds) suggests that lateral accretion processes, typical of meandering stream processes, were of only minor importance during deposition of the Mattagami Formation. The abrupt lower and upper contacts of many of the stack sandstone sequences indicates that channel formation and abandonment was avulsion controlled. Thin lignites are found along channel margins associated with levee and splay deposits. Thick coal accumulations, such as those at Onakawana, appear to have formed only

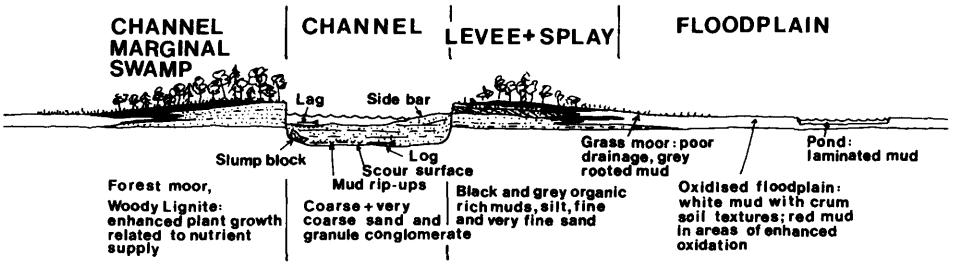

Figure 3. Depositional model for channel-levée-swamp-marsh-lacustrine environments.

in those parts of the floodplain adjacent to contemporary topographic highs developed upon the underlying Devonian bedrock. These marginal areas were more protected than the interchannel floodplains, allowing only limited flood inundation and uninterrupted peat accumulation.

Examination of distribution of major lithofacies (Figure 4) indicates that the ESOOM River (Moose spelled backwards) represents a major trunk stream system which flowed to the west-northwest, draining higher ground to the east. Rocks in the headwaters were not exclusively Precambrian metamorphic rocks as now occur to the east, but included Paleozoic-age carbonates and other sedimentary rocks isolated outliers of which still occur in the vicinity of Lake Temiskaming and Lake St. John, Quebec. An additional source for limestone and shale clasts in the channel sandstones and conglomerates may have been local bedrock highs. The main river system occupied a tract about 50 km wide in which avulsion generated channels predominated (Figure 4). The presence of a local bedrock high (Grand Rapids High) to the east of this trunk system probably influenced the eastward migration of the channel belt. To the east of the high floodplain and lacustrine and swamp deposits, including some thick lignites at Onakawana, predominate, although all holes indicated in Figure 1 contain minor sandstone bodies representing tributary river systems. An Archean inlier along the Pivabiska River may represent another geomorphic high on the western side of the basin during deposition of the Mattagami Formation. Exploration for kimberlite plugs west and north of this area indicates a low potential for preservation of thick coal bodies below the Pleistocene.

During Albian time, an epeiric sea transgressed central North America from the north (Figure 5). Fluvial and estuarine sandstone are now explored for hydrocarbons in Alberta. The size of the interpreted ESOOM River suggests the Moose River Basin outlier of Cretaceous sediments is a fragment of a continuous blanket once connected to the Cretaceous farther west. The marine transgression stopped short of the Moose River Basin, the sediments of which are totally continental.

ADAM CREEK AREA

"ADAM CREEK ANTICLINE"

In 1966, Ontario Hydro built several dams along the Mattagami River near Smoky Falls to provide reservoirs for power stations. An overflow dam was built near the headwaters of Adam Creek. Subsequent water outflow has changed a small stream draining muskeg into a small canyon up to 30 m deep and 50 m wide. The banks expose Pleistocene glacial sediments, Mattagami Formation clays and sands, and near the dam, Archean metamorphic rocks. At locality A (Figure 6 and Figure 8), lignite boulders occur on the gravel bars; lignite is not exposed in situ but is reported to occur below water level. At locality B (Figure 7), dark grey shales, some with rooted zones and white unconsolidated sand, dip, up to 70°, into each bank indicating an anticlinal axis parallel to the stream. The concentration of red boulders occurs symmetrically, relative to the middle of the stream. The stratigraphic succession of about 16 m is the same

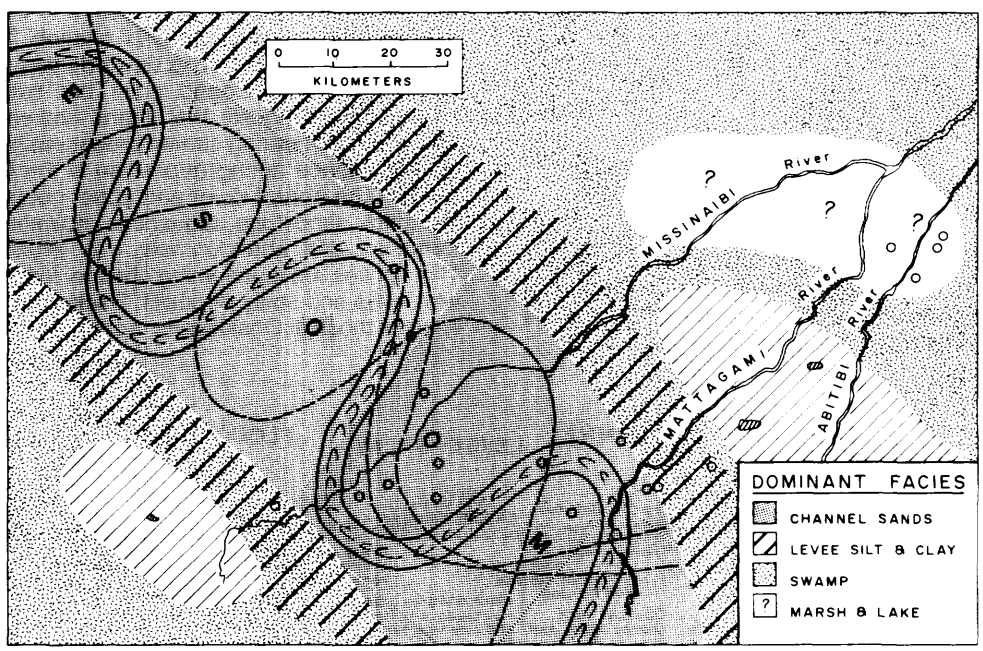

Figure 4. General application of the channel lacustrine model to paleogeography of Mattagami Formation deposits.

toward each bank. The configuration of the outcrop on one bank is semi-circular. In the Moose River Basin, where the general structure consists of flat-lying sediments, these high angle dips suggest a local phenomenon. All exposures of the Mattagami white sand also indicate dips into the banks of the stream.

Drillholes OGS 78-01 and OGS 78-08 were put down to elucidate the stratigraphy near Adam Creek. Projecting the Mattagami Formation (Figure 9) between these 2 holes places its top at least 5 m below the bottom of the creek. Norris and Dobell (1980) reported that the palynomorphs from lignite on Adam Creek probably represent their lowest Zone 1. Their cross-section (Norris and Dobell 1980, Figure 4) shows Zone 1 at least 30 m below the bottom of the creek.

The reservoirs on the Mattagami River at elevations of 98, 132, and 198 m above sea level, are from 18 to 118 m above the outcrops of the Mattagami Formation along Adam Creek. The surface muskeg is water saturated. The friable white sand, which occurs in all drillholes in the area, also should be saturated and have a hydraulic head. A unit thickness of Mattagami Formation shale, friable sand, and lignite is less dense than an equivalent thickness of overlying Pleistocene clays and till. When reservoir overflow along Adam Creek erodes Pleistocene sediments, the underlying Mattagami Formation would become unstable as a result of the density differential. The hydraulic pressure in the friable sand would exert upward vertical pressure. Wetting of the Mattagami shales would reduce internal friction. The average annual temperature of 0°C means regular freezing and thawing would reduce the strength of the rock. The periodic sudden overflow from the reservoir in Adam Creek would cause vibrations and initiate upward movement of the unstable Mattagami sediments. The semi-circular outcrop configuration (Figure 7) suggests a local diapir, possibly coinciding with a subsurface channel sand.

Figure 8 (upper) shows the Mattagami outcrop at point A (Figure 6) in October 1981. The white sand is about 2 m above the water. Figure 8 (lower) is the same outcrop in September 1982. The sand is about 5 m above the water. The facing surface of sand shows smooth vertical grooving. These sands must still be oozing upward.

Martison (1953, p.47) reported that during stripping operations in the Onakawana field "mining difficulties are already present in the form of folding".

"DEVONIAN"

Map 2440 (Ontario Geological Survey 1981) shows a Devonian outcrop on Adam Creek. Telford and Verma (1979, Figure 2.4a) have illustrated the Devonian Sextant Formation on Adam Creek 3 km from the mouth.

Figure 10 illustrates the outcrop at point C (Figure 6) identified as Devonian sandstone. This massive, rusty weathering, coarse sandstone contains conglomerate lenses with pebbles of black chert and white quartzite. "Coloured" metamorphic rocks typical of Archean basement are noticeably absent. Lithologically, the massive sandstone is quite different from the unconsolidated sands of the Mattagami Formation. The underlying material is not consolidated as should be expected for an outcrop, but represents a bar of river gravel. The massive sandstone is broken along joints running parallel to the stream, so the slab appears drooped over the gravel bar. The sandstone contains fragments of coalified wood. Paul Copper (personal communication to D.G.F. Long) has identified a small porous fragment as typical of reptilian bone structure. The evidence suggests this mass is not outcrop, and not Devonian, but a huge slab of Mesozoic rock probably moved from elsewhere by glaciation.

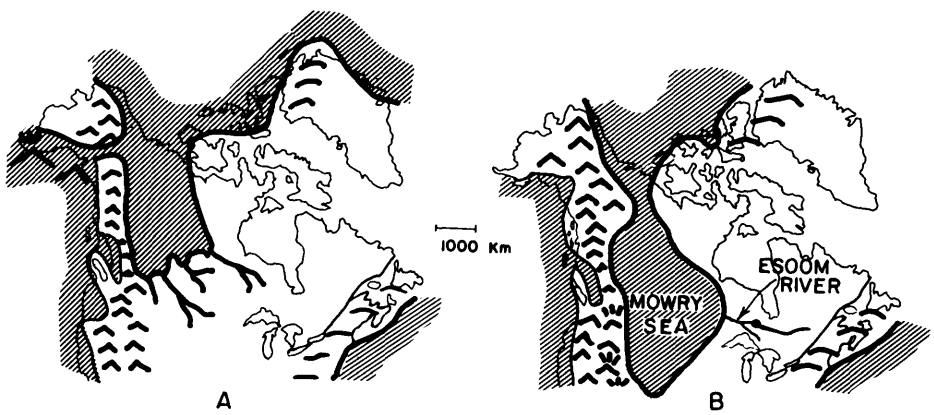

Figure 5. Transgression of the Lower Cretaceous sea and continental drainage including the ESOOM River. (A) - early Albian; (B) - middle Albian (Modified from Williams and Stelck 1975, Putnam 1982).

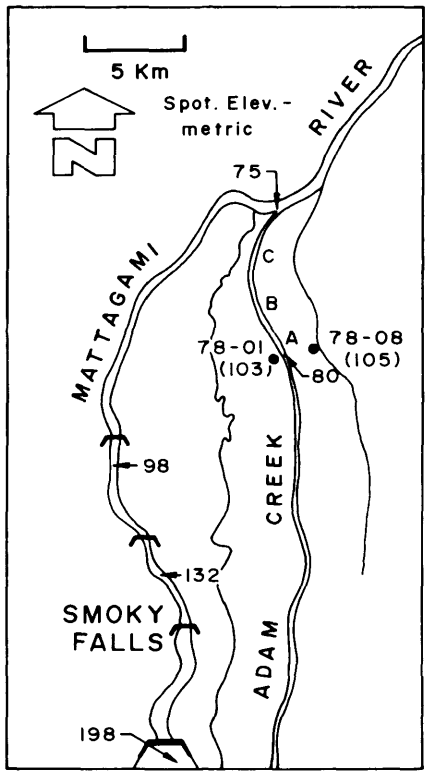

Figure 6. Adam Creek and Mattagami River, stream and reservoir elevations, drill locations, and spot localities.

Figure 7. Adam Creek, locality B, with anticlinal axis at the middle of the stream, and concentrations of red boulders (RB). Grey shales on each bank dip up to 70°. Coarse white sand (WS) occurs directly above the grey shales. Thin lignite (L) occurs on both sides of stream. The outcrop of grey shale is semi-circular.

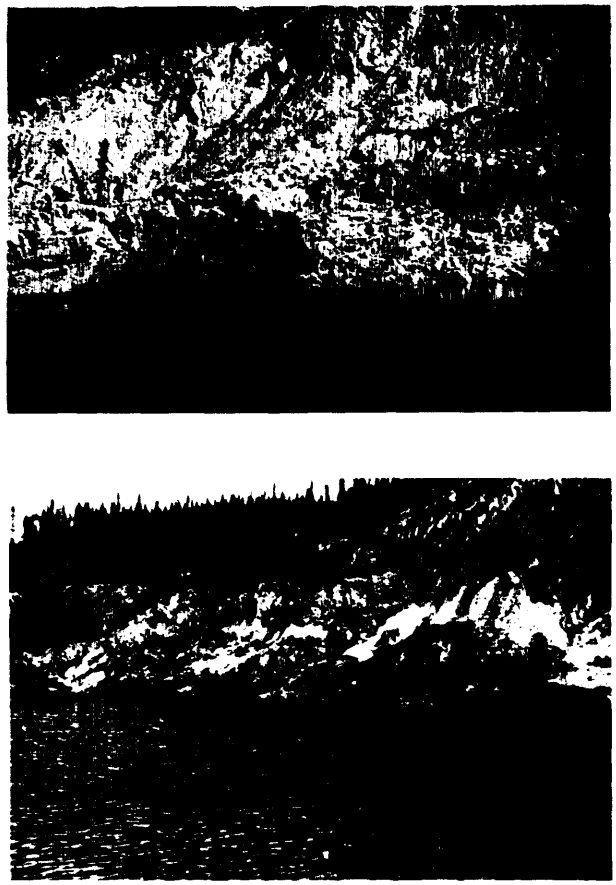

Figure 8. Adam Creek, locality A. Note the differences in height and lateral extent of the white sand. Upper picture taken October 1981. Lower picture taken September 1982.

GEOCHEMISTRY

INTRODUCTION

Coal is material showing extreme geochemical variability. Numerous features may contribute to this variability and include:

1. The nature of plant debris which forms the primary coal deposit. The classic work of Goldschmidt (1954) showed how selective various plants could be in concentrating metals.
2. The diagenetic processes associated with the transition from plants to a carbon-rich residue.
3. Ground water input into the essentially reducing environment of a coal seam. Note, that as plant debris passes to coal, the volume reduction is large and coal seams may be excellent aquifers (Freeze and Cherry 1979).

4. The elevation of the region through time, which may determine the input from descending or ascending ground waters. It is well known that coal deposits near sea level may be influenced by both rising continental waters and marine incursions which may determine features such as the sulphur content.
5. Secondary biological influences, for example the actions of sulphate reducing bacteria in pyrite formation.

The basic geochemistry of coal is important for combustion technology and the "acid rain" problem. If technology for gasification or conversion to liquid fuels is considered, trace metals may act as catalyst poisons or accelerators. Many trace elements (U, Rn, As, S, Hg) may concentrate in fly ash or combustion gases while other toxic species (U, Th, Cd, Tl) may be easily leached from glassy ash debris. Before a coal deposit is utilized, all such factors should be evaluated. This is rarely done, as most coal deposits are developed long before appropriate geochemical studies are conducted.

SOLID-SOURCE SPARK-SOURCE MASS SPECTROMETRY

Most analytical techniques depend on specific selection of elements to be studied. The great advantage of spark-source mass spectrometry is that all elements are detected from Li-U in a single analysis. The technique can be sensitive to the parts per billion level. Thus, spark-source methods are excellent for the detection of particular anomalous concentrations of elements over a very wide spectrum.

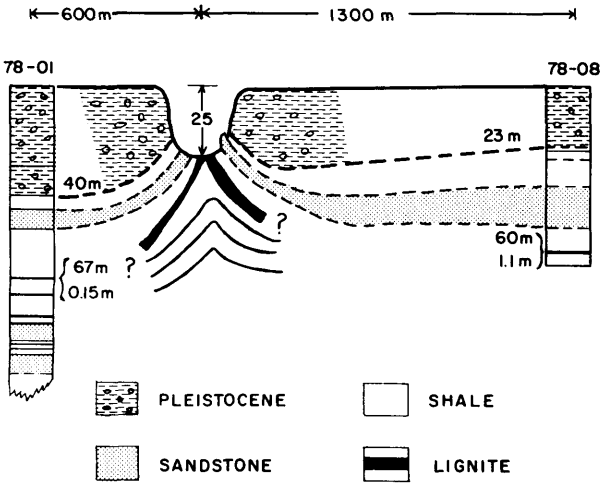

Figure 9. Section across Adam Creek showing the level of the Mattagami Formation in wells as lower than in the creeks, and showing how unloading of Pleistocene sediments allowed the Mattagami sediments to rise by hydraulic pressure within the coarse white sands.

Samples of Mattagami lignite analyzed by spark source mass spectroscopy (SSMS) were prepared by first ashing, where necessary, to remove organic carbon, then mixing with graphite in a 1:1 ratio (the ash from a low temperature asher (LTA) is almost pure calcite). Clay samples were mixed directly with graphite. The addition of graphite is to increase the electroconductivity of the sample. The sample-graphite mixture is then pressed into electrodes and sparked under high vacuum. The composition of the resultant ionized vapour is assumed to be representative of the solid sample. The data are collected on photographic plates which are analyzed semi-quantitatively. The concentrations of the elements are estimated to within a factor of 3. Hence upper and lower limits on a 10 ppm reading are 3 ppm and 30 ppm respectively. United States Geological Survey rock standards were used as references for calculations of element concentrations.

Because the sample size actually analyzed is small (0.1 mg), concentration values are not necessarily representative of the bulk composition; but the analytical record does reflect the in situ association of the elements. The precision in SSMS analysis of geological materials is normally within the variation attributed to sampling constraints.

The 2 Onakawana lignite samples, OL(L) and OL(H) (Table 2) were taken from a large bulk sample. It was found that consolidated "chunks" of lignite, say 3 cm by 3 cm, had a much lower ash content that the loose "crumbled" lignite, (5.7% ash and 15.3% respectively), possibly due to a higher woody content. Therefore, these 2 types of lignite were ashed and analyzed separately by SSMS.

Adam Creek samples AC-07-82 to AC-10-80 incude a fine brown clay overlain by a lignite seam with a pyrite zone at the top. The total section was 1.10 m thick. All but the clay, sample AC-07-82, were ashed. Table 3 includes 2 other clay samples from Adam Creek, a weathered red clay AC-36-82, and a green chloritic clay AC-37-82. Table 4 contains limited element concentrations from a drill core several kilometres east from Adam Creek.

Figure 10. Adam Creek, locality C, slab of a rusty coarse sandstone erratic considered to be Mesozoic.

TABLE 2 CONCENTRATION OF TRACE ELEMENTS (ppm) BY SSMS.

Trace Element	Sample Number OL(L)	OL(H)	AC-07-82	AC-08-82	AC-09-82	AC-10-82
B	600	200	200	600	60	0.2
F	430	1290	129	1290	1290	129
S	240	240	24	75	75	75
Cl	500	1500	17	50	50	17
Sc	12	12	37	37	37	3.7
V	354	120	354	354	3540	3.5
Cr	23	7	23	23	70	0.07
Mn	260	260	9	90	90	3
Co	20	20	2	5.5	5.5	550
Ni	51	170	1.5	15	15	5
Cu	117	117	35	117	117	1
Zn	28	85	8.5	28	85	28
Ga	76	23	23	75	230	0.2
Ge	35	3.5	1	12	36	1
As	7.5	2.5	0.3	2.5	7.5	2.5
Se	2	0.7	0.7	0.7	0.2	0.7
Br	3	0.3	0.1	1	1	0.03
Rb	17	56	0.2	0.6	0.6	0.06
Sr	4,800	1,600	50	4,800	1600	5
Y	400	12	120	400	120	1
Zr	300	300	30,000	3,000	900	3
Nb	40	13.5	135	135	40	0.4
Mo	36	3.5	1	4	4	1
Ag	0.1	0.1	0.05	0.05	0.5	0.05
Cd	ND	.06	ND	ND	0.4	ND
Sn	5	5	5	50	5	ND
Sb	1	0.3	0.3	1	0.3	0.1
I	<3, >1	ND	< 1	<10, >3	< 1	ND
Cs	1.4	5	0.1	1.4	1.4	0.03
Ba	1870	1870	190	560	560	6
La	96	96	32	960	96	1
Ce	150	150	50	1500	500	1.5
Pr	19	6	2	60	19	0.2
Nd	200	60	20	600	200	2
Sm	21	7	7	240	73	ND
Eu	4.5	0.5	1.5	50	5	ND
Gd	50	5	5	50	17	ND
Tb	5	0.5	0.5	2	2	ND
Dy	26	3	9	27	9	ND
Ho	4	1	4	12	1	ND
Er	>13	>4	>13	>13	>4	ND
Tm	> 3	>0.5	>3	>3	>1	ND
Yb	> 8	>1.2	>9	>9	>2.7	ND
Hf	70	7	74	7.4	7.4	ND
Pb	31	31	9	31	9	3
Th	75	7.5	75	240	75	ND
U	60	6.0	20	60	20	ND
Ti	0.5	0.5	ND	ND	0.3	3

SAMPLE DESCRIPTION

OL(H) - Ashed Onakawana lignite - high ash content (15.3%)

OL(L) - Ashed Onakawana lignite - low ash content (5.7%)

SAMPLE FROM ADAM CREEK

AC-10-82 - ashed pyrite and wood from top of seam (90% ash)

AC-09-82 - ashed woody material from top of lignite (10.4% ash)

AC-08-82 - ashed lignite (20.3% ash)

AC-07-82 - Brown clay with root remnants below lignite layer

TABLE 3 ONAKAWANA LIGNITE AND ADAM CREEK SAMPLES – CONCENTRATION (in ppm) OF As, Cd, Hg, Zr, Th, U, AND Ti BY SSMS.

SAMPLE	As	Cd	Hg	Zr	Th	U	Ti	SAMPLE DESCRIPTION
OL(L)	7.5	ND	ND	300	75	60	0.5	ashed Onakawana lignite (low ash)
OL(H)	2.5	>0.06	1	300	7.5	6.0	0.5	ashed Onakawana lignite (high ash)
AC-36-82	2.5	ND	ND	90	24.5	2.0	0.3	weathered red clay
AC-37-82	2.5	ND	ND	300	24	2.0	1.0	green chloritic clay
AC-07-92	0.3	ND	ND	30,000	75	20	<0.3	brown clay, bottom of sequence
AC-08-82	2.5	ND	ND	3,000	240	60	<0.3	ashed lignite (20.3% ash)
AC-09-82	7.5	>0.4	ND	900	75	20	0.3	ashed woody material above lignite (10.4% ash)
AC-10-82	2.5	ND	ND	3	ND	ND	3	ashed pyrite and wood from top of sequence (90% ash)

XRD Results of AC-07-82, AC-08-82, AC-36-83, AC-37-82

AC-07-82 - quartz kaolinite
AC-08-82 - quartz kaolinite
AC-36-82 - calcite, dolomite, quartz, muscovite (possible feldspar?)
AC-37-82 - calcite, quartz, muscovite (possible feldspar?)

Data for various materials are shown in Tables 2, 3, 4.

Features we would stress include:

1. Vanadium is highly concentrated in some lignites.
2. Strontium and barium also are highly concentrated.
3. Some samples are very highly enriched in zirconium (up to 0.3%). It is known that zirconium can be present in organic materials.
4. Uranium is well above crustal abundance and in fly ash could reach levels of several hundred ppb. But in general, uranium is correlated with thorium which suggests concentration in a common mineral phase, zircon.

Values for elements of environmental concern are shown in Tables 3 and 4. It will be noted that arsenic and uranium can reach high levels, but there is little evidence for high mercury and cadmium levels.

URANIUM AND THORIUM

These 2 elements are of particular diagenetic significance, for uranium is easily transported in oxidized ground waters and precipitated in the coal environment, while thorium is a measure of residual heavy minerals.

A variety of sediment and lignite samples were analyzed for U and Th. The material was air-dried, crushed to -200 mesh and sent to Nuclear Activation Services, Hamilton, Ontario for analysis. Uranium was determined by delayed neutron counting and thorium by induced neutron activation analysis. Detection limits are 0.01 and 0.3 ppm for U and Th respectively.

A large range of U and Th values occurs in the samples (*see* Table 5).

The lowest uranium values occur in the gravel/sand samples, averaging 1.18 ppm U. Contents are slightly higher in the wood/lignite samples, averaging 1.66 ppm. The clays contain most U, averaging 4.77 ppm, with highest values occurring in the clays with the most organic material.

Thorium values are lowest in the lignites, averaging 2.57 ppm; are higher in the gravels, averaging 7.25 ppm; and highest in the clays, averaging 10.07 ppm.

Given Th/U ratios of approximately 4:1 for average crustal rocks, from the above values it appears that the clays and lignites in Onakawana have enhanced U values (average Th/U ratios are 2.65 and 2.16 respectively). The gravels, however, are depleted in U, with Th/U ratios averaging 5.47.

Uranium can occur in several ways in lignite; in sorption sites, in organo-uranyl complexes, as small grains of uraninite, or in residual zircons.

Uranium is also readily absorbed onto clays; therefore, considering the reducing environment produced by decaying organic material, the uranyl ion is readily reduced to the insoluble uranous form. This uranium may then be held on the clays or in the lignite.

The data clearly show the great variability of uranium contents and U/Th ratios. But in general the materials are not anomalous in uranium.

WHOLE ROCK GEOCHEMISTRY OF THE SEDIMENTS

At Adam Creek the section can be subdivided into 2 distinct lithological units: (a) an upper quartz-sand channel

TABLE 4 SEDIMENTS FROM DRILLCORE A FEW KILOMETRES FROM ADAM CREEK-CONCENTRATIONS (in ppm) OF As, Cd, Hg, Zr, Th, U, and Ti BY SSMS.

SAMPLE	As	Cd	Hg	Zr	Th	U	Ti	SAMPLE DESCRIPTION
L-2-27	7	ND	ND	190	6.0	>1.7	ND	red clay 28m down core
L-2-28	0.7	ND	ND	57	18	>1.7	ND	white clay 29m
L-2-26	2.1	ND	ND	57	6.0	ND	ND	sandy clay 68.7m
L-2-23	2.1	>0.4	ND	57	ND	ND	ND	gravel 77.2m
L-2-19	0.2	ND	ND	19	6.0	ND	ND	sandstone 90.5m
L-2-18	2.1	ND	ND	190	60	>3	>0.5	lignite clay 90.6m (ashed -37.5%)
L-2-17	20	ND	ND	190	60	>5	>0.5	lignite 90.9m (ashed -4%)

deposit which overlies (b) floodplain and swamp-derived clays and lignite.

Whole rock geochemistry was done on representative samples of each material. Major elements were analyzed by XRF, and trace elements by XRF and atomic absorption. Some representative results are listed in Table 6.

As would be expected, SiO_2, Al_2O_3, and K_2O values are lowest in the lignite, while Loss on Ignition (L.O.I.), P_2O_5, MgO, and CaO values are highest in the lignite. Fe_2O_3 is variable in the materials and TiO_2 contents are highest in the clays.

Although the trace element values tend to be variable, the following trends are apparent. Trace element contents tend to be lowest in the gravels, except for cobalt, which is 95 ppm in the gravel (AC-32B-82) and falls to a minimum of <5 ppm in the lignite. The brown clay has highest values for Cr, Zr, Cu, Zn, Pb, and Ni. The lignite has relatively high Ni, Pb, and Zr values. The lignite has the highest Sr content, 1000 ppm.

It should be noted that some clays are clearly rich in kaolin, and gibbsite has been detected in some samples by X-ray diffraction. Clearly the weathering environment is one which has produced very mature products.

D.C. ARC 30-ELEMENT ANALYSIS

Three lignite samples, 2 clays, 2 indurated red sandstones, and 1 pyrite nodule were analyzed. The materials were ashed in open crucibles and 2 gm sent to X-ray Assay Laboratories Limited in Don Mills, Ontario, for analysis. Of the 30 elements, only 14 were detected in the Onakawana samples. Detection limits were very high for the analyses but varied depending on the element concerned. The results are shown in Table 7.

Beryllium was detected only in sample P3 (black clay) and sample FM-6 (lignite) at <0.01%.

Chromium was detected in all the lignite and clay samples except FM-3 at 0.01 to 0.1%.

Copper was found in all the samples to be <0.01% except for sample P1 (lignite) where the value was 0.01 to 0.1%.

Gallium was present in all the samples at <0.01%.

Manganese values were variable, from a maximum of 0.1 to 1% in sample P4 (green clay) and sample RC1 (red sandstone), to <0.01% in samples P1 (lignite), P3 (black clay), and Py (pyrite nodule).

Molybdenum occurs in samples P1, FM-3, FM-6 (all lignites), and sample P4 with values <0.01%.

Nickel was detected in all samples except FM-3 at values of <0.01%.

Pyrite has the highest Ni content, 0.1 to 1% and is the only sample containing cobalt (0.01 to 0.1%) and tin (<0.01%).

Ti values are variable, from 0.5 to 5% in samples P1 and P3 to <0.01% in the sandstone samples RC1 and RP.

V is ubiquitous at <0.01

Zr is present in most samples at 0.01 to 0.1%.

As one would expect, the pyrite nodule has high values for some of the chalcophile elements: cobalt, tin, nickel. However, copper values are similar to the other samples, as is lead, and manganese values are lower than those of any other samples except the black clay. There is a generaly tendency for chromium, copper, and molybdenum to be higher in the lignites than in the other sediments. Titanium is highest in the black clay, with lowest values in the sandstones.

TABLE 5 U, Th, AND Th/U VALUES FOR ONAKAWANA LIGNITES AND SEDIMENTS.

Sample Number	U ppm	Th ppm	Th/U	
AC-03-82	1.13	2.8	2.48	Wood from red sst
AC-04-82	2.65	6.9	2.60	Laminated mud.silt, org-rich
05	(2.15)	(5.6)	2.60	Wood
06	1.88	7.1	3.78	Laminated mud/silt, org-rich
07	6.35	11.6	1.83	Clay with roots, brown
08	2.97	6.1	2.05	Lignite
09	1.88	3.2	1.70	Wood from lignite
10	0.13	2.1	16.15	Pyrite + wood
11	(0.35)	(1.27)	3.63	Wood
12	0.87	1.8	2.07	Laminated sst + coal
13	0.15	1.2	8.00	Pebbly sst
14	3.46	6.2	1.79	Bonded silt and sand, + roots
15	0.97	2.2	2.27	Sandstone
16	5.29	9.4	1.78	Clay (tan)
17	4.13	9.6	2.32	Clay (tan)
18	6.83	15.2	2.23	Clay (light-brown)
19	8.43	12.7	1.51	Brown clay
20	3.15	10.0	3.17	orange clay
21	4.81	11.0	2.29	Browny/blue clay
22	0.52	3.5	6.73	gravel
23	5.39	9.9	1.84	Brown clay + roots
24	5.95	9.2	1.55	Brown clay
25	3.80	9.2	2.16	silt + sst with roots
26	(2.23)	(2.86)	1.28	Wood
27	5.95	12.4	2.08	Brown clay
28	5.57	11.4	2.05	Clay (White)
29A	1.04	5.9	5.67	gravel with clay
30	(0.43)	(0.66)	1.54	Wood
31	0.42	1.6	3.81	Clay (White)
32B	0.67	5.0	7.46	Gravel
32C	1.57	2.8	1.78	Iron-stained gravel
33	3.05	11.3	3.70	Clay (White)
34	6.72	8.3	1.24	Brown clay
35	(7.2)	(0.14)	0.02	Wood
Py	0.88	NA	-	Pyrite nodule from gravel
RCI	0.59	NA	-	Red sst/gravel + wood
RP	0.24	NA	-	Red sst/gravel with pyrite
OE1	2.56	7.3	2.85	Weathered lignite
OE2	0.07	< 0.3	4.29	Wood stump
OE3	0.29	0.7	2.41	Bark lignite
OE4A	0.33	0.3	0.91	Wood - inside
OE4B	1.10	2.5	2.27	Wood - outer portion
OE6	1.03	2.3	2.23	Wood
OE7	1.21	NA	-	Green clay

TABLE 6 MAJOR AND TRACE ELEMENT ANALYSIS OF SEDIMENTS FROM ADAM CREEK.

%	AC-32B-82 GRAVEL	AC-16-82 WHITE CLAY	AC-19-82 BROWN CLAY	AC-08-82 LIGNITE
SiO_2	90.3	42.4	49.0	22.1
Al_2O_3	6.22	31.6	30.1	7.97
CaO	0.17	0.28	0.48	3.41
MgO	0.07	0.31	0.43	0.73
Na_2O	0.00	0.00	0.00	0.00
K_2O	0.11	0.69	0.43	0.04
Fe_2O_3	0.27	9.03	1.54	1.36
MnO	0.00	0.03	0.00	0.00
LiO_2	0.25	1.03	1.75	0.80
P_2O_5	0.02	0.06	0.09	0.25
L.O.I.	2.62	15.30	16.50	65.20
ppm				
Cr	110	170	320	80
Rb	0	30	10	20
Sr	0	20	90	1000
Zr	150	180	320	260
Co	95	10	35	5
Cu	4	66	108	40
Zn	6	55	79	27
Cd	<.5	<.5	<.5	<.5
Pb	<5	<5	20	10
Mo	<5	<5	<5	<5
Ni	<5	40	75	55

SURFACE ELECTRON SPECTROSCOPY E.S.C.A.

E.S.C.A. spectroscopy was carried out at CANMET, Ottawa on 2 lignite wood fragments and some ashed lignite. The wood appeared very clean with only minor amounts of silicon (0.6 to 0.9 wt.%), S (0 to 0.5 wt. %), Ca (0 to 0.3 wt.%), Al (0 to 0.4 wt.%), and Cl (0 to 0.3 wt.%) detected. To increase the detection limit, the lignite was ashed, and subsequently iron, magnesium, and sodium were observed in the spectrum. Calcium and magnesium values in the ash are high, 12.7 and 9.7 wt.% respectively. Values determined for the other elements observed (*see* Table 8) are as follows: S - 4.4 wt.%, Al - 9.6 wt.%, Si - 3.4 wt.%, Fe - 3.7 wt.%, and Na - 1.1 wt.%. The spectra showed that S is present both as organic S and as sulphate. Of particular interest are the Al/Si ratios in the ash, suggesting the presence of gibbsite.

NOBLE METALS

Noble metals were determined in the ash of several samples of lignite by neutron activation analysis (Table 9). It is worthwile to note that all samples have appreciable gold concentrations (average crust 1 to 3 ppb) while platinum and palladium are also concentrated in several samples. Much more study is required to determine the significance of these data.

MINERAL MATTER ASSOCIATED WITH ONAKAWANA LIGNITES

Lignite from the Onakawana coal field was analyzed by Scanning Electron Microscopy coupled with Energy Dispersive X-ray analysis.

TABLE 7 ARC SPECTROGRAPHIC ANALYSES OF LIGNITE AND SEDIMENTS.

	P_1	P_3	P_4	RCI	RP	PY	FM-3	FM-6
As	-	-	-	-	-	-	-	-
Be	-	FT	-	-	-	-	-	FT
Bi	-	-	-	-	-	-	-	-
Cd	-	-	-	-	-	-	-	-
Ce	-	-	-	-	-	-	-	-
Ni	-	-	-	-	-	-	-	-
Cr	T	T	T	-	-	-	-	T
Co	-	-	-	-	-	T	-	-
Cu	T	FT	FT	FT	FT	FT	FT	FT
Ga	FT	FT	FT	FT	FT	FT	FT	FT
Ge	-	-	-	-	-	-	-	-
Fe	H	M	MH	H	H	H	M	M
Pb	FT	FT	FT	FT	FT	FT	FT	FT
Li	-	-	-	-	-	-	-	-
Mn	T	FT	L	L	TL	FT	T	T
Hg	-	-	-	-	-	-	-	-
Mo	FT	-	-	-	-	FT	FT	FT
Ni	FT	FT	FT	FT	FT	L	-	FT
Ag	-	-	-	-	-	-	-	-
Ta	-	-	-	-	-	-	-	-
Th	-			-	-	-	-	-
Sn	FT	-	-	-	-	FT	-	-
Ti	T	LM	TL	FT	FT	T	TL	TL
Tn	-	-	-	-	-	-	-	-
U	-			-	-	-	-	-
V	FT	FT	FT	FT	FT	FT	FT	FT
Y	-			-	-	-	-	-
Zn	-			-	-	-	-	-
Zr	T	T	T	T	-	T	-	T

Key

H - 10% plus
MH - 5-15%
M - 1-10%
LM - 0.5-5%
L - 0.1-1%

TL - 0.05-0.5%
T - 0.01-0.1%
FT - $\leq$0.01%

DC Arc
30 element
Data - Onakawana

P_1 - lignite
P_2 - lignite
P_3 - black clay
P_4 - green clay

RCI - red sst/gravel + wood
RP - red sst/gravel (pyrite rich)
PY - pyrite nodule from gravel white
FM1 - soily lignite
FM3 - soily lignite
FM4 - soily/woody lignite
FM6 - woody lignite

TABLE 8 E.S.C.A. DATA FOR WOODY FRAGMENTS AND ASH.

	LIGNITE WOOD 1	LIGNITE WOOD 2	ASHED LIGNITE
Si	0.6	0.9	3.4
S	0.5	-	4.4
Ca	0.3	-	12.7
C	73.7	75.6	27.8
O	24.9	22.8	27.6
Al	-	0.4	9.6
Li	-	-	-
Zn	-	-	-
Cl	-	0.3	-
Fe	-	-	3.7
Mg	-	-	9.7
Na	-	-	1.1

All values in wt %

The lignite analyzed in this study was collected from a coal dump site. Large (5 to 10 kg) samples of woody material were selected for analysis. Small pieces (approximately 1 cm in diameter) of the material were mounted on aluminum studs with high purity carbon paint and subsequently carbon coated. These mounts were examined on an I.S.I. D.S.-130 Scanning Electron Microscope with a P.G.T. System III Energy Dispersive X-ray analyzer.

Iron sulphide (pyrite-marcasite) and calcium sulphate (gypsum) are the only 2 mineral phases found in the samples. The iron sulphide occurs as veinlets filling cracks (Figures 11 to 13), as individual crystals within wood pores (Figure 14), and as replacement pseudomorphs of woody structures (Figure 15). The calcium sulphate occurs as crystal aggregates associated with the iron sulphide (Figure 16). Analyses of smooth, clean crystal faces (energy dispersive spectra accompanying the above figures) exhibit low Bremsstrahlungs (continuums) with well-defined peaks for S and Fe, or S and Ca, for iron sulphide or calcium sulphate, respectively. Small peaks associated with these spectra are probably due to surface contamination. Analyses of woody material (cell wall, Figure 17 and matrix, Figure 18) show high Bremsstrahlungs, typical of organic material, with peaks for Mg, Al, Si, S, K, Ca, and Fe.

The occurrence of mineral matter in coal is well documented in the literature, with iron sulphide and calcium sulphate being among the most common (*see for example*, Gluskoter and Lindahl 1973; Nicholls 1968; Pringle and Bradburn 1958; Rao and Gluskoter 1973). Volume changes during coalification (due to the loss of volatile elements, H, O, C, and N) result in high secondary porosity and permeability, which provide for the large volume of groundwater associated with coal (Freeze and Cherry 1979, and references within).

The veinlets of iron sulphide and associated calcium sulphate, appear to be filling cracks in the woody material which were formed during shrinkage and are therefore post-coalification in age. The individual crystals of iron sulphide found in the wood pores could have formed penecontemporaneously with the accumulation of organic material in the swamp, or epigenetically during, or after,

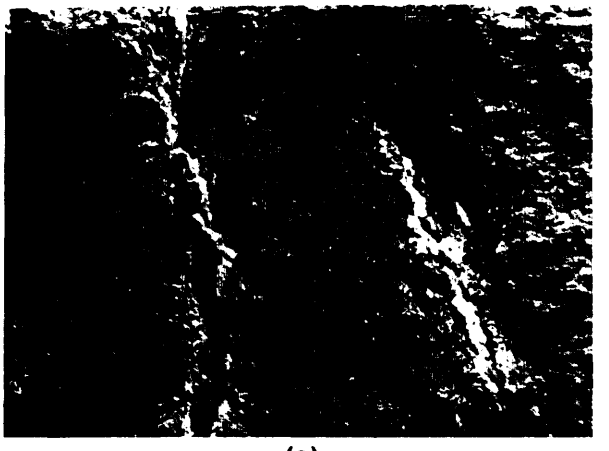

(a)

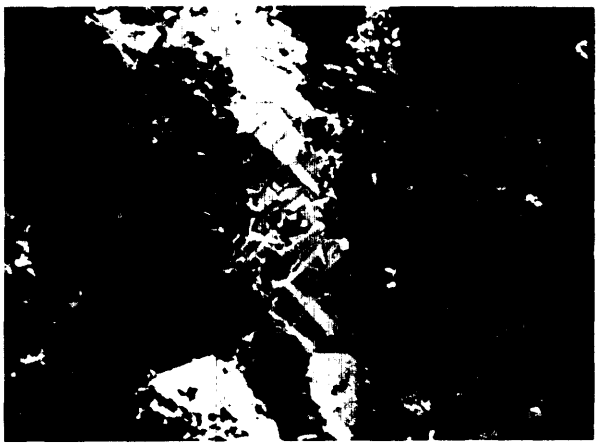

(b)

Figure 11. Photomicrographs of veinlets of iron sulphide lining cracks in woody material (a - 32x; b - 313x).

TABLE 9 NOBLE METALS IN ASH OF LIGNITES (ppb).

	Au	Ru	Rh	Pt	Re	Os	Ir	Pd
RC1	17	<20	<1	<20	<1	<3	0.1	<10
RP	6	<20	<1	<20	<1	<3	0.1	<10
PY	36	<20	<1	<20	1	<3	0.1	10
FM-1	41	<20	<1	80	3	<3	0.1	<10
FM-4	31	<20	1	50	5	<3	0.3	10
P-1	32	<20	<1	<20	<1	<3	0.5	<10
P-2	96	<20	2	35	<1	<3	0.1	250
P-3	55	<20	<1	<20	<1	<3	0.1	10
P-4	8	<20	<1	<20	<1	<3	0.3	<10

Sample code on Table 7.

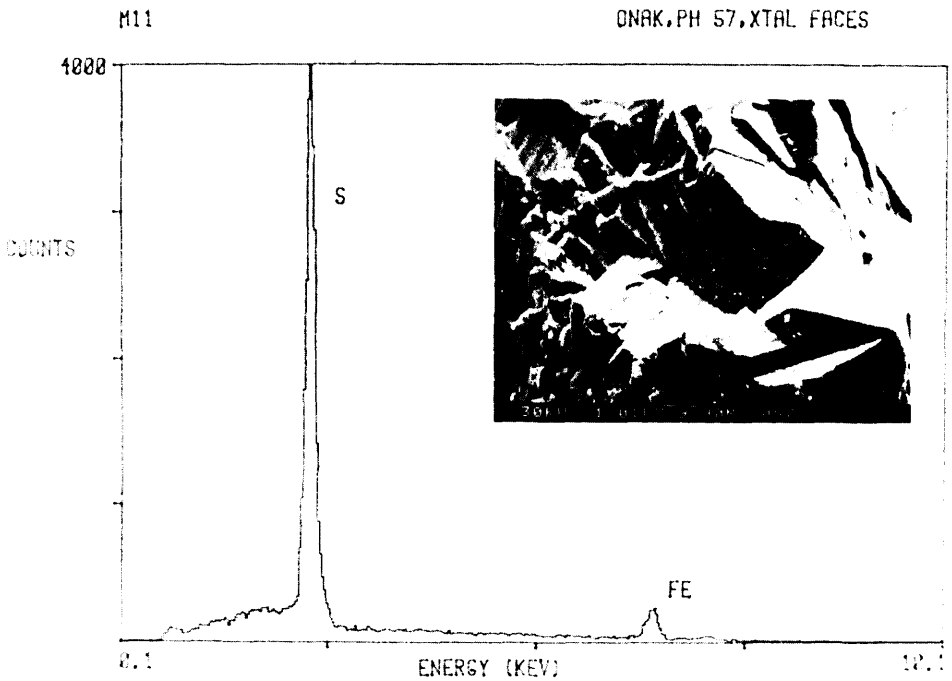

Figure 12. Photomicrograph of iron sulphide crystals in Figure 11b. The spectrum was collected on the crystal faces (1010x).

Figure 13. Photomicrograph of an isolated crystal of iron sulphide growing in the woody material (117x).

coalification. There is no evidence to support either origin. The iron sulphide casts of woody structures must have formed as the plant material was decaying, presumably during the accumulation of material in the swamp. We suspect that sulphate reduction was bacterial.

CONCLUSIONS

From geochemical data so far determined, the Onakawana lignites were formed in an environment of advanced weathering where kaolin-gibbsite materials predominate. Some of the sediments and coals are enriched in detrital zircon and evidence for uranium remobilization and fixation is clear. The coals are anomalous in gold, platinum, and palladium. In general, these are low sulphur coals; but there is evidence for bacterial sulphate reduction, with pyrite even replacing wood structures. In some coals arsenic reaches moderate levels.

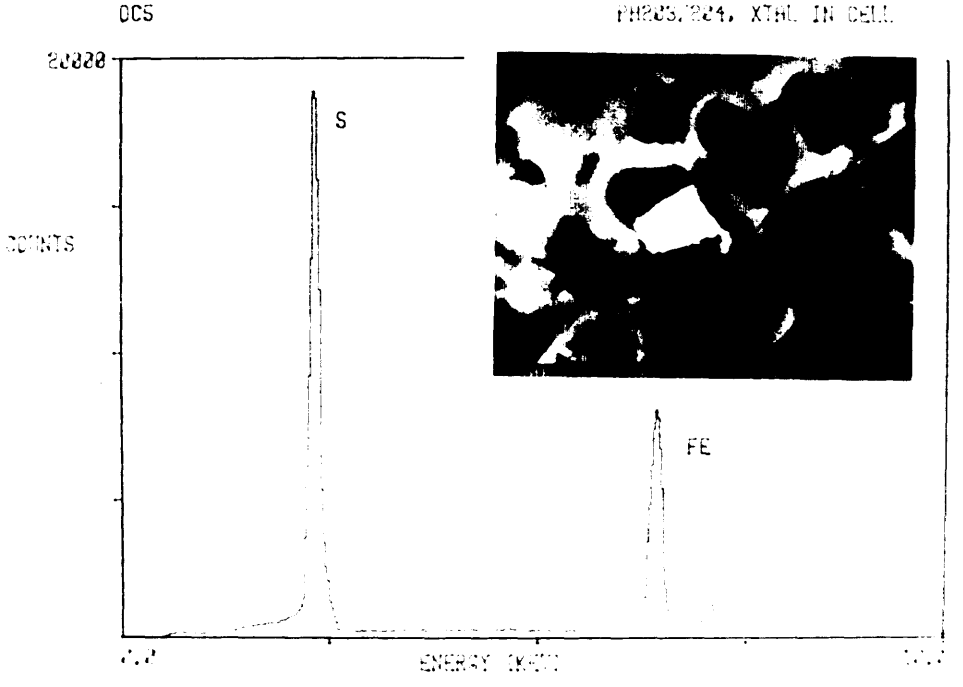

Figure 14. Photomicrograph of an iron sulphide crystal in a cell of the woody material. The spectrum was collected on the surface of the crystal (1200x).

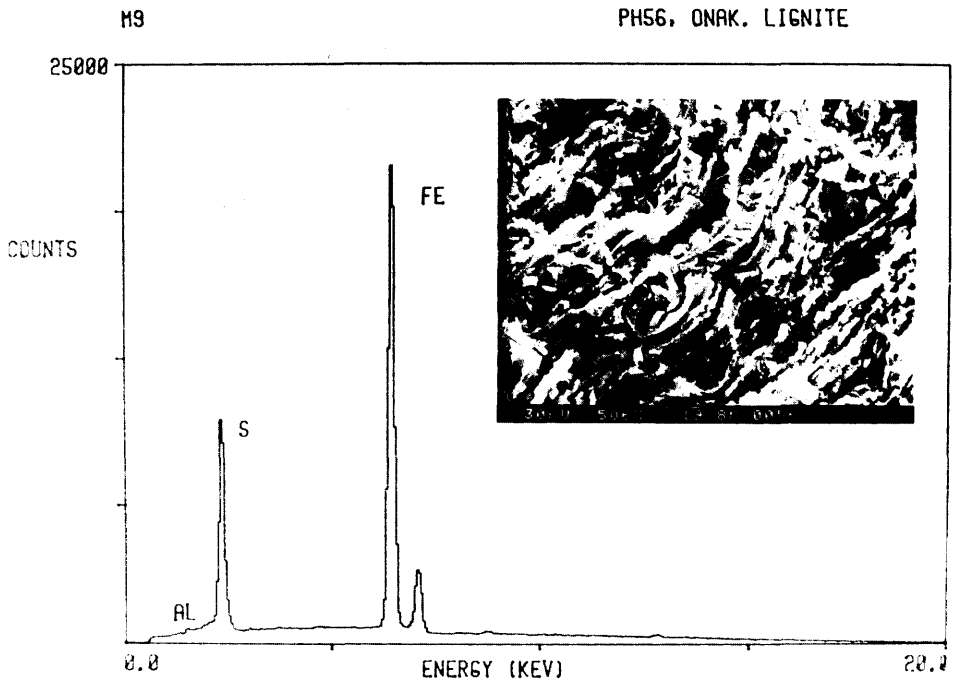

Figure 15. Photomicrograph of convoluted woody structures replaced by iron sulphide (506x).

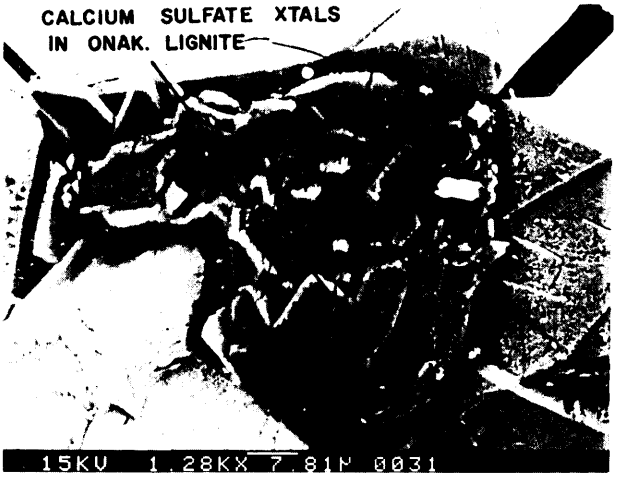

Figure 16. Photomicrograph of calcium sulphate surrounded by iron sulphide (1280x).

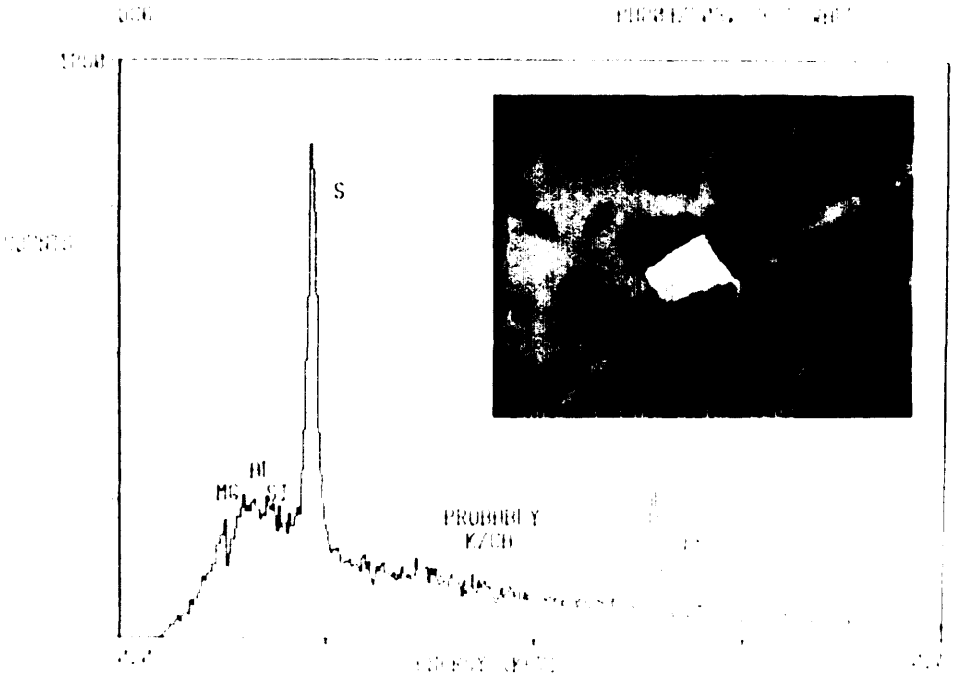

Figure 17. Same photomicrograph as Figure 4. The spectrum was collected on the cell wall adjacent to the iron sulphide crystal. The high Bremsstrahlung and the presence of Mg, Al, Si, K, and Ca are typical of organic material (1190x).

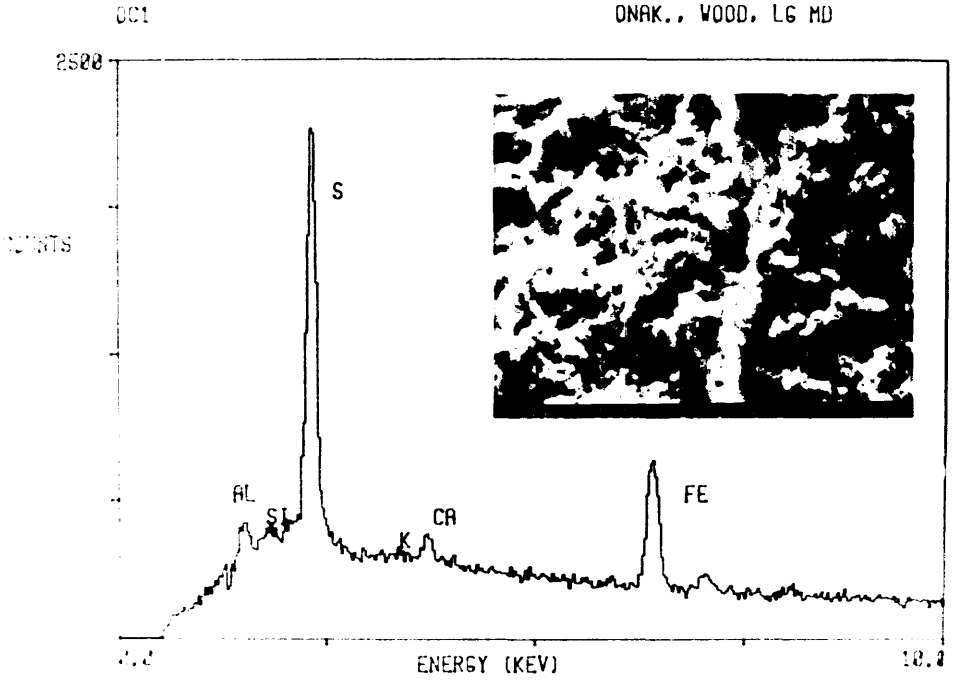

Figure 18. Photomicrograph of woody material to the right of the veinlet in Figure 11b. The high Bremmsstrahlung and the presence of Mg (not labeled), Al, Si, K, and Ca are typical of organic material (387x).

REFERENCES

Freeze, R.A., and Cherry, J.A.
1979: Groundwater; Prentice Hall Incorporated, New Jersey, 604p.

Gluskoter, H.J., and Lindahl, P.C.
1973: Cadmium: Mode of Occurrence in Illinois Coals; Science, Volume 181 (4096), p.264-266.

Goldschmidt, V.M.
1954: Geochemistry; Clarendon Press, Oxford, England, 730p.

Guillet, G.R.
1979: Fossil Fuel Program, Moose River Basin Drilling Project, District of Cochrane; Ontario Geological Survey, Open File Report 5276, 121p., 8 tables, 4 figures, 2 photos, 2 maps.

Hopkins, W.S., and Sweet, A.R.
1976: Miospores and Megaspores from Lower Cretaceous Mattagami Formations of Ontario; Geological Survey of Canada Bulletin 256, p.55-71.

Legault, J.A., and Norris, G.
1982: Palynological Evidence for Recycling of Upper Devonian into Lower Cretaceous of the Moose River Basin, James Bay Lowlands, Ontario; Canadian Journal of Earth Science, Volume 19, p.1-7.

Martison, N.W.
1953: Petroleum Possibilities of the James Bay Lowlands Area; Ontario Department of Mines, Annual Report for 1952, Volume 61, Part 6, p.1-58, map.

Nicholls, G.D.
1968: The Geochemistry of Coal-Bearing Strata; p.267-307 *in* Coal and Coal-Bearing Strata, edited by D.G. Murchison and R.S. Westoll, Oliver and Boyce, Edinburgh and London.

Norris, G., and Dobell, P.
1980: Palynostratigraphic Correlation of Cretaceous Lignitic Strata, Southern Moose River Basin, Ontario; Grant 19, p.179-184 *in* Geoscience Research Grant Program, Summary of Research, 1979-1980, edited by E.G. Pye, Ontario Geological Survey, Miscellaneous Paper 93, 262p.

Norris, G., Telford, P.G., and Vos, M.A.
1976: An Albian Microflora from the Mattagami Formation, James Bay Lowland, Ontario; Canadian Journal of Earth Sciences, Volume 13, p.400-403.

Ontario Geological Survey
1981: Geological Highway Map Northern Ontario; Ontario Geological Survey, Map 2440, scale 1:1 600 000.

Price, L.L.
1978: Mesozoic Deposits of the Hudson Bay Lowlands and Coal Deposits of the Onakawana Area, Ontario; Geological Survey of Canada, Paper 75-13, 39p. 8 figures, 2 maps.

Pringle, W.J.S., and Bradburn, E.
1958: The Mineral Matter in Coal II - The Composition of Carbonate Minerals; Fuel, Volume 37 (2), p.166-180.

Putnam, P.E.
1982: Fluvial Channel Sandstone Within Upper Mannville (Albian) of Lloydminster Area, Canada - Geometry, Petrography, and Paleogeographic Implications; American Associatons of Petroleum Geologists Bulletin, Volume 66, p.436-359, 25 figures, 3 tables.

Rao, C.P., and Gluskoter, H.J.
1973: Occurrence and Distribution of Minerals in Illinois Coals; Illinois State Geological Survey Circular 467, 56p.

Sanford, B.V., Norris, A.W., and Bostock, H.H.
1968: Geology of the Hudson Bay Lowlands (Operation Winisk); Geological Survey of Canada, Paper 67-60, p.1-45, 4 figures, 2 maps.

Stewart, G.A., and MacCallum, G.T.
1978: Athabaska Oil Sands Guidebook; Canadian Society of Petroleum Geologists, 33p.

Telford, P.G., and Verma, H.M. (editors)
1979: Mesozoic Geology and Mineral Potential of the Moose River Basin, District of Cochrane; Ontario Geological Survey, Open File Report 5262, 311p., 6 tables, 38 figures.

Try, C.F., Long, D.G.F., and Winder, C.G.
in press: Sedimentology of the Lower Cretaceous Mattagami Formation, Moose River Basin, James Bay Lowlands, Ontario, Canada; *in* Mesozoic of Middle North America, edited by D.F. Stott, Canadian Society of Petroleum Geologists, Memoir 9.

Williams, G.D., and Stelck, C.R.
1975: Speculations on the Cretaceous Paleogeography of North America; Geological Association of Canada, Special Paper Number 13, p.1-20.

Grant 92 Impact of Groundwater on Surface and Subsurface Mining Activities in the Niagara Escarpment

J.E. Gale[1], R.L. Nadon[2], D.A. McKay[3], and R.A. Sweezey[2]
[1]Department of Earth Science, Memorial University of Newfoundland
[2]Department of Earth Science, University of Waterloo
[3]Ontario Hydro Research Division, Toronto

ABSTRACT

A field, laboratory, and numerical modelling study was undertaken to assess the geotechnical aspects of underground aggregate mining and space development in the Paleozoic rock units of the Niagara Escarpment near Milton, Ontario. Seven holes were drilled at a site next to the Dufferin Quarry, penetrating the Amabel dolostone, the Reynales dolostone, the Cabot Head shale, the Manitoulin limestone, the Whirlpool sandstone, and the top part of the Queenston shale. The results of the hydrogeological studies show no major groundwater problems associated with underground aggregate mining. However groundwater could pose problems for space development in the dolostone cap rock.

This report summarizes the results of the groundwater studies, the rock property measurements, and the in situ stress measurements.

INTRODUCTION

The concept of combining underground aggregate mining and space development within the Paleozoic rock units of the Niagara Escarpment of Southern Ontario has been the subject of much interest in recent years (Procter and Redfern 1974; Acres 1974, 1976; Ontario Mineral Aggregate Working Party 1976). In these reports, underground mining is identified as a possible alternative to aggregate extraction by large scale open pit mining as it is now practiced at several sites along the escarpment. The argument put forward is that underground mining would provide for the protection of the Niagara Escarpment's unique natural environment and at the same time would allow access to a large source of raw material of vital importance to this highly urbanized region.

Although it is more costly to produce aggregate material by underground mining, experience in the Kansas City region (Stauffer 1975) has demonstrated that the economics of underground mining can become very attractive if subsequent use of the mined space for suitable commercial and industrial purposes is introduced. As pointed out by Legget (1978), underground space development in the Hamilton-Niagara area would help slow the rate at which fertile fruitlands are being lost to warehousing and other industrial activity

Another positive factor in the economics of underground space is the energy efficiency of these facilities (McCreath and Mitchell 1978; Stauffer 1975). These authors report on a number of cases where energy savings of 50% to 90% have been achieved by relocating commercial operations such as cold storage facilities in the subsurface.

GEOTECHNICAL CONSIDERATIONS

An evaluation of the technical feasibility of underground aggregate mining and space utilization in the Niagara Escarpment rock units requires data on the engineering properties of the host rockmass and the hydrogeological conditions of the site in question. Previous studies have shown that in the Paleozoic rock units of Southern Ontario, including those making up the Niagara Escarpment, high horizontal stresses present major problems in both surface and subsurface excavations (Palmer and Lo 1976). Rock squeezing due to stress relief has caused cracking of tunnel liners (Bowen *et al.* 1976; Lo and Morton 1976). High horizontal stresses are also considered to be responsible for the formation of pressure ridges observed in the floor of the Dufferin Quarry (White *et al.* 1973). Also, natural erosion of the Niagara Escarpment combined with deformation of the bedrock due to stress relief have created stability problems for the powerhouse and access road at the Sir Adam Beck generating station in Niagara Falls (Carmichael *et al.* 1978).

Although a number of studies have contributed to an understanding of the rock engineering conditions in Southern Ontario, data are required on the hydrogeological conditions, the rock properties, and in situ stress conditions for the rock units in which combined underground mining and space development is considered feasible.

CURRENT STUDY

A field and laboratory study was initiated in May 1980, to provide the information necessary to evaluate the feasibility of underground mining and space development in the Niagara Escarpment rock units. The field work was

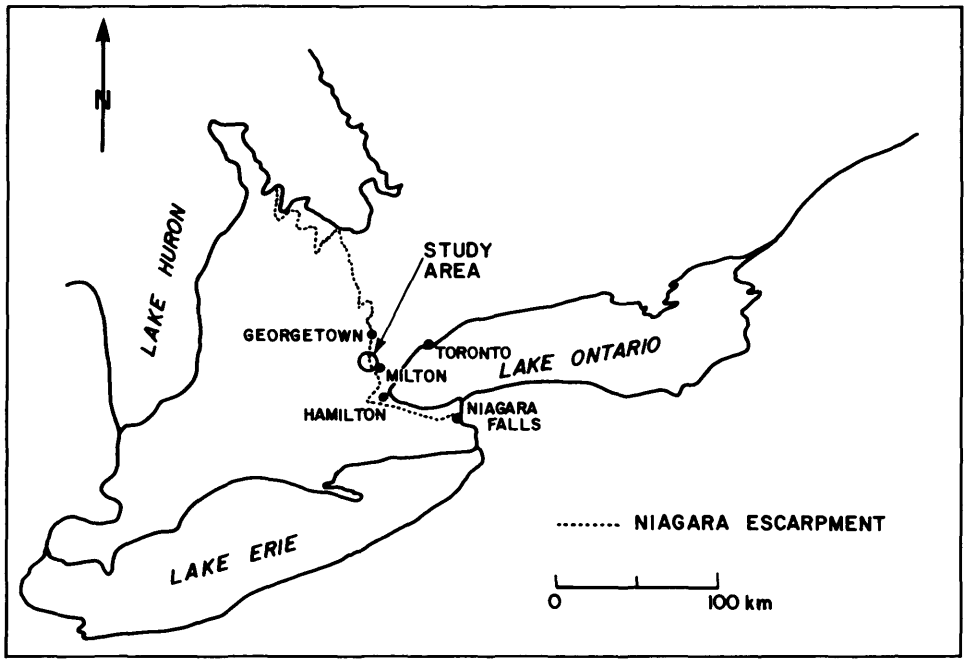

Figure 1. Location of Niagara Escarpment and study area.

carried out at a site on the Niagara Escarpment near Milton, Ontario (Figure 1). The overall project includes an assessment of both the engineering properties of the bedrock units as well as the groundwater conditions at this site. The results of the hydrogeological study have been presented by Nadon and Gale (1983) and are summarized in this report. In the second part of this report, the data collected on the engineering properties of the bedrock units and the results of the in situ stress measurement program are presented.

The test site is located on the Niagara Escarpment between the Dufferin Quarry and the Indusmin Quarry (Figure 2). Five boreholes, DQ-1 to DQ-5, were drilled for the hydrogeological component of this study. The orientation, length, and diameter of the holes are given in Table 1. Three of the boreholes (DQ-1, DQ-2, DQ-5) were diamond drilled and hence provided core samples from the geologic units intersected.

GEOLOGIC SETTING

The Niagara Escarpment is an erosional feature within the geologic structure known as the Michigan Basin. The cap rock of the escarpment is a massive, resistant bed of dolostone which overlies a sequence of thinner shale, limestone, and sandstone beds (Figure 3). This cap rock unit outcrops frequently at the test site with only thin accumulations of surficial materials, consisting mostly of sand and gravel, found in bedrock depressions.

At the test site, the cap rock, which includes the Amabel and Reynales Formations, has a total thickness of about 26 m and is characterized mostly by massive beds, light grey-buff in colour, and composed primarily of fine to medium crystalline dolomite (Figure 4). The beds are highly fossiliferous, composed largely of bioclastic material, which produces in a few layers a highly porous rock matrix. For the most part, the dolostone rock mass is fairly dense and is dissected by frequent horizontal bedding discontinuities and more widely spaced vertical and subvertical fractures. Outcrop and borehole surveys have shown that these fractures have 2 preferred orientations, east-northeast and east-southeast (Nadon and Gale 1983).

Underlying the cap rock is the Cabot Head Formation, which is 18.5 m thick and consists predominantly of grey-green, finely laminated shale. In several locations, the shale is very soft, approaching the consistency of a plastic clay.

At the base of the Cabot Head Formation, the soft shale becomes increasingly calcareous to a point where the rock is more suitably called argillaceous limestone. This somewhat arbitrary point is considered the upper contact of the Manitoulin Formation. The Manitoulin Formation is 5.7 m thick and consists of fine crystalline, argillaceous, dolomitic limestone beds, 50 mm to 600 mm in

TABLE 1 DATA ON TEST BOREHOLES.

BOREHOLE	ORIENTATION BEARING	PLUNGE	LENGTH (m)	DIAMETER (mm)	DRILLING METHOD
DQ – 1	–	90°	55.0	76	DIAMOND CORE
DQ – 2	–	90°	61.0	127	TRICONE
DQ – 3	–	90°	51.3	76	DIAMOND CORE
DQ – 4	–	90°	27.4	203	TRICONE
DQ – 5	309°	52°	76.4	76	DIAMOND CORE

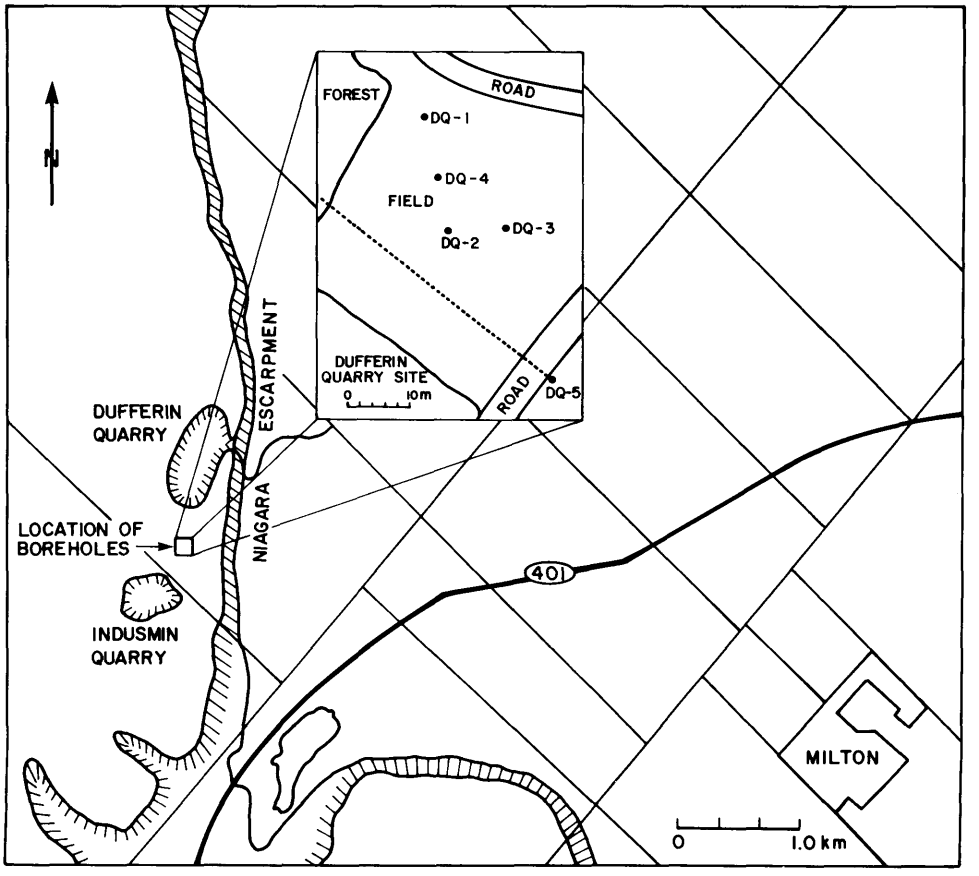

Figure 2. Location of test site and boreholes.

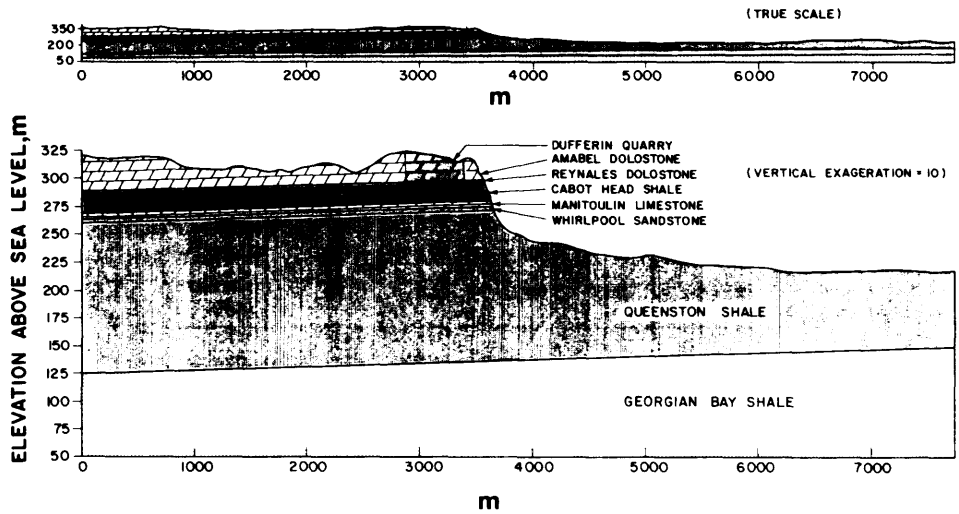

Figure 3. Vertical cross-section through the Niagara Escarpment.

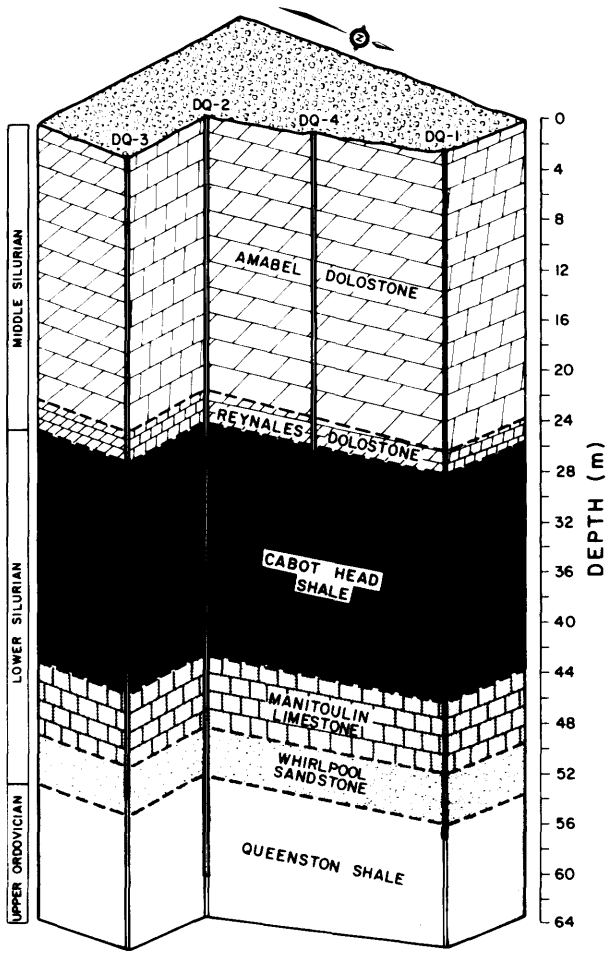

Figure 4. Geologic section through boreholes at test site.

thickness, separated by several thin shale beds. The Manitoulin limestone is underlain by the 4 m thick Whirlpool Formation. This formation is a thick bedded, light brown-grey, fine grained, well sorted, quartz sandstone. Very thin, dark grey to black shale seams occur throughout this sandstone. Few natural fractures were found in the sandstone drillcores although some vertical and horizontal fractures (Nadon and Gale 1983) were found in an exposure near the Indusmin Quarry. Vertical fractures in the Whirlpool sandstone were observed to be spaced up to 5 m apart. The wide spacing of the vertical fractures could explain why none were intersected in the boreholes at the test site.

The Queenstone shale, over 130 m thick in the Milton region (Bolton 1957), underlies the Whirlpool sandstone. Only the top 7 m of the Queenston Formation, consisting mostly of dark red, hematitic, calcareous shale, interbedded with very finely crystalline, grey-green, highly argillaceous limestone, were intersected by the boreholes at the test site.

GROUNDWATER CONDITIONS

Due to the presence of thick shale formations within the Niagara Escarpment, the potential of underground mining for aggregate production and space development is limited to 2 specific zones. One zone is located at the base of the Amabel dolostone cap rock and the other is located within the Whirlpool sandstone and Manitoulin limestone formations. The hydrogeological characteristics of these 2 zones and the adjacent bedrock units have been determined from a series of borehole packer injec-

tion tests, pumping out tests, and laboratory tests. As shown in Figure 5, the packer injection tests gave relatively high hydraulic conductivity values, ranging from 10^{-7} to 10^{-5} m/s, in the dolostone cap rock; low values, ranging from 10^{-11} to 10^{-9} m/s, for the Cabot Head shale and Manitoulin limestone; and intermediate values in the range of 10^{-7} to 10^{-6} m/s in the Whirlpool sandstone and the upper few metres of the Queenston shale (Nadon and Gale 1983).

Based on a knowledge of the hydrogeological properties of each rock type in the Niagara Escarpment and from field observations made in the study area, a conceptual model of the groundwater flow system was developed (Figure 6). Over most of the study area, infiltration of water into the dolostone cap rock unit occurs rapidly. The water, which infiltrates into the saturated portion of the dolostone cap rock, is confined by the underlying Cabot Head shale and thus flows horizontally towards the Escarpment where it discharges, forming several springs located along the contact of the dolostone and shale formations. The Whirlpool sandstone and the top few metres of the Queenston shale are the only other rocks at the test site in which significant groundwater flow occurs. These formations are confined above by the Cabot Head-Mani-

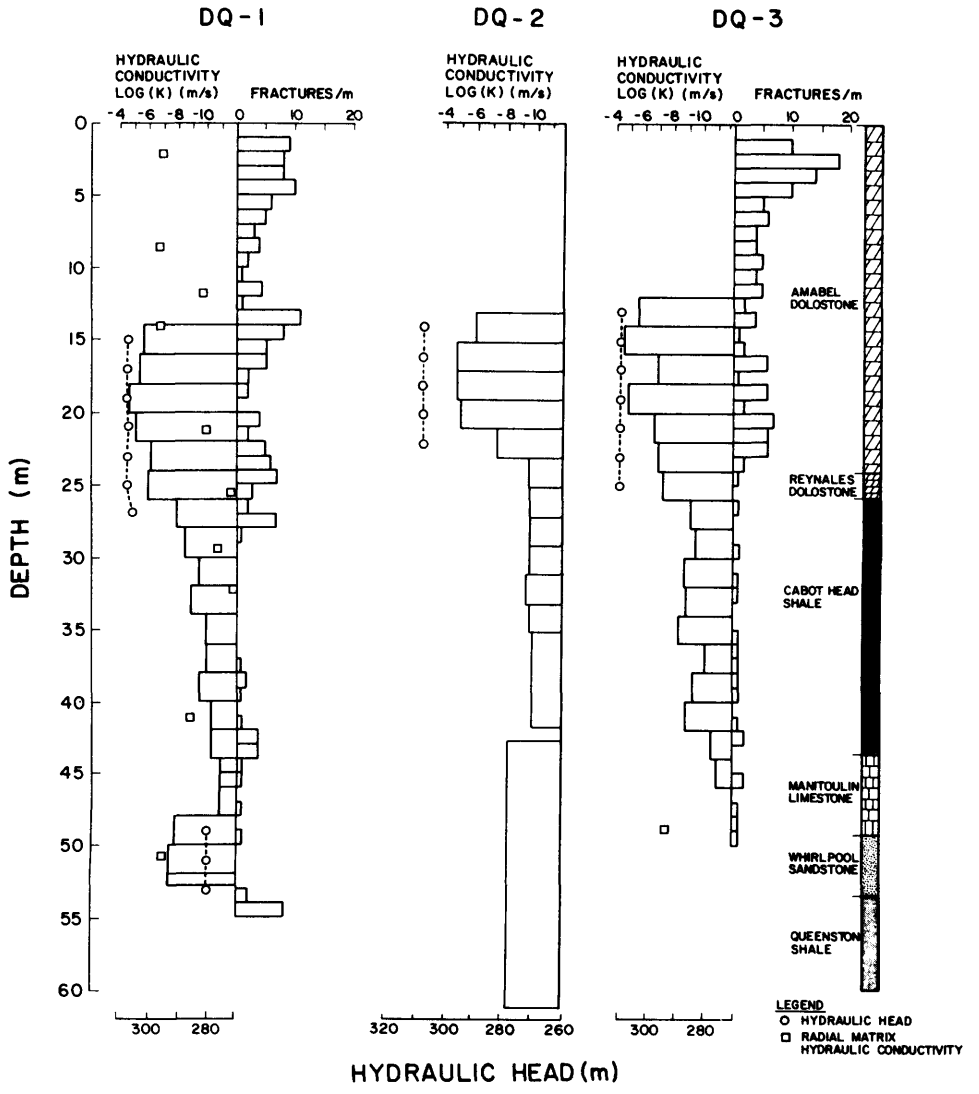

Figure 5. Borehole injection test results, hydraulic conductivity data from laboratory tests on drill core, hydraulic head data, and fracture histrogram for DQ-1, DQ-2, and DQ-3.

toulin unit and below by the Queenston shale. The only source of recharge is downward leakage of groundwater from the dolostone cap rock through the Cabot Head-Manitoulin unit. The unusually high vertical hydraulic gradient which exists across this unit is proof of its low permeability and of its ability to isolate hydraulically the dolostone and sandstone aquifers. From the limited hydraulic head data (Figure 5) available, it appears that the direction of flow is easterly towards the Escarpment.

Based on the conceptual model given in Figure 6, a 2-dimensional finite element model, incorporating the measured hydrogeological properties, was used to calculate the rate of groundwater seepage and the resulting extent of rock mass dewatering for a hypothetical underground mine located within the cap rock and within the Manitoulin-Whirlpool unit. The finite element grid used for groundwater flow simulations in both of these zones is shown in Figure 7. Figure 8 indicates the extent of dewatering in the cap rock unit produced by a hypothetical underground mine about 2 square miles in area. Details of the model simulations are given in Nadon and Gale (1983).

The recharge characteristics and the relatively high permeability of the dolostone cap rock means that considerable inflow of groundwater into underground excavations would be anticipated. For a mine with a floor area in the order of 2 km^2, average inflows as high as 30 to 50 L/s should be anticipated. It is conceivable that, for an extensive underground mine, a suitable layout of trenches could be constructed in order to provide gravity drainage, thus avoiding major pumping expenses. Based on the modelling results, extensive dewatering of the unconfined dolostone acquifer would be restricted to an area located within 1000 m to 2000 m of an underground mine. Therefore, groundwater drainage into a mine could adversely affect nearby shallow wells. However, on a regional scale, no interference problems should be encountered.

For the purpose of underground space development, mining within the Whirlpool sandstone and Manitoulin limestone formations is clearly more desirable than in the Amabel dolostone formation. The low permeability shale units located above and below effectively seal the Whirlpool and Manitoulin Formations from major groundwater movement. The small volume of groundwater that would seep into a mine could be handled with proper ventilation of the rooms.

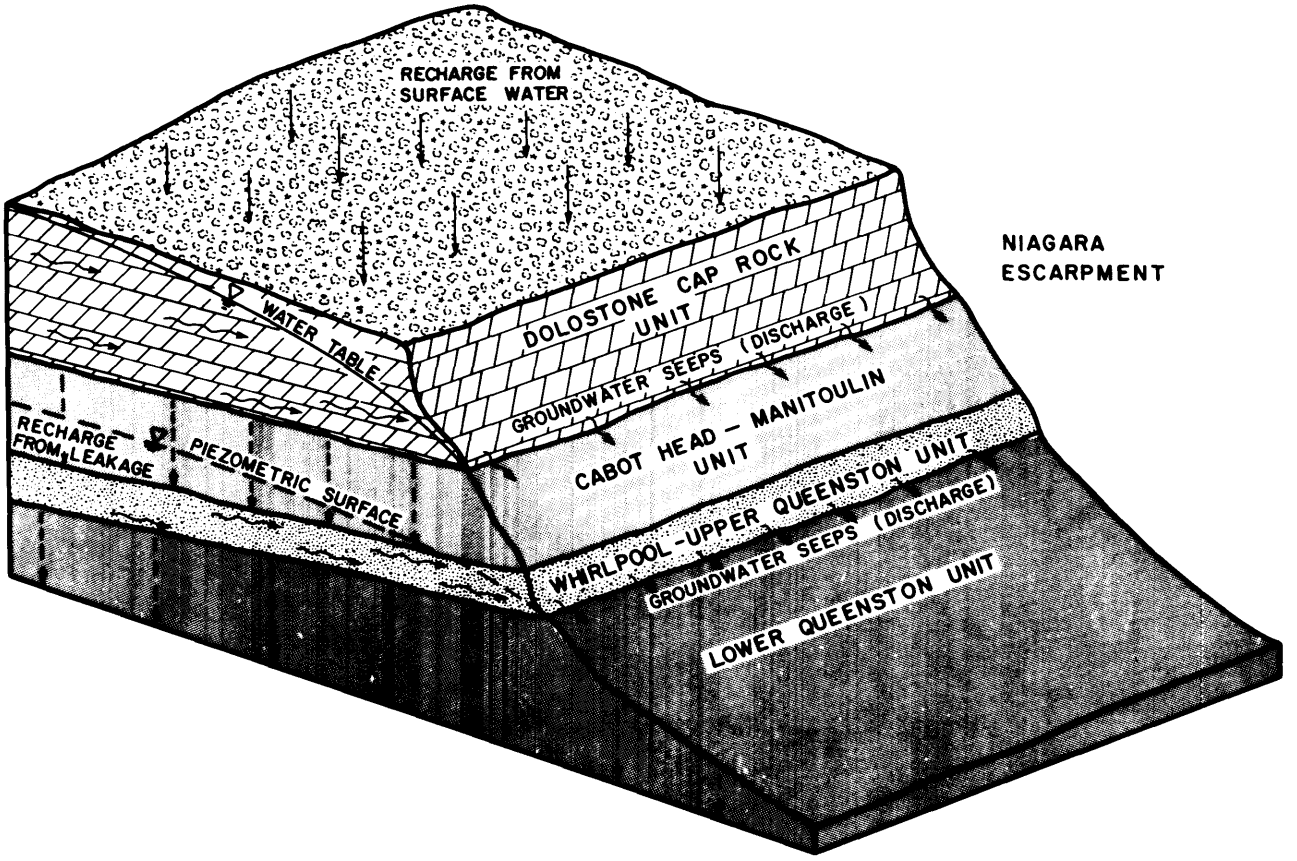

Figure 6. Idealized groundwater flow system for study area.

ROCK PROPERTIES

Rock properties were determined from drillcore samples. Index tests on core samples of the Whirlpool sandstone included 11 uniaxial compression tests, 3 direct tension tests, 5 Brazilian tests, 8 bending tests, and 4 triaxial tests. Both uniaxial compression tests, direct tension tests, and Brazilian tests were performed on sections of drillcore from the cap rock. An obvious concern for mining within the upper or lower zones is the presence of a deformable shale unit below the main cap rock unit and both above and below the Manitoulin-Whirlpool unit. Hence a considerable effort was devoted to determining the geotechnical properties of the Cabot Head and Queenston shales. In addition to the standard index tests, 26 slake durability tests, giving a mean value of 68, were carried out on the Cabot Head shale and 28 slake durability tests, with a mean value of 69, were carried out on sections of the Queenston shale. The same number of direct shear tests were carried out on each of the shale units. These test results will be presented in the final report on this project.

IN SITU STRESS MEASUREMENTS

The high horizontal stresses that exist in the sedimentary rock units of Southern Ontario (White *et al.* 1973) are a

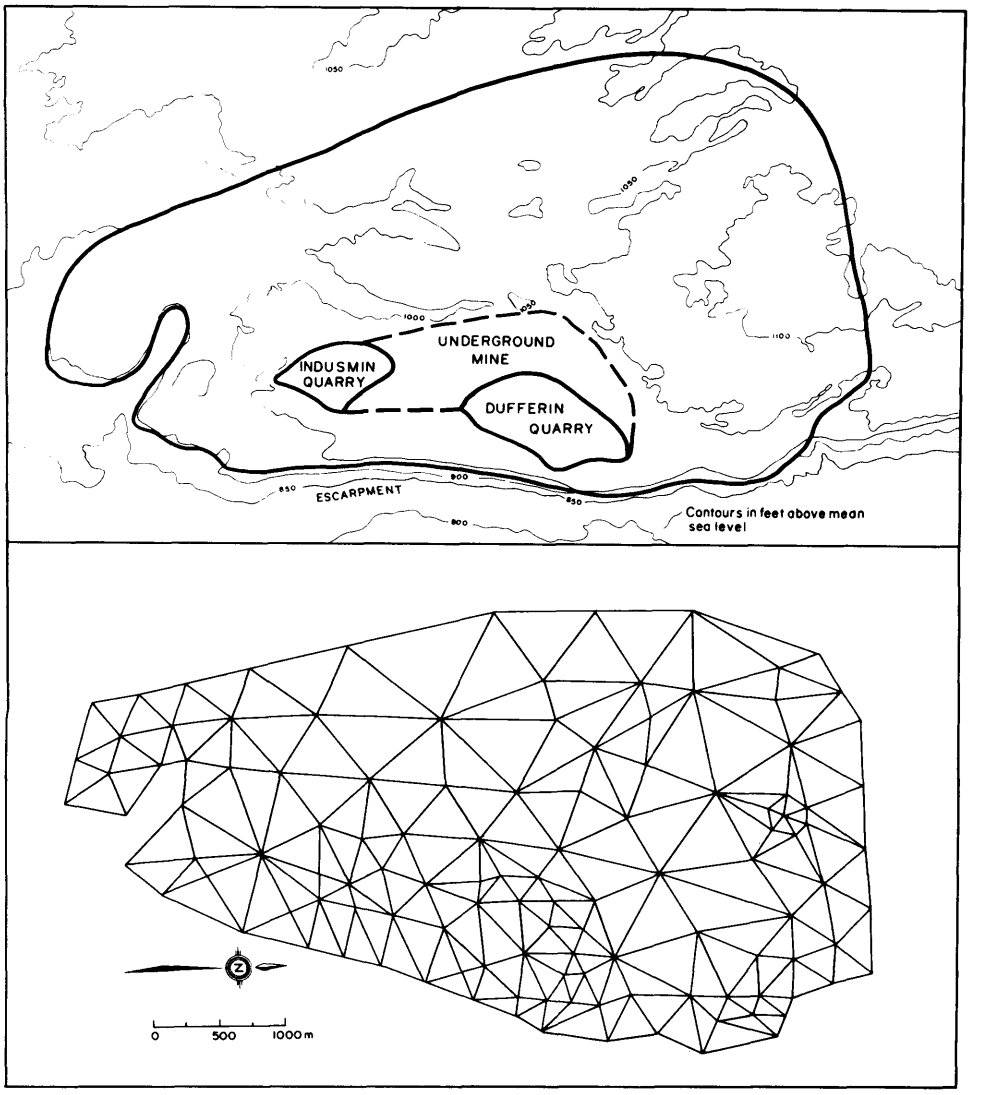

Figure 7. Region of study and finite element grid.

matter of concern to both underground aggregate mining and space development. The floor instability or pop-up structures that have occurred within the Dufferin Quarry indicate the presence of such high horizontal stresses. Given the deformable nature of the shale units that would form the floor and or roof in either of the 2 potential mining horizons, an attempt was made to determine the magnitude and orientation of the stresses existing within the rock mass. During the 1982 field season, in situ stress measurements were carried out at the Dufferin Quarry using professional and equipment resources from both the University of Waterloo and Ontario Hydro Research Division. The in situ stress measurements were made in 2 boreholes using the "USBM gauge method".

The USBM gauge method consists of drilling an HQ diamond corehole (96.0 mm in diameter) to the depth at which a stress measurement is required. At the bottom of this HQ borehole, an EX hole (37.7 mm in diameter) approximately 0.60 m in length is drilled. The USBM gauge is then placed in the EX hole and overcored using a thin wall bit. The strain-gauged, cantilevered arms of the USBM gauge fit tightly against the walls of the EX borehole and are used to monitor the change in diameter of the overcored rock cylinder as it is removed from its in situ stress condition. This rock cyclinder is then reloaded in the laboratory using a biaxial cell system and the Young's modulus of the core determined. Details of the testing procedure used at the Dufferin Quarry are given in McKay (1982).

One of the in situ stress measurement boreholes, DQ-6, was drilled within a few metres of borehole DQ-1, outside the quarry, and the second borehole, DQ-7, was drilled from the main quarry floor. DQ-6 was drilled to a depth of 10.41 m in the dolostone cap rock and 3 stress measurements, at 6.12, 9.50, and 9.60 m depth, were completed. DQ-7 was drilled to a depth 31.17 m, penetrating the Reynales limestone-dolostone, the Cabot Head shale, the Manitoulin Formation, and the top part of the Whirlpool Formation. Overcoring tests were carried out at 24.53 and 24.81 m in the Manitoulin limestone, and at 30.51 and 30.81 m in the Whirlpool sandstone. Results of the individual stress measurements have been tabulated by McKay (1982) and are presented in Table 2. The major horizontal stresses ranged from 7.06 MPa to 10.84 MPa in compression. The major stress orientation varies from N32E to N62E.

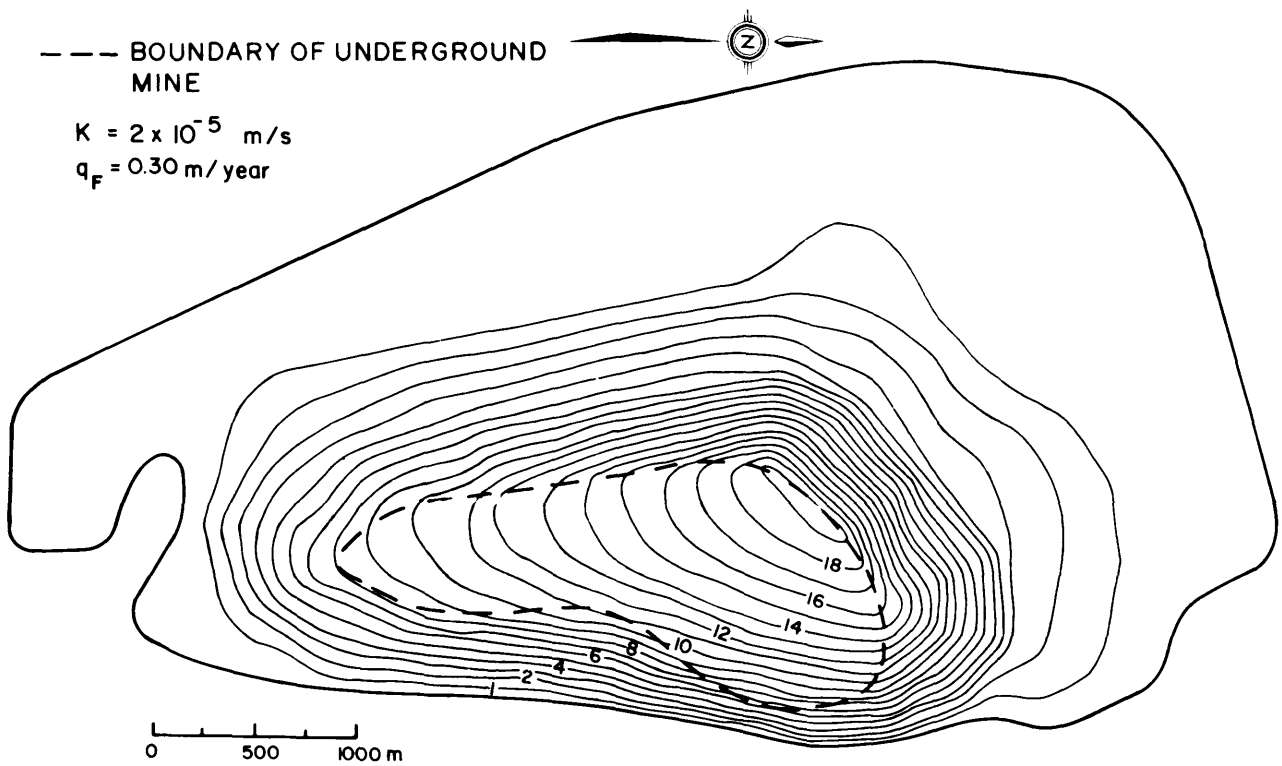

Figure 8. Extent of dewatering, relative to natural hydraulic head, in the Amabel dolostone caused by drainage into an underground mine.

TABLE 2 RESULTS OF IN SITU STRESS MEASUREMENTS.

Borehole	Test	Depth m	Rock Type	P MPa	Q MPa	Azimuth	Young's Modulus MPa
DQ6	1	6.12	Dolostone	8.16	2.41	32	36838
	2	9.50	Dolostone	0.044	-0.82	38	48119
	3	9.61	Dolostone	1.35	0.59	98	48119
DQ7	1	24.53	Shaley Limestone Dolostone	9.09	0.14	242	37703
	2	24.81	Shaley Limestone Dolostone	7.06	0.21	212	37703
	3	30.51	Sandstone	10.84	4.44	215	27083
	4	30.81	Sandstone	NO	TEST		

FUTURE OBJECTIVES

In the final report on this project, the rock property data and the in situ stress data will be analyzed to provide a preliminary assessment of the overall stability of each of the rock units to potential mining operations.

ACKNOWLEDGMENTS

The in situ stress measurements for this project were carried out as a joint effort of the grant program at the University of Waterloo and Ontario Hydro Research Division. Special thanks are extended to Doug Wilson and the staff of Dufferin Materials and Construction Limited for their generous assistance and cooperation during testing at the Dufferin Quarry site. The interest and encouragement provided by Dr. R. Legget during this study is greatly appreciated.

REFERENCES

Acres Consulting Services Limited
1974: Underground Space Utilization; Acres Research and Development Report, (Internal).

1976: Underground Aggregate Mining Preliminary Feasibility Study; Ministry of Treasury, Economics and Intergovernmental Affairs, Niagara Escarpment Commission.

Bolton, T.E.
1957: Silurian Stratigraphy and Paleontology of the Niagara Escarpment in Ontario; Geological Survey of Canada, Memoir 289, 145p.

Bowen, C.F.P., Hewson, F.I., Macdonald, D.H., and Tanner, R.G.
1976: Rock Squeeze at Thorold Tunnel; Canadian Geotechnical Journal, Volume 13, p.111.

Carmichael, T.J., Gorman, G., McKay, D., and Krajewski, J.
1978: Engineering Geology at Niagara Hydroelectric Plants; p.93-102 *in* Field Trip Guidebook, edited by A.L. Currie and W.O. MacKassey, Joint Annual Meeting of Geological Survey America, Geological Association of Canada, Mineralogical Association of Canada, Toronto.

Legget, R.
1978: Energy, Geology and the Underground; Geoscience Canada, Volume 5, Number 3, p.119-123.

Lo, K.Y., and Morton, J.D.
1976: Tunnels in Bedded Rock with High Horizontal Stresses, Canadian Geotechnical Journal, Volume 13, p.216.

McKay, D.A.
1982: In Situ Stress Measurements at the Dufferin Quarry; Ontario Hydro Research Division Report, File Number 844.33.

McCreath, D.R., and Mitchell, D.E.
1978: Build Underground and Conserve Energy: Fact or Fiction; Engineering Journal, Volume 61, Number 2, p.14-16.

Nadon, R.N., and Gale, J.E.
1983: Impact of Groundwater on Mining and Underground Space Development in the Niagara Escarpment Area; Canadian Geotechnical Journal (in press).

Ontario Mineral Aggregate Working Party
1976: A Policy for Mineral Aggregate Resource Management in Ontario; Ontario Ministry of Natural Resources.

Palmer, J.H.L., and Lo, K.Y.
1976: In Situ Stress Measurements in Some Near-Surface Rock Formations Thorold, Ontario; Canadian Geotechnical Journal, Volume 13, p.1.

Proctor and Redfern
1974: Towards the Year 2000 - A Study of Mineral Aggregate in Central Ontario; Ontario Ministry of Natural Resources.

Stauffer, Sr., T.
1975: Kansas City: A Model of Underground Development; Paper Presented at the Seminar - The New Industrial Space - Queen's Park, Toronto, Ontario.

White, O.L., Karrow, P.F., and Macdonald, J.R.
1973: Residual Stress Relief Phenomena in Southern Ontario; Proceedings, 9th Canadian Rock Mechanics Symposium, Montreal, p.323-348.

Grant 128 Subsurface Quaternary Stratigraphy Using Borehole Geophysics

J.P. Greenhouse, P.F. Karrow, and R.N. Farvolden
Department of Earth Sciences, University of Waterloo

ABSTRACT

This project has been undertaken in order to improve the resolution and usefulness of borehole geophysics in deciphering the Quaternary stratigraphy of the Kitchener-Waterloo area. In the fall of 1982, 3 holes were rotary-drilled to bedrock, at intervals of about 1.6 km, along a transect heading southwest from the extensively drilled Greenbrook well field and ending near Homer Watson Park. The holes were geophysically logged, then cased with a 10.2 cm (O.D.) PVC casing, and relogged. A continuously-cored hole was then completed to bedrock beside one of these holes, providing an in situ lithological calibration for the geophysical logs. Further calibration has been undertaken using specially prepared barrels.

The analysis and correlation of these geophysical and geological data sets will continue through 1983-1984. Preliminary results show a good visual identification of the Catfish Creek/Maryhill Till boundary.

INTRODUCTION

Kitchener-Waterloo is typical of cities of southern Ontario in that the Quaternary geology is an important factor in many commercial enterprises. Mining of aggregate, limestone, and clay are important industries. Drainage and foundation conditions plague engineers in both the public and private sectors. The location of sites for landfill disposal of wastes hinges on good geological data, and the groundwater resources of the region are as heavily developed as any in Canada.

In spite of this, the subsurface geology of the region is not well enough known, so the site stratigraphy cannot be predicted. Nor can target horizons be extrapolated beyond test sites—the stratigraphic relationships among units and the distribution of units are poorly understood. A case in point is the Quaternary section on the eastern (urbanized) side of the Waterloo Moraine. Normal drilling (for well development, foundations, etc.) has provided abundant data, but attempts to use these data for subsurface correlation have been disappointing, and we anticipate little progress in the future if we are to rely solely on these methods. Continuous coring is, needless to say, very expensive.

On the other hand, geophysical logging of boreholes in the area has shown promise as a means of correlating these deposits. The Department of Earth Sciences, University of Waterloo, has geophysically logged boreholes throughout the area since 1974, as they became available. The logs were digitally recorded and stored, but no systematic attempt to correlate them to stratigraphy has been made.

This project has as its first objective the careful analysis of the correlation between geophysical logs and adjacent lithology and stratigraphy, with the intention of developing the logging as a useable tool for further exploration of the area geology. As originally proposed, 3 to 4 rotary-drilled and geophysically-logged holes would be completed to bedrock, each year of the 3-year project, with at least 1 continuously-cored hole placed adjacent to a logged hole as a standard. The geophysical log to core correlation will attempt to: (1) recognize stratigraphic sequences on the basis of simple pattern matching (visual or statistical); (2) predict density, porosity, clay content and other physical properties from the suite of geophysical responses; and (3) recognize individual stratigraphic units on the basis of their range of tool responses.

In many ways, we are attempting no more than the modification of long-existing oil industry technology for use in the unconsolidated sediments of southwestern Ontario. That this has not been frequently attempted before reflects the lesser economic importance of the overburden. This attitude is changing, however, as population pressures force us to understand the surficial geology better.

PROGRESS, 1982-1983

Drilling began in late August, and as a result the project has been underway only 8½ months at the time of writing.

FIELD WORK

Three boreholes were rotary drilled to bedrock, which was encountered between 49 and 67 m (160 and 220 feet) below surface. The holes were drilled with a heavy bentonite mud, and in 2 cases redrilled to stabilize the borehole wall prior to logging. The uncased holes were logged with 16-inch normal, 64-inch normal, SP, natural gamma, neutron, and caliper logs, then cased with 0.102 m (O.D.) PVC pipe. The cased holes were then filled with fresh water and relogged with natural gamma and neutron tools, and logged with the gamma-gamma (density) tool. The holes were capped, and thus made

available for repeated logging later. The casing provides a standardized environment for logging each hole, thereby allowing a fair comparison of logs from different boreholes. The variability of borehole conditions in uncased holes in unconsolidated materials makes this standardization necessary. The 3 holes are spaced about 1.6 km apart, and extend along a traverse from the centre of the Greenbrook well field to Homer Watson Park.

A continuously-cored hole was completed immediately adjacent to one of the logged holes, GB3-82. A second logged hole, GB1-82, is situated less than 200 m from a thick exposed section on the western bank of the Grand River at Homer Watson Park. A continuously-cored hole was completed to bedrock on the opposite (and lower) bank of the river to complete the stratigraphy below the exposure. This is a less-than-ideal but useable standard against which to calibrate the geophysical logs at GB1-82.

DATA PROCESSING

To improve the reliability and turnaround time for the digital logging records, we have replaced our old cassette recorders with the CBM 8032 microcomputer and associated double disk drive. The microcomputer logs the data and prompts the operator, and, while there have been "start-up" problems, this system now appears to be functioning as intended. The logged data are sent by telephone line to the IBM 4341 at University of Waterloo for plotting and storage, usually on the day they are recorded.

CALIBRATION

Apart from the core/log comparison, we have attempted over the winter to calibrate the density, neutron, and natural gamma tools in a range of materials using the 0.102 m OD water-filled casing in 45 gallon drums. The drum materials included water, dry sand, wet sand, clay, 2 clay-sand mixtures, and cement. The density, porosity, and clay content were obtained independently in each case and plotted against the tool response. This procedure can not simulate the response of a particular stratigraphic unit (such as the Catfish Creek Till) but it does calibrate for physical properties in the cased borehole environment chosen for the field sites.

These preliminary attempts at calibration were reasonably successful but not as definitive as we believe they could be. We intend to improve our technique during the summer of 1983 (see below).

ANALYSIS

The limited amount of data obtained, and the short time available for its analysis, preclude our drawing any major conclusions from the work to date.

One rudimentary but nevertheless rather useful result is worth noting. Despite many logs having been obtained throughout the southwestern Ontario region over the years, we had not heretofore recognized a distinctive and quite ubiquitous pattern on E logs and neutron logs arising from the upper Catfish Creek Till boundary. Based on the 1982, data we are now able to see this pattern in most of our previous logs and this in itself provides a useful stratigraphic tie for the accumulated well log data.

This pattern, its usefulness, and the general correlation problem we face can perhaps be made clearer in a discussion of the neutron logs shown in Figure 1. The left hand log, GB3-82, was recorded in an uncased borehole immediately adjacent to a continuously-cored borehole. The Maryhill Till, a clay till, shows up characteristically as a zone of low epithermal neutron counts because of the neutron thermalization and absorption by the water in the clay. The Catfish Creek Till below has a comparatively low clay content, and a strong contrast with the Maryhill Till. The base of the Catfish Creek Till is not clearly defined in the cores, but the neutron response typically decays slowly with depth below a 3 to 5 m plateau at the upper boundary.

The right-hand neutron log was recorded in a cased hole at GB2-82, about 1.5 km from GB3-82. No cores are available. The "dog-eared" plateau and drop at the upper boundary of the Catfish Creek Till are readily identifiable, and confirmed by the drillers log (the Catfish Creek Till being hard to drill). This boundary becomes more obvious the more logs one examines.

No other correlatable boundaries are obvious in these 2 logs, but we hope that with experience some similar feature of the pre-Catfish Creek tills may become apparent.

On cannot identify similar units in the 2 logs by actual count levels because the logs are not recorded in the same environment (cased and uncased). When the cased-hole log for GB3-82 is available, the level of the response can be used in matching the 2 patterns.

Finally, one can ask if the Maryhill Till is present at GB2-82. At first glance it would seem to be missing and the response immediately above the Catfish Creek Till at GB2-82 is a better match to that occurring immediately above the Maryhill Till at GB3-82. Until we have some idea of the range of responses in the Maryhill Till, however, we cannot make this judgement. This emphasizes the importance of the stratigraphic calibrations.

FUTURE OBJECTIVES, 1983-1984

A cutback in funding for 1983-1984 will delay the implementation of the second traverse from the Greenbrook well field to the north. Instead, we plan to concentrate on answering the questions raised by the example in Figure 1, namely, how to calibrate responses to stratigraphy and lithology. Our approach, point by point, is as follows:

1. We will relog the existing cased holes many times to establish the variability inherent in a single pass of the borehole, and to experiment with water-filled and dry casings.
2. The "barrel" calibrations will be repeated with larger containers and with better control on the properties of their contents. Properly done, these should allow field logs to be plotted directly in terms of density, apparent porosity, and clay content.
3. We intend to establish in situ calibrations in several shallow boreholes intersecting the prominent tills of the area. This should supplement the core data at GB3-82 and establish the mean and, most importantly, the variability of the physical properties of these tills. This information is vital to any attempt to identify a unit on the basis of its log responses.
4. Two- and three-dimensional cross-plots of the log data will be undertaken to see if the lithology and/or the stratigraphic units can be identified by their position in "response space" as defined by the in situ and core calibrations.
5. We have made arrangments with Pat Killeen of the Geological Survey of Canada, Ottawa, to complete gamma spectroscopy logs of the 3 boreholes this summer, in order to evaluate these responses in "fingerprinting" the stratigraphic units.
6. We have made tentative arrangements with Det Blohm of IFG for a magnetic susceptibility tool to be run in the 3 cased holes this fall. Again, the objective is to evaluate its response as a means of identifying stratigraphy.
7. The results are to be presented at the International Symposium on Borehole Geophysics to be held at the University of Toronto, August 29-31, 1983.

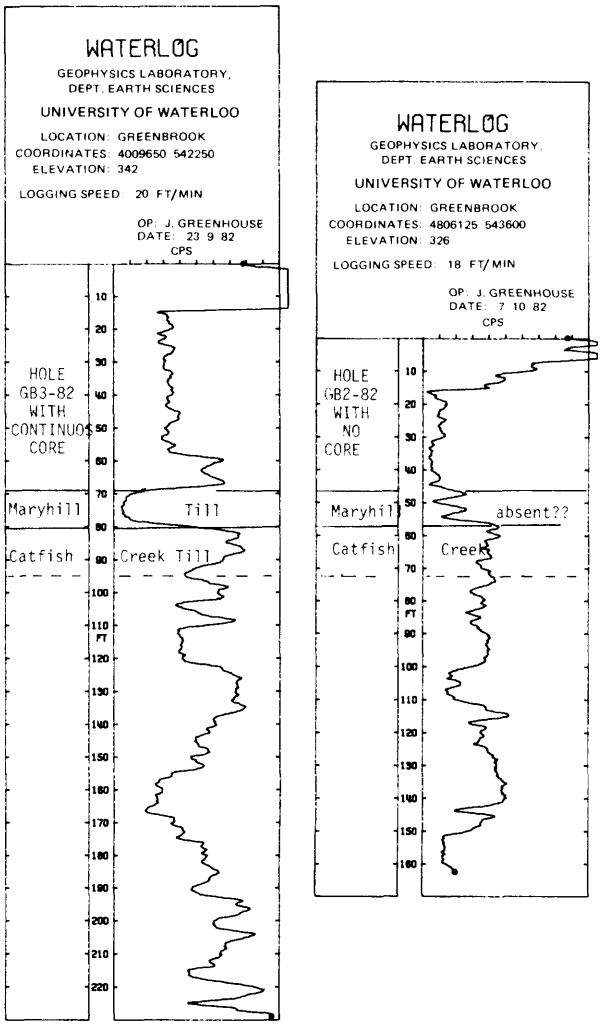

Figure 1. Neutron logs recorded in boreholes GB2-82 (left) and GB1-82 (right). The recording units are counts per second (cps) and there are 100 cps per tick mark on the horizontal scale. The log at GB3-82 was recorded in an uncased hole, and the left-hand vertical axis marks 600 cps. The log at GB2-82 is in a cased hole, and the left-hand axis marks 400 cps. The stratigraphy on the left (GB3-82) is known. At GB2 the stratigraphy is not known. The data are discussed further in the text.

Grant 127 A Gravity Survey of the Dundas Buried Valley West of Copetown, Ontario

J.P. Greenhouse[1] and M. Monier-Williams[2]
[1]Department of Earth Sciences, University of Waterloo
[2]Department of Earth Sciences, University of Waterloo. Now with Waterloo Geophysics, Conestogo, Ontario.

ABSTRACT

A total of 243 Bouguer gravity readings have been completed over a 9 km^2 area covering the terminus of the Dundas Buried Valley. The average error of 47 repeat readings was 0.11 mgals. The contoured gravity data clearly define closure of the buried valley topography west of Copetown, confirming and extending the results of earlier seismic reflection and refraction surveys. An apparent "American Falls" tributary in the contoured gravity data, entering the terminus from the south, is unfortunately poorly resolved. It underlies property for which we could not obtain permission to conduct a survey. The Bouguer gravity readings have been transformed to approximate bedrock elevation contours by fitting a linear model to seismic and borehole control within the survey area.

INTRODUCTION

The Dundas Buried Valley (Figure 1) is a prominent reentrant in the Niagara Escarpment. Its mouth lies beneath the sediments of Lake Ontario to the east of Burlington Bar, and the bedrock valley extends west by southwest to the general vicinity of Copetown. The exposed walls of the reentrant dominate the topography in the Hamilton/Dundas area, but the feature is completely filled in by overburden to the west of Copetown.

Spencer (1881) speculated that the Dundas Valley was eroded by a preglacial channel which drained Lake Erie into Lake Ontario. Karrow (1963) proposed that the valley was cut by an earlier Grand River draining south-central Ontario, and was deepened by glacial action. The walls of the valley are capped by mid-Silurian dolomite of the Lockport Formation, and the axis probably bottoms in upper Ordovician shales of the Dundas Formation. Between the dolomite and the Ordovician shales are a variety of shales, sandstones, mudstones, siltstones, and limestones (Karrow 1963).

Bedrock elevation data along the valley axis are sparse. Borings for the Burlington Bar bridge ("Skyway") penetrated 137 m below lake level (42 m below sea level) without encountering bedrock. Bedrock elevations in the area from Dundas to Copetown, summarized in Figure 2, are based on seismic reflection and refraction data collected by the Geological Survey of Canada (J. Hunter, Geological Survey of Canada, Ottawa, personal communication, 1983) and on borehole data summarized by Miller *et al.* (1979) and Karrow and Sprague (1975). Figure 2 shows that there is a relatively abrupt termination of the Dundas Valley west of Copetown, with the suggestion of an "American Falls" type tributary entering the gorge from the southwest.

The gravity survey described in the present report was undertaken to better define the terminus of the Dundas Buried Valley west of Copetown. Our interest in the valley stems from 2 gravity profiles run by Starkowski (1980) as part of his B.Sc. thesis for the Department of Earth Sciences at the University of Waterloo. The 2 profiles were run across the Burlington and Iroquois Bars, at the eastern and western end of Hamilton harbour respectively. The Bouguer anomaly profile across the Burlington Bar is reproduced in Figure 3b, and shows a prominent 3 milligal anomaly associated with the buried valley, the axis of which lies almost directly beneath the entrance channel to the harbour. Starkowski's modelling of this anomaly suggests that the bedrock elevation on the axis was about 100 m below sea level (180 m below lake level). The survey across the Iroquois Bar produced a similar anomaly.

In her B.Sc. thesis, McLaughlin (1981) began to survey gravity along roads in the Copetown area, and Monier-Williams (1982) extended this coverage off the roads. The present survey combines and extends the data from these 2 theses to produce a gravity map of the shaded area in Figure 1.

Regional gravity for the area can be estimated from the gravity chart for the area (Department of Energy, Mines and Resources 1971), on which Figure 4 is based. The station density for this survey is about 1 station per 20 km^2. The regional gradient indicated near our survey site is approximately 0.2 mgals/km, increasing toward the south or southeast.

THE SURVEY

The 1981-1982 survey was conducted over a grid straddling Highway 99, with Kitchen Road, Powerline Road, and Highway 52 forming its western, southern, and eastern boundaries, respectively (Figure 5). The survey referred to here includes work done in the fall and winter of 1981-1982 as part of Monier-Williams' thesis, and its con-

tinuation in May of 1982 supported by the grant provided through the Ontario Geoscience Research Grant Program. The May 1982 field work employed Monier-Williams and a University of Waterloo undergraduate assistant for the month. A total of 30 km of level survey were completed, for 216 gravity stations. These are combined with the data of McLaughlin (1981) to produce 243 distinct Bouguer anomaly readings. Because several stations were read more than once, a total of 271 readings were recorded. A list of the coordinates, elevations, and Bouger gravity readings, and the estimated bedrock depths at the gravity stations is filed with the Ontario Geoscience Research Fund Administrator, Ontario Geological Survey, Toronto. Stations were sited at approximately 200 m intervals over the area, as access and terrain allowed.

The gravity measurements were made with a Sodin gravimeter having a drift rating of less than 0.15 mgals per hour. Readings were taken in a series of interconnecting loops, each loop having a (temporary) base station which was reoccupied every hour to allow correction for drift.

The reference point for the entire survey is at the base of the telephone pole located 25 m east of the northeastern corner of the intersection of Highway 99 and Kitchen Road. That reference point, hereafter called the "base station", has been assigned an elevation of 1000 m, a northing and an easting of 10 000 m, and a gravity reading of 600 meter units or 60.53 mgals. The true coordinates of the base station, estimated from the topographic map, are: 47487487 m N; 574212 m E; elevation 230 m above sea level.

Stations were sited along lines running N12.5° W, parallel to the local road and fence grid. The lines were chained and staked at 200 m intervals. A transit was used to orient the lines, and to establish elevations. Fence lines and roads also served to establish the survey lines in areas where vegetation and/or topography made sighting difficult. Relief throughout the survey area is mainly gentle and does not exceed 20 m (Figure 6).

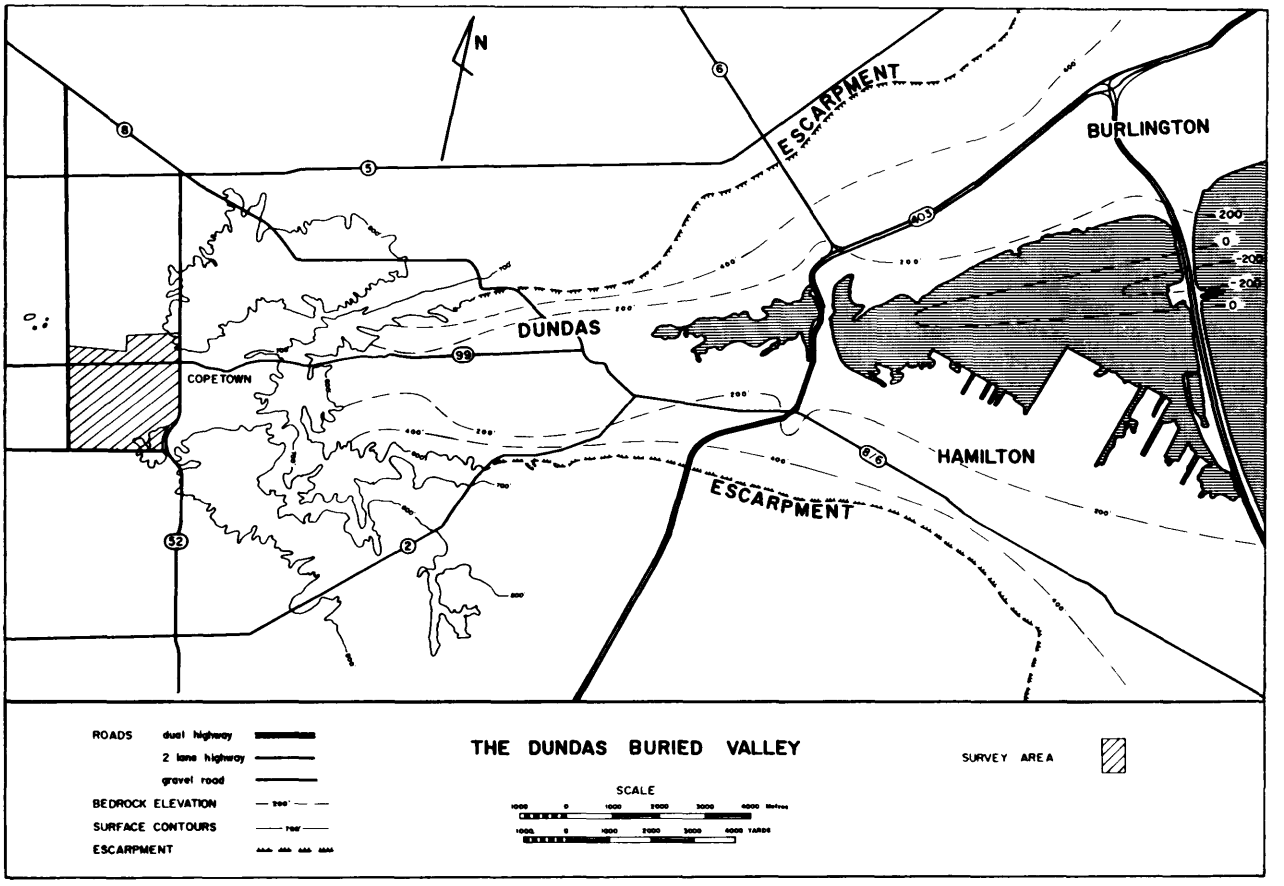

Figure 1. Location map showing the survey area (crosshatched) and the surface and estimated bedrock topography in the Hamilton/Copetown region.

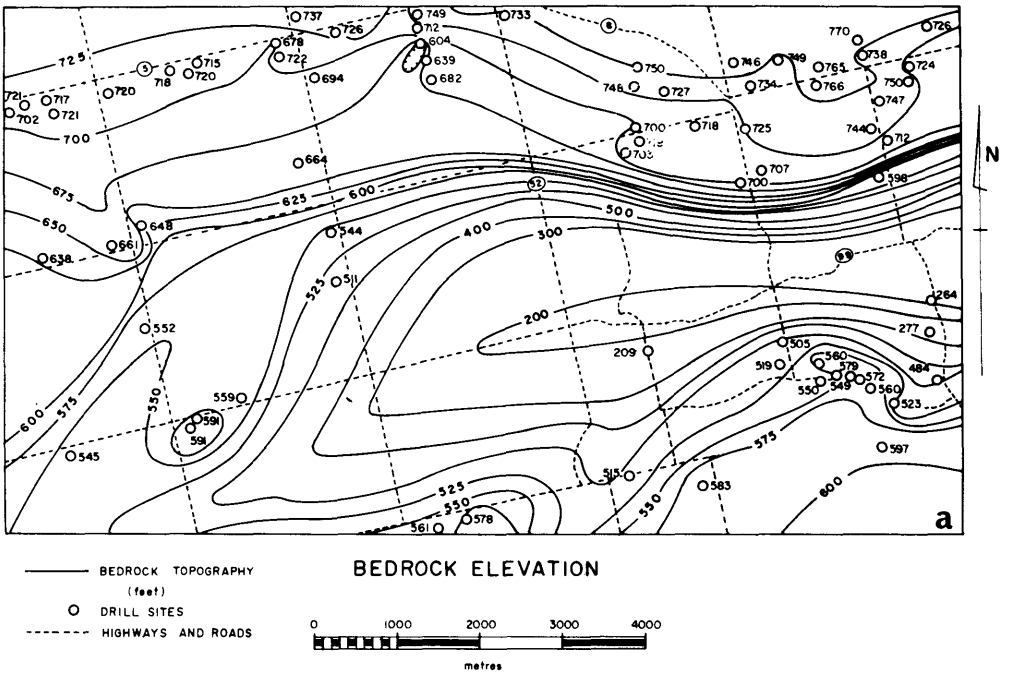

Figure 2a. Bedrock elevation in the vicinity of the survey area compiled from borehole data by Miller et al. (1979) and Karrow and Sprague (1975). Contours and borehole bedrock elevations are given in feet.

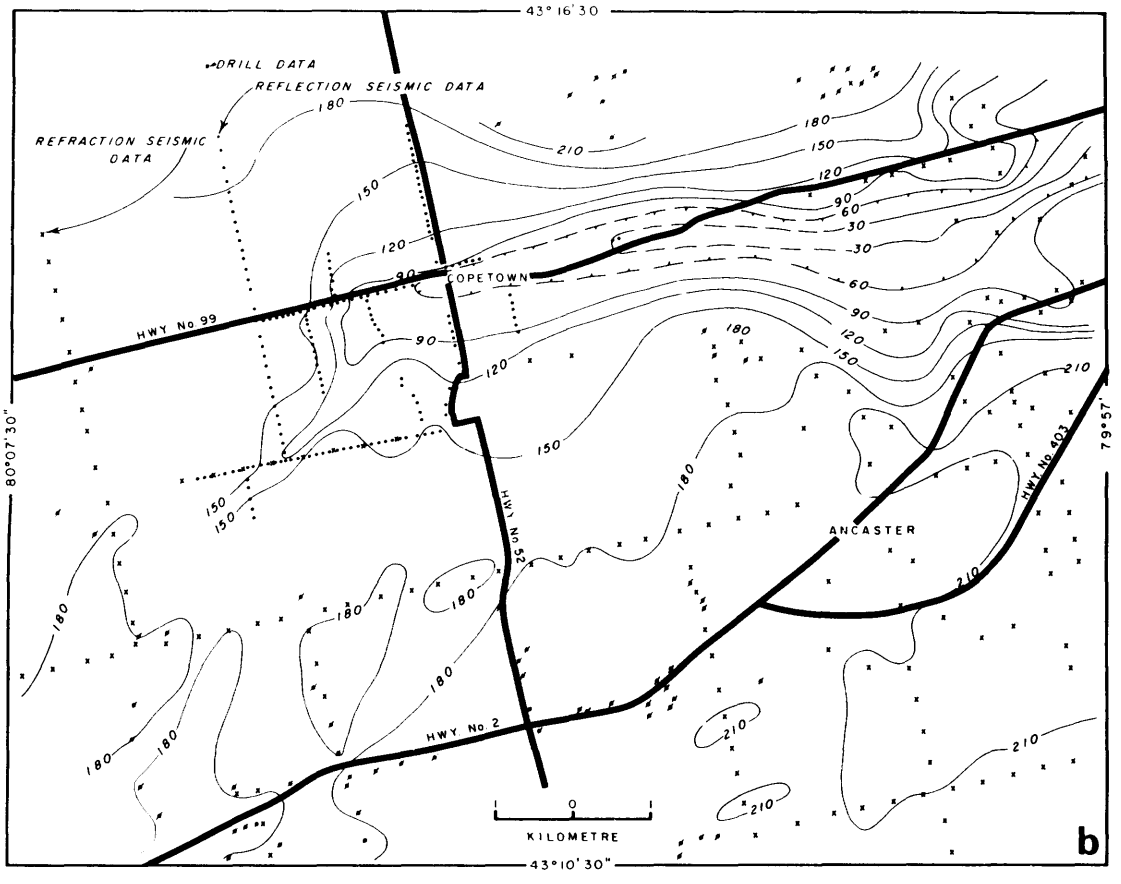

Figure 2b. Bedrock elevation in the vicinity of the survey area compiled from seismic refraction, seismic reflection, and borehole data. The borehole data set is not as complete as that shown in Figure 2a. Contours are in metres. Seismic data were supplied by J. Hunter, Geological Survey of Canada, Ottawa.

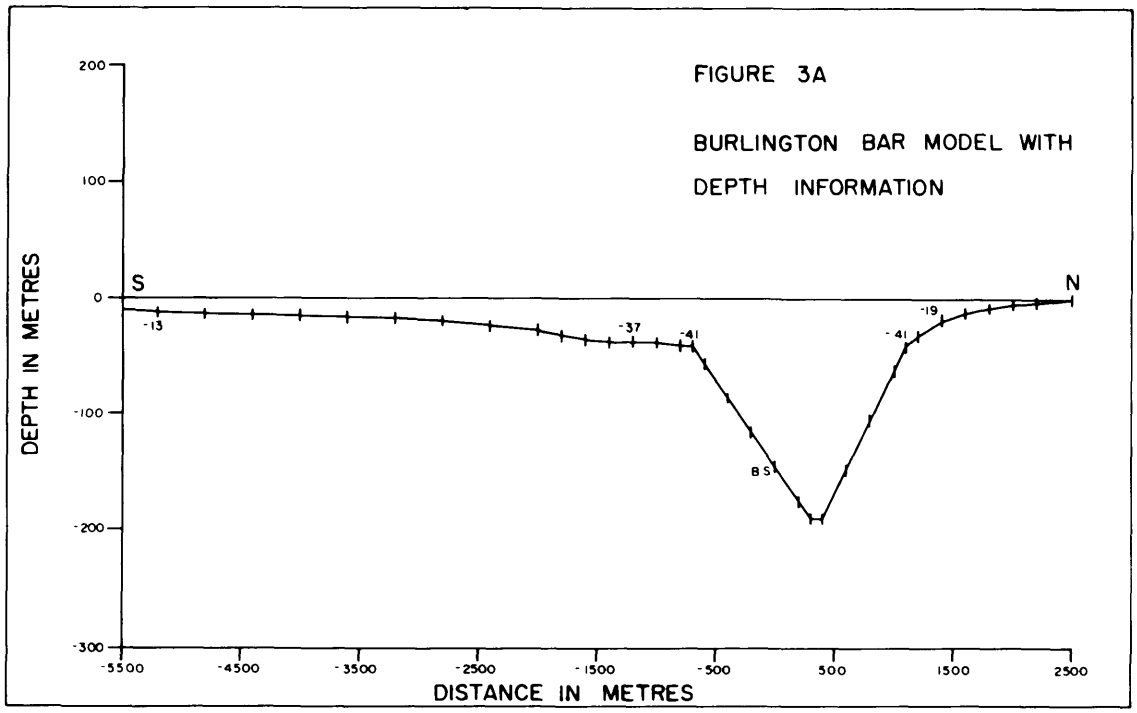

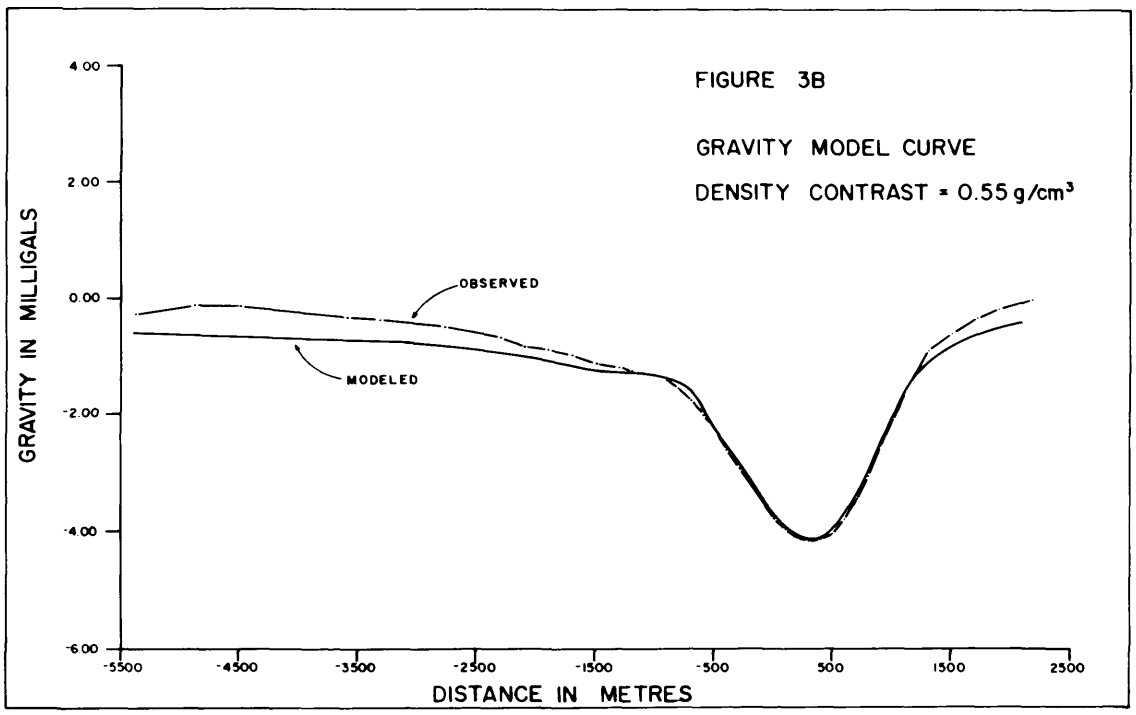

Figure 3. (A) Gravity model for bedrock along Burlington Bar, Hamilton Harbour. Control elevations are shown in metres. Depth is referred to lake level. The entrance channel is at 0 m on the horizontal axis. (B) Model Bouguer gravity profile compared to the observed profile across Burlington Bar (from Starkowski 1981).

Closures of survey loops up to 4 km in length indicate that the errors in northings and eastings are less than 10 m for the gravity stations. Closures on level survey loops shows that station elevation errors (relative to the base) should be less than 15 cm. Coverage of the area is generally satisfactory except for a large property centred on 9500 N, 11200 E to which we were not permitted access. This hole in our coverage unfortunately coincided with a most interesting anomaly, discussed below.

DATA REDUCTION

The coordinates, elevations, and gravity readings of all stations were placed in a computer file and the standard calculations for indicating a Bouguer anomaly performed. Data from McLaughlin's (1981) survey were also incorporated into the file, her base station having been tied to that of the present survey.

The latitude correction at 43.25° N is 8.005 x 10^{-4} mgal per metre north/south. The combined free air and Bouguer corrections are 0.223 mgals per metre elevation, based on an assumed overburden density of 2.05 grams/cc. This density is an average value derived using the gravity-elevation correlation technique of Parasnis (1972) in hilly terrain near Elora. The same technique applied to data along Highway 99 yielded 1.77 gms/cc, but because the elevation range (on which the correlation calculation depends for stability) was small, we have deferred to the more widely-used value. There is no obvious correlation of the resulting Bouguer map and the topography using this overburden density.

Topographic corrections were not applied. The low relief did not in general require this correction. However, 2 reduced gravity values in (separate) areas of high relief were anomalously low compared to the surrounding values, and these have been deleted from the contouring data set.

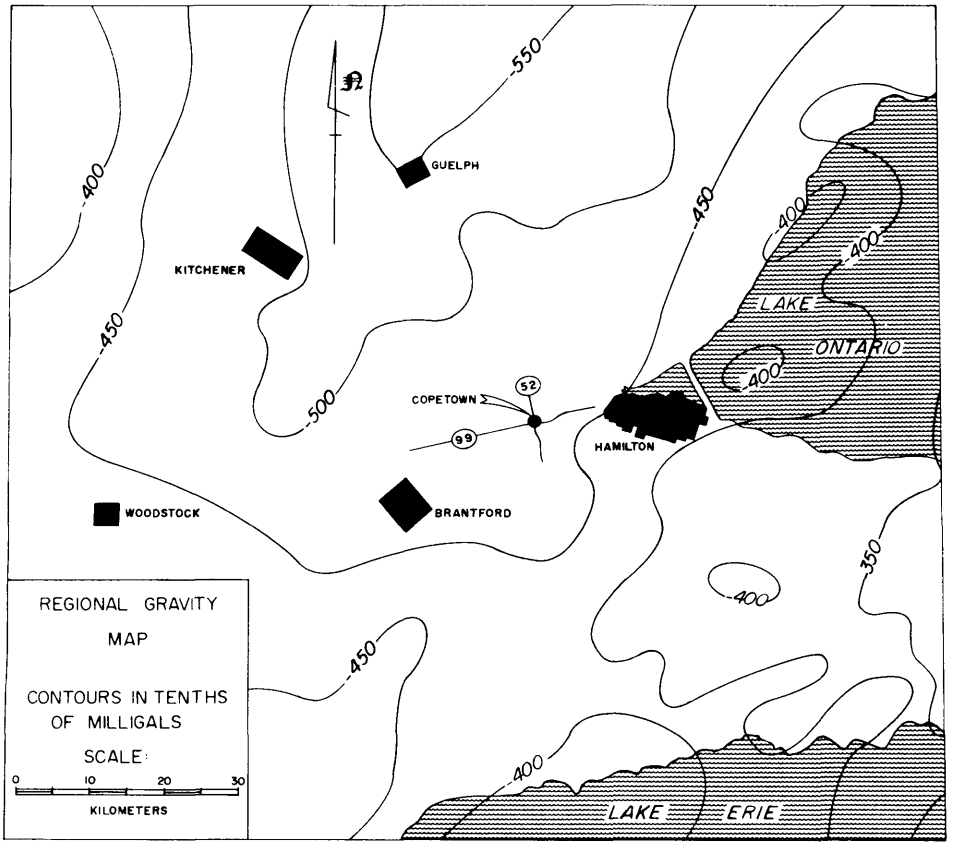

Figure 4. Regional gravity in southwestern Ontario (Department of Energy, Mines and Resources 1971). Contour units are 5 milligals (50 gravity units).

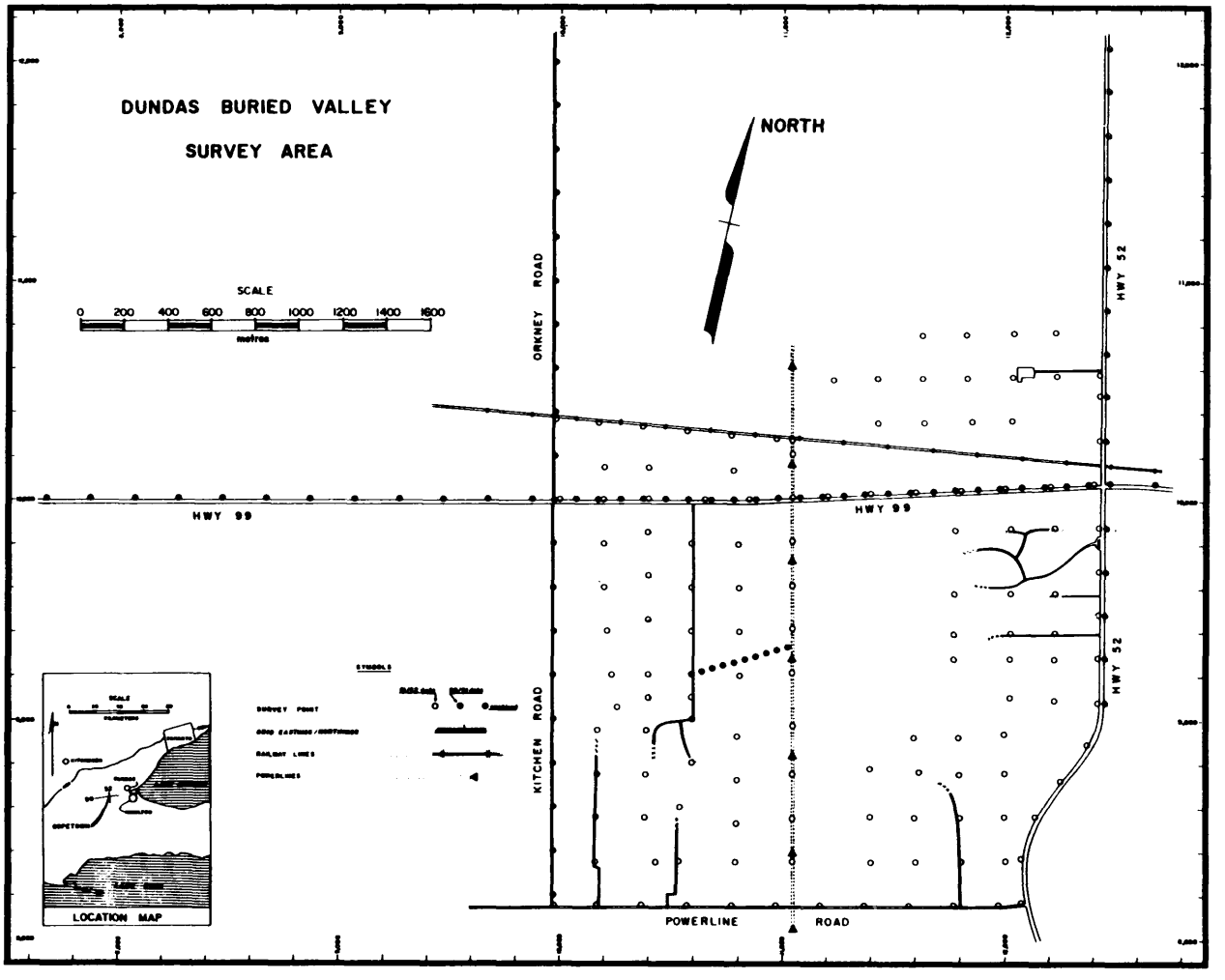

Figure 5. Location of gravity stations in survey area. The grid northings and eastings are given in metres and referred to (10 000, 10 000) at the (open circle) base station on the northeastern corner of the intersection of Kitchen and Orkney Roads and Highway 99.

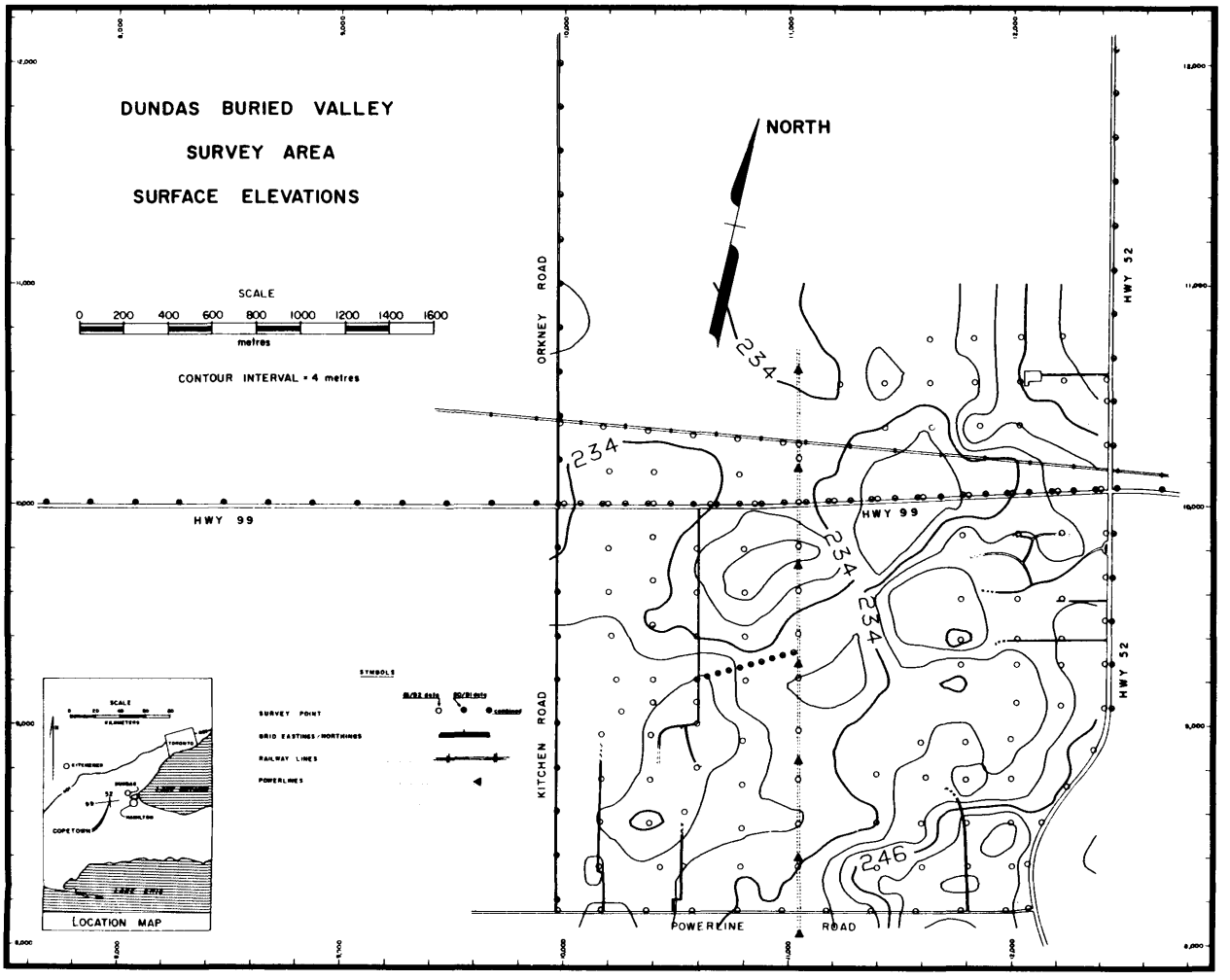

Figure 6. Surface elevation contours over the survey grid, drawn on the basis of level survey data at the gravity stations. The contours are in metres, and referred to a value of 230 m estimated from topographic maps for the base station.

TABLE 1 SOURCES OF ERROR IN GRAVITY READINGS.

Source	Magnitude	Gravity Error (mgals)
Reading	+ .03 metres	+ .03
Elevation	+ .15 metres	+ .038
Position	+ 10 metres	+ $8x10^{-3}$
Bouguer density	+ .2 gms/cc	$+8x10^{-3}$mgals/ m [1]

[1] Maximum relief in the survey area is less than 20 m so that the maximum error due to an incorrect Bouger density would be 0.16 mgals

Apart from the topographic factor, errors in the reduced gravity result from errors in reading, in station elevation, in station position, and in the density used for the Bouguer correction. The approximate magnitude of these errors is shown in Table 1. The average error in 43 independent repetitions of gravity stations was 0.11 mgals, with a standard deviation of 0.08 mgals. We therefore have taken ±0.11 mgals as the probable error in the Bouguer readings.

RESULTS

The Bouguer gravity data are contoured at 0.2 mgal intervals in Figure 7a and shown in relief in Figure 7b. The sharp depression in gravity encountered on the traverse

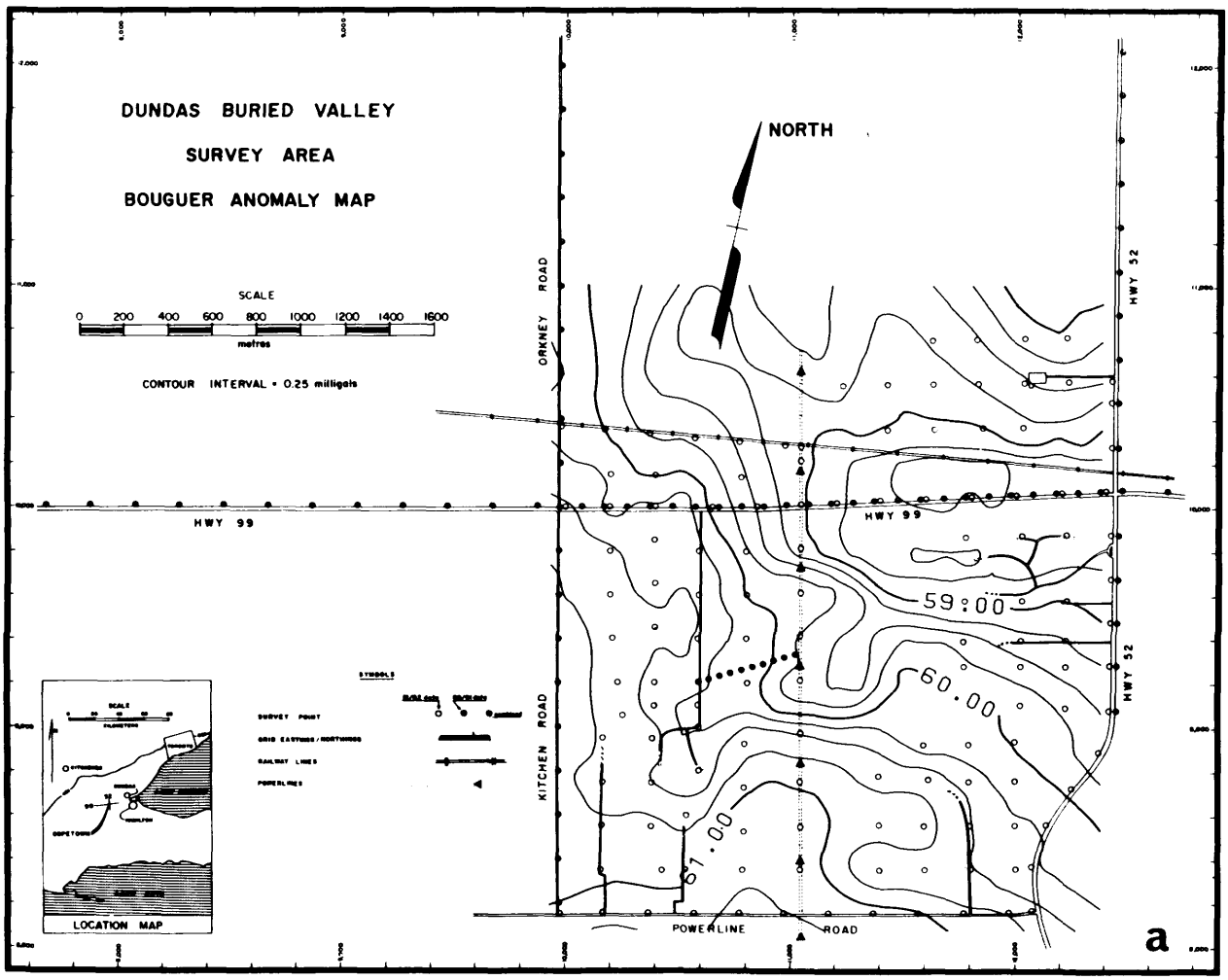

Figure 7a. The contoured Bouguer anomaly over the survey grid.

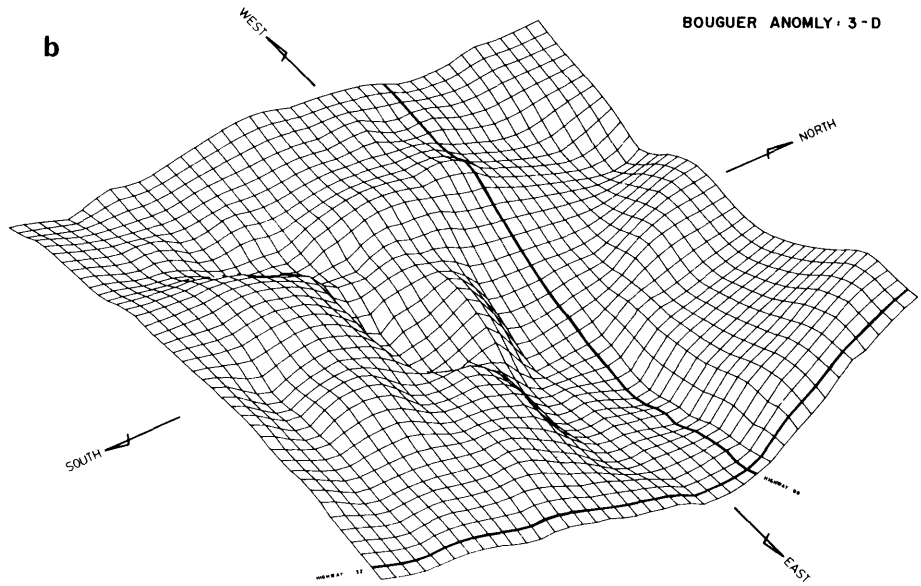

Figure 7b. Perspective view of the Bouguer anomaly over the survey grid.

along Highway 52 near Copetown closes out a kilometre or so to the west under Highway 99. There is good evidence for a tributary valley entering the terminus from the south-southwest. The join of this tributary and the main valley, however, lies beneath the unsurveyed locality in our gravity coverage, so that the contouring here is conjectural. On the other hand, the gravity control of the tributary is good west of 11 000 m east. A second implied tributary, from the northwest, is very poorly defined and merits further station coverage.

INTERPRETATION

A set of 9 bedrock control points, situated throughout the survey area, have been used to derive a linear relationship between bedrock elevation and Bouguer gravity. This is equivalent to the assumption that the overburden has a constant density contrast with the bedrock and that variations in the overburden thickness occur gradually. The assumption is not as good a basis for an interpretation as one might like, but the uncertainties in density contrast and regional gradient render more elaborate 3-dimensional models of questionable significance. We assume, then, an expression of the form:

$$h = ag + bx + cy + d \qquad \text{(i)}$$

where

h = bedrock elevation, metres above sea level
x = northing
y = easting
a,b,c,d are coefficients evaluated by least squares.

In physical terms, this corresponds to solving the equation

$$h = (g - x - By)/(2\pi G\rho) \qquad \text{(ii)}$$

where variations in overburden thickness h are assumed related to variations in Bouguer gravity g through the "infinite slab" relationship (similar to the Bouguer correction) in which ρ is the bedrock/overburden density contrast, G is the Gravitational constant, and B is the coefficient of the regional gravity gradient.

The control points are listed in Table 2, with the regression coefficients and R^2 values obtained in the least squares solution to (i). The control is provided in 3 cases from borehole data, and in the remainder from the seismic reflection data of Hunter (Geological Survey of Canada, Ottawa, personal communication, 1983). The borehole bedrock elevations were matched to the nearest gravity contour; seismic data points were chosen from

TABLE 2 BEDROCK CONTROL USED TO ESTABLISH GRAVITY/BEDROCK ELEVATION RELATION.

Control Point		Bedrock Elevation (h) (m)		Gravity (g) (mgals)	Type of Control
Northing, y (m)	Easting, x (m)	Measured	Predicted		
8,150	10,400	174	171	61.1	Borehole
8,400	10,550	150	134	60.3	Seismic
10,000	11,800	75	79	58.6	Seismic
8,800	12,300	120	130	59.8	Seismic
11,700	9,975	165	158	60.06	Borehole
11,200	9,975	156	151	60.06	Borehole
9,400	12,400	90	93	58.9	Seismic
10,000	7,800	180	183	61.40	Borehole
10,000	8,400	170	181	61.24	Borehole

$h = 51.58\ g + .0098\ x + .0126\ y - 3186$
$R^2 = 0.95$

the map in Figure 2 to be in areas of slow variation. Residuals from the regression are, with one exception, low and the coefficients yield the following with reference to (ii):

Bedrock/Overburden density contrast: 0.46 gms/cc

Regional gradient: 0.31 mgals/km toward S28°W.

Both values are reasonable; the regional gradient in Figure 3 is roughly similar to that deduced here. The resulting interpretation will necessarily be rather crude, however it should provide a reasonable fit to existing borehole and seismic data and fill in the area between control, away from sharp bedrock topography. It will underestimate depths and slopes in regions of sharp bedrock topography, such as the valley walls. The bedrock elevations derived in this way are contoured in Figure 8.

CONCLUSIONS

The bedrock elevation map of Figure 8 represents a significant improvement in our knowledge of the Dundas Buried Valley's morphology. Using other sources of funding we have begun to build a 3-dimensional model in order to put better constraints on the sharpness of the valley terminus, but this will provide at best a second order improvement in bedrock control. The existing map is best used as a guide to further seismic reflection or borehole exploration of the terminus.

RECOMMENDATIONS

If scientific curiosity is to be satisfied, it is essential that the hole in gravity coverage over the join of the southern tributary to the terminus be completed. The field work can easily be completed in a day, and we will undertake it if the Ontario Geological Survey can obtain access to the property. A secondary goal should be to improve the coverage north of the railroad line, near Orkney Road.

The completed gravity and seismic data should be combined for publication at an early date.

ACKNOWLEDGMENTS

The earlier work on this survey was funded through an NSERC Operating Grant to J.P. Greenhouse. Craig Sims and Ellen Leask assisted with the field work. We particularly acknowledge the cooperation of the Geological Survey of Canada in supplying us with their unpublished seismic reflection data in the survey area. We also thank Alan Starkowski and Ann McLaughlin for the initial data that led to this project.

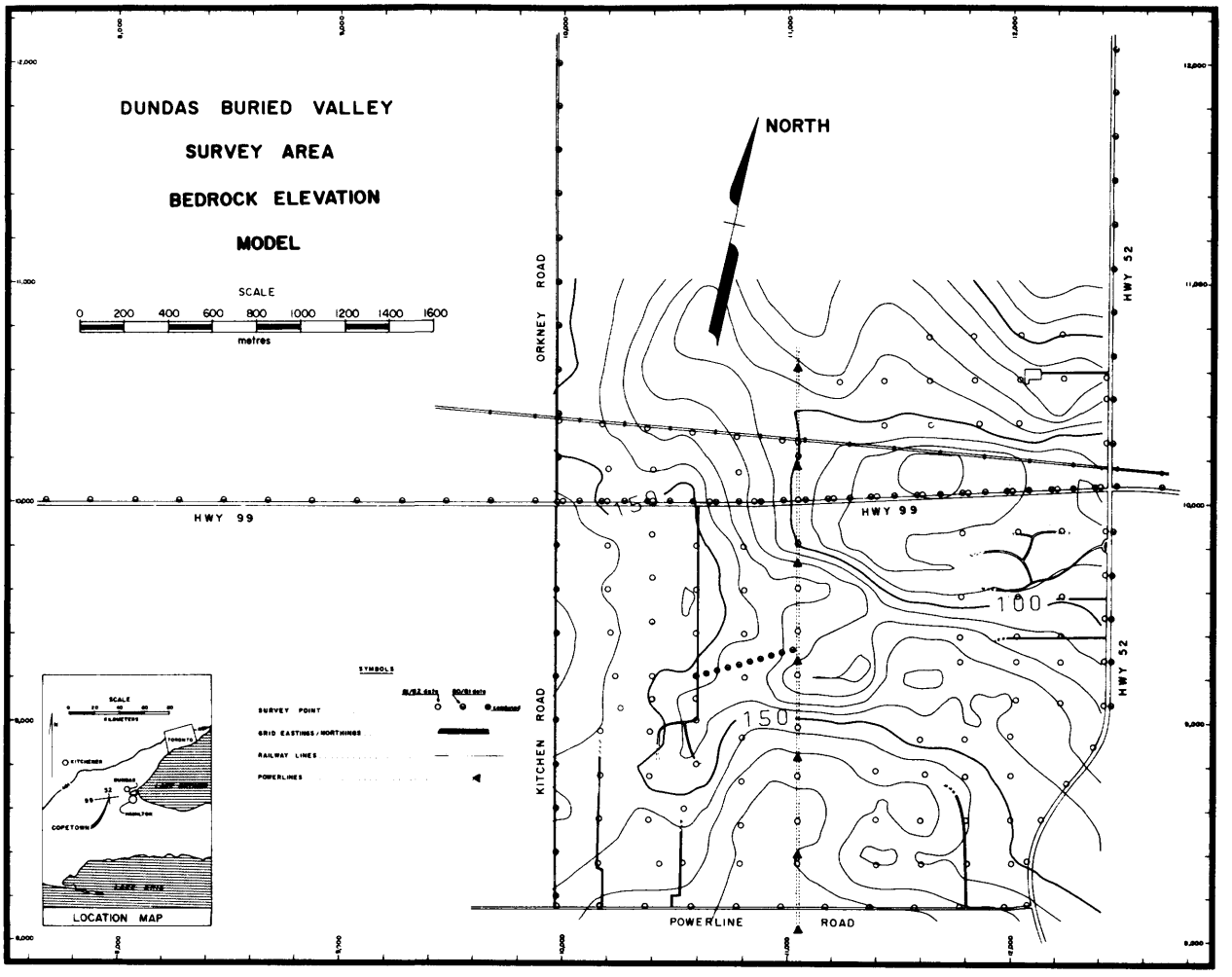

Figure 8. A bedrock elevation model based on the gravity data and tied to borehole and seismic reflection control. Contours are in metres above mean sea level.

REFERENCES

Department of Energy, Mines and Resources
1971: Bouguer Gravity Map of the Windsor Toronto Area; Earth Physics Branch, Gravity Map Series, Number 137.

Karrow, P.F.
1963: Pleistocene Geology of the Hamilton-Galt Area; Ontario Department of Mines, Geological Report 16, 68p. Accompanied by Maps 2029, 2030, 2033, and 2034, scale 1:63 360.

Karrow, P.F., and Sprague, D.J.
1975: Bedrock Topography of the Brantford Area, Southern Ontario; Ontario Division of Mines, Preliminary Map P.1049, Bedrock Topography Series, scale 1:50 000.

McLaughlin, H.A.
1981: Gravity Studies of the Dundas Buried Valley near Copetown, Ontario; B.Sc. Thesis, Department of Earth Sciences, The University of Waterloo, Waterloo, Ontario.

Miller, R.F., Farrell, L., and Karrow, P.F.
1979: Bedrock Topography of the Cambridge Area, Southern Ontario; Ontario Geological Survey, Preliminary Map P.1985, Bedrock Topography Series, scale 1:50 000.

Monier-Williams, M.E.
1982: Gravity Studies Over the Dundas Valley Truncation West of Copetown, Ontario; B.Sc. Thesis, Department of Earth Sciences, The University of Waterloo, Waterloo, Ontario.

Parasnis, D.S.
1972: Principles of Applied Geophysics; Chapman and Hall, London, 214p.

Spencer, J.W.
1881: Discovery of the Preglacial Outlet of Hamilton, Ontario; American Philosophical Society Proceeding, Volume 19, p.300-370.

Starkowski, A.
1980: Geophysical Studies of the Dundas Buried Valley Beneath Hamilton Harbour; B.Sc. Thesis, Department of Earth Sciences, The University of Waterloo, Waterloo, Ontario.

Grant 112 Petrographic Number Re-Evaluation: Phase 2

Peter P. Hudec
Department of Geology, University of Windsor

ABSTRACT

Petrographic Number (PN) is a test used by a number of agencies in Ontario and elsewhere in Canada to judge the suitability of aggregate for use in construction applications. The PN is the sum of the products of percentage of particular rock types in a sample, multiplied by its individual PN factor.

The first phase of the study, done on 31 aggregate types supplied by the Ontario Ministry of Transportation and Communications, indicated that some of the petrographic types have been assigned PN values that do not fit their behaviour in tests. This second phase expanded the study to include a wide variety of rock types obtained from various parts of Canada and the United States. A total of 123 different rock specimens were tested.

The laboratory tests done on the samples included: water absorption, adsorption, and vacuum saturation; density determinations; abrasion tests; freezing and thawing tests; and hardness and grain size determinations. Other parameters were calculated from the tests results. The tests were chosen because the first phase research indicated these to be the best indicators of aggregate quality.

The Estimated Petrographic Number for each rock type was determined as the average of estimates by 5 skilled petrographers. The test results obtained were treated by multivariate statistical analysis—the stepwise regression technique. An empirical relationship was developed which allowed the determination of a Calculated PN for each sample, for comparison with the corresponding Estimated PN. The Calculated PN is considered to be more reliable than the Estimated PN, since it is based on test results of a large number of samples.

The results again indicate that the currently used PN categories are too rigid, and that some of the rock types have been incorrectly classified in their PN values. The application of the proposed PN system to aggregate evaluation will give a much better estimate of the aggregates' performance in service than the current system.

INTRODUCTION

The Petrographic Number method of aggregate evaluation has been used with good success by many agencies in Canada. Notably, the Ontario Ministry of Transportation and Communications (MTC) uses the technique as an 'umpire' test to evaluate an aggregate for use in the Province's construction projects. The successful application of the test depends on the skill, expertise, and familiarity of the technician with the rock types he is testing. It is basically a subjective method of classification of crushed particles of rock aggregate into various categories of good, fair, poor, and bad (deleterious). As such, it suffers considerably from the personal bias of the technician. There is, therefore, some problem with reproducibility of results. However, given familiar rock types, a group of well-trained technicians will come up with results that are reasonably close.

The problem with the current usage of the PN test is not so much in its method, but with the classification of the rock types into the good, fair, poor, and bad categories. Factors of 1, 3, 6, and 10, respectively, are used for the above categories. Thus, if a rock type "X" is given a factor of 6, and it really deserves a factor of 3, it is going to downgrade the sample and may cause rejection of the aggregate if the sample contains a significant amount of the rock type "X". The second objection to the system is its rigidity. The differences in rock properties do not fall into neat categories such as the 1-3-6-10 system would imply. Intermediate, whole number factors can easily be estabished, especially on a regional basis, for a given rock type.

The purpose of this research was to develop techniques by which to examine the established PN factors and their suitability to the given rock type. The ultimate aim was to suggest refactoring of those rocks whose factors were clearly in error when compared to test results.

SAMPLE SELECTION AND PREPARATION

The samples used in the second phase of the research were obtained in part from supply houses, and in part were collected from across Ontario. The samples were chosen to represent as wide a variety of rock types as possible. In most cases, a 1 to 2 kg sample was obtained.

Prior to crushing, the density of the rock, its hardness, and grain size were determined. Whole rock sample splits were also sent to MTC for PN estimates. The rock was then crushed and sieved to -19 mm, $+9.5$ mm size for further laboratory testing. The summary of the test methods are given below.

TESTING METHODS

The following properties and test results were obtained from the samples:

Water adsorption, 95% relative humidity, room temperature

Water absorption, 24 hours

Water absorption, vacuum (boiling method)

Density (specific gravity)

Abrasion (low intensity)

Freeze-thaw resistance (3% salt solution)

Hardness

Grain size.

Many of the above tests are standard, and need not be described in detail.

Vacuum absorption was simulated by boiling the samples in water and allowing them to cool to room temperature before determining their weight in dry surface condition. Boiling displaces the air in rock pores, and cooling the sample under water completely fills the pores.

Water adsorption was determined in a humidity cabinet, where relative humidity was maintained at 95% by a saturated solution of copper sulphate. It was deemed that 72 hours were sufficient to achieve near-equilibrium conditions.

In both of the above, and in normal 24-hour water absorption by immersion, the gain was calculated relative to dry rock weight, and expressed as a percentage of the dry weight.

Density was determined by using a large pycnometer bottle to house the samples.

The freeze-thaw test involved saturating the samples in a 3% by weight NaCl solution for 24 hours, and freezing it, in a saturated condition, in air. The samples were frozen and thawed in an air-tight jar to maintain high humidity and prevent drying. Five cycles of freezing and thawing were used. The samples were back-sieved on a 9.5 mm sieve, and the amounts passing the sieve were considered as loss due to the test. Loss on a 6.7 mm sieve was also determined

The abrasion test used a modified 'Franklin Slake Machine', which normally is used to test the slaking of shales in water. The modification consisted of installing a shelf in the drum of the machine, which allowed the samples to be picked up and dropped a distance of about 8 cm as the drum was rotating. A charge of 5 steel balls, each 2.4 cm in diameter, was introduced to promote abrasion. The samples were rotated for 200 revolutions, and the abraded material was continually removed through the perforated walls of the drum. The difference between the original dry weight and the abraded weight constituted the loss, and was expressed as a percentage of the original weight. The loss was determined both on the samples directly out of the drum, and on the samples retained on the 6.7 mm sieve.

The hardness of each sample was determined on the scale of 1 to 3, where 1 was soft and 3 was hard. Hardness point needles were used to estimate the average hardness of each sample. The needles are tipped with minerals corresponding to the Mohs hardness scale.

The grain size of each sample was determined on a

TABLE 1 SUMMARY OF RESULTS LISTING MEANS OF PN PARAMETERS FOR MAJOR ROCK GROUPS.

		Number	Adsorbed/ Vac.Abs. Ratio	MTC Type	MTC Number	Abrasion 1 - 1.7 mm	Abrasion - 6.7 mm	Freeze-Thaw - 9.5 mm	Freeze-Thaw - 6.7 mm	Hardness	Grainsize	Absorbed %	Vacuum Absorbed %	Adsorbed % 95 R.H.	Spec. Grav.	Void Space Ratio	Bulk Water Ratio
Igneous	Coarse	33	0.255	12.393	1.714	1.580	3.258	1.899	1.481	2.714	4.179	0.562	0.627	0.183	2.806	0.134	0.611
	Fine	29	0.258	11.087	2.130	1.188	2.205	0.357	0.225	2.174	1.652	1.780	2.278	0.352	2.697	0.155	0.595
	Porphyry	4	0.223	8.200	1.400	1.166	2.410	0.167	0.059	2.200	3.200	1.930	2.218	0.237	2.716	0.105	0.673
	Glassy	5	0.362	26.000	3.000	8.015	19.950	13.280	5.185	2.000	1.000	1.690	1.885	0.685	2.350	0.096	0.542
Metamorph.	Gneiss & Schist	10	0.228	12.700	2.600	2.896	5.336	0.575	0.405	2.200	2.700	0.668	0.739	0.163	2.955	0.084	0.688
	Slate	8	0.388	28.200	3.800	1.942	4.272	1.665	0.948	1.000	1.000	1.042	1.134	0.441	2.860	0.086	0.527
	Re-Xllized	13	0.129	14.846	1.154	1.882	3.446	0.333	0.185	2.462	2.615	0.361	0.391	0.055	2.785	0.079	0.792
Sedimentary	Carbonate	4	0.142	13.500	1.500	1.360	2.970	2.114	0.384	2.250	1.250	1.020	1.175	0.134	2.693	0.102	0.756
	Coarse Clastics	20	0.157	27.611	4.000	3.724	5.376	3.629	2.187	1.722	1.556	5.617	7.565	0.396	2.580	0.235	0.641
	Conglomerate	2	0.139	6.333	1.000	0.763	1.433	0.008	0.002	2.667	4.333	0.383	0.493	0.064	2.663	0.149	0.710
	Fine Clastics	5	0.342	38.083	6.667	1.555	4.175	11.136	5.700	1.333	1.167	2.573	2.678	0.625	2.708	0.054	0.577

scale of 1 to 5, where 1 is aphanitic, and 5 is very coarse-grained. The grain size was always applied to the groundmass (in the case of porphyritic or conglomeratic samples).

RESULTS OF THE TESTS

From the results of the water adsorption and absorption tests, secondary parameters such as void space and ratios were calculated. The parameters and the test results were tabulated and stored in computer memory. Added to these were the estimates of PN values by the 4 individual petrographers at the Ministry of Transport and Communications, and by the author. A Estimated PN for the sample was selected that represented the majority or a 'consensus', rather than taking an average. This was done to maintain the PN factor system as it is currently used.

The table of results is too large for publication, and by itself is not particularly significant. However, a summary of the results, grouped according to major rock groups, is given in Table 1. The first column gives the major rock groups into which the samples have been subdivided. The second gives the number of samples in each group. The remaining columns give the mean of the test results for that group.

STATISTICAL EVALUATION OF THE PETROGRAPHIC NUMBER

The principal statistical method used was multivariate stepwise regression. A SAS statistical package at the University of Windsor computer centre provided the required software for the analysis. Simple statistical analyses were done on a TRS-80 microcomputer.

In the stepwise regression analysis, a dependent variable is chosen to which the selected independent variables in the data set are compared. The comparison is by regression, whereby the independent variable, that has the best correlation to the dependent variable, is chosen first. Next, the program searches for the next independent variable that will improve the relationship, and continues to add variables until the model is not significantly improved. The end result is an empirical relationship or equation relating the dependent variable to all the independent variables that have some correlation with it. The equation can then be used to calculate the value of the dependent variable from 2 or more independent variables.

The dependent variable in this case is the Calculated Petrographic Number (PN). The independent variables are all the test results. The empirical relationship developed by the stepwise regression analysis is as follows:

Calculated PN = 4.406 (constant)
+ 0.144 x Abrasion 6.7 mm
+ 1.805 x Adsorbed water
− 0.165 x Grain size
− 2.014 x Adsorbed/Vacuum Absorbed Ratio
− 1.004 x Hardness.

The above are listed in the order of 'goodness of fit' relationship, i.e. abrasion is most related to the PN, whereas hardness has a much lower correlation.

As can be seen, some of the simpler properties of the aggregate determine its PN. Substitution of these properties in the above empirical equation, will give a Calculated PN. This was done for the 123 samples studied. Table 2 gives the comparison of the Estimated or 'consensus' PN, as well as the Calculated PN using the above relationship. The table also gives the rock type tested.

DISCUSSION OF RESULTS

Examination of Table 2 reveals that, for the most part, the Calculated and the Estimated PN values are reasonably close. There are, however, some notable exceptions. These have been highlighted by asterisks. Most notable are the differences between the Calculated and Estimated PN values of some shales, with organic or iron contents that cause them to behave much better in tests than ordinary shales. The PN values of some of the igneous and metamorphic rock types also tend to differ significantly.

Perhaps more significant than the large differences noted above is the 'blending' of Calculated PNs. Instead of the rigid 1-3-6-10 categories, the Calculated PNs show a fuller range. This reinforces the author's earlier assertion that the rigid categories used are unrealistic, and a more flexible approach, based more on the petrographer's experience with the rock type rather than a rigid factor system should be used.

The Calculated PNs have been grouped by rock types in Table 3. The mean of each group was determined, and the significance of the means tested. Thus, for instance, there is a significant difference in the mean Calculated PNs between the coarse- and fine-grained igneous rocks. In fact, the mean Calculated PNs of coarse grained igneous rocks are significantly different than those of all other rock types. The same holds for conglomerates. On the other hand, there is no significant difference in the mean Calculated PNs between fine clastics (shales) and other rock types. These observations, however, must be considered cautiously, since not all rock groups are equally represented, and the results of a small group may be skewed by the extremes of a few samples.

The mean Calculated PNs of all rock groups tend to be much closer than the 1-3-6-10 categories would sug-

TABLE 2 COMPARISON OF ESTIMATED AND CALCULATED PN VALUES FOR VARIOUS ROCK TYPES.

Samp.No.	MTC Type	Est. PN	Calc. PN	Rock Type
9	8	1	1.0	SYENITE
10	29	3	3.6	BLACK ARGILLITE
11	61	10	4.7	*CARBONACEOUS SHALE
12	3	3	3.4	ILMENITE ZIRCON SANDSTONE
13	6	3	2.8	ARKOSE
14	56	10	4.5	*FERRUGINOUS RED SHALE
15	23	1	2.5	WHITE MARBLE
16	1	1	2.6	GRAY LIMESTONE
17	46	3	4.1	ARGILLACEOUS SANDSTONE
18	7	3	3.1	DACITE
19	9	1	1.0	DIABASE
20	8	1	0.6	TONALITE
21	7	1	1.5	RHYOLITE PORPHYRY
22	29	6	3.8	CHLORITOID SLATE
23	29	1	3.1	*TACONITE
24	8	1	0.3	HORNBLENDE GABBRO
25	8	1	0.4	ANORTHOSITE
26	9	1	2.0	ANDESITE PORPHYRY
27	61	10	6.6	*BITUMINOUS SHALE
28	4	1	3.8	*GARNETIFEROUS BIOTITE-GNEISS
29	22	3	2.4	ARKOSE
30	8	3	1.2	RUBELLITE GRANITE
31	29	1	2.9	CALC-SILICATE HORNFELS
32	5	1	0.7	JASPER CONGLOMERATE
33	5	1	0.5	JASPER CONGLOMERATE
34	46	1	2.0	GRAYWACKE
35	36	3	2.5	ARGILLACEOUS SANDSTONE
36	8	1	0.8	ALKALI GRANITE
37	27	3	1.9	HYPERSTHENE GABBRO (NORITE)
38	27	3	3.6	GARNETIFEROUS MICA SCHIST
39	7	1	2.9	HORNBLENDE DIORITE PORPHYRY
40	22	3	2.5	RED SANDSTONE
41	5	1	0.8	QUARTZITE
42	8	1	1.7	DIABASE
43	8	1	1.5	HYPERSTENE GABBRO
44	28	3	2.8	HORNBLENDE ANDESITE
45	9	1	2.9	SCORIA
46	8	1	1.0	APLITE
47	8	1	0.2	GABBRO
48	28	3	3.3	SANIDINE TRACHYTE
49	4	1	2.4	AMPHIBOLITE
50	26	3	2.4	BITUMINOUS SANDSTONE
51	8	1	1.0	SYENITE
52	22	6	4.8	GRAY SANDSTONE
53	9	3	2.6	RHYOLITE PORPHYRY
54	8	1	0.9	ESSEXITE
55	8	1	2.1	CARBONATITE
56	9	3	2.9	OLIVINE BASALT
57	7	1	1.8	DIABASE
58	8	6	0.8	*DIORITE
59	25	1	4.9	*SERPENTINE
61	23	1	1.7	WHITE MARBLE
62	8	1	0.7	SILLIMANITE GARNET GNEISS
63	8	1	1.0	HORNBLENDE GRANITE
65	8	1	1.5	NEPHELINE SYENITE
66	7	1	1.7	BASALT
67	6	3	3.9	GRAYWACKE
68	7	1	1.8	OLIVINE PHONOLITE
69	8	1	0.9	MONZONITE
70	7	1	2.8	BASALT
71	26	6	2.0	*OBSIDIAN (BLACK AND BROWN)
72	22	6	4.6	ARKOSE
73	23	1	1.5	BLUE GRAY MARBLE
74	5	1	1.9	BLACK QUARTZITE
75	48	10	8.2	TUFF
76	27	1	2.2	NEPHELINE-SODALITE SYENITE
77	1	1	3.7	*LITHOGRAPHIC LIMESTONE
78	7	3	3.8	MICA DACITE
79	7	1	2.8	LACTITE PHONOLITE
80	23	1	1.8	DOLOMITE MARBLE
81	7	6	2.2	ARENACEOUS SHALE
82	26	6	1.7	OBSIDIAN
83	23	1	2.6	PINK MARBLE
84	9	1	2.0	CONGLOMERATE META GRAYWACKE
85	56	6	3.5	CATLINITE
86	23	1	1.9	VARIEGATED DOLOMITE MARBLE
87	8	3	4.6	MICA AUGITE PERIDOTITE
88	8	1	1.0	RED GRANITE
89	8	3	0.8	*ECLOGITE
90	26	3	4.2	PERLITE
91	27	3	3.5	QUARTZ SERICITE SHIST
92	9	1	1.9	BASALT
93	8	3	1.3	*ANORTHOSITE
94	8	1	1.6	APLITE
95	7	1	2.3	PHONOLITE
96	8	1	2.3	TRACHYTE
97	9	1	2.1	HORNBLENDE BASALT
98	25	6	1.8	TREMOLITE SCHIST
99	27	3	1.1	PORPHYRITIC BIOTITE GRANITE
100	27	6	2.2	CHIASTOLITE SLATE
101	8	1	1.0	BIOTITE GRANITE
102	8	1	1.2	HORNBLENDE GNEISS
103	29	10	4.5	*GRAY SLATE
104	26	3	3.6	WELDED TUFF
105	8	1	0.9	HORNBLENDE SYENITE
106	46	6	3.9	BROWN SANDSTONE
107	4	6	3.3	GRAPHITE (IN SCHIST)
108	9	6	2.3	*SCORIA
109	8	1	1.0	SYENITE
110	29	10	4.7	*PHYLLITE
111	56	6	5.1	SANDSTONE (BROWN)
112	46	3	3.2	MICACEOUS SANDSTONE (BROWNSTON
113	8	1	0.7	PYROXENITE
114	23	3	2.3	VERD ANTIQUE
115	8	1	2.1	EPIDOSITE
116	8	1	3.0	ECLOGITE
117	29	6	3.3	RED SLATE
118	61	6	3.3	GREEN SLATE
119	26	3	7.1	*PERLITE
120	5	1	1.5	GREEN QUARTZITE
121	7	1	1.9	LAMPROPHYRE
122	9	3	2.0	BASALT
123	27	1	1.2	NORITE
124	7	3	3.0	RHYOLITE
125	28	6	6.5	GREEN LAPILLI TUFF
126	61	6	4.7	*OIL SHALE
127	8	1	1.8	HORNFELD CORDIERITE
128	5	1	1.0	QUARTZITE
129	7	3	5.3	RHYOLITE
130	8	1	0.4	GABBRO
133	26	3	1.3	CALCAREOUS CHERT
135	9	1	0.9	OLIVINE BASALT PORPHYRY
137	26	1	1.7	SILICIOUS DOLOMITE

gest. However, it must be borne in mind that weathering, chert content, excessive porosity, and other variables which normally downgrade a rock, are not taken into account. Also, the samples in each group may not be representative of that group, and certainly are not representative of any region. However, the means do show some interesting differences: coarse grained rocks tend to have lower mean Calculated PNs than those of other rock types, except for conglomerates; fine grained clastics, slate, and fine grained igneous rocks have higher Calculated PNs than other rock types; sandstones as a group have higher PNs.

It must be noted that the range of the numbers obtained for the mean Calculated PNs was dictated by the Estimated PNs used in the dependent variable. Thus, if the Estimated PNs given for a sandstone were consistently high, the mean Calculated PNs will also be, on the average, high. The statistical treatment does not assign new PNs to the rock, but reclassifies the PN somewhere in the range given for that rock type.

The relationship of the Calculated PN to the Estimated PN is shown graphically in Figure 1. A good relationship is seen by the clustering of the low PNs, and to

TABLE 3 CALCULATED PN VALUES GROUPED BY ROCK TYPE SHOWING SIGNIFICANCE OF MEANS (>.95).

	Rock Group	No. of Samples		1	2	3	4	5	6	7	8	9	10	11	Mean PN
Igneous	Coarse	33	1	-	y	y	y	y	y	y	y	y	y	y	1.3
	Fine	29	2	y	_	n	n	n	y	y	n	y	y	n	2.3
	Porphyry	4	3	y	n	-	n	n	y	n	n	y	y	n	1.8
	Glassy	5	4	y	n	n	-	n	n	n	n	n	y	n	3.5
Metamorph	Gneiss & Schist	10	5	y	n	n	n	-	n	n	n	n	y	n	2.8
	Slate	8	6	y	y	y	y	n	-	y	n	n	y	n	3.3
	Re-Xllized	13	7	y	y	n	n	n	y	-	n	y	y	n	1.9
Sedimentary	Carbonate	4	8	y	n	n	n	n	n	n	-	n	y	n	2.3
	Coarse Clastics	20	9	y	y	y	n	n	n	y	n	-	y	n	3.7
	Conglomerate	2	10	y	y	y	y	y	y	y	y	y	-	y	0.6
	Fine Clastics	5	11	y	n	n	n	n	n	n	n	n	y	-	3.7
			Mean PN	1.3	2.3	1.8	3.5	2.8	3.3	1.9	2.3	3.7	0.6	3.7	

y = statistically significant difference between means
n = no statistically significant difference between means

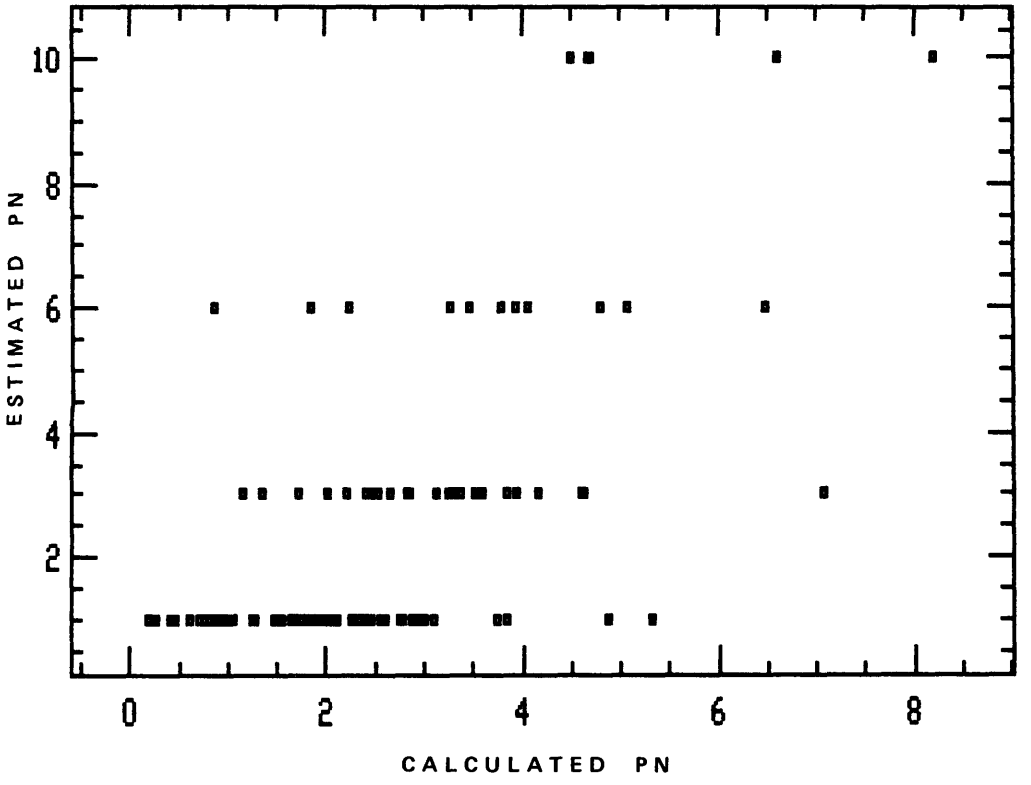

Figure 1. Relationship of Calculated to Estimated Petrographic Number.

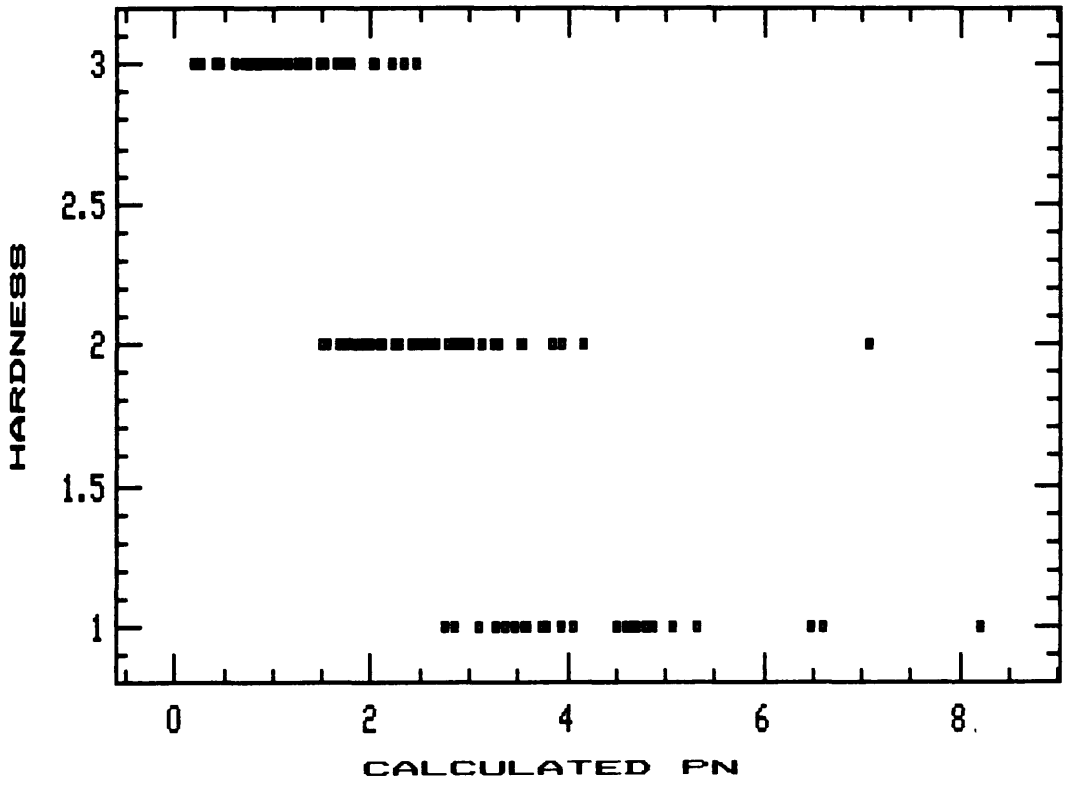

Figure 2. Hardness of the sample related to the Calculated Petrographic Number (Hardness 1 = soft, 3 = hard)

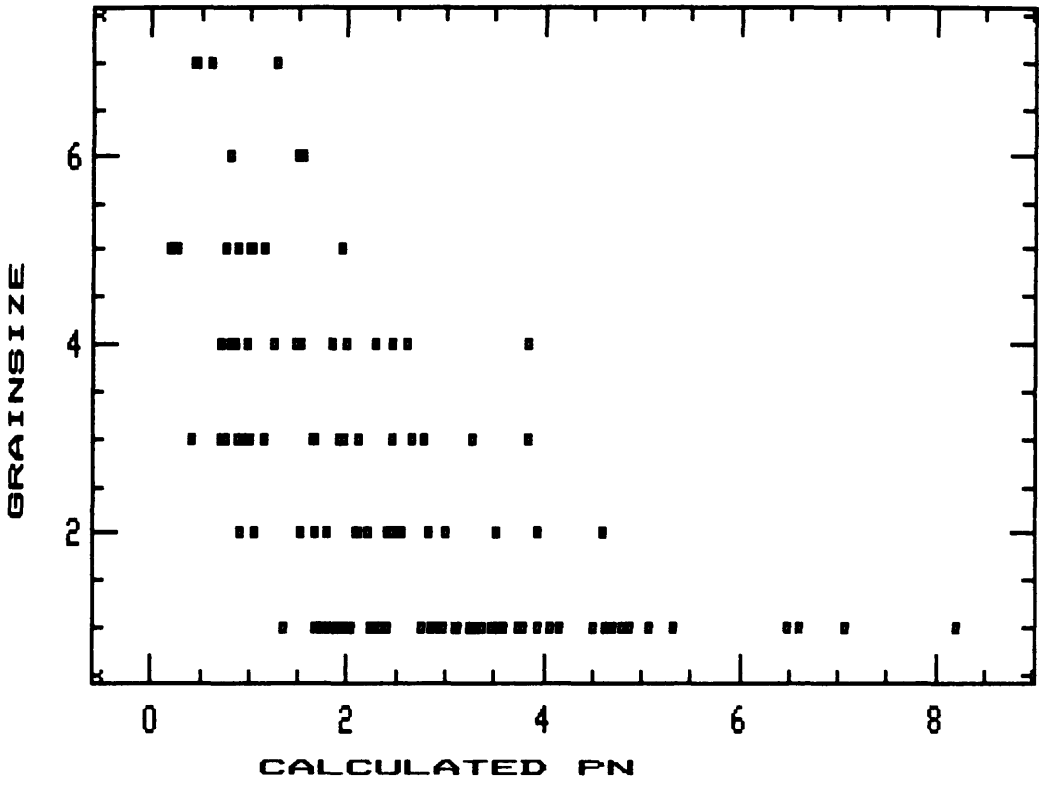

Figure 3. Grain size effect on Calculated Petrographic Number (Grain size 1 = fine grained to aphanitic, 7 = very coarse grained)

some degree, the high PNs. It is the intermediate PNs that are rather indeterminate, and show large differences in values between Estimated and Calculated PNs.

Hardness has a definite influence on the PN. This is not surprising, since the PN testing involves scratching of the sample, the softer samples are put into higher PN categories. This is well illustrated in Figure 2. Some overlap of hardness and PN is seen, but this is to be expected, since PN determination considers other estimated properties of an aggregate as well.

One of these properties is grain size. Figure 3 shows the relationship of grain size to PN. Lower grain size numbers indicate finer grain size (1 is fine grained to aphanitic). The finer the grain size, the higher the PN.

Another property that was shown to have a bearing on PN was water adsorption. Figure 4 illustrates the relationship of water adsorption to calculated PN. Although there is considerable scatter of points, the trend is obvious: the higher the water adsorption percent, the higher the PN.

CONCLUSIONS AND RECOMMENDATIONS

The above results show that some of the Estimated PNs used currently need to be re-evaluated. Since the rock types in the study do not represent any particular region, it is not suggested that the Calculated PNs obtained here be adopted for testing. Rather, it is suggested that the same techniques be applied to specific regions, and the PNs so determined be used to classify the aggregates of that region.

Crushed rock for construction is obtained from quarries and from gravel pits. It is relatively simple to evaluate a quarry, since the rock tends to be uniform. However, crushed gravel contains many lithic types. It is suggested that gravel pits of a region belonging to, or originating from, the same geologic agent(s) be sampled, and the dominant lithic types in the pits separated. Thus, a composite sample of, say, K-spar granite should be obtained

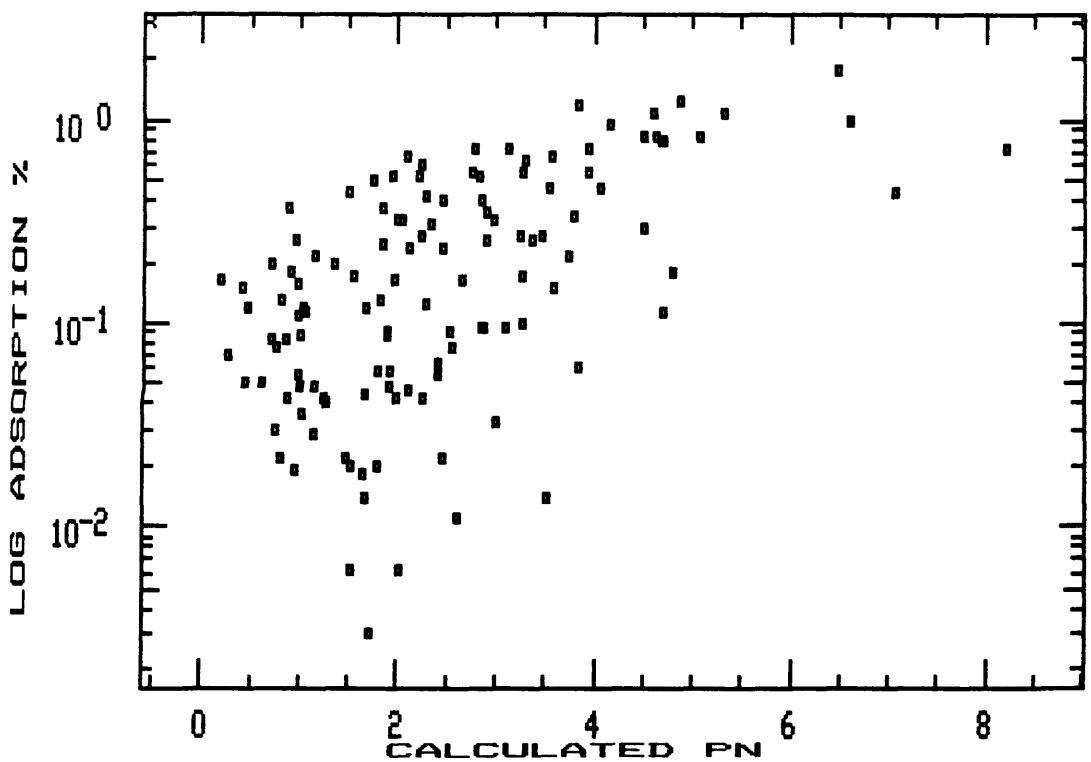

Figure 4. Relationship of adsorbed water percent on Petrographic Number.

from several pits found in the same geologic environment and in the same geographic area. The sample can be tested, its PN determined, and the test results analyzed statistically along with other lithic types. A much more reliable PN for the various lithic types will thus be obtained, and can be applied to any aggregate coming from pits in that area.

The Petrographic Number determination technique is in need of revision. An approach similar to the one outlined above will serve to improve the present system of PN determination, and result in better utilization of resources for more durable structures.

ACKNOWLEDGMENTS

Petrographic Number estimates on the samples were provided by Chris Rogers and his staff in the Petrographic Laboratory of the Ministry of Transportation and Communications, Toronto. Their help is much appreciated.

Much of the laboratory work was done by Irene Hurajt in the aggregate laboratory at the University of Windsor. The author is grateful for her patience and persistence in the routine of lab work.

SELECTED REFERENCES

Bloem, D.L.
1966: Soundness and Deleterious Substances: Significance of Tests and Properties of Concrete and Concrete Aggregates; American Society of Testing and Materials, Special Technical Publication 169-A, p.497-512.

DePuy, G.W.
1965: Petrographic Investigations of Rock Durability and Comparisons of Various Test Procedures; Journal of American Association Engineering Geology, Volume 2, p.31-46.

Dolar-Mantuani, L.
1972: Harmful Constituents in Natural Concrete Aggregates in Ontario; 24th International Geology Congress, Montreal, Proceedings Section 13, p.227-234.

Dolch, W.L.
1966: Porosity: Significance of Tests and Properties of Concrete and Concrete Aggregates; American Society for Testing and Materials, Special Technical Publication 169-A, p.443-461.

Dunn, J.R., and Hudec, P.P.
1965: The Influence of Clays on Water and Ice in Rock Pores; Phase 4 of Physical Research Project No. 4, Acceptability Tests for Coarse Aggregates; Bureau of Physical Research, New York State, Department of Public Works, Report RR65-5.
1966: Water, Clay, and Rock Soundness; Ohio Journal of Science, Volume 66, Number 2.

Hudec, P.P.
1980a: Durability of Carbonate Rocks as Function of Their Thermal Expansion, Water Sorption, and Mineralogy; ASTM Special Technical Publication 691, p.497-508.
1980b: Effect of De-Icing Salts on Deterioration and Dimensional Changes of Carbonate Rocks; American Society for Testing and Materials, Special Technical Publication 691, p.629-640.

Litvan, G.G.
1973: Pore Structure and Frost Susceptibility of Building Materials; Research Paper Number 584 of Division of Building Research, Natural Resource Council, Canada.

Mather, B.
1960: Petrology of Concrete Aggregates; Proceedings, 11th Symposium on Highway Engineering Geology at Florida State University, Florida Geological Survey, p.9-22.

Mielenz, R.C.
1958: Discussion of the Method of Petrographic Examination of Aggregates Employed by the Laboratories of the Department of Highways of Ontario; Internal Report, July 8, 1958.
1978: Petrographic Examination; Significance of Tests and Properties of Concrete and Concrete Aggregates; American Society for Testing and Materials, Special Technical Publication 169-B, p.539-572.

Powers, T.C.
1955: Basic Consideration Pertaining to Freezing and Thawing Tests; American Society for Testing and Materials, Proceedings, Volume 55, p.1132-1155.

Rhoades, R., and Mielenz, R.D.
1948: Petrographic and Mineralogic Characteristics of Aggregates; Symposium on Mineral Aggregates, American Society for Testing and Materials, Special Technical Publication 83.

Rogers, C.A.
1978: Aggregate Durability Tests in Ontario, Precision and Correlation with Field Performance; Ontario Ministry of Transportation and Communications, Materials and Lab Services Section, Unpublished Draft Report.

Stewart, N.B.
1969: Detailed Petrography - An Aid in the Evaluation of Gravel Aggregates for Freeze-Thaw Resistance; Proceedings, 5th Forum on Geology of Industrial Minerals, Harrisburg, Pennsylvania, Pennsylvania Geological Survey, Mineral Resource Report 64, p.55-89.

Verbec, G., and Landgren, R.
1960: Influence of Physical Characteristics of Aggregates on Frost Resistance of Concrete; American Society for Testing and Materials, Proceedings, Volume 60, p.1063-1079.

Grant 113 Investigation of Factors Controlling Changes of Groundwater Pressure in Clay Slopes

T.C. Kenney
Department of Civil Engineering, University of Toronto

ABSTRACT

Research was directed towards answering the question - 'By what magnitudes and at what rates do groundwater pressures change in natural clay slopes?' The answers are important for the prediction of changes of slope stability. They were found to be dependent primarily on the hydraulic boundary conditions in the slopes and the properties of the clays.

Using consolidation theory, predictions were made of changes of groundwater pressure based on the postulate that these changes are the direct result of changes in hydraulic conditions at the ground surface. Two factors which were found to be most influential were changes of hydraulic gradient at the ground surface and the coefficients of consolidation and swelling of the clay. The predictions were in agreement with field measurements taken in a natural clay slope over a time period of 10 years.

On the basis of this work, a method is suggested for estimating the most severe groundwater pressures which a slope can be expected to experience in the future. This would allow estimation of the minimum expected safety factor of the slope.

INTRODUCTION

The objective of this project was to determine, through theoretical and field investigations, the primary factors controlling the rates and magnitudes of change of groundwater pressures in clay slopes.

Temporal changes of stability of a natural slope are dependent in part on the temporal changes of groundwater pressure within the slope. It is generally thought that annual fluctuations of meteorological conditions, such as precipitation and temperature, and possibly short-term weather changes, cause changes of groundwater pressure and of slope stability.

This report presents results from a field investigation in which groundwater pressures were measured in a natural slope of soft varved clay over a 10-year period. From these measurements, it was determined that the flow regime within the slope consisted of infiltration at the ground surface above the slope, and drainage from the area at the bottom of the slope. At depths greater than approximately 5 m below the ground surface, groundwater pressures remained essentially constant, indicating the occurrence of steady-state seepage despite the fact that groundwater pressure conditions were changing at the ground surface. The processes controlling changes of groundwater pressure are analogous to those which control changes of temperature in the ground. It is shown that groundwater pressures are dependent on changes of hydraulic conditions at the ground surface and that their rates of change are controlled by processes of consolidation and swelling (Kenney 1979).

On the basis of these findings a method is suggested to estimate the most severe groundwater pressures a slope can be expected to experience. This method is used to estimate the minimum expected safety factor of the slope at the test site and is compared with calculated values of safety factor based on measured groundwater pressures and river levels during the period 1971 to 1980.

THE SLOPE

Detailed descriptions of the test site have been presented by Chan and Kenney (1973) and Kenney and Chan (1973). The slope is a portion of the eastern bank of Wabi Creek near New Liskeard, Ontario, located within the boundaries of glacial Lake Barlow. Wabi Creek is incised into a broad clay plain which consists of sediments deposited in Lake Barlow.

Figure 1 records the stratigraphy and certain properties of the soils. The soils do not vary in horizontal directions and extend below elevation 145 m. The clay has a jointed structure to a depth of about 2 m from the ground surface, the frequency of jointing decreasing with depth. This was observed in exposures in the area and in shallow excavations at the site. Of considerable importance to the subject of groundwater pressures is the extent to which the joints are open. From visual inspection, the joints seem to be tight below a depth of about 0.5 m. Below the surface weathered zone, the undrained shear strength of the soil is about 30 kPa, and increases with increasing depth; The soil appears to be overconsolidated in the amount of 70 kPa.

Wabi Creek flows into Lake Temiskaming and at the test site the river level is also that of the lake. The level of Lake Temiskaming is controlled for purposes of hydroelectric power generation; it falls during winter, rises

rapidly during spring, and remains relatively constant during summer and autumn (Figure 3).

Precipitation averages about 700 mm of water per year, distributed relatively uniformly throughout the year, as indicated in Figure 3. During the period 1971 and 1980, annual precipitation varied between 600 and 900 mm per year, and during the period 1924 to 1971 it ranged between 450 and 1000 mm per year. The rate of infiltration can be estimated from knowledge of the coefficient of hydraulic conductivity of the soil ($k < 10^{-9}$ m/s) and the hydraulic gradient near the ground surface ($i < 1.0$), giving the value of less than 30 mm per year.

Piezometers were installed in 3 rows perpendicular to the river, about 30 m apart. The measured patterns of piezometric levels indicated that groundwater flow was basically 2-dimensional towards the river (Kenney and Chan 1973). In all, 65 piezometers were installed and measurements have been taken at 2-week intervals since 1971. The locations of some of the piezometers are given in Figure 2.

FIELD MEASUREMENTS

PIEZOMETRIC LEVELS

Some of the field measurements are presented in Figure 3. Piezometers located at 3 sections of the slope, designated A, B, and C in Figure 2, were chosen to provide typical information. Measurements are expressed as piezometric elevations. The piezometers are identified by number and their depths below ground surface are noted. Each piezometric curve has an associated elevation line, and changes of piezometric elevation relative to that line have been drawn to the same elevation scale as used in the graph of river elevations.

The following observations are true for all regions of the slope.

1. Piezometers located close to the river recorded changes of piezometric level which were in harmony with changes of river level. These changes are primarily reflections of changes of total stress caused by the river and will be discussed in a later section.
2. Soils closest to the ground surface experienced the largest annual changes of piezometric level and the most rapid rates of change. These changes and rates of change decreased substantially at increasing depths below the ground surface.
3. Piezometric levels fell during the winter months when the ground was frozen, rose during spring time when melting occurred, and fluctuated randomly during summer and autumn.
4. In addition to short-term changes of piezometric level, it is apparent that during the period 1975 through 1978 there was a steady long-term lowering of piezometric levels in the deep piezometers. No explanation for this can be given.
5. Correlations were sought between precipitation and changes of piezometric level at shallow depths but no such correlation was found to exist for short time periods, such as days, weeks, or months.

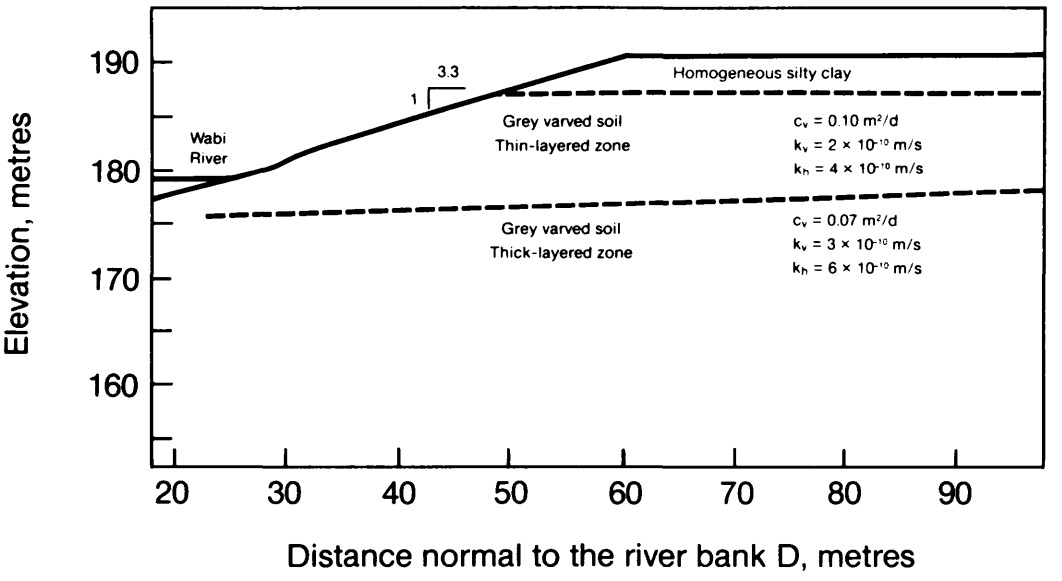

Figure 1. Cross-section of the slope.

GROUNDWATER FLOW

Figure 4 presents a typical pattern of groundwater flow in the Wabi Creek slope on April 15, 1974. Piezometer measurements were used to draw the separate equipotential lines, from which approximate flow directions have been drawn. Profiles of piezometric elevation were extrapolated toward the ground surface to locate approximately the phreatic surface. It is apparent that groundwater flow is initiated by infiltration in the area above the slope and that groundwater discharges into the river channel.

Shown in Figure 2 are regions in which the annual changes of piezometric level are similar in magnitude. A large portion of the slope has groundwater pressures which change very little and therefore correspond to a steady-state seepage condition. In the portion of the slope adjacent to the river, changes of piezometric level are caused by changes of the river level which annually amount to 3 to 4 m. In the absence of the river, the phreatic surface at the toe of the slope would not change position and therefore steady-state seepage conditions would exist in this location also.

CHANGES OF PIEZOMETRIC LEVEL

In Figure 5 are presented the measured ranges of piezometric elevation and positions of the phreatic surface below the area of infiltration at the head of the slope. The data extend over the time period 1972 to 1981. Minimum piezometric elevations occur during late winter and maximum values occur during the summer or autumn period. Maximum changes occur at the ground surface and annual changes do not propagate below a depth of about 5 m. The phreatic surface can rise to the ground surface during the summer or autumn months and falls during the winter period, the maximum fall being about 2.5 m in 1978.

CONCLUSIONS

The following conclusions can be drawn from the results of field measurements presented in Figures 2, 3, 4, and 5.

1. Within this slope at some distance below the ground surface, there is a zone in which groundwater pressures remain essentially constant. This indicates that nearly steady-state seepage conditions exist in equilibrium with average annual hydraulic conditions acting at the surface boundaries.
2. Changes of groundwater pressure within the slope originate at the ground surface as the result of changes in hydraulic conditions or changes in applied total stress. The magnitude and the rate of these pressure changes diminish with increasing distance from the ground surface.
3. In the absence of a fluctuating water body at the toe of a slope, such as Wabi Creek, it would be expected that in the area of groundwater discharge, the annual changes of piezometric level would be very small, to the point of being negligible.
4. Maximum values of piezometric level occur during the summer or autumn period. Minimum values occur during the late winter period, immediately before spring melt.

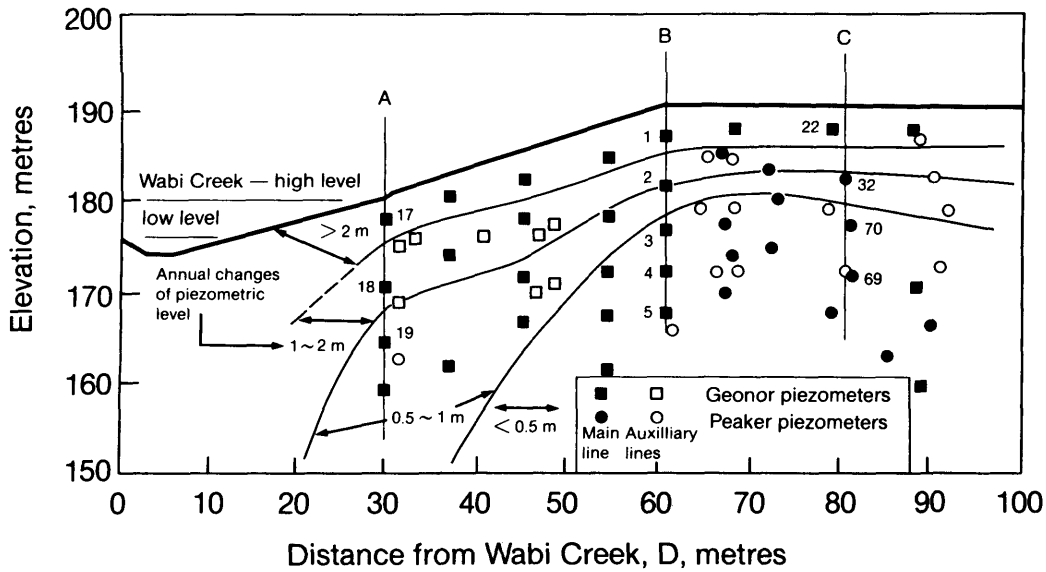

Figure 2. Locations of piezometers and annual changes of piezometric level.

FACTORS INFLUENCING GROUNDWATER PRESSURES

Changes of groundwater pressure cause changes of hydraulic gradient, changes of seepage flux, changes of effective stress, and changes of soil volume. It follows that the propagation of changes of groundwater pressure from one point to another is not the result of pressure transmission through static fluid but rather is the consequence of the process of consolidation or swelling occurring in the soil. The rates of change of groundwater pressures in saturated, isotropic clay can be expressed by the following equation for 2-dimensional consolidation:

$$\delta u/\delta t = (\delta h/\delta t)\gamma_w = (\delta\sigma/\delta t) + (1/m_{\gamma_w})[k_x(\delta^2 u/\delta x^2) + k_z(\delta^2 u/\delta z^2)] \quad (1)$$

where u is groundwater pressure, t is time, h is piezometric elevation, σ is total stress, x and z are coordinate axes in the plane of flow, k is the coefficient of hydraulic conductivity, γ_w is unit weight of water, and m is the coefficient of volume change of clay expressed as change of porosity per unit change of effective stress ($m = -\delta n/\delta\sigma'$). Soils in most slopes are overconsolidated and, therefore, m is small in magnitude and equal for both consolidation and swelling. Therefore, the term k/m_{γ_w} is equal for both consolidation and swelling processes and will be simply referred to as the coefficient of consolidation c_v. The rate of change of groundwater pressure is directly proportional to the magnitude of c_v and decreases rapidly with increasing distance from the boundary where changes of hydraulic conditions occur.

This report is limited to slopes in deep deposits of clay which do not contain aquifers or drainage layers. Within such a slope, changes of groundwater pressure will only result from changes of applied stress and changes of hydraulic conditions occurring at the ground

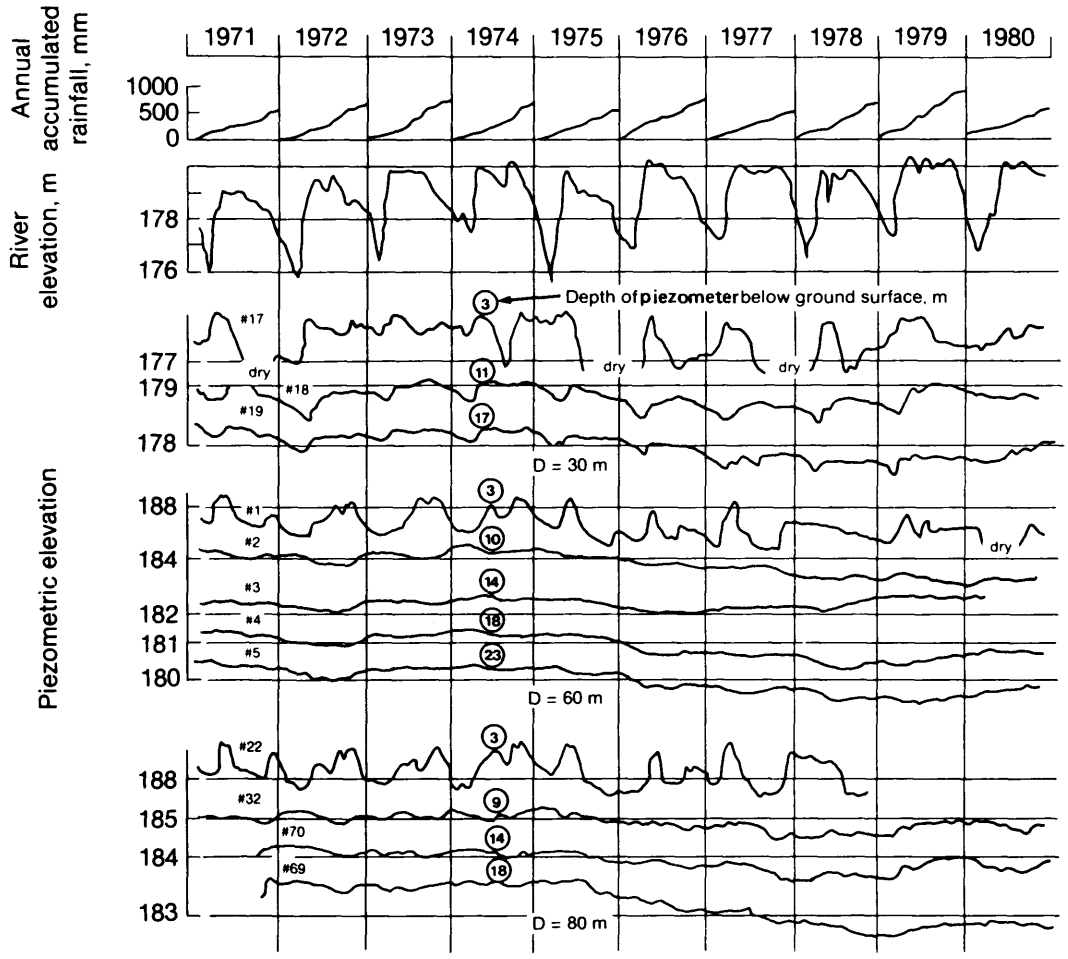

Figure 3. Results of measurements, 1971 to 1980.

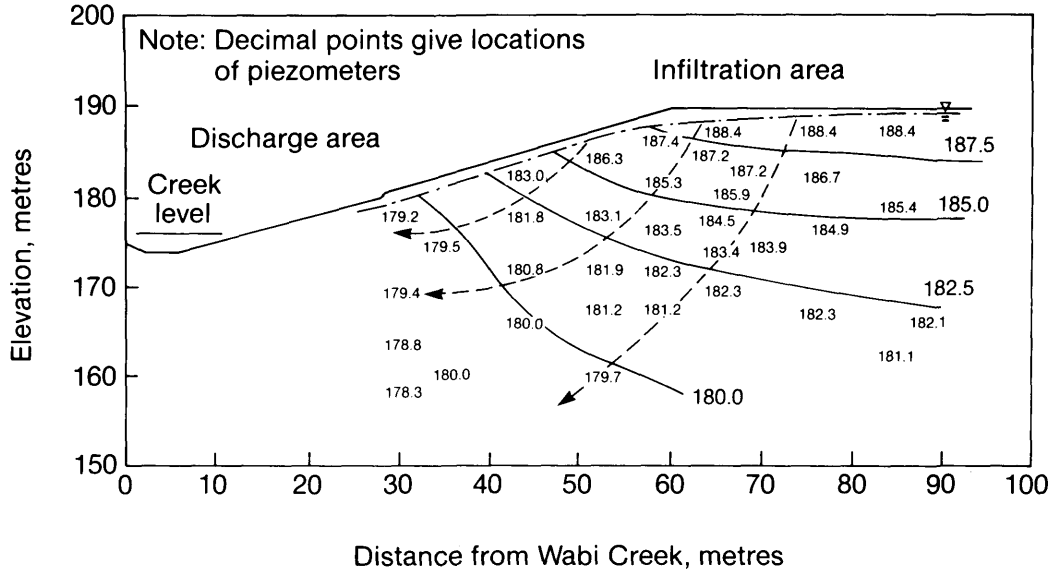

Figure 4. Typical pattern of groundwater flow on 15 April 1974 when river level was 175.8 m. Measured piezometric levels, corresponding equipotential lines, and approximate flow net.

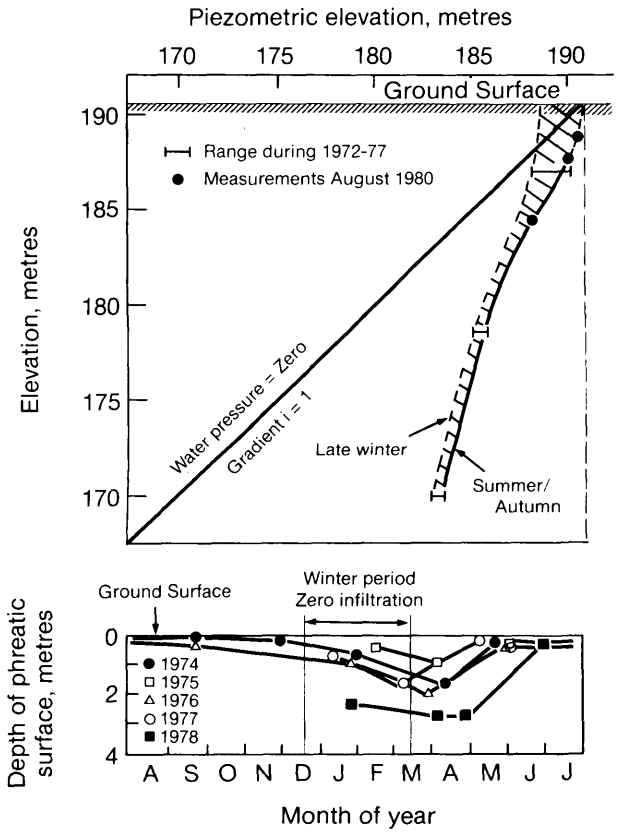

Figure 5. Measured changes of piezometric elevation and phreatic surface below infiltration area.

surface, such as in the area of water infiltration above the slope and in the area of groundwater discharge near the toe of the slope. In the area of infiltration, hydraulic conditions are governed by the availability of water, the hydraulic gradient at the ground surface, and the coefficient of hydraulic conductivity of the clay. During any period of time when the total infiltration flux at the head of the slope is less than the discharge flux at the toe of the slope, such as during winter or during a dry summer period, piezometric elevations in the clay in the area of infiltration will decrease and the phreatic surface will fall. Conversely, when infiltration flux exceeds discharge flux, piezometric elevations in the area of infiltration will increase and the phreatic surface will rise.

The toes of many slopes are not flooded and the hydraulic conditions existing in the region of groundwater discharge remain comparatively constant; that is, the phreatic surface remains stationary at the ground surface and the groundwater pressures remain steady. In cases where the toe of the slope is flooded, changes of boundary conditions are caused by changes of the free water level, having 2 effects: (a) changes of total stress and (b) changes of piezometric elevation along the submerged ground surface. As indicated in Figure 3 by measurements of piezometers 18 and 19, the first effect causes nearly immediate changes of piezometric levels in soil adjacent to the water body, and the second effect causes slower changes through the process of consolidation or swelling.

Figure 6 presents the results of an estimate made of changes of piezometric level below an area of infiltration based on the theory of consolidation (Equation 1). The

calculations were made for a winter period when the ground surface is frozen and there is zero infiltration. Immediately before the ground surface freezes, piezometric levels are at, or close to, their maximum annual values, whereas at the end of winter they are at, or close to, their minimum annual values. Therefore, the changes of piezometric level occurring during the winter period are indicative of maximum annual changes. These estimates can be compared to the results of field measurements summarized in Figure 5. The calculations were based on the following conditions:

1. below the area of infiltration, water movement is vertically downward and volume changes are 1-dimensional
2. hydraulic gradient immediately before freeze-up is $i = 0.5$ (*see* Figures 4 and 5)
3. hydraulic gradient at the ground surface after freeze-up is $i = 0$, corresponding to zero infiltration
4. no account is taken of the penetrating frost line
5. c_v = 0.1 m²/day, determined from field and laboratory tests (Kenney and Lau 1982)

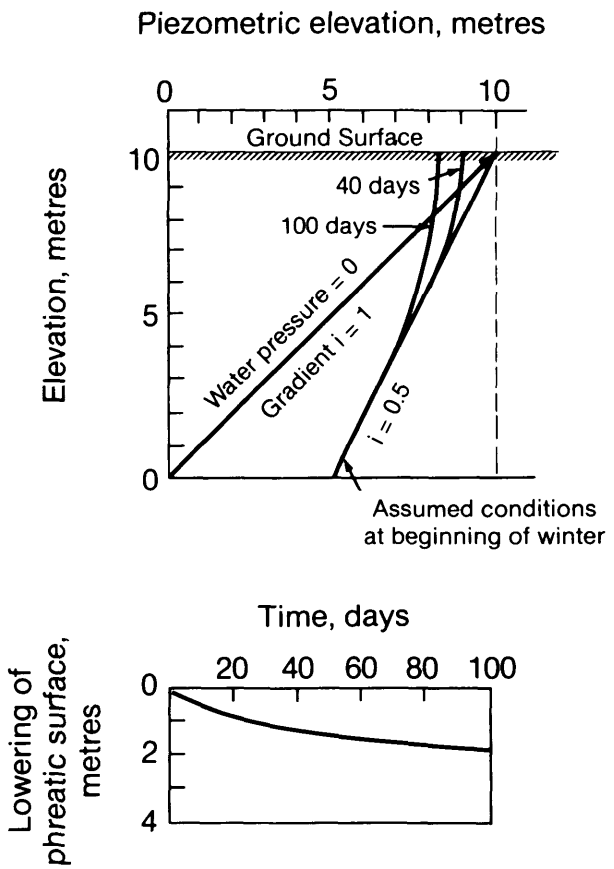

Figure 6. Predicted changes of piezometric elevaion and phreatic surface below infiltration area.

6. soil remains saturated.

In Figure 6, the period of 100 days approximates the maximum length of winter time when infiltration would be zero, and the corresponding changes of piezometric elevation are estimates of the maximum annual changes which would occur. The location of the phreatic surface has been estimated at different times and is shown to be lowered by about 2 m during a 100-day winter period.

The results of field measurements in Figure 5 and of calculations in Figure 6 compare quite closely.

Estimates of rates of increase of groundwater pressure caused by soil swelling following spring melt and the resumption of infiltration were found to be more rapid than the rates of decrease caused by soil consolidation during winter. The reason for this is that near the ground surface, the maximum hydraulic gradient for swelling conditions is larger than the maximum hydraulic gradient for consolidating conditions.

INFLUENCE OF OPEN JOINTS

At the ground surface, clay soils frequently contain open joints. At the Wabi Creek site, the depth to which open joints extend is 0.5 m to perhaps 1 m. At other sites, the depth might be considerably larger. The influence of open, interconnected joints is to increase significantly the bulk permeability of the soil. During periods of rainfall, the joints can become filled with water and the water pressures in the joints approach the hydrostatic condition. During periods of zero infiltration, the joints will aid near-surface drainage of ground water from the jointed clay.

The influence of open joints during periods of precipitation is to increase the groundwater pressures near the ground surface. Should the depth of open joints be small, their influence will be confined to the near-surface soils. Should the depth of open joints be large, their influence on groundwater pressures in the slope could be profound (Silvestri 1980; Lefebvre 1981).

SLOPE STABILITY

RESULTS OF CALCULATIONS

Slope stability calculations were performed using average soil properties of unit weight $\gamma = 17.3$ kN/m³, cohesion $c' = 5$ kPa, and angle of friction $\phi' = 24°$. The test program to determine the strength parameters was not extensive and therefore the accuracy of these parameters is uncertain. This means that the absolute values for safety factor obtained from stability calculations are somewhat uncertain, but the relative changes are correct.

The results are summarized in Figures 7, 8, and 9. It is apparent that the stability of the slope is affected by changes of river level, particularly the rapid rises during spring times (Figure 7). Also, for any particular value of river level, the safety factors can vary because of the ex-

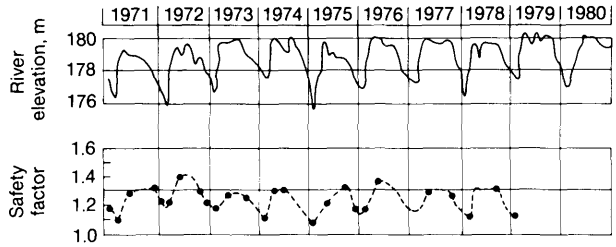

Figure 7. Variation with time of river level and factor of safety of slope.

istance of different conditions of groundwater pressure (Figure 8). The least stable conditions for the slope occur when there is a combination of large groundwater pressures and low river level. During the period 1971 to 1979, the least stable conditions are represented by the lower boundary of the results in Figure 8, curve A.

Approximate locations of critical slip surfaces were obtained from the stability calculations and in Figure 9 it is shown that for a particular value of river elevation, the elevation of the bottom of the critical slip surface is approximately 7 m below the river level.

ESTIMATION OF WORSE CONDITIONS

Consider the general questions of estimating the minimum safety factor of a natural clay slope. Under usual cir-

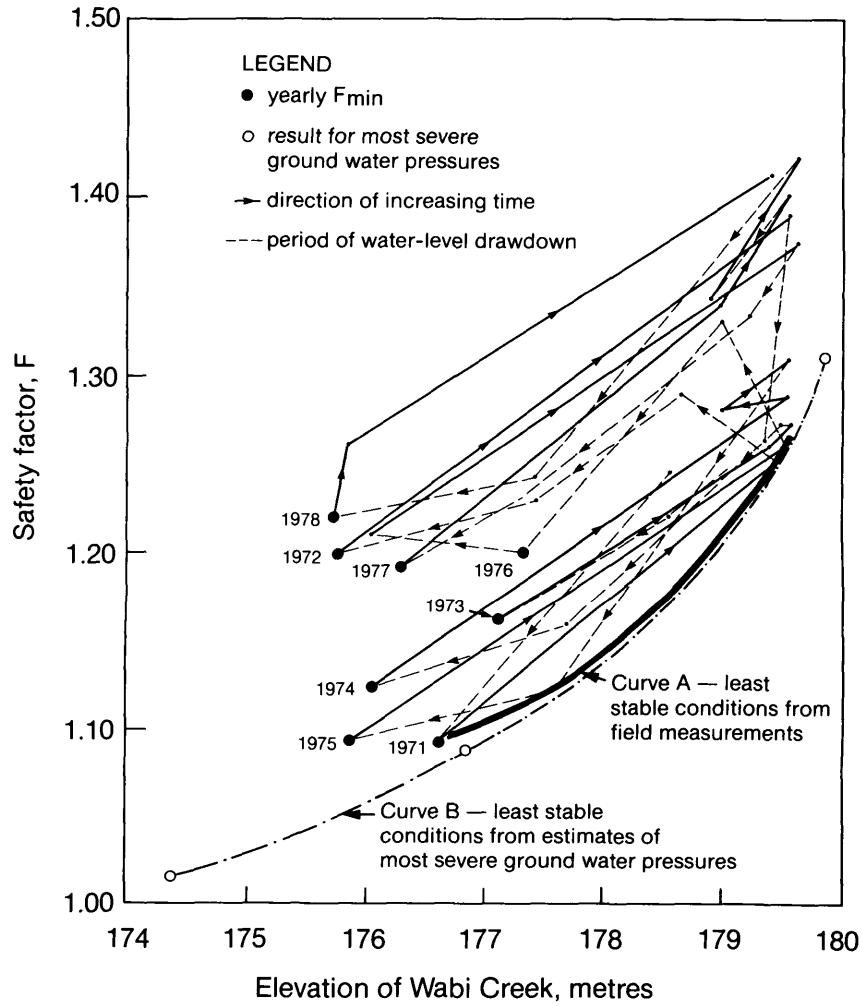

Figure 8. Changes of safety factor of slope relative to changes of river level (1971 to 1979).

cumstances there would be substantially less information about groundwater pressures than has been reported for the Wabi Creek slope. The information might consist of measurements taken over a period of time lasting several months, and very rarely more than a year. How could these measurements be used to estimate the most severe groundwater pressures the slope might experience at some future time? The Wabi Creek slope will be used as an example to describe one method of doing this.

The approach to be taken is to estimate the most severe conditions which might occur along boundaries, shown in Figure 10a, enclosing a region of the slope containing the most likely slip surfaces. The most severe condition at the ground surface would correspond to the phreatic surface being coincident with the ground surface. For this to occur in winter time would require the ground surface to remain unfrozen and infiltration to occur, which are possible. Along the lower boundary, which is remote from the ground surface, the groundwater pressures would remain relatively constant, independent of time. Therefore, in field investigations, piezometric levels would be measured at these depths and used as prescribed heads along the lower boundary. The 2 vertical boundaries can be assumed to be flow lines. On the assumption of steady-state flow conditions within the boundaries, groundwater pressures can be calculated using the Laplace seepage equation (Equation 1 with $\delta u/\delta t$ and $\delta\sigma/\delta t$ set equal to zero) or can be determined by sketching a flownet.

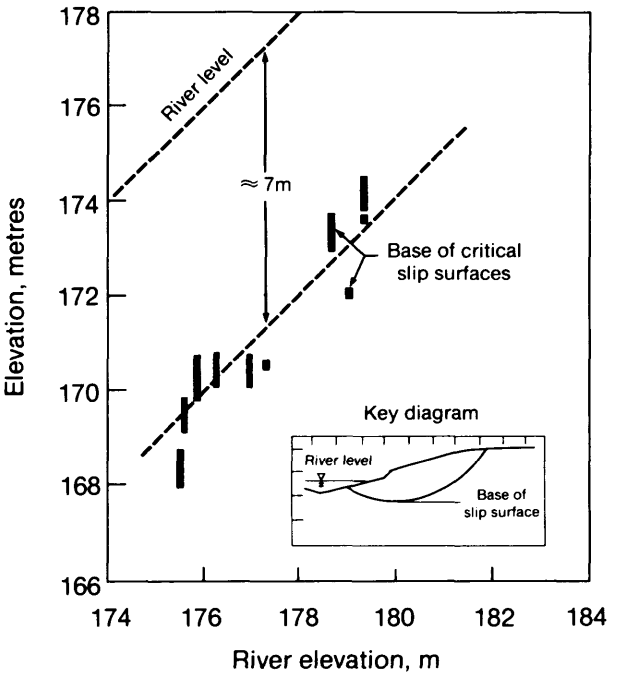

Figure 9. Location of critical slip surfaces relative to river level, 1971 to 1979.

This method was used to estimate the most severe groundwater pressures for the Wabi Creek slope. The resulting equipotential lines corresponding to river elevation 176.7 m are presented in Figure 10b. Three different river levels are chosen and the results of stability calculations, given by curve B in Figure 8, provide an indication of the state of stability of the Wabi Creek slope under the most severe groundwater pressure conditions which can be anticipated.

DETERMINATION OF c_v

Knowledge concerning the magnitudes of c_v within the slope is required if groundwater pressures and changes of pressure are to be estimated on the basis of consolidation theory.

The most convenient approach is to determine this soil property by means of field tests. The usual procedure is to install open-tube piezometers at a number of locations and to allow the water levels in the piezometer tubes to become static. Then, the water levels are either raised or lowered rapidly and subsequent changes of water levels are monitored with time. From the measured response curve and the geometry of the piezometer, an estimate can be made of c_v by means of the method described by Premchitt and Brand (1981).

As part of this research project, a new method for determining c_v from field tests was investigated. It is based on the use of a penetration-cone apparatus instrumented with a rapid-response piezometer. The device has been used before for other purposes and is sometimes called piezometer-friction cone or piezocone. The concept is that insertion of the cone causes an increase of ground-

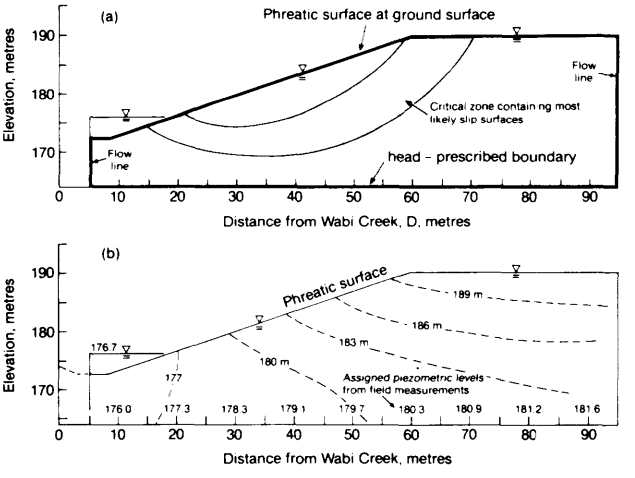

Figure 10. Method to estimate most severe groundwater pressures. (a) General explanation, (b) Typical results for Wabi Creek slope.

water pressure around the cone. The reduction of this pressure by consolidation and swelling is partly controlled by the soil property c_v. Therefore, there is a possibility to use the water pressure decay curve following cone penetration to determine c_v. The results of the research work are described by Sum (1983) but the work is incomplete. It requires further development of the apparatus, further analytical work, and further field trials. However, the method has promise.

DISCUSSION

A field study was made of changes of groundwater pressures in a slope composed of non-fissured clay having a value of coefficient of consolidation $c_v \cong 0.1$ m²/day. The results indicate that, except near the ground surface, the groundwater pressures remain quite steady. Estimates, based on consolidation theory, of changes of piezometric level in soils having similar values of coefficient of consolidation indicate very slow response of groundwater pressures to changes of hydraulic conditions at the ground surface.

The following conclusions can be drawn:

1. Over short periods of time, heavy rainfall will not cause important changes of groundwater pressure in clay soils having values of coefficient of consolidation as small as $c_v = 0.1$ m²/day, except in a narrow zone near the phreatic surface.
2. Conclusion 1 leads to the conclusion that clay soils having small values of c_v will not experience landslides as a direct result of a precipitation event unless the slope is already very close to failure.
3. It is known that some landslides have been triggered by heavy rainfall. If such a landslide occurs, it indicates that the rainfall caused important increases of groundwater pressure, and for this to occur the soil must have a larger value of coefficient of consolidation than $c_v = 0.1$ m²/day. Should the soil be clay, such an occurrence might indicate that the soil was fissured, or was pervious for other reasons, such that the bulk value of coefficient of consolidation was much larger than that of the clay in its intact state.
4. A method has been suggested for estimating the maximum groundwater pressures occurring over the long term. It involves (a) the measurement of groundwater pressures at depths where nearly steady-state conditions exist and (b) the assumption of severe hydraulic conditions at (or near) the ground surface being maintained over a sufficiently long period of time such that seepage equilibrium exists.
5. The presence or absence of fissures and other pervious features, which can lead to rapid changes of groundwater pressure, are of key importance to the question of stability of clay slopes.

REFERENCES

Chan, H.T., and Kenney, T.C.
1973: Laboratory Investigation of Permeability Ratio of New Liskeard Varved Soil; Canadian Geotechnical Journal, Volume 10, Number 3, p.453-472.

Kenney, T.C.
1979: Long-Term Groundwater Pressures in Soft Clay Slopes; VI Panamerican Conference on Soil Mechanics and Foundation Engineering, Lima, Peru, Proceedings, Volume 3, p.83-89.

Kenney, T.C., and Chan, H.T.
1973: Field Investigation of Permeability Ratio of New Liskeard Varved Soil; Canadian Geotechnical Journal, Volume 10, Number 3, p.473-488.

Kenney, T.C., and Lau, K.C.
1982: Horizontal Deep Drains to Stabilize Clay Slopes; Report to Ontario Ministry of Natural Resources, regarding Geoscience Research Grant GR-7.

Lefebvre, G.
1981: Discussion on - The Long-term Stability of a Cutting in an Overconsolidated Sensitive Clay - by V. Silvestri; Canadian Geotechnical Journal, Volume 18, Number 3, p.322-323.

Premchitt, J., and Brand, E.W.
1981: Pore Pressure Equilization of Piezometers in Compressible Soils; Geotechnique, Volume 31, Number 1, p.105-123.

Silvestri, V.
1980: The Long-Term Stability of a Cutting in an Overconsolidated Sensitive Clay; Canadian Geotechnical Journal, Volume 17, Number 3, p.337-351.

Sum, S.
1983: Investigation of Determination of Coefficient of Consolidation of Soils by Means of In Situ Tests; M.Eng. Thesis, University of Toronto, 91p.

Grant 80 Rare Earth Elements in Felsic Volcanic Rocks Associated with Cu-Zn Massive Sulphide Mineralization

C.M. Lesher[1], I.H. Campbell[1], P. Coad[2], J.M. Franklin[3], H.L. Gibson[4], A.M. Goodwin[1], M.P. Gorton[1], T.R. Hart[1], J.M. Sowa[1], and P.C. Thurston[5]

[1]Department of Geology, University of Toronto
[2]Kidd Creek Mines Limited
[3]Economic Geology Division, Geological Survey of Canada
[4]Corporation Falconbridge Copper Limited
[5]Ontario Geological Survey

ABSTRACT

Most felsic volcanic rocks associated with massive Cu-Zn sulphide deposits in the Superior Province (e.g. the Kamiskotia, Kidd Creek, Matagami, and Noranda camps in the Abitibi Belt, and the South Bay deposit in the Uchi Belt) are rhyolites of tholeiitic affinity. They form the felsic members of a bimodal volcanic sequence; they are commonly underlain by intrusions representing subvolcanic magma chambers; and they are characterized by relatively flat chrondrite-normalized REE patterns ([La/Yb]n = 1-4), strong negative Eu anomalies (Eu/Eu* = 0.25-0.90), and high incompatible trace element (HREE, Y, Zr, Hf, U, Th) contents. They probably were derived from partial melting of associated tholeiitic basalts during intrusion of, and subsequent fractional crystallization of magmas in, high level chambers. As the subvolcanic magma chambers probably were important components of the ore-forming hydrothermal systems, the distinctive geochemistry of the tholeiitic felsic volcanic rocks may be used to identify favourable target horizons for mineral exploration.

Other felsic volcanic rocks in the Superior Province are of calc-alkaline affinity and may be further subdivided into 2 types on the basis of trace element geochemistry. Those of the first type (e.g. Bowman Subgroup and Skead Group, Abitibi Belt; Kakagi Lake, Lake of the Woods, and Shoal Lake areas, Wabigoon Belt) are predominantly dacites and rhyodacites. These rocks are not known to contain massive sulphide deposits and are characterized by steep REE patterns ([La/Yb]n = 5-40), weakly negative to moderately positive Eu anomalies (Eu/Eu* = 0.85-1.6), and low incompatible trace element contents. They probably were derived directly from a deep mantle source region, possibly at low degrees of partial melting, with minimal fractional crystallization prior to emplacement and do not represent prospective exploration targets. Those of the second type (e.g. Misema Subgroup, Abitibi Belt; and Sturgeon Lake and Wabigoon areas, Wabigoon Belt) are geochemically transitional between the tholeiitic group and the first calc-alkaline type. Their shallowly sloping REE patterns ([La/Yb]n = 2.5-6), moderate Eu anomalies (Eu/Eu* = 0.55-1.1), and moderate incompatible trace element contents suggest derivation from a shallower mantle source region and/or generation at higher degrees of partial melting with subsequent fractional crystallization. Where subvolcanic magma chambers have been identified (e.g. in the Sturgeon Lake area), the second calc-alkaline type may be mineralized.

INTRODUCTION

The aim of this project has been to use trace element geochemistry, especially the rare-earth elements (REE), to classify the felsic volcanic rocks associated with massive Cu-Zn sulphide deposits, and to evaluate this technique as a tool in mineral exploration. It has been noted that most volcanogenic massive Cu-Zn sulphide deposits in the Superior Province (e.g. the Kam-Kotia, Matagami, and Noranda deposits, Abitibi Belt; the Mattabi deposit, Wabigoon Belt; and probably the South Bay deposit, Uchi Belt) are underlain by intrusions representing large high-level magma chambers. The initial hypothesis was that the magma chambers were an essential component of the ore-forming process, supplying heat to drive the hydrothermal system, and that rocks derived from such high level systems may be geochemically distinguishable from rocks derived from other sources. Thus, the felsic volcanic rocks associated with massive sulphide deposits may have a geochemical signature reflecting high level processes, and may be geochemically distinct from those in "barren" sequences. Previous reports (Campbell *et al.* 1981a, 1982a) have shown this to be the case.

This project has shown that trace element geochemistry can be used to assist in the exploration for massive sulphide deposits by identifying prospective host sequences in the following ways:

1. Area selection can be based on the immobile trace element geochemistry of felsic volcanic rocks.
2. Within a known ore-bearing sequence, felsic volcanic rocks which are petrogenetically related to subvolcanic intrusions may be identified by comparing the trace element geochemistry of the intrusive rocks with the volcanic rocks (Campbell *et al.* 1981b). In a cyclic sequence containing ore-associated and barren felsic volcanic rocks, the ore-associated felsic volcanic rock

units exhibit different chondrite-normalized rare-earth element (REE) patterns from the barren ones (Thurston 1981; Campbell *et al.* 1982b).

3. Target selection based on the geochemistry of alteration zones is possible when normally immobile trace elements, such as Y and the REE, become mobile in alteration pipes beneath large massive sulphide deposits (Campbell *et al.* 1982a), and allow identification of major ore-associated hydrothermal systems.

The aim of this final report on the 3-year project is to summarize the empirical geochemical distinctions between barren and ore-associated felsic volcanic rocks in the Superior Province based on analyses of a large number of samples for the REE and selected trace elements. Felsic volcanic rocks associated with massive Cu-Zn sulphide deposits have been sampled from the Kidd Creek and Corbet (Noranda) Mines, and the Kamiskotia area in the Abitibi Belt; from the South Bay Mine (Uchi Lake area) in the Uchi Belt; and from the Mattabi Mine (Sturgeon Lake area) in the Wabigoon Belt; limited data are also available for the Matagami area in the Abitibi Belt (MacGeehan and MacLean 1980). Felsic volcanic rocks from mineralized sequences, distant from known massive sulphide deposits, have been sampled in the Fly Lake area 8 km south of the South Bay Mine and from throughout the Rouyn-Noranda area. Selecting barren felsic volcanic rocks for comparison is somewhat more problematical, as most sequences contain minor occurrences of mineralization. However, felsic volcanic rocks from sequences not known to contain significant massive sulphide deposits have been sampled from the Bowman, Garrison, and Misema Subgroups of the Blake River Group and the Skead Group in the Abitibi Belt (Goodwin 1979) and from the Kakagi Lake, Lake of the Woods, Shoal Lake, and Wabigoon areas in the Wabigoon Belt, northwestern Ontario (Goodwin 1977).

Campbell *et al.* (1982a) have shown that the major elements normally used to classify igneous rocks (e.g. Si, Al, Fe, Mg, Ca, Na, K, etc.) are mobile in the widespread zones of pervasive low-grade alteration surrounding massive sulphide deposits. However, the REE and high-field-strength (charge/ionic radius) elements such as Y, Zr, Hf, U, and Th appear to have remained immobile except in the alteration pipes which focused the hydrothermal fluids beneath the deposits. We have, therefore, excluded the alteration pipes from this study and have used only the immobile elements to discriminate between ore-associated and barren felsic volcanic rocks. Rare-earth element variations are characterized by fractionation of the light and heavy REE, measures of which are given by the ratio of chondrite-normalized La and Yb ([La/Yb]n) and the chondrite-normalized abundance of Yb ([Yb]n). Other trace element variations are considered relative to Zr, which exhibits a wide range of abundance in these rocks (30 to 800 ppm), is determined with very high analytical accuracy, and is demonstrably one of the least mobile trace elements.

GEOCHEMISTRY

Based on trace element geochemistry, several empirical distinctions may be made between ore-associated and barren felsic volcanic rocks in the Superior Province, the most important of which are summarized below.

Felsic volcanic rocks associated with most massive sulphide deposits in the Superior Province (Figure 1a) are characterized by relatively flat chondrite-normalized REE patterns ([La/Yb]n = 1-6) and by high heavy REE contents ([Yb]n = 10-120). Importantly, samples from mineralized sequences distant from ore exhibit the same geochemical signature as ore-associated samples (cf. Fly Lake vs. Uchi Lake and Rouyn-Noranda vs. Corbet). In contrast, barren felsic volcanic rocks (Figure 1b) exhibit steeper REE patterns ([La/Yb]n = 2-40) and are depleted in heavy REE ([Yb]n = 2-30). Although there is some overlap of REE patterns, especially of the ore-associated Sturgeon Lake and barren Misema and Wabigoon samples (solid symbols in Figures 1a and 1b), rocks with [La/Yb]n < 3 and/or [Yb]n >30 can normally be confidently classified as ore-associated, and those with [La/Yb]n > 5 and/or [Yb]n < 10 as barren. One notable exception is the Garrison samples (*see* Figure 1b), which are unfractionated ([La/Yb]n = 1.1) and strongly enriched in heavy REE ([Yb]n = 90-110). Although no massive sulphide deposits are present in the sampled sequence, Goodwin (1979) reported a relatively high concentration of Cu(-Zn-Au) occurrences in the Garrison Subgroup.

Ore-associated felsic volcanic rocks are also characterized by significant negative Eu anomalies ($Eu/Eu^* = 0.25$ to 0.90, *see* Figure 2). Barren felsic volcanic rocks are more variable ($Eu/Eu^* = 0.55$ to 1.6, excluding Garrison), but are generally less depleted in Eu; the overlapping ratios are again those of the Misema and Wabigoon samples.

Yttrium has a trivalent charge and an ionic radius similar to that of holmium and therefore exhibits close geochemical affinities with the heavy REE. Zirconium on the other hand, has a 4+ charge and behaves more like a light REE. Thus, to a first approximation, the Y content of a rock can be a measure of the Yb content, and the Zr/Y ratio a measure of the La/Yb ratio. As such, Y is also enriched in the ore-associated rocks (Y = 15-200 ppm, *see* Figure 3a) compared to the barren ones (Y = 3-50 ppm, excluding Garrison samples, *see* Figure 3b) and Zr/Y ratios for the ore-associated rocks (Zr/Y = 2-10) are generally lower than those for the barren rocks (Zr/Y = 4-30, excluding Garrison samples). Zr/Y ratios appear to be relatively constant within, and vary systematically between, most individual sample groups; the overlap of ratios between the ore-associated and barren felsic volcanic rocks is similar to that shown by the REE data.

Titanium is depleted in the ore-associated felsic volcanic rocks, especially Kidd Creek Mine samples, compared to the barren ones. The ternary system Zr-Ti-Y has

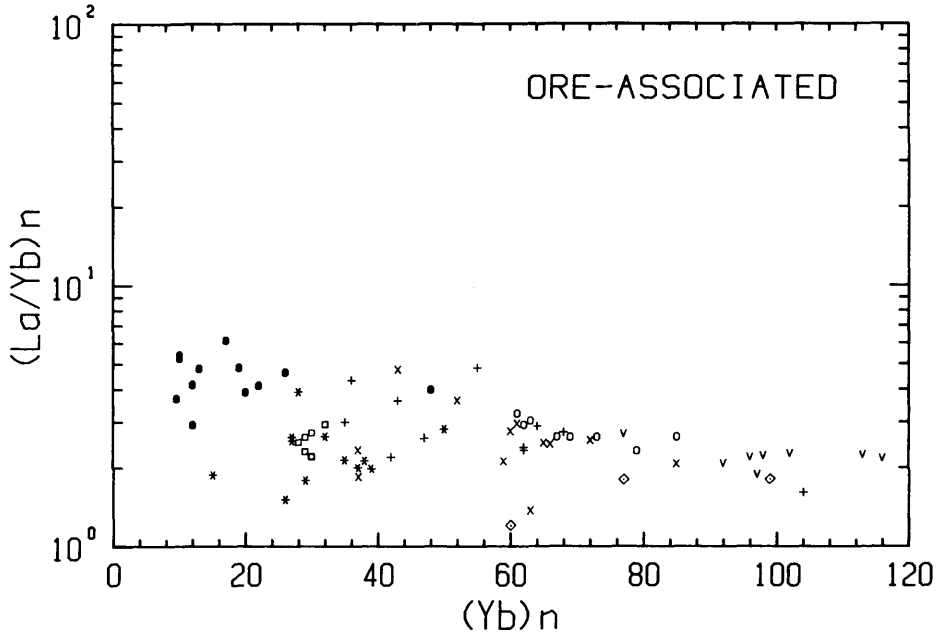

(a)

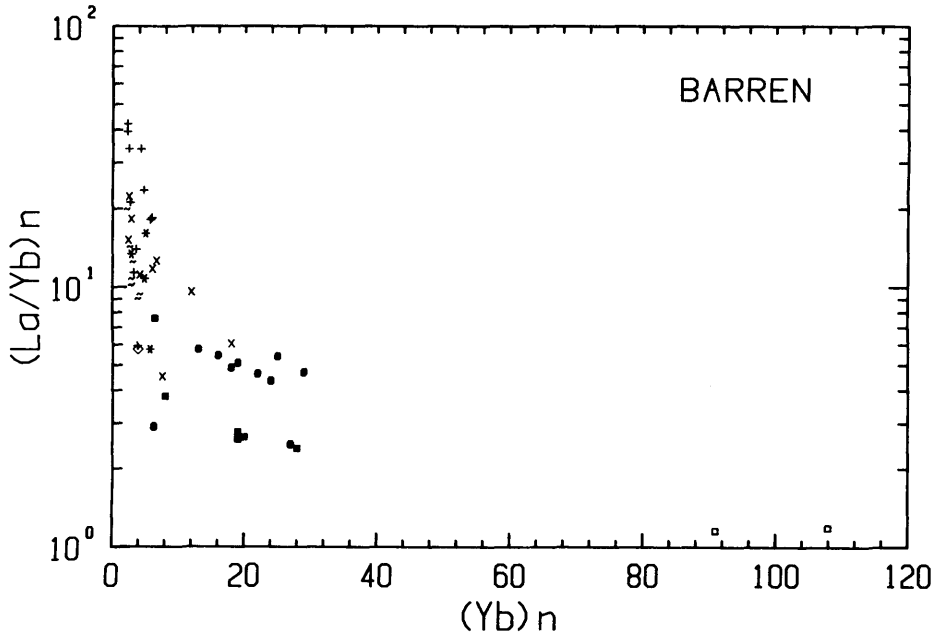

(b)

Figure 1. Chondrite-normalized La/Yb vs Yb plots for felsic volcanic rocks in the Superior Province. **(a) Ore-associated**: x *Kamiscotia,* + *Kidd Creek Mine,* ◈ *Matagami,* □ *Corbet Mine, and* * *Rouyn-Noranda area in the Abitibi Belt;* o *South Bay (Uchi Lake) and* v *Fly Lake in the Uchi Belt; and* • Sturgeon Lake in the Wabigoon Belt. **(b) Barren**: ◇ *Bowman,* ~ *Skead,* □ *Garrison, and* ■ *Misema in the Abitibi Belt; and* * *Kakagi Lake,* + *Lake of the Woods,* x *Shoal Lake, and* • *Wabigoon areas in the Wabigoon Belt.*

been used previously to discriminate between basaltic rocks erupted in different tectonic settings; but when rescaled for felsic rocks, the Zr/10 - Ti/100 - Y projection also discriminates between relatively Y-rich, Ti-poor ore-associated felsic volcanic rocks (Figure 4a) and relatively Ti-rich, Y-poor barren ones (Figure 4b). However, the anomalous and overlapping sample groups (Misema, Sturgeon Lake, Wabigoon) also includes several Rouyn-Noranda samples with relatively high Ti/Y ratios.

Other trace elements such as Hf, U, and Th are also enriched in the ore-associated felsic volcanic rocks relative to the barren ones. Hf and Zr both have 4+ charges as well as very similar ionic radii and should behave similarly under a wide variety of geological processes. Accordingly, Zr/Hf ratios for most sample groups, irrespective of whether associated with ore or barren rocks, are virtually constant (Hf/Zr = *ca* 40). However, the Kidd Creek (Zr/Hf = *ca* 30) and possibly Uchi Lake (Zr/Hf = *ca* 35) sample groups appear to be systematically higher. Zr/U and Zr/Th ratios are also relatively constant within individual sample groups, but there are no systematic differences between ore-associated and barren felsic volcanic rocks.

DISCUSSION

Most of the immobile trace elements are not present in significant amounts in the major mineral phases controlling the chemistry of these rocks. They are incompatible elements, which are concentrated in accessory phases consumed at low degrees of partial melting and are precipitated during the final stages of fractional crystallization. Provided that the degree of partial melting or fraction of liquid remaining during crystallization is greater than the bulk solid/liquid partition coefficient (i.e. F >> D), their absolute abundances in the magma will be controlled by the degree of melting and/or fractionation, and their relative abundances (interelement ratios) by the initial source composition. Exceptions are Eu which is concentrated in plagioclase, and the heavy REE plus Y, which are concentrated in garnet and to a lesser extent in amphibole and clinopyroxene.

In earlier studies, we showed that felsic volcanic rocks associated with massive Cu-Zn sulphide deposits can be divided into 2 types: tholeiitic and calc-alkaline. Most ore-bearing felsic volcanic rocks in the Superior

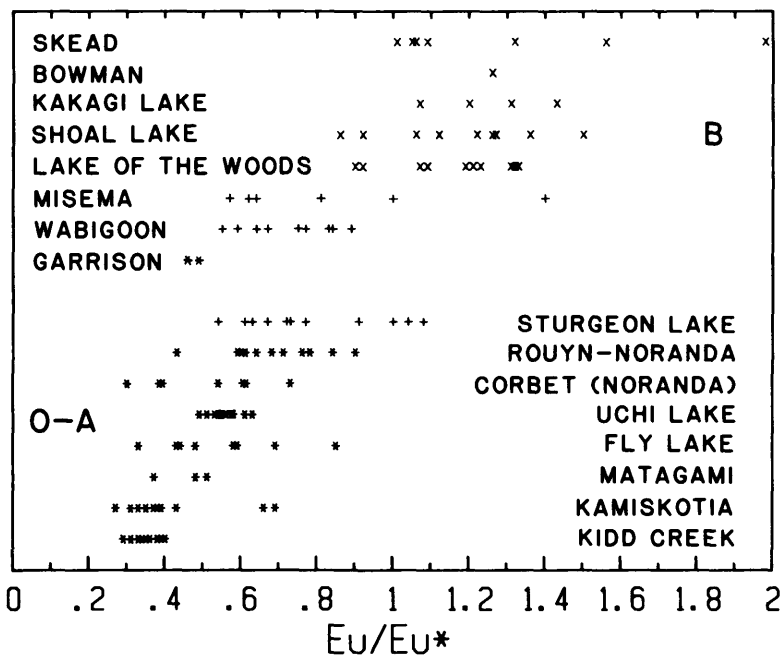

Figure 2. Plot of Eu/Eu for felsic volcanic rocks in the Superior Province; Eu* interpolated from chondrite-normalized Sm and Tb. Sample localities are subdivided into barren (B) and ore-associated (O-A) groups and into rocks of tholeiitic (*) and calc-alkaline (x = type 1 and + = type 2) affinity.*

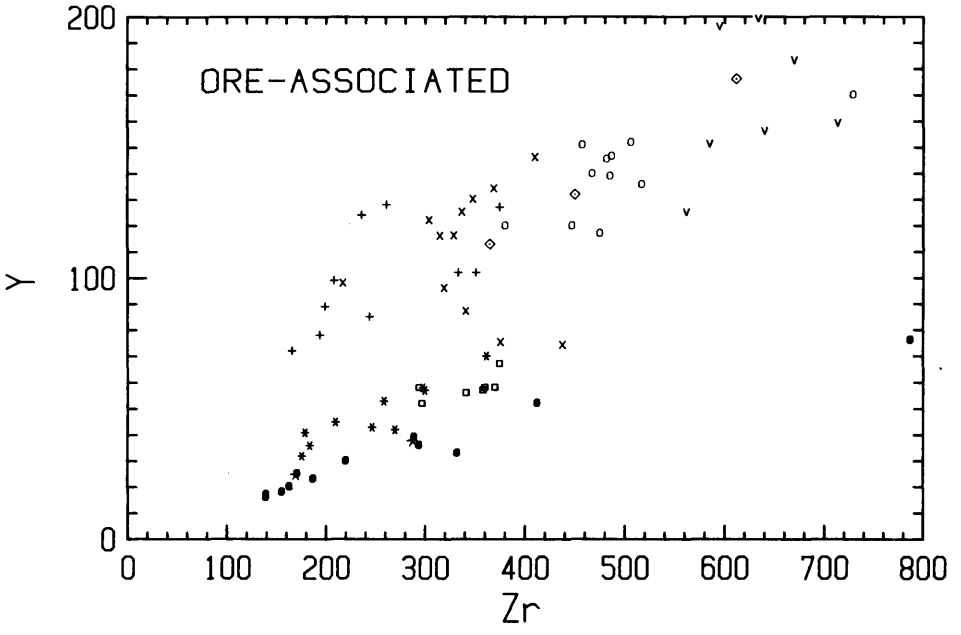

(a)

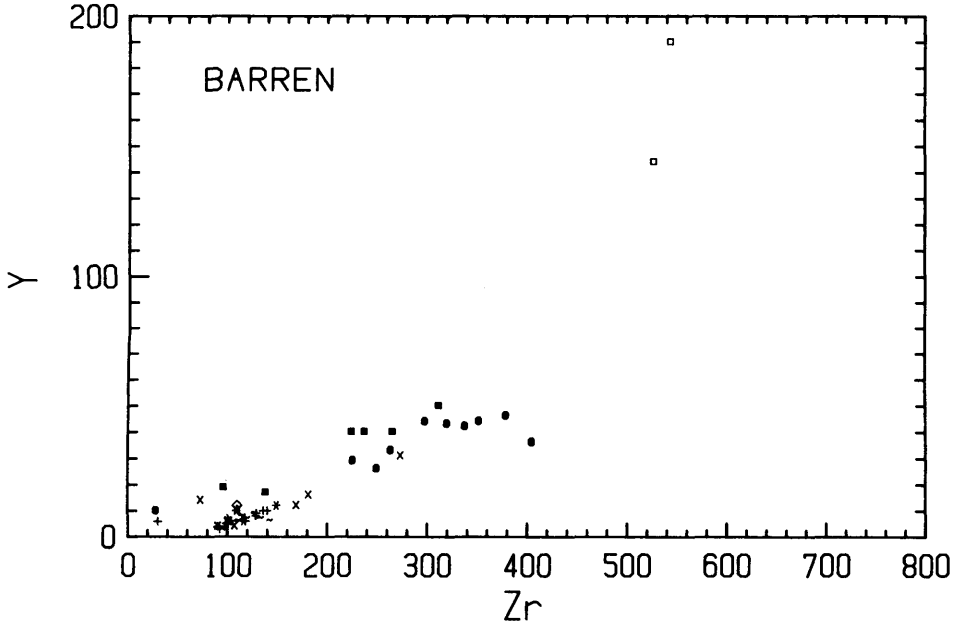

(b)

Figure 3. Y vs. Zr plots for (a) Ore-associated and (b) Barren felsic volcanic rocks in the Superior Province; symbols as in Figure 1.

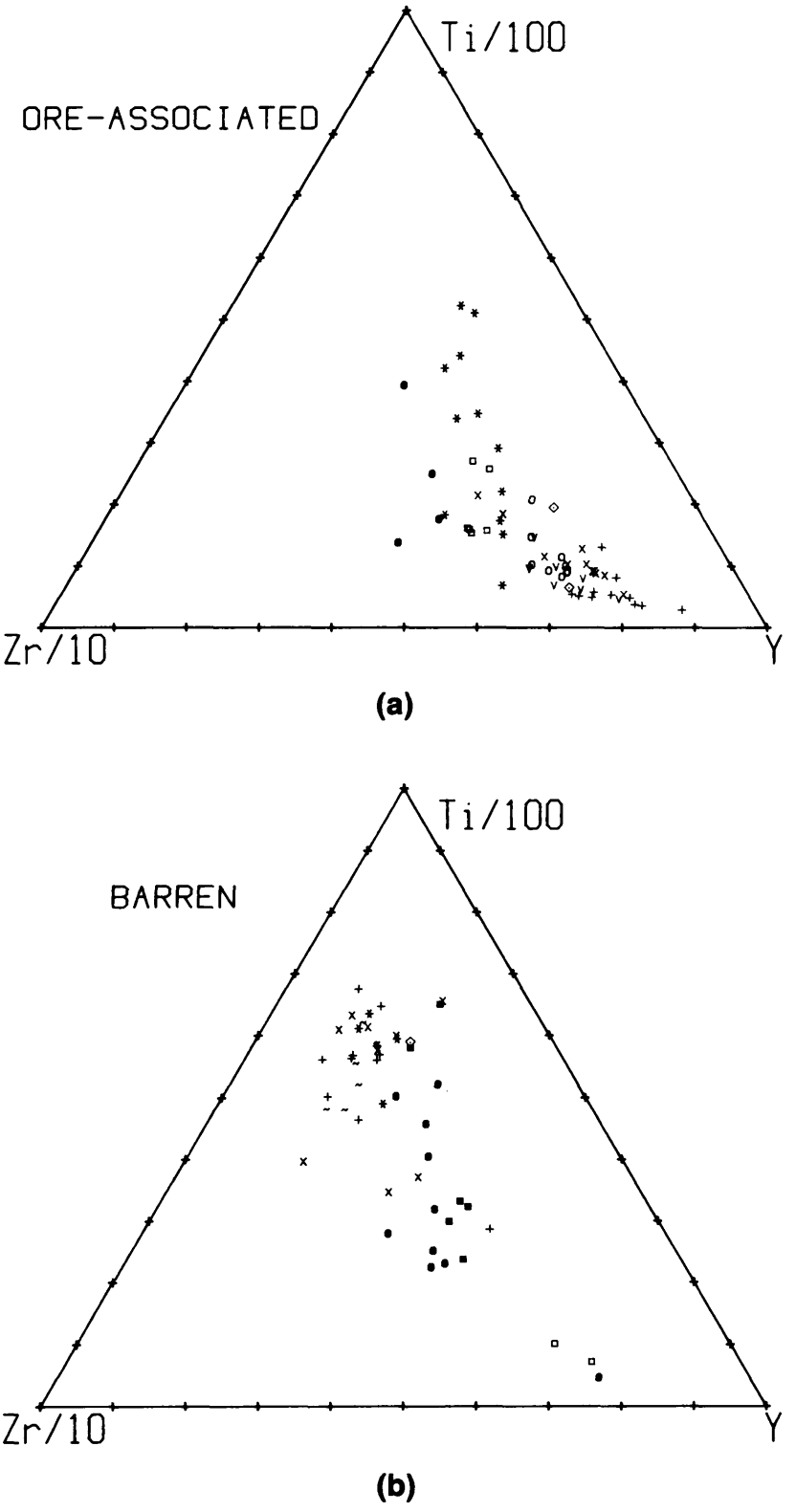

Figure 4. Zr/10 – Ti/100 – Y plots for (a) Ore-associated and (b) Barren felsic volcanic rocks in the Superior Province; symbols as in Figure 1.

Province are of tholeiitic affinity: they form the felsic members of a bimodal rhyolite-basalt volcanic rock sequence and are characterized by relatively flat REE patterns, strong negative Eu anomalies, and high incompatible trace element contents. In some areas (e.g. Kamiskotia, Matagami, Noranda, and possibly Uchi Lake), the volcanic rocks are underlain by intrusive rocks representing subvolcanic magma chambers. The intrusive rocks can be demonstrated to be petrogenetically related to the volcanic rocks (Campbell *et al.* 1981b), and the distinctive geochemistry of the felsic volcanic rocks is consistent with partial melting of the tholeiitic basalts during intrusion. The strong negative Eu anomalies in the felsic volcanic rocks indicate retention of plagioclase in the residue and/or fractional crystallization of plagioclase. The lower Ti/Y ratios of the mineralized felsic volcanic rocks, especially for Kidd Creek samples, suggest fractionation (or retention) of a Ti-rich phase such as ilmenite or titanomagnetite. The slightly lower Zr/Hf ratios of the Kidd Creek samples and possibly the Uchi Lake samples may indicate control by a Zr-rich accessory phase such as zircon. Mobility of the major elements and limited variations within petrogenetically related sample groups precludes more detailed interpretations.

There does not appear to be any systematic relationship between the size of a massive sulphide deposit and the degree of incompatible element enrichment (cf. Kidd Creek and Uchi Lake samples). This is not unexpected, as the distinctive geochemistry of the ore-associated felsic volcanic rocks does not necessarily relate directly to the ore-forming process. The size of an orebody is controlled by the size and thermal characteristics of the magma chamber which supplies heat to the hydrothermal system, and by the efficiency of the ore-forming process.

Most barren felsic volcanic rocks are of calc-alkaline affinity and may be further subdivided into 2 types: (1) dacites with steep REE patterns (high [La/Yb]n), weakly negative to moderately positive Eu anomalies, and low incompatible element contents; and (2) rhyodacites and rhyolites with shallowly sloping REE patterns, weakly to moderately negative Eu anomalies, and moderate incompatible element contents. These rocks generally comprise the upper parts of basalt-andesite-dominated volcanic sequences with only minor rhyolite components (*see* Goodwin 1977). Those of the first type appear to be unique to the Archean and are not known to be associated with any massive Cu-Zn sulphide deposits. Their geochemistry is consistent with derivation directly from a deep mantle source region, possibly at low degrees of partial melting, leaving garnet and no plagioclase in the residue, and involving minimal fractionation during ascent. Those of the second type are more similar to modern calc-alkaline volcanic rocks and their geochemistry suggests a shallower source and/or higher degree of partial melting with subsequent fractional crystallization prior to emplacement. There is considerable overlap in the trace element geochemistry of the ore-associated (Sturgeon Lake) and barren (Misema and Wabigoon) type 2 calc-alkaline felsic volcanic rocks; however, it is probably not fortuitous that the ore-associated rhyolites in the Sturgeon Lake area are underlain by intrusive rocks representing a subvolcanic magma chamber (Beidelman Bay Complex *in* Campbell *et al.* 1981b). The relationship between the 2 calc-alkaline types is uncertain as the different sample groups are not necessarily petrogenetically related. However, the gradations suggest a continuum of lava compositions resulting from varying degrees of partial melting and subsequent fractional crystallization.

We are in the process of extending this study to other Archean areas and to felsic volcanic rocks of younger age. All of the ore-associated felsic volcanic rocks studied to date are of calc-alkaline affinity, making the distinction between ore-bearing and barren felsic volcanic rocks more difficult. The apparent absence of tholeiitic felsic volcanic rocks from other Archean Provinces may reflect a unique tectonic setting for the Superior Province. Alternatively, these rocks may be present in other areas, but fail to outcrop as a consequence of differential weathering in arid areas such as Australia and South Africa.

CONCLUSIONS

Most felsic volcanic rocks associated with massive Cu-Zn sulphide deposits in the Superior Province are of tholeiitic affinity: they form the felsic member of bimodal volcanic sequences, are commonly underlain by intrusive rocks representing subvolcanic magma chambers, and are characterized by relatively flat chondrite-normalized REE patterns ([La/Yb]n = 2-5), strong negative Eu anomalies (Eu/Eu* = 0.25-0.90), and high incompatible element (HREE, Y, Zr, Hf, U, Th) contents. They probably formed by partial melting of associated tholeiitic basalts during emplacement of, and by subsequent fractional crystallization of magma in, high level chambers. As the subvolcanic magma chambers are considered to be an important component of the ore-forming hyrothermal system, the distinctive geochemical signature of the tholeiitic felsic volcanic rocks makes them a favourable target for mineral exploration. The limited data from the Garrison Subgroup places it within this category. Although no massive sulphide deposits are present within the sampled sequence, the sequence does contain a concentration of Cu-(Zn-Au) occurrences and should be considered a prime exploration target.

Other felsic volcanic rocks in the Superior Province are of calc-alkaline affinity: they are predominantly dacites and rhyodacites in volcanic sequences containing only a minor rhyolite component, and may be subdivided into 2 types on the basis of trace element geochemistry. Those of the first type are predominantly dacites which are not known to contain massive sulphide deposits and are characterized by relatively steep REE patterns ([La/Yb]n = 5-40), weakly negative to moderately positive Eu anomalies (Eu/Eu* = 0.85-1.6), and low incompatible element contents. They have probably been derived from a deep mantle source region at low degrees of partial melting with garnet and no plagioclase in the residue and minimal fractional crystallization of magma prior

to emplacement. They do not represent prospective exploration targets. Felsic volcanic rocks of the second type are geochemically transitional between the tholeiitic and type 1 calc-alkaline groups; compared to the latter, the shallowly sloping REE patterns ([La/Yb]n = 1.5-6), weakly to moderately negative Eu anomalies (Eu/Eu* = 0.55-1.1), and moderate incompatible element contents suggest derivation from a shallower source and/or generation at higher degrees of partial melting with subsequent fractional crystallization. Importantly, where subvolcanic magma chambers have been identified, such as at Sturgeon Lake, this type also may be associated with volcanogenic massive Cu-Zn sulphide mineralization.

We thank W.H. MacLean for access to unpublished data from the Matagami area.

REFERENCES

Campbell, I.H., Coad, P., Franklin, J.M., Gorton, M.P., Hart, T.R., Scott, S.D., Sowa, J., and Thurston, P.C.
1981a. Rare Earth Elements in Felsic Volcanic Rocks Associated with Cu-Zn Massive Sulphide Mineralization; Grant 80, p.45-53 *in* Geoscience Research Program Summary of Research, 1980-1981, edited by E.G. Pye, Ontario Geological Survey, Miscellaneous Paper 98, 340p.

Campbell, I.H., Franklin, J.M., Gorton, M.P., Hart, T.R., and Scott, S.D.
1981b. The Roles of Subvolcanic Sills in the Generation of Massive Sulfide Deposits; Economic Geology, Volume 76, p.2248-2253.

Campbell, I.H., Coad, P., Franklin, J.M., Gorton, M.P., Hart, T.R., Scott, S.D., Sowa, J., and Thurston, P.C.
1982a. Rare Earth Elements in Felsic Volcanic Rocks Associated with Cu-Zn Massive Sulphide Mineralization; Grant 80, p.20-28 *in* Geoscience Research Program Summary of Research, 1981-1982, edited by E.G. Pye, Ontario Geological Survey, Miscellaneous Paper 103, 340p.

1982b. Rare Earth Elements in Felsic Volcanic Rocks Associated with Cu-Zn Massive Sulphide Mineralization: A Preliminary Report; Canadian Journal of Earth Sciences, Volume 49, p.619-623.

Goodwin, A.M.
1977. Archean Volcanism in Superior Province, Canadian Shield; p.205-241 *in* Volcanic Regimes in Canada, edited by W.R.A. Barager, L.C. Coleman, and J.M. Hall, Geological Association of Canada Special Paper 16, 476p.

1979. Archean Volcanic Studies in the Timmins-Kirkland Lake-Noranda Region of Ontario and Quebec; Geological Survey of Canada, Bulletin 278, 51p.

MacGeehan, P.J. and MacLean, W.H.
1980. Tholeiitic Basalt-Rhyolite Magmatism and Massive Sulphide Deposits at Matagami, Quebec; Nature, Volume 283, p.153-157.

Thurston, P.C.
1981. Economic Evaluation of Archean Felsic Volcanics Using REE Geochemistry; p.439-452 *in* Archean Geology, edited by J.E. Glover and D.I. Groves, Geological Society of Australia Special Publication 7, 515p.

Grant 57 A Microearthquake Survey of the Gobles Oil Field Area of Southwestern Ontario

R.F. Mereu
Department of Geophysics, University of Western Ontario

ABSTRACT

In August 1980, a 3-station seismic network was installed by the University of Western Ontario in the Gobles oil field in southwestern Ontario. A fourth station was added to this network in November 1982.

During the period from August 1980 to May 1983, over 350 small earth tremors or microearthquakes were detected by the array. Although the average number of events detected per month was approximately 10, the actual number detected per month was rather erratic. Most of the events detected fell within the 1.0 to 2.0 magnitude range. Three events were greater than magnitude 3.0. A detailed analysis of the location of the events showed that they do not correlate with the positions of the oil and gas wells but are confined to 2 main areas, one lying 1.5 km northwest of the Town of Gobles, and the other just to the southeast of the town. With the aid of the fourth station, the areal coverage was improved resulting in more precise determinations of epicentre locations. The observed first motion pattern also indicated that at least 2 active faults almost perpendicular to each other are present in the area. The observations to date are consistent with the hypothesis that the events are induced or triggered by fluids which are being pumped in and out of wells from secondary recovery activities.

INTRODUCTION

A few years ago, the Geophysics Department of the University of Western Ontario received reports of a number of "felt vibrations" or minor tremors from residents of the Gobles oil field area just east of Woodstock, Ontario. Further information of the preliminary studies of these events was given by Mereu (1980, 1982). In this report, the results of the previous reports are brought up to date.

In August 1980, the installation of a 3-station seismic network over the oil field was completed. A fourth station was added last year and became operational in November 1982. This additional station was established to improve the areal coverage and hence the precision in the determination of the locations of the epicentres. The instrument package at each station is made up of a 1 Hz vertical Mark Products seismometer, an amplifier, and a voltage-to-frequency converter. Power is derived from a set of large dry cells which need to be replaced once a year and have excellent low temperature characteristics. The frequency-modulated signals are multiplexed and telemetered directly to the laboratories of the Geophysics Department of the University of Western Ontario via a long distance telephone line. These signals are at present being monitored on a 24-hour basis with magnetic tape. Events of interest are then saved on an edited tape.

RESULTS

The array network has now been in operation for almost 3 years from August 1980 to May 1983. During this time, a total of 350 earth tremors or microearthquakes in the 0.5 to 3.5 magnitude range were detected. Figure 1 is a plot which shows that the number of events which occurred per month is rather erratic. Most of these events have been in the 1.0 to 2.0 magnitude range. Three events have been greater than magnitude 3.0 and were felt by local residents.

A detailed analysis was made of the location of the well-recorded events. These are shown in Figure 2 which shows that most of the events are confined to roughly 2 separate areas, one lying 1 to 1.5 km northwest of the Town of Gobles, and the other just to the southeast of the town. The precision of the locations is about 0.1 km. Depth calculations also confirmed that the epicentres were at the depth of the oil-bearing layer just above the Cambrian (880 m). Observations of the first motion pat-

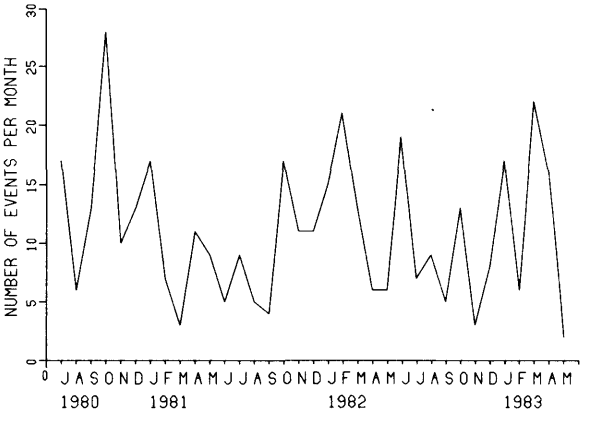

Figure 1. Variation of number of earthquake events per month with time at the Gobles oil field.

terns obtained from the individual seismic traces indicated that at least 2 faults, roughly perpendicular to each other, are active in the area. An example of a recent event recorded on March 5, 1983, is shown in Figure 3. Other examples were given in earlier annual summaries of research (Mereu 1980, 1982).

DISCUSSION AND CONCLUSIONS

The oil field near Gobles, Ontario, now operated by Rayrock Resources Limited, has been producing oil and gas from about 70 wells since 1960, from a depth of 880 m in the Gull River Formation just above the Cambrian. Secondary recovery operations began in the late 1960s. All our observations to date are consistent with the hypothesis that the seismic events are induced or triggered by fluids which are pumped in and out of the wells from the secondary recovery activities in a manner similar to the induced events which were observed in recent years in Denver, Colorado (Evans 1966; Rayleigh *et al.* 1976), or in New York State (Fletcher and Sykes 1977). Our results indicate that the events are being generated along at least 2 active faults. The causes of earthquakes, their prediction, and their prevention by fluid injection are world problems which are still not well understood. The study outlined in this report may provide information to help solve some of these problems.

ACKNOWLEDGMENTS

The author would like to thank J. Brunet, B. Price, A. Yapp, S. Ojo, T. Mok, F. Aibangee, and J. Baerg of the University of Western Ontario, Geophysics Department for their technical assistance in connection with the instrumentation and operation of the seismic network at Gobles. Special thanks are also given to Mr. Gregor, Mr. Birtch, Mr. Dyk, and Mr. Swick for giving us permission to install seismic instruments on their properties. The author would also like to thank Dr. P.A. Palonen and Mr. R. Rebansky of the Ontario Ministry of Natural Resources at London, and Mr. Gaizwinkler of Rayrock Resources Limited for the very helpful discussions and technical information received in connection with the activities at the Gobles oil field.

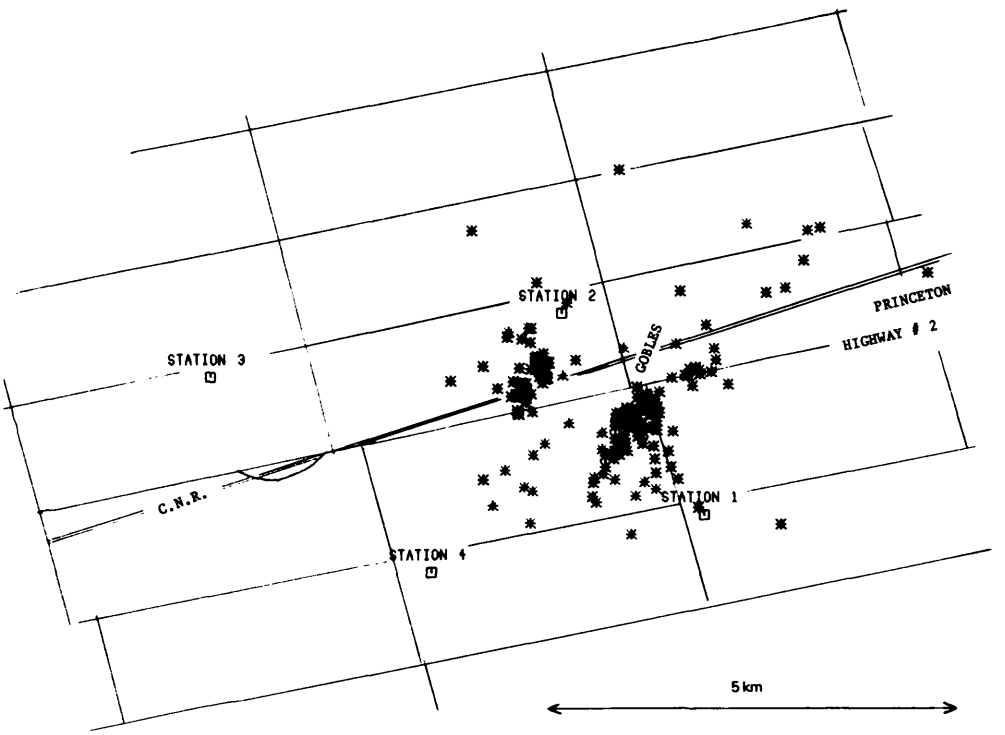

Figure 2. Gobles earthquake epicentre map.

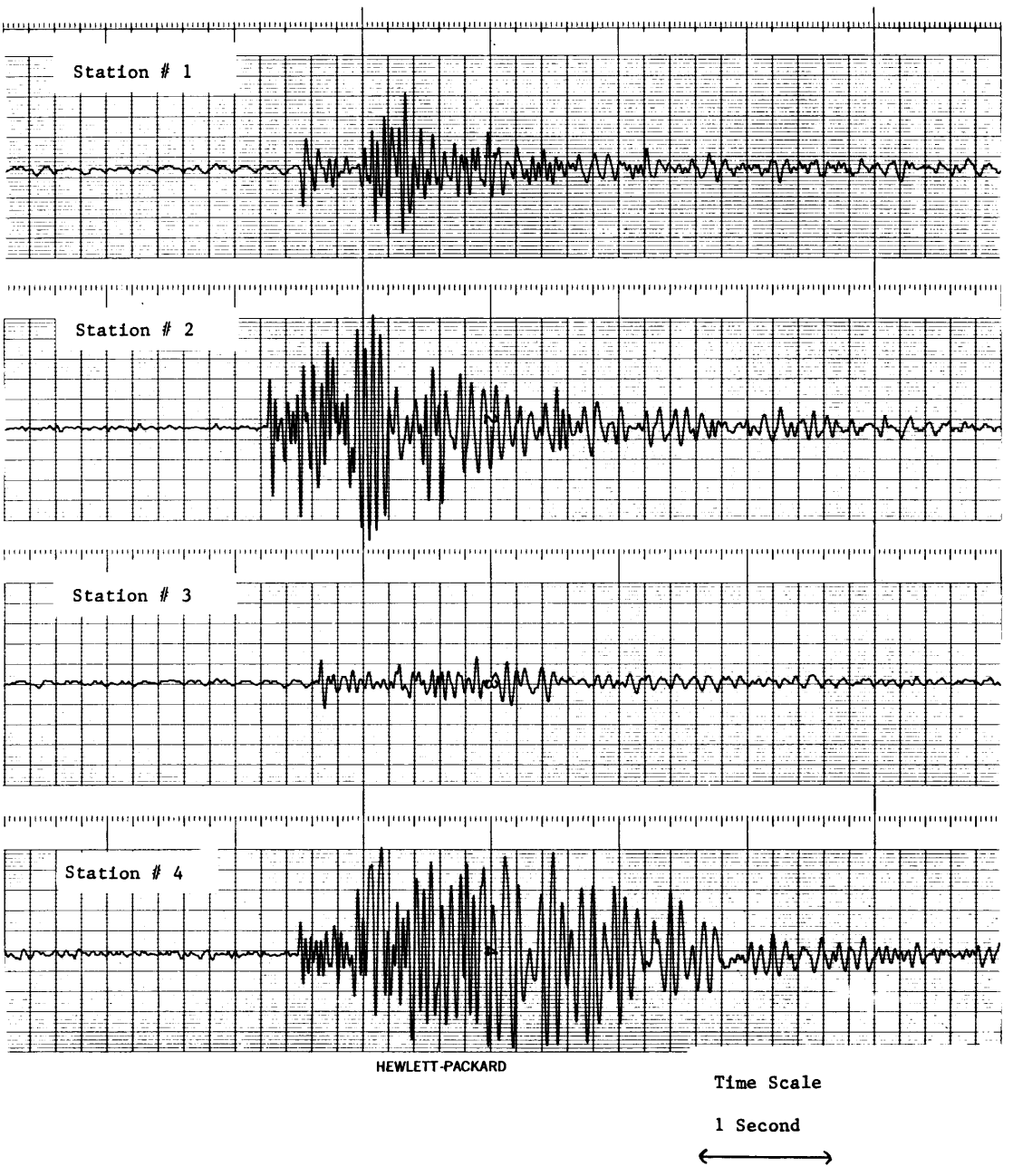

Figure 3. An example of a recent event recorded on March 5, 1983.

REFERENCES

Evans, D.M.
1966: The Denver Area Earthquake and Rocky Mountain Disposal Well; Mountain Geologist, Volume 3, p.23-26.

Fletcher, J.D., and Sykes, L.R.
1977: Earthquakes Related to Hydraulic Mining and Natural Activity, Western New York State; Journal of Geophysical Research, Volume 82, p.3767-3780.

Mereu, R.F.
1980: A Microearthquake Survey of the Woodstock-Kitchener Area; Grant 57, p.163-169 *in* Geoscience Research Grant Program, Summary of Research, 1979-1980, edited by E.G. Pye, Ontario Geological Survey, Miscellaneous Paper 93, 262p.

1982: A Microearthquake Survey of the Gobles Oil Field Area of Southern Ontario; Grant 57, p.126-130 *in* Geoscience Research Grant Program, Summary of Research, 1981-1982, edited by E.G. Pye, Ontario Geological Survey, Miscellaneous Paper 103, 219p.

Rayleigh, C.B., Healy, J.H., and Bredehoeft, J.D.
1976: An Experiment in Earthquake Control at Rangely, Colorado; Science, Volume 191, p.1230-1237.

Grant 146 Contamination and Genesis of the Sudbury Ores

B.V. Rao[1], A.J. Naldrett[1], N.M. Evensen[1], and B.O. Dressler[2]
[1]Department of Geology, University of Toronto
[2]Precambrian Geology Section, Ontario Geological Survey

ABSTRACT

The Ni-Cu ores in the Sudbury area, Ontario, are primarily associated with the "Sublayer" which is considered as a separate series of intrusions along the outer margin of the Sudbury Igneous Complex. The Sublayer consists of rocks ranging in composition from gabbro-norite to quartz diorite. The major and trace element character of the Sublayer suggests extensive contamination of magma by crustal rocks, probably through bulk assimilation. The Sublayer samples display spatial variation in their composition, especially in regard to their La/Yb ratio and, to a certain extent, in their Rb, Sr, Th, and Zr contents. The trace element trends probably resulted from varying degrees of simultaneous assimilation-fractional crystallization processes.

INTRODUCTION

The nickel-copper sulphides associated with the Sudbury Igneous Complex (Figure 1) in Ontario are economically the most important deposits of this type in the world. Some of the significant features that characterize the Sudbury Igneous Complex and distinguish it from other layered intrusions are:

1. fine-scale layering is absent, which has been attributed by Naldrett and MacDonald (1980) to the quartz-rich nature of the magma
2. for a given degree of fractionation, as indicated by the Fe/(Fe + Mg) ratio of pyroxenes and the An content of plagioclase, the cumulus rocks of the Sudbury Igneous Complex are significantly poorer in normative olivine

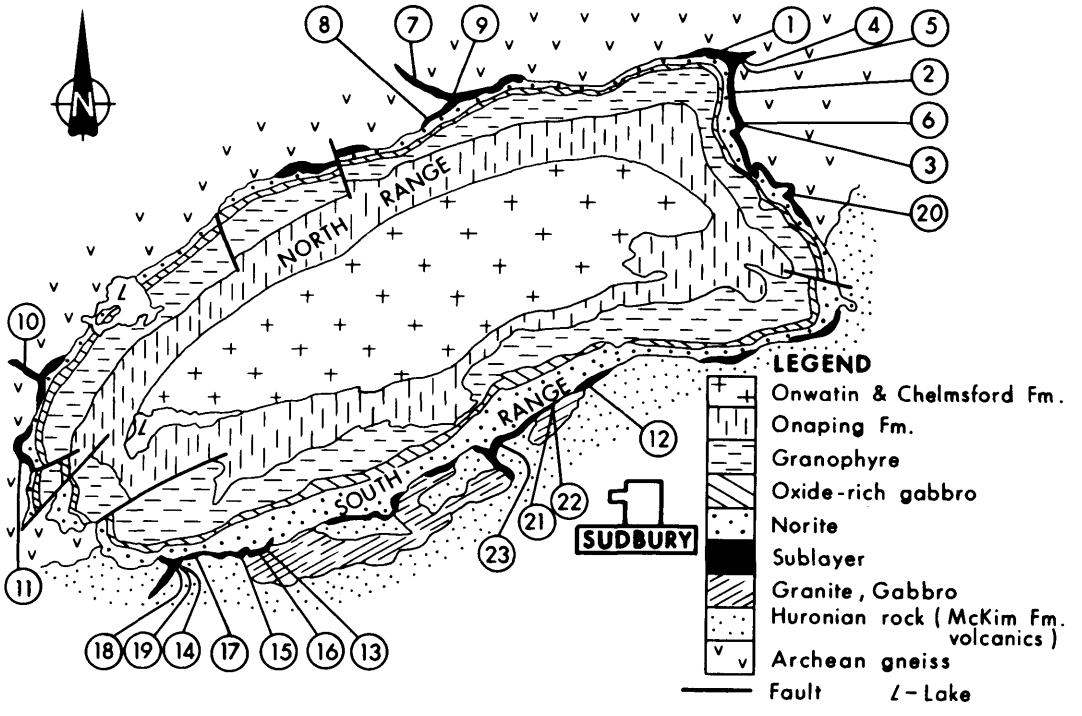

Figure 1. Geological Map of the Sudbury Structure. Numbers refer to the sample numbers in Tables 1-5 (prefix BVR is omitted here).

and richer in normative (and modal) quartz (Naldrett *et al.* 1982)

3. higher $^{87}Sr/^{86}Sr$ values (Gibbins and McNutt 1975) occur than would be expected for magmas derived wholely from a mantle source.

The above characteristics, together with field evidence of the presence of abundant xenoliths of country rocks, point towards an extensive interaction of the Sudbury magma with crustal components. This study aims at a comprehensive and integrated study of field, major and trace elements (including the REE), and a combined Sr, Nd, O-isotope study of the complex as a whole to fully document the nature and extent of this contamination. The norites of the Sudbury Igneous Complex and the Sublayer rocks afford an excellent opportunity to establish criteria for recognizing crustal contamination, and for evaluating any given body as a potential host for ore.

As a part of the first phase of the project, we have studied the major, REE, and other trace element (Zr, Y, Rb, Sr, Th, Ta, Hf, Sc) contents of the Sublayer rocks with which the major mineralization is associated. The results of analyses of selected samples are presented, and are discussed in relation to the nature and extent of crustal contamination of the Sublayer magma.

RELEVANCE OF CONTAMINATION TO SULPHIDE GENESIS

Silica depresses the solubility of sulphur in mafic magmas (Irvine 1975). Irvine (1975), and subsequently Naldrett and MacDonald (1980), attributed the prevalence of Ni-Cu ores at Sudbury to such silicification. The effect of assimilation of siliceous material on a mafic magma is illustrated in Figure 2. As shown in Figure 2, the addition of a small amount of SiO_2 will change the bulk composition of a melt A, to that of melt B. Unlike A, B lies in a 2-liquid field; this consists of an FeO-FeS liquid, containing a very small amount of silica (composition represented by X), that coexists with a silica-rich liquid (composition represented by Y) which contains less sulphide than the former composition represented by A. Addition of SiO_2 to A will cause sulphide saturation, and, depending on how much SiO_2 is added, result in the precipitation of a significant proportion of the dissolved sulphide.

Further, Naldrett *et al.* (1982) have shown that the sulphide liquids responsible for different types of Sudbury ore deposits vary widely in their compositions. These compositional variations are due to separation of sulphides from different batches of a single parental magma that have undergone different evolutionary processes. Many of the compositional differences are due to processes by which the individual batches of magma segregated varying proportions of different sulphides (Naldrett 1981). Thus, varying degrees of assimilation could have resulted in varying proportions of dissolved sulphide being forced to segregate.

GEOLOGIC AND PETROGRAPHIC NOTES

The Sudbury Igneous Complex (Figure 1), which resulted either from 'explosive volcanism' or 'meteorite impact', is a differentiated layered tholeiitic intrusion (Naldrett *et al.* 1970). The complex outcrops in a northeast-trending elliptical ring, 58 km long and 26 km wide. It is dated at 1849 Ma. (Krogh *et al.* 1982). The complex is essentially divided into 3 units: Norite, Quartz Gabbro, and Granophyre. Spatially associated with the Sudbury Igneous Complex, and hosting the major sulphide mineralization, is a group of inclusion-bearing rocks collectively called the Sublayer (Souch *et al.* 1969). A detailed account of the field relationships of the Sublayer rocks to the overlying main Igneous Complex and various theories of its origin have been given by Pattison (1979).

The Sublayer occurs discontinuously around the base of the main mass of the Sudbury Igneous Complex

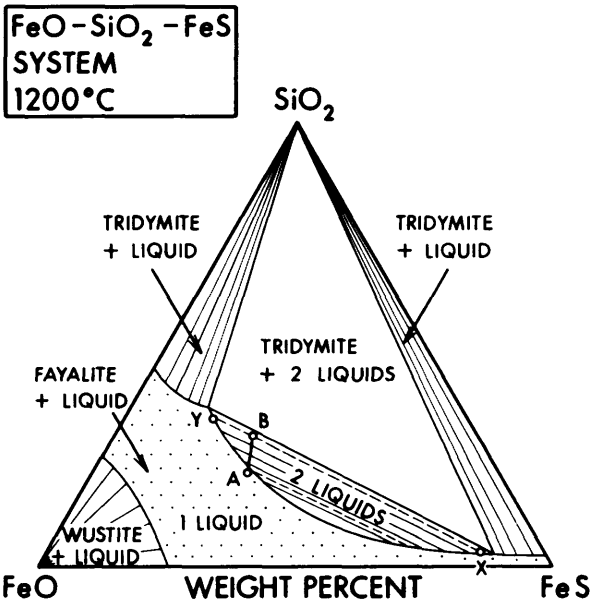

Figure 2. The 1200°C isotherm of the FeO-SiO_2-FeS system illustrating the effect of addition of SiO_2 to a liquid represented by point A. Notice that A lies within a single-liquid field representing complete miscibility between compositions on the FeO-SiO_2 join (analogous to a silicate melt, free from sulphide) and the FeO-FeS join (analogous to a sulphide-rich but not sulphide-saturated silicate melt). (After Naldrett and MacDonald 1980).

as lateral sheets, irregular flat lenses, small bodies occupying embayments and troughs, and as dikes (offsets) that extend several kilometres into the surrounding country rocks. The inclusion population in the Sublayer consists of various footwall rocks (e.g. feldspathic quartzites of the Huronian Supergroup, and Levack Complex gneisses) and a group of mafic to ultramafic rocks. Scribbins *et al.* (in press) contend that the mafic and ultramafic inclusions within the Sublayer represent disrupted fragments of a layered intrusion that may have been genetically related to the Sudbury Igneous Complex. It is generally agreed that the Sublayer is a series of separate intrusions from the overlying main Igneous Complex. Evidence has been accumulating with increasing frequency that the Sublayer postdates the main mass of the Sudbury Igneous Complex, although this is still a contentious issue amongst Sudbury geologists.

The immediate footwall rocks for the Sublayer on the North Range, in general, are rocks of the Levack Complex (age> 2500 Ma), which ranges in composition from diorite or quartz diorite to quartz monzonite, metamorphosed under pyroxene granulite facies conditions (Card 1978), and contain significant quantities of mafic material in the form of layers and inclusions. The Levack Complex and Superior Province felsic plutonic rocks (quartz monzonites, granites, and granodiorites) constitute the basement upon which the succeeding Early Proterozoic supracrustal rocks of the Huronian Supergroup (essentially consisting of pelitic and psammatic sedimentary rocks) were deposited. On the South Range, the Sublayer rocks are generally found in contact with rocks of the Huronian Supergroup and granitic rocks (e.g. Creighton and Murray Granites).

Petrographically, the Sublayer comprises a group of 2-pyroxene gabbros and norites with abundant quartz. Hewin's (1971) study indicates the absence of any cryptic variation in the Sublayer. He suggests that the Sublayer is the result of several batches of magma having different compositions. Petrographically, the matrix of fresh Sublayer samples consists of zoned tabular plagioclase laths, ophitic to subophitic and prismatic crystals of ortho- and clinopyroxenes, primary biotite and hornblende, interstitial quartz (its abundance varies from sample to sample), micrographic intergrowths of quartz and feldspar, and sulphide minerals. The textural characters suggest that the Sublayer rocks are not cumulates and probably approximate a primary magma composition.

RESULTS

MAJOR ELEMENTS

The major element analyses for the Sublayer samples from the North and South Ranges are given in Tables 1 and 2. Relevant statistics are also provided. The Sublayer rocks are characterized by the following major element characteristics:

1. There are no smooth variations of major oxides with MgO/(MgO + FeO) ratio (mg′ number). This is also reflected by the poor correlation coefficients of major oxides with the mg′ number.
2. Although the mean chemical compositions of samples from the North and South Ranges are remarkably similar, the North Range samples show a larger spread as seen from the high standard deviations (Table 1). On mg′ *vs* oxide scatter diagrams, the North Range fall within at least 2 distinctly separated fields. In the combined data, SiO_2 shows a fairly high correlation with CaO (r = −0.85), FeO (r = −0.81), and K_2O (r = 0.77).

TABLE 1 MAJOR ELEMENT ANALYSIS OF SUBLAYER SAMPLES FROM THE NORTH RANGE (RECALCULATED TO 100 ON H_2O-FREE BASIS).

Sample No.	BVR-1	BVR-2	BVR-3	BVR-4	BVR-5	BVR-6	BVR-7	BVR-8	BVR-9	BVR-10	BVR-11	BVR-20	Mean	Std Dev	Corr with mg'num
SiO2	62.93	52.87	52.92	62.00	63.11	52.48	61.44	60.39	63.42	61.76	51.66	59.49	58.74	5.0	-0.04
TiO2	0.93	1.20	1.32	0.75	0.92	1.30	0.50	0.78	0.97	0.81	1.31	1.08	1.01	0.22	0.18
Al2O3	14.90	15.51	13.71	14.73	14.55	14.50	15.26	12.68	14.59	15.25	14.67	15.39	14.63	0.71	0.73
FeO*	6.90	11.11	12.61	9.14	8.41	12.67	7.60	8.94	7.06	8.16	12.84	8.73	9.51	2.16	0.08
MnO	0.11	0.16	0.18	0.13	0.13	0.19	0.11	0.17	0.11	0.18	0.17	0.14	0.15	0.19	0.06
MgO	3.71	6.18	6.79	3.69	3.95	6.04	3.81	8.37	3.91	4.07	6.21	4.07	5.08	1.56	-0.71
CaO	4.59	8.66	8.76	4.58	2.73	8.41	5.25	4.94	5.15	3.15	9.52	5.93	5.96	2.24	0.03
Na2O	2.96	3.15	2.35	2.73	3.00	2.76	3.17	1.83	2.41	3.42	2.81	3.23	2.83	0.41	0.71
K2O	2.28	1.16	1.16	2.25	3.20	1.56	2.56	1.90	2.39	3.20	0.81	1.98	2.03	0.76	0.12
mg'	0.35	0.36	0.35	0.29	0.32	0.32	0.33	0.48	0.35	0.33	0.33	0.32			
CI	0.35	0.21	0.21	0.35	0.48	0.29	0.40	0.31	0.36	0.49	0.15	0.20			

Sample numbers refer to the locations in Figure 1 (prefix BVR is omitted)
* Total iron as FeO
mg'=MgO/(MgO+FeO)
CI is used as a contamination index (CI=K2O/(K2O+SiO2) x 10)

TABLE 2 MAJOR ELEMENT ANALYSIS OF SUBLAYER SAMPLES FROM THE SOUTH RANGE (RECALCULATED TO 100 ON H_2O-FREE BASIS).

Sample No.	BVR13	BVR14	BVR15	BVR16	BVR17	BVR18	BVR19	BVR12	BVR21	BVR22	BVR23	Mean	Std. Dev.	Corr with mg'
SiO2	54.45	58.96	59.78	58.81	57.43	58.78	56.38	57.72	56.75	53.91	58.87	57.43	1.84	0.39
TiO2	1.07	0.99	0.85	1.09	0.80	0.88	0.79	0.55	1.60	1.49	0.80	0.99	0.31	0.70
Al2O3	17.81	15.36	15.17	15.74	16.87	12.95	15.54	16.19	15.87	17.93	16.44	15.93	1.32	0.31
FeO*	8.80	8.92	7.77	8.86	9.01	10.14	9.50	8.48	9.74	11.50	7.68	9.13	1.13	0.79
MnO	0.14	0.13	0.12	0.14	0.13	0.15	0.11	0.10	0.14	0.13	0.12	0.13	0.01	0.46
MgO	5.76	4.93	5.99	4.13	5.02	5.76	5.71	6.54	5.37	3.81	5.13	5.28	0.80	-0.86
CaO	8.09	5.91	5.84	6.51	5.54	7.27	6.09	6.40	6.36	6.48	6.75	6.48	0.71	-0.01
Na2O	3.22	2.68	2.90	2.99	2.71	2.47	3.77	2.79	2.96	3.37	2.50	2.95	0.43	0.27
K2O	1.25	2.10	1.58	1.73	2.49	1.61	2.11	1.23	1.21	1.37	1.36	1.67	0.42	0.09
mg'	0.40	0.36	0.44	0.32	0.36	0.36	0.38	0.44	0.36	0.25	0.40			
Cl	0.22	0.34	0.26	0.28	0.41	0.27	0.37	0.21	0.21	0.25	0.22			

Sample numbers refer to the locations in Figure 1 (the prefix BVR is omitted)
* Total iron as FeO
mg' and Cl are the same as in Table 1

3. The samples are characterized by relatively high SiO_2 and K_2O contents when compared to other continental tholeiitic rocks of similar mg' number.
4. When shown as a $(Na_2O + K_2O)$ *vs* SiO_2 plot (Figure 3A), the data fall within the tholeiitic and high alumina basalt fields.
5. The analyses do not define any discernable trend on the AFM diagram in Figure 3B and the majority of the analyses fall within the calc-alkaline field of Irvine and Baragar (1971).

TRACE ELEMENTS

The rare earth elements (REE) and other trace element data, together with pertinent statistical information, are listed separately for the North and South Range samples in Tables 3 and 4 respectively. The Sublayer gabbro-norites have very high ΣREE (=La+Ce+Nd+Sm+Eu+Yb+Lu) contents, ranging from 93 ppm to 206 ppm, with the chondrite-normalized (Haskin *et al.* 1968) patterns displaying a distinct light REE (LREE) enrichment and no fractionation of heavy REE (HREE). There are no significant Eu anomalies in their patterns. The REE patterns for the North and South Range samples are shown separately in Figures 4A and 4B. The La/Yb ratios range from 9.5 to 29, as compared to 4.7 for the Skaergaard "chilled" gabbro. Although the absolute REE contents vary widely, the Sublayer samples from all localities have strikingly similar chondrite-normalized REE patterns. Furthermore, the REE patterns exhibited by the Sublayer samples have a remarkable resemblance to the marginal norites of the overlying main Igneous Complex (Figure 4C). Kuo and Crocket (1978) consider the REE patterns of these marginal norites as representing the liquid composition parental to the Sudbury Igneous Complex and suggest extensive crustal contamination of the Sudbury magma as being responsible for the LREE enrichment patterns. Typical REE patterns for possible contaminants (Levack Complex gneisses and Huronian pelitic rocks) are also shown in Figure 4C. The Skaergaard "chilled" gabbro REE pattern is also shown for comparison (Frey *et al.* 1968).

In general, the North Range samples are characterized by higher La/Yb ratios than the samples from the South Range. Such a grouping is evident in Figure 5A. However, a few samples from the North Range also plot in the field for the South Range samples. The relationships between the La/Yb ratios and Sr, Th, Zr, and Rb are shown in Figure 5B; the differences in the trace element trends between the North and the South Range samples are apparent. Although the major and trace element variations suggest plagioclase and clinopyroxene fractionation, the entire range of trace element variation cannot be explained solely by crystal fractionation processes.

Shown in Figure 6 is a correlation pattern diagram, which represents the correlation coefficients between particular elements (in this case K_2O and SiO_2) and a series of other elements (in this case Th, Rb, Zr, Hf, La, Ba, Sc, Co, Sr, and Y). This diagram indicates that K_2O and SiO_2 have very similar correlations and both bear strong to moderate positive correlations with all the 'hygromagmatophile' (HYG) elements. La, Zr, Th, and Hf display strong positive correlations among themselves.

Wood (1980) employed Th-Hf-Ta diagrams for tectonomagmatic classification, and to establish the nature and extent of crustal contamination of basaltic lavas of the British Tertiary Volcanic Province (BTVP). Th, Ta, and Hf have a typical hygromagmatophile behaviour during partial melting and crystal fractionation processes and they are insensitive to secondary processes (Wood 1980). When plotted on Wood's Th-Hf-Ta diagram (Figure 7), the Sublayer samples fall within the field of calc-alkaline lavas thought to have resulted from extensive sialic crustal assimilation. Also shown in Figure 7 is the field

occupied by "melt rocks" that underly the Onaping Formation (Figure 1). Peredery (1972) considers the melt rocks as having crystallized from melts produced by meteorite impact, emphasizing that their chemical compositions approximate those of the older "target rocks" in the area. The "melt rock" data plotted on Figure 7 were obtained as a part of the present investigation.

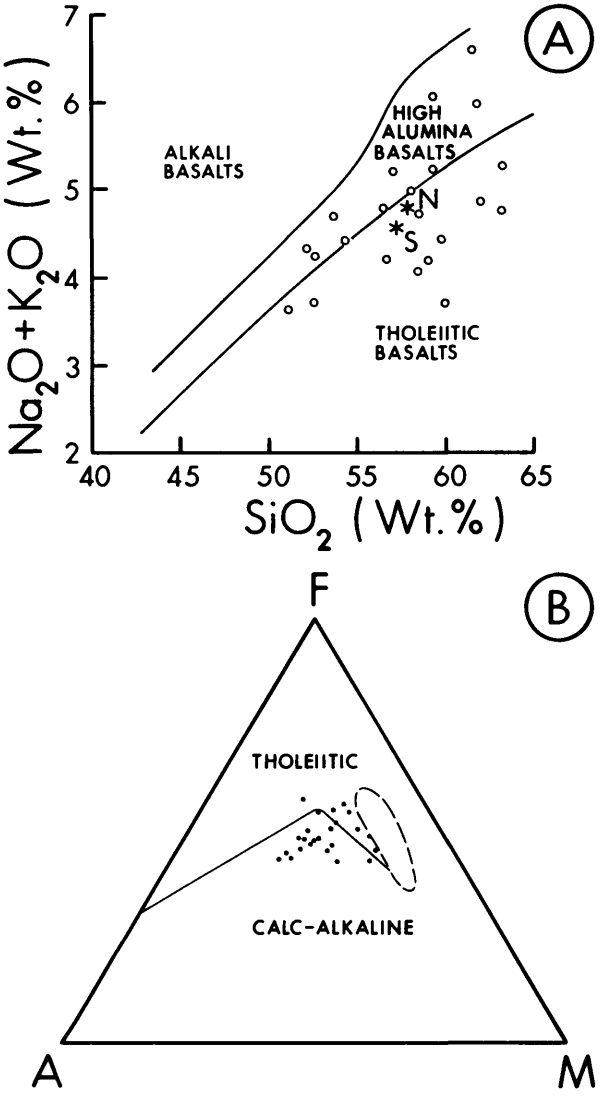

Figure 3. (A) SiO_2 vs Na_2O+K_2O (H_2O-free basis) plot. N *and* S *(shown as asterisks) refer to the mean compositions of the North and South Range Sublayer samples. (B) AFM diagram for the Sublayer samples. The solid line separates the tholeiitic and calcalkaline fields (Irvine and Baragar 1971). The field (indicated in dashed line) for gabbros and norites of the Wanapitei layered intrusion (Finn* et al. *1982) in the Sudbury area, Ontario, is also plotted for comparison.*

DISCUSSION AND MODELS

Watson's (1982) recent experiments convincingly suggest that ascending magmas can be selectively contaminated with K_2O by interaction with wall rocks because of the very high diffusivity of K_2O relative to other components. However, in such a situation (selective contamination by wall rock reaction) once the K_2O content of the magma reaches its transient equilibrium value (about ⅓ the concentration in the crust-derived felsic melts or roughly 1 to 1.5 weight % K_2O), there could not be any further enrichment in K_2O content (Watson 1982). Further increase beyond this value of K_2O would require the bulk assimilation of wall rocks. With bulk assimilation, a rise in K_2O is reflected in the SiO_2 content. The observed data on K_2O and SiO_2 in the Sublayer samples indicate the possibility of such bulk assimilation of silicic crustal rocks. Thomson *et al.* (1982) also report a tendency for the highest K abundances to occur in those samples of the Skye Main Lava Series (SMLS) which, on isotopic evidence, appear to have experienced the highest assimilation of crustal components.

A least squares modelling technique (Wright and Doherty 1970) was used to test the bulk assimilation hypothesis. A model calculation is presented in Table 5. One of the least contaminated samples (on the basis of $K_2O/(K_2O+SiO_2)$ ratio) was used as the initial liquid to model the most contaminated sample. The contaminants have been chosen arbitrarily to yield a reasonably good fit. The contaminants selected for the model here are geologically realistic components in the sense that the country rocks in the area closely approximate the compositions of the contaminants used in the calculation. The calculation suggests bulk assimilation of an unusually large amount of pelitic sediment (about 50 weight %).

The Th-Hf-Ta diagram (Figure 7) also indicates high Th-bearing rocks as major components of assimilation. The possible candidates are rocks of the Huronian Supergroup. Because of the uncertainties in the composition of the initial magma, no quantitative estimates of the extent of contamination were attempted on the basis of this diagram. But this diagram certainly suggests an extensive interaction of the Sublayer magma with sialic crustal rocks. Also, numerous calculations have been done using the least squares technique to model other samples from the Sublayer suite with the above contaminants. The calculations show that the compositions of contaminants, as well as their mixing proportions, vary significantly from sample to sample. Thus the assimilation process may not be a simple 2 or 3 end-member type of mixing.

Further, in the case of bulk assimilation of a single crustal component of perfectly uniform composition, the interelement correlation coefficients are high and significant ($r=0.8$ or more). The scattered trends in the Sublayer data may be the result of interaction of the magma with crustal rocks of variable composition (for a detailed discussion of the use of correlation coefficients in petrogenetic interpretations *see* Cox and Clifford 1982).

TABLE 3 TRACE ELEMENT ANALYSIS OF SUBLAYER SAMPLES FROM THE NORTH RANGE (VALUES ARE IN ppm).

Sample No.	BVR-1	BVR-2	BVR-3	BVR-4	BVR-5	BVR-6	BVR-7	BVR-8	BVR-9	BVR10	BVR11	BVR20	Mean	Std. Dev.
La	33.80	27.24	28.24	34.76	32.70	32.0	38.25	27.12	38.12	34.72	17.96	43.50	32.37	6.63
Ce	72.40	68.30	66.00	88.20	67.00	70.80	97.83	55.40	94.40	72.50	48.20	84.14	73.76	14.95
Nd	28.40	24.90	27.80	39.40	26.90	38.90	21.72	21.10	33.00	29.20	17.83	34.20	28.61	6.82
Sm	5.50	5.52	6.36	5.26	4.50	7.31	5.57	4.28	6.03	4.90	4.65	5.92	5.49	0.85
Eu	1.60	1.73	1.81	0.99	1.05	1.93	1.48	1.25	1.51	1.52	1.96	1.51	1.57	0.27
Tb	0.65	0.71	0.77	0.74	0.52	0.67	0.73	0.50	0.46	0.53	0.76	0.67	0.64	0.11
Yb	1.84	1.41	2.05	2.42	1.58	2.57	1.70	1.32	2.13	1.74	1.43	1.50	1.80	0.41
Lu	0.32	0.18	0.35	0.43	0.27	0.41	0.18	0.25	0.28	0.27	0.27	0.26	0.29	0.08
ΣREE	144.5	130.0	133.4	172.2	134.5	154.6	167.5	111.2	175.9	145.4	93.1	171.7	144.5	
Th	5.7	1.7	2.0	5.5	6.5	2.0	6.0	4.3	6.3	6.3	1.1	4.8	4.3	
Hf	2.9	1.8	1.3	4.6	6.1	1.9	3.3	3.0	5.0	2.4	1.5	4.1	3.4	2.16
Ta	0.44	0.10	0.18	0.43	0.43	0.17	0.30	0.35	0.40	0.40	0.18	0.32	0.31	0.11
Ba	1000	650	550	700	990	640	730	540	800	1000	-	1000	800	185
Sc	18	29	36	17	15	31	18	19	19	17	34	21	22.6	7.62
Co	24	39	55	19	19	47	32	51	27	25	59	35	36	14.1
Zr	148	88	85	152	173	76	167	123	200	166	52	188	134	48.7
Y	20	14	22	19	18	23	19	16	19	20	17	20	19	2.47
Sr	420	580	456	387	263	477	398	288	379	281	602	496	419	110
Rb	48	24	28	45	65	43	70	68	55	146	21	36	54	33.4
Ratios														
La/Yb	18.37	19.32	13.77	14.36	20.69	12.45	22.50	20.54	17.90	19.95	12.55	29.0		
Zr/Y	7.4	6.28	3.86	9.61	9.60	3.30	7.67	7.69	10.50	8.30	3.01	9.40		
Rb/Sr	0.114	0.04	0.06	0.12	0.25	0.09	0.18	0.24	0.14	0.52	0.03	0.07		
Y/Sr	0.05	0.024	0.048	0.049	0.068	0.048	0.048	0.055	0.050	0.070	0.028	0.040		
Zr/Hf	51.60	48.09	65.40	31.45	28.40	40.86	50.60	41.00	40.00	69.10	33.70	45.80		
Th/Hf	1.98	0.93	1.54	1.61	1.41	0.86	1.82	1.40	1.26	2.60	0.71	1.17		

Sample numbers refer to the numbers in Figure 1 (prefix BVR is omitted)

TABLE 4 TRACE ELEMENT ANALYSIS OF SUBLAYER SAMPLES FROM THE SOUTH RANGE (VALUES ARE IN ppm).

Sample No.	BVR12	BVR13	BVR14	BVR15	BVR16	BVR17	BVR18	BVR19	BVR21	BVR22	BVR23	Mean	Std. Dev.
La	20.30	18.90	29.35	27.65	34.72	24.98	25.30	36.10	43.30	37.30	30.40	29.51	7.24
Ce	46.50	49.50	64.00	74.10	91.60	54.70	65.80	99.80	93.00	78.30	69.50	71.54	17.93
Nd	25.70	21.72	22.47	23.50	25.00	17.43	22.40	28.20	54.80	30.50	43.90	28.69	11.04
Sm	3.36	4.63	5.01	4.83	6.14	4.46	4.54	6.30	8.16	6.14	5.00	5.32	1.28
Eu	1.16	1.50	1.46	1.18	1.55	1.37	1.08	2.02	2.40	2.64	1.02	1.52	0.74
Tb	0.58	0.57	0.38	0.64	0.65	0.47	0.91	1.44	0.86	1.03	0.47	0.67	0.36
Yb	1.09	1.99	1.83	2.13	2.30	1.93	2.10	2.45	3.77	3.42	1.89	2.26	0.75
Lu	0.18	0.30	0.35	0.24	0.34	0.24	0.37	0.42	0.55	0.57	0.32		
ΣREE	98.87	99.11	124.85	134.30	162.30	105.60	122.50	176.70	206.80	159.90	152.50		
Th	5.1	2.0	5.0	3.8	4.4	4.0	2.5	5.9	3.0	1.5	4.8	3.76	1.42
Hf	3.5	3.4	3.6	3.0	3.0	2.2	3.2	6.8	2.3	2.2	3.4	3.32	1.27
Ta	0.65	0.31	0.45	0.34	0.40	0.38	0.31	0.71	0.65	0.64	0.34	0.46	0.16
Ba		480	635	610	640	784	490	600	635	820	685		150
Sc	19	25	23	20	24	23	25	33	25	27	19	24	4.01
Co	26	34	34	38	30	35	40	44	37	38	30	35	5.11
Zr	139	145	150	107	132	94	117	170	149	168	109	134	25.14
Y	16	19	23	19	21	19	20	29	34	35	22	23.4	6.4
Sr	466	484	323	427	418	425	356	315	388	393	428	402	54
Rb	34	43	67	54	57	143	50	76	44	41	56	60.5	29.90
Ratios													
La/Yb	18.6	9.50	16.04	12.98	15.10	12.94	12.05	13.18	11.48	10.90	16.10		
Zr/Y	8.69	7.60	6.50	5.60	6.28	4.95	5.85	5.86	4.38	4.80	4.95		
Rb/Sr	0.07	0.09	0.21	0.13	0.14	0.34	0.14	0.24	0.11	0.10	0.13		
Y/Sr	0.034	0.04	0.07	0.044	0.05	0.045	0.056	0.09	0.087	0.089	0.05		
Zr/Hf	39.70	42.40	41.70	35.40	43.56	42.70	36.30	25.0	63.90	74.70	32.06		
Th/Hf	1.46	0.58	1.34	1.26	1.45	1.82	0.77	0.86	1.30	0.66	1.41		

Note: Sample numbers refer to the sample numbers in Figure 1 (prefix BVR is omitted)

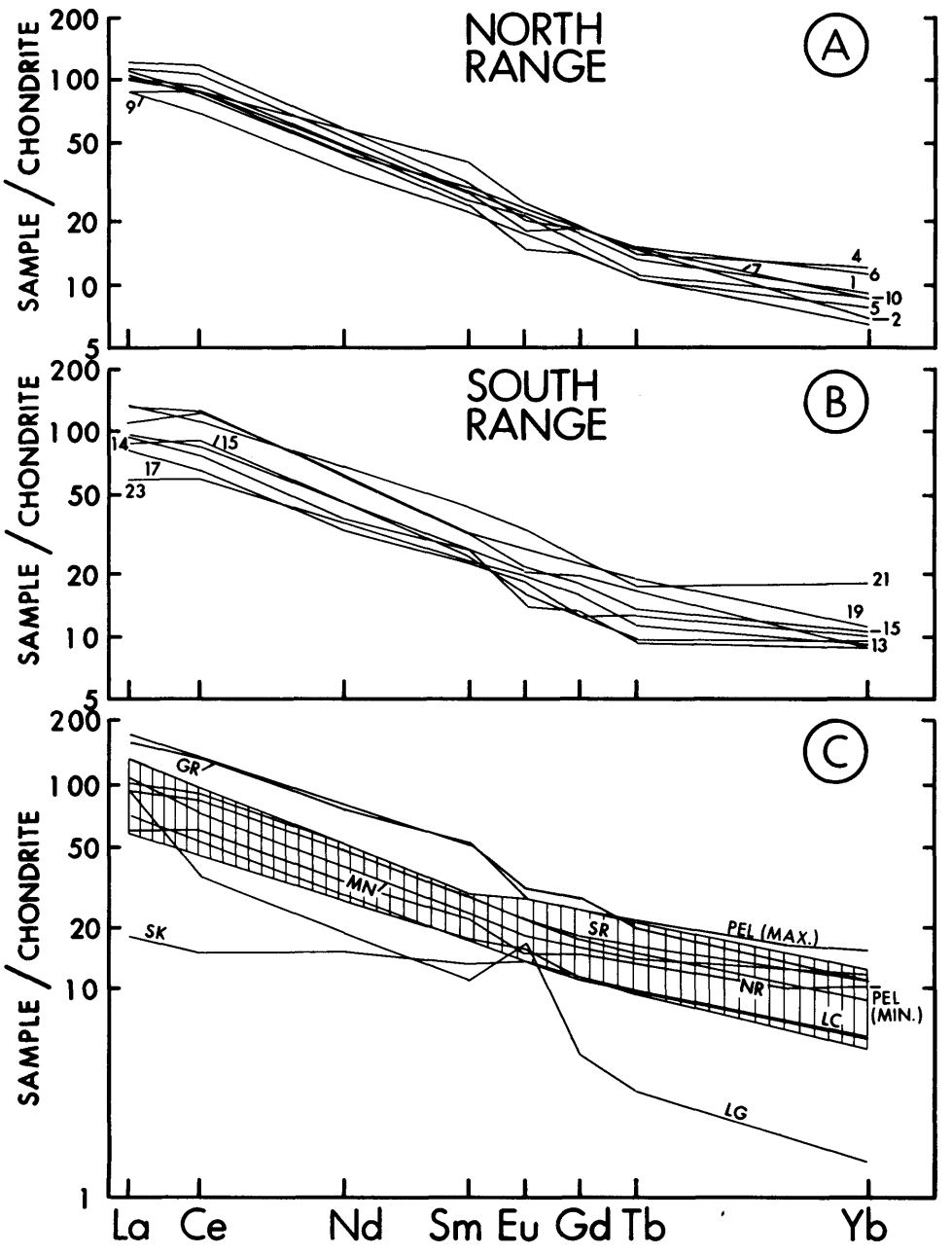

Figure 4. (A) and (B) show the chondrite-normalized rare earth element fractionation patterns for the Sublayer samples from the North and South Ranges respectively. Numbers indicated for each pattern refer to the sample numbers in Tables 3 and 4, and Figure 1 (prefix BVR is omitted). (C) shows the chondrite-normalized patterns for: Levack gneiss (LG), lower crustal rocks (LC) (represented by the average Lewisian granulite in Scotland, data from Wood 1980), marginal mafic norites of the Sudbury Igneous Complex (MN), McKim pelites of the Huronian Supergroup (PEL, max and min indicate the maximum and minimum values, data from McLennan et al. 1979). The mean REE fractionaton patterns for the North and South Range Sublayer samples are represented by NR and SR, respectively, and the range for the Sublayer (combined data) by vertical lines.

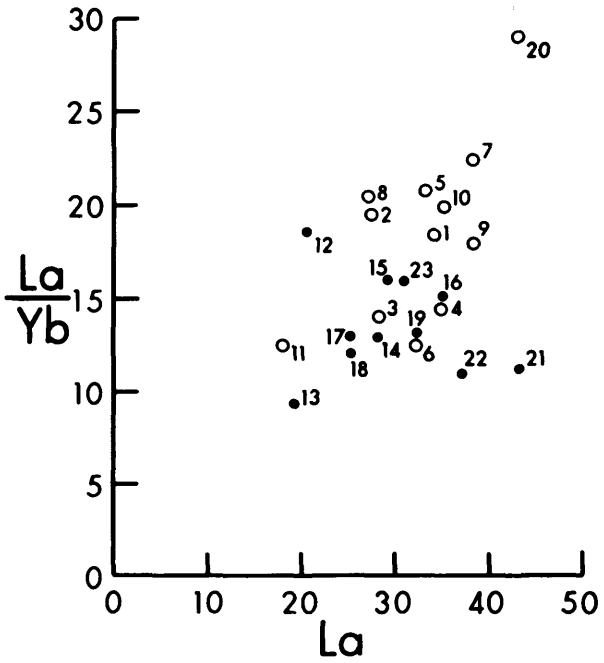

Figure 5A. La/Yb vs La plot. Open circles represent the samples from the North Range and filled circles from the South Range. The numbers refer to the sample numbers in Tables 3 and 4 (prefix BVR is omitted).

Ratio-ratio plots of hygromagmatophile elements, and mixing calculations of the type used by Langmuir *et al.* (1978), also preclude simple 2-component mixing models but suggest involvement of additional end-members of differing nature.

Taylor (1980) and DePaolo (1981) ruled out assimilation as a simple 2-component mixing mechanism. The heat balance considerations suggest that assimilation should be accompanied by concurrent fractional crystallization to provide the necessary heat. Taylor (1980) showed that the resulting effects from such a simultaneous fractional crystallization-assimilation process are significantly different from those predicted by a simple 2 end-member type of mixing process.

DePaolo (1981) has recently derived the equations predicting the effects of concurrent assimilation and fractional crystallization on the distribution of trace elements and isotope ratios. The equations of DePaolo have been used to evaluate whether the trace element distributions in the Sublayer samples are consistent with such a process. Model calculations have been performed and are presented in Figure 8. Calculations have been performed for various values of r (ratio of assimilated rock to the magma crystallized), using a composition similar to the least contaminated Sublayer from the North Range as the initial liquid composition. The contaminant chosen has the composition: La = 40, Yb = 1.7, Th = 25, Zr = 100, Rb = 75, and Sr = 100; and the bulk partition coefficients used are D(La) = 0.08, D(Yb) = 0.1, D(Th) = 0.01, D(Zr) = 0.2, D(Rb) = 0.01, and D(Sr) = 2.0. The calcula-

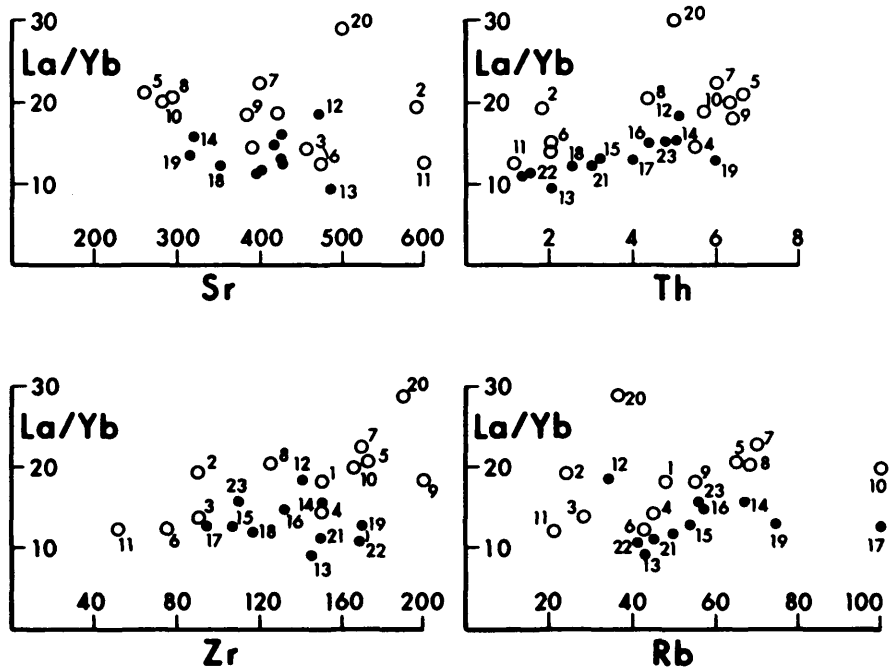

Figure 5B. Plot showing the relationship between La/Yb ratio and Sr, Zr, Th, and Rb. Symbols are the same as in Figure 5A.

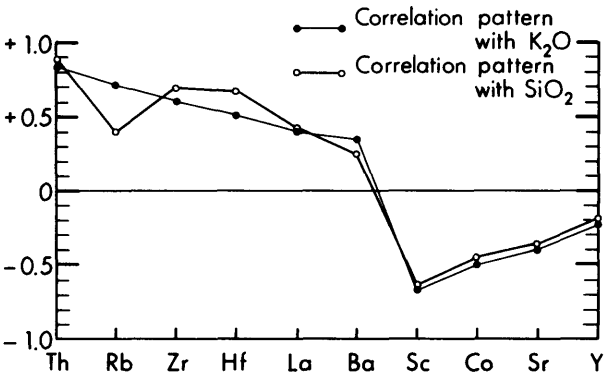

Figure 6. Correlation coefficient patterns showing how SiO_2 and K_2O correlate with Th, Rb, Hf, La, Ba, Sc, Co, Sr, and Y.

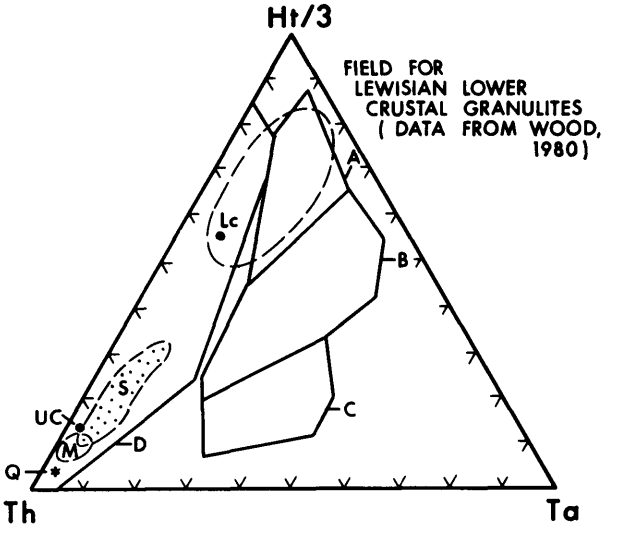

Figure 7. The Th-Hf-Ta diagram of Wood (1980). The fields for different tectonomagmatic environments are : (A) N-type MORB; (B) E-type MORB and within-plate tholeiitic basalts and differentiates; (C) alkaline within-plate basalts and differentiates; (D) destructive plate-margin basalts (calc-alkaline) and differentiates. The field occupied by the Sublayer samples is stipled (S). The Lewisian basic, intermediate, tonalitic, and trondhjemitic granulites (data from Wood 1980), which are similar in composition to the Levack Complex gneisses, occupy a well-spread field. One available analysis of the Huronian (Mississagi) quartzite is also plotted. (M) is the field for the melt rocks.

TABLE 5 RESULTS OF LEAST SQUARES MODELLING.

Oxide	Calc.	Obs. BVR-10	Diff.	BVR-11	Contaminants 1	2	3
SiO_2	61.63	61.77	0.14	51.65	62.25	73.35	61.60
TiO_2	0.81	0.81	0	1.30	0.50	0.79	0.84
Al_2O_3	17.49	15.21	2.28	14.68	15.06	13.62	19.84
FeO	7.36	8.16	0.80	12.85	6.02	1.28	7.31
MnO	0.11	0.18	0.07	0.17	0.10	0.08	0.10
MgO	3.39	4.07	0.68	6.21	4.02	0.68	2.61
CaO	3.54	3.17	0.37	9.52	6.02	0.68	0.92
Na_2O	3.07	3.43	0.36	2.80	4.52	4.72	2.09
K_2O	3.30	3.21	0.09	0.81	1.51	4.80	4.70
Total	100.70	100.00		100.00	100.00	100.00	100.00
	Weight percent mixing			13.99	28.02	6.92	51.77
	Sensitivity			0.61	0.80	0.93	1.01

Notes: BVR-11 is the initial liquid composition(least contaminated sample from the North Range)
Contaminants:
1. Composition similar to Levack gneiss
2. Composition similar to quartz monzonites from the North North Range
3. Pelitic sediment similar to the composition of McKim pelites

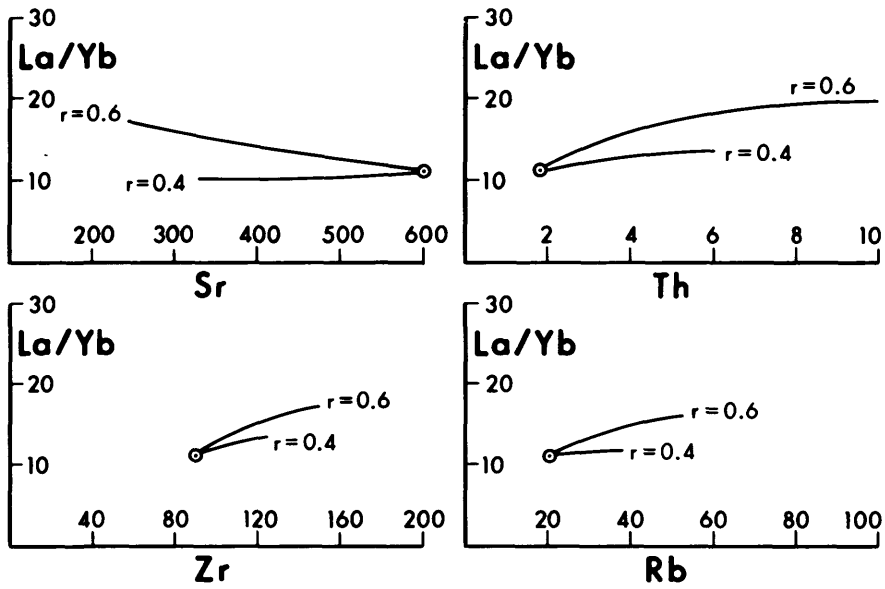

Figure 8. The results of model calculations showing the effect of concurrent assimilation-fractional crystallization; the calculations are for F (fraction of magma crystallized) = 0.2.

TABLE 6 RESULTS OF FACTOR ANALYSIS. THE COLUMNS OF VALUES OF VARIMAX ROTATED FACTORS (1 TO 4) REPRESENT THE FACTOR LOADINGS BY THE CORRESPONDING VARIABLES IN THE MATRIX.

Variable	Mean	Std.Dev.	Factor 1	Factor 2	Factor 3	Factor 4
La	30.99	6.92	0.4072	0.7995	0.0842	0.1645
Ce	72.69	16.09	0.3944	0.8181	-0.0418	-0.1239
Nd	28.64	8.87	0.0508	0.7215	0.1551	0.2124
Sm			-0.2587	0.9102	0.0963	-0.0710
Eu	2.60	3.39	0.0106	-0.1051	0.1279	-0.2534
Yb	2.02	0.63	-0.1757	0.7285	0.5124	-0.2005
Th	4.05	1.74	0.9189	-0.0029	0.0075	0.1260
Hf	3.40	1.75	0.6465	0.1681	-0.0355	-0.0424
Ta	0.38	0.15	0.3735	0.2161	0.7169	-0.0301
Ba	736	170	0.2566	-0.1516	0.0632	0.7367
Sc	23.26	6.06	-0.8024	0.1363	0.0551	-0.2657
Co	35.56	10.55	-0.7545	-0.0535	-0.0271	-0.3414
Zr	134.7	38.41	0.7504	0.3152	0.2194	0.1284
Y	21.04	5.18	-0.1476	0.6303	0.7430	-0.1216
Sr	392	121	-0.7149	-0.0212	-0.4055	0.3689
Rb	57.13	31.21	0.4390	-0.2166	0.2423	-0.1150

Factor	Eigenvalue	Percent Variance	Cumulative Percent
1	5.10	46.20	46.20
2	3.89	35.20	81.40
3	1.31	11.90	93.30
4	0.74	6.70	100.00

tions indicate that the higher the ratio of the assimilated rock to magma crystallized (***r***), the faster the La/Yb ratio increases. Comparison with Figure 5B shows that the observed differences in the trace element trends between the 2 Sublayer groups could probably result from different degrees of assimilation (as indicated by ***r***). Although the model presented here is not exactly a best-fit of the data, it serves to suggest a possible mechanism by which the trace elements trends could have evolved.

Even the least contaminated sample in the Sublayer suite has a very high La/Yb ratio, which is unusual for mantle-derived tholeiitic magmas. Further, the very high Sr contents suggest that the magma had probably experienced prior contamination by lower crustal rocks or rocks similar to the Levack Complex gneisses. Calculations of the AFC type (combined assimilation-fractional crystallization), described above, suggest that to increase the La/Yb ratio from about 5 (Skaergaard "chilled gabbro") to 11 (least contaminated sample) requires simultaneous assimilation and fractional crystallization of magma in the ratio $r = 0.2$, and about 40 weight % of the total magma to be crystallized.

Factor analysis has been performed on the combined trace element data of the Sublayer suite (*see* Joreskog *et al.* 1976 for principles of Geological Factor Analysis). A 4-factor model, which accounts for more than 80% of the total variance in the data, has been chosen to test the influence of contamination on the trace element abundances in the magma. Varimax-rotated factor loadings and other statistics are given in Table 6. Graphical representation of the rotated factors is shown in Figure 9. The significant features to observe in these graphs are: (1) the relative distance of a variable from the 2 axes; (2) the direction of a variable in relation to the axes; and (3) the clustering of the variables and their relative positions.

From the factor loadings in Table 6 and the plots in Figure 9, the following factor-model features are apparent:

1. Factor 1 (F1) is characterized by significant positive loadings by Th, Hf, Zr, Rb and negative loadings by Sc, Co, and Sr. All the other elements have insignificant loadings on this factor. Further, this factor contributes about 46% of the variance in the data in a 4-factor model.
2. Only the REE as a group and Y load significantly on Factor 2 (F2); this accounts for about 35% of the variance.

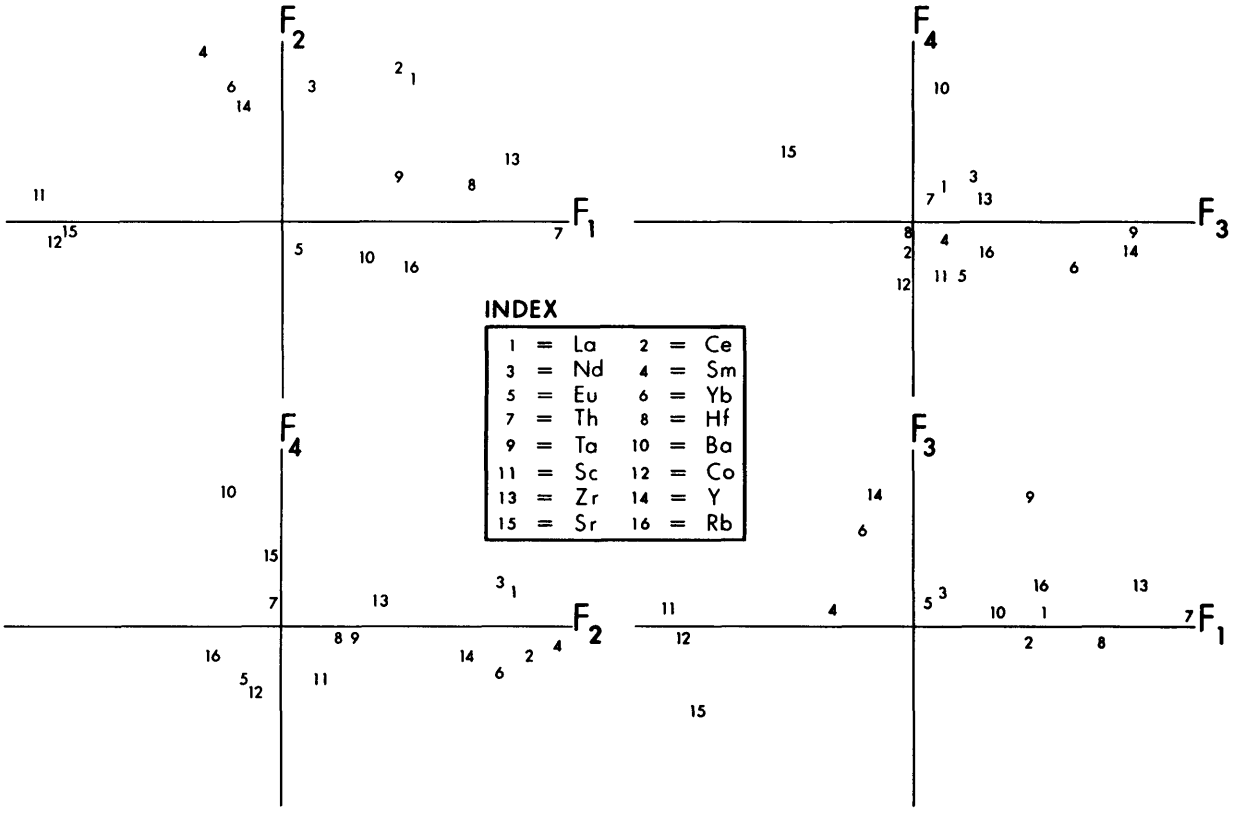

Figure 9. Graphical presentation of factor loadings of different variables on each factor in a 4-factor model.

3. Factors 3 and 4 (F3 and F4) together contribute to only a minor fraction (20%) of the total variance in the data. Yb, Ta, and Y load on Factor 3 moderately and Sr and Ba load on Factor 4.

It is interpreted here that Factor 1 (F1) represents the contamination process and the remaining 3 factors signify the fractionation of ferromagnesian minerals (F2 and F3), and plagioclase (F4).

CONCLUSIONS AND FUTURE OBJECTIVES

The data presented here suggest that the Sublayer magma experienced considerable contamination, probably through bulk assimilation of crustal rocks. Although there is considerable uncertainty in the type of modelling done, the results presented indicate that the observed chemical trends in the Sublayer can be produced by a combined assimilation-fractional crystallization process. In conjunction with such a model, the differences between the North and South Ranges may be explained by varying degrees of simultaneous assimilation and fractional crystallization. Such a model has important implications for the magmatic genesis of sulphides as described by Naldrett (1981).

Contamination of magmas by assimilation of crustal materials is a difficult process to detect conclusively. Field studies, major and trace element, and even simple isotope studies may suggest the possibility of contamination; but a comprehensive integrated study of major and trace elements, and of Sr, Nd, and O-isotopes is necessary to establish a mixing relation between magma and crustal rocks, distinct from the alternate possibility of magma derivation from an anomalous source.

Our future thrust will be mainly on the combined Sr, Nd, O-isotope study of Sublayer rocks from various geographic locations, particularly from mineralized zones. A similar isotope study of the rocks of the Sudbury Igneous Complex will also be undertaken to establish the extent to which these were also contaminated. If the isotopic characters of the magma are due to crustal contamination, it should be reflected in the Sr, Nd, and O-isotope values. A similar evolutionary history of the Rb-Sr and Sm-Nd systems would produce strongly negative correlations between $^{87}Sr/^{86}Sr$ and $^{143}Nd/^{144}Nd$ values because the crust is enriched in Rb relative to Sr, and depleted in Sm relative to Nd. Currently, we are setting up the isotope facility at the University of Toronto.

Further major and trace element (including the REE) work will also be continued to acquire additional data.

ACKNOWLEDGMENTS

The senior author has benefitted from his discussion with W.V. Peredery (Inco Limited) and M.P. Gorton. The help received from officials of Inco Limited and Falconbridge Limited is appreciated.

REFERENCES

Card, K.D.
1978: Geology of the Sudbury-Manitoulin Area, Districts of Sudbury and Manitoulin; Ontario Geological Survey, Report 166, 238p. Accompanied by Map 2360, scale 1:126 720 or 1 inch to 2 miles.

Cox, K.G., and Clifford, P.
1982: Correlation Coefficient Patterns and Their Interpretation in Three Basaltic Suites; Contributions to Mineralogy and Petrology, Volume 79, p.268-278.

DePaolo, D.J.
1981: Trace Element and Isotopic Effects of Combined Wallrock Assimilation and Fractional Crystallization; Earth and Planetary Science Letters, Volume 53, p.189-202.

Finn, G.C., Edgar, A.D., and Rowell, W.F.
1982: Petrology, Geochemistry, and Economic Potential of the Nipissing Diabase; Grant 100, p.43-58 *in* Geoscience Research Grant Program, Summary of Research, 1981-1982, edited by E.G. Pye, Ontario Geological Survey, Miscellaneous Paper 103, 219p.

Frey, F.A., Haskin, M.A., Poetz, J.A., and Haskin, L.A.
1968: Rare Earth Abundances in Some Basic Rocks; Journal of Geophysical Research, Volume 73, p.6085-6098.

Gibbins, W.A., and McNutt, R.H.
1975: The Age of the Sudbury Nickel Irruptive and the Murray Granite; Canadian Journal of Earth Science, Volume 12, p.1970-1989.

Haskin, L.A., Wilderman, T.R., and Haskin, M.A.
1968: An Accurate Procedure for Determination of Rare Earth Element by Neutron Activation; Journal of Radioanalytical Chemistry, Volume 1, p.337-348.

Hewins, R.H.
1971: The Petrology of Some Marginal Mafic Rocks along the North Range of the Sudbury Irruptive; Ph.D Thesis, University of Toronto.

Irvine, T.N.
1975: Crystallization Sequence of the Muskox Intrusion and Other Layered Intrusions-11. Origin of Chromitite Layers and Similar Deposits of Other Magmatic Ores; Geochemica et Cosmichimica Acta, Volume 39, p.991-1020.

Irvine, T.N., and Baragar, W.R.A.
1971: Guide to the Chemical Classification of the Common Volcanic Rocks; Canadian Journal of Earth Sciences, Volume 8, p.523-548.

Joreskog, K.G., Klovan, J.E., and Reyment, R.A.
1976: Geological Factor Analysis; Elsevier Scientific Publishing Company, p.175.

Krogh, T.E., McNutt, R.H., and Davis, G.L.
1982: Two High Precision U-Pb Zircon Ages for the Sudbury Irruptive; Canadian Journal of Earth Science, Volume 19, p.723.

Kuo, H.Y., and Crocket, J.H.
1978: Rare Earth Elements in the Sudbury Nickel Irruptive: Comparison with Layered Gabbros and Implications for Nickel Irruptive Petrogenesis; Economic Geology, Volume 79, p.590-605.

Langmuir, C.H., Vocke, R.D., Hanson, G.N., and Hart, S.R.
1978: A General Mixing Equation: Applied to the Petrogenesis of Basalts from Iceland and Reykjanes Ridge; Earth and Planetary Science Letters, Volume 37, p.380-392.

McLennan, S.M., Fryer, B.J., and Young, G.M.
1977: Rare Earth Elements in Huronian (Lower Proterozoic) Sedimentary Rocks: Composition and Evolution of the Post-Kenoran Upper Crust; Geochimica et Cosmochimica Acta, Volume 43, p.375-388.

Naldrett, A.J.
1981: Nickel Sulfide Deposits: Classification, Composition, and Genesis; Economic Geology, 75th Anniversary Volume, p.628-685.

Naldrett, A.J., Bray, J.G., Gasparrini, E.L., Podolsky, T., and Rucklidge, J.C.
1970: Cryptic Variation and the Petrology of the Sudbury Nickel Irruptive; Economic Geology, Volume 65, p.122-155.

Naldrett, A.J., and MacDonald, A.J.
1980: Tectonic Settings of Some Ni-Cu Sulfide Ores: Their Importance in Genesis and Exploration; Geological Association of Canada Special Paper 20, p.633-657.

Naldrett, A.J., Innes, D.G., Sowa, J., and Gorton, M.P.
1982: Compositional Variations Within and Between Five Sudbury Ore Deposits; Economic Geology, Volume 77, p.1519-1534.

Pattison, E.F.
1979: The Sudbury Sublayer: Its Characteristics and Relationship with the Main Mass of the Sudbury Irruptive; Canadian Mineralogist, Volume 17, p.257-274.

Peredery, W.V.
1972: The Origin of Rocks at the Base of the Onaping Formation, Sudbury, Ontario; Ph.D Thesis, University of Toronto.

Scibbins, B.T., Rae, D.R., and Naldrett, A.J.
(in press): Mafic and Ultramafic Inclusions in the Sublayer of the Sudbury Igneous Complex.

Souch, B.E., Podolsky, T., and Geological Staff
1969: The Sulfide Ores of Sudbury: Their Particular Relationship to Distinctive Inclusion-Bearing Facies of the Nickel Irruptive; p.252-261 *in* Magmatic Ore Deposits, edited by H.D.B. Wilson, Economic Geology Monograph 4, 366 p.

Taylor, Jr. H.P.
1980: The Effects of Assimilation of Country Rocks by Magmas on $^{18}O/^{16}O$ and $^{87}Sr/^{86}Sr$ Systematics in Igneous Rocks; Earth and Planetary Science Letters, Volume 47, p.243.

Thomson, R.N., Dicken, A.P., Gibson, I.L., and Morison, M.A.
1982: Elemental Fingerprints of Isotopic Contamination of Hebridean Palaeocene Mantle-Derived Magmas by Archaean Sial; Contributions to Mineralogy and Petrology, Volume 79, p.159-168.

Watson, E.B.
1982: Basalt Contamination by Continental Crust: Some Experiments and Models; Contributions to Mineralogy and Petrology, Volume 80, p.73.

Wood, D.A.
1980: The Application of a Th-Hf-Ta Diagram to Problems of Tectonomagmatic Classification and to Establishing the Nature of Crustal Contamination of Basaltic Lavas of the British Tertiary Volcanic Province; Earth and Planetary Science Letters, Volume 50, p.11-30.

Wright, T.L., and Doherty, P.C.
1970: A Linear Programming and Least Squares Computer Method for Solving Petrologic Mixing Problems; Bulletin of the Geological Society of America, Volume 81, p.1995-2008.

Grant 100 Petrology, Geochemistry, and Economic Potential of the Nipissing Gabbro

W.F. Rowell and A.D. Edgar
Department of Geology, University of Western Ontario

ABSTRACT

The economic potential of a Nipissing intrusion in the Lake Wanapitei-Portage Bay area of Ontario has been assessed in light of a previous study which detected a zone of slight precious metal enrichment near its base. The "enriched" zone was of particular interest as it was thought to be part of an extensive "gold reef" which includes the small, but precious metal-rich, Rathbun Lake sulphide Deposit. Precious metal analyses of 64 samples from the base of the intrusion, including the "enriched" zone, yielded only typical background levels of Au, Pd, and Pt. This discrepency appears to have been due to differences in the analytical methods used. As our results have been confirmed by the author of the original report, it is apparent that any economic potential is restricted to sulphide-bearing portions of the intrusion, such as the Rathbun Lake Deposit. A study of precious metals in the Rathbun Lake sulphides is currently in progress.

INTRODUCTION

In a preliminary geochemical study of a gabbronorite intrusion located in the Lake Wanapitei-Portage Bay area of Ontario (Figure 1), Dressler (1982) noted 2 anomalies:

1. an anomalous or "reverse" differentiation of both major and trace elements, for example, increasing MgO, Fe_2O_3, Ni, Cr, and Cu with increasing vertical height
2. a slight Au and Pd enrichment in a zone near the intrusion's basal contact.

Finn *et al.* (1982) have provided a comprehensive description of the "reverse" differentiation trend and attributed it to successive injections of a mantle-derived magma undergoing differentiation in 1 or more underlying auxillary magma chambers. In this report, we have summarized our attempt to delineate the extent of the proposed zone of slight precious metal enrichment, and also assess its economic potential. Included in the report are preliminary data concerning the next phase of our study, which focuses on precious metals in sulphide-bearing gabbronorite.

GEOLOGICAL SETTING

The Wanapitei intrusion is 1 of over 90 tholeiitic intrusions distributed across northern Ontario and is part of the Nipissing Diabase intrusive suite (Miller 1911). Nipissing dikes, sills, and irregularly-shaped bodies occur primarily within the Southern Structural Province and generally intrude the less competent Gowganda and Bruce Formations (Card and Pattison 1973). Whole rock Rb/Sr age determinations of 2160 ± 60 Ma (Fairbairn *et al.* 1969) and 2150 ± 50 Ma (Van Schmus 1965) have been obtained for Nipissing intrusions in the Cobalt and Blind River areas, respectively. A K/Ar age determination obtained in this study placed the age of the Wanapitei intrusion at 2109 ± 40 Ma. This age verifies that the Wanapitei intrusion is part of the Nipissing intrusive suite and is not a Sudbury offset.

Arcuate in shape, the Wanapitei intrusion is centred around Portage Bay on the northeastern shore of Lake Wanapitei (Figure 2). It intrudes Gowganda wacke, arkose, and conglomerate, and is cut by an olivine dike of the Sudbury Swarm. Gabbronorite is the predominant rock type, while monzodiorite, quartz diorite, granodiorite, and granite are minor constituents (Finn *et al.* 1982). All rocks have been subjected to lower greenschist facies metamorphism and the gabbronorite has in places been altered due to the addition of water (Dressler 1982).

GEOCHEMISTRY

The Wanapitei intrusion is best exposed in a cliff face on the western side of the peninsula between Portage Bay

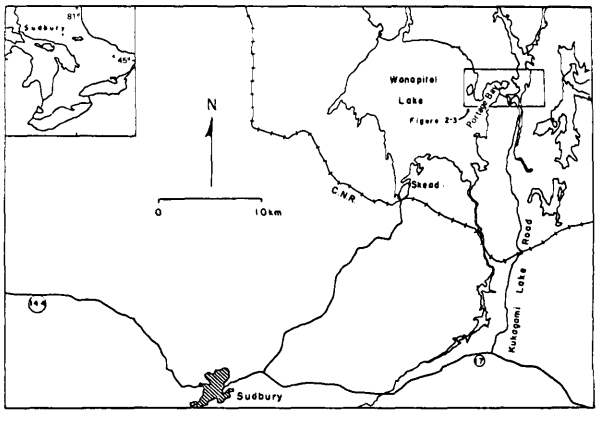

Figure 1. Location of Lake Wanapitei-Portage Bay area, Ontario.

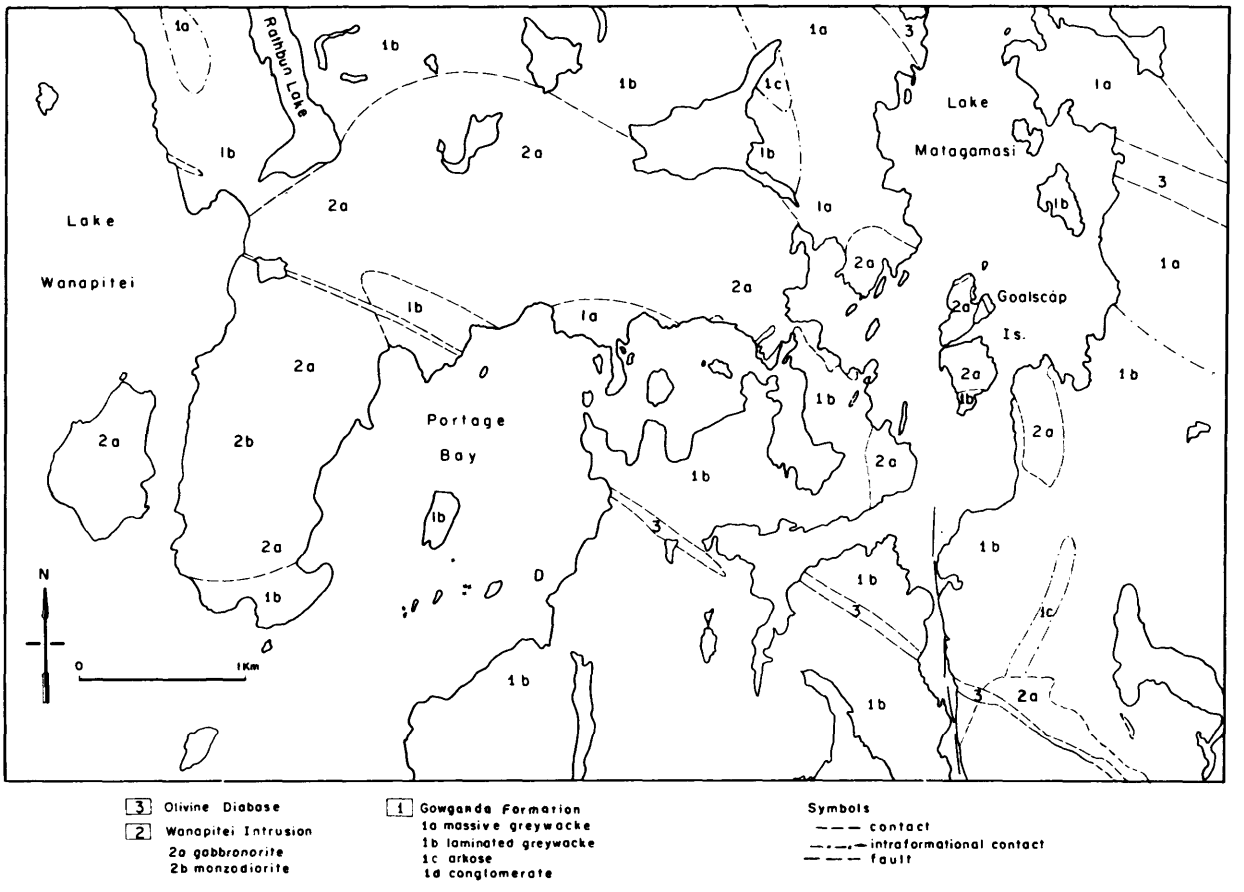

Figure 2. Geology of the Lake Wanapitei-Portage Bay area (after Dressler 1978).

and Lake Wanapitei. It is near the base of sample sections 2, 3, and 4 along this cliff (Figure 3) that Dressler (1982) detected Au values commonly 5 times greater than the typical background content of <10 ppb. Two samples from section 3 and 1 from section 2 appeared to be significantly enriched, with Au >100 ppb. In addition, it was found that Au-enriched samples in section 3 also contained Pd in excess of background amounts (Dressler 1982).

The basal location of most of the precious metal-enriched samples led Dressler (1982) to speculate that they may be part of an extensive "gold reef" which includes a precious metal-rich sulphide deposit located at the southern end of Rathbun Lake (Figure 4). This hypothesis was one of the primary reasons for undertaking a more detailed study of the intrusion's precious metal content.

To determine the extent of precious metal enrichment along the base of the intrusion, 64 samples were collected from 5 localities near its lower contact. These samples included both altered and unaltered gabbronorite, as well as a few sulphide-rich rocks from the Rathbun Lake Deposit. The most extensive sampling was undertaken along the cliff face within the gold-enriched zone delineated by Dressler. Some cliff samples were approximately from the same sample sections as Dressler's study while others were from nearby accessible outcrop. After collection, all samples were analyzed for Pt, Pd, and Au contents at X-Ray Assay Laboratories Limited in Don Mills, using combined fire assay and direct current plasma techniques.

With the exception of the Rathbun Lake sulphide ores, precious metal contents of the gabbronorite samples did not differ from typical background amounts (Figure 5). At each locality Pt, Pd, and Au values were found to be uniformly low (Table 1) and no preferential enrichment of either altered or unaltered gabbronorite was evident. From Figure 6, it is apparent that the Au contents are low even within the proposed "gold reef" along the cliff face. In this zone, precious metal values ranged from 2 to 20 ppb Au, 10 to 37 ppb Pt, and <2 to 50 ppb Pd (Figure 5).

As these results failed to support the concept of precious metal enrichment along the base of the intrusion, 6 of Dressler's "gold reef" samples were reanalyzed. In contrast to the original analyses, Au was detected at only the background level of <10 ppb in each sample (Table 2).

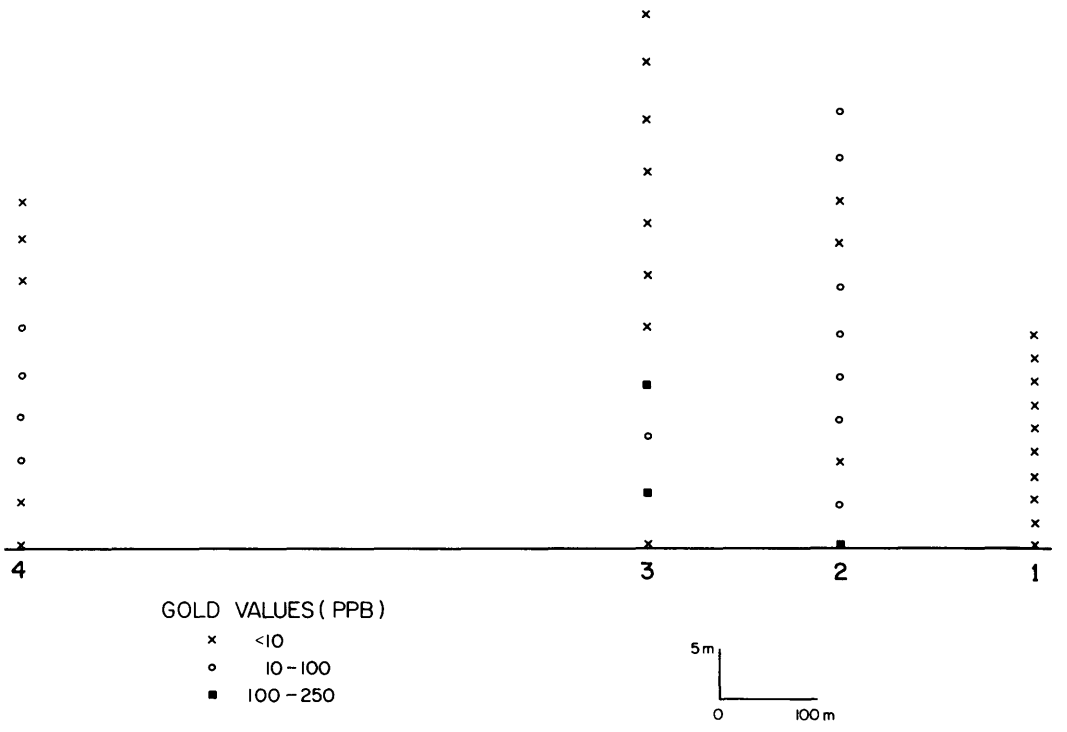

Figure 3. Dressler's (1982) Au values for samples from 4 cliff sections facing Lake Wanapitei.

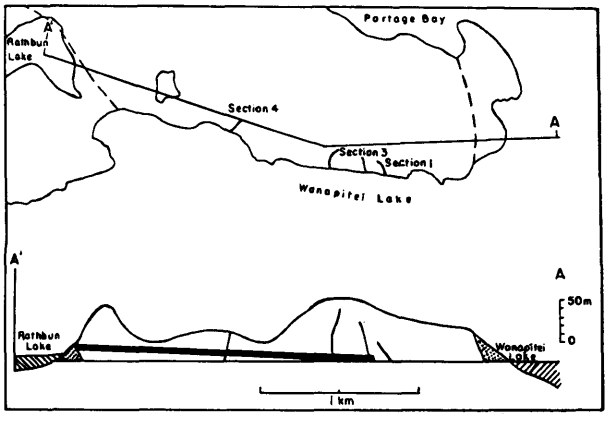

Figure 4. Cross-section and plan view of the Wanapitei intrusion showing the location of Dressler's (1982) sample sections. Heavy line is Dressler's "gold reef". Circle is location of Rathbun Lake sulphide mineralization.

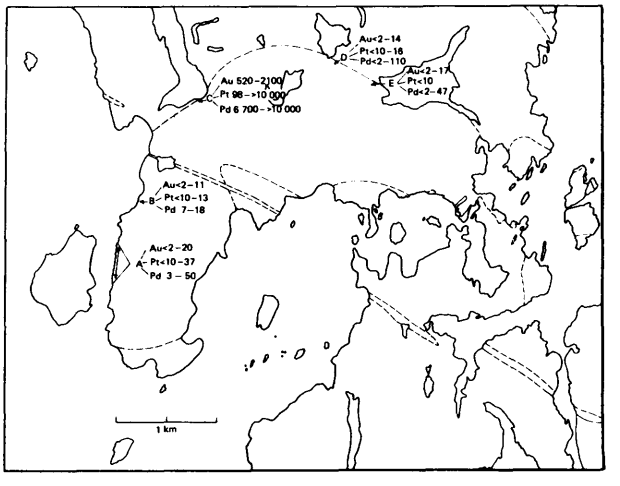

Figure 5. Map of the Lake Wanapitei-Portage Bay area showing locations of sample areas and ranges of precious metal values in ppb. Letters indicating each sample site are referred to in Table 1.

TABLE 1 Au, Pt, AND Pd VALUES OF GABBRONORITE SAMPLES FROM LOCALITIES A, B, C, D, AND E OF FIGURE 5.

Section A

Sample No.	Au	Pt	Pd	Sample No.	Au	Pt	Pd
W2-2	8	25	23	W3-2	<2	<10	3
W6-1	3	12	16	W8-1	<2	<10	5
W8-2	<2	<10	7	W8-3	6	24	14
W8-4	<2	<10	10	W9-2	4	30	40
W9-3	3	<10	5	W10-3	3	20	25
W10-4	8	24	32	W11-4	4	18	15
W11-5	<2	<10	3	W11-6	2	<10	3
W12-2	3	<10	5	W12-3	4	37	38
W12-4	3	22	24	W13-2	<2	18	22
W13-3	3	<10	10	W14-3	<2	21	17
W14-4	2	23	26	W15-2	<2	14	22
W15-3	<2	12	15	W15-4	<2	13	17
W16-2	<2	<10	5	W16-3	<2	19	14
W16-4	<2	17	11	MH4-1	14	<10	12
MH4-2	6	11	14	MH4-3	10	15	16
MH5-1	5	13	37	MH5-2	9	12	30
MH5-3	5	17	39	MH5-4	7	19	26
S-2A	5	28	23	S-5A	15	30	27
S-23A	3	16	29	S-10B	4	22	50
S-43C	<2	13	27	S-28D	2	<10	<2
S-52D	7	35	22	S-54D	20	20	15
S-57D	<2	<10	70	S-58D	11	19	12

Section B

Sample No.	Au	Pt	Pd	Sample No.	Au	Pt	Pd
W17-2	<2	10	7	W17-3	<2	<10	6
W17-4	<2	13	18	W17-5	2	13	12
W18-2	3	11	11	W18-3	11	13	11

Section C

Sample No.	Au	Pt	Pd	Sample No.	Au	Pt	Pd
S59E	1200	>10000	6700	S60E	21000	2400	>10000
41-E-98	520	98	>10000				

Section D

Sample No.	Au	Pt	Pd	Sample No.	Au	Pt	Pd
MH1-1	3	<10	7	MH1-2	3	<10	47
MH1-3	<2	<10	<2	MH1-4	4	<10	<2
MH1-5	2	<10	<2	MH1-6	17	<10	10

Section E

Samples No.	Au	Pt	Pd	Sample No.	Au	Pt	Pd
MH2-1	2	<10	7	MH2-2	<2	<10	28
MH2-3	6	15	110	MH2-4	14	10	6
MH2-5	14	16	13	MH2-6	4	<10	<2

DISCUSSION

The discrepency between Dressler's results and those obtained in this study appears to have been due to the use of different analytical methods. In Dressler's geochemical investigation, precious metal values were determined only by fire assay. As mentioned previously, samples in this study were analyzed by X-Ray Assay Laboratories Limited using fire assay and direct current plasma techniques. The lower detection limits of this method are 2 ppb for Au, 10 ppb for Pt, and 2 ppb for Pd

TABLE 2 COMPARISON OF DRESSLER'S (1982) Au VALUES WITH PRECIOUS METAL VALUES OBTAINED IN THIS STUDY. ALL VALUES ARE IN ppb.

	Reanalysis Values			Dressler's Values
Sample No.	Au	Pt	Pd	Au
G-1-I	<2	<10	3	140
G-1-II	<2	20	7	40
G-1-IV	<2	10	12	40
G-1-V	4	20	14	20
G-1-XI	5	20	16	40
W-3	14	12	47	40

(X-Ray Assay Laboratories Limited, Analytical and Consulting Services 1982).

Using an improved method of precious metal detection, Dressler recently had several samples from his 1982 study reanalyzed. In all cases, reanalysis yielded only background precious metal values (B.O. Dressler, Geologist, Ontario Geological Survey, personal communication, 1982).

CONCLUSIONS AND FUTURE OBJECTIVES

Our results indicate that an extensive zone of slight precious metal enrichment does not exist along the base of the Wanapitei gabbronorite intrusion. Significant Au and particularly Pt and Pd values were detected only in sulphide-bearing gabbronorite samples from the southern end of Rathbun Lake (Table 1). This suggests that any economic potential of the Wanapitei intrusion is dependent on the discovery of more of these small, but precious metal-rich sulphide deposits.

Although mining has removed much of the Rathbun Lake sulphide mineralization, samples from the dump indicate that chalcopyrite, pyrrhotite, and magnetite were the primary ore minerals (Dressler 1982). As part of the next phase of our study of the Wanapitei intrusion, separates of each of these minerals were obtained and analyzed for Platinum Group Elements (Pt, Pd, Ru, Rh, Re, Os, and Ir) and Au content.

Preliminary results of these analyses indicate that Pt and particularly Pd are preferentially associated with chalcopyrite, while Au and Ir are most abundant in pyrrhotite. A Au value of 24 000 ppb in pyrrhotite appears to be anomolously high and may result from the presence of a discrete particle of gold or from an analytical error. Further analyses will be conducted to determine any more definite patterns of precious metal partition.

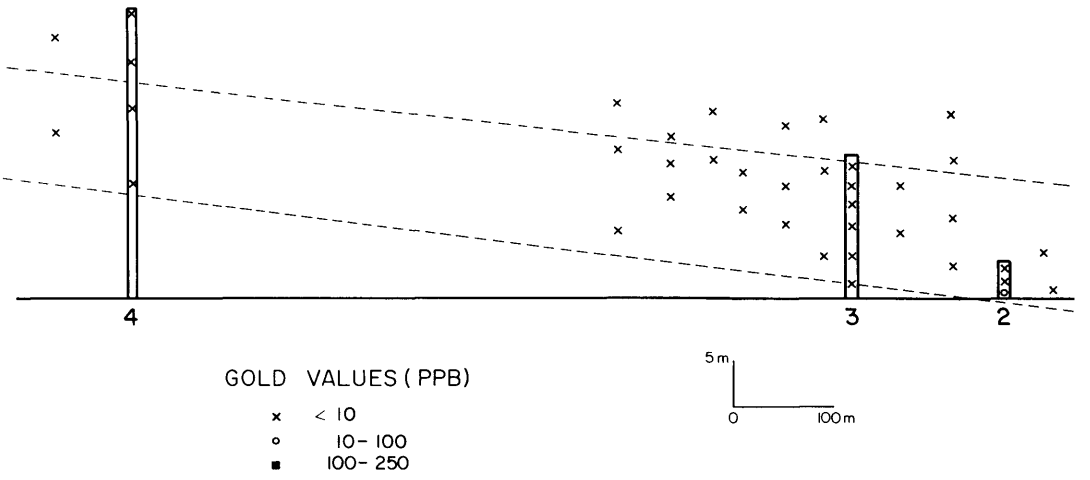

Figure 6. Cliff section Au values obtained in this study. Dashed lines indicate location of Dressler's (1982) "gold reef". Sections 2, 3, and 4 are approximately in the same positions as in Figure 3.

Additional work on the sulphide-bearing gabbronorite will involve:

1. use of an electron microprobe to identify any platinum group minerals present
2. an oxygen isotope study to determine the source of fluids associated with the sulphide mineralization.

REFERENCES

Card, K.D., and Pattison, E.F.
1973: Nipissing Diabase of the Southern Province, Ontario; Geological Association of Canada, Special Paper 12, p.7-30.

Dressler, B.O.
1978: Rathbun Township, District of Sudbury, Ontario; Ontario Geological Survey, Preliminary Map P.1609, scale 1 inch to ¼mile.

1982: Geology of the Wanapitei Lake Area, District of Sudbury; Ontario Geological Survey, Report 213, 131p. Accompanied by Maps 2450, 2451, scale 1:31 680 (1 inch to ½ mile).

Fairbairn, H.W., Hurley, P.M., Card, K.D., and Knight, C.J.
1969: Correlation of Radiometric Ages of Nipissing Diabase and Huronian Metasediments with Proterozoic Orogenic Events in Ontario; Canadian Journal of Earth Sciences, Volume 6, p.489-497.

Finn, G.C., Edgar, A.D., and Rowell, W.F.
1982: Petrology, Geochemistry, and Economic Potential of the Nipissing Diabase; Ontario Geological Survey, Miscellaneous Paper 103, p.43-58.

Miller, W.G.
1911: Notes on the Cobalt Area; Engineering and Mining Journal, Volume 92, p.645-649.

Van Schmus, W.R.
1965: The Geochronology of the Blind River-Bruce Mines Area, Ontario, Canada; Journal of Geology, Volume 73, p.755-780.

X-Ray Assay Laboratories Limited
1982: Analytical and Consulting Services Catalogue, Don Mills, Ontario.

Grant 118 Surface Electromagnetic Mapping in Selected Positions of Northern Ontario, 1982-1983

D.W. Strangway, O.M. Ilkisik, and J.D. Redman
Department of Geology, University of Toronto

ABSTRACT

Audiomagnetotelluric (AMT) data have been collected at 114 stations from 3 different locations during a multiyear electromagnetic mapping study in the clay-covered regions of Northern Ontario.

In Moody and Marathon Townships near Lake Abitibi, the resistivity at all stations shows an anistropic behaviour related to metasediments and to metamorphosed ultramafic rocks. This can be detected even when the ultramafic rocks are covered by conductive clays. One-dimensional models show approximately a 100 m thickness of overburden, with an average resistivity of 450 ohm-m. Underlying Precambrian metavolcanics have resistivity values in the range of 10 000 to 50 000 ohm-m. Conductors within the metavolcanics can be detected.

The Night Hawk Lake geophysical test site is located in the northeastern corner of Thomas Township, near Timmins. There is a conductive graphitic zone in the bedrock under about 90 m of glacial overburden (Barlow *et al.* 1982). A total of 73 AMT measurements were made in this area. Thirty-six (36) were on a rectangular grid with 150 by 200 m spacing. On the grid, the dominant feature is that the high frequency (8570, 5050 Hz) resistivities are around 100 ohm-m in the western portion of the area. This is related to increasing clay content in the glacial overburden towards the west. However, as we examine lower frequencies, we can see the presence of the conductive body within the rhyolite, with an east-west strike. The body appears to be traceable westward at lower frequencies, which are more effective at penetrating the conductive clay.

Measurements were made in Morrisette, Bisley, and Arnold Townships near Kirkland Lake along an east-west profile perpendicular to the Munro Esker. The dominant pattern shows high resistivities, up to 10 000 to 50 000 ohm-m, underneath the esker.

Measurements of the electrical resistivity and its frequency dependence have been made on representative samples of clays and sands. In the laboratory, clays have an average resistivity (at 50 Hz) of 24 ohm-m; silty clays - 45 ohm-m; and loams - 87 ohm-m. These results are similar to results measured in the AMT field work and using local in situ measurements. The frequency dependence is quite small in these samples, although 1 sample shows an unusual negative percent frequency effect.

INTRODUCTION

During the 1982 field season, work continued on a multiyear electromagnetic mapping study in northern Ontario. Parts of the glaciated Canadian Shield have very high resistivities beneath a thin and relatively conductive surface material. We applied the audiomagnetotelluric (AMT) technique to define vertical and horizontal changes within this surficial unit and to map characteristics of the bedrock.

An interference analyzer described by Strangway *et al.* (1973) was used to measure the scalar resistivities at discrete frequencies of 13, 25, 36, 83, 140, 210, 473, 858, 2140, 5050, and 8750 Hz. Electrode spacing was 100 m during normal surveys and 50 m for detailed surveys.

This report presents a summary of progress based on audiomagnetotelluric measurements made in Moody and Marathon Townships near Lake Abitibi (A), the Night Hawk Lake geophysical test range east of Night Hawk Lake (F), and Morrisette, Bisley, and Arnold Townships near Kirkland Lake (G).

Two resistivity soundings were carried out, using a Schlumberger array, at the Night Hawk Lake test site. Thirty-five (35) additional samples were collected from the Cochrane, Timmins, and Elk Lake areas for laboratory measurements. In situ measurements of low frequency resistivity, using a small Wenner array, were made at these sample sites.

DATA PROCESSING AND INTERPRETATION

The data were processed for presentation in several formats. A cubic polynomial was fitted by least-squares to measured ρ_a values versus discrete frequencies. The polynomial fitted 10 log ρ_a values were then computed as a function of log f (decreasing downward) and distance along the lines, and then contoured as pseudosections. These figures illustrate lateral and vertical variations simultaneously. Although not presented here, residual resistivity plots (difference of observed and averaged resistivity at each particular frequency along the line) were also prepared. These plots are especially useful in locating the low resistivity zones. Plots of the ratio of the east-west to north-south components illustrate the anisotropy.

We have interpreted the apparent resistivity smoothed data with the Bostick transformation algorithm. Transformation of the apparent resistivities from frequency domain to depth domain can be done using

$$h_B = \left(\frac{\rho_a}{\omega\mu_o}\right)^{1/2} \cong 356\left(\frac{\rho_a}{f}\right)^{1/2} \quad (1)$$

(Bostick 1977; Jones in press). This formula for the effective depth h_B became popular after Bostick (1977) formulated the concept of the "Bostick resistivity" ρ_B corresponding to depth h_B

$$\rho_B = \rho_a \frac{1-m}{1+m} \quad (2)$$

where m is the gradient of the (ρ_a vs f) data on a logrithmic scale.

Combining the top of 2 layers using Kirchoff's Law into a single fictitious layer with the same total conductivity, i.e.

$$S' = S_1 + S_2 \quad \text{where} \quad S = \frac{h}{\rho}$$

we can calculate the effective resistivity

$$\rho_{Ei} = \frac{\Delta h_{Bi}}{\Delta S_i} \quad (3)$$

These resistivity values of ρ_E are almost identical to the Bostick resistivity values.

By taking into account the energy attenuation of the electromagnetic waves at a certain depth interval, and assuming that ρ_{Ei} represents only a given portion of the true resistivity, it is possible to calculate an almost true resistivity corresponding to that depth interval by

$$\rho_{I1} = \rho_{a1}$$

$$\rho_{Ii} = \frac{\rho_{Ei}}{e^{\frac{-2(fi)^{1/2}(\sum_{n=1}^{i-1}\Delta h_{Bn})}{503}} - e^{-(2)^{1/2}}} \quad (4)$$

$$i = 2, N$$

where N is the number of observations (Ilkisik and Strangway in preparation). Figure 8b is an example of the application of this technique.

The calculations of ρ_B or ρ_E and ρ_I are very simple and can be done in the field using a hand calculator. This provides a quick real-time quantitative interpretation using only the scalar apparent resistivities. These calculations are also useful as an initial guess for expensive inversion and 2-dimensional model programs.

We have derived a set of contour maps for the grid areas. These maps are useful presentations of the observations as a single frequency slice through the region; and together with pseudosections they represent a 3-dimensional 'picture' of the area.

Another technique, singular value decomposition (SVD) analysis of AMT data, gives us the important model parameters and their effects through the frequency range for a certain geologic section (Edward *et al.* 1980; Jones 1982).

We have been using a nonlinear, least-squares estimation method (Marquardt 1963; ZXSSQ routine from IMSL) to invert AMT data. Although the applicability of 2-dimensional models depends on real geologic structures, especially in Precambrian terrain, along some lines we attempted to use mostly E perpendicular responses. For 2-dimensional calculations, a computer program was used, based on impedance networks (Madden and Swift 1969).

DISCUSSION OF RESULTS MOODY AND MARATHON TOWNSHIPS

In Moody and Marathon Townships between Lake Abitibi and Cochrane, 15 AMT stations were surveyed during the summer of 1981 (Ilkisik *et al.* 1982). During the summer of 1982, an additional 28 AMT stations were completed. The oldest basement material is early Precambrian mafic metavolcanics which underlie much of the map area (unit 1 in Table 1). The geologic strike of the bedrock is east-west which is approximately perpendicular to the profile. Most of the stations lie along the northern part of the Munro esker. Conductive clays cover the regions east and west of this roughly north-south oriented esker.

By using the audiomagnetotelluric system at the lower frequencies, we are able to map the electrical resistivity of the basement beneath the clay and/or esker cover. The resistivity curves from the sites which are located on the metasediments and metamorphosed ultramafic rocks (units G5 and G7 respectively in Figure 1a) show, without exception, an anisotropic behaviour in the low frequency range. This is true even in the areas covered by conductive glacial clay as at sites A-33 and A-34.

The measured scalar resistivities in the east-west orientation tend to be lower than in the north-south orientation. Pseudosections in both directions give rise to the sketched geologic section. The anisotropy plot is given in Figure 2. We assume that this lower resistivity is associated with the presence of foliation in anisotropically distributed minerals such as biotite, or with water-filled cracks, which may be parallel to the fabric of steeply dipping metasediments.

We measured a low resistivity anomaly for both the east-west and north-south orientations at site A-15 (Figure 1a) on metavolcanics. In addition, A-14, A-27, and A-28 show strong anisotropy. This suggests a low resistivity structure within the metavolcanics with an east-west strike at station A-15.

Fitted models for isotropic resistivity curves (as at site A-18) were obtained by using Bostick transformation and 1-dimensional inversion techniques. These models show roughly a 100 m thick overburden with an average resistivity of 450 ohm-m. Underlying Precambrian metavolcanics have resistivity values in the range from 8000 to 50 000 ohm-m. Most of the models imply that there is a relatively low resistivity layer at a depth of 8 km.

THE NIGHT HAWK LAKE GEOPHYSICAL TEST RANGE

The Night Hawk Lake geophysical test range is located in the northeastern corner of Thomas Township, east of Timmins. A total of 73 AMT measurements were made during the survey in this area. Thirty-six (36) of them were on a

TABLE 1 TABLE OF LITHOLOGIC UNITS FOR THE STUDY AREAS (*see* FIGURE 1) (AFTER PYKE ET AL. 1973).

Period	Short Description	Unit No. (+)
PHANEROZOIC		
Paleozoic		
Silurian	Limestone, sandstone, shale	18
Ordovician	Shale, limestone	17
PRECAMBRIAN		
Late Precambrian		
Mafic Intr. R.	Diabase: dikes	16
Middle Precambrian		
Alkalic Intr. R.	Syenite, nepheline, syenite	15
Mafic Intr. R.	Diabase, granophyre, sheets and dikes	14
Huronian	Lorrain form, quartzite, arkose	13
"	Gowganda form, arkose, greywacke	12 a,b
Early Precambrian		
Mafic Intr. R.	Diabase: dikes	11
Felsic Intr. R.	Granodiorite,qz. monzonite, pegmatite	10 a,b,c
"	Syenite, feldspar porphyry	9
Metamorphosed Ultramafic R.	Gabbro, diorite, lamporphyre	8
"	Peridotite, dunite, serpentinite	7
Metasediments	Conglomerate, greywacke	6
"	Greywacke, siltstone, argillite	5
Metavolcanics	Trachyte, flows, tuff, breccia	4
"	Serpentinized peridotite flows	3
"	Pyroclastic rocks (Rhyolitic, dacitic)	2 a,b
"	Basaltic and andesitic flows, tuffs	1 a,b,c

(+) The letter "G" preceding rock unit no. on the maps indicates interpretation from geophysical data in drift covered areas.

rectangular grid with 150 by 200 m spacing. In Figure 3, the apparent resistivity contour map is given for a frequency of 473 Hz. As we examine the maps at each frequency, it is noted that there is a surface layer which usually has a moderate resistivity of about 500 ohm-m. At the lower frequencies, the apparent resistivity rises to about 10 000 ohm-m. At the centre of the map, the graphitic conductive zone is well defined with a resistivity value of less than 500 ohm-m (Figure 3).

In Figures 4a and 4b, we present north-south and east-west pseudosections for averaged resistivity values. Along the north-south profile (F/NS, Figure 4a) the major feature is the zone of low resistivity at the middle. This zone reflects the graphitic conductor. Low resistivities in the south result from the presence of clay-rich surficial material. Figure 4b is an east-west pseudosection (F/EW) which corresponds to the location of the clay-covered areas. The high resistivity zone around sites F-40 and F-41 correspond to measurements made on bedrock outcrops of strongly carbonatized volcanic rocks (unit 1c).

On the grid, the dominant feature is that the high frequency (8570 Hz) resistivities are around 100 ohm-m in the western part of the area (Figure 5a) and around 500 ohm-m in the east. This is related to the increasing clay content in the glacial overburden towards the west. However, as we examine maps for lower frequencies carrying information about greater depths, we can see the presence of the east-striking conductive body within the rhyolite. The body appears to be traceable westward at lower frequencies (Figure 5b). These frequencies are capable of penetrating the conducting clay. Figure 5c illustrates the Bostick resistivity distribution at 200 m depth from the surface. This corresponds to the approximately true bedrock resistivity values. The length of the conductive body is about 700 m.

In Figures 6a and 6b, pseudosections and Bostick transforms of resistivity data up to 1000 m in depth are given along 100E (Line #1E). The low resistivity anomaly

on the sections is well correlated with the known graphitic conductive zone. We originally used 150 m station separation. Later we added detailed measurements using 25 m station separation. This detail in the vicinity of the conductor suggests that there is a broad body with a limited depth extent and that the northern and southern edges of the conductor are at about 100N and 200S. We made many attempts to find the true shape of the body. The most important problem for a 2-dimensional interpretation of our data is a clay-rich layer, which lies along the western side of the grid, perpendicular to the strike of the graphitic zone. Two-dimensional model calculations for this clay-rich unit of the glacial overburden show that there is no significant effect of the clay-rich layer at high frequencies 200 m from its edge. We found the "Y"-shaped body (Figure 6c) 2-dimensional response (Figure 6d) gave better fits than rectangular or "V"-shaped bodies. The anomaly found using the Bostick resistivity cross-section (Figure 6b) corresponds well to a full 2-dimensional model (Figure 6c).

We applied 1-dimensional inversion to the data from the north of the grid area which displays an isotropic behaviour. The layered earth section indicates a 95 m thick overburden with 30 m of clay-rich material at the west. Beneath the overburden, the resistivity is in the range of 15 000 to 60 000 ohm-m. Although our data might have higher noise at the lowermost frequencies, there appear to be lower resistivities at a depth of around 6 to 7 km. The existence of clay-rich material at the surface could also affect this interpretation of the structure (Kaufman and Keller 1981).

Two resistivity soundings were carried out using a Schlumberger array at the test site. The results for station 00 on line 500W (50 m south of AMT site F-4) are given in Figure 7a. It was not possible to obtain as good a fit for this station. The 2-layer and 4-layer models give different thicknesses of the clay-rich layer (50 and 30 m respectively). The results for station 200N on line 300E (F-34) are given in Figure 7b. These data can be fitted with a lay-

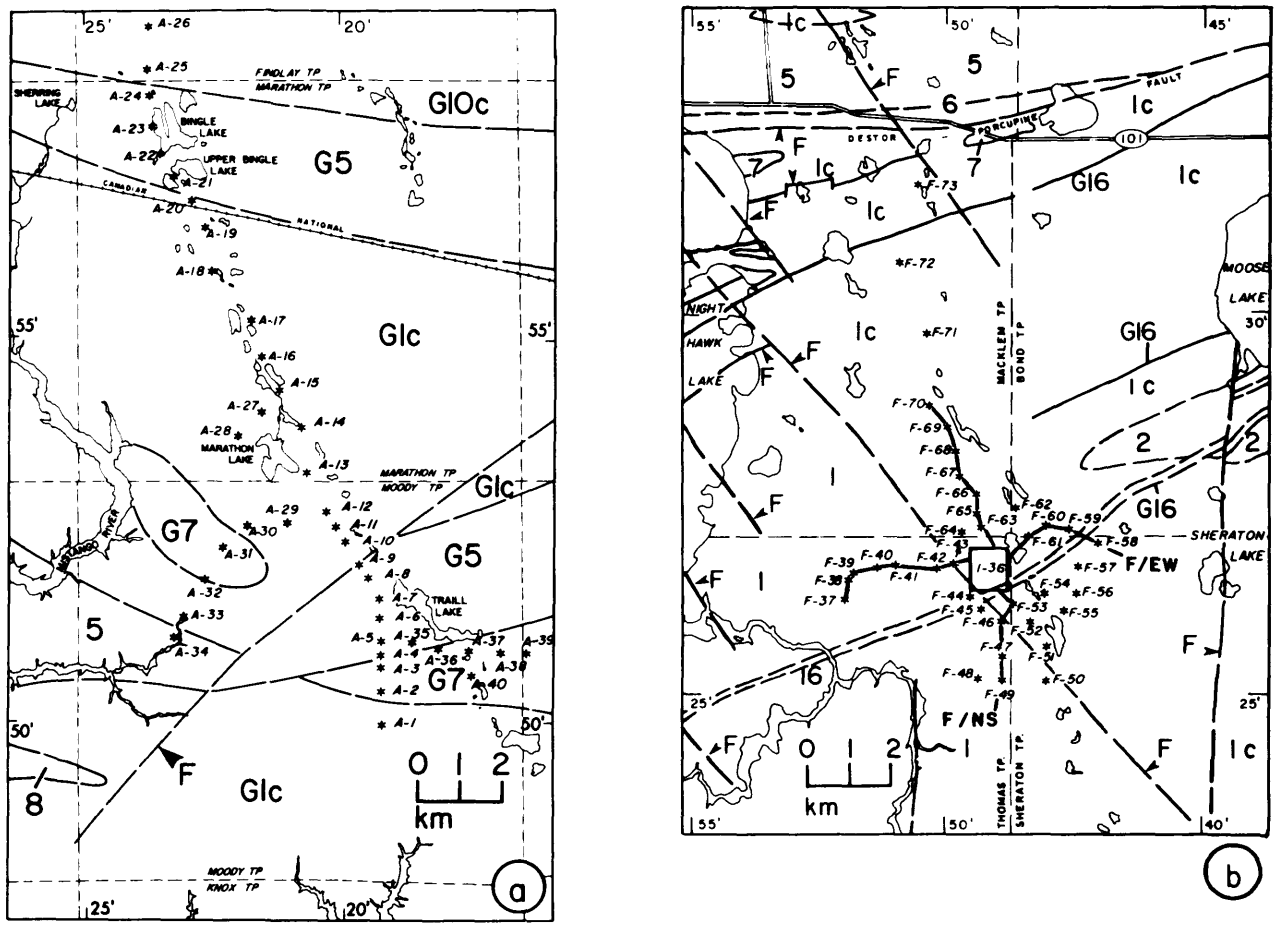

Figure 1. The bedrock geology map of: (a) Moody and Marathon Townships; (b) the area east of Night Hawk Lake (after Pyke et al. 1973). Legend is given in Table 1.

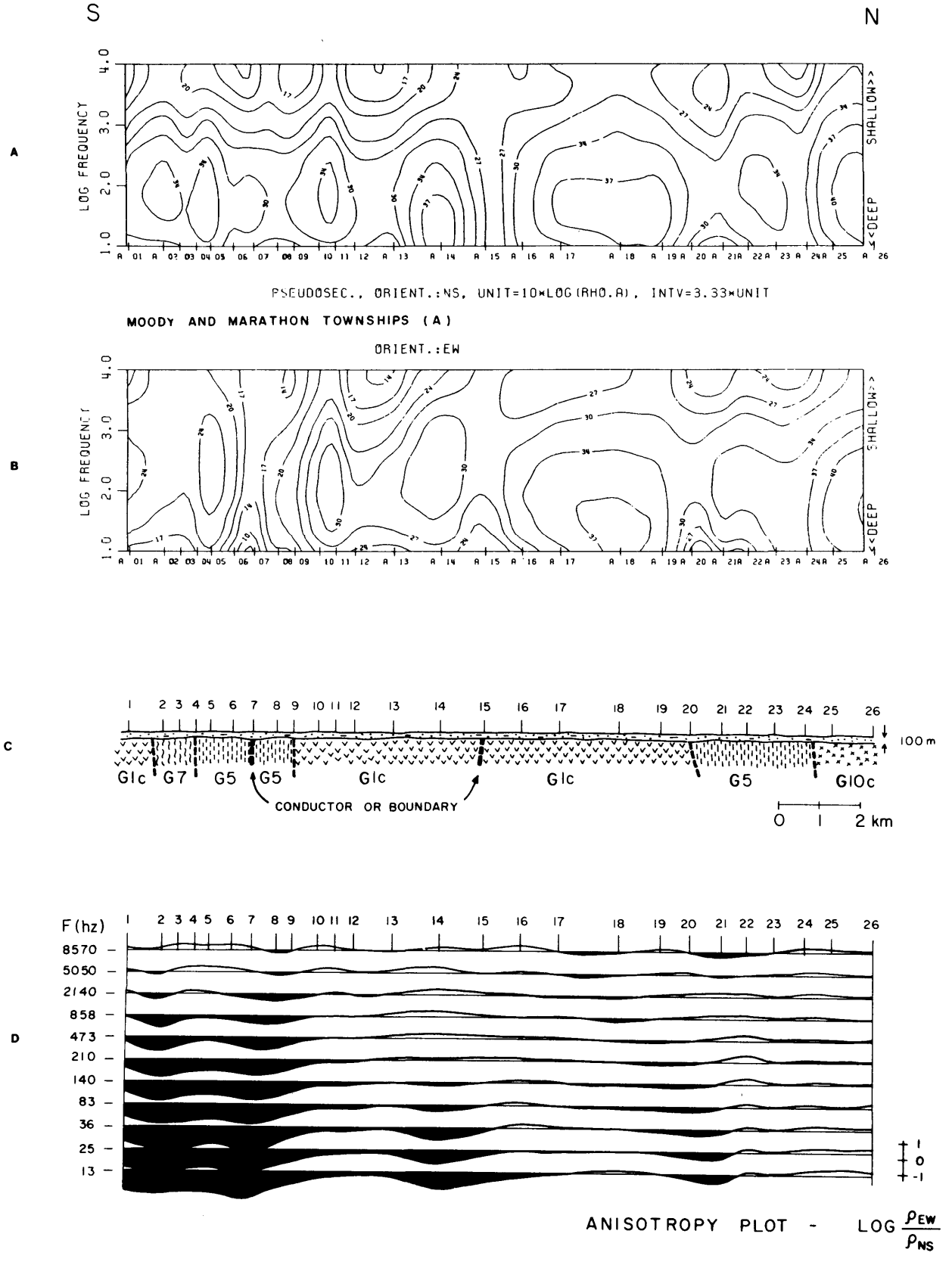

Figure 2. The pseudosections from Moody and Marathon Townships along north-south orientation in NS and EW modes, (a) and (b) respectively; a sketch geologic section (c), and the anisotropy plot (d).

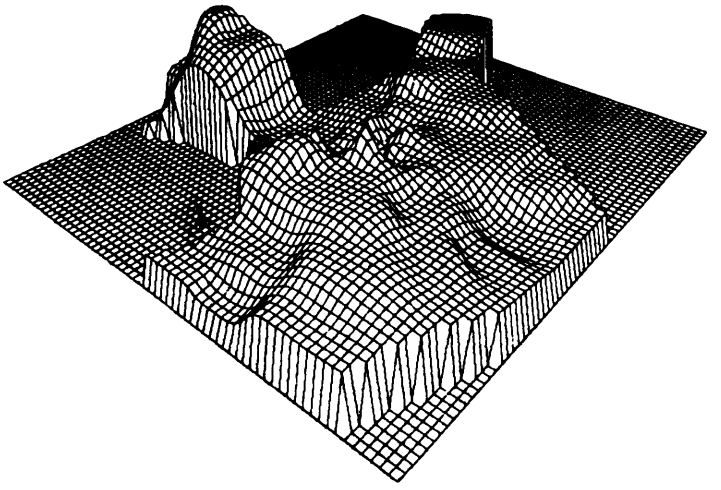

AZIM = 40.0 ELEV = 30.0

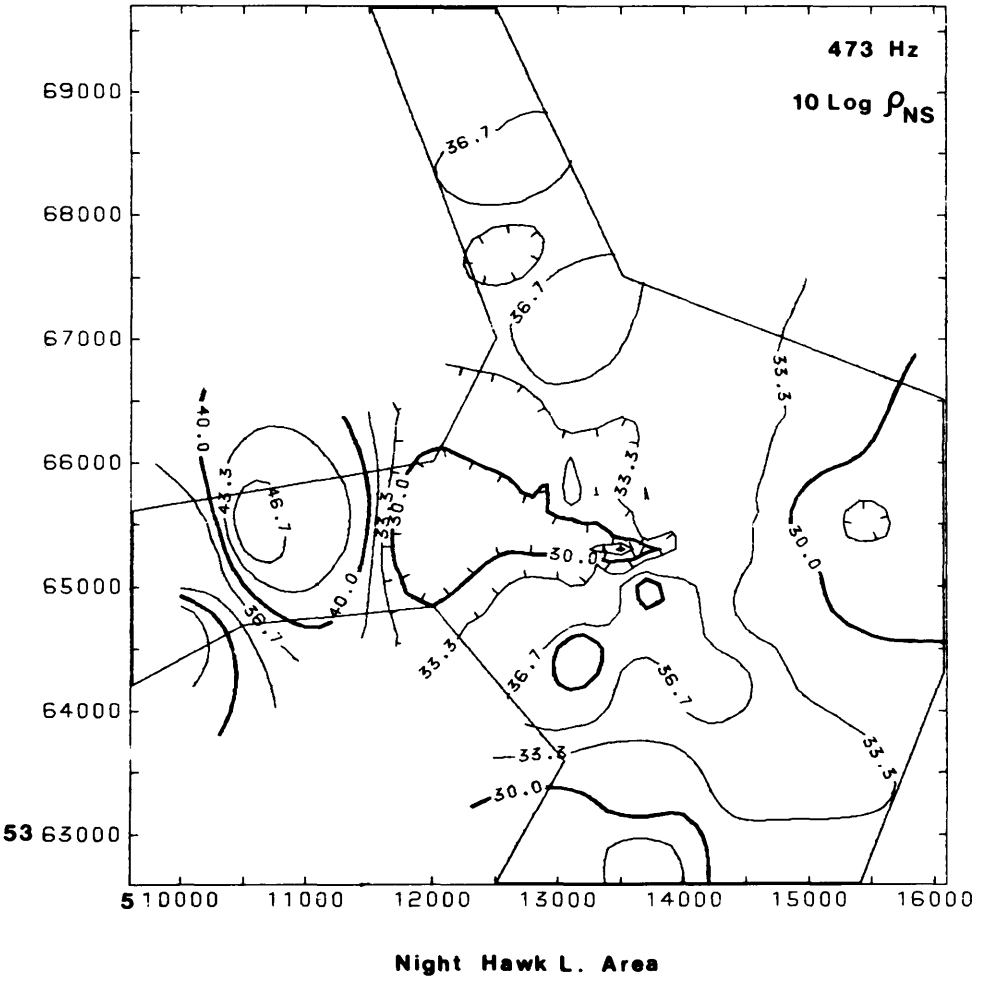

Figure 3. The apparent resistivity map at 473 Hz from east of Night Hawk Lake.

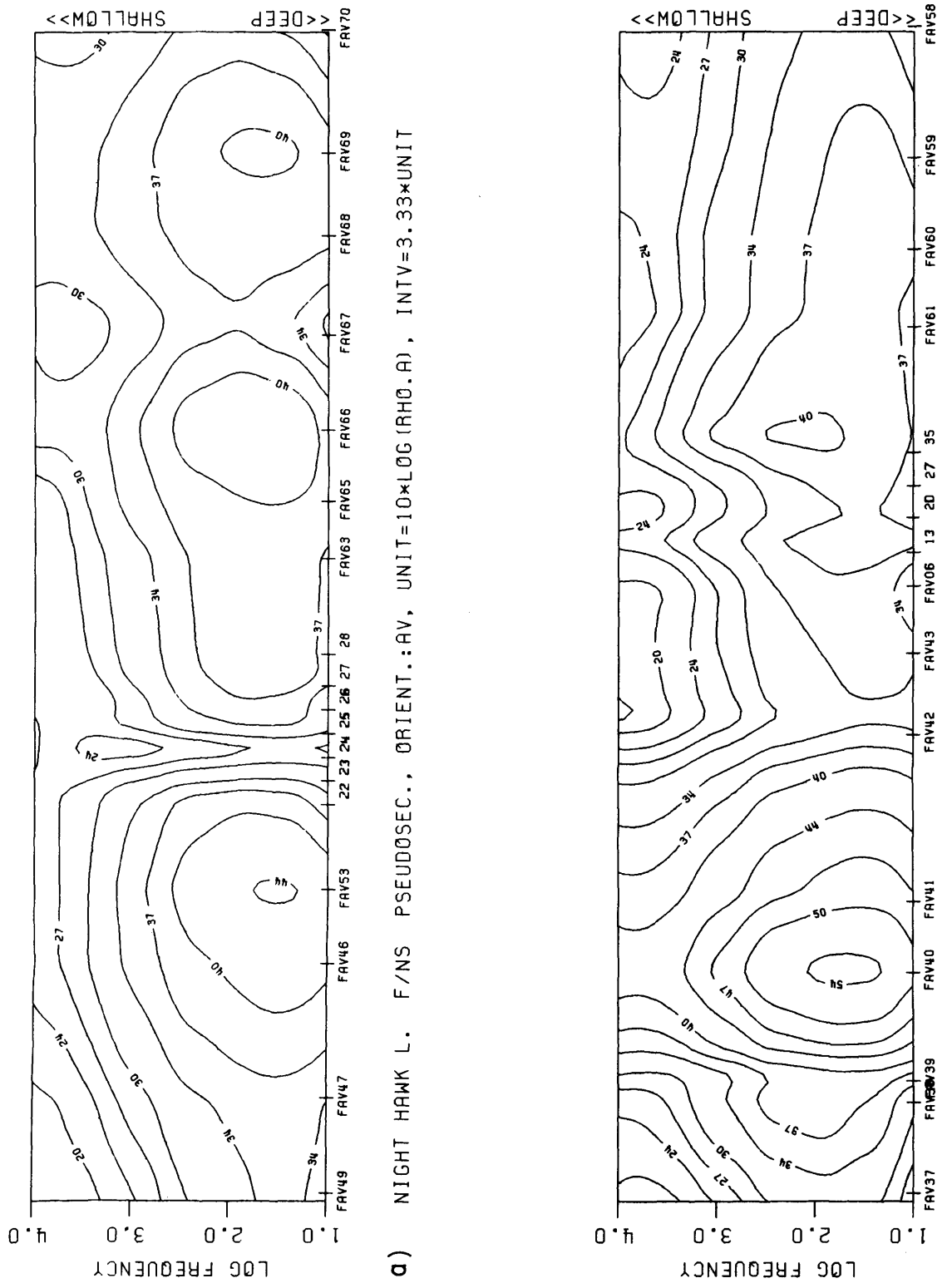

Figure 4. The averaged apparent resistivity pseudosections along north-south (F/NS) orientation (a), and east-west (F/-EW) orientation (b), from Night Hawk Lake area.

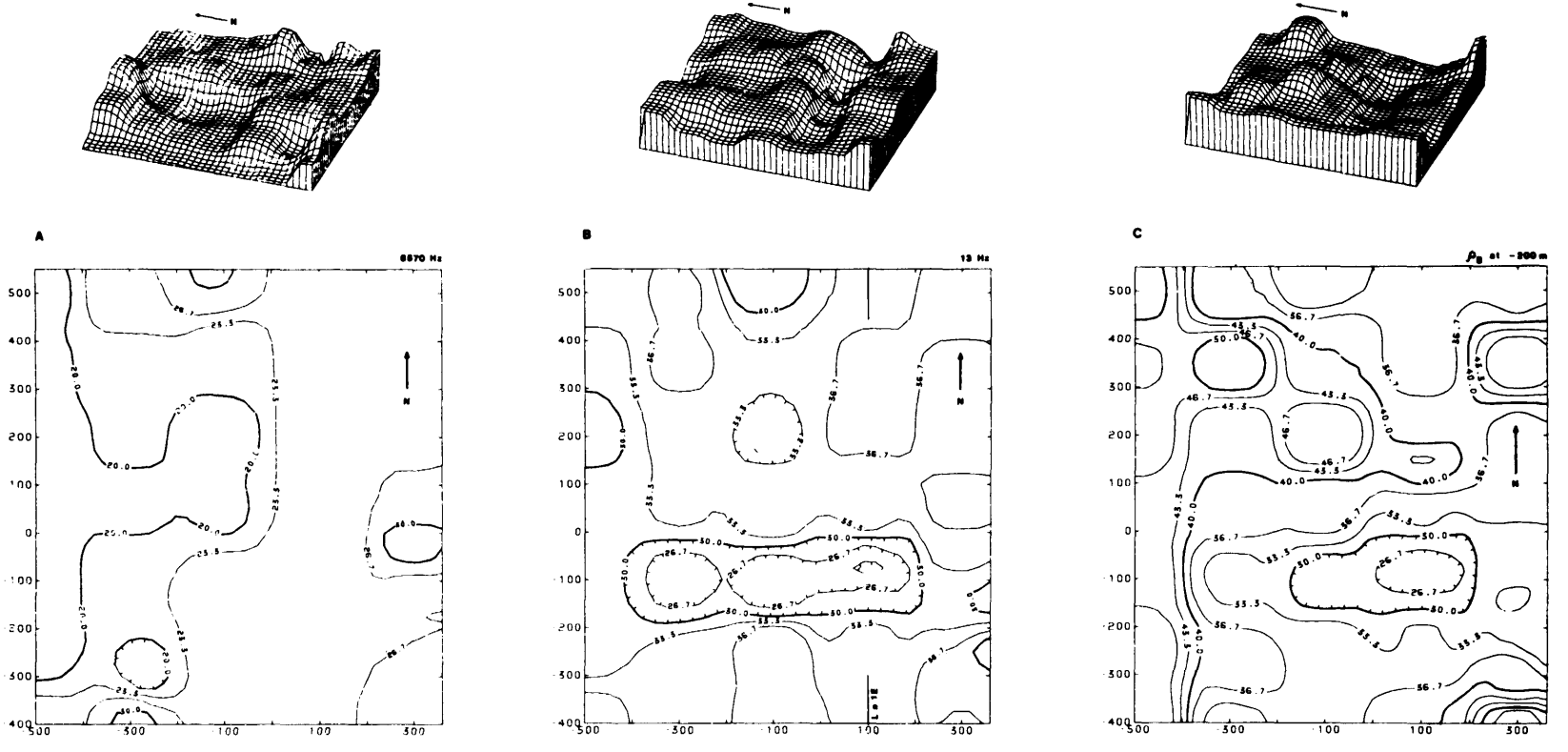

Figure 5. The apparent resistivity contour maps of the Night Hawk Lake geophysical test site; (a) for 8570 Hz which corresponds to the shallow information; (b) for 13 Hz which is the deeper information, and (c) Bostick resistivity map at 200 m depth. Low resistivity anomaly in (b) and (c) corresponds to graphitic conductor. (Contour labels are 10 logρ).

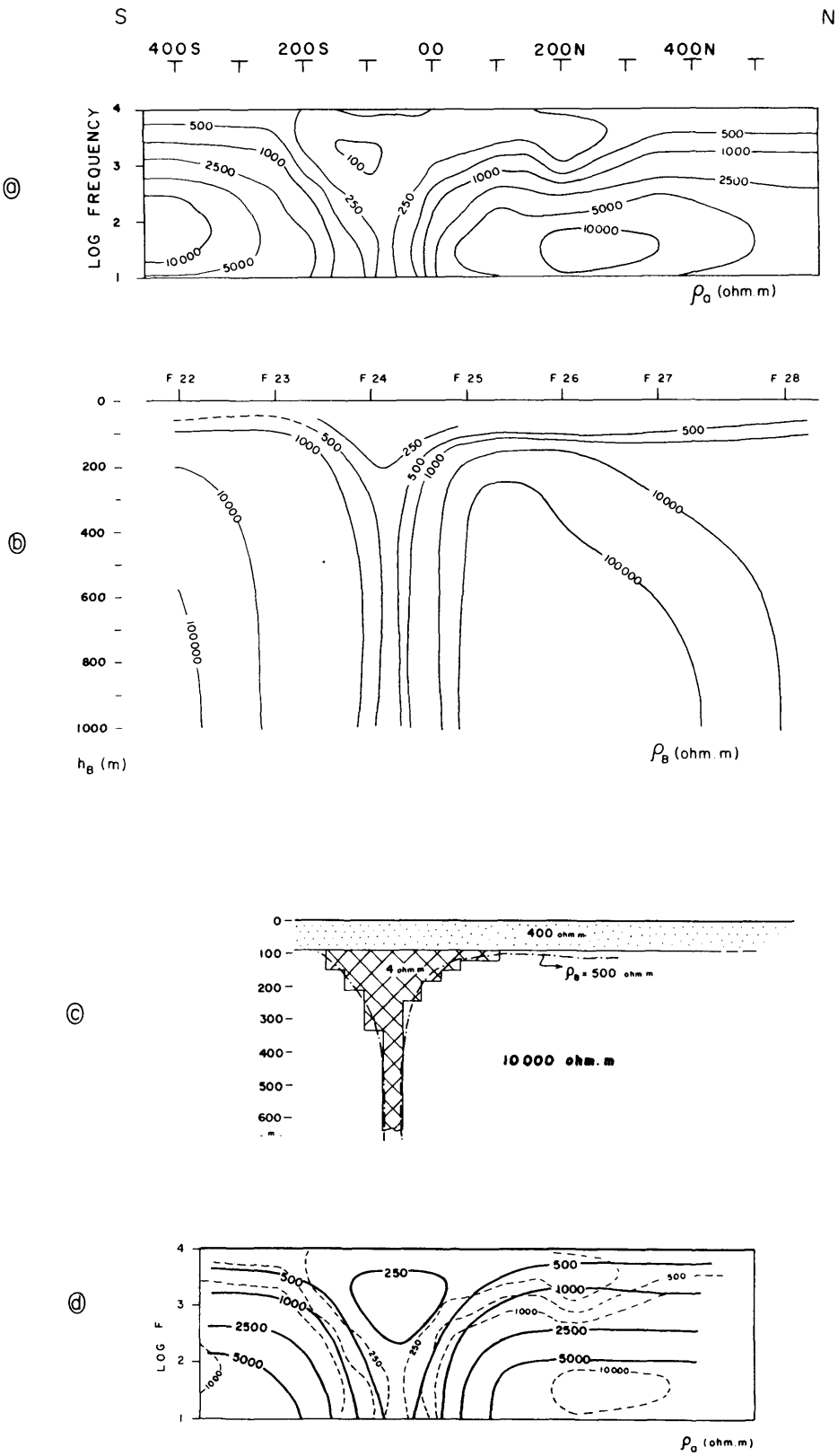

Figure 6. The pseudosections (a) and the Bostick resistivity cross-section (b) along 100E (Line #1E). The northern and southern edges of the body are at about 100 N and 200 S. (c) The fitted 2-dimensional model of the graphitic conductor. (d) 2-dimensional model response (full lines) and the measured data (dashed lines).

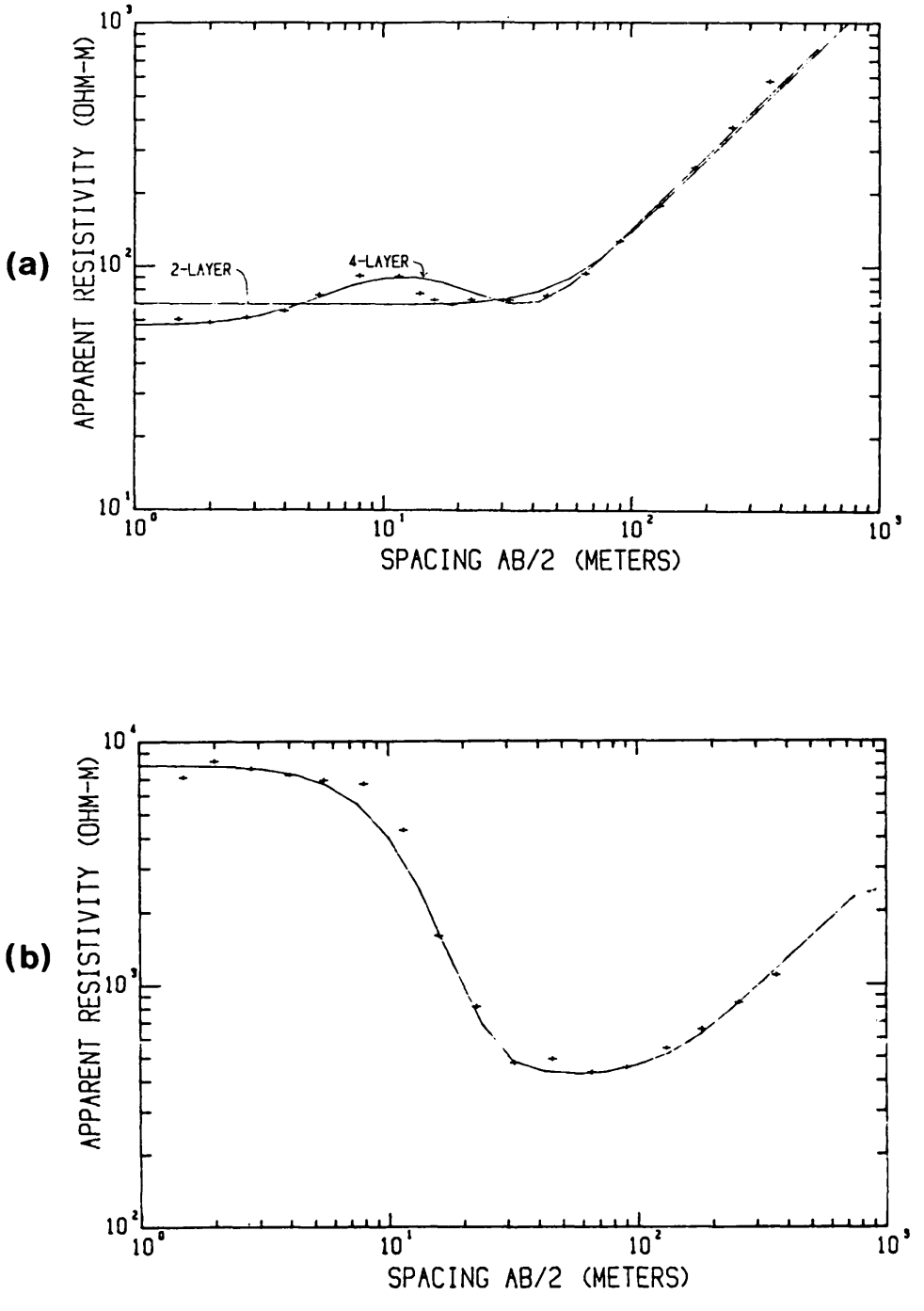

Figure 7. Resistivity sounding at Night Hawk Lake test site, using a Schlumberger array: (a) at Line 500W station 00 (50 m south of F-4); (b) at line 300E station 200N (F-34).

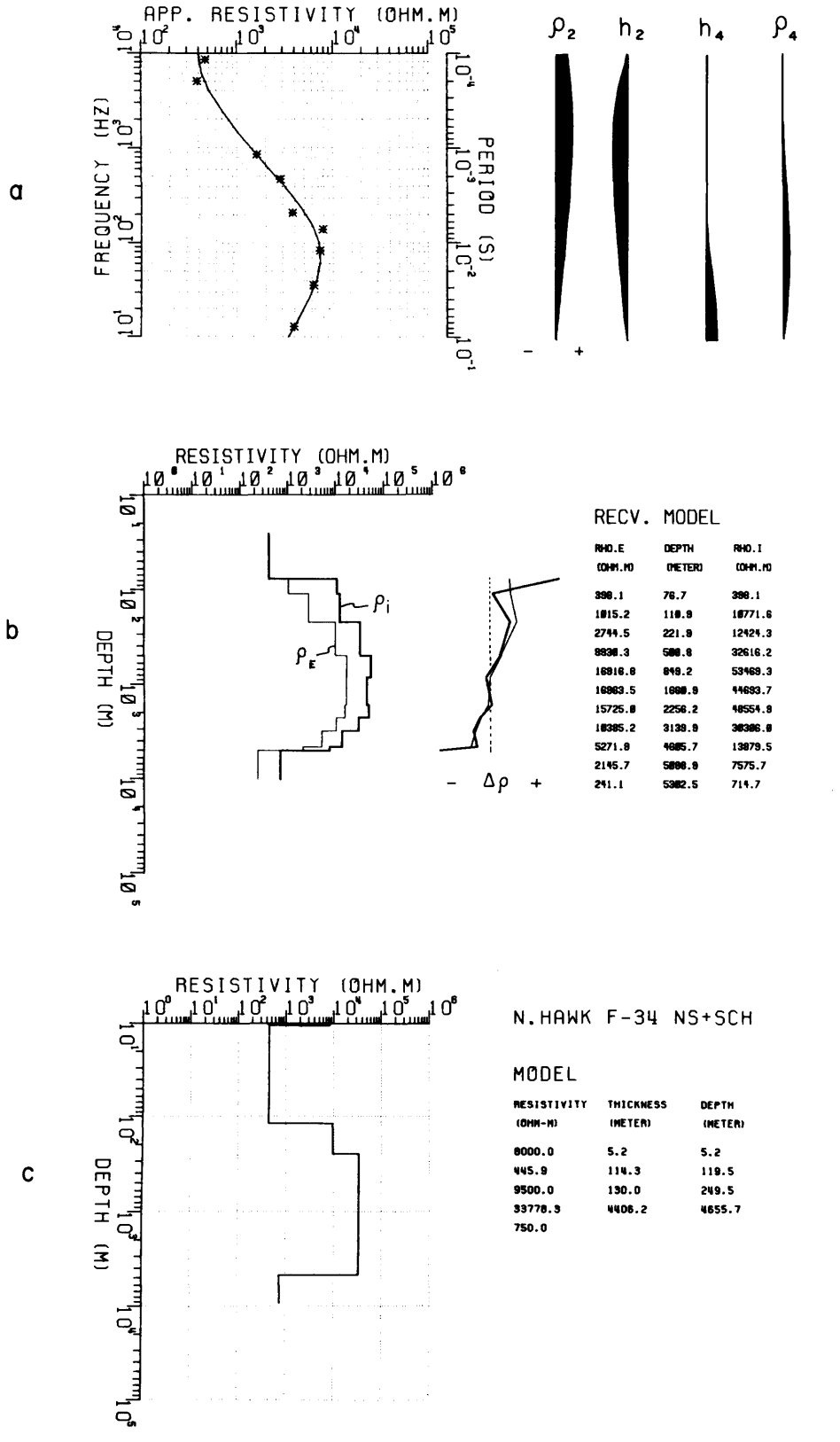

Figure 8. (a) AMT measurements vs. frequency at line 300E station 200N (asterisks), together with the best model response (full line) and the effects of the most important model parameters derived from SVD analysis. (b) Illustration of directly recovered model from data. ρ_E, effective resistivity; ρ_i interval resistivity. The plot of $\Delta\rho$ gives an approximate depth to the layers. This model is used to guess initial model for inversion together with SCH results; (c) Best fitted inverse model based on AMT and Schlumberger measurements.

TABLE 2 THE COMPARISON OF INVERSION RESULTS OF AMT DATA WITH AND WITHOUT SCHLUMBERGER RESISTIVITY MEASUREMENTS FROM SITE F-34 (LINE 300E-STATION 200N, ORIENTATION NORTH-SOUTH).

Inverted model based on:

1) The effective and interval resistivity calculations and only AMT data

Layer	ρ(ohm-m)	h(m)
-	-	-
1	396.3	93.6
2	9429.6	169.8
3	33564.4	4230.0
4	750.0	

2) The effective and interval resistivity calculations, AMT data and Schlumberger resistivity data

Layer	ρ(ohm-m)	h(m)
1	8000.0	5.2
2	445.9	114.3
3	9500.0	130.0
4	33778.3	4406.2
5	750.0	

ered earth model consisting of a very resistive 8000 ohm-m upper layer corresponding to a thin sandy layer (5.2 m), a 120 m thick intermediate layer with a resistivity value of 410 ohm-m, and the very resistive bedrock ($\rho >$ 10 000 ohm-m). The inversion results of AMT data from the same site (F-34) with the inversion results of AMT and Schlumberger information are given in Table 2.

Figure 8 illustrates some stages in the 1-dimensional interpretation at site F-34. The plots of apparent resistivity versus frequency (and period) are given together with the best model response in Figure 8a. The most important model parameters around site F-34 are found by singular value decomposition (SVD) analysis. Total conductivity *(h/ρ)* of the overburden is the most important parameter at high frequencies (500 to 10 000 Hz). Using the effective and interval resistivity calculations (Figure 8b) together with some geologic information from the area, we can calculate the thickness and the resistivity of the overburden. Even the thickness or the resistivity of the Precambrian bedrock is well defined at frequencies of 200 Hz or less. Using the AMT data, interval resistivity calculations, SVD analysis, and combining the results of Schlumberger resistivity sounding at site F-34, our best 1-dimensional result is given in Figure 8c. This model gives a 5.2 m thick resistive (8000 ohm-m) layer at the top. The next layer is less resistive (446 ohm-m) and 114 m thick, representing sandy (which might have some clay content) overburden. The depth to the bedrock is 120 m at this site. We found 9500 ohm-m for the top 130 m of the bedrock, compared to 34 000 ohm-m at greater depths. This might represent weathered or fractured bedrock. It appears that the deeper parts of Precambrian basement at a depth of 5 to 6 km have relatively low resistivity values.

KIRKLAND LAKE AREA

We have done a total of 13 measurements along an east-west profile in Morrisette and Arnold Townships near Kirkland Lake. Most of the stations are at very sandy locations on the Munro esker and are fairly resistive. A surface resistivity value of about 250 ohm-m is representative of the relatively clay-rich overburden at the western boundary of the esker, while very high resistivities of 10 000 to 50 000 ohm-m are found at sites on the esker.

ELECTRICAL RESISTIVITY OF SURFICIAL DEPOSITS

In our previous report (Ilkisik *et al.* 1982), we presented the results of laboratory measurements on the electrical properties of clays. This work has been extended to include laboratory and in situ measurements of all overburden components (clay, silt, sand, and till). The purpose of these measurements was to characterize the "typical" resistivities and the frequency dependence of resistivity for the overburden components. The clays, being the most conductive overburden component of the Abitibi clay belt, have been given the most attention in our work, since they provide the greatest hindrance in the useful application of electromagnetic exploration techniques.

The surface expression of the surficial deposits has been well mapped in the Abitibi clay belt by the Ontario Geological Survey (Northern Ontario Engineering Geology Terrain Study); however, the vertical electrical section of the overburden can be quite complicated. The glaciolacustrine deposits of the Abitibi clay belt were formed in proglacial Lake Abitibi-Ojibway and consist of horizon-

tally stratified sand, silt, and clay layers. The clay and silt layers are commonly varved, showing a seasonal deposition pattern. In the northern part of the region around Cochrane, the clays are covered by a clayey to silty till acquired during a local readvance of an ice lobe. The varved clays in other areas may be masked by sand plains from outwash deposits or derived from eskers. In some areas, the clays lie in pockets or channels between bedrock outcrops.

The esker ridges which are composed principally of sands and gravels can extend through the complete vertical section of the glaciolacustrine plain and may have, at their margins, lacustrine clay and silt lenses interfingering with their sands and gravels.

The depth to bedrock and the thickness of the clay layers within the overburden are quite variable. In the Timmins area, a seismic survey (Killeen and Hobson 1974) has shown that the bedrock togography buried beneath the clay cover is quite rugged with variations of 40 m in 1 km (with an average overburden thickness of 30 m). In fact, the overburden can be quite variable in thickness. Drilling results and exposures for areas of glaciolacustrine plain in the Abitibi clay belt indicate that the clay layer thickness within the overburden is quite variable with 30 m being a typical value (Averill and Thompson 1981; Hughes 1961; Desaulniers 1982).

RESISTIVITY MEASUREMENTS

Samples to be used for the resistivity measurements were collected from gravel pits, road cuts, and from exposures along rivers. The procedure used in collecting the samples and the technique for measuring the complex resistivities in the frequency range 5 Hz to 1 MHz are discussed in Ilkisik *et al.* (1982). The complex resistivities were measured at a current density of .1 A/m. The sand (>45 μm), silt (4 μm - 45 μm), and clay (>4 μm) size fractions were determined by sieving and sedimentation analysis.

A summary of the complex resistivity measurements and grain size analysis for samples from the Matheson, Larder Lake, and Englehart areas is given in Table 3. The percent frequency effect (PFE) observed is generally small but significant for some samples.

The 50 Hz resistivities for all the samples are shown in Figure 9 along with their clay contents. For samples from the Larder Lake dump site, it can be seen that the silt (silt loam) samples with low clay content have high resistivities that are on the order of 120 to 140 ohm-m, whereas the clays have resistivities of 30 to 60 ohm-m. These silt samples are from a varved layer in which the clay content increases from bottom to top. When one includes samples from other areas, then even the silt samples have resistivites of the same order as the clay samples. This variability is probably related to the change in pore water resistivity for different environments. For samples from the same environment, one would expect that the clay samples would have lower resistivities, as seen for the Larder Lake dump site samples. In general, the measurements show that the silts are more likely to have higher resistivities than the clays and tend to have a larger variability.

TABLE 3 CLAY SILT AND SAND FRACTIONS DETERMINED BY SIEVING AND SEDIMENTATION ANALYSIS, THE RESISTIVITY AT 50 Hz, AND THE PERCENT FREQUENCY EFFECT (PFE). CLAY FRACTION < 4 μm, SILT FRACTION FROM 4 μm TO 45 μm, AND SAND > 45 μm. PFE = $(\rho_{5\,Hz} - \rho_{50\,Hz})/\rho_{5\,Hz} \times 100$.

Sample #	Site	Clay %	Silt %	Sand %	Soil Class	Resistivity (ohm-m)	PFE
81-2	M	87.6	10.9	1.5	clay	25	.67
81-3	M	79.4	14.3	6.3	clay	35	1.0
81-4	M	93.8	6.1	.1	clay	17	-4.2
81-5	M	80.7	19.2	.1	clay	13	1.7
81-7	M	81.1	17.6	1.3	clay	30	2.0
81-8	L	55.5	40.8	3.7	silty clay	31	.9
81-11	L	77	16	7	clay	37	.4
81-12	L	80.1	16.3	3.6	clay	32	1.0
81-13	L	66.4	25.9	7.7	clay	31	1.9
81-14	L	78.4	21.0	.6	clay	31	1.4
81-15	L	59.2	38.9	1.9	clay	41	2.4
81-16	L	44.9	51.4	3.7	silty clay	37	.5
81-17	L	54.5	42.0	3.5	silty clay	53	.1
81-18	L	13.3	66.7	20.0	silt loam	125	.9
81-19	L	14.5	66.5	19.0	silt loam	132	2.0
81-21	L	59.1	39.1	1.8	clay	33	.7
81-22	L	73.9	23.9	2.2	clay	32	-0.2
81-23	L	74.3	25.4	.3	clay	57	.5
81-24	L	62.2	32.9	4.9	clay	30	.1
81-25	L	49.9	45.6	4.5	silty clay	58	.1
81-29	L	9.2	62.6	28.2	silt loam	137	1.4
81-30	E	62.0	37.4	.6	clay	23	1.0
81-31	E	21.8	25.6	52.6	loam	33	.8
81-32	E	13.6	33.6	52.8	sandy loam	36	1.3
81-33	E	75.5	16.0	8.5	clay	15	-0.3
81-35	E	26.9	66.1	7.0	silt loam	41	.5
81-36	E	26.0	67.5	6.5	silt loam	24	1.2
81-39	E	14.2	42.3	14.1	loam	175	3.8
81-40	E	14.1	29.6	56.3	sandy loam	125	3.0

L - Larder Lake dump site
M - Matheson area
E - Englehart area

The average resistivity at 50 Hz for the different soil classes at the sites studied was 24 ohm-m for clays (16 samples), 45 ohm-m for silty clay (4 samples), and 87 ohm-m for loams (9 samples of loam, sandy loam, and silt loam). In situ measurements at 1.1 Hz using a small Wenner array with a = .5 m where it was possible and *a* = .05 m for thin layers gave an average resistivity for clays and silty clays of 59 ohm-m (21 sites) and 3700 ohm-m for sands (9 sites). AMT surveys which we have carried out in these same areas typically give resistivities of 20 to 50 ohm-m for the conductive clay layer.

In general, the soil samples have resistivities that are relatively independent of frequency from 5 Hz to 1 MHz and have a small phase. For a few samples, the complex resistivity was also measured in the range .01 Hz to 5 Hz (Figure 10). At frequencies less than 5 Hz, the resistivity was also relatively independent of frequency with small phase. Sample 81-13 is typical of the clays measured in that the phase and PFE are small. Sample 81-4 has an unusual frequency dependence in that the phase angle is positive at the lowest frequencies and the magnitude increases with frequency at the lowest frequencies. Nega-

tive PFE values similar to that observed in this sample have been reported previously (Roy and Elliot 1980) for clay soils with clay content greater than 90%. The silty clays that we have measured, typified by sample 18-16, have small phase and PFE. The loams have a relatively large PFE and phase as shown by sample 81-40. Only 1 peat sample (81-1), which has a significant phase and PFE, has been measured. From the work that we have completed, there is an indication that there may be significant differences in the frequency response for different soil classes. In addition, we have observed that there is considerable variation in frequency response within each soil class.

The principle clay minerals contained in the clay size fraction for samples 81-3, 81-4, and 81-13 are chlorite (40%) and illite (30%). These clay minerals are typical for immature glaciolacustrine clays.

CONCLUSIONS

The results reported here show the effectiveness of the AMT technique for mapping of conductivity structure in the Precambrian bedrock in glacial drift areas.

In Moody Township near Lake Abitibi, steeply dipping metasediments show a strong anisotropy even when covered by conductive clay-rich drift. A conductive fracture zone with an east-west strike was detected within the metavolcanics at station A-15.

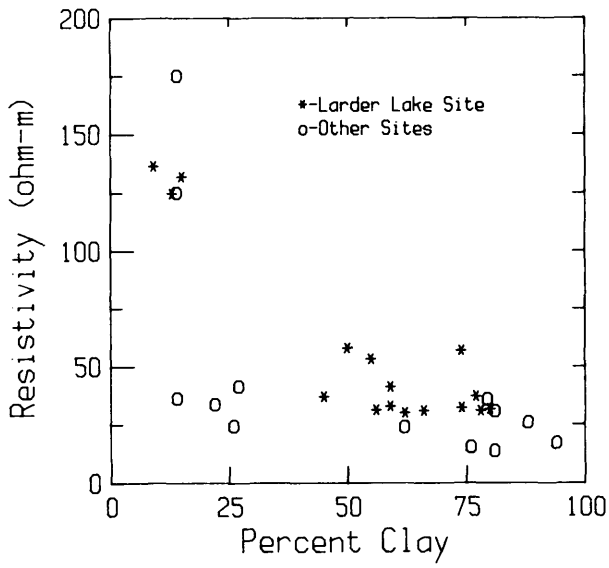

Figure 9. The magnitude of the resistivity at 50 Hz is plotted as a function of the sample clay content (<4μm). The Larder Lake samples were collected from different depths within 1 varved clay layer.

At the Night Hawk Lake geophysical test site, the apparent resistivity at high frequencies clearly illustrates clay-rich overburden along the western side of the grid area. The apparent resistivity maps for lower frequencies and the Bostick resistivity map for a 200 m depth shows the known graphitic conductor with an east-west strike. The detailed pseudosections, Bostick resistivity cross-sections, and 2-dimension model calculation suggest that there is a "Y"-shaped broad body with a limited depth extent and that the northern and southern edges of the conductor are at about 100 N and 200 S.

One-dimensional inversion of AMT data in the northern part of the grid and the results of Schlumberger resistivity measurements indicate a 90 to 120 m thick overburden with 30 m of clay-rich material at the western side of

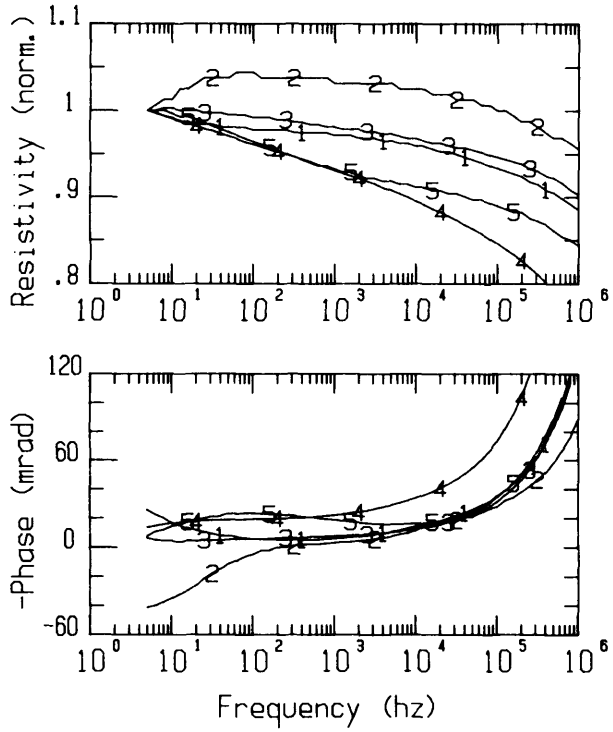

Figure 10. The typical frequency dependence of the phase and magnitude (normalized to the resistivity at 5 Hz) of the complex resistivity of soil samples from the Abitibi belt are shown. The individual data points of which there are 10 per decade in frequency have been joined with straight line segments. The numbers given on the plots are for identification purposes: 1 Clay (varved), Larder Lake (81-13); 2 - Clay, Matheson (81-4); 3 - Silty Clay, Larder Lake (81-16); 4 - Sandy loam, Englehart (81-40); 5 - Peat, Matheson (81-1). Resistivities (ohm-m) at 5 Hz: 1 - 32 ohm-m; 2 - 16 ohm-m; 3 - 37 ohm-m; 4 - 129 ohm-m; 5 - 28 ohm-m.

the grid. Beneath the overburden, the resistivity is in the range of 15 000 to 60 000 ohm-m.

Our study and Singular Value Decomposition analysis of typical models show that the most important and hence best predicted model parameter is total conductance of the glacial material. The low resistivity zones, faults, or anisotropy in the bedrock are also detectable, since the AMT technique is very sensitive to lateral resistivity variations.

Previous studies of the Abitibi Clay Belt have demonstrated that one can expect to have complicated electrical sections for the overburden. In our work we have obtained "typical" resistivities, from laboratory and in situ measurements, for the different units within the overburden, and have shown that, while in general the frequency dependence of the resistivity is small, there is a significant percent frequency effect (PFE) and phase observed in some of the samples.

ACKNOWLEDGMENTS

The authors would like to thank R. Barlow for cooperation and many ideas. S. Dawson and P. Halewood assisted us in the field work. M. Ilkisik wishes to thank Dr. N. Edwards for his kind permission to use the 2-dimensional model program. Geophysical data processing was done using the University of Toronto Computer Services IBM computers and the Physics and Astronomy VAX Research Computer.

REFERENCES

Averill, S.A., and Thompson, I.
1981: Reverse Circulation Rotary Drilling and Deep Overburden Geochemical Sampling in Marter, Catherine, McElroy, Skead, Gauthier, and Hearst Townships, District of Timiskaming; Ontario Geological Survey, Open File Report 5335.

Barlow, R.B., Pitcher, D.H., and Wadge, D.R.
1982: Night Hawk Geophysical Test Range Results, Night Hawk Lake, District of Cochrane; p.152-161 *in* Summary of Field Work, 1982, by the Ontario Geological Survey, edited by John Wood, Owen L. White, R.B. Barlow, and A.C. Colvine, Ontario Geological Survey, Miscellaneous Paper 106, 235p.

Bostick, F.X., Jr.
1977: A Simple and Almost Exact Method of MT Analysis (Abstract); Workshop on Electrical Methods in Geothermal Exploration, Utah.

Desaulniers, D.E.
1982: Clayey Quaternary Deposits in Northern Ontario: A Review; Atomic Energy of Canada, TR-305.

Edwards, R.N., Bailey, R.C., and Garland G.D.
1980: Crustal and Upper Mantle Conductivity Studies With Natural and Artifical Sources; p. *in* The Continental Crust and its Mineral Deposits, edited by D.W. Strangway, Special Paper 20, Geological Association of Canada, p.273-301.

Hughes, O.L.
1961: Preliminary Report on Borings Through Pleistocene Deposits, Cochrane District, Ontario; Geological Survey of Canada, Paper 61-16.

Ilkisik, O.M., Hsu, D.T., Redman, J.D., and Strangway, D.W.
1982: Surface Electromagnetic Mapping in Selected Positions of Northern Ontario; Grant 118, p.98-114 *in* Geoscience Research Grant Program, Summary of Research 1981-1982, edited by E.G. Pye, Ontario Geological Survey, Miscellaneous Paper 103, 219p.

Ilkisik, O.M., and Strangway, D.W.
in preparation: On the Recovery of the True Resistivity Distribution Using Scalar Resistivity Values in AMT (Audiomagnetotellurics).

Jones, A.G.
1982: On the Electrical Crust-Mantle Structure in Fennoscandia: No Moho and the Asthonosphere Revealed?; Geophys. J.R. Astr. Soc. 68, 371-388.

in press: On the Equivalence of the "Niblett" and "Bostick" Transformations in the Magnetotelluric Method; Journal of Geophysics.

Kaufman, A., and Keller, G.V.
1981: The Magnetotelluric Sounding Method; Elsevier, New York, 595p.

Killeen, P.G., and Hobson, G.D.
1974: Project EGMA Seismic, Timmins, Ontario to Val d'Or, Quebec; Geological Survey of Canada, Paper 74-44.

Madden, T.R., and Swift, C.M.
1969: Magnetotelluric Studies of the Electrical Conductivity Structure of the Crust and Upper Mantle; p.469-479 *in* American Geophysical Union Monograph 13, The Earth's Crust and Upper Mantle.

Marquardt, D.W.
1963: An Algorithm for Least Squares Estimation of Nonlinear Parameters; J. Soc. Indust. Appl. Math. 11, 431-441.

Northern Ontario Engineering Terrain Study Data Base Maps
1979: Ontario Geological Survey

Pyke, D.R., Ayres, L.D., and Innes, D.G.
1973: Timmins-Kirkland Lake, Districts of Cochrane, Sudbury, and Timiskaming; Ontario Geological Survey, Map 2205, Geological Compilation Series, Scale 1 inch to 4 miles.

Roy, K.K., and Elliot, H.M.
1980: Model Studies on Some Aspects of Resistivity and Membrane Polarization Behaviour Over a Layered Earth; Geophysical Prospecting, Volume 28, 759-775.

Strangway, D.W., Swift, C.M., and Holmer, R.C.
1973: The Application of Audio-Frequency Magnetotellurics (AMT) to Mineral Exploration; Geophysics, Volume 38, 1159-1175.

Grant 143 Analysis of Aeromagnetic Anomalies over Algoman-Type Iron Formations

D.T.A. Symons and M. Stupavsky
Department of Geology, University of Windsor

ABSTRACT

Magnetic anomalies over Algoman-type banded iron formations cannot be analyzed in a realistic way using conventional interpretation models, because of the effects of their anisotropy of magnetic susceptibility, demagnetizing factor, and natural remanence. Using a test area in northeastern Ontario, about 500 anomalies over known or possible iron formations have been analyzed to correct for these magnetic properties. The results of the study will be presented in tabular form in the final report emphasizing the interpreted geological parameters such as the percentage of magnetite, thickness, dip, strike length, and depth to top.

INTRODUCTION

The authors recently completed a series of studies on the component magnetization of Algoman-type Archean banded iron formations (BIF) of the Sherman Mine at Temagami (Symons and Stupavsky 1979, 1980), the Adams Mine at Kirkland Lake (Symons *et al.* 1981), the Moose Mountain Mine at Capreol (Symons *et al.* 1980), and the Griffith Mine at Ear Falls, Ontario (Symons *et al.* 1983). This research involved the measurement of the specific gravity (SG), bulk magnetic susceptibility (BMS), anisotropy of magnetic susceptibility (AMS), natural remanence (NRM), and remanence decay (viscous, alternating field, thermal, and chemical demagnetization) of some 1500 to 2000 specimens of BIF and host rock (HR) for each deposit. The results of this research are summarized in Symons and Stupavsky (1983).

From this study, it is clear that the AMS and the demagnetizing factor (DF) to a greater extent, and the NRM to a lesser extent, significantly modify the magnitude and shape of the resulting aeromagnetic anomaly profile over a BIF deposit. This modification is sufficiently great that conventional anomaly interpretation models utilizing only the BMS, the geometry of the deposits, and the Earth's magnetic field data may give an incorrect and unrealistic interpretation of the deposit parameters. The objectives of this study are to examine anomalies within the test area in order to better evaluate their potential as economic deposits.

TEST AREA AND METHODOLOGY

The test area is bounded on the east by the Ontario-Quebec border, on the south by Latitude 46°N, on the west by Longitude 82°W, and on the north by the Hudson Bay Lowlands. The area includes rocks of the Superior, Southern, and Grenville Provinces. Within this area, a dual approach was used to select anomalies of possible economic interest.

One approach was to locate all known BIF deposits within the test area using the compilation of Shklanka (1968) and more recent sources. Using the existing Ontario Geological Survey - Geological Survey of Canada aeromagnetic maps, the principal profiles, X and Y, for the resulting anomalies were digitized for computer processing on an Apple II+ system. This information, along with known available geological parameters (grade, strike, dip, thickness, strike length, depth to top) and geophysical parameters (EMF intensity and orientation, EMS, AMS, SD, NRM) were used to determine the fit of the predicted response to the known aeromagnetic response. Using an interactive computer system, the geological parameters were then modified to obtain the optimum fit within a standard deviation of 10% for both profiles. The resulting geological parameters were then output in catalogue format. Approximately 150 anomalies were analyzed in this manner.

The second approach was to identify all aeromagnetic anomalies in the test area which exceed background by $> +500$ or $< -500\nu$. Except for BIF deposits that are perfectly perpendicular to the Earth's magnetic field (EMF) and have no edge effect anomalies, this should include all BIF anomalies of possible commerical interest. The principal profiles were digitized for analysis and "fitted" on the assumption that the causative source was a BIF, with the resulting geologic parameters output in tabular form. At this point, the available geological maps for the area were also examined to see if there was a possible spatial coincidence of the aeromagnetic anomaly with another geologic source such as a dike or basic pluton. If an alternative source was present, then this information was added to the tabulation. Approximately 350 anomalies were analyzed in this manner.

CONCLUSIONS

From the previous work on known deposits, it is apparent that BIF anomalies will typically be exaggerated or diminished in magnitude by up to 50%, relative to a conventional analysis, when the banding is respectively parallel or perpendicular to the Earth's magnetic field because of the anisotropy of magnetic susceptibility, demagnetizing factor, and natural remanence contributions. Also, these factors cause the shape of the anomaly to become nearly symmetrical so that all BIF deposits appear to be very steeply dipping in northern Ontario regardless of the actual dip. Correcting for these factors has led to a more realistic range of thicknesses, dips, and depths-to-top for known and possible BIF deposits in the test area, as will be shown in the final report.

REFERENCES

Shklanka, R.
1968: Iron Deposits of Ontario; Ontario Department of Mines, Mineral Resources Circular 11, 287p.

Symons, D.T.A., Osmani, I.A., and Stupavsky, M.
1983: Magnetization Characteristics of the Algoman Iron Formation and Host Rocks at the Griffith Mine, Red Lake, Ontario; Ontario Geological Survey, Open File Report 5447, Part II, p.19-57.

Symons, D.T.A., Quick, A.W., and Stupavsky, M.
1981: Magnetic and Paleomagnetic Characteristics of the Archean Iron Formation and Host Rocks at the Adams Mine, Ontario; Grant 5, p.293-307 *in* Geoscience Research Grant Program, Summary of Research, 1980-1981, edited by E.G. Pye, Ontario Geological Survey, Miscellaneous Paper 98, 340p.

Symons, D.T.A., and Stupavsky, M.
1979: Magnetic Characteristics of the Iron Formation Near Temagami, Ontario; Grant 5, p.133-147 *in* Geoscience Research Grant Program, Summary of Research, 1978-1979, edited by E.G. Pye, Ontario Geological Survey, Miscellaneous Paper 87, 152p.

1980: Magnetic Anomaly Type Curves and Paleomagnetism of the Algoman-Type Iron Formation near Temagami, Ontario; Grant 5, Part 2, p.215-219 *in* Geoscience Research Grant Program, Summary of Research, 1979-1980, edited by E.G. Pye, Ontario Geological Survey, Miscellaneous Paper 93, 262p.

1983: Component Magnetization of Algoman Banded Iron Formations and Deposits in Ontario; Ontario Geological Survey, Open File Report 5447, Part I, p.1-18.

Symons, D.T.A., Walley, D.A., and Stupavsky, M.
1980: Component Magnetization of the Algoman Iron Formation and Host Rocks, Moose Mountain Mine, Ontario; Grant 5, Part 1, p.198-214 *in* Geoscience Research Grant Program, Summary of Research, 1979-1980, edited by E.G. Pye, Ontario Geological Survey, Miscellaneous Paper 93, 262p.

Grant 140 Direct Trace Elemental Analysis of Solid Samples by Techniques of Atomic Spectrometry

Jon C. Van Loon
Department of Geology, University of Toronto

ABSTRACT

A method is being developed for the insertion of solid samples into flames and plasmas for direct trace element analysis by the techniques of atomic spectrometry. A furnace is used to produce an aerosol (vapour) of the solid by ramping the temperature to approximately 2800°C. This aerosol is carried into the flame or plasma atomizer in a stream of inert gas. Experimental parameters such as carrier gas flow rate, volatilization temperature, and pre-volatilization heating treatment have been studied. Samples of National Bureau of Standards, Standard Reference Materials, and United States Geological Survey, and Scandinavian Standard rocks have been analyzed using a flame atomizer.

INTRODUCTION

The direct elemental analysis of solids (methods not requiring chemical pretreatment) is an important priority for methods development in analytical geochemistry. This is to avoid the time consuming and error prone steps of wet chemical treatment prior to analysis. In the case of trace element determinations, techniques of valence electron atomic spectrometry (i.e. atomic absorption spectrometry (AAS), atomic emission spectrometry (AES), and atomic fluorescence spectrometry (AFS)), many strategies for direct solid sample analysis have been proposed. However, with the exception of arc and spark AES, no approach to direct solid sample analysis for these spectrometric techniques has received widespread acceptance. In addition, most of the proposed methods for solid sample analysis, including arc and spark AES, are plagued by poor precision and difficulties with standardization. Recently, interest in the inductively coupled plasma technique (ICP), has renewed research activity into methods for direct analysis of solid samples.

Table 1 presents a summary of the methods for direct trace analysis of solids by atomic spectrometry.

Ideally, a method for the direct analysis of solid geochemical samples should possess the following attributes:

1. It should be applicable to a wide range of sample compositions.
2. It must be relatively fast.
3. To avoid inhomogeneity problems, it should be capable of handling fairly large samples.
4. Simultaneous multielement determinations are desirable.
5. Cost per analysis should be low.
6. Precision and accuracy should be suitable for geochemical purposes.

None of the methods listed in Table 1 satisfies these needs adequately.

This research proposal is for the development of a method for direct solid sample analysis by atomic absorption and plasma emission spectrometry.

Of the approaches listed in Table 1, the hybrid ones have the following potential advantages:

1. Some time resolution of analyte and background signals occurs.
2. They are generally applicable to a wider compositional range of samples.
3. Generally. larger sample weights can be employed (less problem due to inhomogeneity).
4. Samples may readily be mixed with or treated with substances to improve analyte volatility.

Specifically, we are investigating a furnace-flame (AAS) and furnace-ICP (AES) approach to direct geo-

TABLE 1 SUMMARY OF DIRECT SOLID SAMPLE TRACE ANALYSIS BY ATOMIC SPECTROMETRY.

	Conventional	Hybrid Techniques
Emission	solid-in-flame solid-in-plasma arc electrothermal laser glow discharge	furnace-arc chloride generator laser-plasma spark-plasma
Absorption	solid-in-flame arc spark electrothermal laser cathode sputtering	capsule-in-flame hollow graphite "T" tube furnace-flame arc/spark-flame chloride generator
Fluorescence	laser laser-spark electrothermal	furnace-flame

chemical solid sample analysis. To aid in the volatilization of the more refractory elements, a substance containing a halogen is injected into the furnace (e.g. freon). Since the nature of the sample matrix may affect the volatility of the analyte constituent, a matrix modifer such as ammonium sulphate is added. Initially, a Perkin-Elmer type furnace with large furnace element (HGA 2000) will be used (to accomodate large samples).

Inductively coupled plasma emission has recently developed into a widely used technique for trace element analysis (approximately ⅓ of the atomic spectrometry papers at the recent 9th International Conference on Atomic Spectrometry, Tokyo, September 1981 were on plasma emission). This approach can be used for simultaneous multielement analysis. The very high temperature of the plasma (approximately 7000°K in the zone of observation) makes it particularly attractive as an atomizer for solid samples.

EXPERIMENTAL

APPARATUS

The apparatus used was as follows:

1. HGA 2000 (Perkins-Elmer graphite Furnace) or HGA 2100 (Perkins-Elmer graphite Furnace) modified so that one end of the furnace has a quartz 'T' tube extended into a flame of a Perkin-Elmer 603 atomic absorption spectrometer. The other end of the furnace is fitted with a tube which is connected to an argon gas cylinder (Figure 1).
2. Same furnace as above, but interfaced by a quartz tube with the base of an ARL ICP torch (Figure 2). This is used with an ARL 34000 optical emission spectrometer.

A variety of geological solid samples was used to evaluate the set-up. Standard reference materials employed were United States Geological Survey sample G-2, Scandinavian Standard ASK-3, and NBS Bovine Liver (organic samples).

REAGENTS

Standard solutions were prepared from Spec-Pure metal salts and metals dissolved in a minimum of acid. Final acid content of stock solution was 5%.

The procedure tested for aerosol production was as follows: the weighed solid was placed in the centre of the furnace by using either a special home-made sample spoon or a graphite boat (which is left in during heating); the furnace was reconnected to the argon supply and purged with argon; the sample was heated in the furnace using 1 to 3 heating cycles; during the highest tempera-

Figure 1. Quartz tube in flame furnace interface.

ture stage (about 2700°C), the sample was converted into an aerosol which was swept into the flame or plasma in the inert gas flow; the atomic-absorption (flame) or inductively coupled plasma emission signal was recorded.

STUDY OF CARRIER GAS FLOW RATE

Carrier gas flow rate was found to be a critical factor. The optimum rates for Cd, Sb, Hg, and Se in Bovine Liver and AKS-3 sulphide are given in Table 2. These values clearly indicate the dependence of the optimum flow rate on the type of sample matrix. For Cd in ASK-3 sulphide ore, a second maximum was observed at a flow rate of about 1 L/min (Figure 3). At this flow rate, the peak height sensitivity was lower and the precision was poorer than at the optimum flow rate (0.1 L/min).

Both Sb and Se in ASK-3 sulphide ore gave double peaks when volatilized without a charring step (Figure 4a). Since the ore sample contains a number of different minerals including pyrite and sphalerite, the double peaks are due to the release of the Sb and Se from the different minerals at different temperatures. This effect could be used to give important information on the associations of the elements, e.g. sulphide bound vs. silicate bound. However, it was also possible to remove the double peak for both elements by using a proper charring step; Figure 4b shows this behaviour for Se in ASK-3 sulphide ore. This would allow quantitative data for "total" trace elements to be obtained.

TABLE 2 OPTIMUM CARRIER GAS FLOW RATE RANGE.

ELEMENT	OPTIMUM FLOW RATE L/MIN BOVINE LIVER	ASK-3 SULFIDE ORE
CADMIUM	0.07-0.13	0.08-0.16
ANTIMONY	0.36-0.46	0.10-0.16*
MERCURY	0.60-0.74	0.64-0.74
SELENIUM	0.07-0.12	1.20-1.30+

* Obtained using a charring step
\+ Obtained without a charring step

EFFECTS OF VOLATILIZATION TEMPERATURE ON SENSITIVITY

The effect of the temperature of volatilization on the analyte signal was examined for volatile and refractory elements. Figure 5 presents data on the sensitivity of Cr, Cu,

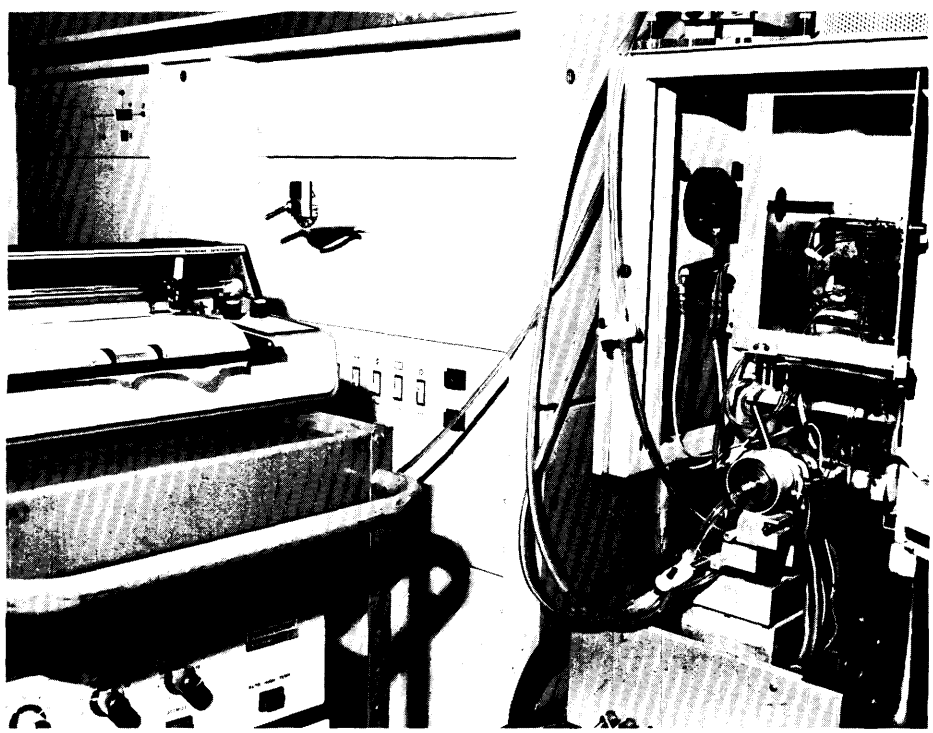

Figure 2. Furnace-ICP interface.

Pb, Cd, and Se (introduced as standard solutions) at different volatilization temperatures when uncoated graphite tubes were used. All elements except lead showed a steady increase in the analyte signal with increasing volatilization temperature. Below 2300°C, the lead signal occurred as a double peak. There was a sharp increase in the lead signal at 2300°C and the signal occurred as a single lead peak. When pyrolytic graphic-coated tubes were used for lead, single peaks were obtained at all temperatures. For the other elements, the dependence of the analyte signals on the volatilization temperature was similar for both standard and pyrolytic graphite-coated tubes.

Table 3 presents sensitivity data measured with the "HGA 2100/quartz T-tube in flame method" for 6 elements (taken as solutions) at a volatilization temperature of 2700°C. These values are compared with the data given by Perkin-Elmer for their HGA 2200 using the maximum power mode of operation. The present method of analysis is about 10 to 200 times less sensitive than conventional graphite furnace techniques. The lower sensitivity makes it possible to use relatively large weights (up to 15 mg for most elements) of solid material without the analyte absorption being too high for accurate analysis. This is advantageous in the analysis of most solids. The use of larger sample weights reduces the previously discussed errors due to sample weighing and inhomogeneity.

Larger sample weights, up to 35 mg, have been used with a charring step. When an HGA 2000 furnace is used instead of the HGA 2100 furnace, very large sample weights, up to 300 mg can be analyzed.

TABLE 3 SENSITIVITY COMPARISON (in pg/0.00044A).

ELEMENT	(nm)	HGA-2100 Quartz T-tube 2800°C	HGA-2200
As	193.7	2000	21
Cd	228.8	30	1
Cr	357.9	2000	11
Cu	324.7	900	15
Pb	283.4	1000	15
Se	196.0	800	60

ICP OPERATING CONDITIONS

The optimum carrier gas flow rate as required for Cu and Pb was 0.3 L/min. The coolant gas and plasma gas pressures were 50 and 35 psi respectively. The nebulizer was left in the system to provide a needed pressure drop. The flow rate through the nebulizer was 0.4 L/min. An incident power of 1300 W was employed and the reflected power, which had to be tolerated under these operating conditions, was 210 W.

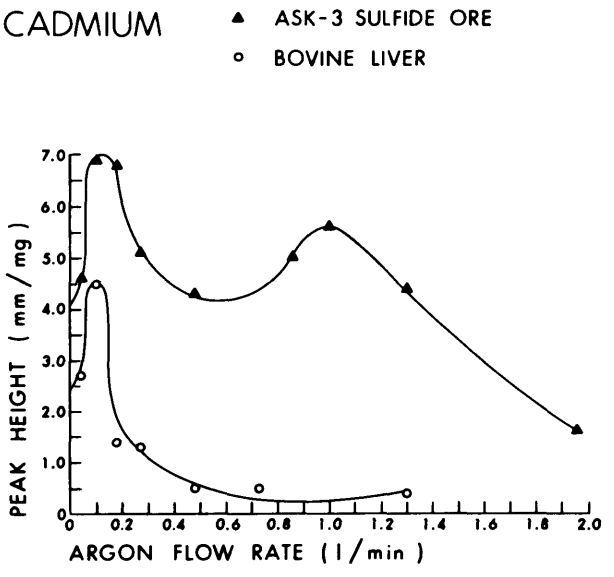

Figure 3. Study of carrier gas flow rate.

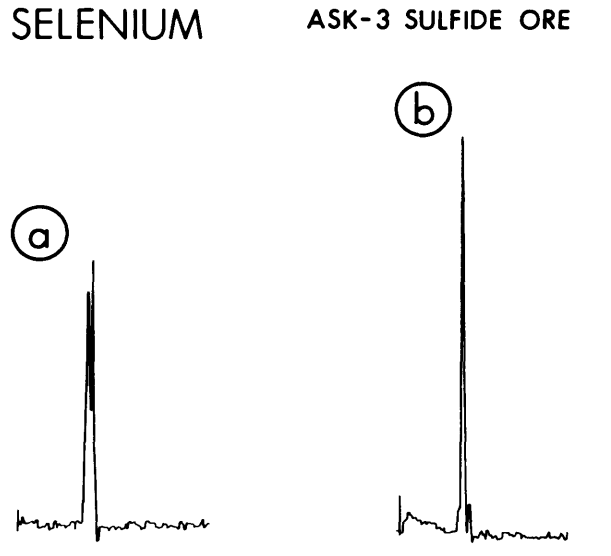

Figure 4. Signals for Se in ASK-3 sulphide ore: (a) without char; (b) with char

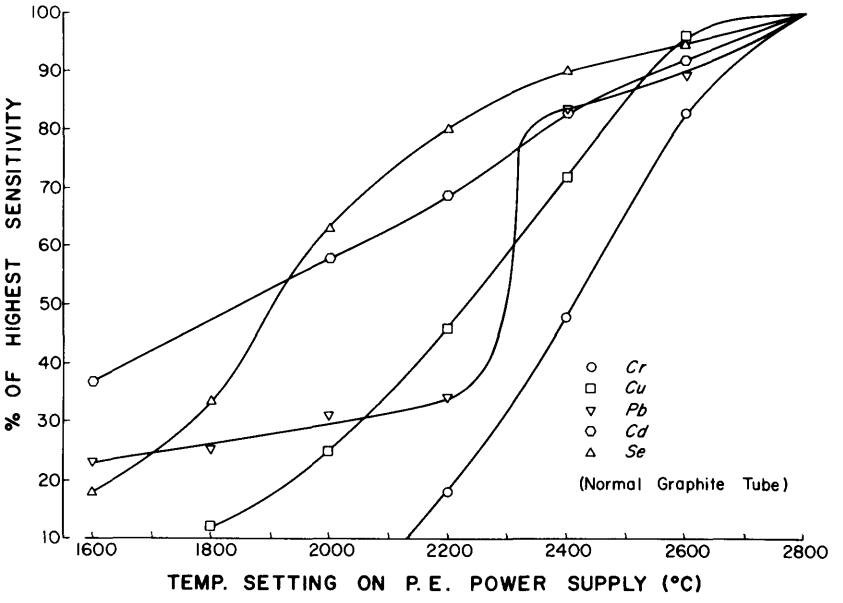

Figure 5. Effect of temperature on signal.

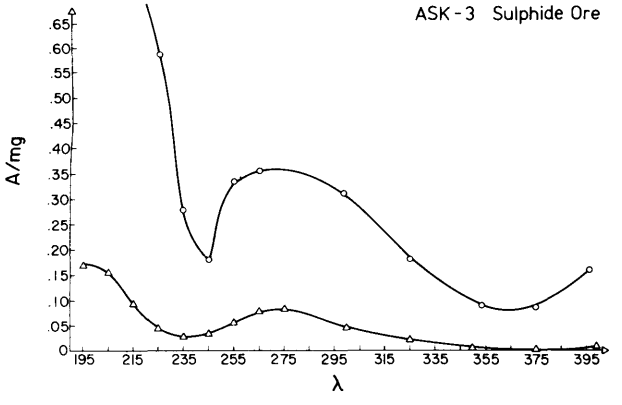

Figure 6. Wave length dependency of background: Top trace - conventional furnace approach; bottom trace - proposed approach.

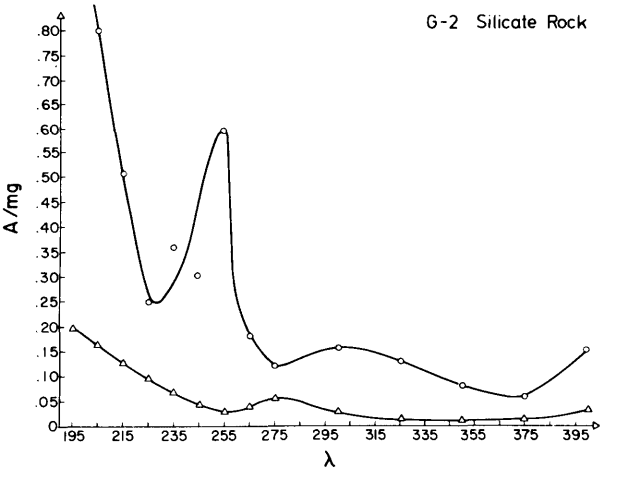

Figure 7. Wave length dependency of background: Top trace - conventional furnace approach; bottom trace - proposed approach.

SOLID SAMPLE ANALYSIS

Figures 6 and 7 show the variation in nonspecific absorption with wavelength for ASK-3 sulphide ore and G-2 granite respectively, for both the proposed and conventional graphite furnace methods of analysis. Using the proposed method, the nonspecific absorption signals are reduced to levels which are compensated by the deuterium (D_2) arc background correction system. In contrast, the levels of background signal occurring for the conventional method are too high to be corrected using the D_2 arc. The low level of background signal observed using

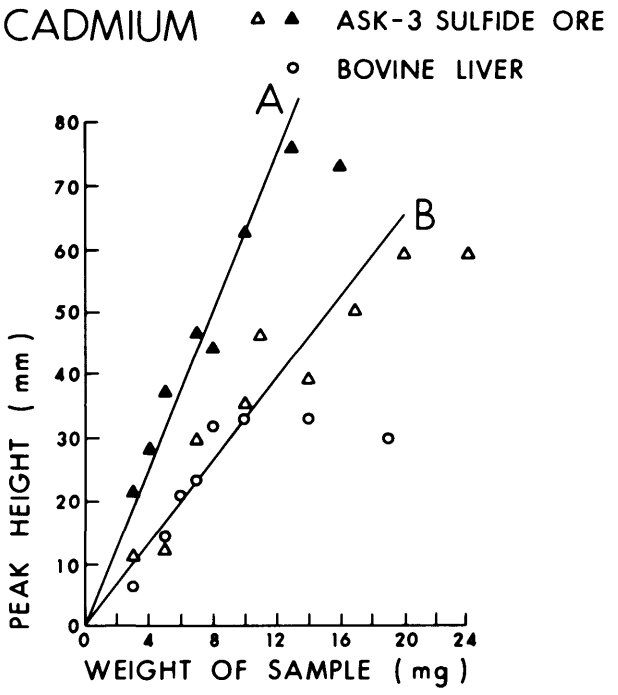

Figure 8. Variation of Cd peak height with sample weight for ASK-3 sulphide ore and Bovine Liver.

TABLE 4 DETECTION LIMITS IN μg OF ELEMENT.

ELEMENT	BOVINE LIVER (NBS)	ASK-3 ORE
Cadmium	7.00×10^{-5}	—
Antimony	0.24×10^{-5}	—
Mercury	1.99×10^{-5}	2.02×10^{-2}
Selenium	82.10×10^{-5}	—

the proposed method occurs primarily because the active chemical environment existing in a flame readily promotes dissociation of particles and absorbing molecular species. Despite the fact that constant temperature atomization (i.e. the flame atomizer) reduces the vapour phase reactions to a large extent, the interferences during the volatilization step (in the HGA 2100) still occur.

In general, there is a satisfactory linear relationship between peak heights of the analyte signal and the sample weight, provided the weights are below 15.0 mg. In Figure 8, Curves A and B both represent Cd in ASK-3 sulphide ore. Curve A was recorded at a carrier gas flow rate of 0.1 L/min. The curve for Cd in Bovine Liver is linear up to 10.0 mg and bends towards the concentration axis beyond that value. However, as mentioned earlier, the linearity of these plots can be extended for larger sample weights with proper charring steps. These weights are much higher than those which can be used in conventional graphite furnace analysis (about 1 to 3 mg). Detection limits for these elements in the same samples are given in Table 4.

At present, it is necessary that standardizations for the proposed method be carried out using solid samples with matrices roughly corresponding to those of the samples under investigation.

Grant 107 Platinum Group Elements in the Eastern Gabbro, Coldwell Complex, Northwestern Ontario

D.H. Watkinson, P.J. Whittaker, and P.L. Jones
Department of Geology, Carleton University and Ottawa-Carleton Centre for Geoscience Studies

ABSTRACT

Platinum-group-element concentrations in the eastern gabbro of the Coldwell Complex in the Thunder Bay District, Ontario, occur with chalcopyrite + pyrrhotite + cubanite + pentlandite in heterogeneous, massive gabbroic rocks at or near the contact with Archean country rocks. Much of the heterogeneous massive gabbro which contains sulphides is inclusion-rich, biotite-bearing, and contains pegmatitic pods. Layered gabbro occurs above the massive unit. Gabbro containing a few percent sulphides has copper, platinum, and palladium contents of about 0.48%, 400, and 1400 ppb respectively. Pt/(Pt + Pd) and Cu/(Cu + Ni) ratios are consistently near 0.22 and 0.94 respectively.

INTRODUCTION

Platinum-group-element (PGE) concentrations are known to occur with copper-nickel-iron sulphides at or near the contact of gabbros of the Coldwell Complex with the Archean country rocks (Wilkinson 1983; Wilkinson and Colvine 1978; Naldrett 1982). There has been no detailed examination of the occurrence and petrographic relationships of PGE to the host rock gabbro at the Coldwell Complex, and it is the purpose of this research project to examine the relationships, and to propose a model for PGE concentration in this and other alkalic rock complexes.

The Coldwell Complex (Figures 1 and 2) is located in the Thunder Bay District, northwestern Ontario, approximately bounded by Latitudes 48°41'N to 48°53'N and Longitudes 86°12'W to 86°40'W. According to Wilkinson and Colvine (1978), there is in excess of 50 million tonnes averaging >0.4% Cu and significant Ni and PGE in 2 occurrences.

The base and precious metals occur as disseminations to net-textured concentrations of chalcopyrite + pyrrhotite + cubanite + pentlandite, with minor sphalerite, pyrite, mackinawite, bornite, galena, and valleriite (Puskas 1967; Watkinson *et al.* 1973; Wilkinson 1983). In the latter studies, it has been concluded that sulphide concentrations are magmatic segregations, saturation of the gabbroic magma with sulphur having been effected by contamination and assimilation of Archean country rocks by the magma at or near its contact. The common occurrence of sulphides with xenoliths, hybrid gabbro, patches of pegmatitic gabbro, and biotite-rich gabbro are compatible with this interpretation.

GEOLOGY OF THE EASTERN GABBRO NEAR TWO DUCK LAKE

The Coldwell Complex (Figure 2) is a composite intrusion of at least 3 interlocking successions of ring dikes and cone sheets (Currie 1980). The eastern gabbro ring dike, containing the sulphide concentrations, is the earliest phase of the complex. The eastern gabbro consists of a heterogeneous unit at the contact (Wilkinson 1983) and an overlying layered succession (Puskas 1967). Two main areas of sulphide concentration (Bamoos Lake and Coubran Lake areas) and a minor area near Middleton (Figure 2) have been described by Wilkinson (1983). The area examined in this study (Figure 3), in the Bamoos Lake area, is a part of the complex extensively examined for Cu and PGE by Anaconda Exploration Company Limited. Data on some of the sulphide-bearing outcrop and drillcore from properties of Anaconda Exploration Company Limited have been presented by Lum (1973). Mapping and sampling in this study was confined to 4 trenches (Figure 3).

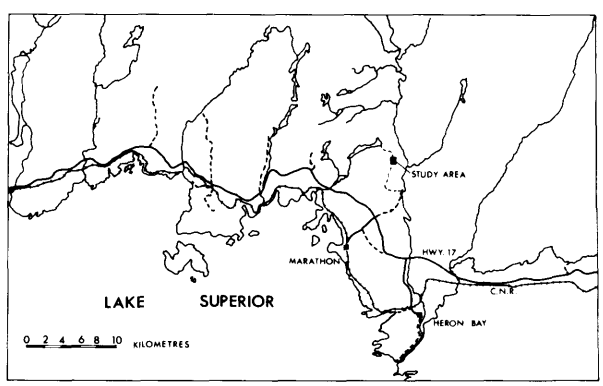

Figure 1. Location of the study area near Two Duck Lake, Coldwell Complex, northwestern Ontario.

GEOLOGY OF THE EASTERN GABBRO IN TRENCHES NEAR TWO DUCK LAKE

TRENCH 1

Trench 1 (Figure 4) is located 50 m north of the southern end of Two Duck Lake on the eastern shore. Massive gabbro underlies the trenched outcrop area and consists of 70% plagioclase, 25% clinopyroxene, and 3 to 5% biotite. Fine grained disseminated sulphides and oxides (magnetite) form 0 to 2% of the rock

Plagioclase is grey-white to grey-green on fresh surfaces and where weathered it is stained reddish brown. Plagioclase ranges from medium grained euhedral laths to coarse grained subhedral to euhedral phenocrysts. Where medium grained laths predominate, usually in 5 to 10 cm patches, they define a subophitic to ophitic texture. Clinopyroxene forms medium- to coarse-grained tabular grains up to 1.5 cm in size and subhedral to euhedral in form. On fresh and weathered surfaces, clinopyroxene is black-green. Biotite occurs as fine to coarse-grained plates up to 1 cm wide and 3 to 4 mm thick. It is randomly oriented and evenly distributed throughout the trench.

Sulphide mineralization causes rusty hematite-limonite staining on weathered surfaces. This colouration penetrates the friable outcrop to a depth of several feet. Sulphides occur as fine grained disseminations ranging in shape from angular to round.

A foliation strikes about 101° and generally has a shallow dip up to 34° alternating from east to west. Several joints cut the foliated gabbro. They strike between 124° and 150° with near vertical dips.

TRENCH 2

Disseminated sulphide mineralization in Trench 2 (Figure 4) is hosted by massive medium grained equigranular gabbro. Small, 10 to 30 cm patches of slightly felsic gabbro are fine grained and equigranular. Scattered coarse grained to pegmatitic patches up to 30 cm across also occur.

Plagioclase ranges from medium grained to pegmatitic and is generally subhedral to anhedral. Euhedral plagioclase is usually confined to fine grained gabbroic patches where it forms subophitic to ophitic texture. Clinopyroxene exhibits a wide range in grain size from fine grained to 2.5 cm pegmatitic phenocrysts. Biotite occurs as an accessory phase forming 3 to 5% of the gabbro and can be medium- or coarse-grained; euhedra up to 1.5 cm were observed. Magnetite is an accessory phase (about 1 to 2%) in the gabbro and is fine grained and subhedral to euhedral.

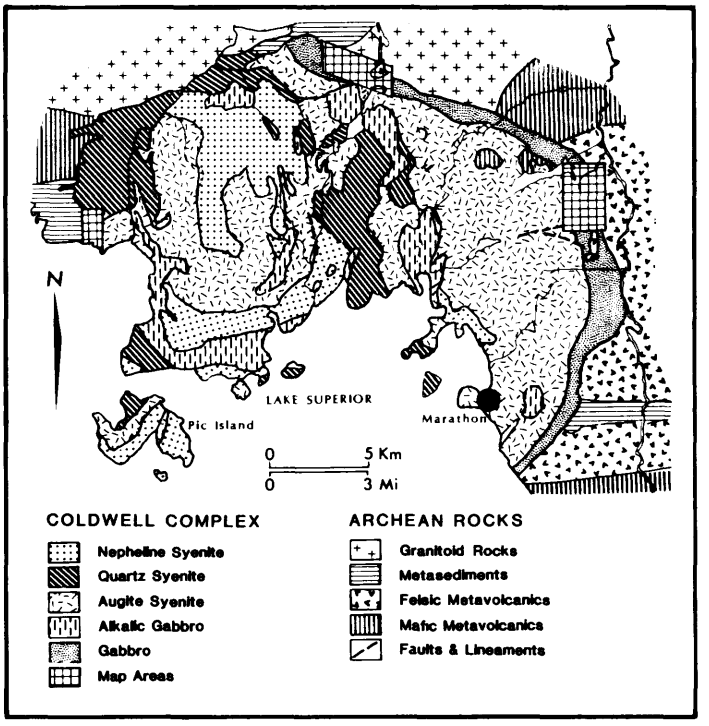

Figure 2. Generalized geology of the Coldwell Complex, from Wilkinson (1983).

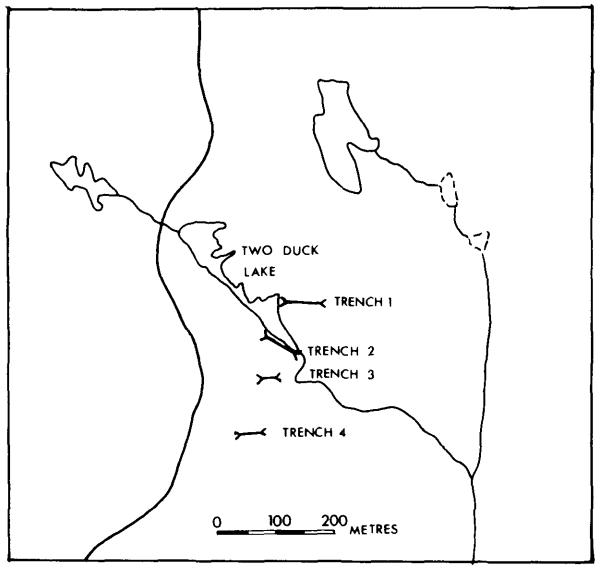

Figure 3. Location of trenches examined in the Two Duck Lake area, Coldwell Complex, northwestern Ontario.

Sulphides (dominantly chalcopyrite + pyrrhotite) occur throughout the trenched area and form 3 to 5% of the gabbro. In coarse grained and pegmatitic patches, sulphides correspondingly occur as coarser disseminations. All sulphides observed were disseminated and, in coarser grained gabbroic patches, are more concentrated, forming 10 to 12% of the patch. Incomplete development of net-textured sulphides was apparent in some of the more sulphide-rich and coarser gabbroic to pegmatitic patches. Coarser grained and pegmatitic gabbro patches are up to 15 cm across, but more commonly are 5 to 7 cm, and irregular in shape. Chalcopyrite was often seen to form rims around pyrrhotite cores.

The rock exposed in the trench is generally massive with some foliated zones which are friable and deeply weathered. Jointing is widely spaced and exhibits a steeply dipping southeast strike. A platy surface exfoliation of 3 to 5 cm thick slabs has also developed.

TRENCH 3

Layered gabbro in Trench 3 (Figure 4) outcrops at the western end of the trenched area, the remainder of which is medium grained equigranular gabbro. The layering strikes 020° and dips 22° west. The medium grained equigranular gabbro contains 7 to 10% disseminated sulphides and the layered gabbro, 2 to 3%.

Layers in the outcrop are:

1. Fine- to medium-grained glomeroporphyritic gabbro with 50% subhedral clinopyroxene and 50% subhedral plagioclase. Glomeroporphyritic plagioclase forms 15 to 20% of the layer. Individual plagioclase grains in the clusters are euhedral laths, 1 to 2 mm by 5 to 8 mm long and form 1 cm diameter rosettes. Disseminated sulphide blebs, up to 4 mm in size, form 2% or less of the layer.
2. Fine grained equigranular gabbro contains equal amounts of subhedral clinopyroxene and plagioclase. Sparse and wispy glomeroporphyritic plagioclase forms 1% or less of the layer.
3. Fine- to medium-grained anorthositic gabbro forms the third type of layer. Clinopyroxene is approximately 15% of the layer, and is subhedral, as is plagioclase.

Layer boundaries are sharply defined, as is the contact between layered and massive gabbro. Sulphides in the layered gabbro are sparsely disseminated in the lower glomeroporphyritic layer and decrease upward.

Medium grained massive gabbro underlies the remainder of the trenched area. An equigranular and fine grained gabbro layer is one exception. The layer is 3 to 5 cm thick and sharply bordered by medium grained gabbro. No sulphides were observed in the fine grained layer.

Plagioclase is unaltered throughout the trench and ranges from fine grained in some layers to medium grained elsewhere. It is mostly subhedral to anhedral but also occurs as fine grained, euhedral laths defining ophitic texture. Clinopyroxene is fine- to medium-grained and subhedral to anhedral. It is finer grained in the layered gabbro. Biotite was not observed in the layered fine grained gabbro. In the massive, equigranular, medium grained gabbro, biotite forms up to 3% of the rock. It is euhedral, forming books up to 4 mm thick and 1 cm thick.

Sulphides (dominantly chalcopyrite + pyrrhotite) are sparsely disseminated in the layered gabbro and are only evident in outcrop in the basal layer in contact with massive gabbro. In the massive equigranular gabbro, disseminated sulphides form up to 7% of the rock. Disseminated blebs are fine- to medium-grained and occur interstitially. Near the eastern end of the trench, an area of gabbro 30 cm across contains coarser clots of sulphides up to 2 cm in size. These clots are angular to round in shape and contain as much as 100% sulphide.

Foliation is weak to absent and jointing is widely spaced.

TRENCH 4

Trench 4 is located 150 m south of Two Duck Lake and is up to 2 m wide. It trends 082° for 35 m. The middle ⅔ of the trench is blasted outcrop and the larger blocks (1 m) are assumed to be in place (Figure 4).

The gabbro which underlies the Trench 4 area consists primarily of medium grained equigranular and massive gabbro. Scattered fine grained and pegmatitic patches form approximately 10% of the outcrop. Fine grained gabbro patches are small, 5 to 15 cm across, and pegmatitic patches occur up to 1 m in size, all being irregular in shape.

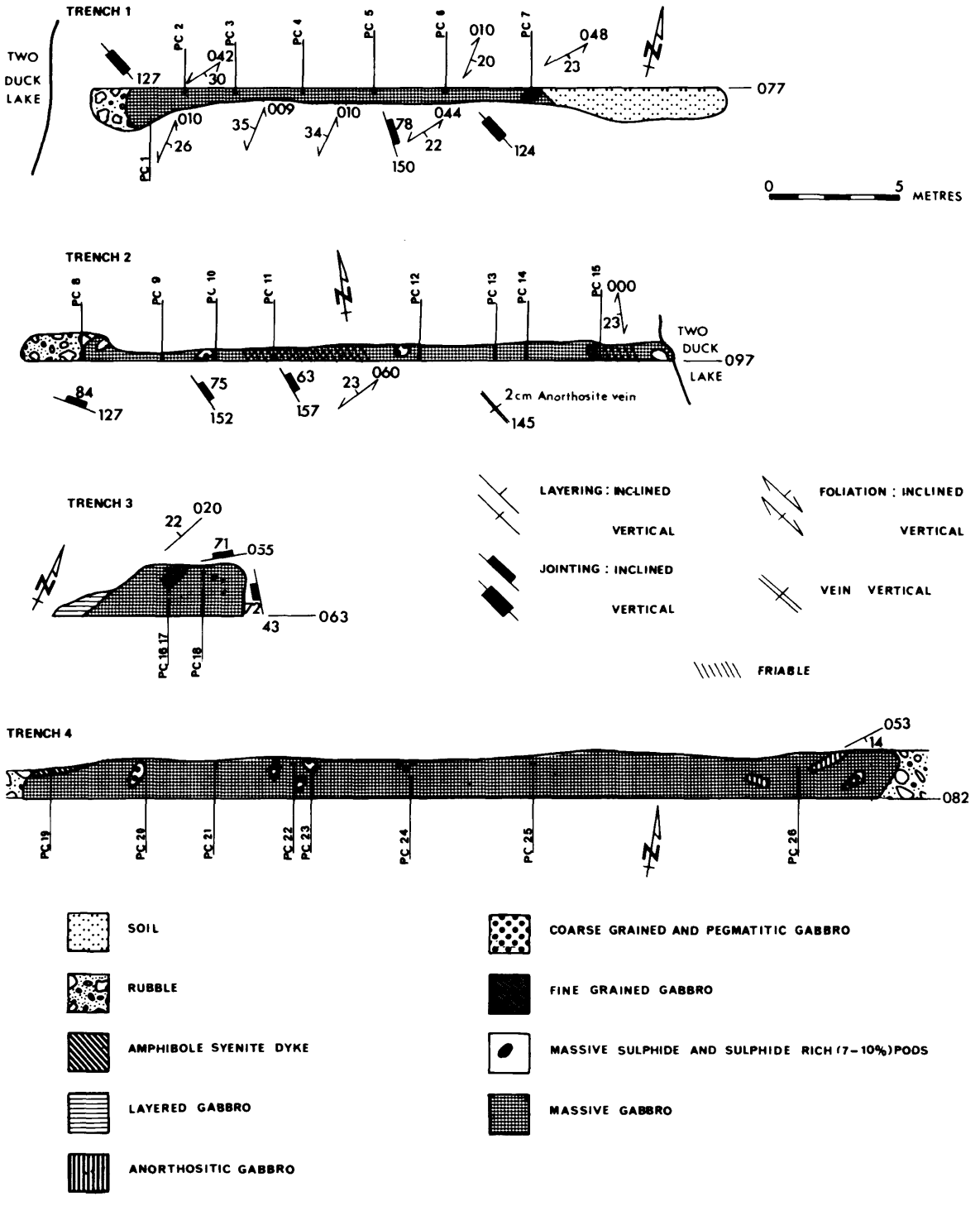

Figure 4. Geological relationships and specimen locations in Trenches 1,2,3, and 4, Two Duck Lake area, Coldwell Complex, northwestern Ontario.

At the western end of the trench, coarse grained amphibole syenite (sulphide-free) cuts massive gabbro. Subhedral and euhedral medium grained quartz forms 10% of the syenite.

Toward the eastern end of the trench, a layer of pegmatitic anorthositic gabbro is sharply bordered by the massive gabbro. Subhedral clinopyroxene forms the mafic phase (15%) and about 1% euhedral potassic-feldspar also occurs. No sulphides were noted in this layer.

Pegmatitic patches in the gabbro are anorthositic gabbro with 10 to 15% subhedral to euhedral clinopyroxene. Individual tabular clinopyroxene grains up to 7 cm long were observed. Medium grained subhedral quartz (3 to 4%) is usually present in pegmatitic patches.

Patches of fine grained anorthositic gabbro contain about 15% subhedral clinopyroxene. These patches together with pegmatitic patches form approximately 25% of the outcrop area.

Plagioclase is unaltered throughout the trenched area. In medium grained gabbro, plagioclase is subhedral to euhedral, and in some instances forms subophitic and ophitic textures. Clinopyroxene is subhedral throughout the massive medium grained gabbro and in fine grained patches. In pegmatitic patches, it is subhedral. Biotite forms 3 to 4% of the massive gabbro and occurs as euhedral books 3 to 4 mm thick and 1 cm wide. In fine-grained patches, it is less common; in pegmatitic patches, biotite occurs up to 2 cm in size.

Sulphides (dominantly chalcopyrite + pyrrhotite) form 7 to 10% of the gabbro as medium- to coarse-grained disseminations. Disseminated sulphides are less abundant in fine grained equigranular gabbro patches. In coarse grained and pegmatitic gabbro patches, disseminated sulphides are as large as 1.5 cm. Disseminated sulphides range in shape from angular to round blebs. Within medium grained massive gabbro, disseminated sulphides are also of medium grain size and many angular disseminations are uniform. Larger individual sulphide patches are sparsely distributed in the massive gabbro. Sulphide patches are irregular and up to 4 cm by 2 cm in size. They consist of up to 75% sulphides with enclosed plagioclase and clinopyroxene. Chalcopyrite is predominant (75%) with minor pyrite and pyrrhotite.

The outcrop area is underlain by massive rocks with widely separated jointing. A weathered surface, about 5 cm thick, is present on undisturbed outcrop.

PETROGRAPHY OF SULPHIDE-BEARING GABBRO

Preliminary petrographic analysis has been made of polished thin sections of specimens assayed for Cu, Ni, Pt, and Pd; the modal compositions are presented in Table 1 and generalized information on constituent minerals is summarized in Table 2. Detailed examination for platinum group minerals is underway, as is microprobe analysis of silicates and sulphides.

Platinum group minerals are not easily found in polished sections of these sulphides; hollingworthite, RhAsS, and merenskyite, $Pd(Bi,Te)_2$, (Figure 5) are the only ones yet identified (Wilkinson 1983).

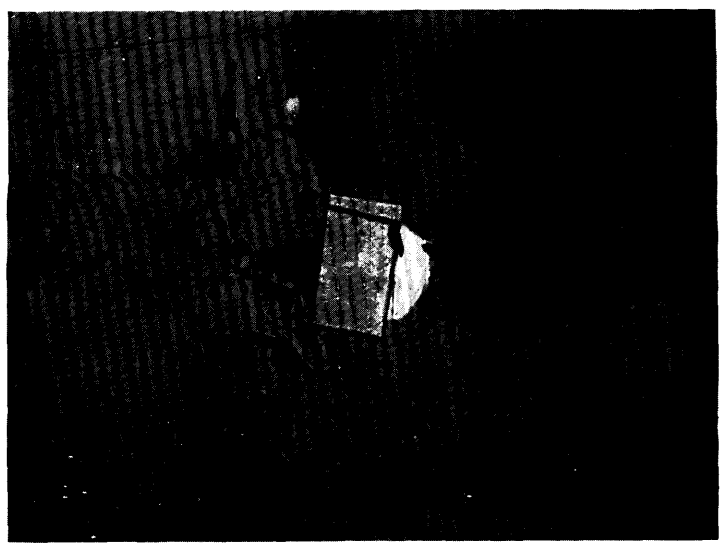

Figure 5. Photomicrograph of euhedral hollingworthite (RhAsS) and anhedral merenskyite $Pd(Bi,Te)_2$ in pyrrhotite, chalcopyrite, cubanite, and pentlandite; width of photo 90 μm.

TABLE 1 MINERALOGY OF GABBROIC ROCKS FROM THE EASTERN GABBRO, COLDWELL COMPLEX.

	plag.	cpx.	ol.	opx.	biot.	amphib.	apat.	serp.	chl.	ser.	qtz.	cpy.	po.	pent.	py.	cub.	mag.
Trench #1																	
PC1	20	45	15	-	5	-	1	1	2	tr	-	1	1	-	tr	tr	7
PC2	49	24	12	-	9	-	tr	tr	1	tr	-	tr	tr	-	-	-	1
PC3	43	24	8	3	9	-	tr	2	7	tr	-	2	1	-	tr	-	2
PC4	33	37	10	-	7	-	tr	2	tr	tr	-	1	-	-	1	-	8
PC5	44	28	7	3	3	-	tr	7	tr	tr	-	1	1	-	-	tr	5
PC6	40	39	5	-	8	-	tr	3	tr	tr	-	2	tr	-	-	-	3
Trench #2																	
PC8	38	37	8	4	4	-	tr	3	-	tr	-	1	tr	-	-	tr	4
PC9	40	42	5	-	2	-	tr	tr	2	tr	-	1	1	-	-	-	6
PC10	32	41	-	3	4	8	tr	tr	3	3	-	4	tr	-	-	tr	1
PC11	41	33	4	3	3	5	1	2	2	2	1	1	-	-	-	tr	1
PC12	42	39	-	-	5	3	tr	1	1	tr	-	5	2	-	-	tr	2
PC13	34	32	12	4	2	1	tr	tr	4	1	-	6	1	tr	tr	1	1
PC14	37	32	12	-	5	-	tr	tr	4	1	-	2	tr	-	tr	-	7
PC15	38	43	-	4	5	-	1	-	tr	4	-	tr	-	-	-	-	4
Trench #3																	
PC16	32	27	23	3	2	5	tr	3	2	2	-	3	2	tr	-	-	1
PC17	39	26	22	3	2	-	tr	3	tr	tr	-	2	3	tr	-	tr	tr
PC18	37	30	10	-	5	-	tr	2	3	tr	-	1	6	tr	-	tr	6
Trench #4																	
PC19	55	-	-	-	-	30	-	-	-	-	15	-	-	-	-	-	-
PC20	34	22	12	-	4	5	tr	4	4	4	-	5	4	tr	-	tr	2
PC21	44	29	4	-	3	6	tr	4	3	1	2	2	tr	-	-	-	3
PC22	43	30	3	-	5	6	tr	-	3	2	-	3	1	tr	tr	-	1
PC23	41	30	10	-	3	3	tr	3	2	2	-	1	-	-	-	-	5
PC25	43	31	4	-	2	-	tr	1	2	tr	-	5	3	1	-	tr	8
PC26	43	29	4	-	2	-	-	1	2	2	-	5	3	1	-	-	5

COPPER, NICKEL, PLATINUM, AND PALLADIUM CONTENTS OF THE EASTERN GABBRO

Sixteen sulphide-rich grab samples from Trenches 1 to 4 were submited to Bondar-Clegg and Company Limited for assay. Cu and Ni were analyzed by Atomic Absorption after HNO_3-HCL hot extraction (lower detection limits 1 and 2 ppm respectively). Pt and Pd were analyzed by Fire Assay-Atomic Absorption techniques after aqua regia extraction (lower detection limits 15 and and 2 ppb respectively). Results, along with Cu/(Cu + Ni) and Pt/(Pt + Pd) ratios, are presented in Table 3; location of sample numbers is shown on Figure 4. Average values (standard deviation) for the elements and ratios are Cu 4837(3314) ppm, Ni 304(262) ppb, Pt 402(233) ppb, Pd 1396(969) ppb, Cu/(Cu + Ni) 0.943(0.021), Pt/(Pt + Pd) 0.220(0.057).

The data vary considerably, in general as a function of the amount of sulphide minerals in the specimen. However, the contents are probably quite homogeneous as the consistent ratios would appear to suggest. As shown in Figure 6, the ratios cluster well in the vicinity of other data from the eastern gabbro (Wilkinson 1983; Naldrett 1982) derived from other methods of analysis. Further analytical data are being obtained, including sulphur analyses, to more carefully determine the control on metal distribution.

The high Cu/(Cu + Ni) ratio and departure from the general tholeiitic trend (Figure 6) shown by Naldrett and Cabri (1976) may result from the alkalic nature of the original magma which was somewhat different from typical tholeiitic compositions. However, olivine is an early cumulus phase in many of the eastern gabbros, and Ni may have been camouflaged in the olivine structure, giving rise to Cu-rich intercumulus liquid. It is unlikely that Cu has been added to the magma during the inclusion and assimilation of country rocks.

TABLE 2 SUMMARY OF PETROGRAPHIC DESCRIPTIONS OF HYBRID GABBROS, TWO DUCK LAKE AREA, COLDWELL COMPLEX.

Mineral	Range	Average	Remarks
Plagioclase	20-55	39.6	An range 38-60. An average -52. Ubiquitous, anhedral to euhedral, equant to tabular, cumulate and intercumulate (to a lesser extent), randomly oriented grains. Sizes range from minute to 6 mm. Apparently unzoned, variably saussuritized, grain boundaries regular to embayed (particularly by olivine). Poikilitically enclosing cpx, apatite, ol, earlier plag. grains, biotite. Rarely the plagioclase grains are extensively altered to chlorite.
Clinopyroxene	0-46	30.9	Generally anhedral intercumulus grains, 0.1-3.5 mm with poikilitic inclusions of plag, ol, mag, sulphides, apatite. Clinopyroxene grain boundaries where in contact with plagioclase grains are serrated and embayed. Alteration to biotite or amphibole common. Twinning occurs rarely.
Olivine	0-23	8.1	Equant, anhedral grains, 0.5-5 mm, always fractured, often extensively altered to chlorite, serpentine and possibly iddingsite. Olivine may be rimmed by amphibole, chlorite, fractures often filled with oxide, often associated with opaque grains. Olivine usually embays plagioclase grains.
Biotite	0-9	4.1	Anhedral, intercumulus, interstitial grains, 0.1-2 mm in size. Poikilitically enclosed in clinopyroxene, opaques and rarely plagioclase, also occurs along fractures and is associated with opaques and amphiboles.
Amphibole	0-30	3.3	Not very common alteration mineral, 0.3-8 mm in size, occurs in very rarely as euhedral or circular grains associated with opaque grains.
Serpentine	0-7	1.8	Brown-green alteration product of olivine, generally occurs along fractures but in some cases entire olivine grains have been altered. (Some of the serpentine may in fact be iddingsite).
Chlorite	0-7	2.1	Blue and green varieties occur as mats in interstitial pockets, also occurs as circular grains along opaque grain boundaries in plag, ol, and cpx grains.
Orthopyroxene	0-4	1.3	Similar habit to cpx.
Sericite	0-4	1	Alteration product of plagioclase. Some grains are extensively altered, others are very fresh. There is no apparent zonation of sericite within single plagioclase grains.
Magnetite	0-8	3.8	Occurs as small (euhedral to subhedral intercumulus grains and as longer cumulus grains (0.2-6 mm). It poikilitically encloses sulphides and olivine. Oxyexsolution flames of ilmenite are common.
Apatite	0-1	0.2	Small elongate grains with high relief occur as poikilitic inclusions in plagioclase and clinopyroxene.
Quartz	0-15		Quartz occurs in only (PC11 + 19). Occurs as small grains associated with plag (PC11) or as large monominerallic intergrowths with serrated grain boundaries.
Sulphides	0-9	3.8	Sulphides composed of cpy po pent py cub (2.4-1.1-0.2-trace-trace). They occur as single and multiple component aggregates and intergrowths and as individual interstitial grains. They are often associated with mafic minerals or magnetite. Cpy is the most common, occurring as intergrowths up to 6 mm across, often enveloping po and pent, alteration to covellite occurs along grain boundaries and fractures. Po occurs in intergrowths with other sulphides and in fractures with oxides. A complex intergrowth of po and cpy occurs rarely where flames of po and cpy are interelated and do not appear to be discrete grains. Pent. always occurs in association with po and cpy and usually forms a core surrounded by po. In some cases pent appears to have altered to po along grain boundaries and fractures. Cubanite grains occur in association with cpy and along Pyrite generally occurs alone as minute grains. Possible mackinawite lamellae occur rarely in cpy and po grains.

TABLE 3 Cu, Ni, Pt, AND Pd CONTENTS OF SELECTED SULPHIDE-RICH SPECIMENS FROM TRENCHES IN THE TWO DUCK LAKE AREA, COLDWELL COMPLEX. SPECIMEN LOCATIONS ARE SHOWN IN FIGURE 4.

SAMPLE NUMBER	Cu ppm	Ni ppm	Pt ppb	Pd ppb	Pt/(Pt+Pd)	Cu/(Cu+Ni)
PC-8	2770	110	309	1285	0.194	0.962
PC-9	6520	263	442	2033	0.179	0.961
PC-10	4860	256	184	870	0.175	0.950
PC-11	1410	120	50	238	0.214	0.922
PC-12	6050	96	403	1407	0.223	0.984
PC-13	5535	559	500	1905	0.208	0.908
PC-14	2200	116	221	706	0.238	0.950
PC-15	3320	70	796	1257	0.388	0.979
PC-18	5100	442	320	1705	0.158	0.924
PC-19	104	11	<10	5		
PC-20	3110	180	315	817	0.278	0.945
PC-21	10940	784	810	3190	0.203	0.933
PC-22	12300	864	715	3325	0.177	0.934
PC-23	1720	125	110	408	0.212	0.932
PC-25	7300	555	525	2275	0.188	0.929
PC-26	4150	313	335	915	0.268	0.930

CONCLUSIONS

The base-metal sulphide concentrations and contained precious metals are interpreted to be of magmatic derivation. The metals and sulphur both may have been juvenile and magmatic, and may have been concentrated due to simple saturation of the magma with respect to a sulphide liquid, with resultant precipitation of monosulphide solid solution, intermediate solid solution, and titanomagnetite (and eventually exsolution and slight alteration to produce the present sulphide mineralogy). However, the consistent occurrence of sulphides with xenoliths, hybrid gabbro, pegmatitic patches, micaceous gabbro, and, to a minor extent, hydrous and carbonate alteration of gabbro, are compatible with a process of saturation of magma, with respect to sulphide liquid, resulting from wall-rock contamination. Magma mixing may explain some features at the interface of hybrid and layered, magnetite-rich gabbros (Wilkinson 1983), but such a process is not clearly related to sulphide concentrations.

The possibility that sulphur was not juvenile, but added during hybridization (Mainwaring and Naldrett 1977) was considered by Watkinson *et al.* (1973), but not established. The occurrence of magmatic sulphides in gabbro around the periphery of the complex, regardless of the type of enclosing Archean rocks (Wilkinson 1983), is one argument for rejection of this hypothesis. However, if the sulphur was of extraneous origin and the metals juvenile, then in areas where early sulphide precipitation did not occur, metals (especially precious metals) may have been concentrated in magma residual to the marginal gabbro; and perhaps precipitated by events such as later magma mixing, assimilation, hybridization, oxidation, hydration, sulphidization, or other processes that might cause PGE-rich, reef-like concentrations such as those of the Bushveld or Stillwater Complexes. This latter hypothesis is under investigation as the concluding part of this project. The extensive occurrence of magnetite-rich rocks at the interface of marginal and layered gabbros, and the concentrations of 2.2 ppm Pd, and 0.31 ppm Pt, reported by Wilkinson (1983) (sample B-12-2 *in* Figure 6) in the magnetite layer at the base of the layered gabbro, make this an interesting possibility.

ACKNOWLEDGMENTS

This project on base and precious metals in the Coldwell Complex was initiated with the permission of Anaconda Exploration Company Limited. Paul R. Mainwaring provided much of the impetus for this work and his contribution to petrological interpretations was invaluable. Field work by and discussions with P. Whittaker, R. Sage, S. Wilkinson, and S. Colvine are greatly appreciated.

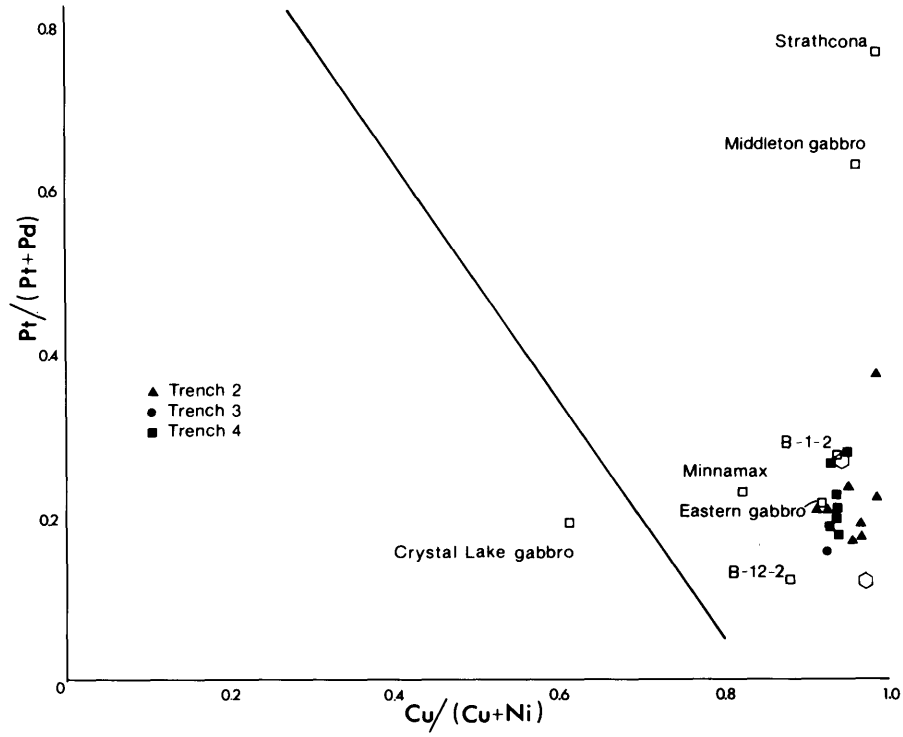

Figure 6. Scatter plot of Cu/(Cu + Ni) versus Pt/(Pt + Pd) for data from Table 3, with data from other Proterozoic Cu-rich sulphides in mafic rock complexes. Hexagons are unpublished data from the Coldwell Complex (Mainwaring, P.R. Canmet, Ottawa, personal communications 1983). Open squares are from Naldrett (1982) and Wilkinson (1983). Line is approximate tholeiitic trend (Naldrett and Cabri 1976).

REFERENCES

Currie, K.L.
1980: A Contribution to the Petrology of the Coldwell Alkaline Complex, Northern Ontario; Geological Survey of Canada, Bulletin 187, 43p.

Lum, H.K.
1973: Petrology of the Eastern Gabbro and Associated Sulphide Mineralization of the Coldwell Alkalic Complex, Ontario; B.Sc. Thesis, Carleton University, Ottawa.

Mainwaring, P.R., and Naldrett, A.J.
1977: Country-Rock Assimilation and Genesis of Cu-Ni Sulphides in the Water Hen Intrusion, Duluth Complex, Minnesota; Economic Geology, Volume 72, p.1269-1284.

Naldrett, A.J.
1982: Platinum Group Metals in Ontario; Ontario Geological Survey, Open File Report 5380, 76p.

Naldrett, A.J., and Cabri, L.J.
1976: Ultramafic and Related Mafic Rocks: Their Classification and Genesis with Special Reference to the Concentration of Nickel Sulphides and Platinum-Group Elements; Economic Geology, Volume 71, p.1131-1158.

Puskas, F.P.
1967: Geology of the Port Coldwell Area, District of Thunder Bay; Ontario Department of Mines, Open File Report 5014, 94p.

Watkinson, D.H., Mainwaring, P.R., and Lum, H.K.
1973: Petrology and Copper Mineralization of the Coldwell Complex, Ontario; Geological Society of America Abstracts, Volume 5, p.856.

Whittaker, P.J.
1979: Geology of the East Central Port Coldwell Complex from Pic River to Red Sucker Cover; M.Sc. Thesis, McMaster University, Hamilton.

Wilkinson, S.
1983: Geology and Sulphide Mineralization of the Marginal Phases of the Coldwell Complex, Northwestern Ontario; M.Sc. Thesis, Carleton University, Ottawa.

Wilkinson, S., and Colvine A.C.
1978: Sulphide Mineralization in the Marginal Phases of the Coldwell Alkalic Complex; p.210-215 *in* Summary of Field Work, 1978, by the Ontario Geological Survey, edited by V.G. Milne, O.L. White, R.B. Barlow, and J.A. Robertson, Ontario Geological Survey, Miscellaneous Paper 82, 235p.

Grant 138 Mineralogy and Geochemistry of the Chrysotile Asbestos Deposits of Ontario

F.J. Wicks, E.S. Schandl, Judit Ozoray, and Wan Pu
Department of Geology, University of Toronto

ABSTRACT

The principal chrysotile asbestos deposits in the Ontario part of the Abitibi Belt have been found to have undergone 2 stages of serpentinization. The first stage was a retrograde serpentinization that produced lizardite-*1T* ± magnetite pseudomorphic textures after primary olivine and pyroxene. This type of serpentinization was not restricted to the asbestos deposits alone, but has been found in most of the other serpentinized ultramafic rocks examined. The second stage of serpentinization that has affected the asbestos deposits was prograde. It commonly produced antigorite ± brucite ± magnetite as well as other serpentine minerals, and was associated with the development of the chrysotile asbestos veins.

Rodingites, calcium-rich metasomatic rocks composed of grossular, diopside, prehnite, and in some cases epidote, were found in all asbestos deposits examined. These rodingites appear to have developed due to calcium-rich fluids released from ultramafic rocks mainly during the second stage of serpentinization. A variety of rocks have been altered to rodingite, including a mafic dike and irregular blocks of mafic volcanic rocks and gabbros within the serpentinites, and mafic volcanic rocks at the contacts with the serpentinites. A prominant chlorite-rich reaction rim separates the rodingites from the serpentinites. In the case of the mafic dike, relict biotite and tremolite within a chlorite-rich reaction rim indicate that the dike intruded and reacted with the ultramafic rocks before and at a higher temperature than the serpentinization. Studies of the fluid inclusions in some of the diopsides in the rodingites indicates a fluid composition of almost pure H_2O, with no more than 1% NaCl and temperatures of entrapment of the fluid inclusions of 270°C at 1 kbar pressure or 350°C at 2 kbars pressure.

INTRODUCTION

The chrysotile asbestos deposits that form the basis of this study occur in the sequence of komatiite flows and sills that form the basal group of the Upper Supergroup in the Abitibi Belt in Ontario (Jensen and Pyke 1982). In recent years these have been extensively investigated (Pyke *et al.* 1973; Fleet and MacRae 1975; Arndt 1976; Jolly 1982), but the serpentinization and the development of chrysotile asbestos deposits in these rocks have not been examined systematically or in detail.

Microbeam X-ray diffraction camera studies (Wicks and Zussman 1975) of asbestos deposits from other areas have indicated that the ultramafic rocks hosting chrysotile asbestos deposits have experienced 2 stages of serpentinization (Wicks and Whittaker 1977; Wicks and Plant 1979). The first is a retrograde serpentinization that produces lizardite ± brucite ± magnetite pseudomorphs after olivine and pyroxene in the host rocks and relatively minor serpentine veins dominated by lizardite. The second is a prograde serpentinization that produces mineralogically varied assemblages dominated by chrysotile ± brucite ± magnetite or antigorite + brucite ± magnetite having non-pseudomorphic textures and abundant veins of cross-fibre chrysotile asbestos.

The project was initiated in the 1982 field season with 2 objectives: (1) to collect representative suites of samples with which to characterize the various chrysotile asbestos deposits in the Abitibi Belt; and (2) to select areas for detailed mapping in the following field season. Suites of chrysotile asbestos, associated non-fibrous vein serpentine, and host serpentinite were collected from the Munro Mine, both A and B pits; the Garrison Deposit, both underground ore zones and the surface pit; the Bowman Mine, both main and subsidiary pits; and the Reeves Mine, both east and west pits. Talc-carbonate alteration zones, that form an envelope around the ore bodies, were found to be well-exposed in Munro A pit and the Reeves west pit. At all localites the ultramafic rocks outside the pits and, where possible, the associated gabbroic and volcanic rocks were also sampled. Permission to visit the Hedman Mine (Vos 1971) was denied by the owners, but loose fragments of serpentinite and rodingite which had falled off ore trucks were collected from the road.

Serpentinized ultramafic rocks that do not contain abundant chrysotile asbestos veins were also sampled to provide a basis for comparison between asbestos-bearing and non-asbestos-bearing serpentinites. These included Fred's flow (Arndt 1975), Pyke's Hill (Pyke *et al.* 1973), the Centre Hill layered intrusion and the underlying komatiites (MacRae 1969), all in Munro Township, and the Alexo Mine (Naldrett 1966) and the Dundonald sill (Naldrett and Mason 1968) in Dundonald and Clergue Townships.

Rodingites occur frequently in Paleozoic serpentinites, such as those in the Eastern Townships, Quebec, but have rarely been described and never studied in detail in Archean serpentinites. Pyke *et al.* (1978) have

noted small isolated blocks of what is apparently rodingite at the Bowman Mine, and Pyke (personal communication, 1983) has described rodingitized dikes in the Midlothian asbestos Mine. Rodingites are calcium-rich metasomatic rocks consisting mainly of grossular-hydrogrossular, diopside, prehnite, vesuvianite, sodic plagioclase, and tremolite. They are formed through the metasomatic reaction of calcium, released by serpentinization of pyroxene, on dikes or inclusions contained within serpentinized ultramafic rocks. In ophiolite complexes it is generally believed that the processes of rodingitization takes place during 2 separate stages of serpentinization (Honnorez and Kirst 1975; Capedry *et al.* 1978; Adib and Pamic 1980; Laurent 1980; Trommsdorff and Evans 1980; Wares and Martin 1980a and 1980b). The first stage of serpentinization takes place on the ocean floor where dikes and inclusions are weakly rodingitized; the second stage takes place during the obduction of the ocean floor onto the continent. During the 1982 field season rodingites were found and collected from the 4 chrysotile asbestos deposits visited in the Abitibi Belt and these, plus the material from the Hedman Mine, have been studied in detail.

GEOLOGY

The basic geology and mining history of the asbestos deposits in the Abitibi Belt are given by Vos (1971). The Munro Mine is located 16 km east of Matheson in the southwest corner of Munro Township. The ultramafic rocks in this township were mapped by Satterly (1952), and through further detailed mapping (Pyke *et al.* 1973; Arndt 1975) have become well known as the classic komatiite locality in Canada. Arndt (1975) feels that the Munro Mine is located in a large komatiite flow or sill. The mine occurs in the fault block between the Munro and Pipestone faults zones and has been described geologically by Hendry and Conn (1957) and Kretschmar and Kretschmar (1982) and mineralogically by Grubb (1962). Rodingites were found during the 1982 field season in the area of the B pit, both as a vertical dike of what was probably mafic rock < 30 cm wide exposed over 35 m, and as an elongate block, 1 m by 2 m, of unknown origin.

The Garrison chrysotile asbestos Deposit occurs in the northern part of Garrison Township (Satterly 1949; MacRae 1969; Kretschmar and Kretschmar 1982) 23 km east of the Munro Mine. Exposure of the ultramafic rock is poor in this area but the samples collected from this deposit are very important for the present study. One of the main problems in trying to collect representative ore samples from mined-out or inactive mines is that the ore has been removed or is inaccessible because of flooding of the open pit. When the Canadian Johns-Manville Company Limited drove its exploration drift through the Garrison Deposit, 46 bulk samples were collected from the major ore zones and stockpiled on the surface. These samples present a unique opportunity to systematically sample the Garrison ore body. Rodingite blocks were also collected by the authors but, as they occurred as loose blocks in the ore stockpiles, their mode of occurrence could not be determined.

The Bowman Mine occurs in the centre of Deloro Township, 9.6 km southeast of Timmins, and has recently been described by Pyke *et al.* (1978) and Kretschmar and Kretschmar (1982) as a peridotitic-dunitic sill with pyroxenite and gabbro differentiates lying at the top of the sill. A system of well-developed chrysotile asbestos veins is well exposed in the southernmost outcrops (Hewitt and Satterly 1953). Rodingite has formed at the expense of small, rounded lenses, less than 30 cm across, of what appears to have been coarse gabbroic material.

The Reeves Mine is located 63 km southwest of Timmins in the southern part of Reeves Township. The geology of the mine has been described by Milne (1972), prior to the recognition of komatiites. However, the former mine geologist has observed spinnifex textures in the pit and in rocks south of the mine (John Goodger, personal communication). The central part of the ultramafic body is cut by a near vertical, north-trending diabase dike and a near-vertical, north-trending pyroxenite dike. These dikes divide the east pit from the west pit and present an opportunity to study the effect of thermal metamorphism on the serpentine minerals. In the northeastern corner of the east pit, a 1.4 m wide rodingite zone has developed in the volcanic rocks at the serpentinite-metavolcanic rocks contact. Although this is an unusual location for the development of rodingite, the final product is similar to rodingites enclosed within serpentinites.

RESULTS

SERPENTINITES

The 4 chrysotile asbestos deposits examined, Garrison, Munro, Bowman, and Reeves, have all experienced 2 stages of serpentinization; an early retrograde serpentinization and a later prograde serpentinization (Wicks and Whittaker 1977). The early retrograde serpentinization has produced, as identified by X-ray microbeam camera, lizardite-*1T* ± magnetite mesh textures pseudomorphic after olivine, and lizardite-*1T* bastites pseudomorphic after pyroxene. This stage is related to the prehnite-pumpellyite facies of metamorphism described by Jolly (1982) and is widespread throughout the Abitibi Belt. All the serpentinites that were collected for comparative purposes, because they were relatively chrysotile-asbestos free, also have been altered to the lizardite-*1T* ± magnetite assemblage. The degree of serpentinization in these low-grade sperpentinites is usually advanced but it is variable and occasionally is only slightly developed.

The prograde serpentinization is complex and microbeam X-ray diffraction studies are still in progress to identify the various components. Antigorite is common and varies from very abundant in the Reeves Mine to only moderately abundant in the Munro Mine. Brucite is abundant in the Garrison Deposit but it is much less abundant

to rare in the other chrysotile-asbestos deposits. The occurrence of prograde chrysotile textures in the rocks has not been established as yet by microbeam X-ray camera but several possible textures are being prepared for diffraction. Thin section studies indicate that the development of the chrysotile-asbestos veins was intimately associated with the development of the prograde textures in the host rocks. The X-ray fibre diffraction studies of the chrysotile-asbestos to date indicate that most of the asbestos is chrysotile-*2* M_{c1} (clinochrysotile) with some minor chrysotile-*2* $0r_{c1}$ (orthochrysotile) and traces of parachrysotile occurring mainly in the Munro Mine asbestos. This prograde serpentinization coincides with the lower greenschist facies described by Jolly (1982), but it is a unique type of metamorphism and structural environment that leads to the development of the chrysotile-asbestos. Some of the low-grade serpentinites studied for comparison with the asbestos deposits also contain some prograde serpentine textures but do not contain significant chrysotile asbestos.

Whole-rock samples have been prepared for X-ray fluorescence and polished thin sections for electron microprobe studies, but as yet the data on whole-rock chemistry and mineral compositions are not available. Thermoanalysis has been carried out on a number of chrysotile-asbestos and associated vein serpentines but analysis of the data was not complete at the time this report was prepared.

RODINGITES

The small number of samples of rodingite, in comparison to the large number of serpentinite samples, has allowed the study of the rodingites to progress relatively rapidly.

The rodingites are fine-grained and in most cases appear to have formed through the metasomatism of fine-grained rocks. In the Garrison Deposit, glomeroporphyritic textures have been preserved in some samples and suggest that the original rock was a mafic volcanic. In the rodingitized dike at the Munro Mine, the presence of small, strongly zoned relict plagioclase in the chloritic rim suggests a fine-grained mafic parent rock. The rodingite at the contact of serpentinite in the Reeves Mine clearly formed from the adjacent mafic volcanic rocks. In a few cases, mainly at the Bowman and Garrison Deposits, relict coarse grained equigranular textures suggest that the parent rocks were gabbros.

The mineral assemblages in the rodingites consist predominantly of diopside, grossular, prehnite, and in some cases, epidote. Plagioclase has been completely replaced by grossular, prehnite, and in some cases, epidote. The replacement of plagioclase suggests an advanced stage in the rodingitization process (Coleman 1977). Textural and mineralogical evidence indicates that two sets of reactions may have been involved in the replacement of plagioclase in these rocks. These reactions are as follows (*from* Coleman 1977):

(1) 3 anorthite + Ca^{2+} + $2H_2O \rightarrow$ zoisite + $2H^+$

then

4 zoisite + 0.5 Ca^{2+} + $13H_2O \rightarrow$ 3 hydrogrossular + $10H^+$

(2) 1.5 anorthite + 0.5 Ca^{2+} + $1.5H_2O \rightarrow$ 2 prehnite + H^+ + $0.5Al_2O_3$

then

2 prehnite + 4 Ca^{2+} + Al_2O_3 + $6H_2O \rightarrow$ hydrogrossular + $8H^+$

In the Garrison, Munro, and Bowman rodingites, prehnite coexists with grossular, whereas in the Reeves Mine rodingite, zoisites are abundant and coexist with minor grossular. Prehnite occurs in two different forms; in veins, crosscutting the rodingite; and as globular aggregates intimately associated with grossular.

The unit cell parameter *a* was calculated (Appleman and Evans 1973) from the X-ray powder diffraction data of 12 garnets carefully picked from thin sections. The value of *a* ranged from 11.857 to 11.898 Å with an average value of 11.874 Å. Typical data for 6 of these grossulars are given in Table 1, and chemical compositions are shown in Figure 1 for garnets in the Timmins rodingites. Results indicate that the garnet is grossular and not hydrogrossular which commonly occurs in Paleozoic rodingites.

Cell parameters (Table 1) and chemical composition (Figure 2) indicate that the pyroxene is diopside. The Fe contents of the diopsides from the Garrison Deposit and Reeves Mine is relatively high. According to Wares and Martin (1980a), this may be due to an arrest in the process of rodingitization; however, it also may be a reflection of the original Fe content of the parent rock.

A chlorite-rich reaction rim of a few centimetres width commonly separates the rodingitized rocks from the ultramafic host rocks. These reaction rims are believed to be formed as the result of the gain and loss of elements between adjacent but greatly contrasting lithologic units (Jahns 1967). The mineral assemblage in the rim is dominated by chlorite, but also contains a few zoned, euhe-

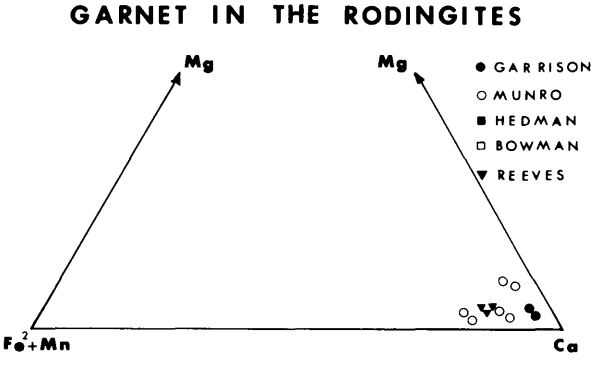

Figure 1. Chemical composition of garnets in the Timmins rodingites.

TABLE 1 CELL PARAMETERS OF MINERALS IN THE ABITIBI RODINGITES.

Sample	a, Å	b, Å	c, Å	β, °	Std. Error 2θ	No. of Peaks Indexed
Grossular						
W82-136	11.871(2)				0.023	7
W82-137	11.871(1)				0.022	13
W82-138	11.865(1)				0.016	9
W82-158	11.870(3)				0.027	9
W82-236	11.898(2)				0.020	5
W82-307	11.857(4)				0.030	4
Diopside						
W82-123A	9.764(5)	8.947(4)	5.256(3)	105.65(6)	0.023	11
W82-137	9.768(5)	8.947(4)	5.273(3)	105.90(5)	0.016	8
W82-306	9.790(4)	8.973(3)	5.263(2)	105.59(5)	0.016	11
Epidote						
W82-307	8.869(8)	5.621(0)	10.139(8)	115.47(7)	0.028	8

dral, relict grains of plagioclase, zoisite, and relict biotite and tremolite. Apparently, prior to chloritization, the plagioclases were saussuritized, changing anorthite-rich phases to more albitic composition. Biotite has been almost completely replaced by chlorite. A few relics and the intact core of several grains indicate that a biotite-rich zone a few millimetres wide existed prior to the development of the chlorite. Corroded, chloritized minor amphibole coexists with the biotite. Chlorite that pseudomorphs and replaces the biotite and amphibole has high Al_2O_3 and FeO, whereas the chlorite that is interstitial to the plagioclase grains and occurs in the rodingitized part of the rock is higher in SiO_2 and MgO.

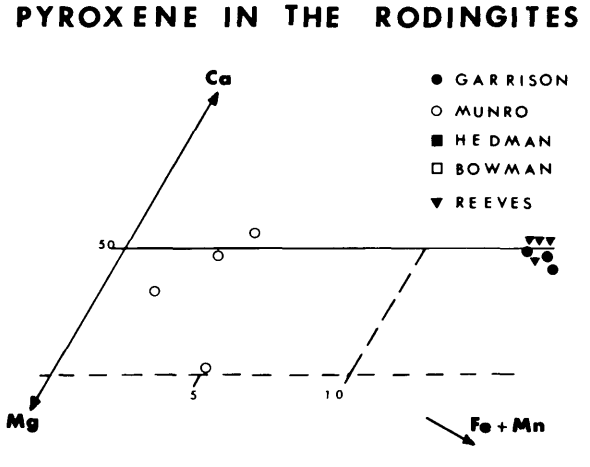

Figure 2. Chemical composition of pyroxenes in the Timmins rodingites.

Sixteen rocks were analyzed by XRF. These included rodingites, chlorite-rich reaction rims, and the host serpentinites. Results are shown in Table 2. The chemical compositions indicate that the rodingites are within or very close to the rodingite field on the ACF diagram determined by Coleman (1977) and shown in Figure 3. The chlorite-rich reaction rims cluster close to the Mg apex of the diagram. The path of rodingitization followed by the metavolcanics from the Reeves Mine is shown in Figure 3 by the line joining the 3 Reeves samples.

Chemical variations within the serpentinites, the reaction rims and rodingites are shown on Figure 4. It is apparent that during the process of rodingitization, the rocks were substantially enriched in calcium. Other chemical changes involved in the reaction were a probable decrease in SiO_2, K_2O, and Na_2O relative to the original mafic composition, and an increase in H_2O.

Fluid inclusions were found in some diopsides in the Bowman Mine rodingites. The inclusions were frozen with liquid nitrogen, then heated to their melting point of between 0° and -2.4°C (after corrections) on a Linkam TH600 heating and freezing stage. When this temperature range is plotted on the depression curve, it gives the fluid composition of almost pure H_2O to H_2O with 1%

TABLE 2 BULK-ROCK COMPOSITIONS OF RODINGITES, THE CHLORITE-RICH CONTACT ZONES, AND HOST SERPENTINITES.

Sample	116-R	116-C	116-S	123-R	123-C	123-S	146-R	146-C	146-S	158-R	159-R	238-R	305-R	306-R	307-R
SiO_2	40.57	38.59	43.47	40.71	40.78	40.42	39.85	40.06	37.28	41.57	40.72	38.15	40.11	43.16	44.30
TiO_2	0.58	0.66	0.11	0.56	0.85	0.35	0.37	0.47	0.31	2.06	1.18	0.46	2.72	1.37	1.32
Al_2O_3	11.89	11.88	3.28	10.68	9.00	7.88	13.65	11.40	9.48	13.28	13.58	16.50	22.06	13.56	9.85
Fe_2O_3*	6.42	7.72	7.62	6.64	3.69	7.96	5.77	4.84	6.74	4.61	6.32	6.98	10.60	10.06	10.66
Cr_2O_3	0.06	0.09	0.19	0.05	0.09	0.29	0.04	0.09	0.10	0.00	0.00	0.04	0.02	0.01	0.01
MnO	0.21	0.62	0.15	0.19	0.79	0.35	0.31	0.46	0.35	0.84	0.26	0.39	0.12	0.28	0.33
MgO	8.30	37.74	43.52	9.36	42.45	41.39	9.51	42.14	39.64	8.57	4.04	12.35	1.72	5.84	8.17
CaO	29.38	1.40	0.05	28.39	0.93	0.27	29.37	0.31	5.99	27.80	32.56	24.08	23.71	23.97	23.12
Na_2O	0.28	0.18	0.15	0.22	0.07	0.37	0.13	0.02	0.01	0.10	0.00	0.08	0.33	0.26	0.21
K_2O	0.02	0.03	0.03	0.02	0.01	0.10	0.02	0.02	0.02	0.02	0.01	0.01	0.07	0.02	0.06
P_2O_5	0.43	0.47	0.04	0.43	0.62	0.20	0.02	0.04	0.01	0.17	0.01	0.11	0.18	0.09	0.12
SO_3	0.03	0.05	0.13	0.02	0.05	0.11	0.03	0.07	0.08	0.01	0.01	0.02	0.03	0.01	0.01
Total	98.18	99.43	98.74	97.29	99.33	99.69	99.07	99.92	100.01	99.03	98.69	99.97	101.67	98.59	98.16
L.O.I.**	1.76	12.38	12.88	1.83	13.13	12.41	3.81	13.07	15.43	2.96	0.75	5.27	2.80	1.81	1.70

*Total Fe as Fe_2O_3

**Loss on ignition (samples were heated to 1000°C prior to analysis)

R=rodingite C=contact S=serpentinite 116,123 Munro; 146 Garrison; 158,159 Hedman; 238 Bowman; 305,306,307 Reeves mines

NaCl. The homogenization temperature (after corrections) for the inclusions, ranges between 199°C and 218°C. From these results the temperature of entrapment of the fluid inclusions in the diopsides would have been 270°C at 1 kbar pressure and 350°C at 2 kbars pressure.

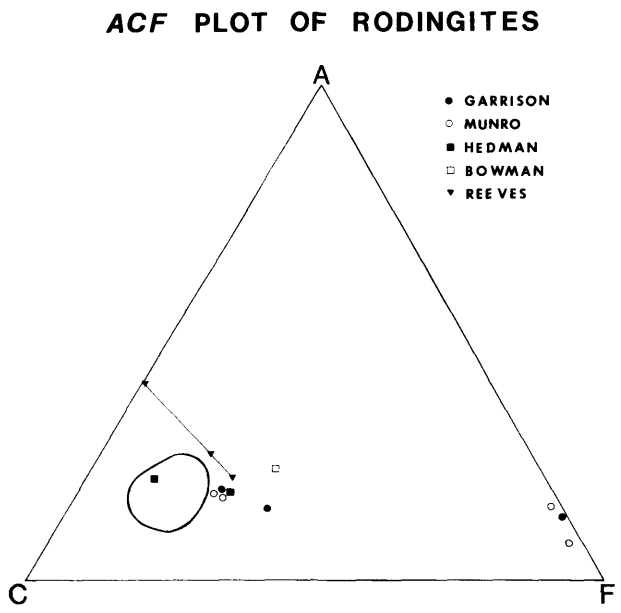

Figure 3. ACF plot of the Timmins rodingites, showing the rodingite field as delineated by Coleman (1977).

DISCUSSION

Although not all the data are available to make a comprehensive interpretation, it has been established that the 4 asbestos deposits have been affected by both retrograde and a subsequent prograde serpentinization. It is the prograde serpentinization that is associated with the development of the chrysotile-asbestos veins.

The blocks of parent rock that were replaced to form rodingite must have been incorporated in the ultramafic bodies at the time of the latter's intrusion or extrusion. The probable mafic dike at the Munro Mine must have intruded prior to serpentinization and is probably a feeder dike related to later basaltic flows. Once water penetrated the sill, while it was still at relatively high temperatures above serpentine stability, the biotite and tremolite reaction rim would have developed.

In all cases the rodingites have developed to an advanced degree, as indicated by the complete replacement of plagioclase by grossular and prehnite, and by the position of these rocks on the ACF diagram (Figure 3). The presence of grossular rather than both grossular and hydrogrossular is unusual in comparison with Paleozoic rodingites. The absence of hydrogrossular in the Abitibi rodingites could mean that the clinopyroxenes in the peridotites were not serpentinized during retrograde serpentinization, so that calcium was not available for rodingite formation. Alternatively, the hydrogrossular could have formed but have been replaced by grossular during the final prograde serpentinization that produced the chrysotile-asbestos.

Jolly (1982) has suggested that the pressure during metamorphism in the Abitibi Belt was low. As yet we do not have an accurate measurement of pressure. However, the open fractures in the olivine, along which serpentinization has progressed, and the open fractures within which the chrysotile-asbestos has developed, suggest pressures of less than 2 kilobars. Fluid inclusion data from the diopsides in the rodingites would indicate entrapment temperatures of 275 and 350°C at 1 and 2 Kbars pressure, respectively.

ACKNOWLEDGMENTS

The sampling of the Munro, Garrison, and Reeves chrysotile-asbestos Deposits was greatly facilitated by the help of F.J. Eveleigh, Canadian Johns-Manville Company Limited, Matheson, Ontario, and W.C. Streib, Manville Service Corporation, Denver, Colorado. The assistance of Craig Boogers, Steetley Talc, Limited, Timmins, Ontario for access to the Reeves property is appreciated. E.T.C. Spooner, University of Toronto, kindly provided access to the freezing and heating stage for the fluid inclusion study. Our thanks to Gloria Nelson for her careful typing of the manuscript.

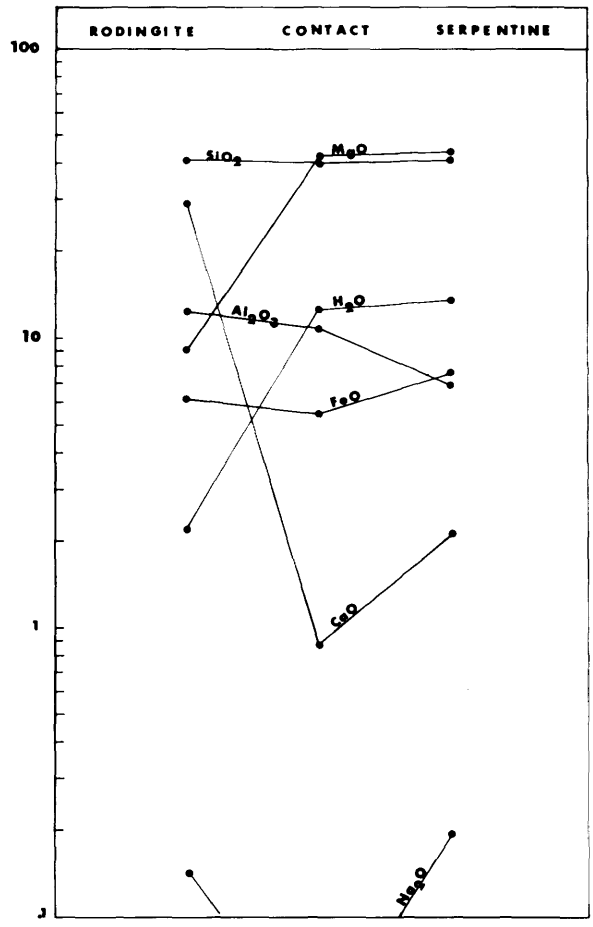

Figure 4. Average chemical variations within rodingites, reaction zones, and host serpentinites in the Munro Mine and the Garrison Deposit.

REFERENCES

Adib, D., and Pamic, J.
1980: Rodingites from the Southeastern Parts of the Neyriz Ophiolite Complex in the Zagros Range, Iran; Archives des Sciences (Societe des Physique et d'Histoire Naturelle de Geneve), Volume 33, Number 2-3, p.281-289.

Appleman, D.E., and Evans, H.T., Jr.
1973: Job 9214: Indexing and Least Square Refinement of Powder Diffraction Data; United States Geological Survey, Computer Contribution, Volume 20.

Arndt, N.T.
1975: Ultramafic Rocks of Munro Township and Their Volcanic Setting; Ph.D. Thesis, University of Toronto, Toronto, Canada.

1976: Ultramafic Rocks of Munro Township; Economic and Tectonic Implications; Geological Association of Canada, Special Paper 14, p.617-657.

Capredi, S., Garuti, G., and Ross, A.
1978: Rodingites from Pindos. Constraints on the 'Rodingite Problem'; Neues Jahrbuch fur Mineralogie, Abhandlung, Volume 132, Number 3, p.242-263.

Coleman, R.G.
1977: Ophiolites; Ancient Oceanic Lithosphere?; Springer-Verlag, New York.

Fleet, M.E., and MacRae, N.D.
1975: A Spinifex Rock from Munro Township, Ontario; Canadian Journal of Earth Sciences, Volume 12, p.928-939.

Grubb, P.L.C.
1982: Serpentinization and Chrysotile Formation in the Matheson Ultrabasic Belt, Northern Ontario; Economic Geology, Volume 57, p.1228-1246.

Hendry, N.W., and Conn, H.K.
1957: The Ontario Asbestos Deposit of Canadian Johns-Manville Company Limited; p.36-45 *in* Geology of Canadian Industrial Mineral Deposits, 6th Commonwealth Mining and Metallurgical Congress.

Hewitt, D.F., and Satterly, J.
1953: Asbestos in Ontario; Ontario Department of Mines, Industrial Mineral Circular 1, Revised Edition.

Honnorez, J., and Kirst, P.
1975: Petrology of Rodingites from the Equatorial Mid-Atlantic Fracture Zones and their Geotectonic Significance; Contributions of Mineralogy and Petrology, Volume 49, p.233-257.

Jahns, R.H.
1967: Serpentinites of the Roxbury District, Vermont; p.137-160 *in* Ultramafic and Related Rocks, edited by P.J. Wyllie, John Wiley and Sons, Inc., New York.

Jensen, L.S. and Pyke, D.R.
1982: Komatiites in the Ontario Portion of the Abitibi Belt; *in* Komatiites; edited by N.T. Arndt and E.G. Nisbet, George Allen and Unwin, London.

Jolly, W.T.
1982: Progressive Metamorphism of Komatiites and Related Archean Lavas of the Abitibi Area, Canada; *in* Komatiites, edited by N.T. Arndt and E.G. Nisbet, George Allen and Unwin, London.

Kretschmar, U., and Kretschmar, D.
1982: Talc, Magnesite and Asbestos Deposits in the Kirkland Lake-Timmins Area; Ontario Geological Survey, Open File Report 5391.

Laurent, R.
1980: Regimes of Serpentinization and Rodingitization in Quebec Appalachian Ophiolites; Archives des Sciences (Societe des Physique et d'Histoire Naturelle de Geneve), Volume 33, Number 2-3, p.311-320.

MacRae, N.D.
1969: Ultramafic Intrusions of the Abitibi Area, Ontario; Canadian Journal of Earth Sciences, Volume 6, p.281-301.

Milne, V.G.
1972: Geology of the Kukatush-Sewell Lake Area, District of Sudbury; Ontario Division of Mines, Geological Report 97. Accompanied by Maps 2230 and 2231, scale 1:31 680 or 1 inch to ½ mile.

Naldrett, A.J.
1966: The Role of Sulphurization in the Genesis of Iron-Nickel Sulphide Deposits of the Porcupine District, Ontario; Transactions of the Canadian Institute of Mining and Metallurgy, Volume 69, p.147-155.

Naldrett, A.J. and Mason, G.D.
1968: Contrasting Archean Ultramafic Igneous Bodies in Dundonald and Clergue Townships, Ontario; Canadian Journal of Earth Sciences, Volume 5, p.111-143.

Pyke, D.R., MacVeigh, J.G., and Middleton, R.S.
1978: Volcanic Stratigraphy and Geochemistry in the Timmins Mining Area; *in* Toronto 78 Field Trip Guidebook, Joint Annual Meeting of the Geological Society of America, Geological Association of Canada, and Mineralogical Association of Canada, Toronto.

Pyke, D.R., Naldrett, A.J., and Eckstrand, O.R.
1973: Archean Ultramafic Flows in Munro Township, Ontario; Geological Society of America, Bulletin 84, p.955-978.

Satterly, J.
1949: Geology of Garrison Township, Cochrane District; Ontario Department of Mines, Annual Report for 1949, Volume 58, Part 4. Accompanied by Map 1949-1, scale 1:12 000 or 1 inch to 1000 feet.

1952: Geology of Munro Township, Cochrane District; Ontario Department of Mines, Annual Report for 1951, Volume 60, Part 8.

Trommsdorff, V., and Evans, B.W.
1980: High Grade Rodingites from the Central Alps: Metamorphism and Geochemistry; Archives des Sciences (Societe des Physique et d'Histoire Naturelle de Geneve), Volume 33, Number 2-3, p.181-184.

Vos, M.A.
1971: Asbestos in Ontario; Ontario Department of Mines and Northern Affairs, Industrial Minerals Report 36.

Wares, R.P., and Martin, R.F.
1980a: Rodingitization of Dyke Rocks and Enclosing Serpentinites in the Jeffrey Mine, Quebec Appalachians; Archives des Sciences (Societe des Physique et d'Histoire Naturelle de Geneve), Volume 33, p.301-310,

1980b: Rodingitization of Granite and Serpentinite in the Jeffrey Mine, Asbestos, Quebec; Canadian Mineralogist, Volume 18, p.231-240.

Wicks, F.J., and Plant A.G.
1979: Electron Microprobe and X-Ray Microbeam Studies of Serpentine Minerals; Canadian Mineralogist, Volume 17, p.785-830.

Wicks, F.J., and Whittaker, E.J.W.
1977: Serpentine Textures and Serpentinization; Canadian Mineralogist, Volume 15, p.459-488.

Wicks, F.J., and Zussman, J.
1975: Microbeam X-Ray Diffraction Patterns of the Serpentine Minerals; Canadian Mineralogist, Volume 13, p.244-258.

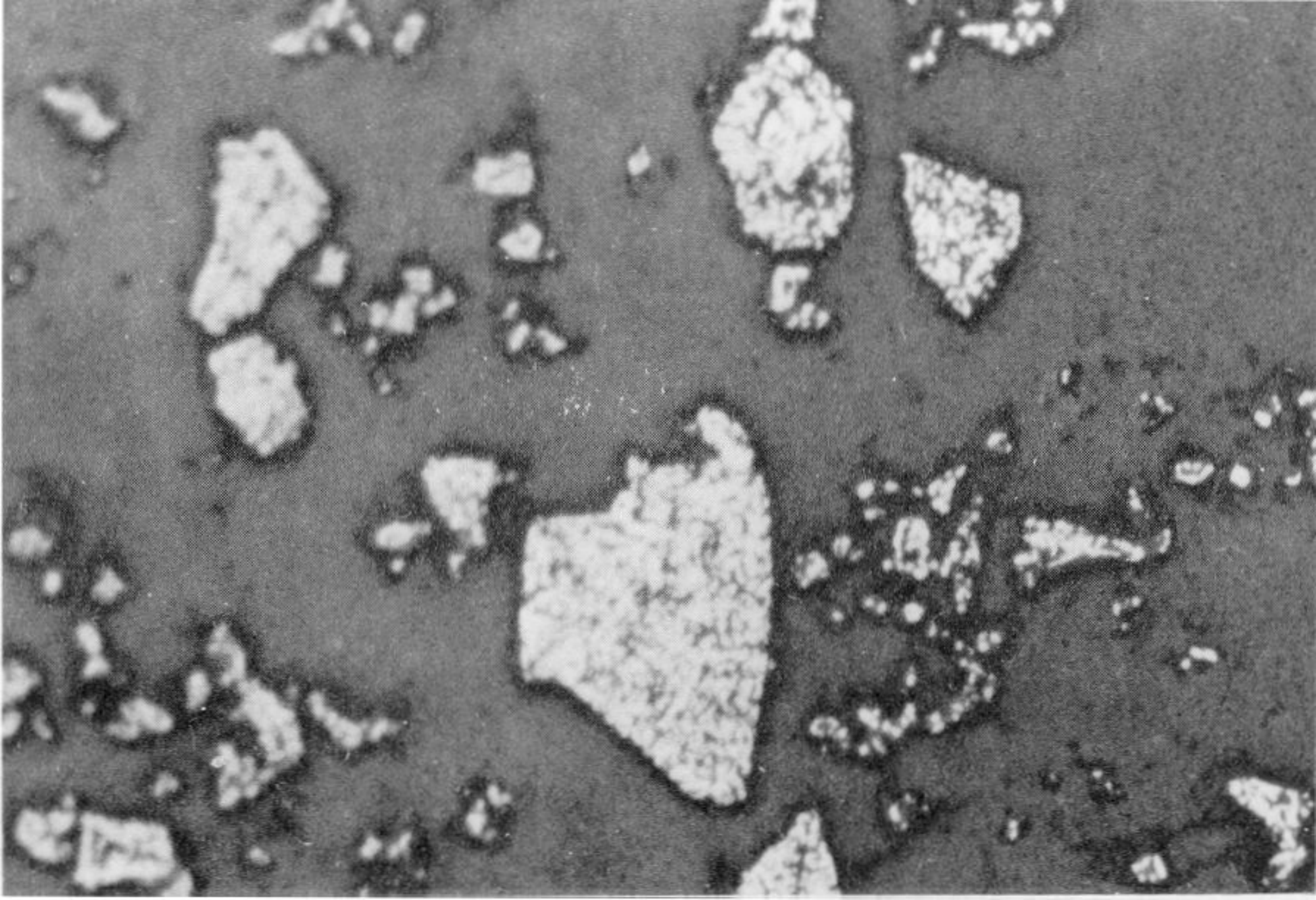

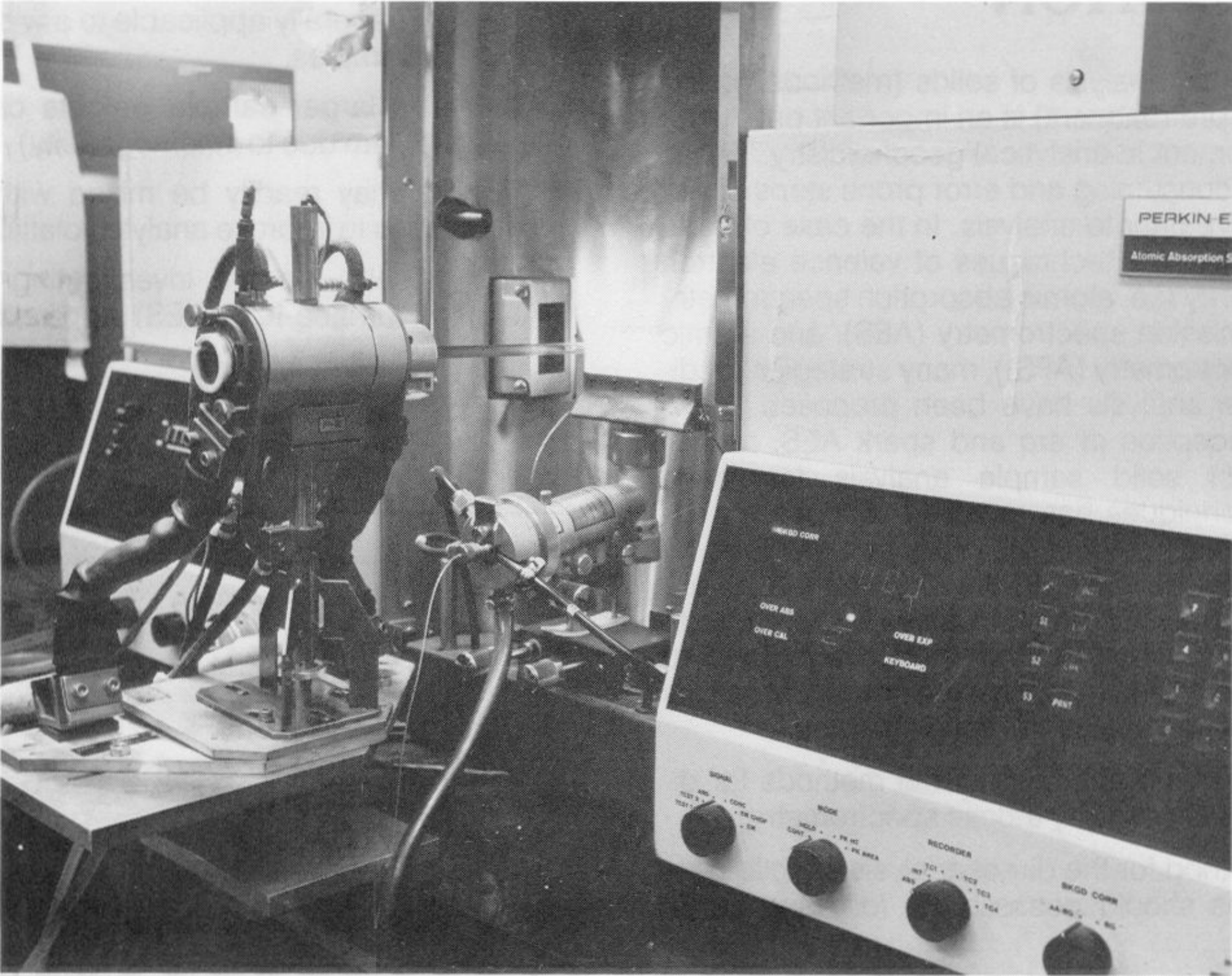
PERKIN-E
Atomic Absorption
OVER ABS
OVER CAL
OVER EXP
KEYBOARD
PRINT
SIGNAL
MODE
RECORDER
BKGD CORR

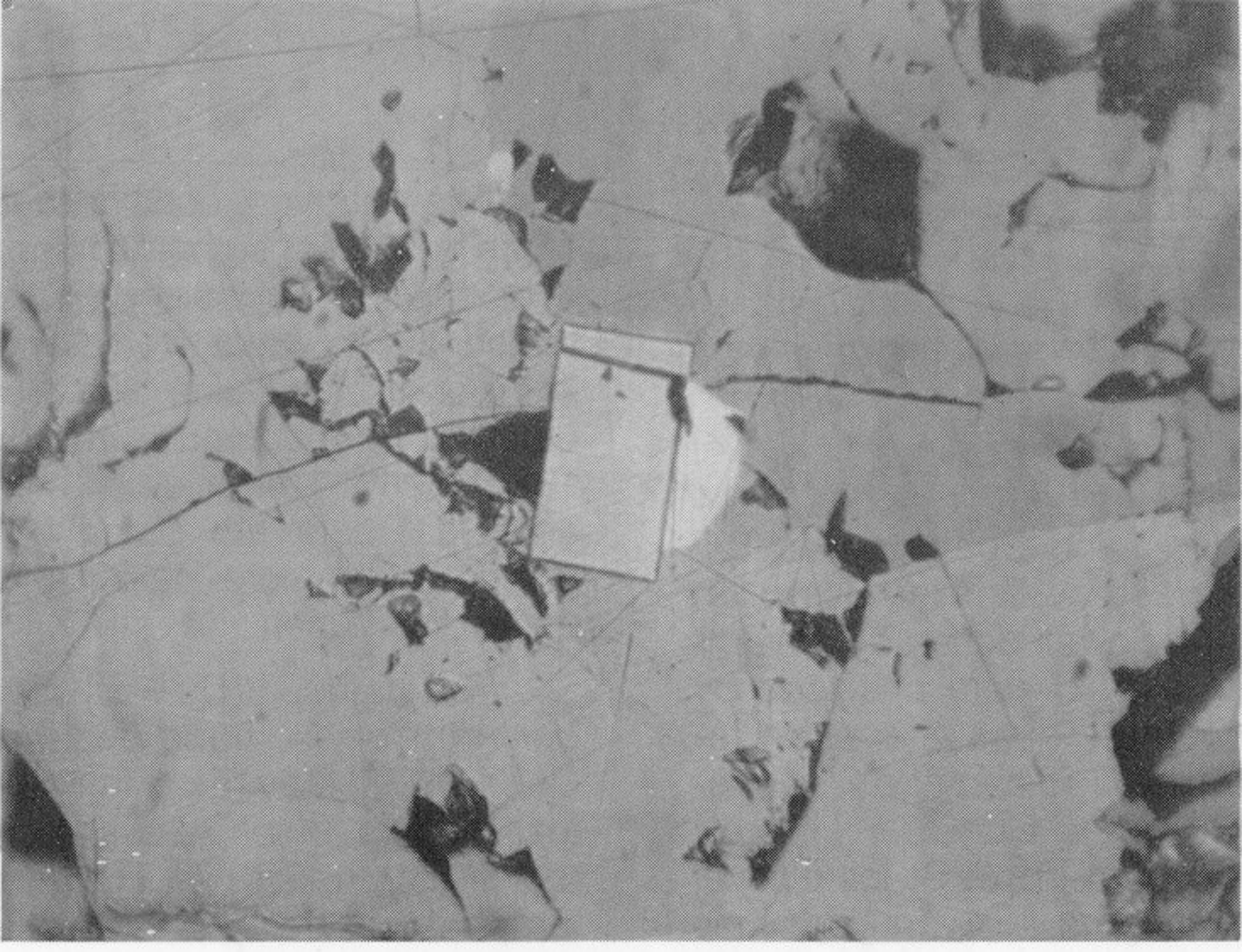

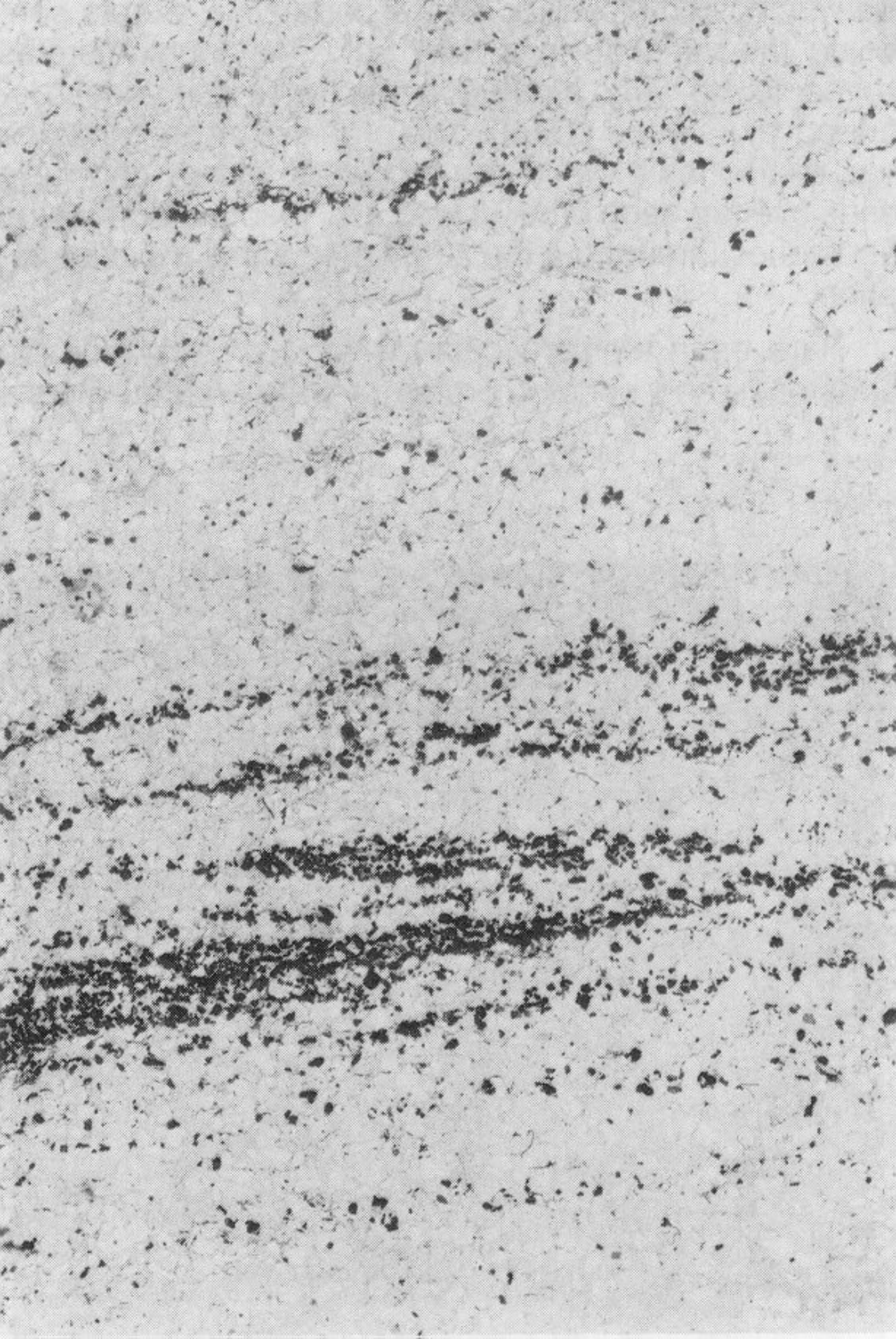

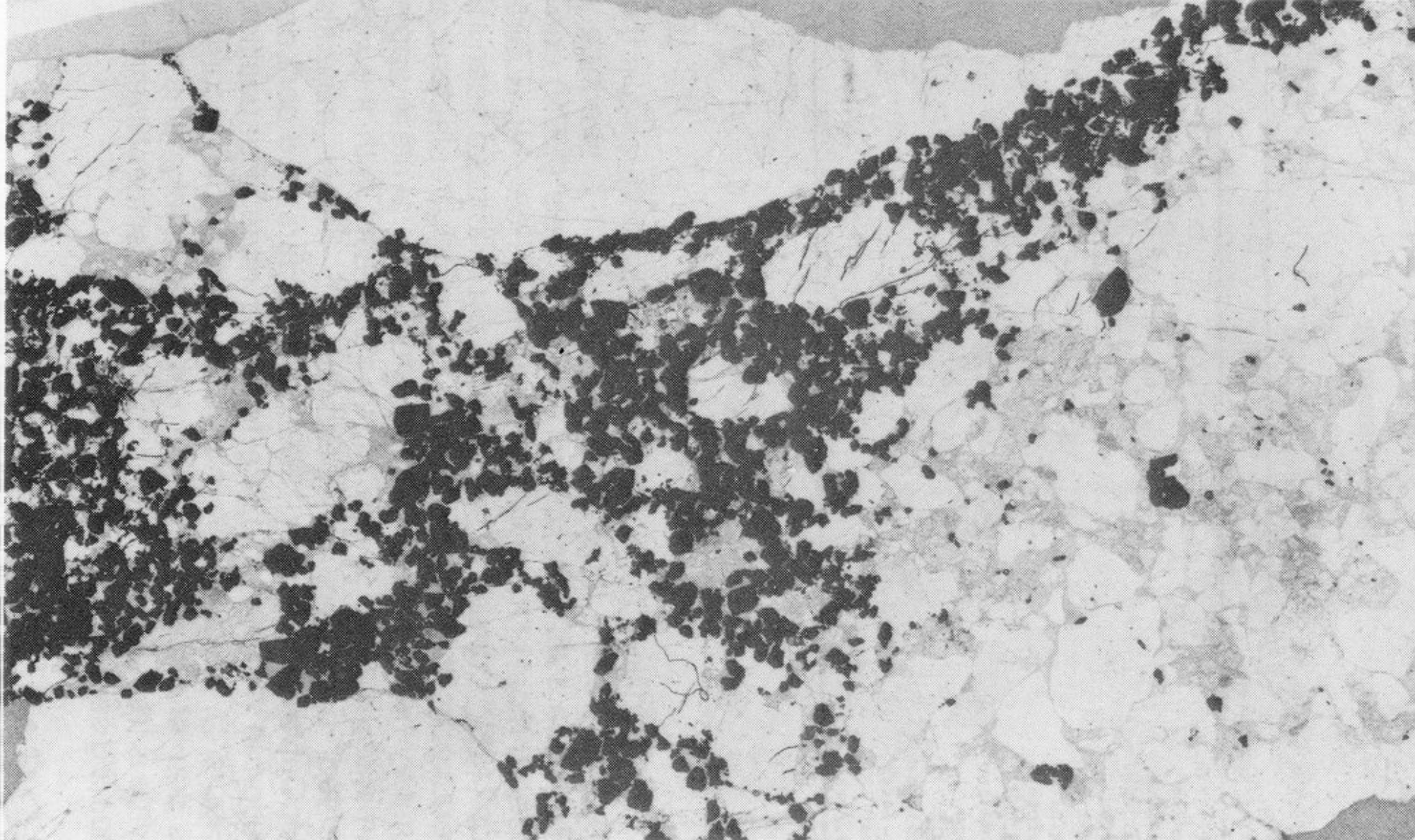

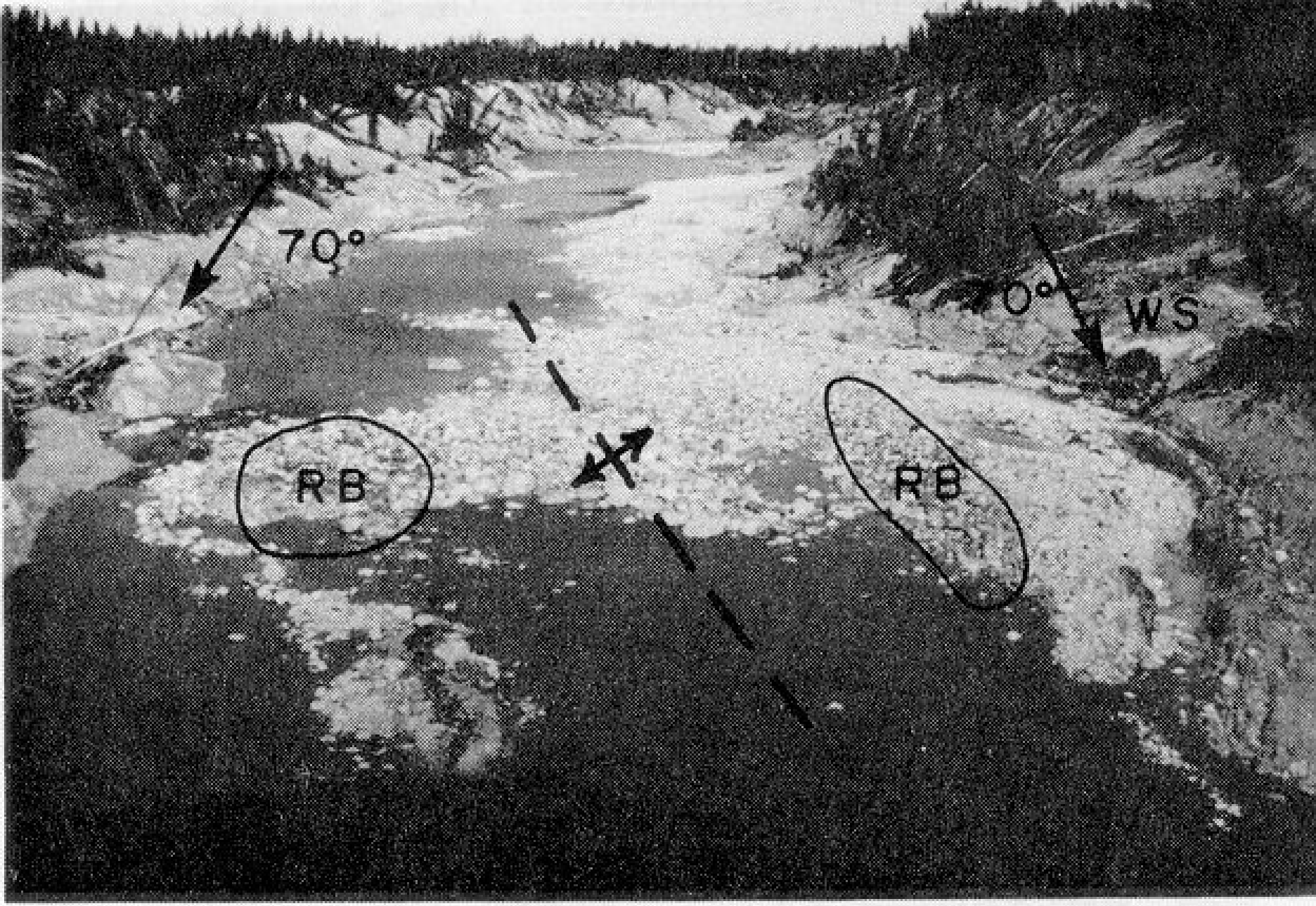
70°
70°
WS
RB
RB

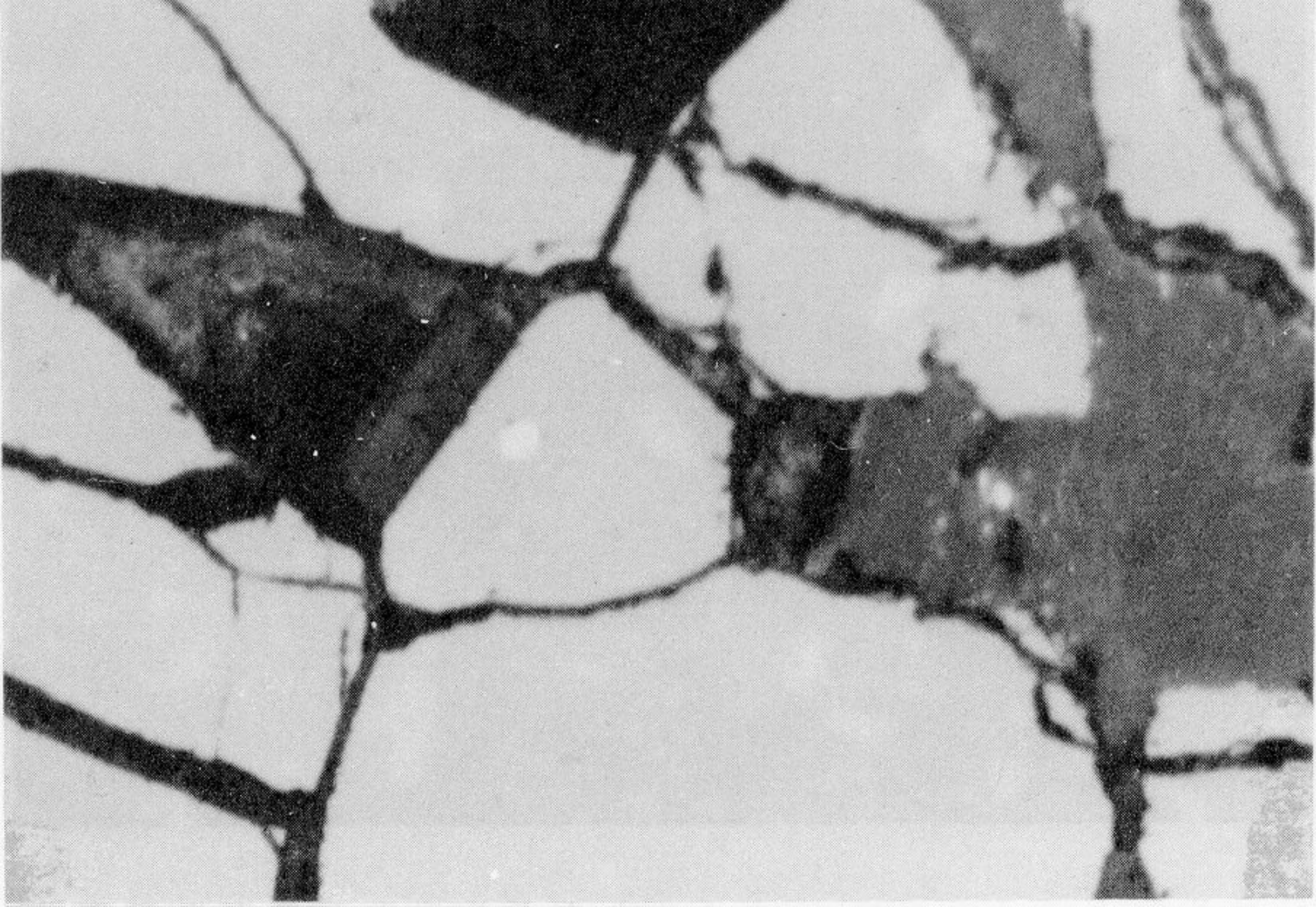

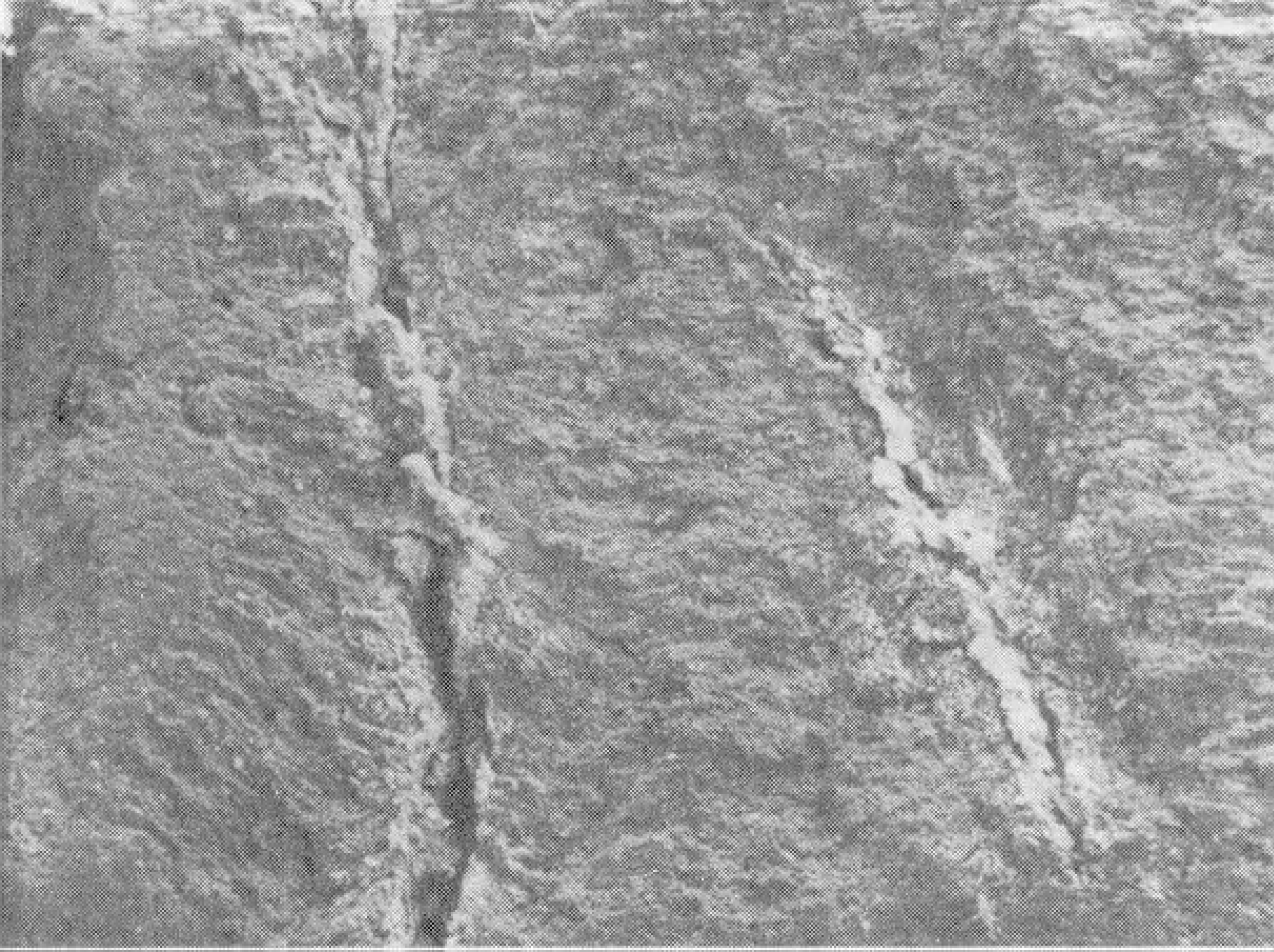

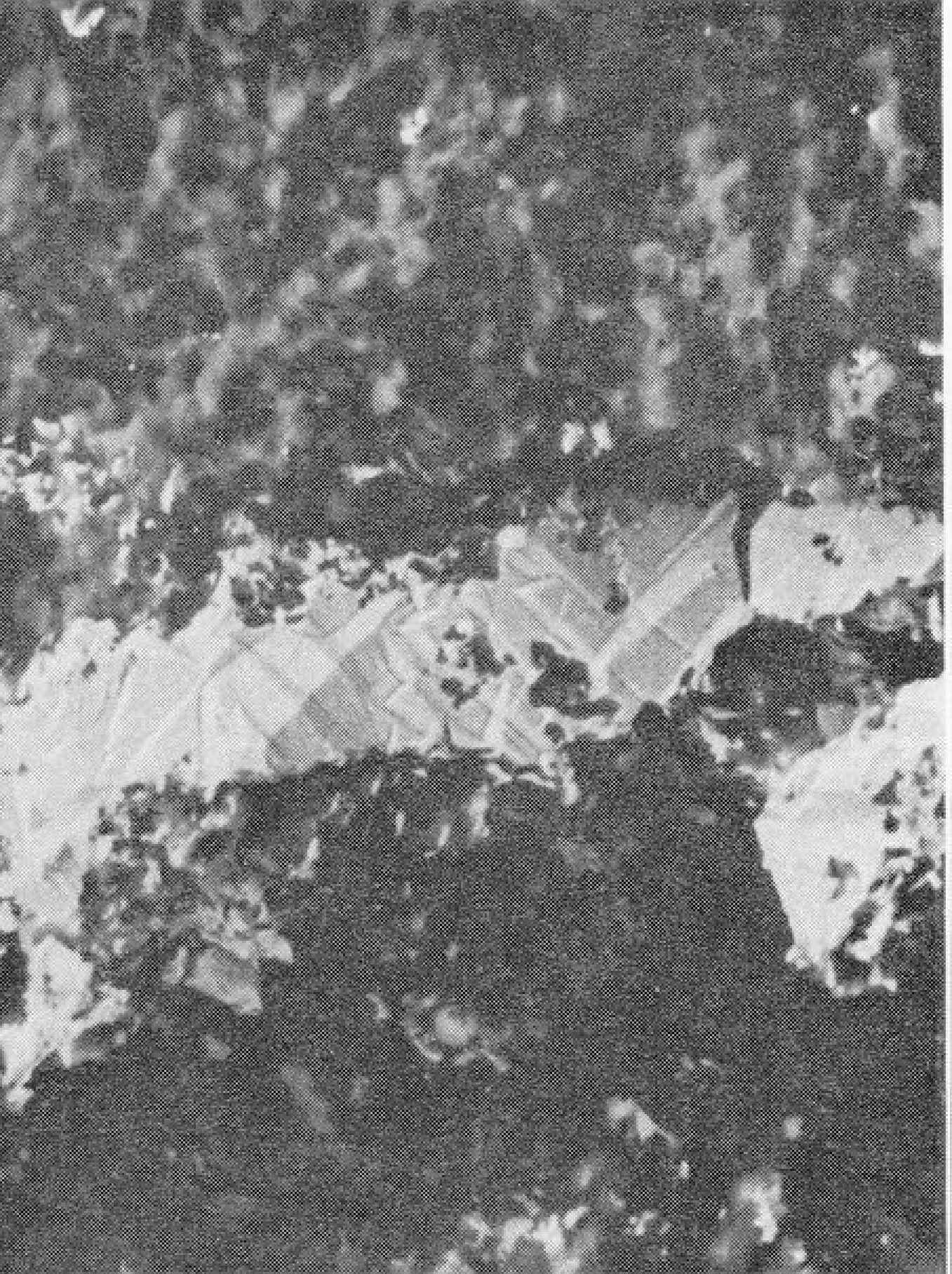

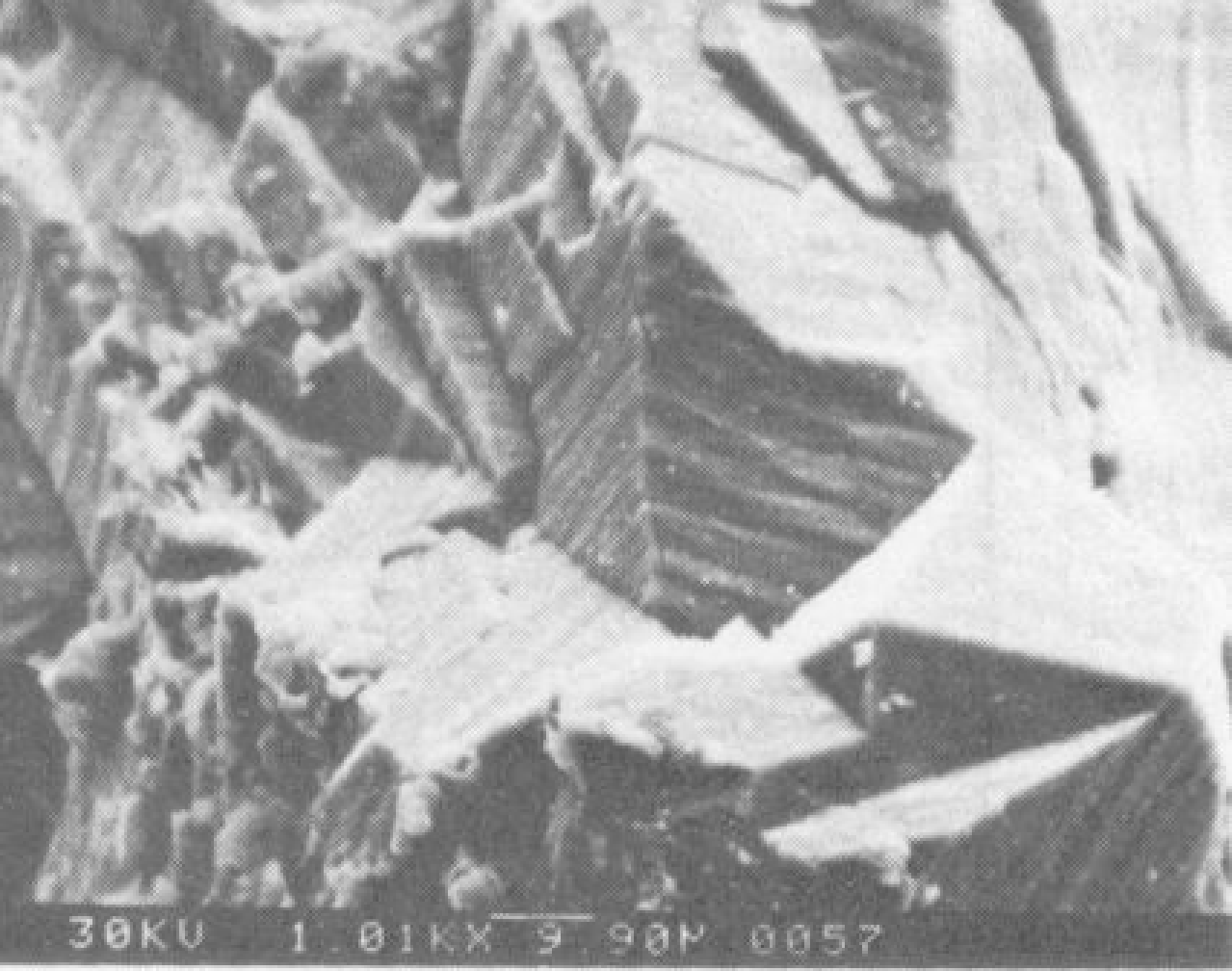
30KV 1.01KX 9.90U 0057


30KV 117X 85.5U 0193

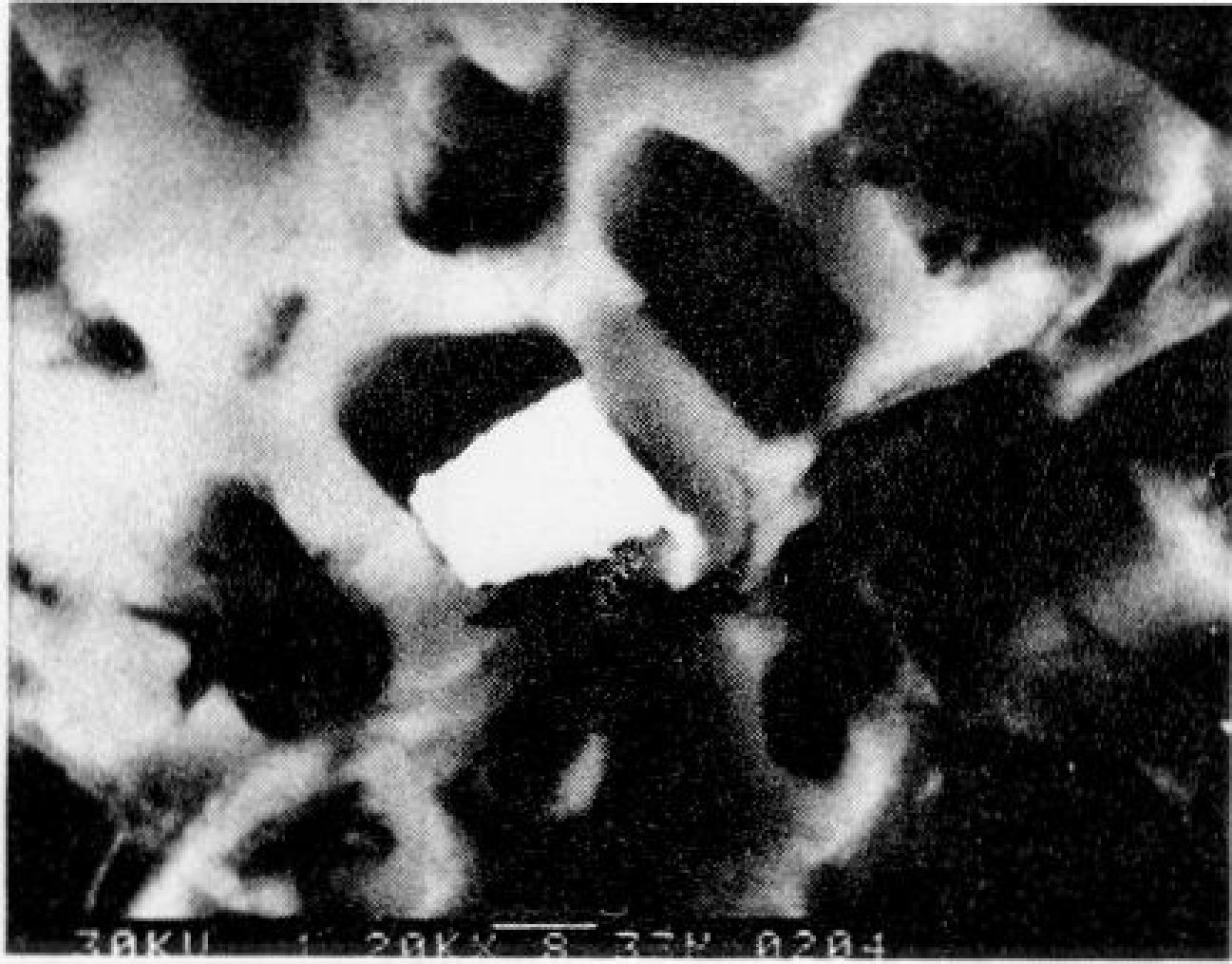
30KV 20KX 8 35M 0204

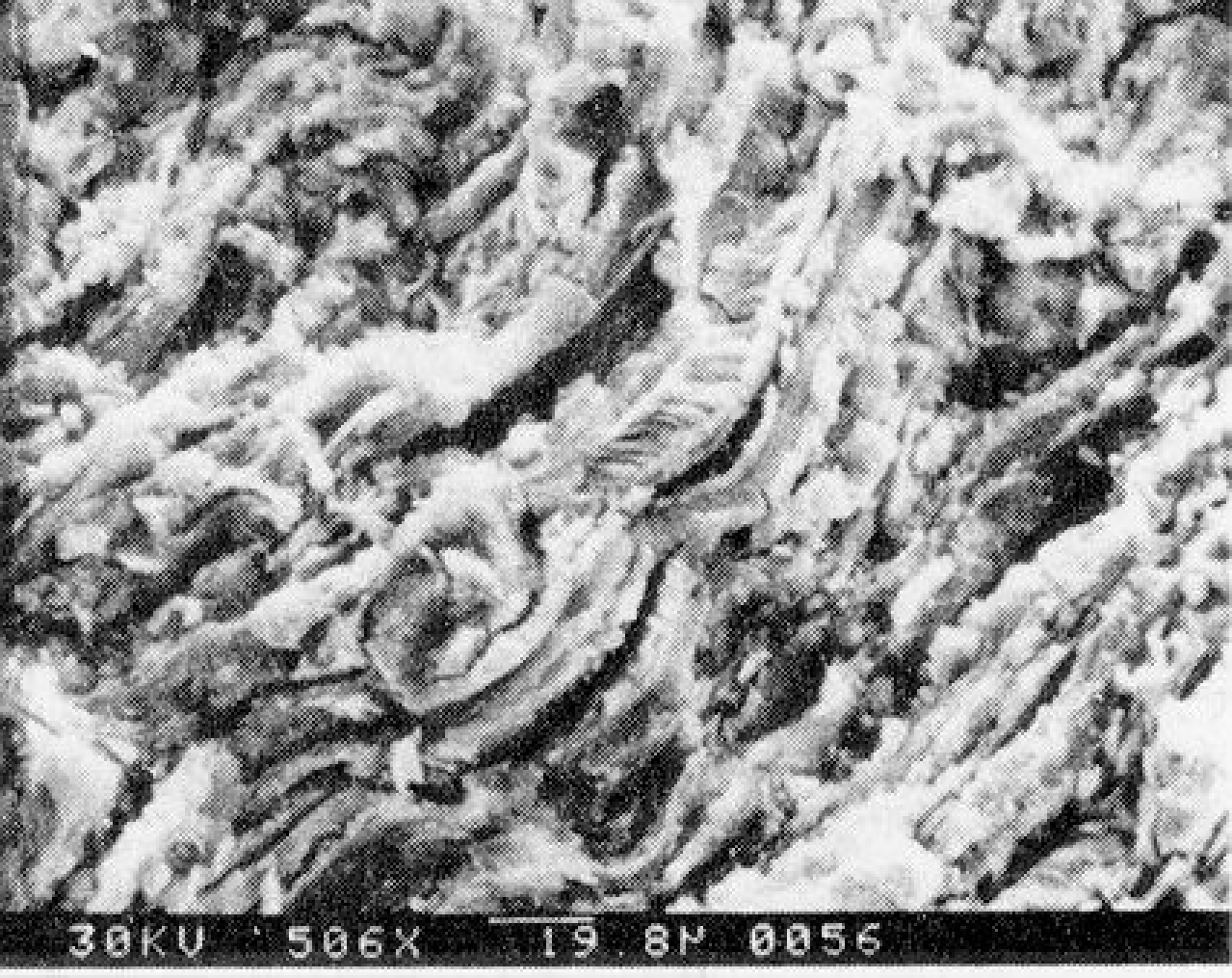
30KV X506X 19.8µ 0056

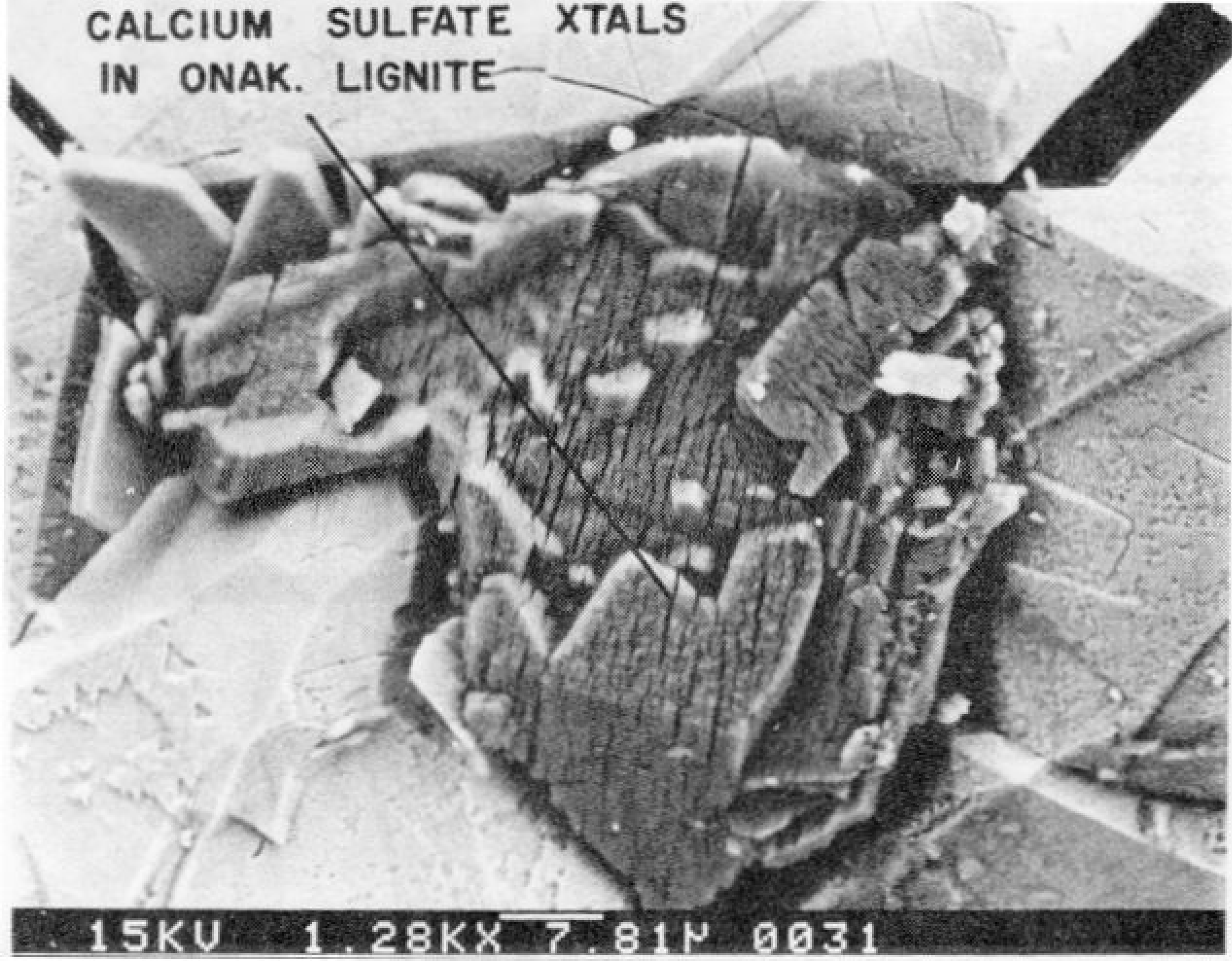
CALCIUM SULFATE XTALS
IN ONAK. LIGNITE
15KV 1.28KX 7.81µ 0031

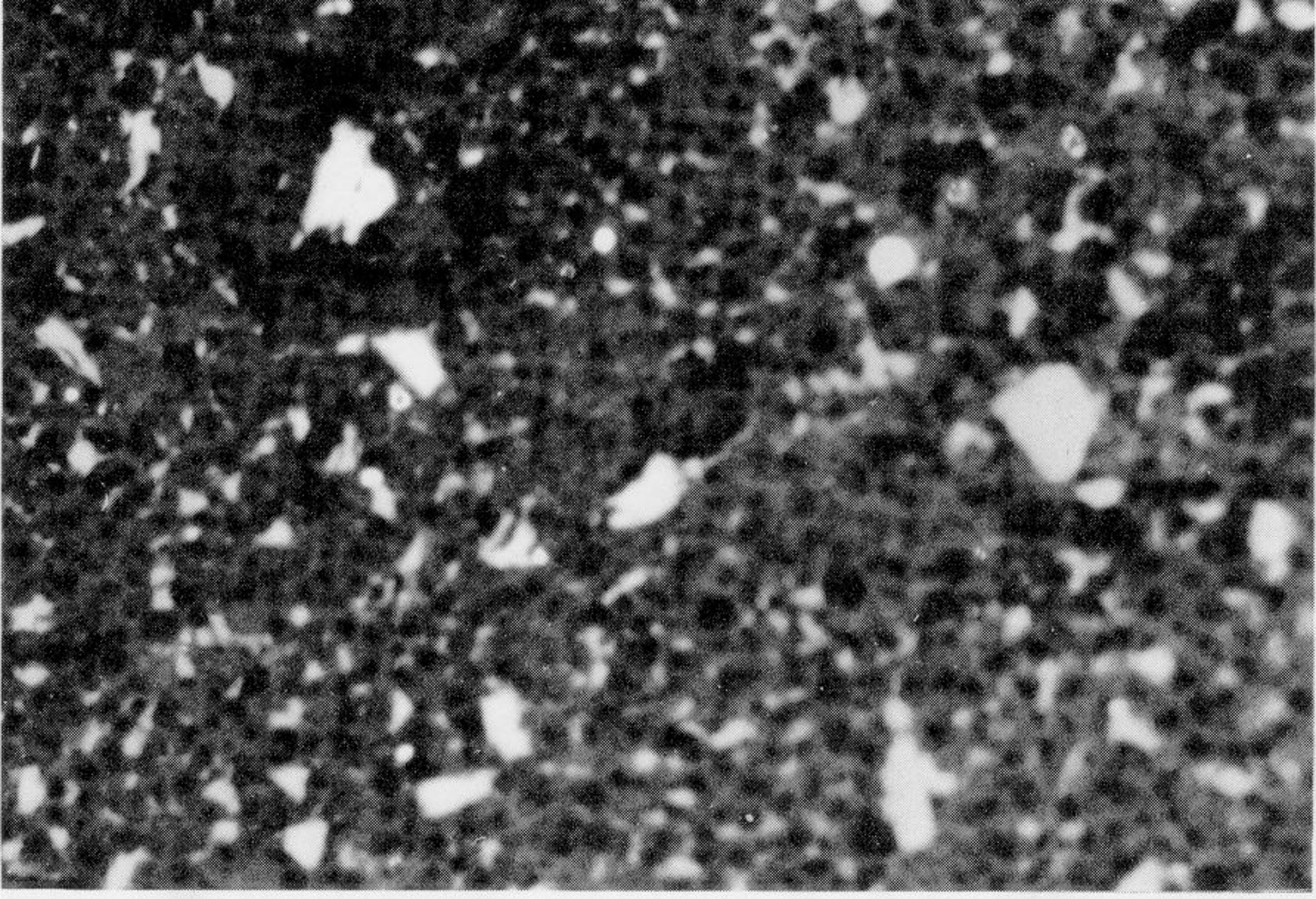

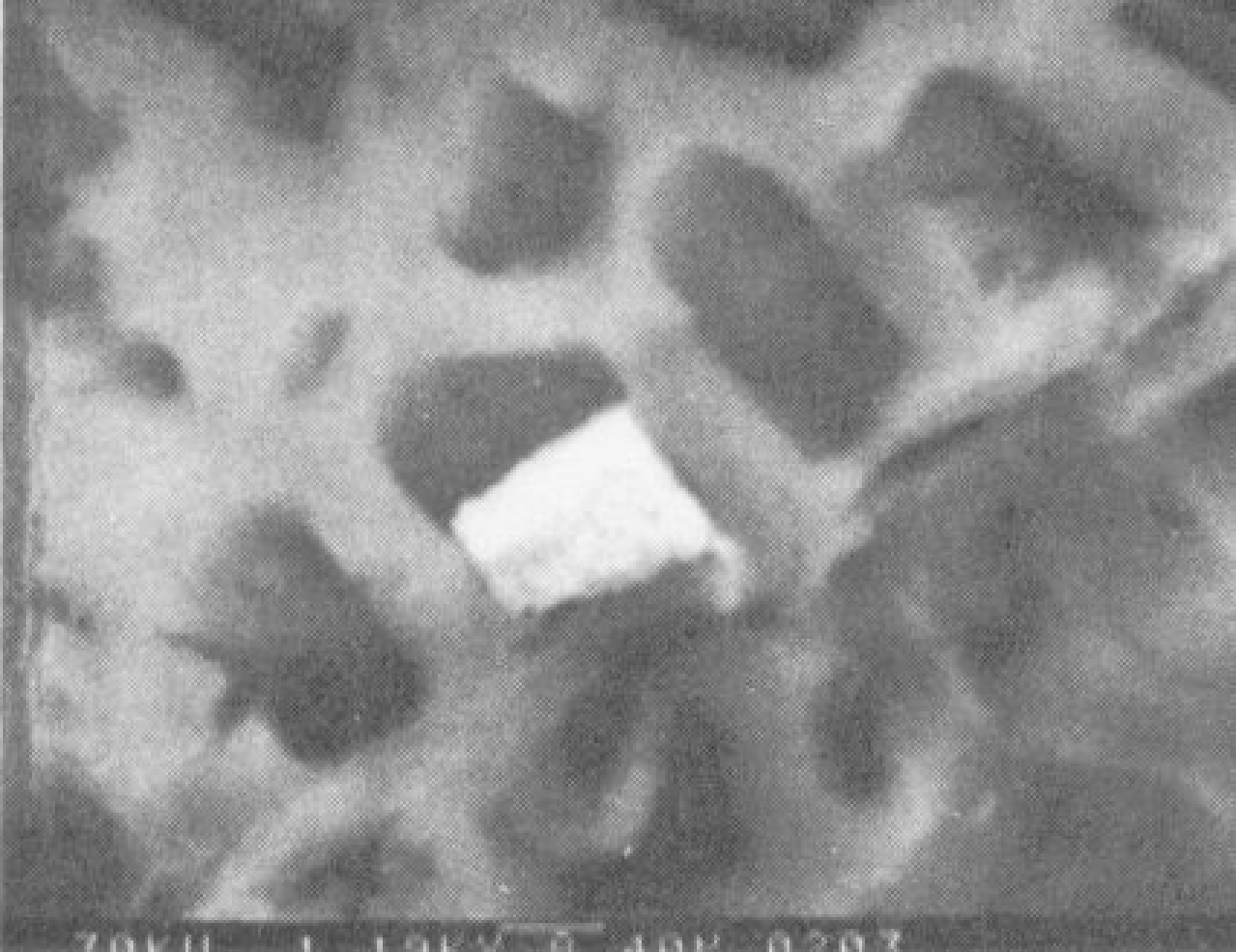


30KV 387X 25 8µ 0185